労災疾病臨床研究事業費補助金

悪性中皮腫に対するヒト化抗 CD26 抗体を基盤とする安全かつ有効な新規併用療法の確立

平成 29 年度　総括・分担研究報告書

研究代表者　森本　幾夫

平成 30(2018)年 3 月

目　　次

Ⅰ．　総括研究報告

労災疾病臨床研究事業費補助金
総括研究報告書

悪性中皮腫に対するヒト化抗 CD26 抗体を基盤とする安全かつ有効な新規併用療法の確立

研究代表者　　森本　幾夫　順天堂大学大学院医学研究科
免疫病・がん先端治療学講座客員教授

研究要旨

悪性胸膜中皮腫はアスベストばく露によって起こる胸膜中皮由来の難治性悪性腫瘍であり、現時点で満足できる治療法はなく、新たな治療法の確立が望まれる。我々は、新規治療標的分子として悪性胸膜中皮腫細胞に発現する CD26 に着目し、ヒト化 CD26 抗体を開発しフランスにて第 I 相臨床試験を行った。安全性が確認されるとともに治療薬としての有効性を示唆する結果も得られ、平成 29 年 6 月から国内での第 I/II 相臨床試験をスタートした。しかしながら、CD26 抗体単剤投与では、Stabilized Disease が認められるも完全寛解までは得られず、悪性胸膜中皮腫患者に完全寛解と肺機能改善をもたらす安全かつ有効な CD26 抗体との革新的な併用療法の開発が望まれる。Y-box binding protein (YB-1)はがんの浸潤・転移促進に関与することから、有用な治療標的として着目されている分子であり、近年、共同研究者の中野賢二博士により良質な YB-1 antisense oligonucleotide (YB-1 AON)が開発された。In vitro 及び in vivo study 解析において、YB-1 AON と CD26 抗体の併用の有用性が示唆されたが、そのメカニズムとして YB-1 AON 及び CD26 抗体それぞれは cyclophilin A 発現を抑制し、さらに併用でより強く cyclophilin A 発現を抑制することによる可能性が示唆された。更に、免疫沈降法、共焦点顕微鏡および STED（誘導放出制御）顕微鏡で CyA と CD26 が共局在していることを明らかにし、YB-1 と CD26 が CyA を介して腫瘍増殖と浸潤に働いている可能性が示された。

中皮腫検体における YB-1 の発現評価方法および半定量的解析法を確立した。その結果、84 例（上皮型 65 例、二相型 10 例、肉腫型 9 例）において 81%の症例について CD26 と YB-1 の共発現が明らかとなり、細胞内局在においても細胞質内での共在が示された。

悪性胸膜中皮腫患者 T 細胞のフェノタイプ解析について悪性胸膜中皮腫患者 11 例の末梢血および胸水中 T 細胞の解析を行った結果、悪性胸膜中皮腫患者の末梢血 CD8T 細胞では、健常者の末梢血 CD8T 細胞よりも Terminal Effector の割合が予想に反して顕著に増加しており、一方で、胸水中 CD8T 細胞では免疫チェックポイント分子の中で PD1 や BTLA、CD39 の発現上昇や Perforin GranzymeB の著明な発現低下が見られた。このことから、胸水中 T 細胞は、近位に存在する悪性胸膜中皮腫からの影響を受けて機能不全になっている可能性が示唆された。

研究分担者

岸本　卓巳：岡山労災病院・副院長

山田　健人：埼玉医科大学医学部
病理学 教授

研究協力者

青江　啓介：山口宇部医療センター
内科系診療部長

藤本　伸一：岡山労災病院
第二呼吸器内科部長

大沼　　圭：順天堂大学大学院医学研究科
免疫病・がん先端治療学講座
准教授

波多野　良：順天堂大学大学院医学研究科
免疫病・がん先端治療学講座
博士研究員

山崎　裕人：順天堂大学大学院医学研究科
免疫病・がん先端治療学講座
研究員

中野　賢二：福岡大学医学部 寄付研究連携
がん薬物療法研究講座　教授

A. 研究目的

悪性中皮腫は、アスベストばく露により発生する難治性悪性腫瘍である。アスベストばく露から悪性中皮腫発生までの潜伏期間は約 30～50 年とされ本邦においても患者数は今後ますます増加すると予想されている。悪性胸膜中皮腫に対する治療法としては手術療法、放射線療法、化学療法などが施行されているが、いずれも満足できる治療成績ではない。更に化学療法の標準治療とされているアリムタ、シスプラチンなどの抗がん剤治療では日本人では副作用が強く、その治療を完遂できる患者は約半数に満たず、生存期間は約 1 年と極めて予後不良である。また悪性中皮腫はアスベストばく露により発症するため労災疾病行政上も病態解明と安全で有効な新規治療法開発が急務とされている。

CD26 分子は T 細胞共刺激分子で DPPIV 酵素活性を有し、研究代表者の森本らは CD26cDNA の単離から CD26 抗体の開発を世界に先駆けて行い当分野では最先端に位置している。CD26 は正常中皮には発現しないが上皮型悪性中皮腫では約 8 割に発現しており、中皮腫細胞の増殖・浸潤に重要な役割を果たすことから、抗腫瘍作用を有する良質なヒト化 CD26 抗体を開発し、悪性中皮腫の新規治療法として有効な可能性が示唆された(Clin Cancer.Res.2007)。

アリムタ、シスプラチンなど抗がん剤治療抵抗性の悪性中皮腫及びその他 CD26 陽性悪性腫瘍を対象に、フランスで本抗体の第 1 相臨床試験を施行し、その安全性が確認され、更に悪性中皮腫 19 例中 10 例が Stabilized Disease(SD)となり、その内 6 例で 3 ヶ月以上(5 例は 6 ヶ月以上)SD が継続し、その有効性が示唆され本邦でも 2017 年 6 月から第Ⅰ/Ⅱ臨床試験がスタートし、現時点では順調に経過している。フランスでの臨床試験ではヒト化 CD26 抗体の単独投与のため完全寛解は得られず、症状緩和、肺の機能改善、治癒を目指す安全かつ有効な新規治療薬との併用療法の確立が望まれる。

Y-box binding protein-1(YB-1)は癌細胞の増殖、浸潤に関与する転与因子で悪性中皮腫でも高発現している(Oncology2014)。研究協力者九州大学中野賢二博士らは YB-1 発現を阻害する架橋型核酸アンチセンス(YB-1 antisense oligonucleotide :

YB-1 AON)を開発し、膵癌モデルの系で有効かつ毒性も低いことを報告した(特願2012-89772)。更に中皮腫組織での CD26 陽性度評価がアリムタを含む化学療法剤の効果予測として有用なことを我々はすでに報告している(Clin Cancer Res 2012)。

本研究では(1)ヒト化 CD26 抗体と YB-1 アンチセンスとの併用による副作用の少ない安全で有効な悪性中皮腫の焦学的治療法の確立を目指し、YB-1 AON および CD26 抗体の中皮腫細胞株での増殖、浸潤への併用効果およびその分子メカニズムの解明(2)悪性中皮腫における CD26 と YB-1 の組織発現と治療反応性や予後を含む臨床パラメーターとの相関を明らかにする。また最近 CTLA-4 抗体や PD-1/PD-L1 抗体が免疫チェックポイント阻害薬として悪性黒色腫や肺癌治療薬として注目されつつあるが、CD26 抗体も免疫チェックポイント阻害薬として作用する可能性を示唆するデータも得られている(J.Immnnol.2015)。そこで、(3)悪性胸膜中皮腫患者の末梢血および胸水中 T 細胞の CD26 発現、免疫チェックポイント分子の発現、細胞傷害性分子の発現、細胞傷害性エフェクター細胞の割合に特に注目して解析を行った。

B. 研究方法

各分担研究報告書に著述

(倫理面への配慮)

ヒト化 CD26 抗体及び YB1-ASO の抗腫瘍効果を評価するためのマウスを用いた動物実験は、順天堂大学医学部実験動物委員会の審査を受け承認されている(承認番号 270138)。

患者検体などについては研究対象者に対する人権擁護上の配慮及び研究により研究対象者が受ける不利益、利益等の説明を患者及び遺族に対して行い、書面でのインフォームド・コンセントを得ている。また病理組織について免疫染色して CD26 発現を解析する研究については、慶應義塾大学医学部および埼玉医科大学の倫理委員会の審査にて承認されている（承認番号 20120100 および 734）。

成人健常者ならびに岡山労災病院、山口宇部医療センターの悪性中皮腫患者、良性石綿胸水患者の末梢血および胸水を用いた研究については、順天堂大学医学部研究等倫理委員会の審査を受け承認されている(承認番号 2017090)。末梢血および胸水の提供を受ける際には、研究対象者に対する人的擁護上の配慮及び研究により研究対象者が受ける不利益、利益等の説明を行い、書面でのインフォームド・コンセントを得ている。

C. 研究結果

1. ヒト化CD26抗体とYB-1阻害アンチセンスとの併用療法およびその分子メカニズムの検討

   Y-box binding protein (YB-1) はがんの浸潤・転移促進に関与することから、有用な治療標的として着目されている分子で、近年、共同研究者の中野賢二博士により、良質な YB-1 antisense oligonucleotide (YB-1 AON)が開発された。一昨年度の研究では、YB-1 AON 処理により YB1 の発現が減少するとともに CD26 の発現も低下することが示され、in vitro 及び in vivo ともに CD26 抗体と YB-1 AON と

の併用の有用性を示唆する実験結果が得られた。また昨年度は、CD26 ノックダウン及び CD26 抗体処理中皮腫細胞株の DNA マイクロアレイデータから、様々な癌で予後因子として知られる cyclophilin A（CyA）を見出したたが、CyA の発現が CD26 抗体及び YB-1 AON それぞれ単剤で抑制され、両者の併用によりさらに抑制されることがわかり、両者の併用効果に CyA が深く関与している可能性が示唆された。本年度は、免疫沈降法で CyA と CD26 の association を明らかにし、さらに共焦点顕微鏡および STED（誘導放出制御）顕微鏡で、細胞内での共局在を証明した。今後は YB-1 AON と CD26 抗体投与のさいの最適プロトコルの決定、また CyA を介した腫瘍抑制メカニズム、また CD26 陽性細胞における CyA の役割、さらには中皮腫病理組織における CyA の発現と予後因子としての可能性について検討する予定である。

2. 悪性中皮腫における CD26 および YB-1 発現について

悪性中皮腫の新規治療法として期待されるヒト化 CD26 抗体療法および YB-1 アンチセンス療法においては、腫瘍組織における CD26 および YB-1 分子の発現の適確な評価が重要である。本研究では、すでに確立された CD26 発現評価方法とともに、新たに YB-1 発現評価方法の確立を通じて、中皮腫検体における本分子群の免疫染色での発現評価法について検討した。その結果、84 症例において、CD26 および YB-1 は、それぞれ 69、79 症例で陽性であり、CD26 陰性 15 症例中では 4 症例で YB-1 陰性であった。また肉腫型中皮腫では CD26 発現頻度は低く 9 症例中陽性は 2 例であったが、YB-1 は 9 症例中 9 例陽性と高率に発現していることを見出した。また、画像解析から CD26 は細胞膜および細胞質に 95%、核に 1-2%の発現があり、一方、YB-1 は細胞質に 90%の発現が認められ、核内に 2-3%の発現が観察された。

3. ヒト化 CD26 抗体の抗腫瘍メカニズムの新たな可能性：悪性中皮腫患者 T 細胞のフェノタイプ解析

有効かつ安全な CD26 抗体との併用療法の開発とともに、CD26 抗体の抗腫瘍作用メカニズムの更なる解明は極めて重要である。CD26 は T 細胞に活性化シグナルを伝達する共刺激分子としても機能するため、CD26 抗体は免疫系にも影響する可能性が考えられる。これまでに、CD26 シグナルによって免疫チェックポイント分子 BTLA と LAG3 の高発現、抑制性サイトカイン IL-10 高産生が誘導されることを報告した。今年度は、悪性胸膜中皮腫患者の胸水中 T 細胞の機能解析を行い、健常者及び中皮腫患者の末梢血 T 細胞と比較して、免疫チェックポイント分子の中で特に PD1, BTLA, CD39 の発現が上昇していること、細胞傷害性分子の Perforin, Granzyme B の発現、エフェクターT 細胞の割合が顕著に低下していることを明らかにした。このことから、悪性胸膜中皮腫患者の胸水中 T 細胞は、近位に存在するがん細胞からの影響を受けて機能不全になっている

可能性が示唆された。

D. 考察

昨年までの研究で中皮腫細胞株においてin vitro, in vivoともにYB-1 AONとCD26抗体との併用での抗腫瘍効果の有用性を示唆する実験結果を報告した。

更にYB-1 AONによる増殖・浸潤抑制作用に、CD26の発現抑制が関与していることが示唆されたため、我々はまずCD26ノックダウン及びCD26抗体処理後のマイクロアレイ解析データを用いて、新規関連分子の探索を行った。その結果、候補分子の一つとしてcyclophilin A (CyA)に着目した。

蛍光顕微鏡の観察では、CyAは細胞質に局在していたが、YB-1 AONまたはCD26抗体処理により、その蛋白発現が抑制された。両者を併用することにより、さらに抑制が増強されたが、CyAのノックダウン実験で、CyAも増殖及び浸潤を促進していることが示された。したがって中皮腫細胞においては、YB-1 AONとCD26抗体の併用による増殖・浸潤抑制作用に、CyAが深く関与している可能性が示唆された。

また免疫沈降実験では、CyAはYB-1とは共沈してこなかったが、CD26とは共沈した。蛍光抗体法による共焦点顕微鏡とSTED（誘導放出制御）顕微鏡で細胞内の局在を観察したところ、両者は共局在していることが確認された。さらに、CyA mRNAの発現制御について検討すると、YB-1 AON、CD26抗体、CD26-siの処理では、すべて影響しなかった。このことをcycloheximide chase assayで確認すると、これらの処理がCyA蛋白のstabilityを低下させることがわかった。つまりCD26は、CyA蛋白に直接結合することで、それを安定化させていることが示唆された。

これまでの研究で、CyAはがん細胞の増殖や浸潤を促進することが報告されており(Nat Med 21:572 2015; Nat Chem Biol 12:117 2016)、子宮癌、食道扁平上皮癌、腎明細胞癌などにおいては、予後予測因子であることが報告されている (Mol Cell Proteomics 7:1810 2008; Genet Test Mol Biomarkers 19:182 2015; Cancer Biol Ther 11:535 2011)。今回、中皮腫細胞においてYB-1 AONとCD26抗体が、CyAの発現を抑制することがわかったが、中皮腫においてCyAが予後予測因子であれば、YB-1 AONやCD26抗体を中皮腫の治療に用いる意義も、さらに強くなると考えられる。

それゆえ中皮腫病理組織でのCyAの発現や、予後因子としての可能性の検討も、今後は必要になると予想された。また、CD26陽性細胞でのCyAの役割や、YB-1 AONやCD26抗体がCyA発現を抑制するメカニズムについても、より詳しく調べる必要があると考えられた。

YB-1は、転写・翻訳に関わる分子であるが、興味深いことに免疫染色での観察では、YB-1タンパク質の主たる局在部位は細胞質であり、核の陽性像は明らかではなかった。しかし、画像解析では、核内に少量の局在が認められたことは、これまでの試験管内でのデータと合致するものである。一方、CD26は、細胞膜貫通型の細胞表面に局在する糖蛋白質であるが、細胞内での局在は、細胞膜のみならず細胞質でのライソゾームや核内と広範囲であり、今回の画像解析の結果も同様であった。これらの二つの分子のがん細胞における局在は重要な意

味を持つが、免疫染色での観察では、CD26 と YB-1 が中皮腫細胞の細胞質において、類似した瀰漫性の局在を示すことは、これらの分子の相互作用の可能性がある。CD26 を標的とした抗体療法は、抗体による免疫学的細胞傷害や CD26 機能の抑制が主体であり、腫瘍細胞の細胞表面 CD26 は抗体により細胞質内に内在化される。一方、YB-1 を標的としたアンチセンス療法は、アンチセンスによる YB-1 蛋白発現抑制が主体である。従って併用療法においては、抗体により CD26 は細胞質内での増加とその核内移行が惹起され、一方、YB-1 蛋白はアンチセンスにより減少することが想像されため、この状況での中皮腫細胞における細胞増殖や細胞死の変化がどうなるか、さらなる詳細な検証が期待される。

また悪性中皮腫における CD26 および YB-1 発現について細胞局在、陽性率、陽性強度などの各種パラメーターで詳細に定量評価することで、抗体療法の効果や予後などとの関連性あるいは臨床パラメーターを検証する基礎を構築していくことが重要と考える。

これまでの結果から、CD26 共刺激は CD4 T 細胞に対して BTLA と LAG3 の高発現、IL-10 の高産生を誘導し、CD8 T 細胞に対しても CD28 共刺激と比較して BTLA の発現を顕著に誘導することが示された。また、がん細胞周囲に多く存在すると考えられる免疫抑制性因子のうち、TGF-□は PD1 の、PGE_2、L-Kynurenine、Adenosine は TIM3 の、PGE_2 は 2B4 (CD244)と CD39 の発現を顕著に増強させることが示された。興味深いことに、PGE_2、L-Kynurenine、Adenosine は CD26 の発現も顕著に増強することが示唆され、がん細胞周囲に浸潤した T 細胞は CD26 の発現が増強している可能性が考えられる。

CD26 抗体が免疫系に及ぼす影響を解析する方法として、平成 29 年 6 月から開始したヒト化 CD26 抗体の国内第 I/II 相臨床試験に参加した患者検体を用いて、CD26 抗体投与による血清中の可溶性 CD26 濃度/DPPIV 酵素活性値や IL-10 濃度の変動、末梢血 T 細胞のエフェクター機能、BTLA や LAG3 などの免疫チェックポイント分子の発現の変動を経時的に解析することを計画している。

今回はまだ悪性胸膜中皮腫患者 11 例、良性石綿胸水患者 2 例での検討結果だが、悪性胸膜中皮腫患者の胸水中 CD4 T 細胞、CD8 T 細胞ともに健常者の末梢血 T 細胞、悪性胸膜中皮腫患者の末梢血 T 細胞と比較して、CD26 の発現や免疫チェックポイント分子の発現、細胞傷害性機能が明らかに異なることが示された。今後、良性石綿胸水患者や肺がん患者といった対照症例のデータを増やし、悪性胸膜中皮腫に特徴的な免疫チェックポイント分子の発現パターンや CD26 の発現、T 細胞のサブセット解析を進め、悪性胸膜中皮腫の影響を受けた T 細胞の特性を解明する予定である。また、病理組織の免疫染色により、実際に悪性胸膜中皮腫周囲に浸潤した T 細胞の性質についても解析を行う。

われわれは強い CD26 共刺激シグナルによって BTLA の発現が CD4・CD8 両 T 細胞に特徴的に誘導されることを明らかにしたが、そのシグナル伝達経路、及び転写因子についても解析が必要となる。一部の悪性胸膜中皮腫患者では胸水中 T 細胞に

BTLA の高発現が認められるため、このサブセットをセルソーターで分離・精製し、DNA マイクロアレイ解析を行う。in vitro の実験で CD26 共刺激に特徴的な発現上昇が見られる転写因子との比較解析を行い、BTLA の発現制御に関わる転写因子の絞り込みを行う。また、悪性胸膜中皮腫患者の中で、BTLA が高発現している患者の臨床的な特徴についても、検体数を増やしてより詳細に検討していく予定である。

更に血清中の可溶性 CD26 濃度/DPPIV 酵素活性値や IL-10 濃度、末梢血 T 細胞の BTLA、LAG3 の発現の経時的なモニタリングが、ヒト化 CD26 抗体の治療有効性を予測するバイオマーカーになりうる可能性も考えられるため、その点にも着目して解析を行う。

E. 結論

1. In vitro および in vivo 解析において、YB-1 AON と CD26 抗体の併用の有用性が示唆されたが、そのメカニズムとして、YB-1 と CD26 が、CyA を介して腫瘍の増殖と浸潤に働いている可能性が示された。

2. 中皮腫検体における YB-1 の発現評価方法および半定量的解析法を確立した。その結果、81%の症例において CD26 と YB-1 の共発現が明らかとなり、細胞内局在においても細胞質内での共在が示された。

3. 悪性胸膜中皮腫患者 11 例の末梢血および胸水中 T 細胞の解析を行った結果、悪性胸膜中皮腫患者の末梢血 CD8 T 細胞では、健常者の末梢血 CD8 T 細胞よりも Terminal Effector の割合が予想に反して顕著に増加しており、一方で、胸水中 CD8 T 細胞では PD1 や BTLA、CD39 の発現上昇や Perforin、Granzyme B の著明な発現低下が見られた。このことから、胸水中 T 細胞は、近位に存在する悪性胸膜中皮腫からの影響を受けて機能不全になっている可能性が示唆された。

F. 健康危険情報

現時点では特記すべき健康危険情報はない。

G. 今後の展望

YB-1－AON については中野教授らにより前臨床毒性試験は終了して、現在 First in Man 第 1 相臨床試験を計画中である。またヒト化 CD26 抗体は 2017 年 6 月から悪性中皮腫をターゲットにして国内で第 1/2 相臨床試験がスタートした。

YB-1 AON 及び CD26 抗体の併用の、最適投与プロトコルの確立を行う。また、それらによる CyA の発現抑制メカニズムと、CD26 陽性細胞における CyA の役割を、より詳細に調べる。さらに、中皮腫病理組織における CyA の発現と、予後因子としての可能性を検討する。

悪性中皮腫自身やその周囲の細胞に BTLA や LAG3、そのリガンドである HVEM や MHC class II が発現しているか免疫組織染色で検討する。また、CD26 共刺激に特徴的な BTLA の発現誘導に関わるシグナル伝達経路、及び転写因子についての解析が必要となる。さらに、本年度に引き続き、悪性中皮腫患者の末梢血 T 細胞、胸水 T 細胞、悪性中皮腫周囲に浸潤した T 細胞を用いて、各種免疫チェックポイント分子の発現パターンやエフェクター分子、CD26 の発現を解析するとともに、CD26

抗体の国内第 I/II 相臨床試験検体を用いて、CD26 抗体投与による血清中可溶性 CD26 濃度/DPPIV 酵素活性値、IL-10 濃度、末梢血 T 細胞上の BTLA、LAG3 の発現変動を経時的にモニタリングしていく予定である。

H. 研究発表

1. 論文発表

1) Ohnuma K, Hatano R, Komiya E, Otsuka H, Itoh T, Iwao N, Kaneko Y, Yamada T, Dang NH, Morimoto C. A novel role for CD26/dipeptidyl peptidase IV as a therapeutic target in selected immune disorders and cancers. Front Biosci. in press.
2) Hiromura M, Nohtomi K, Mori Y, Kataoka H, Sugano M, Ohnuma K, Kuwata H, Hirano T. Caveolin-1, a binding protein of CD26, is essential for the anti-inflammatory effects of dipeptidylpeptidase-4 inhibitors on human and mouse macrophages. Biochem Biophys Res Commun. 2018; 495: 223-229.
3) Angevin E, Isambert N, Trillet-Lenoir V, You B, Alexandre J, Zalcman G, Vielh P, Farace F, Valleix F, Podoll T, Kuramochi Y, Miyashita I, Hosono O, Dang NH, Ohnuma K, Yamada T, Kaneko Y, Morimoto C. First-in-Human phase 1 of YS110, a monoclonal antibody directed against CD26 in advanced CD26-expressing cancers.Br.J.Cancer.2017;116:1126-1134.
4) Komiya E, Hatano R, Otsuka H, Itoh T, Yamazaki H, Yamada T, Dang NH, Tominaga M, Suga Y, Kimura U, Takamori K, Morimoto C, Ohnuma K. A possible role for CD26/DPPIV enzyme activity in the regulation of psoriatic pruritus.J Dermatol Sci. 2017; 86:212-221.
5) Kim KM, Noh JH, Bodogai M, Martindale JL, Yang X, Indig FE, Basu SK, Ohnuma K, Morimoto C, Johnson PF, Biragyn A, Abdelmohsen K, Gorospe M. Identification of senescent cell surface targetable protein DDP4.Genes Dev. 2017;31:1529-1534.
6) Ikeda T, Kobayashi S, Morimoto C. Gene expression microarray data from mouse cerebrum treated with rTMS for 30 days.Data Brief. 2017; 15: 948-969.
7) Doonan BP, Ohnuma K, Dang LH, Morimoto C, Dang NH. Current and Emerging Therapy for Malignant Pleural Mesothelioma: Focus on CD26/Dipeptidyl Peptidase IV as a Therapeutic Target. Current Cancer Therapy Reviews. 2017; 13: 1-13.
8) Murakami R, Saisho Y, Watanabe Y, Inaishi J, Tsuchiya T, Kou K, Sato S, Kitago M, Kitagawa Y, Yamada T. Pancreas fat and beta cell mass in humans with and without diabetes: An analysis in the Japanese population. J Clin Endocrinol Metab 2017;102:3251-3260.

9) Aida S, Hozumi M, Ichikawa D, Iida K, Yonemura Y, Tabata N, Yamada T, Matsushita M, Sugai T, Yanagawa H, Hattori Y. A novel phenylphthalimide derivative, pegylated TC11, improves pharmacokinetic properties and induces apoptosis of high-risk myeloma cells via G2/M cell-cycle arrest. BBRC 2017;493:514-520.
10) Kushitani K, Amatya VJ, Mawas AS, Suzuki R, Miyata Y, Okada M, Inai K, Kishimoto T, Takeshima Y. Utility of Survivin, BAP1, and Ki‐67 immunohistochemistry in distinguishing epithelioid mesothelioma from reactive mesothelial hyperplasia. Oncology Letters.2018;15:3540-3547.
11) Ninomiya T, Nogami N, Kozuki T, Harada D, Kubo T, Ohashi K, Kuyama S, Bessho A, Fujimoto N, Aoe K, Shibayama T, Takigawa N, Sugimoto K, Kudo K, Fukamatsu N, Hotta K, Kiura K. A phase I trial of afatinib and bevacizumab in chemo-naïve patients with advanced non-small-cell lung cancer harboring EGFR-mutations: Okayama Lung Cancer Study Group Trial 1404. Lung Cancer. 2018;115:103-108.
12) Sato H, Sakaguchi M, Yamamoto H, Tomida S, Aoe K, Shien K, Yoshioka T, Namba K, Torigoe H, Soh J, Tsukuda K, Tao H, Okabe K, Miyoshi S, Pass HI, Toyooka S. Therapeutic potential of targeting S100A11 in malignant pleural mesothelioma. Oncogenesis. 2018;7:11.
13) Hotta K, Aoe K, Kozuki T, Ohashi K, Ninomiya K, Ichihara E, Kubo T, Ninomiya T, Chikamori K, Harada D, Nogami N, Hirata T, Hinotsu S, Toyooka S, Kiura K. A Phase II Study of Trastuzumab Emtansine in HER2-positive Non-Small-Cell Lung Cancer. J Thorac Oncol. 2018;13:273-279.
14) Katakami N, Uchino J, Yokoyama T, Naito T, Kondo M, Yamada K, Kitajima H, Yoshimori K, Sato K, Saito H, Aoe K, Tsuji T, Takiguchi Y, Takayama K, Komura N, Takiguchi T, Eguchi K. Anamorelin (ONO-7643) for the treatment of patients with non-small cell lung cancer and cachexia: Results from a randomized, double-blind, placebo-controlled, multicenter study of Japanese patients (ONO-7643-04). Cancer. 2018;124:606-616.
15) Kushitani K, Amatya VJ, Okada Y, Katayama Y, Mawas AS, Miyata Y, Okada M, Inai K, Kishimoto T, Takeshima Y. Utility and pitfall of Immunohistochemistry in the Differential Diagnosis between Epithelioid Mesothelioma and Poorly Differentiated Lung Squamous Cell Carcinoma. Histopathology. 2017;70:375-384.
16) Amatya VJ, Kushitani K, Mawas AS, Miyata Y, Okada M, Kishimoto T, Inai

K, Takeshima Y. MUC4, a novel immunohistochemical marker identified by gene expression profiling, differentiates pleural sarcomatoid mesothelioma from lung sarcomatoid carcinoma. Mod Pathol. 2017;30:672-681.

17) Kuraoka M, Amatya VJ, Kushitani K, Mawas AS, Miyata Y, Okada M, Kishimoto T, Inai K, Nishisaka T, Sueda T, Takeshima Y. Identification of DAB2 and Intelectin-1 as Novel Positive Immunohistochemical Markers of Epithelioid Mesothelioma by Transcriptome Microarray Analysis for its Differentiation From Pulmonary Adenocarcinoma. Am J Surg Pathol. 2017; 41: 1045-1052

18) 岸本卓巳、藤本伸一.石綿ばく露によるびまん性胸膜肥厚と中皮腫・肺癌発生に関する検討.日職災医誌. 2017; 65: 153-159.

19) 岸本卓巳.アスベストの発がん機序　環境による健康リスク.日本医師会雑誌.2017;146:S253.

20) Kuyama S, Ochi N, Bessho A, Hotta K, Ikeda G, Kishino D, Kubo T, Harada D, Fujimoto N, Nakanishi M, Umeno T, Okada T, Chikamori K, Yamagishi T, Ohashi K, Ichihara E, Takigawa N, Tanimoto M, Kiura K. A Phase II trial of carboplatin plus S-1 for elderly patients with advanced non-small-cell lung cancer with wild-type epidermal growth factor receptor: The Okayama Lung Cancer Study Group Trial 1202. Lung Cancer 2017;112: 188-194.

21) Ozeki T, Asano M, Fujimoto N, Nishimura J, Takada K, Miyamoto Y, Fuchimoto Y, Wada S, Ozaki S, Kishimoto T. Esophagobronchial fistula in a patient with squamous cell carcinoma of the lung: A case report. Case Rep Oncol. 2017;10:553-557.

22) Nishimura J, Miyamoto Y, Fujimoto N, Ozeki T, Takada K, Asano M, Fuchimoto Y, Wada S, Ozaki S, Kishimoto T. Adenocarcinoma of the lung acquiring resistance to afatinib by transformation to small cell carcinoma: A case report. Case Rep Oncol. 2017;10:666-670.

23) Murata Y, Aoe K, Mimura-Kimura Y, Murakami T, Oishi K, Matsumoto T, Ueoka H, Matsunaga K, Yano M, Mimura Y. Association of IgG4 and free light chain with idiopathic pleural effusion. Clin Exp Immunol. 2017;190:133-142.

２．著書

1) Hatano R, Ohnuma K, Yamada T, Okamoto T, Komiya E, Otsuka H, Itoh T, Yamazaki H, Iwao N, Kaneko Y, Dang NH, Morimoto C. The use of the humanized anti-CD26 monoclonal antibody YS110 as a novel targeted therapy for refractory cancers and immune disorders. Advances in Medicine and Biology

(Nova Science Publishers, Inc.). in press.

2) Ohnuma K, Hatano R, Yamazaki H, Kaneko Y, Dang NH, Morimoto C. CD26-targeted therapy: A new horizon in malignant pleural mesothelioma management. Horizons in Cancer Research (Nova Science Publishers, Inc.). 2017; Volume 64: Chapter 6: 129-161.

３．学会発表

1) 岩尾憲明、大沼圭、大塚春奈、波多野良、古宮栄利子、伊藤匠、森本幾夫. 急性 GVHD マウスモデルにおける HMGB1 の動態に関する検討.第 40 回日本造血細胞移植学会、2018 年 2 月、札幌.

2) Eriko Komiya, Ryo Hatano, Haruna Otsuka, Takumi Itoh, Hiroto Yamazaki, Mitsutoshi Tominaga, Kenji Takamori, Kei Ohnuma, Chikao Morimoto. CD26/DPPIV regulates mechanical itch in a mechanistically distinct manner from chemical itch. 第 42 回日本研究皮膚科学会、2017 年 12 月、高知.

3) Takumi Itoh, Ryo Hatano, Haruna Otsuka, Noriaki Iwao, Satoshi Iwata, Taketo Yamada, Chikao Morimoto. IL-26 facilitates angiogenesis and skin inflammation via inducing FGF2 production in a murine model of imiquimod-induced psoriasis. 第 46 回日本免疫学会、2017 年 12 月、仙台.

4) Eriko Komiya, Ryo Hatano, Haruna Otsuka, Takumi Itoh, Hiroto Yamazaki, Taketo Yamada, Yasushi Suga, Utako Kimura, Mitsutoshi Tominaga, Kenji Takamori, Kei Ohnuma, Chikao Morimoto. The regulation of pruritus in psoriasis and atopic dermatitis-a possible role for CD26/DPPIV. 9th World Congress on Itch, 2017 ,October.Wrocław, Poland.

5) 波多野良、大沼圭、石井智徳、岩田哲史、奥村康、関川巖、森本幾夫. 全身性エリテマトーデスのステロイド治療抵抗性と CD26 陰性 T 細胞サブセットとの関係性について. 第 61 回日本リウマチ学会、2017 年 4 月、福岡.

6) Nishida H, Hayashi M, Morimoto C, Sakamoto M, Yamada T. Humanized anti-CD26 monoclonal antibody, YS110, has anti-myeloma efficacy for the treatment of high-risk multiple myeloma. The 59th American Society of Hematology Annual Meeting and Exposition. 2017, December, Atlanta, GA, USA.

7) Yamada T, Madokoro H, Nishida H, Morimoto C, Sakamoto M, Hayashi M. Anti-CD26 humanized monoclonal antibody conjugated to triptolide is transported into nucleus and impairs RNA polymerase II. 2017 年 12 月、生命科学系学会合同年次大会（ConBio2017）神戸.

8) Nishida H, Hayashi M, Morimoto C, Sakamoto M, Yamada T. Humanized

anti-CD26 monoclonal antibody has a therapeutic potentiality against multiple myeloma. 第 79 回日本血液学会、2017 年 10 月、東京国際フォーラム.

9) 土居美枝子、稲田博輝、細沼沙紀、政岡秀彦、瀬山幸子、金野美年子、石澤圭介、茅野秀一、山田健人、佐々木惇 腺癌との鑑別を要したリンパ腫様型/形質細胞腫様浸潤性尿路上皮癌の 1 例. 第 58 回日本臨床細胞学会総会、平成 29 年（2017 年）5 月、大阪.

10）李治平，山田健人，金玲，市村隆也，石澤圭介，佐々木惇　関節リウマチのエタネルセプト治療中に UIP 型間質性肺炎併発した一剖検症例．第 106 回日本病理学会総会 2017 年 4 月、東京

11）金　玲，李　治平，市村隆也，石澤圭介，茅野秀一，佐々木惇，山田健人　百日咳肺炎から肺高血圧症を併発し死亡した新生児剖検症例．第 106 回日本病理学会総会 2017 年 4 月、東京.

12）Yamada T, Madokoro H, Yamada K, Nishida H, Morimoto C, Sakamoto M, Hayashi M. Anti-tumor effects of humanized anti-CD26 monoclonal antibody against hepatocellular carcinoma. 第 106 回日本病理学会総会　2017 年 4 月、東京.

13）Aida S, Ichikawa D, Iida K, Hozumi M, Nakamura M, Uozaki R, Hashimoto N, Okayama M, Yonemura Y, Tabata N, Yamada T, Matsushita M, Sugai T, Yanagawa H, Hattori Y. PEG(E)-TC11, a novel polyethylene glycol-linked phthalimide derivative, inhibited high-risk MM cell growth in vivo and in vitro via cell cycle G2/M arrest in a CRBN-independent manner. American Association for Cancer Research (AACR) Annual Meeting, 2017, April, Washington D.C., USA.

14）Fujimoto N, Kojima Y, Kishimoto T. Secretary leukocyte peptide inhibitor (SLPI) in pleural fluid is useful as a diagnostic marker of malignant pleural mesothelioma. ASCO2017(American Society of Clinical Oncology Annual Meeting) 2017 年 6 月 3－7 日 Chicago.

15）Kato K, Gemba K, Ashizawa K, Kishimoto T, Fujimoto N, Aoe K, Takeshima Y, Inai K. CT Findings of Malignant Pleural Mesothelioma and Correlation with the Survival Period .The 4th World Congress of Thoracic Imaging（WCTI）2017 年 6 月 18－21 日　Boston.

16）藤本伸一、児島葉子、宮本洋輔、浅野美智子、渕本康子、和田佐恵、小崎晋司、岸本卓巳．胸膜中皮腫の診断における胸水 Secretary leukocyte peptide inhibitor (SLPI) の有用性について．第 15 回日本臨床腫瘍学会学術集会 2017 年 7 月 27 日　神戸.

17）尾瀬功、長松康子、青江啓介、加藤勝也、堀田勝幸、中川淳子、原桂子、岸本卓巳、藤本伸一．悪性胸膜中皮腫患者の QOL 調査結果．第 15 回日本臨床

腫瘍学会学術集会　2017 年 7 月 28 日　神戸.

18）中川淳子、小林幸以、石丸直樹、野村伽奈子、亀谷友里恵、藤本伸一、岸本卓巳. 胸膜中皮腫患者の経時的ケアニーズ. 第 15 回日本臨床腫瘍学会学術集会　2017 年 7 月 29 日　神戸.

19）藤本伸一、長松康子、青江啓介、堀田勝幸、加藤勝也、尾瀬功、中川淳子、原桂子、岸本卓巳. 「患者と家族のための胸膜中皮腫ハンドブック」の作成　第 15 回日本臨床腫瘍学会学術集会　2017 年 7 月 29 日　神戸.

20）Oze I , Nagamatsu Y, Aoe K, Hotta K, Kato K, Nakagawa J, Hara K, Kishimoto T, Fujimoto N. Evaluation of quality of life in survivors with malignant pleural mesothelioma in Japan. EUROPEAN SOCIETY FOR MEDICAL ONCOLOGY 2017 Congress （ESMO2017） 2017 年 9 月 8－12 日　MADRID.

21）倉岡正嗣、アマティア　ヴィシュワジート、櫛谷桂、Amany S.Mawas、宮田義浩、岡田守人、岸本卓巳、井内康輝、西阪隆、末田泰二郎、武島幸男. 網羅的遺伝子発現解析から同定した DAB2 と Intelectin-1 の上皮型中皮腫と肺腺癌の鑑別診断における有用性. 第 24 回石綿・中皮腫研究会　2017 年 10 月 7 日　大阪.

22）西村泰光　李順姫、松﨑秀紀、武井直子、吉留敬、岡本賢三、岸本卓巳. 包括的免疫機能解析による悪性中皮腫とびまん性胸膜肥厚との判別指標の探索. 第 24 回石綿・中皮腫研究会　2017 年 10 月 7 日　大阪.

23）藤本伸一、西村淳、宮本洋輔、浅野美智子、渕本康子、和田佐恵、小崎晋司、伊賀徳周、西英行、岸本卓巳. 「胸水のみ」を呈する胸膜中皮腫症例の検討. 第 58 回日本肺癌学会学術集会　2017 年 10 月 14 日　横浜.

24）Kuraoka M, Amatya VJ, Kushitani K, Mawas AS, Miyata Y, Okada M, Kishimoto T, Inai K, Nishisaka T, Sueda T, Takeshima Y. Identification of DAB2 and Intelectin-1 as Novel Positive Immunohistochemical Markers of Epithelioid Mesothelioma. 18th World Conference on Lung Cancer　2017 年 10 月 16 日　Yokohama.

25）Kishimoto T. Clinical Evaluation for Asbestos-Induced Diffuse Pleuralthickening (DPT) in JAPAN. CHEST 2017. 2017 年 11 月 1 日　Toronto.

26）岸本卓巳、藤本伸一. 胸膜中皮腫の診断時胸部 CT 所見の検討. 第 65 回日本職業・災害医学会学術大会　2017 年 11 月 25 日　北九州.

27）藤本伸一、岸本卓巳、青江啓介、加藤勝也、堀田勝幸、尾瀬功、長松康子. 胸膜中皮腫に対する新規治療法の臨床導入に関する研究. 第 65 回日本職業・災害医学会学術大会　2017 年 11 月 25 日　北九州.

28）藤本伸一、宮本洋輔、和田佐恵、野上尚之、久山彰一、別所昭宏、堀田勝幸、青江啓介、南大輔、木浦勝行. EGFR 遺伝子変異陽性非小細胞肺癌に対する

afatinib・bevacizumab 併用療法の第Ⅰ相試験：OLCSG1404．第 58 回日本肺癌学会学術集会。平成 29 年 10 月 14 日、横浜.

29）坂本健次、近森研一、村田順之、青江啓介、前田忠士、亀井治人、松本常男．両側肺動脈腫瘍の肺浸潤に対し、TBLB で悪性軟部腫瘍と診断した一例．第 57 回日本呼吸器学会学術講演会、平成 29 年 4 月 22 日、東京.

30）村田順之、青江啓介、宇都宮利彰、三村雄輔、松本常男．胸膜に IgG4 陽性形質細胞を認めた胸水症例の解析．第 57 回日本呼吸器学会学術講演会．平成 29 年 4 月 23 日、東京.

31）坂本健次、村田順之、近森研一、青江啓介、前田忠士、亀井治人、丸山治彦．肺結核、結核性胸膜炎との鑑別を要したウェステルマン肺吸虫症の一例．第 40 回日本呼吸器内視鏡学会学術集会、平成 29 年 6 月 10 日、長崎.

32）近森研一、関千尋、青江啓介、前田忠士、坂本健次、村田順之、宇都宮利彰、亀井治人．ニボルマブ使用後に薬剤性肺障害を発症した非小細胞肺がん症例の当院での臨床的特徴. 第 58 回日本肺癌学会学術集会、平成 29 年 10 月 15 日、横浜.

33）関千尋、前田忠士、青江啓介、近森研一、坂本健次、村田順之、宇都宮利彰、亀井治人．ニボルマブを早期肺障害で中止したが、ペムブロリズマブへ変更し、効果が得られた進行肺腺癌の一例．第 58 回日本肺癌学会学術集会、平成 29 年 10 月 14 日、横浜.

34）坂本健次、村田順之、大畑秀一郎、宇都宮利彰、近森研一、青江啓介、前田忠士、亀井治人、松本常男．肺 MAC 症に MALT リンパ腫を併発した一例．第 26 回日本呼吸器内視鏡学会中国四国支部会、平成 29 年 10 月 28 日、広島.

I.知的財産権の出願・登録状況（予定を含む）

1. 発明者：森本幾夫、波多野良、山田健人、大沼圭.
   出願番号：特許出願中
   名称：抗ヒト CD26 モノクローナル抗体
   出願人：学校法人 順天堂、埼玉医科大学（共同出願）
   出願年月日：2018 年 3 月予定(PCT 出願)
2. 発明者：森本幾夫、波多野良、大沼圭、伊藤匠.
   出願番号：特願 2017-231439
   名称：抗ヒト IL-26 抗体
   出願人：学校法人 順天堂
   出願年月日：2017 年 12 月 1 日(PCT 出願)

Ⅱ．　分担研究報告

労災疾病臨床研究事業費補助金
分担研究報告書

ヒト化 CD26 抗体と YB-1 阻害アンチセンスとの悪性中皮腫における併用療法の可能性

研究代表者　森本　幾夫　順天堂大学大学院医学研究科
免疫病・がん先端治療学講座 客員教授

研究協力者　岡本　俊博　免疫病・がん先端治療学講座 研究補助員

研究協力者　波多野　良　免疫病・がん先端治療学講座 博士研究員

研究協力者　山崎　裕人　免疫病・がん先端治療学講座 協力研究員

研究協力者　中野　賢二　福岡大学医学部 寄付研究連携　がん薬物療法研究講座　教授

研究要旨

悪性胸膜中皮腫はアスベストばく露によって起こる胸膜中皮由来の難治性悪性腫瘍であり、現時点で満足できる治療法はなく、新たな治療法の確立が望まれている。我々は、新規治療標的分子として、中皮腫細胞に発現する CD26 に着目し、自ら開発したヒト化 CD26 抗体で、フランスにて第 I 相臨床試験を行った。その結果、ヒトでの安全性が確認されるとともに、治療薬としての有効性を示唆する結果も得られたため、平成 29 年 6 月から国内でも第 I/II 相臨床試験を開始した。フランスの第 I 相臨床試験での CD26 抗体単剤投与では、Stabilized Disease が認められるも、完全寛解までは得られなかった。そのため安全かつ有効な、中皮腫患者に完全寛解と肺機能改善をもたらす、CD26 抗体との革新的な併用療法の開発が望まれる。一方、Y-box binding protein (YB-1) は、がんの浸潤・転移促進に関与することから、有用な治療標的として着目されている分子で、近年、共同研究者の中野賢二博士により、良質な YB-1 antisense oligonucleotide (YB-1 AON)が開発された。一昨年度の研究では、YB-1 AON 処理により YB1 の発現が減少するとともに CD26 の発現も低下することが示され、in vitro 及び in vivo ともに CD26 抗体と YB-1 AON との併用の有用性を示唆する実験結果が得られた。また昨年度は、CD26 ノックダウン及び CD26 抗体処理中皮腫細胞株の DNA マイクロアレイデータから、様々な癌で予後因子として知られる cyclophilin A（CyA）を見出したたが、CyA の発現が CD26 抗体及び YB-1 AON それぞれ単剤で抑制され、両者の併用によりさらに抑制されることがわかり、両者の併用効果に CyA が深く関与している可能性が示唆された。本年度は、免疫沈降法で CyA と CD26 の association を明らかにし、さらに共焦点顕微鏡および STED（誘導放出制御）顕微鏡で、細胞内での共局在を証明した。今後は YB-1 AON と CD26 抗体投与の際の最適プロトコルの決定、また CyA を介した腫瘍抑制メカニズム、また CD26 陽性細胞における CyA の役割、さらには中皮腫病理組織における CyA の発現と予後因子としての可能性について検討する予定である。

A.研究目的

悪性胸膜中皮腫はアスベストばく露によって起こる胸膜中皮由来の難治性悪性腫瘍である。アスベストばく露から発症までの潜伏期間は 30-50 年とされ、日本を含めアジアやヨーロッパなど世界規模で胸膜中皮腫患者数は、今後ますます増加すると考えられている。悪性胸膜中皮腫に対しては手術療法、化学療法、放射線療法などが行われるが、いずれも満足できる治療成績ではなく、化学療法の標準治療法とされているアリムタ・シスプラチンの併用投与でも生存期間中央値は約 1 年と非常に短い。

このことから、新たな治療法の確立が切望されているが、我々は新規治療標的分子として悪性胸膜中皮腫細胞に発現する CD26 に着目した。その目的で、我々はヒト化 CD26 抗体を開発し、フランスにて悪性胸膜中皮腫を中心とした CD26 陽性腫瘍に対する第 I 相臨床試験を行った。特記すべき副作用もなく、その安全性が確認されたが、その後抗がん剤抵抗性の悪性胸膜中皮腫患者 19 例中、10 例が Stabilized Disease (SD)となり、治療薬としての有効性を示唆する結果も得られた。平成 29 年 6 月からは、国内での第 I/II 相臨床試験がスタートしている。ヒト化 CD26 抗体単剤投与を行ったフランスの第 I 相臨床試験では、SD が認められるも完全寛解までは得られなかった。それゆえ副作用の少ない、安全かつ有効な CD26 抗体との併用療法の開発が望まれる。

一方、Y-box binding protein (YB-1) はコールドショック蛋白族メンバーに属し、RNA の転写・翻訳の制御に関係するタンパク質で、ヒト癌細胞の核内と細胞質に局在することが知られている。また P-糖蛋白質 (MDR1, ABCB1) などの ABC トランスポーターや DNA 修復関連酵素の発現を上昇させ、広く薬剤耐性の獲得について重要な鍵を握るとされている分子である。

YB-1 はさまざまな癌種において、その核内局在や発現レベルが、がんにおける薬剤耐性や予後の有用な予測因子とも報告されており、さらにがん細胞の上皮間葉転換(EMT)を誘発し、浸潤、転移の促進にも関与することから、がんの有用な治療標的として注目されるようになった。そして近年、共同研究者の福岡大学・中野賢二博士により、生物活性や安定性に優れた良質な YB-1 antisence oligonucleotide (YB-1 AON) が開発され、膵がんに対して増殖抑制効果、浸潤・転移抑制効果を示すことが報告された (特願 2012-89772)。

そこで本研究では、悪性胸膜中皮腫患者に完全寛解、及び肺機能改善をもたらす、CD26 抗体との革新的な併用療法の確立を目指し、まず中皮腫細胞株の浸潤及び増殖に対するヒト化 CD26 抗体と YB-1 AON の併用効果を検討した。さらに、その分子メカニズムについても、新規関連蛋白の探索と解析により、分子細胞生物学的に検討することにした。

B. 研究方法

1) 細胞株

本研究ではすべて、CD26 陽性ヒト悪性胸膜中皮腫細胞株として H226 及び JMN を用いた。

2) 抗体及び試薬

ヒト化 CD26 抗体 YS110 (Isotype: Human IgG1)は Y's therapeutics により開発された。

Goat anti-Human CD26 pAb (AF1180)は R&D Systems より購入した。Rabbit anti-Human YB1 pAb (clone ab12148)は abcam より購入した。Mouse anti-Human Cyclophilin A mAb (clone ab58144)は abcam より購入した。YB-1 antisense oligonucleotide (AON) は九州大学・中野賢二博士により開発されたもので、本人から提供を受けた。Control siRNA は Qiagen より購入した。Cyclophilin A siRNA は Sigma-Aldrich より購入した。YB-1 AON 及び control-siRNA は最終濃度が 5, 10, 15, 20 nM、cyclophilin A は 20 nM の濃度で、Lipofectamine RNAiMAX Reagent (Invitrogen) を用いて transfection を行った。

3) In vitro 浸潤アッセイ及び増殖アッセイ
In vitro の浸潤は、10%ウシ胎児血清(FCS)を誘引物質として用い、Boyden chamber assay で測定した。具体的にはマトリゲルでコーティングされたインサートウェルを用い、細胞に control-siRNA 及び YB-1 AON を transfection 後、48 時間目に $3x10^4$ /ウェルの細胞を播種した。一方 CD26 抗体は、細胞の播種と同時に添加した。浸潤した細胞はディフ・クイック（シスメックス）を用いて染色し、それぞれ 24, 48, 72 時間後における細胞浸潤を測定した。In vitro 増殖アッセイは 96 well プレートを用い、細胞に control-siRNA 及び YB-1 AON を transfection 後、48 時間目に $2\text{-}2.5x10^3$ /ウェルの細胞を播種した。CD26 抗体は細胞の播種と同時に添加した。それぞれ 24, 48, 72 時間後に MTT アッセイを行い、細胞増殖を測定した。

4) in vivo での腫瘍増殖評価
YB-1 AON とヒト化 CD26 抗体の腫瘍増殖抑制効果を in vivo で評価するために、雌の C.B17-scid マウスの dorsal region にそれぞれ H226 および JMN 細胞株を 1 匹あたり $5x10^3$ cell 皮下移植し、翌日からヒト化 CD26 抗体を 200μg/dose で週 2 回腹腔内投与、また YB-1 AON 200μg を週 1 回尾静脈より注射した。腫瘍移植後 14 日目にマウスを安楽死させて解剖し、生じた腫瘍を摘出して重量を測定した。

5) Flow cytometry
細胞を trypsin 処理して回収した後、FACS buffer (2%FCS 含有 PBS)で懸濁した。細胞膜上の CD26 の発現は、PE-conjugated Mouse anti-Human CD26 mAb (clone M-A261, BD Biosciences)または、PE anti-mouse CD26(Pharmingen)を用いて染色し、FACS Calibur (BD Biosciences)にて解析を行った。

6) 免疫沈降及び Western Blot
細胞溶解液で細胞を処理後、SD-buffer を加えて denature を行い、western blot 用のサンプルを準備した。免疫沈降では、細胞溶解液に mouse anti-CD26 抗体(1F7) 10 μg あるいは mouse anti-cyclophilin A mAb 10μg を 4^oC で 24 時間反応させ、protein G カラムで回収した。
サンプルは 1 レーンあたり 5-10 μg の蛋白質を SDS-PAGE で電気泳動し、ウェット式ブロッティングで membrane に transfer した後、各種抗体を用いてウェスタンブロットを行った。検出には LAS4000 (GE Healthcare)を用いた。

7) Real-Time RT-PCR
Total RNA は RNeasy Mini Kit (Qiagen)を用いて抽出し、PrimeScript II first strand cDNA

synthesis kit (Takara Bio)により cDNA を作製した。Human HPRT1 を内因性コントロールとして、7500 Real-Time PCR System と SYBR Select Master Mix (Applied Biosystems) を用いて mRNA の定量を行った。

8)　Polysome の分画

Polysome はショ糖密度勾配超遠心法により分画した。Control-siRNA あるいは YB-1 AON (20 nM)を細胞に transfection し、48 時間後に溶解液を作成した。それぞれ 50, 40, 30, 20, 10%のショ糖を含む polysome extraction buffer を 2 ml ずつ重層したステップグラディエントを作成し、そこに細胞溶解液 1ml を重層してから、超遠心機(Hitachi Himac CP100α)及び P40ST ローターを用いて 38000 rpm 2 時間の超遠心を行った。遠心後、上層より 1 ml ずつ溶液をピペットで吸い取り、フラクションに分けた。450 nm で吸光度を測定し、translation-inactive 及び -active のフラクションを確認した。各フラクション(0.5 ml)より phenol/ choloroform/ isoamyl alcohol を用いてタンパクを除去したのち、3 M sodium acetate (pH 5.2)で RNA を沈殿後、70%エタノールで精製した。CD26 mRNA 発現の測定には、RT-PCR を用いた。

9) マイクロアレイ解析

CD26 ノックダウン細胞のマイクロアレイ解析は、細胞にそれぞれ control-siRNA または CD26-siRNA を transfection し、24 時間後に抽出した RNA を用いた。CD26 抗体処理のマイクロアレイ解析は、細胞にヒト化 CD26 抗体(10μg/ml)を添加し、24 時間後に抽出した RNA サンプルを用いた。変動遺伝子の解析は、東レの 3D-Gene マイクロアレイ解析に委託した。

10) 蛍光抗体法

適切な細胞数の中皮腫細胞を Lab-Tek II chamber slide (Thermo Fisher)に撒き増殖させ、細胞を 4% paraformaldehyde で固定(4℃ 30min)。PBS で wash した後、0.1% Triton X-100 により細胞の透過処理を行った。2 次抗体の non-specific binding を防止するために正常血清(donkey serum、1/10 希釈)による処理を行った(室温 30min)。一次抗体として Rb anti-Human YB-1 pAb (abcam 既出), anti-CD26 pAb（R&D 既出）、anti-cyclophilin A mAb (abcam 既出)を用いた。2 次抗体として anti-Rabbit Alexa 488 標識 2 次抗体(A11034 Thermo Fisher)、anti-Mouse Alexa 555 標識 2 次抗体(A21432 Thermo Fisher)、anti-Goat Alexa 647 標識 2 次抗体(A21245 Thermo Fisher)を用いた。免疫染色では western で使用した 1 次抗体を用いてラベルした 2 次抗体を用いた。サンプルは Leica TCS-SP5 共焦点レーザー顕微鏡を用いて解析を行った。

11) STED 顕微鏡による CD26 と CyA の結合の解析

細胞の増殖は厚さ 0.16-0.19mm のカバーガラス上で行った。細胞を 4% paraformaldehyde で固定(4℃ 30min)し、PBS で wash した後、0.1% Triton X-100 により細胞の透過処理を行った。抗体の non-specific binding を防止するためは、BSA (1/10 希釈、室温 30min)処理を行った。CD26 の検出には anti-mouse CD26 (1F7)を Oregon Green 488(Invitrogen)で直接ラベルした。CyA の検出には CyA 抗体(既出)を Alexa Fluor 532 (Thermo Fisher)で直接ラベルし、Leica STED 顕微鏡を用いて CD26 と CyA の結合を解析した。

12）Cycloheximide (CHX) chase assay

中皮腫細胞を 48 時間、各種処理(上記の YB-1

AON, CD26-si, CD26 抗体)をした後、蛋白合成阻害剤 Cycloheximide(CHX)を加え(最終濃度 50μ/ml)、0, 1, 2, 4 時間の時点で経時的に sampling した。コントロール実験は、すべて正常マウス IgG 添加で行い、抗 CyA、抗 Actin を用いて Western blot で検出した。

13) 統計処理

統計解析には t 検定を用い、併用効果の解析には two-way ANOVA を用いた。

(倫理面への配慮)

ヒト化 CD26 抗体及び YB-1 AON の抗腫瘍効果を評価するためのマウスを用いた動物実験は、順天堂大学医学部実験動物委員会の審査を受け承認されている(承認番号 290131)。

C. 研究結果

1) 悪性中皮腫細胞株に対する、YB-1 AON 単剤での抗腫瘍効果

中皮腫細胞株では、CD26 と YB-1 はともに細胞質で強く発現が見られる蛋白であるが(図 1 A)、我々はまず、YB-1 AON 単剤での細胞増殖及び浸潤に対する効果を検討した。細胞に control- siRNA (5, 10, 15, 20 nM) あるいは YB-1 AON (5, 10, 15, 20 nM)を transfection し、48 時間後に細胞からタンパク質を抽出して、ウェスタンブロットを行ったところ、YB-1 AON 5 nM では、H226、JMN ともにわずかに YB-1 発現を抑制したが、15 nM 及び 20 nM では 80 %以上抑制した(図 1B)。

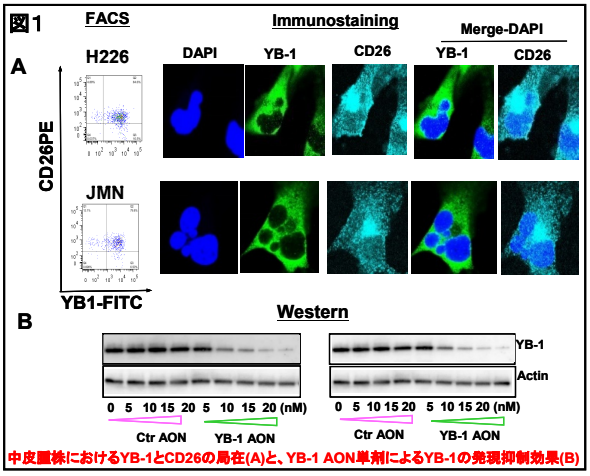

次に細胞増殖増殖への効果を検討したが、YB-1 AON transfection 後 48 時間の細胞を 96 well plate に播種し、それぞれ 24、48、72 時間後に MTT アッセイを行ったところ、H226、JMN ともに YB-1 発現の減少に応じて in vitro の増殖が.抑制された。

H226 では、YB-1 AON 15, 20 nM は 48 時間で、それぞれ 81%、92%増殖を抑制し、72 時間ではそれぞれ 83、91%抑制した。JMN では YB-1 AON 15、20 nM は、48 時間でそれぞれ 55、58%抑制し、72 時間ではそれぞれ 69、73%抑制した(図 2)。

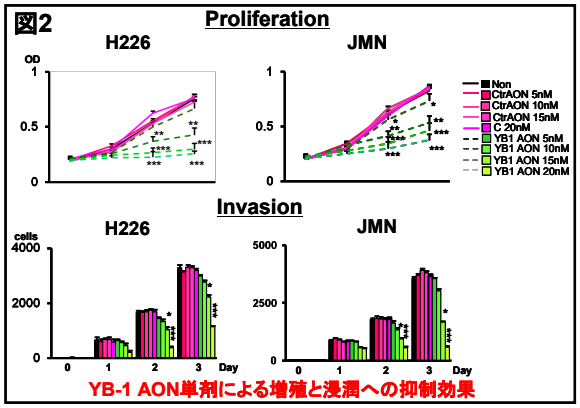

さらに YB-1 AON transfection 後 48 時間の細胞を Boyden chamber に播種し、24, 48, 72 時間後にアッセイを行ったところ、H226、JMN ともに YB-1 発現のノックダウンに応じて浸潤が抑制された。H226 では YB-1

AON 15、20nM は 48 時間でそれぞれ 47、32%抑制し、72 時間ではそれぞれ 78、66%抑制した。JMN では YB-1 AON 15、20nM は 48 時間でそれぞれ 49、51%抑制し、72 時間ではそれぞれ 64、68%抑制した(図 2)。

2) YB-1 AON 処理と CD26 抗体処理による、両者の発現に対する影響

我々は次に、YB-1 AON と CD26 抗体の併用において、YB-1 AON の CD26 発現に対する作用及び CD26 抗体の YB-1 発現に対する作用の検討を行った。その目的で、コントロールとして、CD26 とともに中皮腫のがん幹細胞マーカーである CD24 の発現も調べたが、YB-1 は CD24 の発現には影響を与えず、CD26 の発現を抑制することがわかった。

さらに我々は、CD26 抗体処理による YB-1 への影響も調べた。H226 及び JMN に control IgG (5, 10, 15, 20) μg/ml、CD26 抗体(5, 10, 15, 20) μg/ml を添加後、1、2、3 日目にサンプルを採取し、ウェスタンブロットを行ったが、CD26 抗体処理では、YB-1 の発現は影響を受けなかった。

そのため、次に YB-1 AON による CD26 発現抑制の濃度検討を行った。中皮腫細胞を control- siRNA (5、10、15、20 nM)、及び YB-1 AON(5、10、15、20 nM)で transfection した後、48 時間に細胞表面における CD26 発現を検出したところ、YB-1 発現の減少に応じて CD26 発現が減少していた。同時に、細胞全体の CD26 発現をウェスタンブロットで測定したところ、同様に YB-1 発現の減少に応じて CD26 発現が減少していた(図 3)。

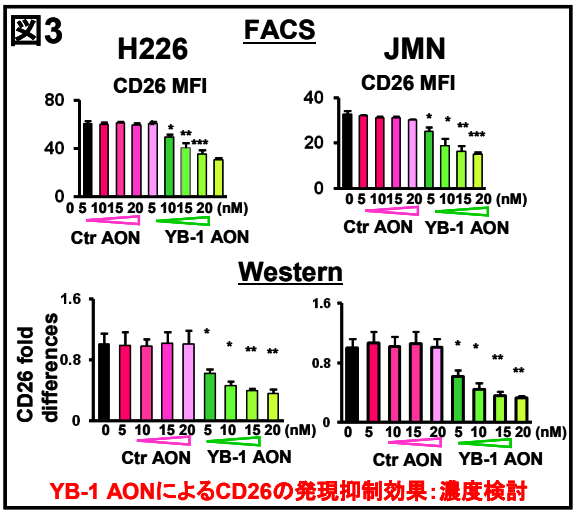

また、以上の実験と平行し、YB-1 AON の YB-1 発現に対するノックダウン効果の検証と、CD26 の発現減少に対する time course study を行った。細胞に control- siRNA (20 nM),あるいは YB-1 AON (20 nM)を transfection し、1、3、7、14 日後にサンプリングを行い、FACS と Western blot で解析したその結果両細胞株とも、YB-1 AON により YB-1 の発現は 1 日目から減少したが、14 日目には回復していた。一方で CD26 発現は、細胞表面及び細胞全体において、ともに 3 日目から特に低下が見られたが、14 日目では回復傾向が見られた(図 4)。

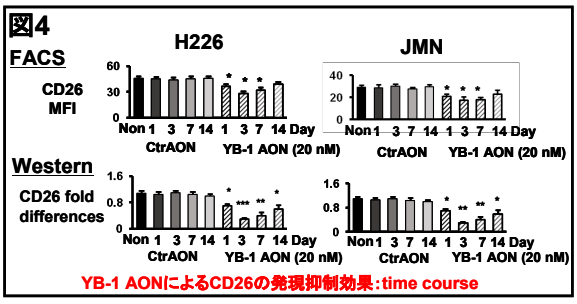

ちなみに mRNA は、タンパク質の発現変化より前に変動すると考えられている。そのため、細胞を control-siRNA 及び YB-1 AON (5、10、15、20 nM)で transfection した後、24 時間目に CD26 mRNA の発現を測定した

が、YB-1 AON 処理によっては変化しなかった。

この理由を明らかにするため、次にショ糖密度勾配法により、中皮腫細胞株から polysome を分画し、translation active における CD26 の mRNA 発現を測定した。その結果、両株ともに polysome における CD26 発現は、YB-1 AON 20 nM 処理により減少していた。一方 polysome 分画をプールして CD26 発現を測定したところ、YB-1 AON 処理で CD26 mRNA の Total 量は変化しなかった。しかし translation active な polysome 分画では、YB-1 AON 処理により CD26 の mRNA が減少していた(図 5)。これらの結果より、YB-1 AON は CD26 のタンパク質発現を抑制するが、それは translation レベルであることが示唆された。

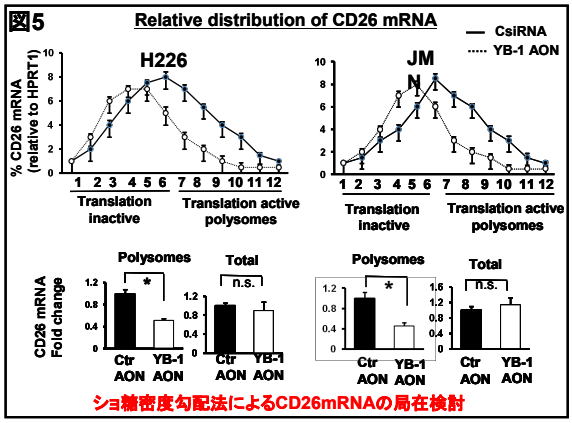

3) CD26 抗体と YB-1 AON との併用効果

次に我々は、YB-1 AON と CD26 抗体の併用効果の検討を行った。細胞増殖に対しては、図 6 で YB-1 AON の用量検討を行った結果を参考にし、最適量以下の 5 および 15 nM の YB-1 AON を transfection した。48 時間後に 96 well plate に細胞を播種し、それと同時に suboptimal dose の CD26 抗体(10 μg/ml)を添加し、さらに 48 時間後に MTT アッセイを行った。その結果、H226、JMN ともに YB-1 AON の増殖抑制効果は、CD26 抗体の添加によって増強された(図 6)。

浸潤に対する併用効果では、最適量以下の 15nM YB-1 AON を細胞に transfection し、48 時間後に Boyden chamber に播種した。同時に CD26 抗体(10, 20 μg/ml)を添加し、48 時間後に浸潤した細胞を測定したところ、YB-1 AON と CD26 抗体との併用により、浸潤能の抑制が増強された(図 6)。

さらに、in vivo growth における YB-1 AON と CD26 抗体の併用についての検討を行った。雌 SCID マウスに H226 あるいは JMN ($1x10^5$ cells/mouse)を皮下移植したのち、翌日より suboptimal dose (200 μg/mouse)の CD26 抗体週 2 回腹腔内投与、YB-1AON (200 μg/mouse)週 1 回尾静脈投与で観察を行った。移植後 14 日に腫瘍を摘出し、重量を測定したところ、移植実験においても YB-1 AON と CD26 抗体の併用により、腫瘍抑制効果の増強が見られた(図 6)。

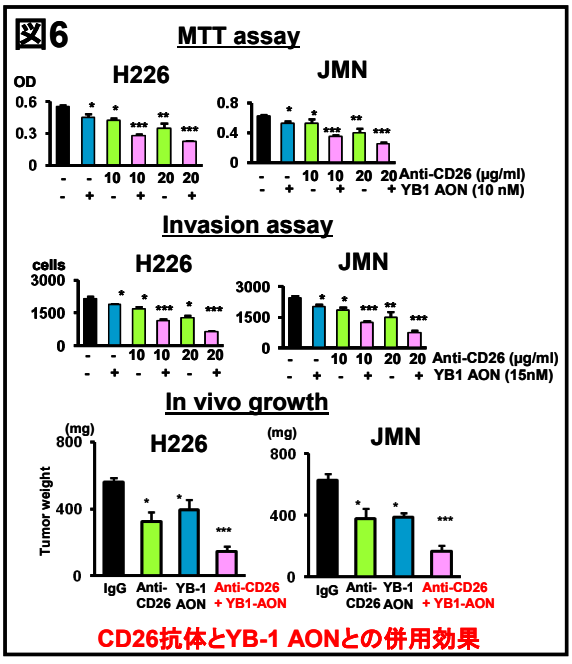

4) CD26 抗体と YB-1 AON の併用効果の分子メカニズム

以上の実験結果から、中皮腫細胞では YB-1 AON により、細胞の増殖及び浸潤が抑制され、同時に CD26 のタンパク質発現が抑制されることが明らかとなった。また YB-1 AON と CD26 抗体には、併用効果も観察されたため、二つのタンパク質は細胞内でも密接に関係していることが示唆された。それゆえ、これらに関与する新たなタンパク質の存在も考えられたため、次に我々は、CD26 ノックダウン、または CD26 抗体処理をした中皮腫細胞のマイクロアレイ解析データを用いて、新規関連分子の探索を行った。

データから遺伝子発現が 2 倍以上抑制される浸潤関連分子を抽出したところ、CD26 ノックダウン細胞では H226 で 22 個、JMN では 16 個の候補が見つかった。そのうち両株で共通に 2 倍以上発現が抑制されている遺伝子として、PPIA、HGF および SFRP1 が残った。このうち種々の癌で過剰発現するだけでなく、増殖や浸潤に関与し、さらには予後予測因子としても報告されている、分子量 18 kD の PPIA (Cyclophilin A, CyA) に着目した。

この CyA は、蛍光抗体法で観察すると、CD26 と同様に細胞質で強く発現していたが、CD26- siRNA によるノックダウンを行うと、その発現が抑制されることがわかった **(図 7)**。そのため我々は、次に YB-1 AON と CD26 抗体の、CyA 発現への併用効果の検討を行った。まず中皮腫細胞株を CD26 抗体 (10 μg/ml)を 48 時間処理し、ウェスタンブロットしたところ、両株ともに CyA 発現の抑制が見られた。YB-1 AON (20 nM)単独の場合では、transfection 後 48 時間に採取したサンプルで、CD26 の発現が抑制されていただけでなく、CyA の発現も抑制されていた。さらに CD26 抗体と YB-1 AON の併用では、YB-1 AON (20 nM)の transfection 後 48 時間に播種し、同時に CD26 抗体(10 μg/ml)を添加して 48 時間後に回収したサンプルで、CyA 発現はそれぞれ単独処理よりも、併用した場合の方がより強く抑制された**(図 7)**。

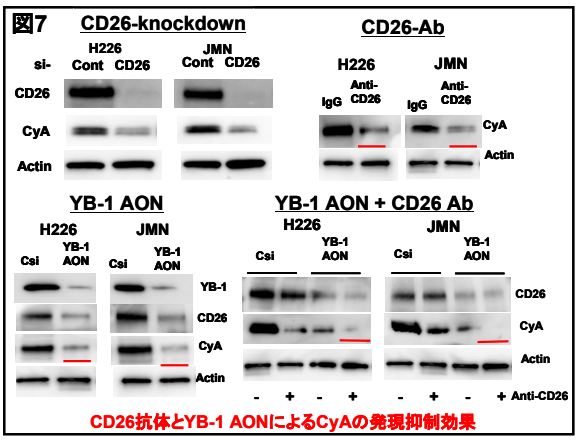

その効果を、蛍光抗体法でも調べた結果、YB-1 AON、CD26 抗体により、実際に CyA の発現減少がみられたが、さらに我々は、中皮腫細胞においても CyA は、増殖及び浸潤を促進しているかどうかを、2 種類の CyA-siRNA を用いて検討した。細胞に siRNA (20 nM)を transfection し、48 時間後に 96 well plate または Boyden chamber に播種したのち、その 48 時間後に MTT アッセイと invasion アッセイを行った結果、CyA-siRNA は 2 種類とも増殖及び浸潤を抑制し、CD26 や YB-1 と同様の働きがあることが示された**(図 8A)**。

5) CD26 と CyA の association

以上の結果から、YB-1 と CD26 と CyA は密接に関連する分子で、共同して抗腫瘍効果を発揮すると予想された。そのため次に、我々はこれらのタンパク質の細胞内での

association の可能性を検討した。

細胞溶解液をまず、抗 CD26 抗体(1F7)または抗 CyA 抗体でそれぞれ免疫沈降し、CD26 抗体または YB-1 抗体で western blot を行ったところ、CyA 抗体により CD26 が共沈し、また CD26 抗体でも CyA が共沈してくることがわかった。一方で YB-1 と CyA は、いずれの抗体でも共沈してこなかった。このことから、CD26 と CyA は in vivo で associate しており、YB-1 は CD26 を介して、間接的に CyA に影響していることが示唆された(図 8B)。

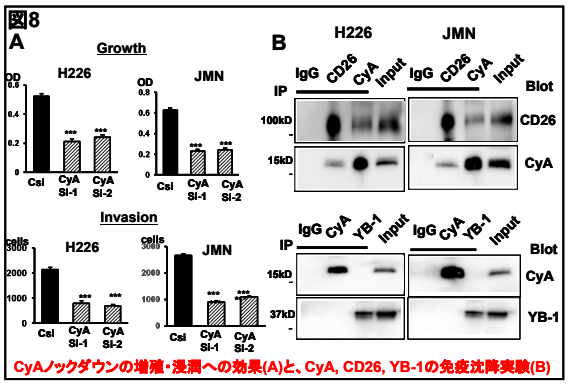

CyAノックダウンの増殖・浸潤への効果(A)と、CyA, CD26, YB-1の免疫沈降実験(B)

このことをさらに確認するために、我々は次に共焦点蛍光顕微鏡で、CD26 と CyA の局在を検討した。すると両者は、cytosol で colocalize していることが示された。さらに我々は、STED(誘導放出制御)顕微鏡でも同様に解析を行ったが、これは分子間の結合距離(20-30nm)とほぼ同程度の解像度を誇る、超高解像度の蛍光顕微鏡として近年実用化された。観察の結果、CD26(青)と CyA(赤)はともに cytosol で強く発現し、また Merge 画像では、共局在を意味する白からピンクの領域が広く分布しており、実際に CD26 と CyA は、細胞質で結合していることが強く示唆された(図 9)。

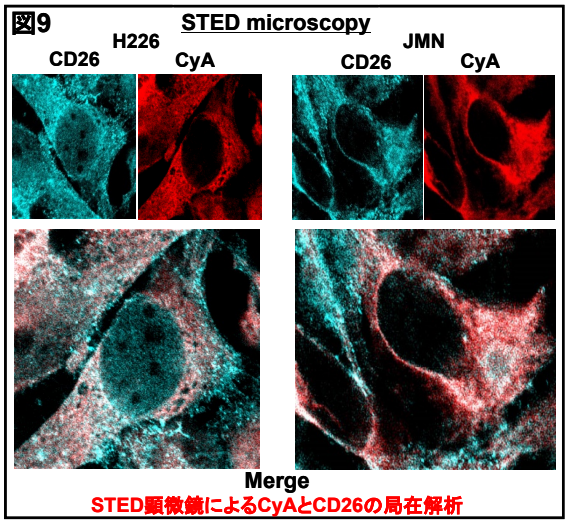

STED顕微鏡によるCyAとCD26の局在解析

6) CD26-si、YB-1AON および CD26 抗体による、CyA の発現抑制

最後に我々は、YB-1 AON と CD26 抗体の、CyA 発現に対する効果の検討を行った。これまでの実験で、CyA の蛋白発現は CD26-si、YB-1 AON、CD26 抗体処理のすべてで抑制されることがわかったが、RT-PCR で CyA の mRNA の発現を測定したところ、これらの処理では影響を受けないことがわかった(図 10A)。

このことは CyA の発現が、蛋白質の翻訳レベルで制御されていることを意味しているが、そのことを確かめるために、CyA 蛋白の stability を、Cycloheximide chase assay を行った。細胞を 48 時間、上記の処理をしたのち、蛋白合成阻害剤である cycloheximide(最終濃度 50μg/ml)を加え、経時的にサンプリングを行った。細胞内では、安定性の低い蛋白ほど早く分解されるが、それぞれの処理で CyA 蛋白が急速に減少していくことがわかった(図 10B)。YB-1 AON については、CD26 への間接的効果と推測されたが、このことから CD26 が、細胞内で CyA 蛋白を安定させる役割を持つ可能性が考え

られた。

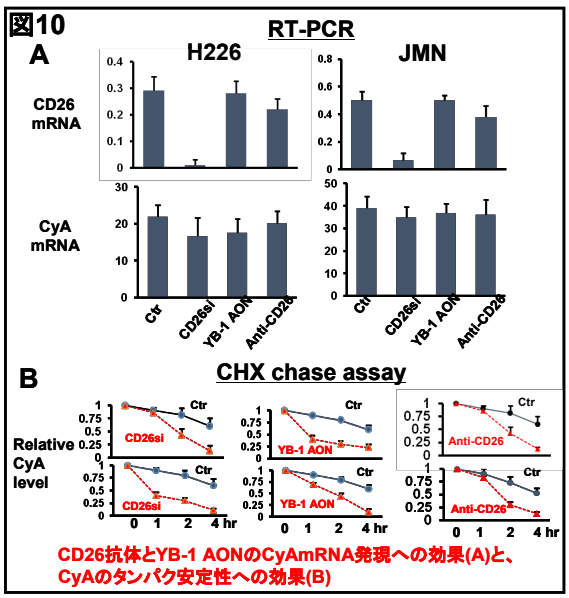

D. 考察

本研究では、前半で中皮腫細胞における YB-1 AON と CD26 抗体との併用効果についての検討を行った。そして後半では、その併用効果の鍵となりうる蛋白を発見し、その分子メカニズムの解明を行った。

我々はまず、CD26 発現に対する YB-1 AON の作用を検討したが、CD26 のタンパク質発現は、YB-1 のノックダウンに濃度依存的に抑制され、それとともに強い増殖抑制効果、浸潤抑制効果が見られた。そしてこの結果より、YB-1 AON による増殖及び浸潤の抑制には、CD26 の発現抑制が関与している可能性が示唆された。

一方 YB-1 は、EMT 関連因子である snail1 や HIF1α の発現を translation レベルで制御していることが報告されているが(Cancer Cell 15:402 2009; Cancer Cell 2:682 2015)、YB-1 AON による CD26 発現の抑制においても、YB-1 AON は translation レベルで CD26 発現を抑制していることが示唆された。

YB-1 AON の time course study では、YB-1 AON は少なくとも transfection 後 7 日間は YB-1 に対するノックダウン効果があり、濃度依存的に CD26 の発現抑制が見られた。この結果により、生体に使用する場合は少なくとも週 1 回以上の頻度で、YB-1AON の投与が必要であると考えられた。

ところが細胞を CD26 抗体で処理しても、YB-1 の発現には影響しなかった。このことから、シグナル伝達系において YB-1 は、CD26 の上流側に位置する分子である可能性が示唆された。

また YB-1 AON と CD26 抗体は、それぞれ単独でも in vitro で中皮腫細胞の増殖と浸潤を抑制するが、両者を併用することで、それらの効果が増強された。さらに in vivo での移植実験においても、YB-1 AON の増殖抑制効果は、CD26 抗体の併用により増強されることが判明した。

以上の結果より、中皮腫患者においても YB-1 AON と CD26 抗体との併用で、より強い治療効果が得られる可能性があると考えられたが、本研究の後半で、我々はその分子メカニズムの解明も試みた。

YB-1 AON による増殖・浸潤抑制作用に、CD26 の発現抑制が関与していることが示唆されたため、我々はまず CD26 ノックダウン及び CD26 抗体処理後のマイクロアレイ解析データを用いて、新規関連分子の探索を行った。その結果、候補分子の一つとして cyclophilin A (CyA)に着目した。

蛍光顕微鏡の観察では、CyA は細胞質に局在していたが、YB-1 AON または CD26 抗体処理により、その蛋白発現が抑制された。両者を併用することにより、さらに抑制が増強されたが、CyA のノックダウン実験で、

CyA も増殖及び浸潤を促進していることが示された。したがって中皮腫細胞においては、YB-1 AON と CD26 抗体の併用による増殖・浸潤抑制作用に、CyA が深く関与している可能性が示唆された。

また免疫沈降実験では、CyA は YB-1 とは共沈してこなかったが、CD26 とは共沈した。蛍光抗体法による共焦点顕微鏡と STED（誘導放出制御）顕微鏡で細胞内の局在を観察したところ、両者は共局在していることが確認された。さらに、CyA mRNA の発現制御について検討すると、YB-1 AON、CD26 抗体、CD26-si の処理では、すべて影響しなかった。このことを cycloheximide chase assay で確認すると、これらの処理が CyA 蛋白の stability を低下させることがわかった。つまり CD26 は、CyA 蛋白に直接結合することで、それを安定化させていることが示唆された。

これまでの研究で、CyA はがん細胞の増殖や浸潤を促進することが報告されており (Nat Med 21:572 2015; Nat Chem Biol 12:117 2016) 、子宮癌、食道扁平上皮癌、腎明細胞癌などにおいては、予後予測因子であることが報告されている (Mol Cell Proteomics 7:1810 2008; Genet Test Mol Biomarkers 19:182 2015; Cancer Biol Ther 11:535 2011)。今回、中皮腫細胞において YB-1 AON と CD26 抗体が、CyA の発現を抑制することがわかったが、中皮腫において CyA が予後予測因子であれば、YB-1 AON や CD26 抗体を中皮腫の治療に用いる意義も、さらに強くなると考えられる。

それゆえ中皮腫病理組織での CyA の発現や、予後因子としての可能性の検討も、今後は必要になると予想された。また、CD26 陽性細胞での CyA の役割や、YB-1 AON や CD26 抗体が CyA 発現を抑制するメカニズムについても、より詳しく調べる必要があると考えられた。

E. 結論

In vitro および in vivo 解析において、YB-1 AON と CD26 抗体の併用の有用性が示唆されたが、そのメカニズムとして、YB-1 と CD26 が、CyA を介して腫瘍の増殖と浸潤に働いている可能性が示された。

F. 次年度以降の計画

YB-1 AON 及び CD26 抗体の併用の、最適投与プロトコルの確立を行う。また、それらによる CyA の発現抑制メカニズムと、CD26 陽性細胞における CyA の役割を、より詳細に調べる。さらに、中皮腫病理組織における CyA の発現と、予後因子としての可能性を検討する。

G. 研究発表

1. 論文発表

1) Ohnuma K, Hatano R, Komiya E, Otsuka H, Itoh T, Iwao N, Kaneko Y, Yamada T, Dang NH, Morimoto C. A novel role for CD26/dipeptidyl peptidase IV as a therapeutic target in selected immune disorders and cancers. Front Biosci. in press.

2) Hiromura M, Nohtomi K, Mori Y, Kataoka H, Sugano M, Ohnuma K, Kuwata H, Hirano T. Caveolin-1, a binding protein of CD26, is essential for the anti-inflammatory effects of dipeptidylpeptidase-4 inhibitors on human and mouse macrophages.

Biochem Biophys Res Commun. 2018; 495: 223-229.

3) Angevin E, Isambert N, Trillet-Lenoir V, You B, Alexandre J, Zalcman G, Vielh P, Farace F, Valleix F, Podoll T, Kuramochi Y, Miyashita I, Hosono O, Dang NH, Ohnuma K, Yamada T, Kaneko Y, Morimoto C. First-in-Human phase 1 of YS110, a monoclonal antibody directed against CD26 in advanced CD26-expressing cancers.Br.J.Cancer.2017;116:1126-1134.

4) Komiya E, Hatano R, Otsuka H, Itoh T, Yamazaki H, Yamada T, Dang NH, Tominaga M, Suga Y, Kimura U, Takamori K, Morimoto C, Ohnuma K. A possible role for CD26/DPPIV enzyme activity in the regulation of psoriatic pruritus.J Dermatol Sci. 2017; 86:212-221.

5) Kim KM, Noh JH, Bodogai M, Martindale JL, Yang X, Indig FE, Basu SK, Ohnuma K, Morimoto C, Johnson PF, Biragyn A, Abdelmohsen K, Gorospe M. Identification of senescent cell surface targetable protein DDP4.Genes Dev. 2017;31:1529-1534.

6) Ikeda T, Kobayashi S, Morimoto C. Gene expression microarray data from mouse cerebrum treated with rTMS for 30 days.Data Brief. 2017; 15: 948-69.

7) Doonan BP, Ohnuma K, Dang LH, Morimoto C, Dang NH. Current and Emerging Therapy for Malignant Pleural Mesothelioma: Focus on CD26/Dipeptidyl Peptidase IV as a Therapeutic Target. Current Cancer Therapy Reviews. 2017; 13: 1-13.

２．著書

1) Hatano R, Ohnuma K, Yamada T, Okamoto T, Komiya E, Otsuka H, Itoh T, Yamazaki H, Iwao N, Kaneko Y, Dang NH, Morimoto C. The use of the humanized anti-CD26 monoclonal antibody YS110 as a novel targeted therapy for refractory cancers and immune disorders. Advances in Medicine and Biology (Nova Science Publishers, Inc.). in press

2) Ohnuma K, Hatano R, Yamazaki H, Kaneko Y, Dang NH, Morimoto C. CD26-targeted therapy: A new horizon in malignant pleural mesothelioma management. Horizons in Cancer Research (Nova Science Publishers, Inc.). 2017; Volume 64: Chapter 6: 129-162.

３．学会発表

1) 岩尾憲明、大沼圭、大塚春奈、波多野良、古宮栄利子、伊藤匠、森本幾夫. 急性 GVHD マウスモデルにおける HMGB1 の動態に関する検討.第 40 回日本造血細胞移植学会.2018 年 2 月、札幌.

2) Eriko Komiya, Ryo Hatano, Haruna Otsuka, Takumi Itoh, Hiroto Yamazaki, Mitsutoshi Tominaga,

Kenji Takamori, Kei Ohnuma, Chikao Morimoto. CD26/DPPIV regulates mechanical itch in a mechanistically distinct manner from chemical itch. 第 42 回日本研究皮膚科学会、2017 年 12 月、高知.

3) Takumi Itoh, Ryo Hatano, Haruna Otsuka, Noriaki Iwao, Satoshi Iwata, Taketo Yamada, Chikao Morimoto. IL-26 facilitates angiogenesis and skin inflammation via inducing FGF2 production in a murine model of imiquimod-induced psoriasis. 第 46 回日本免疫学会、2017 年 12 月、仙台.

4) Eriko Komiya, Ryo Hatano, Haruna Otsuka, Takumi Itoh, Hiroto Yamazaki, Taketo Yamada, Yasushi Suga, Utako Kimura, Mitsutoshi Tominaga, Kenji Takamori, Kei Ohnuma, Chikao Morimoto. The regulation of pruritus in psoriasis and atopic dermatitis-a possible role for CD26/DPPIV. 9th World Congress on Itch, 2017 ,October.Wrocław, Poland.

5) 波多野良、大沼圭、石井智徳、岩田哲史、奥村康、関川巖、森本幾夫. 全身性エリテマトーデスのステロイド治療抵抗性と CD26 陰性 T 細胞サブセットとの関係性について. 第 61 回日本リウマチ学会、2017 年 4 月、福岡.

H.知的財産権の出願・登録状況（予定を含む）

1. 発明者：森本幾夫、波多野良、山田健人、大沼圭.
   出願番号：特許出願中
   名称：抗ヒト CD26 モノクローナル抗体
   出願人：学校法人 順天堂、埼玉医科大学（共同出願）
   出願年月日：2018 年 3 月予定(PCT 出願)

2. 発明者：森本幾夫、波多野良、大沼圭、伊藤匠.
   出願番号：特願 2017-231439
   名称：抗ヒト IL-26 抗体
   出願人：学校法人 順天堂
   出願年月日：2017 年 12 月 1 日(PCT 出願)

労災疾病臨床研究事業費補助金
分 担 研 究 報 告 書

中皮腫におけるCD26およびYB-1発現について

研究分担者　山田　健人　埼玉医科大学 病理学・教授
研究分担者　岸本　卓巳　岡山労災病院アスベスト関連疾患研究センター・センター長
研究協力者　藤本　伸一　岡山労災病院アスベスト関連疾患研究センター・副センター長
研究協力者　青江　啓介　国立病院機構山口宇部医療センター・内科系診療部長

研究要旨
悪性中皮腫の新規治療法として期待されるヒト化 CD26 抗体療法および YB-1 アンチセンス療法においては、腫瘍組織における CD26 および YB-1 分子の発現の適確な評価が重要である。本研究では、すでに確立された CD26 発現評価方法とともに、新たに YB-1 発現評価方法の確立を通じて、中皮腫検体における本分子群の免疫染色での発現評価法について検討した。その結果、84 症例において、CD26 および YB-1 は、それぞれ 69、79 症例で陽性であり、CD26 陰性 15 症例中では 4 症例で YB-1 陰性であった。また肉腫型中皮腫では CD26 発現頻度は低く 9 症例中陽性は 2 例であったが、YB-1 は 9 症例中 9 例陽性と高率に発現していることを見出した。また、画像解析から CD26 は細胞膜および細胞質に 95%、核に 1-2%の発現があり、一方、YB-1 は細胞質に 90%の発現が認められ、核内に 2-3%の発現が観察された。

A. 研究目的

フランスで施行されたヒト化 CD26 抗体療法の第 I 相臨床試験では、特記すべき有害事象なく、26 症例中 13 症例で「安定」(Stable Disease;SD)への導入が可能であり、安全性のみならず、その腫瘍効果も期待される成果が得られた。本研究課題では、この CD26 抗体療法とともに中皮腫細胞の増殖・細胞死を司る他の分子メカニズムを阻害することで、相加相乗効果を狙った新規治療法を目指している。その標的分子が、YB-1 である。YB-1 は、Ybox (CAAT/ATTG)と呼ばれる塩基配列を認識して標的遺伝子に結合する転写因子の一つであり、cold shock domain 蛋白スーパーファミリーに属する。本分子は、細胞周期関連分子や癌抑制分子などの細胞増殖や腫瘍悪性化に関与する転写・翻訳を制御するとともに、DNA-RNA との結合を介して翻訳にも関わる多機能分子である。この YB-1 は、ヒトがんにおける発現解析から、肺癌や乳癌の抗がん剤感受性や予後と相関するとの報告がなされている。また研究協力者・中野賢二博士は、この YB-1 に対するアンチセンス療法の開発にすでに成功している。

そこで本研究においては、まず悪性中皮腫症例における CD26 と YB-1 発現を詳細に明

らかにし、CD26 とともに YB-1 が中皮腫における標的分子としてどのような発現パターンを示すのかを明らかにし、CD26 抗体および YB-1 アンチセンスの併用療法にそなえた基礎的検討を行った。また CD26 発現は現在用いられているアリムタ、シスプラチンなど化学療法剤の治療効果予測バイオマーカーとしても有望な結果を得て報告(Clin Cancer Res 18:1447, 2012)してきたが、さらに CD26 および YB-1 発現を細胞局在、陽性率、陽性強度など様々な要素で解析し、各種の臨床パラメーターとの相関を明らかにすることで、バイオマーカーとなりうるかどうかを検討することを目的とした。

B. 研究方法

YB-1 の発現解析には、抗 YB-1 抗体（Rabbit monoclonal antibody(EP2708Y), ABCAM 社 ab76149）を用いた。本抗体は、ヒト YB-1 の C 末端領域を抗原として作成されたものであり、ヒトおよびげ齧歯類の YB-1 と反応する。YB-1 陽性対照標本としては、ヒト癌細胞株（HeLa, SW480, A549, MCF7）を免疫不全マウス（NOD/SCID）皮下に移植して形成された腫瘍をホルマリン固定したものを用いた。またヒト組織としては、ホルマリン固定したパラフィン切片（CD26 陽性である正常ヒト腎、肝、前立腺及び悪性中皮腫の組織および肺）を用いた。抗原賦活化として、オートクレーブ処置（120℃、20 分、0.01M Citrate Buffer pH8.0）を行い、二次抗体は、Peroxidase 付加抗ラビット IgG 抗体(ImmPRESS 社製)を用い、発色は、DAB 液（Simple Stain DAB, Histofine）を用いた。

岡山労災病院および山口宇部医療センターにおける中皮腫 84 症例の腫瘍の病理組織（生検及び手術材料、10%ホルマリン固定、パラフィン切片）について、CD26 の免疫染色を行った。抗原賦活化は、オートクレーブ処置（120℃、20 分、0.01M Citrate Buffer pH8.0)を行った。抗 CD26 抗体は、仏の臨床試験で使用した R&D 社製抗 CD26 ヤギ・ポリクロナール抗体(Lot.No. JOQ107061）を用いた。二次抗体は、Peroxidase 付加抗ヤギ IgG 抗体(ImmPRESS 社製)あるいは Peroxidase 付加抗マウス IgG 抗体(ImmPRESS 社製)を用い、発色は、DAB 液（Simple Stain DAB, Histofine）を用いた。いずれの染色においても、陽性対照には、正常ヒト腎、肝、前立腺及び悪性中皮腫を用い、陰性対照には、これらの正常組織切片内の各種組織（平滑筋、脂肪組織、結合組織など）と CD26 陰性肺癌組織を用いた。

（倫理面への配慮）

患者検体などについては研究対象者に対する人権擁護上の配慮及び研究により研究対象者が受ける不利益、利益等の説明を患者及び遺族に対して行い、書面でのインフォームド・コンセントを得ている。また病理組織について免疫染色して CD26 発現を解析する研究については、慶應義塾大学医学部および埼玉医科大学の倫理委員会の審査にて承認されている（承認番号 20120100 および 794）。

C. 研究結果

中皮腫組織 84 例（上皮型 65 例、二相型 10 例、肉腫型 9 例）について、同様に YB-1 の免疫染色を行った。その結果、中皮腫組織

において、YB-1 は腫瘍細胞の細胞質に瀰漫性に強陽性となり、その頻度は 84 例中 79 例が陽性であった（図 1 および表 1）。また腫瘍組織における腫瘍血管の内皮細胞において、細胞質に YB-1 発現を認めた。次にこれらの中皮腫組織における YB−1 陽性所見が真に YB−1 蛋白であるかどうかを確認するために、一次抗体について YB−1 蛋白に

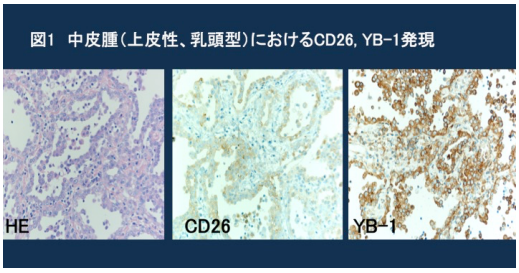

よる吸収実験を行った。ラビット抗ヒト YB-1 モノクローナル抗体と YB-1 蛋白を 4℃で 3 時間反応させた後、同様に免疫染色を施行した。その結果、中皮腫組織および血管内皮細胞における YB−1 陽性像がほぼ完全に消失したことから、この YB-1 の免疫染色は特異的に切片上の YB-1 蛋白発現を認識していると考えられた。

次に上記の中皮腫 84 症例について、ヒツジ抗ヒト CD26 ポリクローナル抗体を用いて同一検体での CD26 染色を行った（図 1 および表 1）。その結果、CD26 陽性症例は 84 例中 69 例であり、CD26 陰性 15 症例中 4 症例は YB-1 も陰性であった。一方、CD26 陽性 69 例中、YB-1 陰性例は 1 例であった。

また CD26 陰性症例において、YB-1 と機能的に関連する p53 の発現を解析したところ、12 症例中 6 症例で核内 p53 が強陽性であった（図 2）。これらの p53 陽性症例においては、p53 変異が示唆され、YB-1 を治療

表1 中皮腫におけるCD26・YB−1発現
84症例（上皮型65例、二相型10例、肉腫型9例）

		YB−1発現	
		陽性(79) C/N = 79/0	陰性(5)
CD26	陽性(69) M/M+C/N = 28/37/4	68 / 84	1 / 84
	陰性(15)	11 / 84	4 / 84

M:Membrane C:Cytoplasmic N:Nuclear

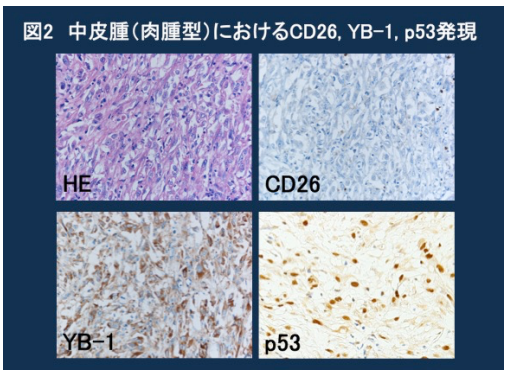

標的とする場合に p53 変異の有無がその効果と関わる可能性が考えられる。

次に、これらの染色標本をデジタル画像とし、imageProPlus プログラムにて詳細に半定量的に発現解析を行った。その結果、CD26 は細胞膜および細胞質に 95%が、核内に 1-2%の発現が認められた。一方、YB-1 は細胞質に 90%、核内に 2-3%の発現が認められることを明らかにした。現在、このデータベースを元に臨床パラメーターとの相関について検討している。

D. 考察

YB-1 は、転写・翻訳に関わる分子であるが、興味深いことに免疫染色での観察では、YB-1 タンパク質の主たる局在部位は細胞質であり、核の陽性像は明らかではなかった。

しかし、画像解析では、核内に少量の局在が認められたことは、これまでの試験管内でのデータと合致するものである。一方、CD26は、細胞膜貫通型の細胞表面に局在する糖蛋白質であるが、細胞内での局在は、細胞膜のみならず細胞質でのライソゾームや核内と広範囲であり、今回の画像解析の結果も同様であった。これらの二つの分子のがん細胞における局在は重要な意味を持つが、免疫染色での観察では、CD26 と YB-1 が中皮腫細胞の細胞質において、類似した瀰漫性の局在を示すことは、これらの分子の相互作用の可能性がある。CD26 を標的とした抗体療法は、抗体による免疫学的細胞傷害や CD26 機能の抑制が主体であり、腫瘍細胞の細胞表面 CD26 は抗体により細胞質内に内在化される。一方、YB-1 を標的としたアンチセンス療法は、アンチセンスによる YB-1 蛋白発現抑制が主体である。従って併用療法においては、抗体により CD26 は細胞質内での増加とその核内移行が惹起され、一方、YB-1 蛋白はアンチセンスにより減少することが想像されため、この状況での中皮腫細胞における細胞増殖や細胞死の変化がどうなるか、さらなる詳細な検証が期待される。

また悪性中皮腫における CD26 および YB-1 発現について細胞局在、陽性率、陽性強度などの各種パラメーターで詳細に定量評価することで、抗体療法の効果や予後などとの関連性あるいは臨床パラメーターを検証する基礎を構築していくことが重要と考える。

E. 結論

中皮腫検体における YB-1 の発現評価方法および半定量的解析法を確立した。その結果、81%の症例において CD26 と YB-1 の共発現が明らかとなり、細胞内局在においても細胞質内での共在が示された。

F. 研究発表

1. 論文発表

1) Angevin E, Isambert N, Trillet-Lenoir V, You B, Alexandre J, Zalcman G, Vielh P, Farace F, Valleix F, Podoll T, Kuramochi Y, Miyashita I, Hosono O, Dang NH, Ohnuma K, Yamada T, Kaneko Y, Morimoto C. First-in-Human phase 1 of YS110, a monoclonal antibody directed against CD26 in advanced CD26-expressing cancers.Br.J.Cancer.2017;116:1126-1134.

2) Komiya E, Hatano R, Otsuka H, Itoh T, Yamazaki H, Yamada T, Dang NH, Tominaga M, Suga Y, Kimura U, Takamori K, Morimoto C, Ohnuma K. A possible role for CD26/DPPIV enzyme activity in the regulation of psoriatic pruritus.J Dermatol Sci. 2017; 86:212-221.

3) Murakami R, Saisho Y, Watanabe Y, Inaishi J, Tsuchiya T, Kou K, Sato S, Kitago M, Kitagawa Y, Yamada T. Pancreas fat and beta cell mass in humans with and without diabetes: An analysis in the Japanese population. J Clin Endocrinol Metab. 2017;102:3251-3260.

4) Aida S, Hozumi M, Ichikawa D, Iida K, Yonemura Y, Tabata N, Yamada T, Matsushita M, Sugai T, Yanagawa H,

Hattori Y. A novel phenylphthalimide derivative, pegylated TC11, improves pharmacokinetic properties and induces apoptosis of high-risk myeloma cells via G2/M cell-cycle arrest. BBRC. 2017;493:514-520.

5) Kushitani K, Amatya VJ, Mawas AS, Suzuki R, Miyata Y, Okada M, Inai K, Kishimoto T, Takeshima Y. Utility of Survivin, BAP1, and Ki‐67 immunohistochemistry in distinguishing epithelioid mesothelioma from reactive mesothelial hyperplasia. Oncology Letters.2018;15:3540-3547.

6) Ninomiya T, Nogami N, Kozuki T, Harada D, Kubo T, Ohashi K, Kuyama S, Bessho A, Fujimoto N, Aoe K, Shibayama T, Takigawa N, Sugimoto K, Kudo K, Fukamatsu N, Hotta K, Kiura K. A phase I trial of afatinib and bevacizumab in chemo-naïve patients with advanced non-small-cell lung cancer harboring EGFR-mutations: Okayama Lung Cancer Study Group Trial 1404. Lung Cancer. 2018;115:103-108.

7) Sato H, Sakaguchi M, Yamamoto H, Tomida S, Aoe K, Shien K, Yoshioka T, Namba K, Torigoe H, Soh J, Tsukuda K, Tao H, Okabe K, Miyoshi S, Pass HI, Toyooka S. Therapeutic potential of targeting S100A11 in malignant pleural mesothelioma. Oncogenesis. 2018;7:11.

8) Hotta K, Aoe K, Kozuki T, Ohashi K, Ninomiya K, Ichihara E, Kubo T, Ninomiya T, Chikamori K, Harada D, Nogami N, Hirata T, Hinotsu S, Toyooka S, Kiura K. A Phase II Study of Trastuzumab Emtansine in HER2-positive Non-Small-Cell Lung Cancer. J Thorac Oncol. 2018;13:273-279.

9) Katakami N, Uchino J, Yokoyama T, Naito T, Kondo M, Yamada K, Kitajima H, Yoshimori K, Sato K, Saito H, Aoe K, Tsuji T, Takiguchi Y, Takayama K, Komura N, Takiguchi T, Eguchi K. Anamorelin (ONO-7643) for the treatment of patients with non-small cell lung cancer and cachexia: Results from a randomized, double-blind, placebo-controlled, multicenter study of Japanese patients (ONO-7643-04). Cancer. 2018;124:606-616.

10) Kuraoka M, Amatya VJ, Kushitani K, Mawas AS, Miyata Y, Okada M, Kishimoto T, Inai K, Nishisaka T, Sueda T, Takeshima Y. Identification of DAB2 and Intelectin-1 as Novel Positive Immunohistochemical Markers of Epithelioid Mesothelioma by Transcriptome Microarray Analysis for its Differentiation From Pulmonary Adenocarcinoma. Am J Surg Pathol. 2017; 41: 1045-1052

11) 岸本卓巳、藤本伸一.石綿ばく露によるびまん性胸膜肥厚と中皮腫・肺癌発生に関

する検討.日職災医誌. 2017; 65: 153-159.
12) 岸本卓巳.アスベストの発がん機序　環境による健康リスク.日本医師会雑誌.2017;146:S253.
13) Kuyama S, Ochi N, Bessho A, Hotta K, Ikeda G, Kishino D, Kubo T, Harada D, Fujimoto N, Nakanishi M, Umeno T, Okada T, Chikamori K, Yamagishi T, Ohashi K, Ichihara E, Takigawa N, Tanimoto M, Kiura K. A Phase II trial of carboplatin plus S-1 for elderly patients with advanced non-small-cell lung cancer with wild-type epidermal growth factor receptor: The Okayama Lung Cancer Study Group Trial 1202. Lung Cancer 2017;112: 188–194.
14) Ozeki T, Asano M, Fujimoto N, Nishimura J, Takada K, Miyamoto Y, Fuchimoto Y, Wada S, Ozaki S, Kishimoto T. Esophagobronchial fistula in a patient with squamous cell carcinoma of the lung: A case report. Case Rep Oncol. 2017;10:553-557.
15) Nishimura J, Miyamoto Y, Fujimoto N, Ozeki T, Takada K, Asano M, Fuchimoto Y, Wada S, Ozaki S, Kishimoto T. Adenocarcinoma of the lung acquiring resistance to afatinib by transformation to small cell carcinoma: A case report. Case Rep Oncol. 2017;10:666-670.
16) Murata Y, Aoe K, Mimura-Kimura Y, Murakami T, Oishi K, Matsumoto T, Ueoka H, Matsunaga K, Yano M, Mimura Y. Association of IgG4 and free light chain with idiopathic pleural effusion. Clin Exp Immunol. 2017;190:133-142.

２．著書

1) Hatano R, Ohnuma K, Yamada T, Okamoto T, Komiya E, Otsuka H, Itoh T, Yamazaki H, Iwao N, Kaneko Y, Dang NH, Morimoto C. The use of the humanized anti-CD26 monoclonal antibody YS110 as a novel targeted therapy for refractory cancers and immune disorders. Advances in Medicine and Biology (Nova Science Publishers, Inc.). in press

３．学会発表

1) Takumi Itoh, Ryo Hatano, Haruna Otsuka, Noriaki Iwao, Satoshi Iwata, Taketo Yamada, Chikao Morimoto. IL-26 facilitates angiogenesis and skin inflammation via inducing FGF2 production in a murine model of imiquimod-induced psoriasis. 第 46 回日本免疫学会、2017 年 12 月、仙台.
2) Eriko Komiya, Ryo Hatano, Haruna Otsuka, Takumi Itoh, Hiroto Yamazaki, Taketo Yamada, Yasushi Suga, Utako Kimura, Mitsutoshi Tominaga, Kenji Takamori, Kei Ohnuma, Chikao Morimoto. The regulation of pruritus in psoriasis and atopic dermatitis-a possible role for CD26/DPPIV. 9th World Congress on Itch, 2017 ,October.Wrocław, Poland.
3) Nishida H, Hayashi M, Morimoto C,

Sakamoto M, Yamada T. Humanized anti-CD26 monoclonal antibody, YS110, has anti-myeloma efficacy for the treatment of high-risk multiple myeloma. The 59th American Society of Hematology Annual Meeting and Exposition. 2017, December, Atlanta, GA, USA.

4) Yamada T, Madokoro H, Nishida H, Morimoto C, Sakamoto M, Hayashi M. Anti-CD26 humanized monoclonal antibody conjugated to triptolide is transported into nucleus and impairs RNA polymerase II. 2017 年 12 月、生命科学系学会合同年次大会（ConBio2017）神戸.

5) Nishida H, Hayashi M, Morimoto C, Sakamoto M, Yamada T. Humanized anti-CD26 monoclonal antibody has a therapeutic potentiality against multiple myeloma. 第79回日本血液学会 2017 年 10 月、東京国際フォーラム.

6) 土居美枝子、稲田博輝、細沼沙紀、政岡秀彦、瀬山幸子、金野美年子、石澤圭介、茅野秀一、山田健人、佐々木惇 腺癌との鑑別を要したリンパ腫様型/形質細胞腫様浸潤性尿路上皮癌の 1 例 第 58 回日本臨床細胞学会総会、平成 29 年（2017 年）5 月、大阪.

7) 李治平，山田健人，金玲，市村隆也，石澤圭介，佐々木惇 関節リウマチのエタネルセプト治療中に UIP 型間質性肺炎併発した一剖検症例 第 106 回日本病理学会総会 2017 年 4 月、東京

8) 金 玲, 李 治平, 市村隆也, 石澤圭介, 茅野秀一, 佐々木惇, 山田健人 百日咳肺炎から肺高血圧症を併発し死亡した新生児剖検症例 第 106 回日本病理学会総会 2017 年 4 月、東京.

9) Yamada T, Madokoro H, Yamada K, Nishida H, Morimoto C, Sakamoto M, Hayashi M. Anti-tumor effects of humanized anti-CD26 monoclonal antibody against hepatocellular carcinoma. 第106回日本病理学会総会 2017 年 4 月、東京.

10) Aida S, Ichikawa D, Iida K, Hozumi M, Nakamura M, Uozaki R, Hashimoto N, Okayama M, Yonemura Y, Tabata N, Yamada T, Matsushita M, Sugai T, Yanagawa H, Hattori Y. PEG(E)-TC11, a novel polyethylene glycol-linked phthalimide derivative, inhibited high-risk MM cell growth in vivo and in vitro via cell cycle G2/M arrest in a CRBN-independent manner. American Association for Cancer Research (AACR) Annual Meeting, 2017, April, Washington D.C., USA.

11) Fujimoto N, Kojima Y, Kishimoto T. Secretary leukocyte peptide inhibitor (SLPI) in pleural fluid is useful as a diagnostic marker of malignant pleural mesothelioma. ASCO2017(American Society of Clinical Oncology Annual Meeting) 2017 年 6 月 3－7 日 Chicago.

12) Kato K, Gemba K, Ashizawa K, Kishimoto T, Fujimoto N, Aoe K,

Takeshima Y, Inai K. CT Findings of Malignant Pleural Mesothelioma and Correlation with the Survival Period .The 4th World Congress of Thoracic Imaging（WCTI）2017 年 6 月 18－21 日　Boston.

13）藤本伸一、児島葉子、宮本洋輔、浅野美智子、淵本康子、和田佐恵、小崎晋司、岸本卓巳. 胸膜中皮腫の診断における胸水 Secretary leukocyte peptide inhibitor (SLPI) の有用性について　第 15 回日本臨床腫瘍学会学術集会　2017 年 7 月 27 日　神戸.

14）尾瀬功、長松康子、青江啓介、加藤勝也、堀田勝幸、中川淳子、原桂子、岸本卓巳、藤本伸一. 悪性胸膜中皮腫患者の QOL 調査結果　第 15 回日本臨床腫瘍学会学術集会　2017 年 7 月 28 日　神戸.

15）中川淳子、小林幸以、石丸直樹、野村伽奈子、亀谷友里恵、藤本伸一、岸本卓巳. 胸膜中皮腫患者の経時的ケアニーズ　第 15 回日本臨床腫瘍学会学術集会　2017 年 7 月 29 日　神戸.

16）藤本伸一、長松康子、青江啓介、堀田勝幸、加藤勝也、尾瀬功、中川淳子、原桂子、岸本卓巳. 「患者と家族のための胸膜中皮腫ハンドブック」の作成　第 15 回日本臨床腫瘍学会学術集会　2017 年 7 月 29 日　神戸.

17）Oze I , Nagamatsu Y, Aoe K, Hotta K, Kato K, Nakagawa J, Hara K, Kishimoto T, Fujimoto N. Evaluation of quality of life in survivors with malignant pleural mesothelioma in Japan. EUROPEAN SOCIETY FOR MEDICAL ONCOLOGY 2017 Congress （ESMO2017） 2017 年 9 月 8－12 日　MADRID.

18）倉岡正嗣、アマティア　ヴィシュワジート、櫛谷桂、Amany S.Mawas、宮田義浩、岡田守人、岸本卓巳、井内康輝、西阪隆、末田泰二郎、武島幸男. 網羅的遺伝子発現解析から同定した DAB2 と Intelectin-1 の上皮型中皮腫と肺腺癌の鑑別診断における有用性　第 24 回石綿・中皮腫研究会　2017 年 10 月 7 日　大阪.

19）西村泰光　李順姫、松﨑秀紀、武井直子、吉留敬、岡本賢三、岸本卓巳. 包括的免疫機能解析による悪性中皮腫とびまん性
胸膜肥厚との判別指標の探索　第 24 回石綿・中皮腫研究会　2017 年 10 月 7 日　大阪.

20）藤本伸一、西村淳、宮本洋輔、浅野美智子、淵本康子、和田佐恵、小崎晋司、伊賀徳周、西英行、岸本卓巳. 「胸水のみ」を呈する胸膜中皮腫症例の検討　第 58 回日本肺癌学会学術集会　2017 年 10 月 14 日　横浜.

21）Kuraoka M, Amatya VJ, Kushitani K, Mawas AS, Miyata Y, Okada M, Kishimoto T, Inai K, Nishisaka T, Sueda T, Takeshima Y. Identification of DAB2 and Intelectin-1 as Novel Positive Immunohistochemical Markers of Epithelioid Mesothelioma. 18th World Conference on Lung Cancer　2017 年 10 月 16 日　Yokohama.

22）Kishimoto T. Clinical Evaluation for

Asbestos-Induced Diffuse Pleuralthickening (DPT) in JAPAN. CHEST 2017. 2017 年 11 月 1 日 Toronto.

23）岸本卓巳、藤本伸一．胸膜中皮腫の診断時胸部 CT 所見の検討　第 65 回日本職業・災害医学会学術大会　2017 年 11 月 25 日　北九州.

24）藤本伸一、岸本卓巳、青江啓介、加藤勝也、堀田勝幸、尾瀬功、長松康子．胸膜中皮腫に対する新規治療法の臨床導入に関する研究　第 65 回日本職業・災害医学会学術大会　2017 年 11 月 25 日 北九州.

25）藤本伸一、宮本洋輔、和田佐恵、野上尚之、久山彰一、別所昭宏、堀田勝幸、青江啓介、南大輔、木浦勝行。EGFR 遺伝子変異陽性非小細胞肺癌に対する afatinib・bevacizumab 併用療法の第 I 相試験：OLCSG1404。第 58 回日本肺癌学会学術集会。平成 29 年 10 月 14 日、横浜.

26）坂本健次、近森研一、村田順之、青江啓介、前田忠士、亀井治人、松本常男．両側肺動脈腫瘍の肺浸潤に対し、TBLB で悪性軟部腫瘍と診断した一例．第 57 回日本呼吸器学会学術講演会、平成 29 年 4 月 22 日、東京.

27）村田順之、青江啓介、宇都宮利彰、三村雄輔、松本常男．胸膜に IgG4 陽性形質細胞を認めた胸水症例の解析．第 57 回日本呼吸器学会学術講演会、平成 29 年 4 月 23 日、東京.

28）坂本健次、村田順之、近森研一、青江啓介、前田忠士、亀井治人、丸山治彦．肺結核、結核性胸膜炎との鑑別を要したウェステルマン肺吸虫症の一例．第 40 回日本呼吸器内視鏡学会学術集会、平成 29 年 6 月 10 日、長崎.

29）近森研一、関千尋、青江啓介、前田忠士、坂本健次、村田順之、宇都宮利彰、亀井治人. ニボルマブ使用後に薬剤性肺障害を発症した非小細胞肺がん症例の当院での臨床的特徴．第 58 回日本肺癌学会学術集会、平成 29 年 10 月 15 日、横浜.

30）関千尋、前田忠士、青江啓介、近森研一、坂本健次、村田順之、宇都宮利彰、亀井治人. ニボルマブを早期肺障害で中止したが、ペムブロリズマブへ変更し、効果が得られた進行肺腺癌の一例．第 58 回日本肺癌学会学術集会、平成 29 年 10 月 14 日、横浜.

31）坂本健次、村田順之、大畑秀一郎、宇都宮利彰、近森研一、青江啓介、前田忠士、亀井治人、松本常男．肺 MAC 症に MALT リンパ腫を併発した一例．第 26 回日本呼吸器内視鏡学会中国四国支部会、平成 29 年 10 月 28 日、広島.

G.知的財産権の出願・登録状況（予定を含む）

1. 発明者：森本幾夫、波多野良、山田健人、大沼圭.
   出願番号：特許出願中
   名称：抗ヒト CD26 モノクローナル抗体
   出願人：学校法人 順天堂、埼玉医科大学（共同出願）
   出願年月日：2018 年 3 月予定(PCT 出願)

2. 発明者：森本幾夫、波多野良、大沼圭、
伊藤匠.
出願番号：特願 2017-231439
名称：抗ヒト IL-26 抗体
出願人：学校法人 順天堂
出願年月日：2017 年 12 月 1 日(PCT
出願)

労災疾病臨床研究事業費補助金
分担研究報告書

ヒト化 CD26 抗体の抗腫瘍作用メカニズムの新たな可能性：悪性胸膜中皮腫患者 T 細胞のフェノタイプ解析

研究代表者　森本　幾夫　順天堂大学大学院医学研究科
免疫病・がん先端治療学講座 客員教授
研究分担者　岸本　卓巳　岡山労災病院
ｱｽﾍﾞｽﾄ関連疾患研究ｾﾝﾀｰｾﾝﾀｰ長
研究分担者　山田　健人　埼玉医科大学医学部 病理学 教授
研究協力者　波多野　良　順天堂大学大学院医学研究科
免疫病・がん先端治療学講座 博士研究員
研究協力者　大沼　　圭　順天堂大学大学院医学研究科
免疫病・がん先端治療学講座 准教授
研究協力者　藤本　伸一　岡山労災病院 ｱｽﾍﾞｽﾄ関連疾患研究ｾﾝﾀｰ副ｾﾝﾀｰ長
研究協力者　青江　啓介　山口宇部医療センター 腫瘍内科 内科系診療部長

研究要旨

悪性胸膜中皮腫はアスベストばく露によって起こる難治性悪性腫瘍であり、現時点で満足できる治療法はなく、新たな治療法の確立が望まれる。われわれは、新規治療標的分子として悪性胸膜中皮腫に発現する CD26 に着目し、ヒト化 CD26 抗体を開発しフランスにて第 I 相臨床試験を行った。安全性が確認されるとともに治療薬としての有効性を示唆する結果も得られ、平成 29 年 6 月から国内でも第 I/II 相臨床試験を開始した。有効かつ安全な CD26 抗体との併用療法の開発とともに、CD26 抗体の抗腫瘍作用メカニズムの更なる解明は極めて重要である。CD26 は T 細胞に活性化シグナルを伝達する共刺激分子としても機能するため、CD26 抗体は免疫系にも影響する可能性が考えられる。これまでに、CD26 シグナルによって免疫チェックポイント分子 BTLA と LAG3 の高発現、抑制性サイトカイン IL-10 高産生が誘導されることを報告した。今年度は、悪性胸膜中皮腫患者の胸水中 T 細胞の機能解析を行い、健常者及び中皮腫患者の末梢血 T 細胞と比較して、免疫チェックポイント分子の中で特に PD1, BTLA, CD39 の発現が上昇していること、細胞傷害性分子の Perforin, Granzyme B の発現、エフェクターT 細胞の割合が顕著に低下していることを明らかにした。このことから、悪性胸膜中皮腫患者の胸水中 T 細胞は、近位に存在するがん細胞からの影響を受けて機能不全になっている可能性が示唆された。

A. 研究目的

悪性胸膜中皮腫はアスベストばく露によって起こる胸膜中皮由来の難治性悪性腫瘍である。アスベストばく露から発症までの潜伏期間は 30-50 年とされ、日本を含めアジアやヨーロッパなど世界規模で胸膜中皮腫患者数は今後ますます増加すると考えられている。悪性胸膜中皮腫に対しては手術療法、化学療法、放射線療法などが行われるが、いずれも満足できる治療成績ではなく、新たな治療法の確立が望まれる。われわれは、新規治療標的分子として悪性胸膜中皮腫細胞に発現する CD26 に着目し、ヒト化 CD26 抗体を開発しフランスにて第 I 相臨床試験を行った。特記すべき副作用もなく安全性が確認されるとともに、抗がん剤抵抗性の悪性中皮腫患者 19 例中 10 例が Stabilized Disease (SD)となり治療薬としての有効性を示唆する結果も得られた。平成 29 年 6 月から国内でも第 I/II 相臨床試験を開始したが、有効かつ安全な CD26 抗体との併用療法の開発とともに、CD26 抗体の抗腫瘍作用メカニズムの更なる解明は極めて重要である。

我々はこれまでにヒト化 CD26 抗体の抗腫瘍作用メカニズムとして、抗体医薬特有の抗体依存性細胞傷害(ADCC)活性・補体依存性細胞傷害(CDC)活性に加え、CD26 陽性腫瘍に抗体が結合することによる直接的な作用があることを明らかにしてきた。がん細胞の細胞膜上の CD26 にヒト化 CD26 抗体が結合すると、cyclin dependent kinase inhibitor である p21 や p27 の発現が上昇し cell cycle arrest を起こさせること(Clin Cancer Res. 2001, Immunology. 2002, Clin Cancer Res. 2007, Cancer Cell Int. 2016)、CD26 抗体と CD26 の複合体が細胞膜から細胞質、さらに核内へと移行し、RNA polymerase II のサブユニットである POLR2A 遺伝子の転写領域下流に結合することで POLA2A の転写を抑制し増殖抑制に働くことを明らかにした(PLoS One. 2013)。また、CD26 は collagen や fibronectin との結合タンパクであるが、CD26 抗体が結合することでそれらのタンパクへの接着が阻害され(Clin Cancer Res. 2007)、このことから CD26 抗体が CD26 陽性腫瘍の浸潤・転移の抑制にも働くことが示唆された。

CD26 はヒト T 細胞に活性化シグナルを伝達する T 細胞共刺激分子であり、ヒト化 CD26 抗体は CD26 のリガンドである caveolin-1 の CD26 への結合をブロックする。また、CD26 の機能の一つに dipeptidyl peptidase IV (DPPIV)酵素活性があり、N 末から 2 番目にプロリンまたはアラニンを有するペプチドの 2 アミノ酸を切断する。生体内で様々な生理活性物質がその基質となることが知られているが、いくつかのケモカインも DPPIV による切断を受けその細胞遊走活性が不活性化される。ヒト化 CD26 抗体は DPPIV 酵素活性自体に直接は影響しないが、フランスでの第 I 相臨床試験の結果から CD26 抗体の投与により血中の可溶性 CD26 の量が顕著に低下し、DPPIV 酵素活性も同様に低下することが示されている(Br J Cancer. 2017)。DPPIV 酵素活性の低下により IP-10(CXCL10)などのケモカインの切断と不活性化が抑えられ、免疫細胞が腫瘍組織に遊走しやすくなる可能性が考えられる(Nat Immunol. 2015)。これらの知見から、CD26 抗体は免疫系にも影響する可能性が強く示唆される。

近年、がんの新たな治療法として免疫系に

抑制シグナルを伝達するチェックポイント分子をブロックすることで腫瘍免疫を活性化させる免疫チェックポイント阻害薬が非常に注目されており、CTLA4 抗体や PD1 抗体は既に臨床現場で用いられ始めている。われわれは最近、ヒト CD4 T 細胞に強い CD26 共刺激シグナルが伝達すると免疫チェックポイント分子 LAG3 の発現と代表的な抑制性サイトカイン IL-10 の産生が強く誘導されることを報告した(J Immunol. 2015)。また、これまでの解析から、CD26 共刺激は CD28 共刺激と比較して、CD4 T 細胞・CD8 T 細胞のどちらに対しても免疫チェックポイント分子 BTLA の発現を顕著に増強させること、がん細胞周囲に多く存在すると考えられる免疫抑制性因子のうち TGF-β、PGE_2、L-Kynurenine、Adenosine は免疫チェックポイント分子の発現を増強させるとともに CD26 の発現増強にも作用することを報告した。

ヒト化 CD26 抗体投与が腫瘍免疫に及ぼす影響を解析するうえで、悪性胸膜中皮腫患者の免疫機能に関する基礎情報は不可欠である。そこで今年度は、悪性胸膜中皮腫患者の末梢血及び胸水中 T 細胞の CD26 発現、免疫チェックポイント分子の発現、細胞傷害性分子の発現、細胞傷害性エフェクター細胞の割合に特に着目して解析を行った。

B. 研究方法

1) ヒト T 細胞の調製

順天堂大学医学部研究等倫理委員会での承認を得て、インフォームド・コンセントを書面で得られた成人健常者の末梢血から、Ficoll 密度分離法により末梢血単核球(PBMC)を調製した。PBMC から T 細胞への精製には MACS(磁気細胞分離)システム(Miltenyi Biotec)を用いた。ヒト CD4 T 細胞、CD8 T 細胞への精製には、それぞれ human $CD4^+$ T cell isolation kit, human $CD8^+$ T cell isolation kit (Miltenyi Biotec)を使用し、それぞれ $CD3^+CD4^+$ が 97%以上、$CD3^+CD8^+$ $CD56^{nega}$ が 95%以上であることを FACS Calibur (BD Biosciences)にて確認した。また、岡山労災病院、山口宇部医療センターで倫理委員会での承認を得て、インフォームド・コンセントを書面で得られた悪性中皮腫・良性石綿胸水の患者から末梢血と胸水の提供を受けた。末梢血から Ficoll 密度分離法により PBMC を調製した。胸水を 1800rpm, 7min, 4℃で遠心し、胸水細胞を得た。上記と同様に MACS システムを用いて、PBMC 及び胸水細胞から T 細胞への精製を行った。

2) 抗体と試薬

Flow cytometry には下記のヒト抗原特異抗体を用いた。FITC-labeled anti-CD26 mAb (clone M-A261), FITC-labeled anti-CD28 mAb (clone CD28.2), FITC-labeled anti-Perforin (clone δG9), PE-labeled anti-CD26 mAb (clone M-A261), PE-labeled anti-Granzyme A (clone CB9), APC-labeled anti-CD3 mAb (clone UCHT1), APC-labeled anti-CTLA4 mAb (clone BNI3), Alexa Fluor 647-labeled anti-CCR7 mAb (clone 3D12), Alexa Fluor 647-labeled anti-FOXP3 mAb (clone 259D/C7) 及び Alexa Fluor 647-labeled anti-Granzyme B mAb (clone GB11)は BD Biosciences から購入した。FITC-labeled anti-LAG3 mAb (clone

3DS223H)と PE/Cy7-labeled anti-TIGIT mAb (clone MBSA43)は eBioscience から購入した。FITC-labeled anti-CD8a mAb (clone HIT8a), PerCP/Cy5.5-labeled anti-CD4 mAb (clone RPA-T4), PerCP/Cy5.5-labeled anti-CD73 mAb (clone AD2), PerCP/Cy5.5-labeled anti-CD244 (2B4) mAb (clone C1.7), PE/Cy7-labeled anti-Tim3 mAb (clone F38-2E2), PE/Cy7-labeled anti-CD28 mAb (clone clone CD28.2), PE/Cy7-labeled anti-CD45RA mAb (clone HI100), PE/Cy7-labeled anti-CD160 mAb (clone BY55), APC-labeled anti-PD1 mAb (clone EH12.2H7), APC-labeled anti-BTLA mAb (clone MIH26), APC-labeled anti-CD39 mAb (clone A1), APC-labeled anti-DNAM1 (CD226) (clone 11A8)及び Alexa Fluor 647-labeled anti-CD57 mAb (clone HCD57)は BioLegend から購入した。

3) フローサイトメトリー

末梢血単核球及び胸水中細胞から精製した CD4 T 細胞、CD8 T 細胞の、細胞膜上の免疫チェックポイント分子及び CD26 の発現、細胞傷害性エフェクターT 細胞マーカーの発現を解析した。Perforin、Granzyme A、Granzyme B の細胞内の発現に関しては、BD Cytofix/Cytoperm Plus Fixation/ Permeabilization kit (BD Biosciences)を用いて、付属のプロトコルに従い細胞内染色を行った。FACSCalibur (BD Biosciences)で測定を行い、得られたデータを FlowJo (Tree Star)で解析した。

(倫理面への配慮)

成人健常者ならびに岡山労災病院、山口宇部医療センターの悪性胸膜中皮腫患者・良性石綿胸水患者の末梢血及び胸水を用いた研究については、順天堂大学医学部研究等倫理委員会の審査を受け承認されている(承認番号 2017090)。末梢血及び胸水の提供を受ける際には、研究対象者に対する人的擁護上の配慮及び研究により研究対象者が受ける不利益、利益等の説明を行い、書面でのインフォームド・コンセントを得ている。

C. 研究結果

1) 健常者末梢血、悪性胸膜中皮腫患者末梢血及び胸水中 CD4 T 細胞、CD8 T 細胞における CD26 の発現解析

免疫チェックポイント阻害薬が腫瘍免疫活性化に働くことを証明するための研究では、がん患者の末梢血及び腫瘍内浸潤リンパ球(Tumor Infiltrating Lymphocyte; TIL)における、免疫チェックポイント分子の発現と Perforin や Granzyme などの細胞傷害性因子、TNF-αや IFN-γなどのサイトカイン産生の発現といったエフェクター機能の解析が主に行われている。しかしながら、悪性胸膜中皮腫患者の腫瘍細胞塊を新鮮な状態で、研究に足りるだけの十分な細胞数得ることは難しく、一方で、胸水に関しては検査目的で採取する機会も多く、また末梢血と比べて量も多く得やすい。そこで、悪性胸膜中皮腫患者の末梢血と、悪性胸膜中皮腫の近位に存在しがん細胞の影響をより受けていることが予想される胸水を用いて、T 細胞の機能解析を行った。

まず、CD4 T 細胞、CD8 T 細胞の CD26 の発現を解析した。CD26 は健常者の末梢血 CD4 T 細胞、CD8 T 細胞ともに、CD26 高

発現(CD26^{high})・CD26 低発現(CD26$^{low/int}$)・CD26 陰性(CD26^{nega})の三相性の特徴的な発現パターンを示し、それぞれが Naive・Central Memory・Effector Memory・Terminal Effector といった T 細胞の分化段階と密接に関係している(Immunology. 2013)。代表的な T 細胞共刺激分子である CD28 と組み合わせて CD26/CD28 の発現分布を調べる方が、より詳細な情報を得られるため、CD26/CD28 の発現分布を解析した結果、図 1 に示すように、健常者の末梢血 CD4 T 細胞及び悪性胸膜中皮腫患者の末梢血 CD4 T 細胞は、いずれの提供者も同等の発現パターンを示し、CD26$^{low/int}$CD28^{+}に大部分が属する結果であった。悪性胸膜中皮腫患者の胸水中 CD4 T 細胞に関しても、11 例中 9 例は末梢血と同様の発現パターンを示したが(図 1 中 Type A)、1 例は CD26$^{low/int}$CD28^{nega} に一部が属し(Type B)、1 例は CD26^{high}CD28^{nega} に大部分が属する発現パターンを示した(Type C)。

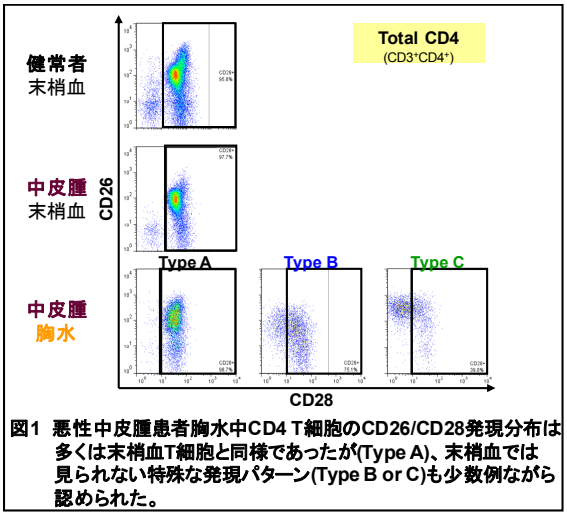

図1 悪性中皮腫患者胸水中CD4 T細胞のCD26/CD28発現分布は多くは末梢血T細胞と同様であったが(Type A)、末梢血では見られない特殊な発現パターン(Type B or C)も少数例ながら認められた。

次に、CD8 T 細胞の CD26/CD28 の発現分布を解析した結果、CD4 T 細胞とは異なり CD8 T 細胞は健常者でも Naive・Memory・Effector の割合の個人差は大きいが、図 2 に代表的な末梢血 CD8 T 細胞の発現パターンを示す。主に 4 つのサブセットに分類することができ、CD26^{high}CD28^{+}は早期 Effector Memory、CD26$^{low/int}$CD28^{+}は Naive、CD26^{nega}CD28^{+}は全ての分化段階の混合、CD26^{nega}CD28^{nega} は主に Terminal Effector に属することを、以前報告した(Immunology. 2013)。意外なことに、悪性胸膜中皮腫患者の末梢血 CD8 T 細胞は、Terminal Effector の CD26^{nega}CD28^{nega} に属する割合が非常に高く、健常者と比較して末梢血中の CD8 T 細胞が異常に活性化した状態にあることが示唆された(図 2)。一方で、悪性胸膜中皮腫患者の胸水中 CD8 T 細胞は、CD26$^{int/high}$CD28^{+}に多くが属するパターン(図 2 中 Type A)、CD26^{nega}CD28^{+}に多くが属するパターン(Type B)、CD26^{nega}CD28^{nega} に大部分が属するパターン(Type C)のいずれかが 11 例中それぞれ複数例で見られ、Type B と Type C は少なくとも健常者の末梢血 CD8 T 細胞では見られない発現パターンであった。これらの結果から、悪性胸膜中皮腫患者の胸水中 T 細胞、特に CD8 T 細胞は CD26/CD28 の発現パターンや分化段階が末梢血とは明らかに異なることが示唆され、さらに患者内でも多様性が認められた。

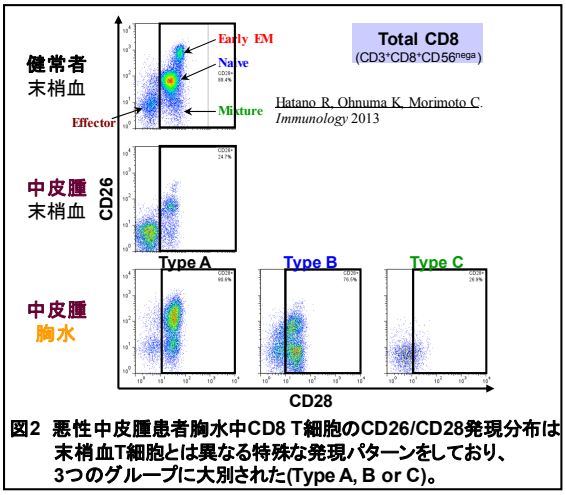

図2 悪性中皮腫患者胸水中CD8 T細胞のCD26/CD28発現分布は末梢血T細胞とは異なる特殊な発現パターンをしており、3つのグループに大別された(Type A, B or C)。

2) 健常者末梢血、悪性胸膜中皮腫患者末梢血及び胸水中 CD4 T 細胞、CD8 T 細胞における免疫チェックポイント分子と細胞傷害性エフェクター分子の発現解析

近年、免疫系に抑制シグナルを伝達するチェックポイント分子をブロックすることで腫瘍免疫を活性化させる免疫チェックポイント阻害薬が新たながん治療法として非常に注目されている。一昨年度・昨年度に引き続き、近年着目されている免疫チェックポイント分子 10 種の解析を行った(それぞれのリガンドとの関係を図 3 にまとめた)。

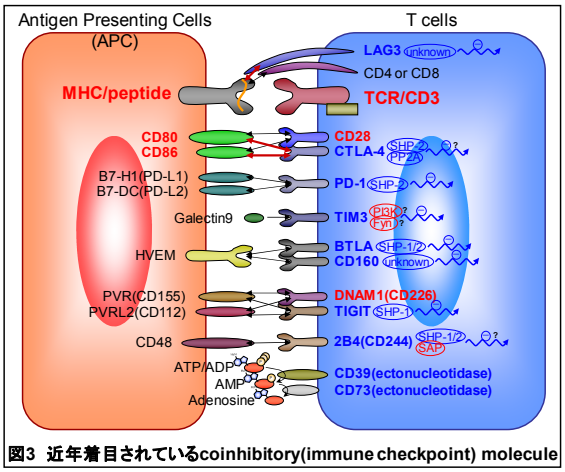

図3 近年着目されているcoinhibitory(immune checkpoint) molecule

免疫応答を負に制御する免疫チェックポイント分子は、慢性的な免疫応答の持続を制御するために生体内に本来備わっている機構であり、抗原感作されて活性化した T 細胞に発現が誘導されることが多い。健常者の末梢血 CD4 T 細胞、CD8 T 細胞に in vitro で T cell receptor (TCR)刺激を与えると、CD73 と CD160 を除く PD1、LAG3、TIM3、BTLA、CTLA4、TIGIT、2B4(CD244)、CD39 では、代表的な T 細胞活性化刺激である CD28 共刺激または CD26 共刺激による発現上昇が認められた。中でも CD4 T 細胞の BTLA と LAG3、CD8 T 細胞の BTLA は CD28 共刺激と比較して CD26 共刺激によって顕著に発現が増強することが示された(一昨年度・昨年度報告書参照)。

がん細胞の周囲に浸潤した T 細胞では各種免疫チェックポイント分子の発現が上昇していることが報告されている。がん微小環境に多く存在すると考えられる TGF-βやプロスタグランジン、キヌレニン、アデノシンなどの免疫抑制性因子が、PD1 や TIM3、2B4(CD244)、CD39 など様々な免疫チェックポイント分子の発現を増強し得ることを昨年度報告した。また、それらの免疫抑制性因子は CD26 の発現増強にも作用することが示唆され、このことからがん細胞周囲では CD26 シグナルが増強している可能性が考えられる。

今年度は、悪性胸膜中皮腫患者の T 細胞に関する基礎的な知見を得るべく、悪性胸膜中皮腫の近傍に位置する胸水中 T 細胞の免疫チェックポイント分子の発現を解析した結果、胸水中 CD8 T 細胞では健常者の末梢血 CD8 T 細胞や悪性胸膜中皮腫患者の末梢血 CD8 T 細胞と比較して、PD1、BTLA、

CD39 の 3 種類に、11 例中複数例(3 例以上)で明らかな発現上昇が認められた(図 4)。その他に、LAG3、TIM3 に関しても発現が上昇している患者が少数ながら認められた(データ未掲載)。しなしながら、悪性胸膜中皮腫の対照症例として 2 例解析を行った良性石綿胸水患者の胸水中 CD8 T 細胞においても末梢血 T 細胞と比較して、PD1 や CD39 の発現上昇が見られた(図 4)。今後、対照症例の症例数を増やして、免疫チェックポイント分子の発現上昇ががん細胞による影響を受けての変化なのかを明らかにする。また、肺がん患者の胸水中 T 細胞における免疫チェックポイント分子の発現に関しても同様に解析を行い、悪性胸膜中皮腫に特異的に発現が誘導される免疫チェックポイント分子が存在するかについても明らかにする。

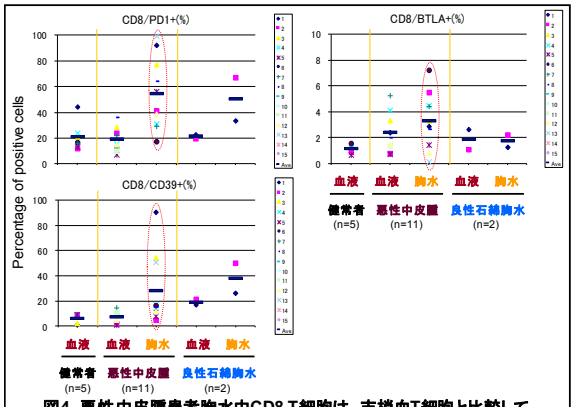

図4 悪性中皮腫患者胸水中CD8 T細胞は、末梢血T細胞と比較して、PD1, BTLA, CD39の発現が上昇している可能性が示唆された。

次に、悪性胸膜中皮腫患者の胸水中 CD8 T 細胞のエフェクター機能の解析を行った。Perforin と Granzyme B を高発現する Terminal Effector CD8 T 細胞のマーカーとして CD28 陰性と CD57 陽性が報告されている。そこで、悪性胸膜中皮腫患者の末梢血及び胸水中 CD8 T 細胞における CD28 陰性の割合、CD57 陽性の割合を解析した結果、図 2 でも示したように、悪性胸膜中皮腫患者の末梢血 CD8 T 細胞は、健常者の末梢血 CD8 T 細胞と比較して CD28 陰性の割合が顕著に高く、同様に CD57 陽性の割合も顕著に高かった(図 5)。一方で、悪性胸膜中皮腫患者の胸水中 CD8 T 細胞では末梢血 CD8 T 細胞と比較して CD28 陰性の割合、CD57 陽性の割合がどちらも健常者の末梢血 CD8 T 細胞と同等のレベルまで低下していることが示された(図 5)。細胞傷害活性における中心的なエフェクター分子の一つである Perforin と Granzyme B の細胞内発現も解析した結果、悪性胸膜中皮腫患者の末梢血 CD8 T 細胞では、健常者の末梢血 CD8 T 細胞よりも Perforin 陽性の割合、Granzyme B 陽性の割合が非常に高く、一方で、悪性胸膜中皮腫患者の胸水中 CD8 T 細胞では Perforin 陽性の割合、Granzyme B 陽性の割合の著明な低下が見られ、特に Perforin は健常者の末梢血 CD8 T 細胞よりも陽性率が低いことが示された(図 5)。このことから、悪性胸膜中皮腫患者の胸水中 CD8 T 細胞は、細胞表面マーカーの発現及び細胞傷害性エフェクター分子の発現から、細胞傷害性 T 細胞として十分な機能を果たしていないことが予想される。しかしながら、図 4 の免疫チェックポイント分子の発現でも示したように、現時点でまだ 2 例しか解析を行えていないが、良性石綿胸水の患者においても末梢血 CD8 T 細胞と胸水中 CD8 T 細胞とで、悪性胸膜中皮腫患者と同様の傾向が見られている(図 5)。今後、対照症例の症例数を増やして、胸水中 CD8 T 細胞の細胞傷害活性の低下ががん細胞による影響を受けての変化なのかを明らかにする。

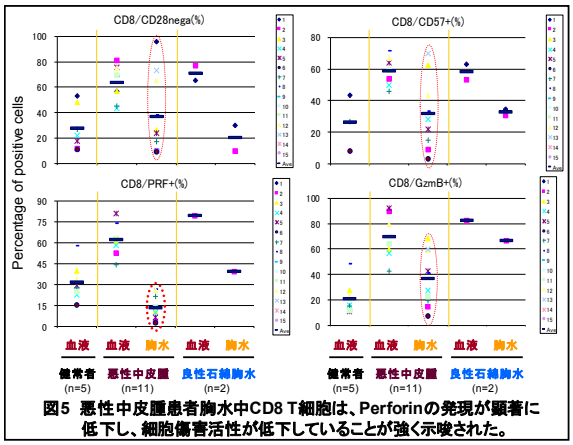

図5 悪性中皮腫患者胸水中CD8 T細胞は、Perforinの発現が顕著に低下し、細胞傷害活性が低下していることが強く示唆された。

悪性胸膜中皮腫患者 11 例と対照症例として良性石綿胸水患者 2 例の解析を行った結果、悪性胸膜中皮腫患者の末梢血 T 細胞の免疫チェックポイント分子の発現は、CD73 以外は健常者の末梢血 T 細胞と大きな違いはなく、Perforin や Granzyme B、Terminal Effector 細胞の割合を示す CD26 陰性、CD57 陽性の割合は健常者と比べて顕著に高く、予想に反して T 細胞が活性化した状態にあることが強く示唆された。一方で、胸水中 T 細胞では PD1、BTLA、CD39 をはじめとした様々な免疫チェックポイント分子の発現が上昇しているとともに、Perforin の発現の劇的な低下など細胞傷害性 T 細胞として十分に機能できない状態にあることが示された。

また、胸水中 T 細胞の CD26 の発現パターンに関しても、悪性胸膜中皮腫患者の中で多様性が見られ、何かしらの病態、臨床情報を反映している可能性が考えられる。今後、検体数をさらに増やし、CD26 の発現パターンの違いが意味することについても検討していきたい。

D. 考察

ヒト化 CD26 抗体の抗腫瘍作用メカニズムの更なる解明を目的として、CD26 抗体の免疫系への影響、腫瘍免疫を亢進する可能性について、一昨年度・昨年度に引き続き検討している。

免疫チェックポイント分子の多くが、その細胞内ドメインに SHP-1/2 をはじめとしたフォスファターゼが会合し、T 細胞受容体からのシグナル伝達(キナーゼカスケード)を阻害することで T 細胞の活性化を負に制御する。CD26 の細胞内ドメインはわずか 6 アミノ酸で構成されており、フォスファターゼが会合することが知られている ITIM や ITSM と呼ばれる既存の配列は存在しない。このことから、CD26 分子の細胞内ドメインを介して直接抑制性のシグナルが伝達する可能性は低いと考えられる。そのため、CD26 分子を介して直接抑制性シグナルが伝達するのではなく、CD26 シグナルによって抑制機能を有する免疫チェックポイント分子を誘導し、それらを介して免疫応答を負に制御する可能性を検討している。これまでの結果から、CD26 共刺激は CD4 T 細胞に対して BTLA と LAG3 の高発現、IL-10 の高産生を誘導し、CD8 T 細胞に対しても CD28 共刺激と比較して BTLA の発現を顕著に誘導することが示された。また、がん細胞周囲に多く存在すると考えられる免疫抑制性因子のうち、TGF-βは PD1 の、PGE_2、L-Kynurenine、Adenosine は TIM3 の、PGE_2 は 2B4 (CD244)と CD39 の発現を顕著に増強させることが示された。興味深いことに、PGE_2、L-Kynurenine、Adenosine は CD26 の発現も顕著に増強することが示唆され、がん細胞周囲に浸潤した T 細胞は CD26 の発現が増強している可能性が考え

られる。

ヒト化 CD26 抗体が腫瘍免疫を増強させることを直接的に証明するためには、腫瘍細胞塊に浸潤したがん抗原特異的な T 細胞のエフェクター機能の解析が望まれるが、メラノーマのようによく研究されているがんとは異なり、悪性中皮腫ではがん抗原が十分に特定されていないうえ、腫瘍細胞塊の入手も難しいなど研究の遂行が難しい要素が多い。そこで、がん細胞に特異的な T 細胞に特化しての解析ではないが、CD26 抗体が免疫系に及ぼす影響を解析する方法として、平成 29 年 6 月から開始したヒト化 CD26 抗体の国内第 I/II 相臨床試験に参加した患者検体を用いて、CD26 抗体投与による血清中の可溶性 CD26 濃度/DPPIV 酵素活性値や IL-10 濃度の変動、末梢血 T 細胞のエフェクター機能、BTLA や LAG3 などの免疫チェックポイント分子の発現の変動を経時的に解析することを計画している。

また、まだ悪性胸膜中皮腫患者 11 例、良性石綿胸水患者 2 例での検討結果だが、悪性胸膜中皮腫患者の胸水中 CD4 T 細胞、CD8 T 細胞ともに健常者の末梢血 T 細胞、悪性胸膜中皮腫患者の末梢血 T 細胞と比較して、CD26 の発現や免疫チェックポイント分子の発現、細胞傷害性機能が明らかに異なることが示された(図 4, 5)。今後、良性石綿胸水患者や肺がん患者といった対照症例のデータを増やし、悪性胸膜中皮腫に特徴的な免疫チェックポイント分子の発現パターンや CD26 の発現、T 細胞のサブセット解析を進め、悪性胸膜中皮腫の影響を受けた T 細胞の特性を解明する予定である。また、病理組織の免疫染色により、実際に悪性胸膜中皮腫周囲に浸潤した T 細胞の性質についても解析を行う。

われわれは強い CD26 共刺激シグナルによって BTLA の発現が CD4・CD8 両 T 細胞に特徴的に誘導されることを明らかにしたが、そのシグナル伝達経路、及び転写因子についても解析が必要となる。一部の悪性胸膜中皮腫患者では胸水中 T 細胞に BTLA の高発現が認められるため、このサブセットをセルソーターで分離・精製し、DNA マイクロアレイ解析を行う。in vitro の実験で CD26 共刺激に特徴的な発現上昇が見られる転写因子との比較解析を行い、BTLA の発現制御に関わる転写因子の絞り込みを行う。また、悪性胸膜中皮腫患者の中で、BTLA が高発現している患者の臨床的な特徴についても、検体数を増やしてより詳細に検討していく予定である。

これらの研究により、悪性胸膜中皮腫の影響を受けた T 細胞の特性を明らかにするとともに、ヒト化 CD26 抗体が免疫系に及ぼす影響についても明らかにする。また、血清中の可溶性 CD26 濃度/DPPIV 酵素活性値や IL-10 濃度、末梢血 T 細胞の BTLA、LAG3 の発現の経時的なモニタリングが、ヒト化 CD26 抗体の治療有効性を予測するバイオマーカーになりうる可能性も考えられるため、その点にも着目して解析を行う。

E. 結論

悪性胸膜中皮腫患者 11 例の末梢血および胸水中 T 細胞の解析を行った結果、悪性胸膜中皮腫患者の末梢血 CD8 T 細胞では、健常者の末梢血 CD8 T 細胞よりも Terminal Effector の割合が予想に反して顕著に増加しており、一方で、胸水中 CD8 T 細胞では PD1 や BTLA、CD39 の発現上昇や Perforin、

Granzyme B の著明な発現低下が見られた。このことから、胸水中 T 細胞は、近位に存在する悪性胸膜中皮腫からの影響を受けて機能不全になっている可能性が示唆された。

F. 今後の展望

悪性中皮腫自身やその周囲の細胞に BTLA や LAG3、そのリガンドである HVEM や MHC class II が発現しているか免疫組織染色で検討する。また、CD26 共刺激に特徴的な BTLA の発現誘導に関わるシグナル伝達経路、及び転写因子についての解析が必要となる。さらに、本年度に引き続き、悪性中皮腫患者の末梢血 T 細胞、胸水 T 細胞、悪性中皮腫周囲に浸潤した T 細胞を用いて、各種免疫チェックポイント分子の発現パターンやエフェクター分子、CD26 の発現を解析するとともに、CD26 抗体の国内第 I/II 相臨床試験検体を用いて、CD26 抗体投与による血清中可溶性 CD26 濃度/DPPIV 酵素活性値、IL-10 濃度、末梢血 T 細胞上の BTLA、LAG3 の発現変動を経時的にモニタリングしていく予定である。

G. 研究発表

1. 論文発表

1) Ohnuma K, Hatano R, Komiya E, Otsuka H, Itoh T, Iwao N, Kaneko Y, Yamada T, Dang NH, Morimoto C. A novel role for CD26/dipeptidyl peptidase IV as a therapeutic target in selected immune disorders and cancers. Front Biosci. in press.

2) Hiromura M, Nohtomi K, Mori Y, Kataoka H, Sugano M, Ohnuma K, Kuwata H, Hirano T. Caveolin-1, a binding protein of CD26, is essential for the anti-inflammatory effects of dipeptidylpeptidase-4 inhibitors on human and mouse macrophages. Biochem Biophys Res Commun. 2018; 495: 223-229.

3) Angevin E, Isambert N, Trillet-Lenoir V, You B, Alexandre J, Zalcman G, Vielh P, Farace F, Valleix F, Podoll T, Kuramochi Y, Miyashita I, Hosono O, Dang NH, Ohnuma K, Yamada T, Kaneko Y, Morimoto C. First-in-Human phase 1 of YS110, a monoclonal antibody directed against CD26 in advanced CD26-expressing cancers.Br.J.Cancer.2017;116:1126-1134.

4) Komiya E, Hatano R, Otsuka H, Itoh T, Yamazaki H, Yamada T, Dang NH, Tominaga M, Suga Y, Kimura U, Takamori K, Morimoto C, Ohnuma K. A possible role for CD26/DPPIV enzyme activity in the regulation of psoriatic pruritus.J Dermatol Sci. 2017; 86:212-221.

5) Kim KM, Noh JH, Bodogai M, Martindale JL, Yang X, Indig FE, Basu SK, Ohnuma K, Morimoto C, Johnson PF, Biragyn A, Abdelmohsen K, Gorospe M. Identification of senescent cell surface targetable protein DDP4.Genes Dev. 2017;31:1529-1534.

6) Ikeda T, Kobayashi S, Morimoto C. Gene expression microarray data from mouse cerebrum treated with rTMS

for 30 days.Data Brief. 2017; 15: 948-69.

7) Doonan BP, Ohnuma K, Dang LH, Morimoto C, Dang NH. Current and Emerging Therapy for Malignant Pleural Mesothelioma: Focus on CD26/Dipeptidyl Peptidase IV as a Therapeutic Target. Current Cancer Therapy Reviews. 2017; 13: 1-13.

8) Murakami R, Saisho Y, Watanabe Y, Inaishi J, Tsuchiya T, Kou K, Sato S, Kitago M, Kitagawa Y, Yamada T. Pancreas fat and beta cell mass in humans with and without diabetes: An analysis in the Japanese population. J Clin Endocrinol Metab. 2017;102:3251-3260.

9) Aida S, Hozumi M, Ichikawa D, Iida K, Yonemura Y, Tabata N, Yamada T, Matsushita M, Sugai T, Yanagawa H, Hattori Y. A novel phenylphthalimide derivative, pegylated TC11, improves pharmacokinetic properties and induces apoptosis of high-risk myeloma cells via G2/M cell-cycle arrest. BBRC. 2017;493:514-520.

10) Kushitani K, Amatya VJ, Mawas AS, Suzuki R, Miyata Y, Okada M, Inai K, Kishimoto T, Takeshima Y. Utility of Survivin, BAP1, and Ki‐67 immunohistochemistry in distinguishing epithelioid mesothelioma from reactive mesothelial hyperplasia. Oncology Letters.2018;15:3540-3547.

11) Ninomiya T, Nogami N, Kozuki T, Harada D, Kubo T, Ohashi K, Kuyama S, Bessho A, Fujimoto N, Aoe K, Shibayama T, Takigawa N, Sugimoto K, Kudo K, Fukamatsu N, Hotta K, Kiura K. A phase I trial of afatinib and bevacizumab in chemo-naïve patients with advanced non-small-cell lung cancer harboring EGFR-mutations: Okayama Lung Cancer Study Group Trial 1404. Lung Cancer. 2018;115:103-108.

12) Sato H, Sakaguchi M, Yamamoto H, Tomida S, Aoe K, Shien K, Yoshioka T, Namba K, Torigoe H, Soh J, Tsukuda K, Tao H, Okabe K, Miyoshi S, Pass HI, Toyooka S. Therapeutic potential of targeting S100A11 in malignant pleural mesothelioma. Oncogenesis. 2018;7:11.

13) Hotta K, Aoe K, Kozuki T, Ohashi K, Ninomiya K, Ichihara E, Kubo T, Ninomiya T, Chikamori K, Harada D, Nogami N, Hirata T, Hinotsu S, Toyooka S, Kiura K. A Phase II Study of Trastuzumab Emtansine in HER2-positive Non-Small-Cell Lung Cancer. J Thorac Oncol. 2018;13:273-279.

14) Katakami N, Uchino J, Yokoyama T, Naito T, Kondo M, Yamada K, Kitajima H, Yoshimori K, Sato K, Saito H, Aoe K, Tsuji T, Takiguchi Y, Takayama K, Komura N, Takiguchi T, Eguchi K. Anamorelin (ONO-7643) for the treatment of patients with

non-small cell lung cancer and cachexia: Results from a randomized, double-blind, placebo-controlled, multicenter study of Japanese patients (ONO-7643-04). Cancer. 2018;124:606-616.

15) Kuraoka M, Amatya VJ, Kushitani K, Mawas AS, Miyata Y, Okada M, Kishimoto T, Inai K, Nishisaka T, Sueda T, Takeshima Y. Identification of DAB2 and Intelectin-1 as Novel Positive Immunohistochemical Markers of Epithelioid Mesothelioma by Transcriptome Microarray Analysis for its Differentiation From Pulmonary Adenocarcinoma. Am J Surg Pathol. 2017; 41: 1045-1052

16) 岸本卓巳、藤本伸一.石綿ばく露によるびまん性胸膜肥厚と中皮腫・肺癌発生に関する検討.日職災医誌. 2017; 65: 153-159.

17) 岸本卓巳.アスベストの発がん機序　環境による健康リスク.日本医師会雑誌.2017;146:S253.

18) Kuyama S, Ochi N, Bessho A, Hotta K, Ikeda G, Kishino D, Kubo T, Harada D, Fujimoto N, Nakanishi M, Umeno T, Okada T, Chikamori K, Yamagishi T, Ohashi K, Ichihara E, Takigawa N, Tanimoto M, Kiura K. A Phase II trial of carboplatin plus S-1 for elderly patients with advanced non-small-cell lung cancer with wild-type epidermal growth factor receptor: The Okayama Lung Cancer Study Group Trial 1202. Lung Cancer 2017;112: 188–194.

19) Ozeki T, Asano M, Fujimoto N, Nishimura J, Takada K, Miyamoto Y, Fuchimoto Y, Wada S, Ozaki S, Kishimoto T. Esophagobronchial fistula in a patient with squamous cell carcinoma of the lung: A case report. Case Rep Oncol. 2017;10:553-557.

20) Nishimura J, Miyamoto Y, Fujimoto N, Ozeki T, Takada K, Asano M, Fuchimoto Y, Wada S, Ozaki S, Kishimoto T. Adenocarcinoma of the lung acquiring resistance to afatinib by transformation to small cell carcinoma: A case report. Case Rep Oncol. 2017;10:666-670.

21) Murata Y, Aoe K, Mimura-Kimura Y, Murakami T, Oishi K, Matsumoto T, Ueoka H, Matsunaga K, Yano M, Mimura Y. Association of IgG4 and free light chain with idiopathic pleural effusion. Clin Exp Immunol. 2017;190:133-142.

２．著書

1) Hatano R, Ohnuma K, Yamada T, Okamoto T, Komiya E, Otsuka H, Itoh T, Yamazaki H, Iwao N, Kaneko Y, Dang NH, Morimoto C. The use of the humanized anti-CD26 monoclonal antibody YS110 as a novel targeted therapy for refractory cancers and immune disorders. Advances in Medicine and Biology (Nova Science Publishers, Inc.). in press

2) Ohnuma K, Hatano R, Yamazaki H, Kaneko Y, Dang NH, Morimoto C.

CD26-targeted therapy: A new horizon in malignant pleural mesothelioma management. Horizons in Cancer Research (Nova Science Publishers, Inc.). 2017; Volume 64: Chapter 6: 129-161.

３．学会発表

1) 岩尾憲明、大沼圭、大塚春奈、波多野良、古宮栄利子、伊藤匠、森本幾夫. 急性 GVHD マウスモデルにおける HMGB1 の動態に関する検討.第 40 回日本造血細胞移植学会.2018 年 2 月、札幌.
2) Eriko Komiya, Ryo Hatano, Haruna Otsuka, Takumi Itoh, Hiroto Yamazaki, Mitsutoshi Tominaga, Kenji Takamori, Kei Ohnuma, Chikao Morimoto. CD26/DPPIV regulates mechanical itch in a mechanistically distinct manner from chemical itch. 第 42 回日本研究皮膚科学会、2017 年 12 月、高知.
3) Takumi Itoh, Ryo Hatano, Haruna Otsuka, Noriaki Iwao, Satoshi Iwata, Taketo Yamada, Chikao Morimoto. IL-26 facilitates angiogenesis and skin inflammation via inducing FGF2 production in a murine model of imiquimod-induced psoriasis. 第 46 回日本免疫学会、2017 年 12 月、仙台.
4) Eriko Komiya, Ryo Hatano, Haruna Otsuka, Takumi Itoh, Hiroto Yamazaki, Taketo Yamada, Yasushi Suga, Utako Kimura, Mitsutoshi Tominaga, Kenji Takamori, Kei Ohnuma, Chikao Morimoto. The regulation of pruritus in psoriasis and atopic dermatitis-a possible role for CD26/DPPIV. 9th World Congress on Itch, 2017 ,October.Wrocław, Poland.
5) 波多野良、大沼圭、石井智徳、岩田哲史、奥村康、関川巖、森本幾夫. 全身性エリテマトーデスのステロイド治療抵抗性と CD26 陰性 T 細胞サブセットとの関係性について. 第 61 回日本リウマチ学会、2017 年 4 月、福岡.
6) Nishida H, Hayashi M, Morimoto C, Sakamoto M, Yamada T. Humanized anti-CD26 monoclonal antibody, YS110, has anti-myeloma efficacy for the treatment of high-risk multiple myeloma. The 59th American Society of Hematology Annual Meeting and Exposition. 2017, December, Atlanta, GA, USA.
7) Yamada T, Madokoro H, Nishida H, Morimoto C, Sakamoto M, Hayashi M. Anti-CD26 humanized monoclonal antibody conjugated to triptolide is transported into nucleus and impairs RNA polymerase II. 2017 年 12 月、生命科学系学会合同年次大会（ConBio2017）神戸.
8) Nishida H, Hayashi M, Morimoto C, Sakamoto M, Yamada T. Humanized anti-CD26 monoclonal antibody has a therapeutic potentiality against multiple myeloma. 第 79 回日本血液学会　2017 年 10 月、東京国際フォーラム.
9) 土居美枝子、稲田博輝、細沼沙紀、政岡

秀彦、瀬山幸子、金野美年子、石澤圭介、茅野秀一、山田健人、佐々木惇　腺癌との鑑別を要したリンパ腫様型/形質細胞腫様浸潤性尿路上皮癌の 1 例　第 58 回日本臨床細胞学会総会、平成 29 年（2017 年）5 月、大阪.

10）李治平，山田健人，金玲，市村隆也，石澤圭介, 佐々木惇　関節リウマチのエタネルセプト治療中に UIP 型間質性肺炎併発した一剖検症例　第 106 回日本病理学会総会 2017 年 4 月、東京

11）金　玲，李　治平，市村隆也，石澤圭介，茅野秀一，佐々木惇，山田健人　百日咳肺炎から肺高血圧症を併発し死亡した新生児剖検症例　第 106 回日本病理学会総会 2017 年 4 月、東京.

12）Yamada T, Madokoro H, Yamada K, Nishida H, Morimoto C, Sakamoto M, Hayashi M. Anti-tumor effects of humanized anti-CD26 monoclonal antibody against hepatocellular carcinoma. 第 106 回日本病理学会総会 2017 年 4 月、東京.

13）Aida S, Ichikawa D, Iida K, Hozumi M, Nakamura M, Uozaki R, Hashimoto N, Okayama M, Yonemura Y, Tabata N, Yamada T, Matsushita M, Sugai T, Yanagawa H, Hattori Y. PEG(E)-TC11, a novel polyethylene glycol-linked phthalimide derivative, inhibited high-risk MM cell growth in vivo and in vitro via cell cycle G2/M arrest in a CRBN-independent manner. American Association for Cancer Research (AACR) Annual Meeting, 2017, April, Washington D.C., USA.

14）Fujimoto N, Kojima Y, Kishimoto T. Secretary leukocyte peptide inhibitor (SLPI) in pleural fluid is useful as a diagnostic marker of malignant pleural mesothelioma. ASCO2017(American Society of Clinical Oncology Annual Meeting) 2017 年 6 月 3－7 日 Chicago.

15）Kato K, Gemba K, Ashizawa K, Kishimoto T, Fujimoto N, Aoe K, Takeshima Y, Inai K. CT Findings of Malignant Pleural Mesothelioma and Correlation with the Survival Period .The 4th World Congress of Thoracic Imaging（WCTI）2017 年 6 月 18－21 日　Boston.

16）藤本伸一、児島葉子、宮本洋輔、浅野美智子、渕本康子、和田佐恵、小崎晋司、岸本卓巳. 胸膜中皮腫の診断における胸水 Secretary leukocyte peptide inhibitor (SLPI) の有用性について　第 15 回日本臨床腫瘍学会学術集会　2017 年 7 月 27 日　神戸.

17）尾瀬功、長松康子、青江啓介、加藤勝也、堀田勝幸、中川淳子、原桂子、岸本卓巳、藤本伸一. 悪性胸膜中皮腫患者の QOL 調査結果　第 15 回日本臨床腫瘍学会学術集会　2017 年 7 月 28 日　神戸.

18）中川淳子、小林幸以、石丸直樹、野村伽奈子、亀谷友里恵、藤本伸一、岸本卓巳. 胸膜中皮腫患者の経時的ケアニーズ　第 15 回日本臨床腫瘍学会学術集会　2017 年 7 月 29 日　神戸.

19）藤本伸一、長松康子、青江啓介、堀田勝幸、加藤勝也、尾瀬功、中川淳子、原桂子、岸本卓巳. 「患者と家族のための胸膜中皮腫ハンドブック」の作成　第15回日本臨床腫瘍学会学術集会　2017年7月29日　神戸.

20）Oze I , Nagamatsu Y, Aoe K, Hotta K, Kato K, Nakagawa J, Hara K, Kishimoto T, Fujimoto N. Evaluation of quality of life in survivors with malignant pleural mesothelioma in Japan. EUROPEAN SOCIETY FOR MEDICAL ONCOLOGY 2017 Congress （ESMO2017） 2017年9月8－12日　MADRID.

21）倉岡正嗣、アマティア　ヴィシュワジート、櫛谷桂、Amany S.Mawas、宮田義浩、岡田守人、岸本卓巳、井内康輝、西阪隆、末田泰二郎、武島幸男. 網羅的遺伝子発現解析から同定したDAB2とIntelectin-1の上皮型中皮腫と肺腺癌の鑑別診断における有用性　第24回石綿・中皮腫研究会　2017年10月7日　大阪.

22）西村泰光　李順姫、松﨑秀紀、武井直子、吉留敬、岡本賢三、岸本卓巳. 包括的免疫機能解析による悪性中皮腫とびまん性
胸膜肥厚との判別指標の探索　第24回石綿・中皮腫研究会　2017年10月7日　大阪.

23）藤本伸一、西村淳、宮本洋輔、浅野美智子、渕本康子、和田佐恵、小崎晋司、伊賀徳周、西英行、岸本卓巳. 「胸水のみ」を呈する胸膜中皮腫症例の検討　第58回日本肺癌学会学術集会　2017年10月14日　横浜.

24）Kuraoka M, Amatya VJ, Kushitani K, Mawas AS, Miyata Y, Okada M, Kishimoto T, Inai K, Nishisaka T, Sueda T, Takeshima Y. Identification of DAB2 and Intelectin-1 as Novel Positive Immunohistochemical Markers of Epithelioid Mesothelioma. 18th World Conference on Lung Cancer　2017年10月16日　Yokohama.

25）Kishimoto T. Clinical Evaluation for Asbestos-Induced Diffuse Pleuralthickening (DPT) in JAPAN. CHEST 2017. 2017年11月1日　Toronto.

26）岸本卓巳、藤本伸一. 胸膜中皮腫の診断時胸部CT所見の検討　第65回日本職業・災害医学会学術大会　2017年11月25日　北九州.

27）藤本伸一、岸本卓巳、青江啓介、加藤勝也、堀田勝幸、尾瀬功、長松康子. 胸膜中皮腫に対する新規治療法の臨床導入に関する研究　第65回日本職業・災害医学会学術大会　2017年11月25日　北九州.

28）藤本伸一、宮本洋輔、和田佐恵、野上尚之、久山彰一、別所昭宏、堀田勝幸、青江啓介、南大輔、木浦勝行。EGFR遺伝子変異陽性非小細胞肺癌に対するafatinib・bevacizumab併用療法の第I相試験：OLCSG1404。第58回日本肺癌学会学術集会。平成29年10月14日、横浜.

29）坂本健次、近森研一、村田順之、青江啓介、前田忠士、亀井治人、松本常男.

両側肺動脈腫瘍の肺浸潤に対し、TBLBで悪性軟部腫瘍と診断した一例．第 57 回日本呼吸器学会学術講演会、平成 29 年 4 月 22 日、東京.

30）村田順之、青江啓介、宇都宮利彰、三村雄輔、松本常男．胸膜に IgG4 陽性形質細胞を認めた胸水症例の解析．第 57 回日本呼吸器学会学術講演会、平成 29 年 4 月 23 日、東京.

31）坂本健次、村田順之、近森研一、青江啓介、前田忠士、亀井治人、丸山治彦．肺結核､結核性胸膜炎との鑑別を要したウェステルマン肺吸虫症の一例．第 40 回日本呼吸器内視鏡学会学術集会､平成 29 年 6 月 10 日、長崎.

32）近森研一、関千尋、青江啓介、前田忠士、坂本健次、村田順之、宇都宮利彰、亀井治人.ニボルマブ使用後に薬剤性肺障害を発症した非小細胞肺がん症例の当院での臨床的特徴．第 58 回日本肺癌学会学術集会、平成 29 年 10 月 15 日、横浜.

33）関千尋、前田忠士、青江啓介、近森研一、坂本健次、村田順之、宇都宮利彰、亀井治人.ニボルマブを早期肺障害で中止したが、ペムブロリズマブへ変更し、効果が得られた進行肺腺癌の一例．第 58 回日本肺癌学会学術集会、平成 29 年 10 月 14 日、横浜.

34）坂本健次、村田順之、大畑秀一郎、宇都宮利彰、近森研一、青江啓介、前田忠士、亀井治人、松本常男．肺 MAC 症に MALT リンパ腫を併発した一例．第 26 回日本呼吸器内視鏡学会中国四国支部会、平成 29 年 10 月 28 日、広島.

H.知的財産権の出願･登録状況（予定を含む）

1. 発明者:森本幾夫､波多野良､山田健人、大沼圭.
   出願番号：特許出願中
   名称：抗ヒト CD26 モノクローナル抗体
   出願人：学校法人 順天堂、埼玉医科大学（共同出願）
   出願年月日：2018 年 3 月予定(PCT 出願)

2. 発明者：森本幾夫、波多野良、大沼圭、伊藤匠.
   出願番号：特願 2017-231439
   名称：抗ヒト IL-26 抗体
   出願人：学校法人 順天堂
   出願年月日：2017 年 12 月 1 日(PCT 出願)

Ⅲ.　研究成果の刊行に関する一覧表

＜研究成果の刊行に関する一覧表＞

【書　籍】

著者氏名	論文タイトル名	書籍全体の編集者名	書　籍　名	出版社名	出版地	出版年	ページ
Hatano R, Ohnuma K, Yamada T, Okamoto T, Komiya E, Otsuka H, Itoh T, Yamazaki H, Iwao N, Kaneko Y, Dang NH, Morimoto C	The use of the humanized anti-CD26 monoclonal antibody YS110 as a novel targeted therapy for refractory cancers and immune disorders	Leon V. Berhardt	Advances in Medicine and Biology	Nova Science Publishers,Inc	USA		In Press
Ohnuma K, Hatano R, Yamazaki H, Kaneko Y, Dang NH, Morimoto C.	CD26-targeted therapy: A new horizon in malignant pleural mesothelioma management	Hiroto S. Watanabe	Horizons in Cancer Research	Nova Science Publishers, Inc.	USA	2017年	129-161

【雑　誌】

発表者氏名	論文タイトル名	発表誌名	巻号	ページ	出版年
Ohnuma K, Hatano R, Komiya E, Otsuka H, Itoh T, Iwao N, Kaneko Y, Yamada T, Dang NH, Morimoto C	A novel role for CD26/dipeptidyl peptidase IV as a therapeutic target in selected immune disorders and cancers	Front Biosci			in press

発表者氏名	論文タイトル名	発表誌名	巻号	ページ	出版年
Hiromura M, Nohtomi K, Mori Y, Kataoka H, Sugano M, Ohnuma K, Kuwata H, Hirano T	Caveolin-1, a binding protein of CD26, is essential for the anti-inflammatory effects of dipeptidylpeptidase-4 inhibitors on human and mouse macrophages	Biochem Biophys Res Commun	495	223-229	2018
Angevin E, Isambert N, Trillet-Lenoir V, You B, Alexandre J, Zalcman G, Vielh P, Farace F, Valleix F, Podoll T, Kuramochi Y, Miyashita I, Hosono O, Dang NH, Ohnuma K, Yamada T, Kaneko Y, Morimoto C	First-in-Human phase 1 of YS110, a monoclonal antibody directed against CD26 in advanced CD26-expressing cancers	Br J Cancer	116	1126-1134	2017
Komiya E, Hatano R, Otsuka H, Itoh T, Yamazaki H, Yamada T, Dang NH, Tominaga M, Suga Y, Kimura U, Takamori K, Morimoto C, Ohnuma K	A possible role for CD26/DPPIV enzyme activity in the regulation of psoriatic pruritus	J Dermatol Sci	86	212-221	2017
Kim KM, Noh JH, Bodogai M, Martindale JL, Yang X, Indig FE, Basu SK, Ohnuma K, Morimoto C, Johnson PF, Biragyn A, Abdelmohsen K, Gorospe M	Identification of senescent cell surface targetable protein DDP4	Genes Dev	31	1529-1534	2017

発表者氏名	論文タイトル名	発表誌名	巻号	ページ	出版年
Ikeda T, Kobayashi S, Morimoto C	Gene expression microarray data from mouse cerebrum treated with rTMS for 30 days	Data Brief	15	948-69	2017
Doonan BP, Ohnuma K, Dang LH, Morimoto C, Dang NH	Current and Emerging Therapy for Malignant Pleural Mesothelioma: Focus on CD26/Dipeptidyl Peptidase IV as a Therapeutic Target	Current Cancer Therapy Reviews	13	1-13	2017
Murakami R, Saisho Y, Watanabe Y, Inaishi J, Tsuchiya T, Kou K, Sato S, Kitago M, Kitagawa Y, Yamada T	Pancreas fat and beta cell mass in humans with and without diabetes: An analysis in the Japanese population	J Clin Endocrinol Metab	102	3251-3260	2017
Aida S, Hozumi M, Ichikawa D, Iida K, Yonemura Y, Tabata N, Yamada T, Matsushita M, Sugai T, Yanagawa H, Hattori Y	A novel phenylphthalimide derivative, pegylated TC11, improves pharmacokinetic properties and induces apoptosis of high-risk myeloma cells via G2/M cell-cycle arrest	BBRC	493	514-520	2017
Kushitani K, Amatya VJ, Mawas AS, Suzuki R, Miyata Y, Okada M, Inai K, Kishimoto T, Takeshima Y	Utility of Survivin, BAP1, and Ki‐ 67 immunohistochemistry in distinguishing epithelioid mesothelioma from reactive mesothelial hyperplasia	Oncology Letters	15	3540-3547	2018

発表者氏名	論文タイトル名	発表誌名	巻号	ページ	出版年
Ninomiya T, Nogami N, Kozuki T, Harada D, Kubo T, Ohashi K, Kuyama S, Bessho A, Fujimoto N, Aoe K, Shibayama T, Takigawa N, Sugimoto K, Kudo K, Fukamatsu N, Hotta K, Kiura K	A phase I trial of afatinib and bevacizumab in chemo-naïve patients with advanced non-small-cell lung cancer harboring EGFR-mutations: Okayama Lung Cancer Study Group Trial 1404	Lung Cancer	115	103-108	2018
Sato H, Sakaguchi M, Yamamoto H, Tomida S, Aoe K, Shien K, Yoshioka T, Namba K, Torigoe H, Soh J, Tsukuda K, Tao H, Okabe K, Miyoshi S, Pass HI, Toyooka S	Therapeutic potential of targeting S100A11 in malignant pleural mesothelioma	Oncogenesis	7	11	2018
Hotta K, Aoe K, Kozuki T, Ohashi K, Ninomiya K, Ichihara E, Kubo T, Ninomiya T, Chikamori K, Harada D, Nogami N, Hirata T, Hinotsu S, Toyooka S, Kiura K	A Phase II Study of Trastuzumab Emtansine in HER2-positive Non-Small-Cell Lung Cancer	J Thorac Oncol.	13	273-279	2018

発表者氏名	論文タイトル名	発表誌名	巻号	ページ	出版年
Katakami N, Uchino J, Yokoyama T, Naito T, Kondo M, Yamada K, Kitajima H, Yoshimori K, Sato K, Saito H, Aoe K, Tsuji T, Takiguchi Y, Takayama K, Komura N, Takiguchi T, Eguchi K	Anamorelin (ONO-7643) for the treatment of patients with non-small cell lung cancer and cachexia: Results from a randomized, double-blind, placebo-controlled, multicenter study of Japanese patients (ONO-7643-04)	Cancer	124	606-616	2018
Kushitani K, Amatya VJ, Okada Y, Katayama Y, Mawas AS, Miyata Y, Okada M, Inai K, Kishimoto T, Takeshima Y.	Utility and pitfall of Immunohistochemistry in the Differential Diagnosis between Epithelioid Mesothelioma and Poorly Differentiated Lung Squamous Cell Carcinoma	Histopathology	70	375-384	2017
Amatya VJ, Kushitani K, Mawas AS, Miyata Y, Okada M, Kishimoto T, Inai K, Takeshima Y	MUC4, a novel immunohistochemical marker identified by gene expression profiling, differentiates pleural sarcomatoid mesothelioma from lung sarcomatoid carcinoma	Mod Pathol.	30	672-681	2017
Kuraoka M, Amatya VJ, Kushitani K, Mawas AS, Miyata Y, Okada M, Kishimoto T, Inai K, Nishisaka T, Sueda T, Takeshima Y	Identification of DAB2 and Intelectin-1 as Novel Positive Immunohistochemical Markers of Epithelioid Mesothelioma by Transcriptome Microarray Analysis for its Differentiation From Pulmonary Adenocarcinoma	Am J Surg Pathol	41	1045-1052	2017
岸本卓巳、藤本伸一	石綿ばく露によるびまん性胸膜肥厚と中皮腫・肺癌発生に関する検討	日職災医誌	65	153-159	2017

発表者氏名	論文タイトル名	発表誌名	巻号	ページ	出版年
岸本卓巳	アスベストの発がん機序 環境による健康リスク	日本医師会雑誌	146	S253	2017
Kuyama S, Ochi N, Bessho A, Hotta K, Ikeda G, Kishino D, Kubo T, Harada D, Fujimoto N, Nakanishi M, Umeno T, Okada T, Chikamori K, Yamagishi T, Ohashi K, Ichihara E, Takigawa N, Tanimoto M, Kiura K	A Phase II trial of carboplatin plus S-1 for elderly patients with advanced non-small-cell lung cancer with wild-type epidermal growth factor receptor: The Okayama Lung Cancer Study Group Trial 1202	Lung Cancer	112	188-194	2017
Ozeki T, Asano M, Fujimoto N, Nishimura J, Takada K, Miyamoto Y, Fuchimoto Y, Wada S, Ozaki S, Kishimoto T	Esophagobronchial fistula in a patient with squamous cell carcinoma of the lung: A case report	Case Rep Oncol	10	553-557	2017
Nishimura J, Miyamoto Y, Fujimoto N, Ozeki T, Takada K, Asano M, Fuchimoto Y, Wada S, Ozaki S, Kishimoto T	Adenocarcinoma of the lung acquiring resistance to afatinib by transformation to small cell carcinoma: A case report	Case Rep Oncol	10	666-670	2017
Murata Y, Aoe K, Mimura-Kimura Y, Murakami T, Oishi K, Matsumoto T, Ueoka H, Matsunaga K, Yano M, Mimura Y	Association of IgG4 and free light chain with idiopathic pleural effusion	Clin Exp Immunol	190	133-142	2017

Ⅳ.　研究成果の別刷

Chapter

THE USE OF THE HUMANIZED ANTI-CD26 MONOCLONAL ANTIBODY YS110 AS A NOVEL TARGETED THERAPY FOR REFRACTORY CANCERS AND IMMUNE DISORDERS

Ryo Hatano[1], PhD, Kei Ohnuma[1,*], MD, PhD,
Taketo Yamada[2], MD, PhD, Toshihiro Okamoto[1], PhD,
Eriko Komiya[1], PhD, Haruna Otsuka[1],
Takumi Itoh[1], PhD, Hiroto Yamazaki[1], MD, PhD,
Noriaki Iwao[3], MD, PhD, Yutaro Kaneko[4],
Nam H. Dang[5], MD, PhD,
and Chikao Morimoto[1], MD, PhD

[1]Department of Therapy Development and Innovation for Immune Disorders and Cancers, Graduate School of Medicine, Juntendo University, Tokyo, Japan
[2]Department of Pathology, Saitama Medical University, Saitama, Japan

[*] Corresponding Author Email: kohnuma@juntendo.ac.jp.

[3]Department of Hematology,
Juntendo University Shizuoka Hospital, Shizuoka, Japan
[4]Y's AC Co., Ltd., Tokyo, Japan
[5]Division of Hematology/Oncology,
University of Florida, Gainesville, FL, US

ABSTRACT

CD26 is a 110 kDa surface glycoprotein with intrinsic dipeptidyl peptidase IV (DPPIV) activity that is expressed on numerous cell types and has a multitude of biological functions. We have had a long-standing interest in the role of CD26 in cancer biology and immune regulation and developed YS110, a humanized monoclonal antibody (mAb) with high affinity to the CD26 antigen. Our group has shown that *in vivo* administration of YS110 inhibits tumor cell growth, migration and invasion, and enhances survival of mouse xenograft models inoculated with malignant mesothelioma (MPM), renal cell carcinoma, non-small-cell lung carcinoma, ovarian carcinoma or T-cell lymphoma via multiple mechanisms of action. The first-in-human (FIH) phase 1 clinical trial of this mAb for CD26-expressing solid tumors, particularly refractory MPM, was conducted from 2009 to 2014, with results being recently published. Our FIH study demonstrates that YS110 therapy exhibits a favorable safety profile and results in encouraging disease stabilization in a number of patients with advanced/refractory CD26-expressing cancers. In addition, we have robust evidence through multiple studies that CD26 functions as a T-cell costimulatory molecule and has an important role in T-cell biology. High CD26 cell surface expression is correlated with enhanced migratory ability through endothelial cells, and $CD26^+$ T cells are present at high levels in the inflammatory site of graft-versus-host disease (GVHD) and various autoimmune diseases such as rheumatoid arthritis, multiple sclerosis and Graves' disease. Our recent work with a xenogeneic GVHD murine model also demonstrates that administration of YS110 decreases GVHD severity and prolongs survival, while preserving the graft-versus-leukemia effect. Furthermore, recent work has shown that infection by the novel Middle East respiratory syndrome coronavirus (MERS-CoV) is mediated by the use of CD26 as a functional receptor. We have identified the domains of CD26 involved in the binding of MERS-CoV and showed that YS110 treatment significantly inhibits viral infection. We herein review novel findings strongly suggesting that YS110 represents a promising novel therapy for refractory cancers, immune disorders and MERS-CoV infection.

Keywords: CD26/DPPIV, YS110, malignant mesothelioma, immune disorders, MERS-CoV

1. INTRODUCTION

CD26 is a 110-kDa, type II transmembrane glycoprotein with known dipeptidyl peptidase IV (DPPIV, EC 3.4.14.5) activity in its extracellular domain and is capable of cleaving N-terminal dipeptides with either L-proline or L-alanine at the penultimate position (Ohnuma et al., 2008a). CD26 activity is dependent on cell type and the microenvironment factors that can influence its multiple biological roles (Ohnuma et al., 2011; Thompson et al., 2007). CD26 is expressed on various tumors including malignant pleural mesothelioma (MPM), renal cell carcinoma (RCC), lung cancer, colorectal cancer (CRC), hepatocellular carcinoma, prostate cancer, gastrointestinal stromal tumor (GIST), thyroid carcinoma, and hematologic malignancies such as T-anaplastic large cell lymphoma, T-lymphoblastic lymphoma and T-acute lymphoblastic leukemia (Havre et al., 2008; Ohnuma and Morimoto, 2013; Thompson et al., 2007). We have had a long-standing interest in the role of CD26 in cancer biology and developed YS110, a humanized monoclonal antibody (mAb) with high affinity to the CD26 antigen. Our group has shown that *in vitro* and *in vivo* administration of YS110 inhibited tumor cell growth, migration and invasion, and enhanced survival of mouse xenograft models inoculated with MPM, RCC, non-small-cell lung carcinoma, ovarian carcinoma or T-cell lymphoma via multiple mechanisms of action (Inamoto et al., 2007; Inamoto et al., 2006; Ho et al., 2001). The first-in-human (FIH) phase 1 clinical trial of this mAb for CD26-expressing solid tumors, particularly refractory MPM, was conducted with results being recently published (Angevin et al., 2017). Our FIH study demonstrated that YS110 therapy exhibits a favorable safety profile and resulted in encouraging disease stabilization in a number of patients with advanced/refractory CD26-expressing cancers.

In addition, we have robust evidence through multiple studies that CD26 functions as a T-cell costimulatory molecule and has an important role in T-cell biology and overall immune function (Morimoto and Schlossman, 1998; Ohnuma et al., 2008a). We identified caveolin-1 as a costimulatory ligand for CD26 in T cells, and showed that CD26-caveolin-1 interaction led to activation of both CD4 T cells and antigen presenting cells (APCs) (Ohnuma et al., 2004; Ohnuma et al., 2005; Ohnuma et al., 2007). Moreover, High CD26 cell surface expression was correlated with enhanced migratory ability through endothelial cells (Masuyama et al., 1992), and $CD26^+$ T cells were present at high levels in the inflammatory site of graft-versus-host disease (GVHD) and various autoimmune diseases such as rheumatoid arthritis (RA), multiple sclerosis and Graves' disease (Hatano et al., 2013a; Ohnuma et al., 2015a; Ohnuma et al., 2011). Our recent work with a xenogeneic GVHD murine model also demonstrated that administration of YS110 decreased GVHD severity and prolonged survival, while preserving the graft-versus-leukemia (GVL) effect (Hatano et al., 2013a).

Furthermore, recent work has shown that infection by the Middle East respiratory syndrome coronavirus (MERS-CoV) is mediated by the use of CD26 as a functional receptor (Raj et al., 2013). MERS-CoV is a novel coronavirus identified in patients with severe lower respiratory tract infections with almost 50% of cases resulting in lethal lower respiratory tract infections (Zaki et al., 2012; Enserink, 2013). We have identified the domains of CD26 involved in the binding of MERS-CoV and showed that YS110 treatment significantly inhibited viral infection (Ohnuma et al., 2013). We recently reviewed our significant findings and the early clinical development of a CD26-targeted therapy for MPM (Ohnuma et al., 2017). We herein review novel findings strongly suggesting that YS110 represents a promising novel therapy not only for MPM but also for other refractory cancers, immune disorders and MERS-CoV infection.

2. CANCERS

2.1. Malignant Pleural Mesothelioma

Our recent in-depth studies of CD26 expression in MPM revealed that CD26 is preferentially expressed in MPM cells but not in normal mesothelial cells (Amatya et al., 2011; Aoe et al., 2012). Our immunohistochemical analysis showed that membranous expression of CD26 was particularly found in epithelioid mesotheliomas, but not in sarcomatoid mesotheliomas (Aoe et al., 2012). In addition, we identified SP (side-population), CD9, CD24, and CD26 as MPM cancer stem cell markers that correlated with primary stem cell signatures (Ghani et al., 2011; Yamazaki et al., 2012). These intriguing findings propelled our development of CD26-targeted therapy for MPM. For this purpose, we had developed a novel humanized anti-CD26 mAb, YS110. We recently reviewed the functional role of CD26 in the neoplastic biology of MPM and our robust *in vitro* and *in vivo* data investigating the anti-tumor effect of YS110 on MPM (Ohnuma et al., 2017). We conducted the FIH phase 1 clinical trial of YS110 for patients with refractory MPM and other CD26-positive solid tumors (Angevin et al., 2017). Thirty-three heavily pre-treated patients with CD26-positive cancers including 22 MPM underwent YS110 administration. Our FIH study conclusively demonstrated that YS110 exhibits a favorable safety profile and substantial clinical activity in heavily pre-treated CD26-positive MPM patients who had previously progressed on conventional standard chemotherapies. Further clinical trial of YS110 for MPM is in progress worldwide (ClinicalTrials.gov, 2017).

2.2. Other Cancers

In contrast to our robust findings regarding the role of CD26/DPPIV on MPM (Ohnuma et al., 2017), the exact role of CD26/DPPIV in other cancers remains to be elucidated, partly due to its variable expression on these tumors. In general, it is strongly expressed on some cancers, while

being absent or present at low levels in others (Thompson et al., 2007). Furthermore, given its multiple biological functions, including its ability to associate with several key proteins and its cleavage of a number of soluble factors to regulate their function, it is likely that the CD26/DPPIV effect on tumor biology is at least partly mediated by the effect of these biological functions on specific tumor types (Havre et al., 2008).

2.2.1. Renal Cancer

CD26 has also been shown to be expressed on RCC (Stange et al., 2000; Inamoto et al., 2006; Hatano et al., 2014), including the cell lines Caki-1, Caki-2, VMRC-RCW, and ACHN (Inamoto et al., 2006). We showed that anti-CD26 mAb inhibition of the Caki-2 cell line was associated with G1/S cell cycle arrest, enhanced $p27^{kip1}$ expression, downregulation of cyclin-dependent kinase 2 (CDK2) and dephosphorylation of retinoblastoma substrate (Rb) (Inamoto et al., 2006). We also found that anti-CD26 mAb therapy attenuated Akt activity (Figure 1D) and internalized cell surface CD26 leading to decreased CD26 binding to collagen and fibronectin (Figure 1A and 1B). Treatment with anti-CD26 murine mAb inhibited the growth of human RCC and significantly enhanced survival in a mouse xenograft model (Figure 1C). Our FIH phase 1 study demonstrated that disease stabilization was observed in heavily pre-treated CD26-positive MPM and RCC patients who had previously progressed on conventional standard therapies (Angevin et al., 2017), suggesting that YS110 treatment may have potential clinical use for CD26-positive RCC.

2.2.2. Lung Cancer

CD26 expression in lung cancer appears to be dependent on the specific histologic subtype. Liu et al., showed that CD26 was highly expressed in poorly differentiated lung adenocarcinomas compared to highly differentiated lung adenocarcinomas utilizing human lung adenocarcinoma tissue microarrays (Liu et al., 2013). These investigators demonstrated that CD26 inhibition by shRNA significantly decreased the invasive and migratory capacity of human lung adenocarcinoma cell line,

SPC-A-1sci cells, while CD26 overexpression increased the invasive and migratory capacity of SPC-A-1 cells (Liu et al., 2013). We are currently investigating *in vitro* and *in vivo* anti-tumor activity of YS110 on lung cancers, and our preliminary data show that treatment with YS110 inhibits the growth of human lung cancer cell lines *in vitro* and *in vivo*. Definitive data will be presented in the near future.

2.2.3. Colorectal Cancer

Pang et al., identified a subpopulation of $CD26^+$ cells uniformly presenting in both primary and metastatic tumors in colorectal cancer, and showed that $CD26^+$ cancer cells are associated with enhanced invasiveness and chemoresistance (Pang et al., 2010). These investigators showed that in $CD26^+$ colorectal cancer cells, mediators of epithelial to mesenchymal transition (EMT) contributed to the invasive phenotype and metastatic capacity. These results suggested that $CD26^+$ cells are cancer stem cells in colorectal cancer, and that CD26/DPPIV can be targeted for metastatic colorectal cancer therapy. More recently, significantly higher CD26 expression has been shown to be correlated with poorly differentiated tumor, late tumor node metastasis (TNM) stage (TNM stage III and stage IV), and development of metastasis (Lam et al., 2014). Moreover, a high CD26 expression level is a predictor of poor outcome after resection of CRC. These findings strongly suggest that CD26 may be a useful prognostic marker in patients with CRC. Other investigators demonstrated in a murine model that lung metastasis of CRC was suppressed by treatment with a DPPIV inhibitor (Jang et al., 2015). They showed a reduction of EMT markers, suggesting that the EMT status of the murine colon cancer cell line MC38 was at least in part affected by DPPIV inhibition, with a diminution in the growth of metastases. They also showed that DPPIV inhibition decreased the growth of lung metastases of colon cancer by downregulating autophagy, increasing apoptosis and arresting the cell cycle.

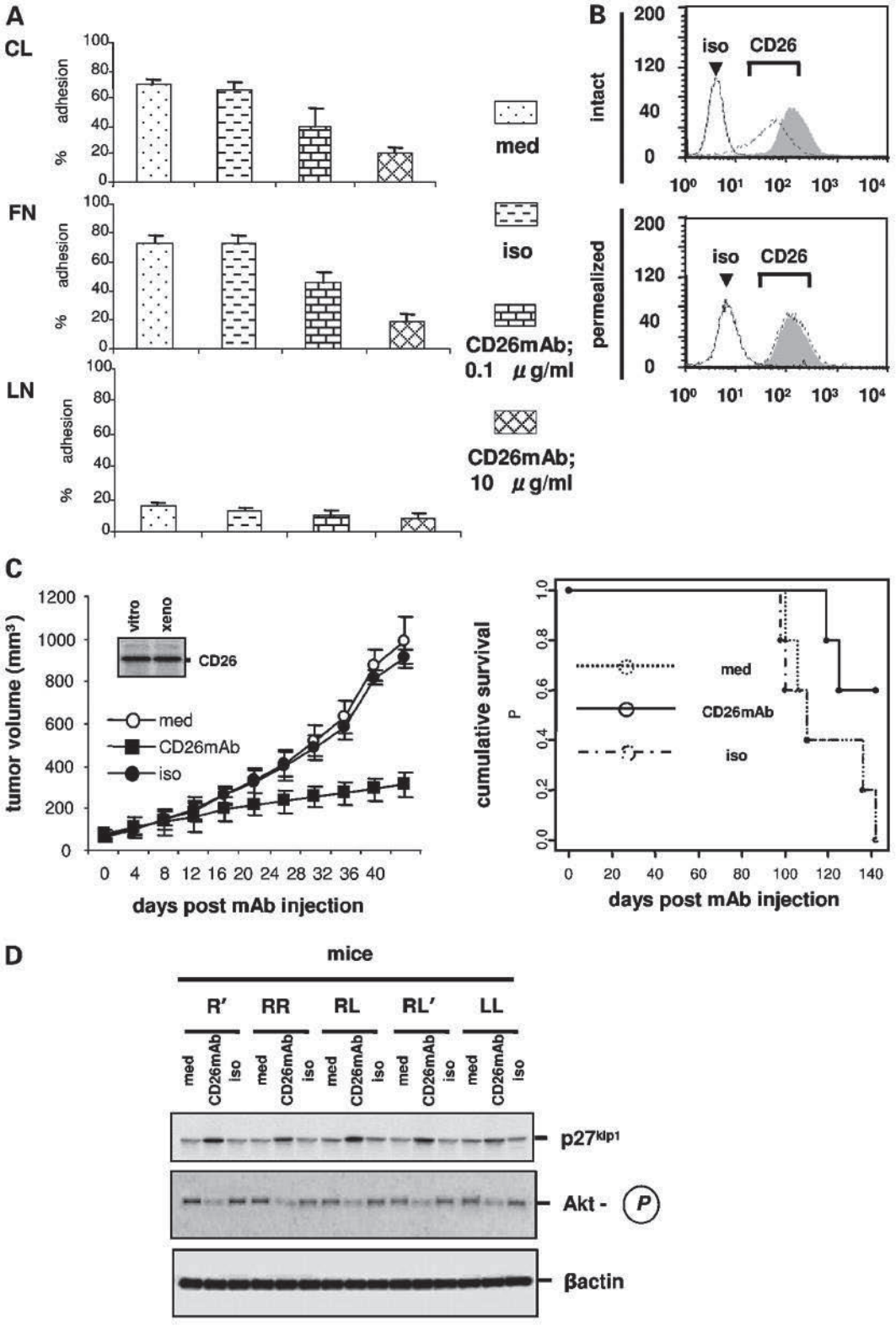

Figure 1. Antitumor effect of anti-CD26 mAb in mouse xenograft model of Caki-2, human renal carcinoma. (A) effect of anti-CD26 murine mAb (14D10) on cell adhesion to ECM. Caki-2 cells treated with medium only, anti-CD26 mAb, or isotype-matched control mAb were plated onto 60-mm dishes (3 x 10^6 per dish) coated with collagen I (*CL*), fibronectin (*FN*), or laminin (*LN*) and cultured for 21 hours. The

adhesive ability of cancer cells was expressed as the mean number of cells that had attached to the bottom surface of the dish. Columns, mean number of cells per field of view; bars, SE. Values for invasion were determined by calculating the average number of adhesive cells per mm^2 over three fields per assay and expressed as an average of triplicate determinations. Adhesive cells (%): adhesive cells / adhesive cells + nonadhesive cells. (B) Caki-2 cells were treated with anti-CD26 mAb on ice, or isotype-matched control mAb, followed by washing in ice-cold PBS twice and subsequently incubated at 37°C for 12 hours. Cells were collected and stained with FITC-conjugated anti-mouse IgG. Expression status of cell surface CD26 was analyzed by flow cytometry. To detect total CD26 level, including the internalized CD26 fraction, cell membrane permeabilization method was used. Filled histogram, positive control, which was incubated 30 minutes with anti-CD26 mAb. Open histogram, status of CD26 after treatment. (C) Caki-2 cells (1×10^6) were inoculated s.c. into the left flank of mice. CD26 expression of Caki-2 cells after tumor implantation into the mouse was similar to its level before tumor implantation. Mice were treated with intratumoral injection of PBS only (medium; $n = 5$), anti-CD26 mAb ($n = 5$), or isotype-matched control mAb ($n = 5$) on the day when the tumor mass became visible (5 mm in size). Tumor size and cumulative survival were monitored. (D) resected specimens were immediately frozen for whole-cell lysate preparation and lysed by lysis buffer. Protein (50 μg) was applied for SDS-PAGE and immunoblotting for $p27^{kip1}$, phosphorylated Akt, and β-actin. R,' RR, RL, RL,' and LL, names of mice in each treatment group. This figure is reprinted with permission from Inamoto T et al., *Clin Cancer Res* 12: 3470-7, 2006.

2.2.4. T-Anaplastic Large Cell Lymphoma and Acute T Cell Leukemia

We showed that treatment with anti-CD26 murine mAb inhibited adhesion of the human $CD30^+$ T-anaplastic large cell lymphoma cell line Karpas 299 to fibronectin. Furthermore, depletion of CD26 in Karpas 299 cells by siRNA decreased tumorigenesis and increased survival of SCID mice inoculated with these cells (Sato et al., 2005). In addition, we demonstrated that anti-CD26 murine mAb treatment of the CD26-positive Karpas 299 resulted in *in vitro* and *in vivo* anti-tumor activity. Administration of anti-CD26 mAb induced cell cycle arrest at the G1/S checkpoint, associated with enhanced p21 expression, and significantly enhanced survival of SCID mice inoculated with Karpas 299 cells by inhibiting tumor formation (Ho et al., 2001). Likewise, we showed that treatment with anti-CD26 murine mAb inhibited the growth of acute T cell leukemia cell line Jurkat transfected with CD26 through G1/S cell cycle arrest, associated with concurrent activation of the ERK signaling pathway and increased p21 expression (Ohnuma et al., 2002). These findings further

support a therapeutic approach involving targeted therapy against CD26 for selected hematological malignancies.

2.2.5. Gastrointestinal Stromal Tumor

Yamaguchi et al., comprehensively investigated gene expression profiles in surgical samples of untreated GIST of the stomach and small intestine. They found that the disease-free survival of patients with CD26-positive GIST of the stomach was worse than that of patients with CD26-negative GIST (Yamaguchi et al., 2008). Moreover, the postoperative recurrence rate of CD26-negative gastric GIST cases was as low as 2.0%. Meanwhile, CD26 expression was not associated with clinical outcome of small intestinal GIST. They concluded that CD26 is a significant prognostic factor of gastric GIST and may also serve as a therapeutic target (Yamaguchi et al., 2008).

2.2.6. Thyroid Carcinoma

The *BRAF*V600E mutation, which results in greater mitogen-activated protein kinase signaling output, is the most predominant oncogenic driver of thyroid cancer (Fagin and Wells, 2016). CD26 expression is upregulated in malignant thyroid tumors, and CD26 can be used as a malignancy marker in fine-needle aspiration cytology of thyroid nodules (de Micco et al., 2008). Recently, CD26, secretogranin V (SCG5) and carbonic anhydrase XII (CA12) are a three-gene signature that can distinguish malignant thyroid cancers, and useful for preoperative diagnosis of thyroid cancer (Zheng et al., 2015). More recently, the function of CD26 in thyroid cancer has been investigated. High CD26 was associated with extrathyroidal extension, *BRAF* mutation, and advanced tumor stage in papillary thyroid cancer (Lee et al., 2017). CD26 silencing by siRNA or treatment with DPPIV inhibitors significantly suppressed colony formation, cell migration, and invasion of thyroid cancer. CD26 expression was suggested to be involved in the transforming growth factor (TGF)-β signaling pathway. Furthermore, *in vivo* experiments revealed that treatment with the DPPIV inhibitor sitagliptin reduced tumor growth and xenograft TGF-β receptor I expression (Lee et al., 2017). These

investigators concluded that increased CD26 expression is associated with cellular invasion and more aggressive disease in papillary thyroid cancer, and targeting CD26/DPPIV may be a therapeutic strategy for CD26-expressing thyroid cancer.

2.2.7. Urothelial Carcinoma

Although there is an increasing number of biomarkers that have prognostic relevance to urothelial carcinoma (UC), factors involved in tumor progression remained largely unclear. Recently, by mining the datasets obtained from the Gene Expression Omnibus (GEO, NCBI, Bethesda) and focusing on the proteolysis pathway, Liang et al., discovered that mRNA level of CD26 is significantly upregulated in advanced-stage human UC and the upregulation of CD26 is most significantly associated with clinical aggressiveness of UC (Liang et al., 2017). CD26 is an independent prognostic biomarker for disease-specific survival and metastasis-free survival. Moreover, CD26 knockdown by shRNA resulted in a significantly decreased cell viability, proliferation, migration, and invasion in urothelial cell lines, J82 and RTCC-1 cells (Liang et al., 2017). These findings strongly suggest that CD26 plays a role in the aggressiveness of UCs, and can serve as a novel prognostic marker and therapeutic target.

2.2.8. Chronic Myeloid Leukemia

Chronic myeloid leukemia (CML) is a stem cell neoplasm characterized by the BCR/ABL1 oncogene. Herrmann et al., recently identified CD26/DPPIV as a novel, specific and pathogenetically relevant biomarker of $CD34^{+}CD38^{-}$ CML leukemic stem cell (LSC) (Herrmann et al., 2014). CD26 was not detected on normal stem cells or LSC in other hematopoietic malignancies. Correspondingly, $CD26^{+}$ LSC decreased to low or undetectable levels during successful treatment with imatinib. $CD26^{+}$ CML LSC engrafted NOD-SCID-IL-2R$\gamma^{-/-}$ (NSG) mice with $BCR/ABL1^{+}$ cells, whereas $CD26^{-}$ LSC from the same patients produced multilineage $BCR/ABL1^{-}$ engraftment. Moreover, targeting of CD26 by gliptins suppressed the expansion of $BCR/ABL1^{+}$ cells. These results

suggest that CD26 is a new biomarker and target of CML LSC, and inhibition of CD26/DPPIV may revert abnormal LSC function and support curative treatment approaches in this malignancy. More recently, Warfvinge et al., extensively defined the heterogeneity within the LSC population in chronic phase CML patients at diagnosis and following conventional tyrosine kinase inhibitor (TKI) treatment. Cell surface expression of the CML stem cell markers CD25, CD26, and IL1RAP was high in all subpopulations at diagnosis but downregulated and unevenly distributed across subpopulations in response to TKI treatment. The most TKI-insensitive cells of the LSC compartment could be captured within the $CD45RA^-$ fraction and further defined as positive for CD26 in combination with an aberrant lack of cKIT expression. These results expose a considerable heterogeneity of the CML stem cell population and propose a $Lin^-CD34^+CD38^{-/low}CD45RA^-cKIT^-CD26^+$ population as a potential therapeutic target for improved therapy response (Warfvinge et al., 2017).

2.3. Mechanisms of Action of YS110 for Cancer Treatment

We had developed a novel humanized anti-CD26 mAb, namely YS110. YS110 is a recombinant DNA-derived humanized mAb that selectively binds with high affinity to the extracellular domain of CD26. The antibody is an $IgG_1\kappa$ with a molecular weight of 144 kDa and was humanized via an *in silico* design based on the amino acid sequence of anti-human CD26 murine mAb (14D10), which inhibited tumor cell growth, migration and invasion, and enhanced survival of mouse xenograft models (Inamoto et al., 2006). YS110 is produced by fermentation in CHO (Chinese hamster ovary) mammalian cell suspension culture with the Glutamine Synthetase Expression System. *In vitro* pharmacologic evaluation of YS110 demonstrated its selective binding to human CD26 on a number of human cancer cell lines and tissues, with no apparent agonistic effect on human CD26-positive lymphocytes and no inhibition of DPPIV activity. Moreover, in the proof-of-concept (POC) studies using preclinical models, *in vivo* administration of YS110 resulted in inhibition of tumor cell growth,

migration and invasion, and enhanced survival of mouse xenograft models inoculated with RCC or MPM (Inamoto et al., 2006; Inamoto et al., 2007; Okamoto et al., 2014; Yamamoto et al., 2014). In addition to our robust *in vitro* and *in vivo* data on antibody-mediated dose-dependent tumor growth inhibition, YS110 exhibited excellent safety and pharmacological profiles in non-human primate models using single and repeated increasing intravenous doses. Other key safety findings were obtained from studies involving cynomolgus monkeys which express YS110-reactive CD26 molecules, with similar tissue distribution profiles and expression levels to human CD26. We therefore conducted the FIH phase 1 clinical trial of YS110 for patients with refractory MPM and other CD26-positive solid tumors (Angevin et al., 2017). Thirty-three heavily pre-treated patients with CD26-positive cancers including 22 MPM, 10 RCC and 1 UC underwent YS110 administration. Our FIH phase 1 study conclusively demonstrated that YS110 exhibits a favorable safety profile and substantial clinical activity in heavily pre-treated CD26-positive MPM and RCC patients who had previously progressed on conventional standard chemotherapies. Further clinical trial of YS110 for MPM is in progress worldwide (ClinicalTrials.gov, 2017).

The role of CD26 in cancer cell biology and the mechanisms of action of YS110 for cancer treatment have been reviewed in detail recently (Ohnuma et al., 2017). In brief, we summarize the mechanisms of action of YS110 as follows; (i) a direct cytotoxic effect on certain human CD26-positive cancer cell lines via antibody-dependent cell-mediated cytotoxicity (ADCC) (Inamoto et al., 2007), (ii) a direct anti-tumor effect through the induction of cell cycle arrest by induction of $p27^{kip1}$ and $p21^{cip1}$ expression (Inamoto et al., 2007; Hayashi et al., 2016), (iii) the nuclear translocation of CD26 molecules by internalization of the CD26-YS110 complexes to inhibit proliferation of tumor cells via suppression of *POLR2A* gene expression, a component of RNA polymerase II (Yamada et al., 2009; Yamada et al., 2013), and (iv) following internalization of the CD26-YS110 complexes, an inhibition of invasion and migration of tumor cells by decreased binding to the collagen/fibronectin microenvironment matrix (Inamoto et al., 2007). We are currently investigating other

mechanisms of action for the observed anti-tumor activity of YS110, especially focusing on the effects of YS110 on tumor immunology.

The FIH phase 1 clinical study of YS110 revealed that an increase in YS110 infusion dose was associated with decreased serum sCD26 level and DPPIV enzyme activity, particularly in cohorts 4-6 (2.0 to 6.0 mg/kg), with an approximately 80% decrease in these levels (Angevin et al., 2017). Although DPPIV inhibitors are clinically used as oral hypoglycemic agents (Drucker and Nauck, 2006), hypoglycemia was not observed during YS110 administration. Of note is the fact that greater than 80% inhibition of serum DPPIV activity was obtained 24 hours after oral administration of clinically available DPPIV inhibitors (drug information published by manufacturers of sitagliptin, vildagliptin, saxagliptin and *etc*.), a level of inhibition comparable to that seen in patients treated with YS110. Our current data would therefore indicate that YS110 therapy is tolerable in the clinical setting. Recent work has demonstrated the functional role of DPPIV-mediated post-translational modification of chemokines in regulating tumor immunity through its interaction with its substrate CXCL10 (Barreira da Silva et al., 2015). Barreira da Silvia et al., used *in vivo* tumor-transplant models to show that DPPIV inhibition reduced tumor growth through the preservation of bioactive CXCL10 in the tumor microenvironment (TME). In the normal physiological state, CXCL10 is rapidly degraded by DPPIV, resulting in decreased recruitment and migration of $CXCR3^+$ T cells into the TME. CXCR3 has been shown to be a functional receptor for CXCL10 (Proost et al., 2001). In contrast, DPPIV inhibition enhanced tumor rejection by preserving the full-length biologically active form of CXCL10, leading to increased trafficking of $CXCR3^+$ T cells into the TME (Ohnuma et al., 2015b). This anti-tumor response is potentiated in combination with other anti-tumor immunotherapeutic approaches including CpG adjuvant therapy, adoptive T cell transfer therapy and checkpoint blockade therapy (anti-CTLA-4 and anti-PD-1) (Barreira da Silva et al., 2015). In view of these recent findings, data from our current trial showing that serum DPPIV activity was decreased following treatment with YS110 in a dose-dependent manner would suggest that anti-tumor activity via DPPIV inhibition may constitute

yet another mechanism of action for the anti-tumor activity of YS110 (Ohnuma et al., 2015b).

Although the cellular and molecular mechanisms involved in CD26-mediated T cell activation have been extensively evaluated by our group and others (Morimoto and Schlossman, 1998; Ohnuma et al., 2008a; De Meester et al., 1999), potential negative feedback mechanisms to regulate CD26-mediated activation still remain to be elucidated. Utilizing human peripheral blood lymphocytes, we recently found that CD26-mediated costimulation induced the development of a population of human type 1 regulatory T (T_{reg}) cells from $CD4^+$ T cells with high level of IL-10 production and lymphocyte-activation gene 3 (LAG3) expression (Hatano et al., 2015). Other investigators have also reported that the $CD26^+CD39^-$ T_{reg} subset among $CD4^+$ T_{reg} exhibits high level of IL-10 expression (Hua et al., 2015). These findings strongly suggest that a specific subset of $CD26^+$ T cells plays a role in immune checkpoint system, and that the CD26 molecule may be a novel target for a therapeutic approach involving immune checkpoint blockade. We are currently investigating whether CD26-mediated signals are associated with the induction of immune checkpoint molecules in the tumor-infiltrating lymphocytes, and definitive data will be presented in the near future.

3. IMMUNE DISORDERS

3.1. Acute Graft-versus-Host Disease

GVHD is a severe complication and major cause of morbidity and mortality following allogeneic hematopoietic stem cell transplantation (alloHSCT) (Giralt, 2012). GVHD results from an immunobiological attack on target recipient organs by donor allogeneic T cells that are transferred along with the allograft (Blazar et al., 2012; Shlomchik, 2007). The pivotal role of donor-derived T cells in acute GVHD (aGVHD) is supported by the complete abrogation of GVHD following T cell depletion from the graft (Giralt, 2012; Tsirigotis et al., 2012). This approach remains

the most effective in preventing aGVHD. However, complications such as graft rejection, loss of GVL effect or increased opportunistic infections can occur. Although new approaches are being developed in the clinical setting for the prevention or treatment of GVHD (Blazar et al., 2012), in-depth understanding of the precise cellular mechanisms of human GVHD is necessary for more effective and less immunocompromising strategies to improve the clinical outcome of alloHSCT.

Costimulatory pathways are required to induce T cell proliferation, cytokine secretion and effector function following antigen-mediated T cell receptor activation (Rudd, 2010), and the important role of costimulatory pathways in transplant biology has been established (Markey et al., 2014). The most extensively studied pathways involve interactions between CD28 and the B7 molecules CD80 and CD86 (Rudd et al., 2009). Initial studies focused on the *in vivo* blockade of interactions between CD28 or cytotoxic T lymphocyte antigen 4 (CTLA4) and their B7 ligands, CD80 and CD86, using a CTLA4-immunoglobulin fusion protein (CTLA4-Ig) or B7-specific antibodies (Lenschow et al., 1992; Saito, 1998). Blockade of CD28 pathways may lead to profound immunosuppression (Blazar et al., 1997). CD26 is also associated with T cell signal transduction processes as a costimulatory molecule, as well as being a marker of T cell activation (Morimoto and Schlossman, 1998; Ohnuma et al., 2008a). In fact, patients with autoimmune diseases such as multiple sclerosis, Grave's disease, and RA have been found to have increased numbers of $CD4^+CD26^+$ T cells in inflamed tissues as well as in their peripheral blood (Eguchi et al., 1989; Gerli et al., 1996; Hafler et al., 1985; Mizokami et al., 1996), with enhancement of CD26 expression in these autoimmune diseases correlating with disease severity (Eguchi et al., 1989; Gerli et al., 1996; Muscat et al., 1994). Moreover, $CD26^{high}CD8^+$ T cells in humans belong to early effector memory T cells, and $CD26^{high}CD8^+$ T cells exhibited increased expression of granzyme B, TNF-α, IFN-γ and Fas ligand, and exerted cytotoxic effect with CD26-mediated costimulation (Hatano et al., 2013b). These findings implied that $CD26^+$ T cells play an important role in the inflammation process and subsequent tissue damage in such diseases, and suggested that

$CD26^+$ T cells belong to the effector T cell population. However, little is known about the effectiveness of CD26-targeting therapy on aGVHD.

To determine whether human $CD26^+$ T cells play a role in an animal model of inflammatory diseases mediated by human effector lymphocytes, we utilized a xenogeneic model of GVHD resulting from the adoptive transfer of human peripheral blood mononuclear cells (PBMCs) into NOD/Shi-*scid*, IL-2Rγ^{null} (NOG) mice (hu-PBL-NOG mice) (Ito et al., 2002). We first conducted a pathological analysis of x-GVHD target organs such as the skin, colon or liver in hu-PBL-NOG mice. The liver, colon and skin of hu-PBL-NOG mice were infiltrated with human $CD3^+$ mononuclear cells (MNCs), with associated organ destruction. Moreover, human $CD3^+$ MNCs reactive to anti-human CD26 Ab were readily visible in all evaluated samples in the liver, colon or skin of x-GVHD mice. The infiltrated $CD26^+$ cells were confirmed to be human $CD3^+$ T cells by co-staining analysis with flow cytometry. These results suggest that donor-derived human $CD26^+$ cells play a role in the pathogenesis of x-GVHD in our hu-PBL-NOG murine model.

We attempted to determine whether treatment with humanized anti-CD26 mAb could ameliorate disease progression and severity in our x-GVHD murine model. As comparison, the clinically available T cell costimulation blocking agent CTLA4-Ig (abatacept) was utilized (Genovese et al., 2005; Gribben et al., 1996). As shown in Figure 2A, anti-CD26 mAb (orange or red lines) or CTLA4-Ig (green or dark green lines) treatment of hu-PBL-NOG mice significantly increased overall survival, as compared with control IgG treatment (blue line). This life-prolonging effect of anti-CD26 mAb was observed at the same low dose as CTLA4-Ig (orange or green lines in Figure 2A, respectively). Moreover, GVHD-associated weight loss for up to 4 weeks post cell inoculation was not significantly different between anti-CD26 mAb and CTLA4-Ig treatment groups (orange or green lines in Figure 2B). These data strongly suggest that anti-CD26 mAb treatment is a promising novel therapeutic agent for x-GVHD, with efficacy comparable to CTLA4-Ig.

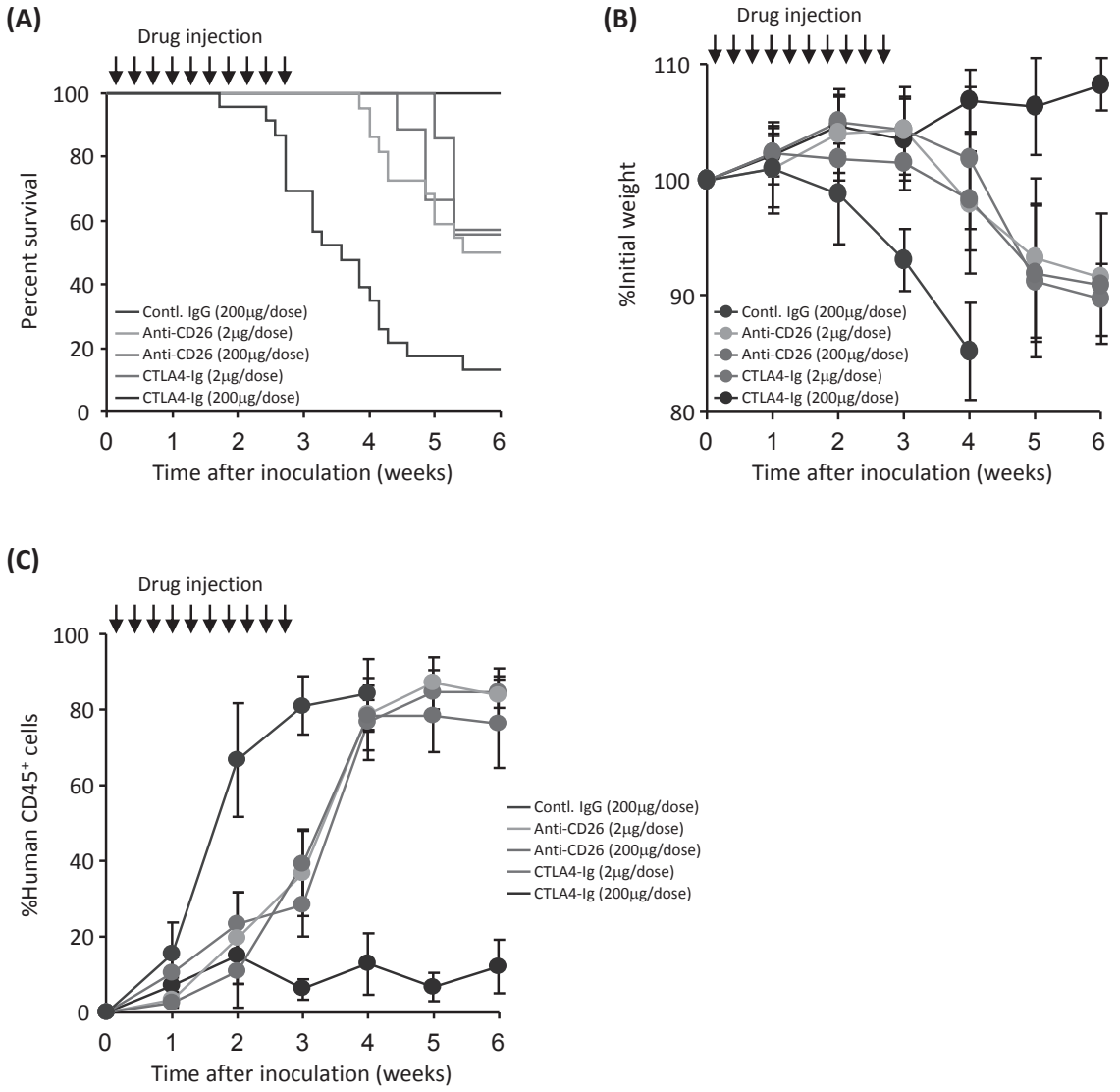

Figure 2. Anti-CD26 mAb treatment reduces x-GVHD-related lethality, and weight loss in hu-PBL-NOG mice without rejection of donor-derived human lymphocytes. After 1 day of inoculation of human PBMCs, Hu-PBL-NOG mice were injected intraperitoneally with humanized anti-CD26 mAb, CTLA4-Ig, or isotype IgG control at indicated doses in 200 μl of sterile phosphate-buffered saline (PBS), and then were injected thrice weekly for a total of 10 doses to assess potency in preventing x-GVHD. (A) Kaplan–Meier survival curves for mice receiving PBMC plus control IgG (200 μg/dose, blue line, n = 23), low dose anti-CD26 mAb (2 μg/dose, orange line, n = 24) (P = 0.0001 vs. control IgG group), high dose anti-CD26 mAb (200 μg/dose, red line, n = 7) (P = 0.0006 vs. control IgG group), low dose CTLA4-Ig (2 μg/dose, green line, n = 9) (P = 0.0005 vs. control IgG group), or high dose CTLA4-Ig (200 μg/dose, dark green line, n = 6) (P = 0.0008 vs. control IgG group). (B) Average weight (percentage ± standard deviation (SD) of initial) for mice surviving on a given day for different groups of mice as shown in (A). (C) Time course changes of average percentage (± SD) of human $CD45^+$ lymphocytes in peripheral blood in mice receiving PBMC

plus control IgG (200 μg/dose, blue line, n = 23), low dose anti-CD26 mAb (2 μg/dose, orange line, n = 24), high dose anti-CD26 mAb (200 μg/dose, red line, n = 7), low dose CTLA4-Ig (2 μg/dose, green line, n = 9), or high dose CTLA4-Ig (200 μg/dose, dark green line, n = 6). This figure is reprinted with permission from Hatano R et al., *Br J Haematol* 162: 263-77, 2013.

We next analyzed circulating human lymphocytes in the peripheral blood of hu-PBL-NOG mice receiving anti-CD26 mAb or CTLA4-Ig. As shown in Figure 2C, at 3 weeks after inoculation, human lymphocyte level was increased in peripheral blood of mice receiving anti-CD26 mAb at both low dose and high dose (orange and red lines of Figure 2C), comparable to low dose CTLA4-Ig (green line of Figure 2C). On the other hand, in mice receiving high dose CTLA4-Ig, most of the inoculated human PBMCs were rejected (dark green line in Figure 2C). These data indicate that while treatment with increasing doses of CTLA4-Ig resulted in the absence of x-GVHD development, graft rejection did occur, potentially analogous to findings in a clinical trial with a new CTLA4-Ig agent, belatacept (Vincenti et al., 2010). On the other hand, increasing doses of anti-CD26 mAb resulted in no graft rejection in hu-PBL-NOG mice with prolonging survival as compared to hu-PBL-NOG mice receiving control IgG.

We next examined human CD26 expression level in the peripheral blood of hu-PBL-NOG mice receiving anti-CD26 mAb or CTLA4-Ig. Higher expression level of human CD26 on both $CD4^+$ and $CD8^+$ human lymphocytes in the peripheral blood of hu-PBL-NOG mice receiving control IgG or CTLA4-Ig was observed from 1 to 3 weeks after inoculation. On the other hand, in hu-PBL-NOG mice receiving anti-CD26 mAb, neither $CD4^+$ nor $CD8^+$ T cells expressed CD26 from 1 to 3 weeks. At 3 weeks after inoculation, very weak expression of human CD26 was observed on $CD4^+$ or $CD8^+$ cells in the peripheral blood of hu-PBL-NOG mice receiving anti-CD26 mAb. Taken together, these data suggest that decreased number of $CD26^{high}$ effector T cells may be responsible for the relative absence of x-GVHD development in mice receiving anti-CD26 mAb.

Since $CD26^{high}$ effector lymphocytes have high capacity for migration into inflamed tissues, we examined liver tissues of hu-PBL-NOG mice for

donor lymphocyte infiltration. In x-GVHD mice receiving control IgG, liver damage was observed with infiltration of human $CD4^+$ or $CD8^+$ MNCs. Moreover, slight inflammation of the portal duct areas in the liver was observed in mice receiving CTLA4-Ig. On the other hand, infiltration of human T cells in the liver was barely detected in mice receiving anti-CD26 mAb. In addition to the pathological changes seen in the liver, significant elevation of serum alanine aminotransferase (ALT) activity was observed in mice receiving control IgG or CTLA4-Ig, while that of mice receiving anti-CD26 mAb was found to be near normal level. Along with lymphocyte infiltration in the GVHD target tissues, the mRNA level of effector cytokines of donor-derived human $CD4^+$ or $CD8^+$ cells in the liver of hu-PBL-NOG mice receiving anti-CD26 mAb was decreased compared to those of hu-PBL-NOG mice receiving control IgG. Taken together, these results indicate that anti-CD26 treatment in hu-PBL-NOG mice ameliorated liver GVHD by decreasing production of proinflammatory cytokines of donor-derived human lymphocytes as well as inhibiting lymphocyte infiltration in the liver.

Since aGVHD and GVL effects are immune reactions highly linked to each other (Wu and Ritz, 2009; Zorn et al., 2002), we evaluated the potential influence of anti-CD26 mAb treatment on GVL effect. NOG mice transplanted with P815 cells along with human PBMCs and control IgG showed minimal signs of tumor growth in the inoculated region, but all mice died around 4 weeks after inoculation due to x-GVHD. On the other hand, mice inoculated with P815 along with human PBMC and anti-CD26 mAb exhibited enhanced survival rate with minimal evidence of GVHD. Importantly, mice in this group showed significantly slow initial tumor growth, suggesting the preservation of GVL effect more than CTLA4-Ig treatment. We examined the expression level of effector cytokines of human $CD8^+$ T cells isolated from the spleens of hu-PBL-NOG mice at 2 weeks after transplantation. Our data suggest that the GVL effect of cytotoxic effector function occurring at the early time period prior to manifestation of x-GVHD was preserved in hu-PBL-NOG mice receiving anti-CD26 mAb, compared to those in hu-PBL-NOG mice receiving CTLA4-Ig. In conclusions, CD26-mediated T cell activation

appears to play a significant role in GVHD. Since full suppression of x-GVHD with interventional therapies is currently a difficult challenge, our data demonstrating that control of x-GVHD can be achieved by modulating $CD26^{high}$ T cells with anti-CD26 mAb are potentially important clinically. Our work also suggests that anti-CD26 mAb treatment may be a novel therapeutic approach for GVHD in the future.

3.2. Chronic Graft-versus-Host Disease

On the basis of differences in clinical manifestations and histopathology, GVHD can be divided into acute and chronic forms (Blazar et al., 2012). aGVHD and chronic GVHD (cGVHD) are traditionally diagnosed primarily by time of onset, with cGVHD occurring after day 100 of transplantation (Deeg et al., 1997). However, cGVHD has distinct clinicopathologic features and is often diagnosed based on these features regardless of time of onset, being characterized by cutaneous fibrosis, involvement of exocrine glands, hepatic disease, and obliterative bronchiolitis (OB) (Filipovich, 2008; Socie and Ritz, 2014). OB, characterized by airway blockade, peribronchiolar and perivascular lympho-fibroproliferation and obliteration of bronchioles, is a late-stage complication of cGVHD (Chien et al., 2010). Patients diagnosed with OB have a 5-year survival rate of only 10 to 40%, compared to more than 80% of patients without OB (Dudek et al., 2003; Nakaseko et al., 2011). Furthermore, while multiple strategies to control cGVHD involving T cell depletion from the graft or global immunosuppression have been developed, cGVHD is still a common clinical outcome in many alloHSCT patients (Socie and Ritz, 2014; Zeiser and Blazar, 2016). In addition, immunosuppression potentially abrogates the GVL effect, associated with increased relapses following alloHSCT (Champlin et al., 1999). Novel therapeutic approaches are thus needed to control cGVHD without eliminating the GVL effect.

Since our aGVHD model described in the preceding section succumbed to aGVHD around 4 weeks after transplantation of human adult

PBL, this early-onset model of aGVHD does not permit the assessment of longer term consequences of interventional therapies, such as their effect on the development of OB, a form of cGVHD of the lung. In contrast to adult PBL, human cord blood (HuCB) lymphocytes have been reported to be immature, predominantly consisting of $CD45RA^+$ naive cells (Kobayashi et al., 2004). We previously showed that, while all HuCB CD4 T cells constitutively express CD26, CD26-mediated costimulation was considerably attenuated in HuCB CD4 T cells, compared to the robust activation via CD26 costimulation of adult PBL (Kobayashi et al., 2004). Based on these findings, we hypothesized that HuCB naive CD4 T cells gradually acquire a xenogeneic response via attenuated stimulatory signaling with indolent inflammation in the target organs, leading eventually to chronic inflammatory changes. We therefore succeeded in developing a humanized murine pulmonary cGVHD model utilizing NOG mice as recipients and HuCB as donor cells (Ohnuma et al., 2015a), and overcame the limitations seen in the humanized murine aGVHD model such as vigorous activation of all engrafted T cells and extensive loss of B cell maturation and activation (Shultz et al., 2012). Whole CB transplant mice exhibited clinical signs/symptoms of GVHD as early as 4 weeks post transplant, and demonstrated significantly decreased survival rate. The lung of whole CB transplant mice showed perivascular and subepithelial inflammation and fibrotic narrowing of the bronchiole. Skin of whole CB transplant mice manifested fat loss, follicular drop-out and sclerosis of the reticular dermis in the presence of apoptosis of the basilar keratinocytes while the liver exhibited portal fibrosis and cholestasis. These findings indicate that whole CB transplant mice develop pulmonary cGVDH as well as concomitant active GVHD in skin and liver. Taken together, our data demonstrate that the lung of whole CB transplant mice exhibits OB as manifestation of pulmonary GVHD (Ohnuma et al., 2015a).

Utilizing this model, we identified IL-26 as a key effector cytokine inducing transplant-related obliterative bronchiolitis. Lung of HuCB mice exhibited obliterative bronchiolitis with increased collagen deposition and predominant infiltration with human $IL\text{-}26^+CD26^+$CD4 T cells. Moreover, although IL-26 is absent from rodents, we showed that IL-26 increased

collagen synthesis in fibroblasts and promoted lung fibrosis in a murine GVHD model using *IL-26* transgenic mice. *In vitro* analysis demonstrated a significant increase in IL-26 production by HuCB CD4 T cells following CD26 costimulation, whereas Ig Fc domain fused with the N-terminal of caveolin-1 (Cav-Ig), the ligand for CD26, effectively inhibited production of IL-26. Administration of Cav-Ig before or after onset of GVHD impeded the development of clinical and histologic features of GVHD without interrupting engraftment of donor-derived human cells, with preservation of the GVL effect (Ohnuma et al., 2015a). These results therefore provide proof of principle that cGVHD of the lungs is caused in part by IL-$26^{+}$$CD26^{+}$CD4 T cells, and that blockade of CD26-caveolin-1 interaction by Cav-Ig or YS110 could be beneficial for cGVHD prevention and therapy.

3.3. Rheumatoid Arthritis

RA is a chronic, inflammatory autoimmune disease that primarily affects the joints, but also has systemic symptoms. RA is characterized by progressive invasion of synovial fibroblasts into the articular cartilage and erosion of the underlying bone, followed by joint destruction (Asif Amin et al., 2017). Several reports on RA patients have shown that concentration of soluble CD26 and DPPIV enzyme activity were significantly decreased in both synovial fluid and serum compared with osteoarthritis patients or healthy donors (Busso et al., 2005; Buljevic et al., 2013; Cordero et al., 2015). Cordera et al., studied serum levels of IL-12, IL-15, and soluble CD26 from 35 patients with active and inactive RA as well as those of healthy controls (Cordero et al., 2001). Patients' sera had higher IL-12 and IL-15 levels, and the level of soluble CD26 was inversely correlated with the number of swollen joints. These findings suggest that these cytokines and CD26 are associated with the inflammation and immune activity in RA. A number of proinflammatory peptides are supposed to be involved in the pathogenesis of RA, and have their biological activity controlled by limited proteolysis mediated by DPPIV and DPPIV-like hydrolytic activity (Wolf

et al., 2008). Several investigators have demonstrated that SDF-1α (CXCL12), a substrate of DPPIV, is a crucial mediator controlling the influx of lymphocytes and monocytes/macrophages into the inflamed synovium of RA and thus triggering joint destruction (Kim et al., 2007; Sromova et al., 2010). DPPIV regulates neuropeptide Y (NPY) and vasoactive intestinal peptide (VIP), recently implicated in RA (Buljevic et al., 2013). However, involvement of DPPIV enzyme activity in the pathology of RA remains controversial. Using CD26/DPPIV-KO mice, Busso et al., demonstrated that damage severity, as indicated by synovial thickness, knee-joint inflammation, and histological grading, was more severe in CD26/DPPIV-KO mice than in wild-type control mice in antigen- and collagen-induced arthritis models (Busso et al., 2005). The authors concluded that decreased circulating CD26/DPPIV levels in arthritis increased the intact active form of SDF-1, associated with increased numbers of CXCR4 (SDF-1 receptor)-positive cells infiltrating arthritic joints. On the other hand, using a type II collagen-induced or alkyldiamine-induced rat model of arthritis, Tanaka et al., showed that treatment with any DPPIV inhibitors examined reduced hind paw swelling, an indicator of disease severity (Tanaka et al., 1997; Tanaka et al., 1998).

In contrast with the decrease in the levels of soluble CD26 in the synovial fluid and serum, patients with active RA displayed higher percentage of peripheral blood $CD26^{+}CD4^{+}$ T cells than inactive RA and control subjects (Muscat et al., 1994; Cordero et al., 2015). RA synovial fluid contained lower percentages of whole $CD26^{+}$ T cells compared with peripheral blood, while the percentage of $CD26^{high}$ T cells in synovial fluid of RA was markedly increased compared with peripheral blood of RA patients and healthy subjects (Mizokami et al., 1996). These findings suggest that $CD26^{+}$ T cells induce the inflammation and tissue destruction characteristic of RA by migrating to and being active in the rheumatoid synovium. We described $CD26^{+}$ T cells infiltrating the rheumatoid synovium using immunohistochemical studies (Ohnuma et al., 2006). We also noted high expression of caveolin-1 in the rheumatoid synovium and synoviocytes. These data suggest that the CD26-caveolin-1-mediated upregulation of CD86 on activated monocytes in addition with CD26-

mediated signal transduction in T cells leads to antigen specific T cell activation in RA, and blockade of this CD26-caveolin-1 interaction by YS110 may be useful for suppressing the immune system in RA.

3.4. Inflammatory Bowel Diseases

In patients with inflammatory bowel diseases (IBD) such as Crohn's disease or ulcerative colitis, $CD26^+$ T-cells and DPPIV activity in serum were examined (Hildebrandt et al., 2001; Rose et al., 2002). In these studies, while the DPPIV activity was reduced in patients with IBD, the number of $CD25^+CD26^+$ T-cells in the peripheral blood was increased in patients with IBD. Moreover, other investigators recently reported that $CD26^{high}$ T cells contain T_H17 cells, and that $CD26^{high}$ T_H17 cells are enriched in the inflamed tissue of IBD patients (Bengsch et al., 2012). In addition, Kappeler et al., showed that activated perforin mRNA expressing T cells are present in close proximity to the intestinal epithelial cells in active stages of ulcerative colitis and Crohn's disease (Kappeler et al., 2000), suggesting an important role of cytotoxic cells in the pathogenesis of IBD. We recently showed that $CD26^{high}CD8^+$ T cells exhibit increased expression of granzyme B, TNF-α, IFN-γ and Fas ligand, and exert cytotoxic effect with CD26-mediated costimulation (Hatano et al., 2013b). Taken together, these data indicate that CD26 may be potentially important for the pathophysiology of IBD, and appears to be a useful therapeutic target for IBD.

3.5. Middle East Respiratory Syndrome Coronavirus

MERS-CoV was first identified in a 60-year-old patient in June 2012 who presented with acute pneumonia, followed by acute respiratory distress syndrome and renal failure with a fatal outcome (Zaki et al., 2012). Between 2012 and September 2017, 2080 laboratory-confirmed cases of MERS-CoV infection were reported to the World Health Organization

(WHO), which has notified of at least 722 deaths (around 35% fatality rate) related to MERS-CoV since September 2012 (WHO, 2017). Efforts to develop effective preventive and therapeutic intervention strategies are currently ongoing. Several treatment modalities have been investigated to develop effective therapies against MERS-CoV, including interferon, ribavirin, cyclosporin A, protease inhibitors, convalescent plasma and immunoglobulins. Several promising anti-MERS-CoV therapeutic agents have recently been reviewed extensively (Mo and Fisher, 2016), while broad spectrum antiviral agents might not be sufficient to treat severe MERS-CoV patients because of its limited effective therapeutic window of opportunity (Zumla et al., 2016).

An alternative approach using prophylactic regimens would be theoretically suitable to limit the spread of MERS-CoV. This scenario includes MERS vaccine and neutralizing MERS-CoV-specific mAb (Zumla et al., 2016). The MERS-CoV genome encodes for 16 non-structural proteins (nsp1-16) and 4 structural proteins, the spike (S), envelope (E), membrane (M), and nucleocapsid (N) (van Boheemen et al., 2012). The viral structural proteins, S and N, show the highest immunogenicity (Agnihothram et al., 2014). While both S and N proteins induce T-cell responses, neutralizing antibodies are almost solely directed against the S protein, with the receptor binding domain (RBD) being the major immunodominant region (Mou et al., 2013). These great challenges have been extensively reviewed previously (Zumla et al., 2016).

Recent reports indicated that the spike protein S1 of MERS-CoV is required for viral entry into human host cells (Gierer et al., 2013; Lu et al., 2013), using CD26/DPPIV as a functional receptor (Raj et al., 2013). Inhibiting virus entry into host cells could also be achieved by targeting the host receptor CD26/DPPIV. While inhibitors of the CD26/DPPIV enzymatic activity are used clinically to treat type 2 diabetes patients, commercially available DPPIV inhibitors would not serve this purpose since these agents have been shown not to inhibit binding of the RBD of MERS-CoV to CD26/DPPIV (Raj et al., 2013). We previously showed that human CD26 is a binding protein for ADA (Kameoka et al., 1993). Currently, it is known that there are two isoforms of ADA, ADA1 and

ADA2. ADA1 is particularly present in lymphocytes and macrophages, while ADA2 is found predominantly in the serum and other body fluids including pleural effusion (Gakis, 1996). CD26/DPPIV binds to ADA1, but not ADA2 (Kameoka et al., 1993). The crystal structure of CD26/DPPIV and the S protein of MERS-CoV allowed for visualization of the interacting amino acid in both proteins. However, our *in vitro* experiments showed that blockade of MERS-CoV binding to CD26/DPPIV by ADA1 is incomplete (Ohnuma et al., 2013). Therefore, mAb-mediated blocking CD26/DPPIV binding to the RBD of MERS-CoV needs to be developed.

CD26/DPPIV, a host receptor for MERS-CoV, is conserved among different species such as bats and humans, partially explaining the large host range of MERS-CoV (Mohd et al., 2016). In addition to being widely expressed in most cell types including T lymphocytes, bronchial mucosa or the brush border of proximal tubules, CD26/DPPIV exists in systemic circulation as soluble form (Ohnuma et al., 2008b). This distribution of CD26 may play a role in the systemic dissemination of MERS-CoV infection in human (Drosten et al., 2013). Therefore, an effective therapy for MERS-CoV is needed not only to block the entry of MERS-CoV into such CD26-expressing organs as the respiratory system, kidney, liver or intestine, but also to eliminate circulating MERS-CoV. In this regard, manipulation of CD26/DPPIV levels or the development of inhibitors that target the interaction between the MERS-CoV S1 domain and its receptor may provide therapeutic opportunities to combat MERS-CoV infection. More recently, the RBD in the S protein was mapped to a 231-amino acid fragment of MERS-CoV S proteins (residues 358-588) (Mou et al., 2013).

We have recently mapped MERS-CoV S protein-binding regions in human CD26 molecule and demonstrated that anti-CD26 mAbs, which had been developed in our laboratory, effectively blocked the interaction between the spike protein and CD26, thereby neutralizing MERS-CoV infectivity. To determine the specific CD26 domain involved in MERS-CoV infection, we chose six different clones of anti-CD26 mAbs (4G8, 1F7, 2F9, 16D4B, 9C11, 14D10), and the humanized anti-CD26 mAb YS110, which recognize 6 distinct epitopes of the CD26 molecule (Dong

et al., 1998; Inamoto et al., 2007), to conduct MERS-CoV S1-Fc (S1 domain of MERS-CoV fused to the Fc region of human IgG) binding inhibition assays (Ohnuma et al., 2013). 2F9 inhibited fully binding of MERS-CoV S1-Fc to JKT-hCD26WT (Jurkat cells transfected with full-length human CD26/DPPIV), while other anti-CD26 mAbs demonstrated certain levels of inhibition (1F7, or YS110) or no significant inhibition (4G8, 16D4B, 9C11 or 14D10). These results strongly suggest that the anti-CD26 mAb 2F9 has better therapeutic potential than recombinant MERS-CoV S1-Fc in preventing viral entry into susceptible cells, and that 1F7 or YS110 also blocks MERS-CoV infection.

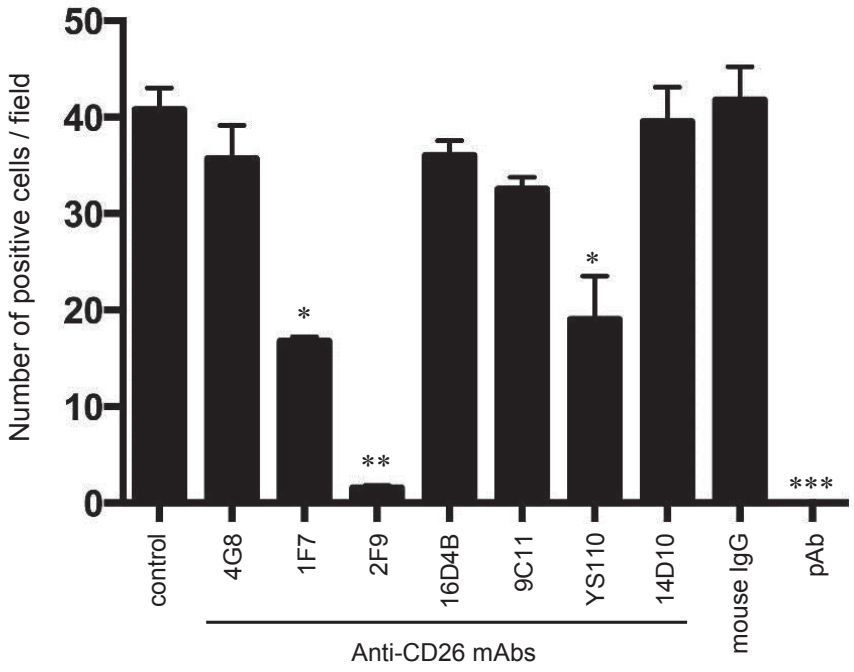

Figure 3. Inhibition of MERS-CoV infection by the anti-CD26 mAb. Huh-7 cells were preincubated with normal mouse IgG, various anti-CD26 mAbs (4G8, 1F7, 2F9, 16D4B, 9C11, or 14D10), humanized anti-CD26 mAb (YS110), or anti-CD26 goat polyclonal antibody (pAb) at a concentration of 40 μg/ml for 0.5 h prior to MERS-CoV virus inoculation (1 h), all at room temperature. Mock-incubated cells (control) were used as controls. Following incubation at 37°C for 8 h, infected cells were detected by immunofluorescence using anti-SARS-CoV NSP4 antibodies that are cross-reactive for MERS-CoV, and infection was quantified as the number of anti-SARS-CoV NSP4-positive cells. Two independent experiments were performed, and data from one representative experiment are shown. Error bars indicate SEMs (two-tailed Student's *t* test; *, **, or ***, $P < 0.05$ versus control. This figure is reprinted with permission from Ohnuma K et al., *J Virol* 87: 13892-9, 2013.

Moreover, we have characterized the CD26 epitope involved in MERS-CoV S1-Fc binding to CD26 through the use of various CD26 mutants with deletion in the C-terminal extracellular region, since CD26 is a type II transmembrane protein (Ohnuma et al., 2008a). Our biological experiments on binding regions of CD26 to MERS-CoV using mAbs showed results comparable to those obtained from crystal structure analysis (Lu et al., 2013; Wang et al., 2013). Our observations strongly suggest that the main binding regions of CD26 to MERS-CoV appear to be close to the 358th amino acid recognized by 2F9, and the regions of CD26 defined by 1F7 and YS110 (248-358th amino acids) are also partially involved in MERS-CoV binding.

To determine whether treatment with anti-CD26 mAbs 2F9 as well as 1F7 and YS110 could inhibit MERS-CoV infection, susceptible cells, Huh-7, were pre-incubated with various anti-CD26 mAbs prior to inoculation with the virus (Ohnuma et al., 2013). In this experimental system, infection was almost completely blocked by 2F9 but not by control IgG or several other anti-CD26 mAbs recognizing other epitopes (4G8, 16D4B, 14D10 or 9C11) (Figure 3). Moreover, the anti-CD26 mAbs 1F7 and YS110 considerably inhibited MERS-CoV infection of Huh-7 cells (Figure 3). These results demonstrate that 2F9 inhibits MERS-CoV entry, and therefore can potentially be developed as a preventive or therapeutic agent for MERS-CoV infection in the clinical setting. More importantly, the humanized anti-CD26 mAb YS110 has been evaluated in patients with CD26-expressing cancers in our FIH phase 1 clinical trial. Since no apparent adverse effects of YS110 have been reported besides transient and tolerable injection reactions, and moreover, the level of circulating soluble CD26 in the serum is decreased following YS110 administration (Angevin et al., 2017), YS110 may be an immediate therapeutic candidate for clinical use as potential treatment for MERS-CoV infection.

CLOSING REMARKS

CD26 is a multifunctional protein with known DPPIV enzyme activity. CD26 is expressed on various tumors including MPM. Although the exact role of CD26/DPPIV in various cancers remains to be elucidated, CD26 serves as a prognostic marker in multiple tumors such as CRC, GIST, thyroid carcinoma and UC. Moreover, in several human malignancies including MPM, CRC and CML, CD26/DPPIV expression is reported to be a marker of cancer stem cells. Our FIH phase 1 clinical trial of YS110 demonstrates that YS110 therapy exhibits a favorable safety profile and results in encouraging disease stabilization in a number of patients with advanced/refractory CD26-expressing MPM and RCC, and further clinical testing of YS110 for MPM is being conducted worldwide. Given the potential role of CD26 surface expression in cancer biology, YS110 therapy may also influence tumor growth through its potential effect on the cancer stem cells of selected tumors.

Besides being a marker of T cell activation, CD26 is also associated with T cell signal transduction processes as a costimulatory molecule and has an important role in T cell biology and overall immune function. Since CD26/DPPIV has a multitude of biological functions in human tumor cells and immune system, further detailed understanding of the role of this molecule in various clinical settings may lead potentially to novel therapeutic approaches not only for MPM but also for other refractory cancers, immune disorders and MERS-CoV infection.

ACKNOWLEDGMENTS

This study was supported in part by a grant of the Ministry of Health, Labour, and Welfare, Japan (Grant Number 150401-01 (C.M.)), JSPS KAKENHI Grant Numbers JP16H05345 (C.M.), JP15H04879 (K.O.), JP17K10008 (R.H.), JP26860760 (R.H.), and a Grant-in-Aid (S1311011) from the Foundation of Strategic Research Projects in Private Universities

from the Ministry of Education, Culture, Sports, Science, and Technology, Japan (K.O. and C.M.).

Figures 1, 2 and 3 are reproduced with permission from Inamoto T et al., *Clin Cancer Res* 12: 3470-7, 2006 (*Copyright 2006. American Association for Cancer Research*), Hatano R et al., *Br J Haematol* 162: 263-77, 2013 (*Copyright 2013. John Wiley & Sons, Inc.*), and Ohnuma K et al., *J Virol* 87: 13892-9, 2013 (*Copyright 2013. American Society for Microbiology*), respectively.

REFERENCES

Agnihothram, S., Gopal, R., Yount, B. L. Jr., Donaldson, E. F., Menachery, V. D., Graham, R. L., Scobey, T. D., Gralinski, L. E., Denison, M. R., Zambon, M., and Baric, R. S. (2014). Evaluation of serologic and antigenic relationships between middle eastern respiratory syndrome coronavirus and other coronaviruses to develop vaccine platforms for the rapid response to emerging coronaviruses. *J Infect Dis* 209, 995-1006.

Amatya, V. J., Takeshima, Y., Kushitani, K., Yamada, T., Morimoto, C., and Inai, K. (2011). Overexpression of CD26/DPPIV in mesothelioma tissue and mesothelioma cell lines. *Oncol Rep* 26, 1369-1375.

Angevin, E., Isambert, N., Trillet-Lenoir, V., You, B., Alexandre, J., Zalcman, G., Vielh, P., Farace, F., Valleix, F., Podoll, T., Kuramochi, Y., Miyashita, I., Hosono, O., Dang, N. H., Ohnuma, K., Yamada, T., Kaneko, Y., and Morimoto, C. (2017). First-in-human phase 1 of YS110, a monoclonal antibody directed against CD26 in advanced CD26-expressing cancers. *Br J Cancer* 116, 1126-1134.

Aoe, K., Amatya, V. J., Fujimoto, N., Ohnuma, K., Hosono, O., Hiraki, A., Fujii, M., Yamada, T., Dang, N. H., Takeshima, Y., Inai, K., Kishimoto, T., and Morimoto, C. (2012). CD26 overexpression is associated with prolonged survival and enhanced chemosensitivity in malignant pleural mesothelioma. *Clin Cancer Res* 18, 1447-1456.

Asif Amin, M., Fox, D. A., and Ruth, J. H. (2017). Synovial cellular and molecular markers in rheumatoid arthritis. *Semin Immunopathol* 39, 385-393.

Barreira da Silva, R., Laird, M. E., Yatim, N., Fiette, L., Ingersoll, M. A., and Albert, M. L. (2015). Dipeptidylpeptidase 4 inhibition enhances lymphocyte trafficking, improving both naturally occurring tumor immunity and immunotherapy. *Nat immunol* 16, 850-858.

Bengsch, B., Seigel, B., Flecken, T., Wolanski, J., Blum, H. E., and Thimme, R. (2012). Human Th17 cells express high levels of enzymatically active dipeptidylpeptidase IV (CD26). *J Immunol* 188, 5438-47.

Blazar, B. R., Murphy, W. J., and Abedi, M. (2012). Advances in graft-versus-host disease biology and therapy. *Nat Rev Immunol* 12, 443-458.

Blazar, B. R., Taylor, P. A., Boyer, M. W., Panoskaltsis-Mortari, A., Allison, J. P., and Vallera, D. A. (1997). CD28/B7 interactions are required for sustaining the graft-versus-leukemia effect of delayed post-bone marrow transplantation splenocyte infusion in murine recipients of myeloid or lymphoid leukemia cells. *J Immunol* 159, 3460-3473.

Buljevic, S., Detel, D., Pucar, L. B., Mihelic, R., Madarevic, T., Sestan, B., and Varljen, J. (2013). Levels of dipeptidyl peptidase IV/CD26 substrates neuropeptide Y and vasoactive intestinal peptide in rheumatoid arthritis patients. *Rheumatol Int* 33, 2867-74.

Busso, N., Wagtmann, N., Herling, C., Chobaz-Péclat, V., Bischof-Delaloye, A., So, A., and Grouzmann, E. (2005). Circulating CD26 is negatively associated with inflammation in human and experimental arthritis. *Am J Pathol* 166, 433-42.

Champlin, R., Khouri, I., and Giralt, S. (1999). Graft-vs.-malignancy with allogeneic blood stem cell transplantation: a potential primary treatment modality. *Pediatr Transplant*, 3 (Suppl 1), 52-8.

Chien, J. W., Duncan, S., Williams, K. M., and Pavletic, S. Z. (2010). Bronchiolitis obliterans syndrome after allogeneic hematopoietic stem cell transplantation-an increasingly recognized manifestation of

chronic graft-versus-host disease. *Biol Blood Marrow Transplant* 16(1 Suppl), S106-14.

ClinicalTrials.gov. (2017). Clinical Study of YS110 in Patients With Malignant Pleural Mesothelioma. https://www.clinicaltrials.gov/ct2/show/NCT03177668?term=YS110&cond=Mesotheliomas+Pleural&rank=1.

Cordero, O. J., Varela-Calviño, R., López-González, T., Calviño-Sampedro, C., Viñuela, J. E., Mouriño, C., Hernández-Rodríguez, Í., Rodríguez-López, M., Aspe de la Iglesia, B., and Pego-Reigosa, J. M. (2015). CD26 Expression on T Helper Populations and sCD26 Serum Levels in Patients with Rheumatoid Arthritis. *PLoS One* 10, e0131992.

Cordero, O. J., Salgado, F. J., Mera-Varela, A., and Nogueira, M. (2001). Serum interleukin-12, interleukin-15, soluble CD26, and adenosine deaminase in patients with rheumatoid arthritis. *Rheumatol Int* 21, 69-74.

De Meester, I., Korom, S., Van Damme J., and Scharpe, S. (1999). CD26, let it cut or cut it down. *Immunol Today* 20, 367-75.

de Micco, C., Savchenko, V., Giorgi, R., Sebag, F., and Henry, J. F. (2008). Utility of malignancy markers in fine-needle aspiration cytology of thyroid nodules: comparison of Hector Battifora mesothelial antigen-1, thyroid peroxidase and dipeptidyl aminopeptidase IV. *Br J Cancer* 98, 818-823.

Deeg, H. J., Lin, D., Leisenring, W., Boeckh, M., Anasetti, C., Appelbaum, F. R., Chauncey, T. R., Doney, K., Flowers, M., Martin, P., Nash, R., Schoch, G., Sullivan, K. M., Witherspoon, R. P., and Storb R. (1997). Cyclosporine or cyclosporine plus methylprednisolone for prophylaxis of graft-versus-host disease: a prospective, randomized trial. *Blood* 89, 3880-7.

Dong, R. P., Tachibana, K., Hegen, M., Scharpe, S., Cho, D., Schlossman, S. F., and Morimoto, C. (1998). Correlation of the epitopes defined by anti-CD26 mAbs and CD26 function. *Mol Immunol* 35, 13-21.

Drosten, C., Seilmaier, M., Corman, V. M., Hartmann, W., Scheible, G., Sack, S., Guggemos, W., Kallies, R., Muth, D., Junglen, S., Muller, M. A., Haas, W., Guberina, H., Rohnisch, T., Schmid-Wendtner, M.,

Aldabbagh, S., Dittmer, U., Gold, H., Graf, P., Bonin, F., Rambaut, A., and Wendtner, C. M. (2013). Clinical features and virological analysis of a case of Middle East respiratory syndrome coronavirus infection. *Lancet Infect Dis* 13, 745-51.

Drucker, D. J., and Nauck, M. A. (2006). The incretin system: glucagon-like peptide-1 receptor agonists and dipeptidyl peptidase-4 inhibitors in type 2 diabetes. *Lancet* 368, 1696-1705.

Dudek, A. Z., Mahaseth, H., DeFor, T. E., and Weisdorf, D. J. (2003). Bronchiolitis obliterans in chronic graft-versus-host disease: analysis of risk factors and treatment outcomes. *Biol Blood Marrow Transplant* 9, 657-66.

Eguchi, K., Ueki, Y., Shimomura, C., Otsubo, T., Nakao, H., Migita, K., Kawakami, A., Matsunaga, M., Tezuka, H., Ishikawa, N., et al., (1989). Increment in the $Ta1^+$ cells in the peripheral blood and thyroid tissue of patients with Graves' disease. *J Immunol* 142, 4233-4240.

Enserink, M. (2013). Emerging diseases. New coronavirus reveals some of its secrets. *Science* 340, 17-8.

Fagin, J. A., and Wells, J. A. Jr. (2016). Biologic and clinical perspectives on thyroid cancer. *N Engl J Med* 375, 1054-67.

Filipovich, A. H. (2008). Diagnosis and manifestations of chronic graft-versus-host disease. *Best Pract Res Clin Haematol* 21, 251-7.

Gakis, C. (1996). Adenosine deaminase (ADA) isoenzymes ADA1 and ADA2: diagnostic and biological role. *Eur Respir J* 9, 632-3.

Genovese, M. C., Becker, J. C., Schiff, M., Luggen, M., Sherrer, Y., Kremer, J., Birbara, C., Box, J., Natarajan, K., Nuamah, I., Li, T., Aranda, R., Hagerty, D. T., and Dougados, M. (2005). Abatacept for rheumatoid arthritis refractory to tumor necrosis factor alpha inhibition. *N Engl J Med* 353, 1114-1123.

Gerli, R., Muscat, C., Bertotto, A., Bistoni, O., Agea, E., Tognellini, R., Fiorucci, G., Cesarotti, M., and Bombardieri, S. (1996). CD26 surface molecule involvement in T cell activation and lymphokine synthesis in rheumatoid and other inflammatory synovitis. *Clin Immunol Immunopathol* 80, 31-37.

Ghani, F. I., Yamazaki, H., Iwata, S., Okamoto, T., Aoe, K., Okabe, K., Mimura, Y., Fujimoto, N., Kishimoto, T., Yamada, T., Xu, C. W., and Morimoto, C. (2011). Identification of cancer stem cell markers in human malignant mesothelioma cells. *Biochem Biophys Res Commun* 404, 735-742.

Gierer, S., Bertram, S., Kaup, F., Wrensch, F., Heurich, A., Kramer-Kuhl, A., Welsch, K., Winkler, M., Meyer, B., Drosten, C., Dittmer, U., von Hahn, T., Simmons, G., Hofmann, H., and Pohlmann, S. (2013). The spike protein of the emerging betacoronavirus EMC uses a novel coronavirus receptor for entry, can be activated by TMPRSS2, and is targeted by neutralizing antibodies. *J Virol* 87, 5502-11.

Giralt, S. (2012). Graft-versus-host disease: have we solved the problem? *J Clin Oncol* 30, 3160-3161.

Gribben, J. G., Guinan, E. C., Boussiotis, V. A., Ke, X. Y., Linsley, L., Sieff, C., Gray, G. S., Freeman, G. J., and Nadler, L. M. (1996). Complete blockade of B7 family-mediated costimulation is necessary to induce human alloantigen-specific anergy: a method to ameliorate graft-versus-host disease and extend the donor pool. *Blood* 87, 4887-4893.

Hafler, D. A., Fox, D. A., Manning, M. E., Schlossman, S. F., Reinherz, E. L., and Weiner, H. L. (1985). In vivo activated T lymphocytes in the peripheral blood and cerebrospinal fluid of patients with multiple sclerosis. *N Engl J Med* 312, 1405-1411.

Hatano, R., Ohnuma, K., Yamamoto, J., Dang, N. H., Yamada, T., and Morimoto, C. (2013a). Prevention of acute graft-versus-host disease by humanized anti-CD26 monoclonal antibody. *Br J Haematol* 162, 263-77.

Hatano, R., Ohnuma, K., Otsuka, H., Komiya, E., Taki, I., Iwata, S., Dang, N. H., Okumura, K., and Morimoto, C. (2015). CD26-mediated induction of EGR2 and IL-10 as potential regulatory mechanism for CD26 costimulatory pathway. *J Immunol* 194, 960-972.

Hatano, R., Yamada, T., Matsuoka, S., Iwata, S., Yamazaki, H., Komiya, E., Okamoto, T., Dang, N. H., Ohnuma, K., and Morimoto, C. (2014).

Establishment of monoclonal anti-human CD26 antibodies suitable for immunostaining of formalin-fixed tissue. *Diagn Pathol* 9, 30.

Hatano, R., Ohnuma, K., Yamamoto, J., Dang, N. H., and Morimoto, C. (2013b). CD26-mediated co-stimulation in human $CD8^+$ T cells provokes effector function via pro-inflammatory cytokine production. *Immunology* 138, 165-172.

Havre, P. A., Abe, M., Urasaki, Y., Ohnuma, K., Morimoto, C., and Dang, N. H. (2008). The role of CD26/dipeptidyl peptidase IV in cancer. *Front Biosci* 13, 1634-45.

Hayashi, M., Madokoro, H., Yamada, K., Nishida, H., Morimoto, C., Sakamoto, M., and Yamada, T. (2016). A humanized anti-CD26 monoclonal antibody inhibits cell growth of malignant mesothelioma via retarded G2/M cell cycle transition. *Cancer cell int* 16, 35.

Herrmann, H., Sadovnik, I., Cerny-Reiterer, S., Rulicke, T., Stefanzl, G., Willmann, M., Hoermann, G., Bilban, M., Blatt, K., Herndlhofer, S., Mayerhofer, M., Streubel, B., Sperr, W. R., Holyoake, T. L., Mannhalter, C., and Valent, P. (2014). Dipeptidylpeptidase IV (CD26) defines leukemic stem cells (LSC) in chronic myeloid leukemia. *Blood* 123, 3951-62.

Hildebrandt, M., Rose, M., Ruter, J., Salama, A., Monnikes, H., and Klapp, B. F. (2001). Dipeptidyl peptidase IV (DPIV, CD26) in patients with inflammatory bowel disease. *Scand J Gastroenterol* 36, 1067-1072.

Ho, L., Aytac, U., Stephens, L. C., Ohnuma, K., Mills, G. B., McKee, K. S., Neumann, C., LaPushin, R., Cabanillas, F., Abbruzzese, J. L., Morimoto, C., and Dang, N. H. (2001). *In vitro* and *in vivo* antitumor effect of the anti-CD26 monoclonal antibody 1F7 on human CD30+ anaplastic large cell T-cell lymphoma Karpas 299. *Clin Cancer Res* 7, 2031-40.

Hua, J., Davis, S. P., Hill, J. A., and Yamagata, T. (2015). Diverse Gene Expression in Human Regulatory T Cell Subsets Uncovers Connection between Regulatory T Cell Genes and Suppressive Function. *J Immunol* 195, 3642-3653.

Inamoto, T., Yamada, T., Ohnuma, K., Kina, S., Takahashi, N., Yamochi, T., Inamoto, S., Katsuoka, Y., Hosono, O., Tanaka, H., et al., (2007).

Humanized anti-CD26 monoclonal antibody as a treatment for malignant mesothelioma tumors. *Clin Cancer Res* 13, 4191-200.

Inamoto, T., Yamochi, T., Ohnuma, K., Iwata, S., Kina, S., Inamoto, S., Tachibana, M., Katsuoka, Y., Dang, N. H., and Morimoto, C. (2006). Anti-CD26 monoclonal antibody-mediated G1-S arrest of human renal clear cell carcinoma Caki-2 is associated with retinoblastoma substrate dephosphorylation, cyclin-dependent kinase 2 reduction, $p27^{kip1}$ enhancement, and disruption of binding to the extracellular matrix. *Clin Cancer Res* 12, 3470-7.

Ito, M., Hiramatsu, H., Kobayashi, K., Suzue, K., Kawahata, M., Hioki, K., Ueyama, Y., Koyanagi, Y., Sugamura, K., Tsuji, K., Heike, T., and Nakahata, T. (2002). NOD/SCID/γc^{null} mouse: an excellent recipient mouse model for engraftment of human cells. *Blood* 100, 3175-3182.

Jang, J. H., Baerts, L., Waumans, Y., De Meester, I., Yamada, Y., Limani, P., Gil-Bazo, I., Weder, W., and Jungraithmayr, W. (2015). Suppression of lung metastases by the CD26/DPP4 inhibitor Vildagliptin in mice. *Clin Exp Metastasis* 32, 677-87.

Kameoka, J., Tanaka, T., Nojima, Y., Schlossman, S. F., and Morimoto, C. (1993). Direct association of adenosine deaminase with a T cell activation antigen, CD26. *Science* 261, 466-9.

Kappeler, A., and Mueller, C. (2000). The role of activated cytotoxic T cells in inflammatory bowel disease. *Histol Histopathol* 15, 167-72.

Kim, K. W., Cho, M. L., Kim, H. R., Ju, J. H., Park, M. K., Oh, H. J., Kim, J. S., Park, S. H., Lee, S. H., and Kim, H. Y. (2007). Up-regulation of stromal cell-derived factor 1 (CXCL12) production in rheumatoid synovial fibroblasts through interactions with T lymphocytes: role of interleukin-17 and CD40L-CD40 interaction. *Arthritis Rheum* 56, 1076-86.

Kobayashi, S., Ohnuma, K., Uchiyama, M., Iino, K., Iwata, S., Dang, N. H., and Morimoto, C. (2004). Association of CD26 with CD45RA outside lipid rafts attenuates cord blood T-cell activation. *Blood* 103, 1002-10.

Lam, C. S., Cheung, A. H., Wong, S. K., Wan, T. M., Ng, L., Chow. A. K., Cheng, N. S., Pak, R. C., Li, H. S., Man, J. H., Yau, T. C., Lo, O. S., Poon, J. T., Pang, R. W., and Law, W. L. (2014). Prognostic

significance of CD26 in patients with colorectal cancer. *PLoS One* 9, e98582.

Lenschow, D. J., Zeng, Y., Thistlethwaite, J. R., Montag, A., Brady, W., Gibson, M. G., Linsley, P. S., and Bluestone, J. A. (1992). Long-term survival of xenogeneic pancreatic islet grafts induced by CTLA4Ig. *Science* 257, 789-792.

Lee, J. J., Wang, T. Y., Liu, C. L., Chien, M. N., Chen, M. J., Hsu, Y. C., Leung, C. H., and Cheng, S. P. (2017). Dipeptidyl peptidase IV as a prognostic marker and therapeutic target in papillary thyroid carcinoma. *J Clin Endocrinol Metab* 102, 2930-2940.

Liang, P. I., Yeh, B. W., Li, W. M., Chan, T. C., Chang, I. W., Huang, C. N., Li, C. C., Ke, H. L., Yeh, H. C., Wu, W. J., and Li, C. F. (2017). DPP4/CD26 overexpression in urothelial carcinoma confers an independent prognostic impact and correlates with intrinsic biological aggressiveness. *Oncotarget* 8, 2995-3008.

Liu, L., Yan, M., Zhao, F., Li, J., Ge, C., Geng, Q., Zhu, M., Sun, L., He, X., Li, J., and Yao, M. (2013). CD26/dipeptidyl peptidase IV contributes to tumor metastasis in human lung adenocarcinoma. *Bangladesh J Pharmacol* 8, 198-206.

Lu, G., Hu, Y., Wang, Q., Qi, J., Gao, F., Li, Y., Zhang, Y., Zhang, W., Yuan, Y., Bao, J., Zhang, B., Shi, Y., Yan, J., and Gao, G. F. (2013). Molecular basis of binding between novel human coronavirus MERS-CoV and its receptor CD26. *Nature* 500, 227-31.

Markey, K. A., MacDonald, K. P., and Hill, G. R. (2014). The biology of graft-versus-host disease: experimental systems instructing clinical practice. *Blood* 124, 354-62.

Masuyama, J., Berman, J. S., Cruikshank, W. W., Morimoto, C., and Center, D. M. (1992). Evidence for recent as well as long term activation of T cells migrating through endothelial cell monolayers in vitro. *J Immunol* 148, 1367-74.

Mizokami, A., Eguchi, K., Kawakami, A., Ida, H., Kawabe, Y., Tsukada, T., Aoyagi, T., Maeda, K., Morimoto, C., and Nagataki, S. (1996). Increased population of high fluorescence 1F7 (CD26) antigen on T

cells in synovial fluid of patients with rheumatoid arthritis. *J Rheumatol* 23, 2022-6.

Mo, Y., and Fisher, D. (2016). A review of treatment modalities for Middle East Respiratory Syndrome. *J Antimicrob Chemother* 71, 3340-3350.

Mohd, H. A., Al-Tawfiq, J. A., and Memish, Z. A. (2016). Middle East Respiratory Syndrome Coronavirus (MERS-CoV) origin and animal reservoir. *Virol J* 13, 87.

Morimoto, C., and Schlossman, S. F. (1998). The structure and function of CD26 in the T-cell immune response. *Immunol Rev* 161, 55-70.

Mou, H., Raj, V. S., van Kuppeveld, F. J., Rottier, P. J., Haagmans, B. L., and Bosch, B. J. (2013). The receptor binding domain of the new Middle East respiratory syndrome coronavirus maps to a 231-residue region in the spike protein that efficiently elicits neutralizing antibodies. *J Virol* 87, 9379-83.

Muscat, C., Bertotto, A., Agea, E., Bistoni, O., Ercolani, R., Tognellini, R., Spinozzi, F., Cesarotti, M., and Gerli, R. (1994). Expression and functional role of 1F7 (CD26) antigen on peripheral blood and synovial fluid T cells in rheumatoid arthritis patients. *Clin Exp Immunol* 98, 252-6.

Nakaseko, C., Ozawa, S., Sakaida, E., Sakai, M., Kanda, Y., Oshima, K., Kurokawa, M., Takahashi, S., Ooi, J., Shimizu, T., Yokota, A., Yoshiba, F., Fujimaki, K., Kanamori, H., Sakai, R., Saitoh, T., Sakura, T., Maruta, A., Sakamaki, H., and Okamoto, S. (2011). Incidence, risk factors and outcomes of bronchiolitis obliterans after allogeneic stem cell transplantation. *Int J Hematol* 93, 375-82.

Ohnuma, K., Dang, N. H., and Morimoto, C. (2008a). Revisiting an old acquaintance: CD26 and its molecular mechanisms in T cell function. *Trends Immunol* 29, 295-301.

Ohnuma, K., Hosono, O., Dang, N. H., and Morimoto, C. (2011). Dipeptidyl peptidase in autoimmune pathophysiology. *Adv Clin Chem* 53, 51-84.

Ohnuma, K., and Morimoto, C. (2013). DPP4 (dipeptidyl-peptidase 4). *Atlas Genet Cytogenet Oncol Haematol* 17, 301-312.

Ohnuma, K., Yamochi, T., Uchiyama, M., Nishibashi, K., Yoshikawa, N., Shimizu, N., Iwata, S., Tanaka, H., Dang, N. H., and Morimoto, C. (2004). CD26 up-regulates expression of CD86 on antigen-presenting cells by means of caveolin-1. *Proc Natl Acad Sci USA* 101, 14186-14191.

Ohnuma, K., Yamochi, T., Uchiyama, M., Nishibashi, K., Iwata, S., Hosono, O., Kawasaki, H., Tanaka, H., Dang, N. H., and Morimoto, C. (2005). CD26 mediates dissociation of Tollip and IRAK-1 from caveolin-1 and induces upregulation of CD86 on antigen-presenting cells. *Mol Cell Biol* 25, 7743-7757.

Ohnuma, K., Uchiyama, M., Yamochi, T., Nishibashi, K., Hosono, O., Takahashi, N., Kina, S., Tanaka, H., Lin, X., Dang, N. H., and Morimoto, C. (2007). Caveolin-1 triggers T-cell activation via CD26 in association with CARMA1. *J Biol Chem* 282, 10117-10131.

Ohnuma, K., Hatano, R., Aune, T. M., Otsuka, H., Iwata, S., Dang, N. H., Yamada, T., and Morimoto, C. (2015a). Regulation of pulmonary graft-versus-host disease by IL-26+CD26+CD4 T lymphocytes. *J Immunol* 194, 3697-712.

Ohnuma, K., Haagmans, B. L., Hatano, R., Raj, V .S., Mou, H., Iwata, S., Dang, N. H., Bosch, B. J., and Morimoto, C. (2013). Inhibition of Middle East respiratory syndrome coronavirus infection by anti-CD26 monoclonal antibody. *J Virol* 87, 13892-9.

Ohnuma, K., Hatano, R., Yamazaki, H., Kaneko, Y., Dang, N. H., and Morimoto, C. (2017). CD26-targeted therapy: a new horizon in malignant pleural mesothelioma management. *Horizons in Cancer Research (Nova Science Publishers, Inc.)* 64, Chapter 6, 129-162.

Ohnuma, K., Hatano, R., and Morimoto, C. (2015b). DPP4 in anti-tumor immunity: going beyond the enzyme. *Nat immunol* 16, 791-792.

Ohnuma, K., Ishii, T., Iwata, S., Hosono, O., Kawasaki, H., Uchiyama, M., Tanaka, H., Yamochi, T., Dang, N. H., and Morimoto, C. (2002). G1/S cell cycle arrest provoked in human T cells by antibody to CD26. *Immunology* 107, 325-333.

Ohnuma, K., Inoue, H., Uchiyama, M., Yamochi, T., Hosono, O., Dang, N. H., and Morimoto, C. (2006). T-cell activation via CD26 and caveolin-1 in rheumatoid synovium. *Mod Rheumatol* 16, 3-13.

Ohnuma, K., Takahashi, N., Yamochi, T., Hosono, O., Dang, N. H., and Morimoto, C. (2008b). Role of CD26/dipeptidyl peptidase IV in human T cell activation and function. *Front Biosci* 13, 2299-2310.

Okamoto, T., Iwata, S., Yamazaki, H., Hatano, R., Komiya, E., Dang, N. H., Ohnuma, K., and Morimoto, C. (2014). CD9 Negatively Regulates CD26 Expression and Inhibits CD26-Mediated Enhancement of Invasive Potential of Malignant Mesothelioma Cells. *PLoS One* 9, e86671.

Pang, R., Law, W. L., Chu, A. C., Poon, J. T., Lam, C. S., Chow, A. K., Ng, L., Cheung, L. W., Lan, X. R., Lan, H. Y., Tan, V. P., Yau, T. C., Poon, R. T., and Wong, B. C. (2010). A subpopulation of CD26+ cancer stem cells with metastatic capacity in human colorectal cancer. *Cell Stem Cell* 6, 603-15.

Proost, P., Schutyser, E., Menten, P., Struyf, S., Wuyts, A., Opdenakker, G., Detheux, M., Parmentier, M., Durinx, C., Lambeir, A. M., Neyts, J., Liekens, S., Maudgal, P. C., Billiau, A., and Van Damme, J. (2001). Amino-terminal truncation of CXCR3 agonists impairs receptor signaling and lymphocyte chemotaxis, while preserving antiangiogenic properties. *Blood* 98, 3554-3561.

Raj, V. S., Mou, H., Smits, S. L., Dekkers, D. H., Müller, M. A., Dijkman, R., Muth, D., Demmers, J. A., Zaki, A., Fouchier, R. A., Thiel, V., Drosten, C., Rottier, P. J., Osterhaus, A. D., Bosch, B. J., and Haagmans, B. L. (2013). Dipeptidyl peptidase 4 is a functional receptor for the emerging human coronavirus-EMC. *Nature* 495, 251-254.

Rose, M., Hildebrandt, M., Fliege, H., Seibold, S., Monnikes, H., and Klapp, B. F. (2002). T-cell immune parameters and depression in patients with Crohn's disease. *J Clin Gastroenterol* 34, 40-48.

Rudd, C. E. (2010). T-cell signaling and immunopathologies. *Semin Immunopathol* 32, 91-4.

Rudd, C. E., Taylor, A., and Schneider, H. (2009). CD28 and CTLA-4 coreceptor expression and signal transduction. *Immunol Rev* 229, 12-26.

Saito, K. (1998). Involvement of CD40 ligand-CD40 and CTLA4-B7 pathways in murine acute graft-versus-host disease induced by allogeneic T cells lacking CD28. *J. Immunol* 160, 4225-4231.

Sato, T., Yamochi, T., Yamochi, T., Aytac, U., Ohnuma, K., McKee, K. S., Morimoto, C., and Dang, N. H. (2005). CD26 regulates p38 mitogen-activated protein kinase-dependent phosphorylation of integrin beta1, adhesion to extracellular matrix, and tumorigenicity of T-anaplastic large cell lymphoma Karpas 299. *Cancer Res* 65, 6950-6956.

Shlomchik, W. D. (2007). Graft-versus-host disease. *Nat Rev Immunol* 7, 340-352.

Sromova L, Mareckova H, Sedova L, Balaziova E, Sedo A. (2010). Dipeptidyl peptidase-IV in synovial fluid and in synovial fluid mononuclear cells of patients with rheumatoid arthritis. *Clin Chim Acta* 411, 1046-50.

Shultz, L. D., Brehm, M. A., Garcia-Martinez, J. V., and Greiner, D. L. (2012). Humanized mice for immune system investigation: progress, promise and challenges. *Nat Rev Immunol* 12, 786-98.

Socie, G., and Ritz, J. (2014). Current issues in chronic graft-versus-host disease. *Blood* 124, 374-84.

Stange, T., Kettmann, U., and Holzhausen, H. J. (2000). Immunoelectron microscopic demonstration of the membrane proteases aminopeptidase N/CD13 and dipeptidyl peptidase IV/CD26 in normal and neoplastic renal parenchymal tissues and cells. *Eur J Histochem* 44, 157-64.

Tanaka, S., Murakami, T., Horikawa, H., Sugiura, M., Kawashima, K., and Sugita, T. (1997). Suppression of arthritis by the inhibitors of dipeptidyl peptidase IV. *Int J Immunopharmacol* 19, 15-24.

Tanaka, S., Murakami, T., Nonaka, N., Ohnuki, T., Yamada, M., and Sugita, T. (1998). Anti-arthritic effects of the novel dipeptidyl peptidase IV inhibitors TMC-2A and TSL-225. *Immunopharmacology* 40, 21-6.

Thompson, M. A., Ohnuma, K., Abe, M., Morimoto, C., and Dang, N. H. (2007). CD26/dipeptidyl peptidase IV as a novel therapeutic target for cancer and immune disorders. *Mini Rev Med Chem* 7, 253-73.

Tsirigotis, P., Or, R., Resnick, I. B., and Shapira, M. Y. (2012). Immunotherapeutic approaches to improve graft-versus-tumor effect and reduce graft-versus-host disease. *Immunotherapy* 4, 407-424.

van Boheemen, S., de Graaf, M., Lauber, C., Bestebroer, T. M., Raj, V. S., Zaki, A. M., Osterhaus, A. D., Haagmans, B. L., Gorbalenya, A. E., Snijder, E. J., and Fouchier, R. A. (2012). Genomic characterization of a newly discovered coronavirus associated with acute respiratory distress syndrome in humans. *MBio* 3, pii: e00473-12.

Vincenti, F., Charpentier, B., Vanrenterghem, Y., Rostaing, L., Bresnahan, B., Darji, P., Massari, P., Mondragon-Ramirez, G. A., Agarwal, M., Di Russo, G., Lin, C. S., Garg, P., and Larsen, C. P. (2010). A phase III study of belatacept-based immunosuppression regimens versus cyclosporine in renal transplant recipients (BENEFIT study). *Am J Transplant* 10, 535-546.

Wang, N., Shi, X., Jiang, L., Zhang, S., Wang, D., Tong, P., Guo, D., Fu, L., Cui, Y., Liu, X., Arledge, K. C., Chen, Y. H., Zhang, L., and Wang, X. (2013). Structure of MERS-CoV spike receptor-binding domain complexed with human receptor DPP4. *Cell Res* 23, 986-93.

Warfvinge, R., Geironson, L., Sommarin, M. N. E., Lang, S., Karlsson, C., Roschupkina, T., Stenke, L., Stentoft, J., Olsson-Strömberg, U., Hjorth-Hansen, H., Mustjoki, S., Soneji, S., Richter, J., and Karlsson, G. (2017). Single-cell molecular analysis defines therapy response and immunophenotype of stem cell subpopulations in CML. *Blood* 129, 2384-2394.

Wesley, U. V., Tiwari, S., and Houghton, A. N. (2004). Role for dipeptidyl peptidase IV in tumor suppression of human non small cell lung carcinoma cells. *Int J Cancer* 109, 855-866.

WHO Programmes and Projects. (2017). Emergencies: Middle East resipratory syndrome cornavirus (MERS-CoV). http://www.who.int/emergencies/mers-cov/en/.

Wolf, M., Albrecht, S., and Märki, C. (2008). Proteolytic processing of chemokines: implications in physiological and pathological conditions. *Int J Biochem Cell Biol* 40, 1185-98.

Wu, C. J., and Ritz, J. (2009). Revealing tumor immunity after hematopoietic stem cell transplantation. *Clin Cancer Res* 15, 4515-4517.

Yamada, K., Hayashi, M., Du, W., Ohnuma, K., Sakamoto, M., Morimoto, C., and Yamada, T. (2009). Localization of CD26/DPPIV in nucleus and its nuclear translocation enhanced by anti-CD26 monoclonal antibody with anti-tumor effect. *Cancer cell int* 9, 17.

Yamada, K., Hayashi, M., Madokoro, H., Nishida, H., Du, W., Ohnuma, K., Sakamoto, M., Morimoto, C., and Yamada, T. (2013). Nuclear localization of CD26 induced by a humanized monoclonal antibody inhibits tumor cell growth by modulating of POLR2A transcription. *PLoS One* 8, e62304.

Yamaguchi, U., Nakayama, R., Honda, K., Ichikawa, H., Hasegawa, T., Shitashige, M., Ono, M., Shoji, A., Sakuma, T., Kuwabara, H., Shimada, Y., Sasako, M., Shimoda, T., Kawai, A., Hirohashi, S., and Yamada, T. (2008). Distinct gene expression-defined classes of gastrointestinal stromal tumor. *J Clin Oncol* 26, 4100-8.

Yamamoto, J., Ohnuma, K., Hatano, R., Okamoto, T., Komiya, E., Yamazaki, H., Iwata, S., Dang, N. H., Aoe, K., Kishimoto, T., Yamada, T., and Morimoto, C. (2014). Regulation of somatostatin receptor 4-mediated cytostatic effects by CD26 in malignant pleural mesothelioma. *Br J Cancer* 110, 2232-45.

Yamazaki, H., Naito, M., Ghani, F. I., Dang, N. H., Iwata, S., and Morimoto, C. (2012). Characterization of cancer stem cell properties of CD24 and CD26-positive human malignant mesothelioma cells. *Biochem Biophys Res Commun* 419, 529-536.

Zaki, A. M., van Boheemen, S., Bestebroer, T. M., Osterhaus, A. D., and Fouchier, R. A. (2012). Isolation of a novel coronavirus from a man with pneumonia in Saudi Arabia. *N Engl J Med* 367, 1814-20.

Zeiser, R., and Blazar, B. R. (2016). Preclinical models of acute and chronic graft-versus-host disease: how predictive are they for a successful clinical translation? *Blood* 127, 3117-26.

Zheng, B., Liu, J., Gu, J., Lu, Y., Zhang, W., Li, M., and Lu, H. (2015). A three-gene panel that distinguishes benign from malignant thyroid nodules. *Int J Cancer* 136, 1646-1654.

Zorn, E., Wang, K. S., Hochberg, E. P., Canning, C., Alyea, E. P., Soiffer, R. J., and Ritz, J. (2002). Infusion of $CD4^+$ donor lymphocytes induces the expansion of $CD8^+$ donor T cells with cytolytic activity directed against recipient hematopoietic cells. *Clin Cancer Res* 8, 2052-2060.

Zumla, A., Chan, J. F., Azhar, E. I., Hui, D. S., and Yuen, K. Y. (2016). Coronaviruses - drug discovery and therapeutic options. *Nat Rev Drug Discov* 15, 327-47.

SCH

In: Horizons in Cancer Research. Volume 64 ISBN: 978-1-53610-512-4
Editor: Hiroto S. Watanabe

Chapter 6

CD26-TARGETED THERAPY: A NEW HORIZON IN MALIGNANT PLEURAL MESOTHELIOMA MANAGEMENT

Kei Ohnuma[1,*], MD, PhD, Ryo Hatano[1], PhD, Hiroto Yamazaki[1], MD, PhD, Yutaro Kaneko[2], Nam H. Dang[3], MD, PhD and Chikao Morimoto[1], MD, PhD

[1]Department of Therapy Development and Innovation for Immune Disorders and Cancers, Graduate School of Medicine, Juntendo University, Tokyo, Japan
[2]Y's AC Co., Ltd., Tokyo, Japan
[3]Division of Hematology/Oncology, University of Florida, Gainesville, FL, US

ABSTRACT

Malignant pleural mesothelioma (MPM) is a rare and aggressive neoplasm deriving from the pleural mesothelial lining. More than 80% of cases are related to previous professional asbestos exposure, with its worldwide incidence being expected to increase in the future. Despite the modest clinical benefit of a multimodality treatment approach including

* Corresponding Author Email: kohnuma@juntendo.ac.jp.

surgery, combination chemotherapy and radiation, prognosis remains grim with poor overall survival. For the vast majority of MPM patients ineligible for potentially curative surgery at diagnosis, systemic chemotherapy is the best option to improve survival. The only treatment with level-one level of evidence for improving clinical outcome is the regimen consisting of a platinum doublet with an antifolate. It is possible that standard cytotoxic therapies for MPM have reached a therapeutic plateau, and new approaches based on deregulated pathways and targeted therapies are required to improve survival of MPM patients. We have had a long-standing interest in the role of CD26 in cancer biology and its suitability as a novel therapeutic target in selected neoplasms. Our previous work demonstrated that CD26 is preferentially expressed in MPM cells but not in normal mesothelial cells, and suggested that CD26 expression level correlates with clinical outcomes. More recently, we showed that the CD26-positive population of $CD24^{+}CD9^{+}$ MPM cells exhibits cancer stem cell features. We also reported robust *in vivo* data on the anti-tumor activity of anti-CD26 monoclonal antibody in mouse xenograft models. We herein review significant novel findings and the early clinical development of a CD26-targeted therapy for MPM, advances that can lead to a more hopeful future for MPM patients.

Keywords: malignant pleural mesothelioma, CD26, DPPIV, YS110

INTRODUCTION

Malignant pleural mesothelioma (MPM) is a rare and aggressive neoplasm arising from the pleural mesothelial lining (Kondola et al., 2016), with more than 80% of cases being related to previous occupational asbestos exposure (Myers, 2012; Shersher and Liptay, 2013). Peak incidence of MPM has been reached in the United States, while its incidence is predicted to increase further in the next decades in developing countries where asbestos has not yet been prohibited (Myers, 2012; Shersher and Liptay, 2013). Worldwide, about 80% of mesothelioma deaths occur in ten countries, with Japan, United Sates and United Kingdom being in the top three (van Meerbeeck and Damhuis, 2011; Robinson, 2012). Despite the modest clinical benefit of a multimodality treatment approach including surgery, combination chemotherapy and radiation, prognosis remains grim with poor overall survival (Abdel-Rahman and Kelany, 2015; Maggioni et al., 2016). For the vast majority of MPM patients ineligible for potentially curative surgery at diagnosis, systemic chemotherapy is the best option to improve survival (Kondola et al., 2016).

The only treatment with level-one level of evidence for improving clinical outcome is the regimen consisting of a platinum doublet with an antifolate (Haas and Sterman, 2013). With this combined chemotherapy, patients with good performance status have a median overall survival (OS) of approximately 1 year, and a median progression free survival (PFS) of less than 6 months (van Meerbeeck et al., 2005). There is no standard second line treatment with documented ability to prolong survival. Due to the lack of efficacy of conventional treatments, novel therapeutic strategies are urgently needed to improve outcomes of MPM (Astoul et al., 2012; Haas and Sterman, 2013; Kondola et al., 2016).

Successful treatment of MPM depends on an in-depth understanding of the biology of mesothelioma. Our group has had a long-standing interest in the role of CD26 in cancer biology and its suitability as a novel therapeutic target in selected neoplasms (Thompson et al., 2007; Havre et al., 2008; Ohnuma and Morimoto, 2013). CD26 is a 110-kDa, type II transmembrane glycoprotein with known dipeptidyl peptidase IV (DPPIV, EC 3.4.14.5) activity in its extracellular domain and is capable of cleaving N-terminal dipeptides with either L-proline or L-alanine at the penultimate position (Ohnuma et al., 2008a). CD26 activity is dependent on cell type and the microenvironment factors that can influence its multiple biological roles (Thompson et al., 2007; Ohnuma et al., 2011). Although CD26 expression is enhanced following activation of resting T cells, $CD4^+$ $CD26^{high}$ T cells respond maximally to recall antigens such as tetanus toxoid (Morimoto et al., 1989; Dang et al., 1990c). Cross-linking of CD26 with CD3 by solid-phase immobilized monoclonal antibodies (mAbs) can induce T-cell costimulation and IL-2 production by $CD26^+$ T cells (Dang et al., 1990a; Morimoto and Schlossman, 1998). In addition, anti-CD26 antibody treatment of T cells enhances activation associated with tyrosine phosphorylation of signaling molecules such as CD3ζ and $p56^{lck}$, while its DPPIV enzyme activity is required for CD26-mediated T cell costimulation (Tanaka et al., 1993; Hegen et al., 1997; Ishii et al., 2001). CD26 therefore has an important role in T cell biology and overall immune function (Morimoto and Schlossman, 1998; Ohnuma et al., 2008a).

CD26 is also expressed on various tumors including MPM, renal cell carcinoma (RCC), colorectal cancer, hepatocellular carcinoma, lung cancer, prostate cancer, gastrointestinal stromal tumor, thyroid cancer, and hematologic malignancies such as T-anaplastic large cell lymphoma, T-lymphoblastic lymphoma and T-acute lymphoblastic leukemia (Thompson et al., 2007; Havre et al., 2008; Ohnuma and Morimoto, 2013). In addition to its

expression in cancer cells, CD26 regulates topoisomerase IIα level in hematological malignancies, affecting sensitivity to doxorubicin and etoposide (Yamochi et al., 2005). Moreover, CD26 itself appears to be a novel therapeutic target, and anti-CD26 mAb treatment resulted in both *in vitro* and *in vivo* anti-tumor activity against selected tumor types including MPM (Ho et al., 2001; Inamoto et al., 2006; Inamoto et al., 2007). Our previous work demonstrated that CD26 is preferentially expressed in MPM cells but not in normal mesothelial cells, and suggested that CD26 expression level correlates with clinical outcomes, while being a potential therapeutic target in MPM (Amatya et al., 2011; Aoe et al., 2012). We herein review mainly our significant novel findings and the early clinical development of a CD26-targeted therapy for MPM.

MOLECULAR CHARACTERIZATION OF CD26

In 1979, a large molecular weight complex composed of adenosine deaminase (ADA) activity was found to be an ADA-binding protein (ADBP), also known as adenosine deaminase complexing protein-2 (ADCP2) (Daddona and Kelley, 1979). In 1992, this ADBP or ADCP2 is determined to be identical to CD26, a T-cell activation molecule and a 110-kD glycoprotein that is present also on epithelial cells of various tissues including the liver, kidney, and intestine (Hopsu-Havu and Glenner, 1966; Marguet et al., 1992; Tanaka et al., 1992). The human CD26 cDNA contains a 3,465 base pair (bp) open reading frame that encodes a 766 amino acid protein. The human CD26 amino acid sequence has 85% amino acid identity with the mouse and rat CD26, and 37% amino acid identity with *D. melanogaster* (Marguet et al., 1992; Tanaka et al., 1992). The 5'-flanking region does not contain a TATA box or CAAT box, commonly found in housekeeping genes (Bohm et al., 1995). CD26 does contain a 300 bp G-C rich region with potential binding sites for NF-κB, AP2, or Sp1 (Erickson et al., 2000b). CD26 expression is activated by interferons (IFNs) and retinoic acid in chronic lymphocytic leukemia via Stat1α and the GAS (IFN-γ activaton site) response element (TTCnnnGAA located at bp -35 to -27) in the CD26 promoter (Bauvois et al., 2000). A hepatocyte nuclear factor 1 binding site at position -150 to -131 of the CD26 gene regulates CD26 expression in human intestinal (Caco-2) and hepatic epithelial (HepG2) cell lines (Erickson et al., 1999; Erickson et al., 2000a).

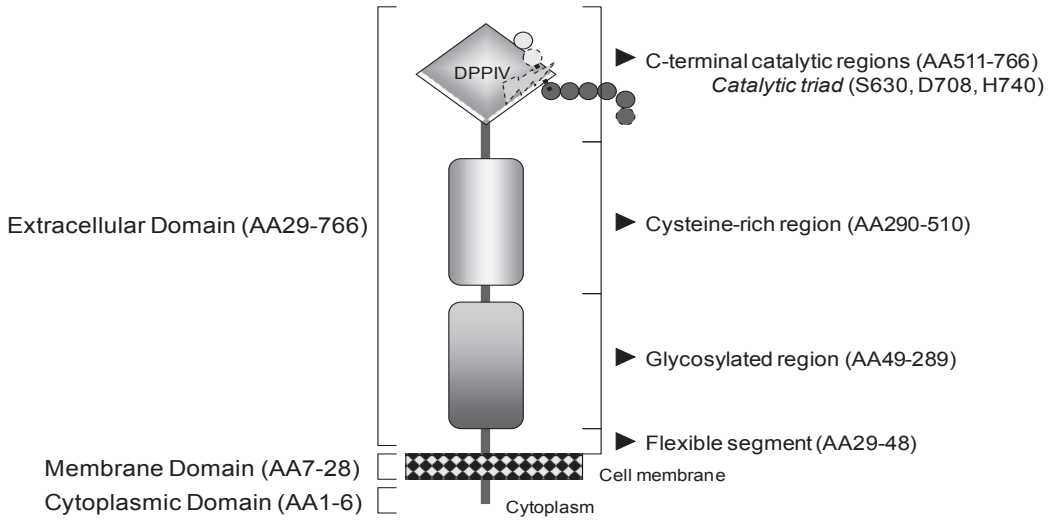

Figure 1. Schematic diagrams of the amino acids of human CD26.
Human CD26 cDNA is composed of 2,301 base pairs, translated to a 766 amino acid protein. DDPIV catalyzes the hydrolysis of N-terminal dipeptides from polypeptides with proline or alanine in the penultimate position. See text for further details.

CD26 is a multifunctional membrane-bound glycoprotein present as a homodimer on the surface of most cell types (Chien et al., 2004; Ohnuma et al., 2008a). Human CD26 is composed of 766 amino acids (Figure 1), including a short cytoplasmic domain of 6 amino acids, a transmembrane region of 24 amino acids, and an extracellular domain with dipeptidyl peptidase activity which selectively removes the N-terminal dipeptide from peptides with proline or alanine at the penultimate position (Heins et al., 1998; Ohnuma et al., 2008a). Analysis of single amino acid point mutations in the β-propeller motif identified Glu205 and Glu206 to be essential for DPPIV enzyme activity, and the central tunnel and α/β-hydrolase domains both participate in DPPIV inhibitor binding (David et al., 1993; Abbott et al., 2000; Rasmussen et al., 2003). CD26/DPPIV was initially considered to cleave peptides only after a proline or alanine residue, but its substrates are now known include hydroxyproline, serine, glycine, valine, threonine, and leucine (Yaron and Naider, 1993; Abbott et al., 2000; Bjelke et al., 2006). CD26 binds to caveolin-1 on antigen presenting cells (APC), and residues 201 to 211 of CD26 along with the serine catalytic site at residue 630, which constitute a pocket structure of CD26/DPPIV, contribute to its binding to the caveolin-1 scaffolding domain (Ohnuma et al., 2004). This region in CD26 contains a caveolin-binding domain ($\Phi X\Phi XXXX\Phi XX\Phi$; Φ and *X* depict aromatic residue and any amino acid, respectively), specifically WVYEEEVFSAY in CD26. These observations strongly support the notion that DPPIV enzyme activity is necessary for CD26-mediated T-cell costimulatory activation, as demonstrated

in our previous work using CD26-targeted mAbs (Tanaka et al., 1993; Morimoto and Schlossman, 1998). Single amino acid point mutation analysis showed that His750 residue is responsible for dimerization (Chien et al., 2004), which is required for T cell costimulation signaling (Ohnuma et al., 2007).

A soluble form of the protein with conserved DPPIV enzyme activity (sCD26 or sDPPIV) is present in the serum and other body fluids, presumably as a result of shedding or secretion from different cell types (Nagatsu et al., 1968; Iwaki-Egawa et al., 1998; Cordero et al., 2009; Rohrborn et al., 2014). The soluble form lacks the transmembrane region and cytoplasmic residues, as it begins at the 39th amino acid residue (Iwaki-Egawa et al., 1998). This form also exists as a dimer and has been detected in seminal fluid as a larger oligomer (>900 kDa) (Iwaki-Egwa et al., 1998). DPPIV enzyme activity is involved in the activation/inactivation of a number of chemokines and cytokines to regulate immune and endocrinological functions as well as cancer cell biology. (De Meester et al., 2000; Thomspn et al., 2007; Havre et al., 2008; Ohnuma et al., 2008a; Ohnuma and Morimoto, 2013). The clinical significance of sCD26 or sDPPIV in MPM patients has been shown in our recent study, which included 80 MPM patients, 79 subjects with past asbestos exposure (SPE), and 134 patients with other benign pleural diseases (OPD) as a control group (Fujimoto et al., 2014). Serum sCD26 levels and sDPPIV enzyme activity in patients with MPM were significantly decreased compared with those in the SPE group. The level of serum sCD26 was significantly decreased in patients with advanced stages of MPM compared with those with earlier stages. The median OS of patients with MPM who had higher DPPIV enzyme activity was significantly longer than that of those with lower DPPIV enzyme activity. The sCD26 levels in the pleural fluid of MPM patients with an epithelioid subtype were significantly increased compared with the OPD cohort. Moreover, DPPIV enzyme activity in the pleural fluid of patients with MPM with an epithelioid subtype was significantly increased compared with that in the OPD cohort. Patients with MPM who had lower specific DPPIV activity, determined as the ratio of DPPIV activity to sCD26 protein quantification, exhibited significantly prolonged survival compared with those with higher specific DPPIV activity. Serum sCD26 and DPPIV enzyme activity appear to be useful biomarkers for differentiating patients with MPM from SPE. In addition, the sCD26 level and DPPIV enzyme activity in pleural fluid appear to be biomarkers in patients with the MPM epithelioid subtype. DPPIV activity in serum or pleural fluid may also be predictive markers for the prognosis of MPM patients (Fujimoto et al., 2014).

CD26 AND IMMUNE FUNCTION

In human peripheral blood, CD26 is found on $CD4^+$ T memory cells and $CD8^+$ effector/memory T cells (Morimoto et al., 1989; Dang et al., 1990c; Hatano et al., 2013). It has been reported that 0-5% of freshly isolated $CD20^+$ B cells do express the CD26 antigen (Buhling et al., 1995). Following stimulation with PMA (phorbol 12-Myristate 13-acetate) or *Streptococcus aureus* protein, the fraction of CD26-positive cells increased to 51% (Morimoto and Schlossman, 1998; Fujimaki et al., 2008). Meanwhile, CD26 is not expressed or is found only at low levels on monocytes of healthy adults (Stohlawetz et al., 1998; Ohnuma et al., 2001). Flow cytometric analysis of dendritic antigen-presenting cells (DC) generated from peripheral blood of normal donors in the presence of granulocyte/macrophage colony-stimulating factor and IL-4 revealed intermediate levels of CD26 expression during a 2-week culture period (Alijagic et al., 1995). Only a small fraction of peripheral NK cells was found to express CD26 (Buhling et al., 1994).

CD26 is a co-stimulatory molecule for T-cell signal transduction. While CD26 expression is enhanced following activation of resting T cells, $CD4^+CD26^{high}$ T cells respond maximally to recall antigens such as tetanus toxoid (Dang et al., 1990c; Morimoto and Schlossman, 1998). Moreover, we have previously reported that effector CD26-mediated costimulatory activity is exerted via its DPPIV enzymatic activity (Tanaka et al., 1993). In addition, $CD4^+$ T cells with *in vitro* transendothelial migratory capacity appear to express high CD26 (Masuyama et al., 1992), and patients with autoimmune diseases such as multiple sclerosis, Grave's disease, and rheumatoid arthritis have been found to have increased numbers of $CD4^+CD26^+$ T cells in inflamed tissues as well as in their peripheral blood, with enhancement of CD26 expression in these autoimmune diseases correlating with disease activity (Ohnuma et al., 2011). Moreover, $CD26^{high}CD8^+$ T cells in humans belong to early effector memory T cells, and $CD26^{high}CD8^+$ T cells exhibit increased expression of granzyme B, TNF-α, IFN-γ and Fas ligand, and exert cytotoxic effect with CD26-mediated costimulation (Hatano et al., 2013).

The cytoplasmic tail of CD26 is responsible for T-cell costimulation induced by anti-CD3 plus caveolin-1 (Ohnuma et al., 2007). Our work found that CARMA1 binds to the cytoplasmic tail of dimeric CD26, and that a PDZ domain in CARMA1 is necessary for binding to CD26 (Ohnuma et al., 2007). Following its phosphorylation, CARMA1 functions as a signaling intermediate downstream of PKCθ (protein kinase θ) and upstream of IKK (IκB kinase) in

the TCR (T cell receptor) signaling transduction pathway, which leads eventually to NF-κB activation. Dimeric CD26, but not monomeric CD26, binds to CARMA1 (Ohnuma et al., 2007). The enzymatic pocket structure of the DPPIV catalytic site is necessary for binding of CD26 to caveolin-1, leading to the upregulation of CD86 expression on APC (Ohnuma et al., 2005). Dimerization of CD26 is therefore not only necessary for binding to caveolin-1, but also serves as a scaffolding structure for the cytoplasmic signaling molecule CARMA1. Overall, CD26 ligation by caveolin-1 on APC recruits CD26-interacting CARMA1 to lipid rafts, resulting in the formation of a CARMA1-Bcl10-MALT1-IKK complex, and this membrane-associated Bcl10 complex then activates IKK through ubiquitination of NEMO (NF-κB essential modulator) (Ohnuma et al., 2008b).

We recently reported that CD3/CD26 costimulation induces the development of a population of human type 1 regulatory T (T_{reg}) cells from $CD4^+$ T cells with high level of IL-10 production and lymphocyte-activation gene 3 (LAG3) expression (Hatano et al., 2015). Other investigators have also reported that the $CD26^+CD39^-$ T_{reg} subset among $CD4^+$ T_{reg} exhibits high level of IL-10 expression (Hua et al., 2015). These findings strongly suggest that a specific subset of $CD26^+$ T cells plays a role in immune checkpoint system, and that the CD26 molecule may be a novel target for a therapeutic approach involving immune checkpoint blockade.

EXPRESSION OF CD26 IN MPM

Our previous work analyzing extracellular matrix interactions and intracellular signaling events demonstrated that the malignant mesothelial cell line JMN expresses CD26 (Dang et al., 1990b). Our recent in-depth studies of CD26 expression in MPM revealed that CD26 is preferentially expressed in MPM cells but not in normal mesothelial cells (Amatya et al., 2011; Aoe et al., 2012). Tissue samples from eighty one epithelioid (49 differentiated and 32 less differentiated), 34 sarcomatoid, 19 biphasic mesothelioma patients and 8 mesothelioma cell lines were examined via immunohistochemistry for membranous and cytoplasmic expression. Cytoplasmic expression of CD26 was observed in all histological types of mesothelioma, being found in 65 of 81 (80%) of epithelioid mesotheliomas, and 17 of 18 (95%) of epithelioid component of biphasic mesothelioma. Meanwhile, membranous expression of CD26 was not found in sarcomatoid mesothelioma or sarcomatoid component

of biphasic mesothelioma (Figure 2). Moreover, 7 out of 8 mesothelioma cell lines (MESO1, MESO4, HMMME, H226, H2452, H28, and H2052), including sarcomatoid types, exhibited CD26 expression, with the MSTO-211H (MSTO) mesothelioma cell line having no expression of CD26 (Amatya et al., 2011). These same 7 mesothelioma cell lines also demonstrated membranous expression of CD26 in cellblock preparation.

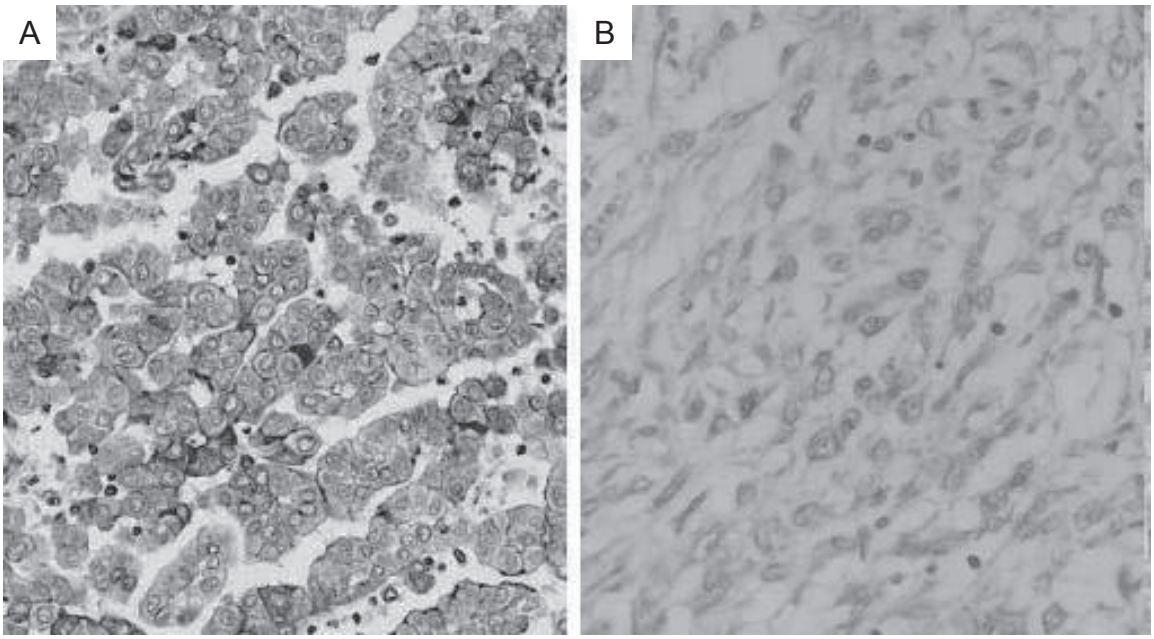

Figure 2. Immunohistochemical staining of MPM with anti-CD26.
Representative serial sections of resected specimens of MPM.
(A) Epithelioid mesothelioma for anti-CD26 immunohistochemistry, showing membranous expression of CD26.
(B) Sarcomatoid mesothelioma for anti-CD26 immunohistochemistry, showing only cytoplasmic expression with inconspicuous membranous expression of CD26.
This figure is reprinted with permission from K Aoe *et al*., *Clin Cancer Res* 18:147-1456, 2012.

CLINICAL RELEVANCE OF CD26 EXPRESSION AND MPM

To explore the role of CD26 for MPM in the clinical setting as a prognostic and therapeutic biomarker, we evaluated 79 MPM cases for CD26 expression and clinical outcome (Aoe et al., 2012). Fifty-eight patients with mesothelioma (73.4%) expressed CD26 on the mesothelioma cell membrane. The majority of patients with epithelioid and biphasic type of mesothelioma expressed CD26 on the mesothelioma cell membrane, whereas none of the patients with the sarcomatoid type did. It should be noted that diffuse staining

for CD26 in the cytoplasm of the mesothelioma cells was observed in all patient samples, even in patients with the sarcomatoid type (Figure 2). We next evaluated the prognostic significance of CD26 membrane expression and other clinicopathological factors in those patients (Aoe et al., 2012). The median survival time (MST) for all mesothelioma patients in the current study was 13.9 months, with the 1-year survival rate being 58.9%. Older age, sarcomatoid histology, advanced stage, absence of extrapleural pneumonectomy (EPP), absence of chemotherapy, and best supportive care were factors associated with poor prognosis. However, no significant relationship between membranous CD26 expression in malignant mesothelioma and survival was observed (MST, 15.0 *vs*. 10.8 months, P=0.1384). Potential relationship between CD26 expression and chemotherapy response and survival was also analyzed. Of the 56 patients treated with chemotherapy, 15 patients had adjuvant chemotherapy, and one patient died prior to evaluation of response to chemotherapy. Therefore, we evaluated the relationship between membranous CD26 expression and response to chemotherapy for 40 patients. The response rate to chemotherapy was marginally associated with membranous CD26 expression (P=0.053). There was a trend toward an association between higher level of CD26 membrane expression and better response to chemotherapy. Univariate analysis of survival time for patients who received chemotherapy demonstrated that membranous CD26 expression was a significant factor associated with better survival (MST, 18.6 *vs*. 10.7 months, P=0.0083). In addition, other clinicopathological factors, including epithelioid histology type, lower stage, EPP or treatment with pemetrexed were also observed to be associated with overall survival. Multivariate analysis for response to chemotherapy showed that epithelioid histology (P=0.016) and EPP (P=0.005) had independent prognostic significance. Membranous CD26 expression showed a hazard ratio of 1.947, but without statistically significant value (P=0.067). Taken together, we concluded that the CD26 molecule is a reliable biomarker for predicting potential therapeutic outcome following chemotherapy (Aoe et al., 2012).

MPM Cancer Cell Biology of CD26

Since CD26 membrane expression on mesothelioma cells appears to be a predictive marker of response to chemotherapy, we next attempted to characterize in details the CD26-positive cells of mesothelioma cell lines. For this purpose we sorted naturally occurring CD26-positive MESO1

mesothelioma cells and subdivided them into CD26-positive and CD26-negative cells. Such cells were subsequently cultured for the indicated days. $CD26^{high}$ cells always exhibited higher level of proliferative activity than CD26-negative cells. Similarly, $CD26^{high}$ cells from other naturally occurring CD26-positive mesothelioma cell lines such as H226 and H28 cell lines consistently had higher level of proliferation than CD26-negative cells from the same cell lines. Moreover, CD26-knockdown of MESO1, JMN and H28 cells resulted in reduced proliferation as compared to wild type CD26-positive MESO-1, JMN and H28 cells, respectively. These results hence suggest that CD26-positive mesothelioma cells have generally robust growth activity (Aoe et al., 2012). Since highly proliferative cells are typically sensitive to chemotherapeutic agents, our present data support the notion that mesothelioma patients with tumors expressing high level of CD26 generally have chemosensitive disease, as discussed in the preceding section.

To extend our previous studies on the relationship between high proliferative activity and invasiveness and high expression level of CD26, we analyzed the signaling events downstream of CD26 in MPM. With the proximal signaling events associated with the cytoplasmic region of CD26 being previously shown in normal human T lymphocytes (Ohnuma et al., 2007), it is conceivable that similar CD26-mediated proximal events may play a role in MPM cell biology. To define the crucial role of the CD26 cytoplasmic region in regulating migratory, invasive or proliferative activity of MPM cells, we used a mutant construct of CD26 in which its cytoplasmic region was replaced with that of human CD10 (CD26-CD10 chimeric receptor), which was shown to abrogate CD26-mediated costimulation in T cells (Ohnuma et al., 2007). CD10, as is the case with CD26, is a type II transmembrane glycoprotein with a relatively short cytoplasmic tail containing signal sequence that has an expected membrane topology similar to CD26 (Ogata et al., 1989; Maguer-Satta et al., 2011). We transfected CD26-negative parental MSTO cells with full-length human CD26 (CD26WT) or CD26-CD10 chimeric receptor (CD26/10Chi) to establish MSTO-CD26WT or MSTO-CD26/10Chi, respectively (Yamamoto et al., 2014). A significant increase in migration was observed in MSTO-CD26WT as compared to MSTO-Mock (vector alone) or MSTO-CD26/10Chi (Figure 3A). Similarly, an increase in invasion was also observed in MSTO-CD26WT as compared to MSTO-Mock or MSTO-CD26/10Chi (Figure 3B). Moreover, a significant increase in colony formation was observed in MSTO-CD26WT as compared

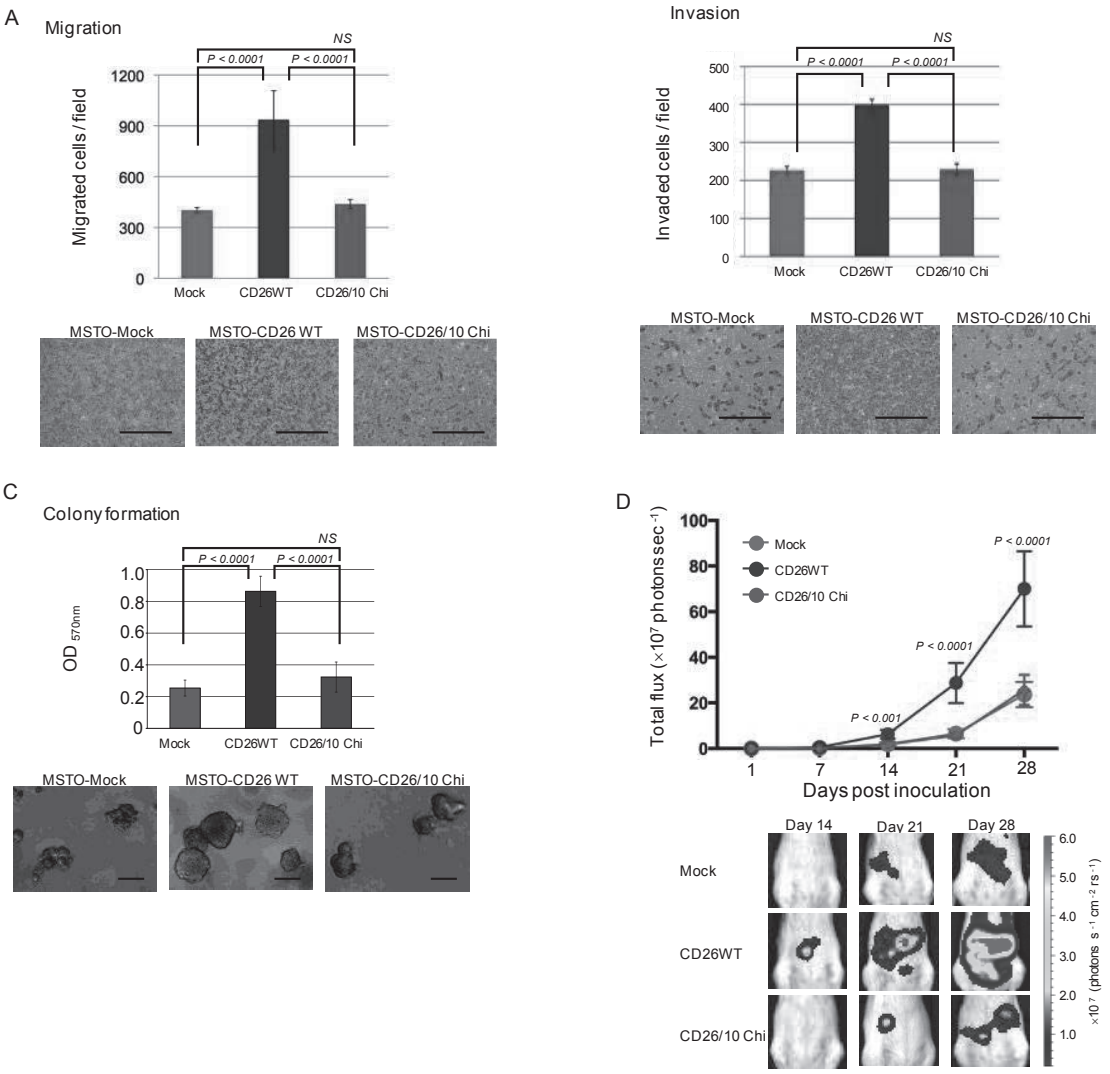

Figure 3. The cytoplasmic region of CD26 is required for cell migration, invasion and colony formation.

(A) Cells were seeded on top of a Boyden chamber. The number of cells that migrated through the uncoated filter in the lower chamber was counted. The mean number of cells per field was determined from 5 fields per filter (mean ± SEM; n=5 experiments with triplicates). A significant increase of MSTO-CD26WT is indicated as $P<0.0001$ (*v.s.* MSTO-Mock or MSTO-CD26/10Chi), as calculated by ANOVA with Tukey-Kramer *post-hoc* test. *NS* denotes 'not significant'. Representative microphotographs of cells migrating through the filter were shown in the lower panels (crystal violet staining). Scale bars indicate 200μm. (B) Cells were seeded on top of Matrigel-coated chamber inserts. The number of cells that invaded through the Matrigel in the lower chamber was counted. The mean number of cells per field was determined from 5 fields per filter (mean ± SEM; n=5 experiments with triplicates). A significant increase of MSTO-CD26WT is indicated as $P<0.0001$ (*v.s.* MSTO-Mock or MSTO-CD26/10Chi), as calculated by ANOVA with Tukey-Kramer *post-hoc* test. *NS* denotes 'not significant'. Representative microphotographs of cells invading through the filter were shown in the lower panels (crystal violet staining). Scale bar indicates 200μm.

(C) Cells were plated in a cell suspension agar matrix between layers of base agar matrix. After 1 week, the agar matrix was solubilized, and cells were stained with MTT solution. Absorbance at 570nm was measured (mean ± SEM; n=5 experiments with triplicates). A significant increase of MSTO-CD26WT is indicated as $P<0.0001$ (*v.s.* MSTO-Mock or MSTO-CD26/10Chi), as calculated by ANOVA with Tukey-Kramer *post-hoc* test. *NS* denotes 'not significant'. Representative microphotographs of cells grown in soft agar just prior to solubilization to indicate cell size and morphology were shown in the lower panels (phase-contrast imaging). Original magnification, ×8. Scale bars indicate 50μm. (D) SCID mice were injected i.p. with 1×10^5 luciferase-expressing MSTO-Mock, MSTO-CD26WT or MSTO-CD26/10Chi cells. Tumor growth was measured by *in vivo* bioluminescence photometry, with imaging data of each cohort being indicated as total flux of photons per second (mean ± SEM; n=20). A significant increase of MSTO-CD26WT is indicated as $P<0.0001$ (*v.s.* MSTO-Mock or MSTO-CD26/10Chi), as calculated by ANOVA with Tukey-Kramer *post-hoc* test. Representative optical bioluminescence imaging of each cohort mice was shown with intensity of luminescence as heat maps in the lower panels. This figure is reprinted with permission from J Yamamoto *et al*., *Br J Cancer* 110:2232-2245, 2014.

to MSTO-Mock or MSTO-CD26/10Chi (Figure 3C). To extend the above *in vitro* results to *in vivo* experimentation, we performed a cell growth assay using xenograft mice. A significant increase in *in vivo* tumor growth was observed with MSTO-CD26WT as compared to MSTO-Mock or MSTO-CD26/10Chi (Figure 3D). These results suggest that the cytoplasmic region of CD26 is important for CD26 function in such MPM biological processes as cell migration, invasion and anchorage-independent cell growth as well as *in vivo* tumor growth, and clinical benefit may be obtained by targeting the CD26 molecule in MPM therapy.

CD26 AND CANCER STEM CELLS IN MPM

The putative existence of cancer stem cell (CSC) is a widely accepted notion at the present time (Reya et al., 2001). CSC proliferates in an asymmetric cell division-like manner, exhibits various stem cell signatures, and is believed to be a potential reason for resistance to therapy. Recent studies have demonstrated the existence of CSCs not only in hematologic malignancies but also solid tumors (Frank et al., 2010; Wang and Dick, 2005). Our recent work identified SP (side-population), CD9, CD24, and CD26 as MPM CSC markers that correlated with primary stem cell signatures (Ghani et al., 2011). SP cells of H226 and H2452 cell lines, and CD24-positive cells of JMN and H226 cell lines proliferated in an asymmetric cell division-like manner. The expression of CD26 closely correlated with that of CD24 in

sarcomatoid type cell lines. In addition, CD9 and CD24-positive cells displayed a higher potential to generate spheroid colony than negative cells in the stem cell medium. Moreover, these marker-positive cells had a clear tendency to generate larger tumors in mouse transplantation assay (Ghani et al., 2011). We further analyzed the CSC properties of CD24 and CD26-positve MPM cells (Yamazaki et al., 2012). We established RNA interference (RNAi) -knockdown MPM cells and found that these markers correlated significantly with chemoresistance, proliferation, and *in vitro* invasion potential. Interestingly, while MESO1 cells expressed both CD24 and CD26, the presence of each of these two markers was correlated with different CSC property. To distinguish intracellular signals downstream of these cell surface antigens, we performed DNA microarray analysis of $CD24^+$ and $CD24^-$ cells of JMN and H226, $CD24^+CD26^+$ and $CD24^-CD26^-$ cells of MESO1, and control-short hairpin RNA (shRNA) and CD24-shRNA cells of MESO1. We found that several genes related to cancer development and stem cell signatures were differentially regulated. Among the genes up-regulated in the positive cells, insulin-like growth factor binding protein 7 (IGFBP7) was commonly up-regulated in all experiments (fold change, JMN-$CD24^+$, 2.5×; H226-$CD24^+$, 3.3×; MESO1-$CD24^+CD26^+$, 27.3×; MESO1-control/CD24-shRNA, 1.9×). In $CD24^+CD26^+$/$CD24^-CD26^-$ cells and control/$CD24^-$ shRNA cells of MESO-1, IGFBP3 (another member of IGFBP, 7.9× and 5.8×, respectively), a cancer gene Wnt5A (5.2× and 6.3×, respectively), and hematopoietic/lymphoid stem cell antigen CD127 (interleukin 7 receptor, IL7R, 10.5× and 3.0×, respectively) were also significantly up-regulated. The microarray data of these genes were further confirmed by RT-PCR in the CD24/CD26-isolated MESO1 cells. Interestingly, expression of IGFBP3 and IGFBP7 was well-correlated with that of CD26, rather than CD24. Meanwhile, expression of Wnt5A and IL7R was correlated with not only CD24 but also CD26 expression, while their expression was completely absent in the $CD24^-CD26^-$ cells. These data suggest that CD24 and CD26 expression correlated with several cancer and stemness genes. In addition to gene expression profiles, our examination of downstream signaling events relating to IGFBP3 and IGFBP7 showed that phosphorylation of ERK (extracellular signal-regulated kinase) by EGF (epidermal growth factor) stimulation was significantly affected by the expression of CD26, but not CD24. Taken together, our data suggest that CD24 and CD26 differentially regulate the CSC potentials of MPM and could be promising targets for CSC-oriented therapy.

ASSOCIATION OF CD26 AND EXTRACELLULAR MATRIX IN MPM

To further explore the molecular mechanisms involved in the highly proliferative activity of CD26-positive MPM cells, we focused on the interaction between CD26 and CD9, and identified as novel markers for cancer stem cells in malignant mesothelioma (Ghani et al., 2011). We found that CD26 and CD9 co-modulated and coprecipitated with each other in the malignant mesothelioma cell lines MESO1 and MSTO (Okamoto et al., 2014). RNAi study revealed that depletion of CD26 led to increased CD9 expression, while depletion of CD9 resulted in increased CD26 expression. Consistent with these findings was the fact that gene transfer of CD26 into CD26-negative MSTO cells reduced CD9 expression. Cell invasion assay showed that overexpression of CD26 or gene depletion of CD9 led to enhanced invasiveness, while CD26 gene depletion resulted in reduced invasive potential. Furthermore, co-precipitation studies demonstrated an association between CD26 and α5β1 integrin, suggesting that this enhanced invasiveness may be partly mediated by α5β1 integrin. Finally, gene depletion of CD9 resulted in elevated protein levels and tyrosine phosphorylation of FAK (focal adhesion kinase) and Cas-L/NEDD9, which are downstream signaling molecules of β1 integrin, while depletion of CD26 led to a reduction in the levels of these molecules. Collectively, our findings suggest that CD26 potentiates tumor cell invasion through its interaction with α5β1 integrin, and CD9 negatively regulates tumor cell invasion by reducing the level of CD26-α5β1 integrin complex through an inverse correlation between CD9 and CD26 expression (Okamoto et al., 2014).

Along with our previous observation that depletion of CD26 by RNAi resulted in the loss of adhesive property, suggesting that CD26 is a binding protein to the extracellular matrix (ECM), the above observation regarding the CD26-α5β1 integrin complex suggests that CD26 regulates the interaction of MPM cells with the ECM via yet-to-be-determined integrin adhesion molecules. More recently, we found that expression of CD26 upregulates periostin secretion by MPM cells, leading to enhanced MPM cell migratory and invasive activity (Komiya et al., 2014). Periostin is a secreted cell adhesion protein of approximately 90kDa, which shares a homology with the insect cell adhesion molecule fasciclin I (FAS1) (Morra and Moch, 2011). Moreover, we showed that upregulation of periostin expression results from the nuclear translocation of the basic helix-loop-helix transcription factor

Twist1, a process that is mediated by CD26-associated activation of Src phosphorylation. In the clinical setting, periostin upregulation has been reported for many cancer types including MPM, and may potentially be a tumor-enhancing factor (Morra and Moch, 2011). Previous work also suggested that periostin expression in MPM cells may be an independent prognostic factor for overall survival (Schramm et al., 2010). Periostin was shown to be not only a marker of epithelial-mesenchymal transition (EMT), but to be itself an inductor of this phenomenon (Yan and Shao, 2006). Our results hence suggest that CD26 expression is associated with EMT via its regulation of periostin.

We demonstrated that CD9 suppresses cell adhesion by inhibiting CD26-α5β1 integrin complex through its negative regulation of CD26 (Okamoto et al., 2014). These observations show that CD26 regulates the interaction of MPM cells with the ECM via the integrin adhesion molecules. Meanwhile, as described above, we have shown that the cytoplasmic 6 amino acid residues of CD26 are required for regulating migratory, invasive or proliferative activity of MPM cells. To define the molecular details involved in the critical role of the CD26 cytoplasmic region, we used affinity purification and LC-MS/MS (liquid chromatography-tandem mass spectrometry) to identify the proteins that are associated with the CD26 cytoplasmic domain (Yamamoto et al., 2014). In these experiments, membrane fractions of MSTO-Mock, MSTO-CD26WT or MSTO-CD26/10Chi were harvested in native conditions and subjected to affinity purification using anti-CD26 mAb. We demonstrated that the cytoplasmic region of CD26 plays a crucial role in MPM tumor biology through its linkage to somatostain receptor 4 (SSTR4) and SHP-2 protein tyrosine kinase in cell membrane lipid rafts, leading to cytostatic effects in MPM cells without direct association of the ECM to CD26 (Yamamoto et al., 2014).

In view of the findings above, we propose that CD26 forms macromolecular complexes in the cell surface of MPM (Figure 4), and plays a pivotal role in the malignant activity of MPM by connecting periostin and ECM to intracellular signaling events. It is therefore conceivable that targeting CD26 may be a novel and effective therapeutic approach for MPM.

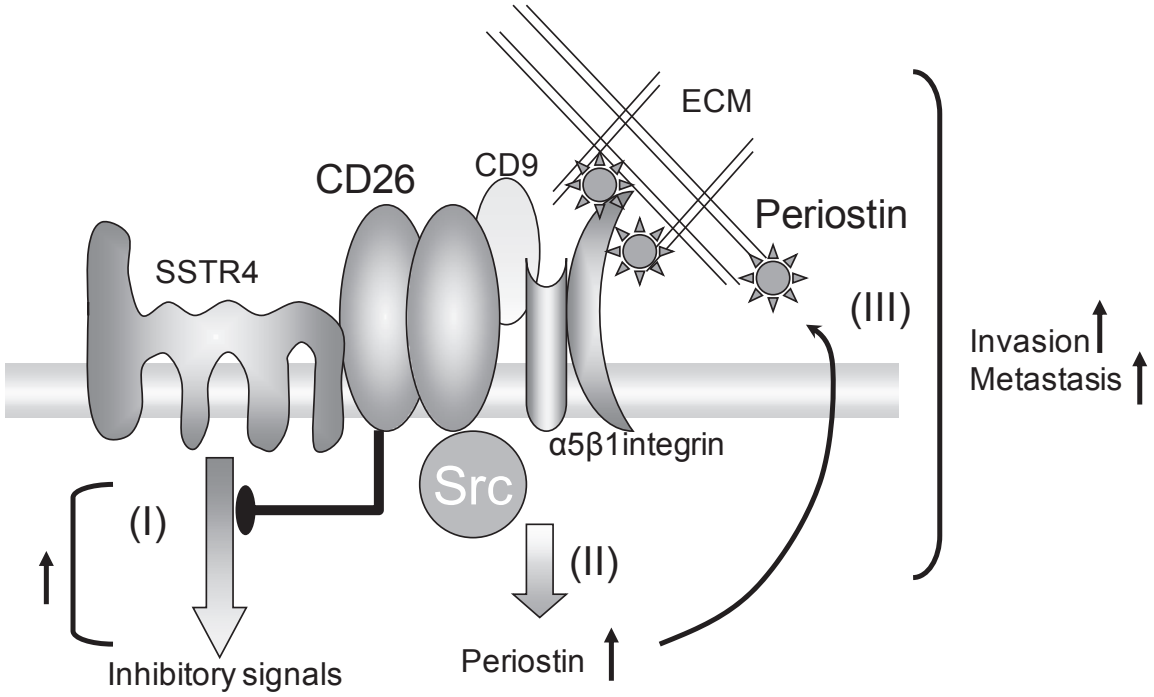

Figure 4. Macromolecular complex associated with cell surface CD26 in MPM.
(I) In CD26-negative MPM cells, SSTR4 mediated inhibitory signaling to suppress cell proliferation and motility. In contrast, by locking the signaling domain of SSTR4 with CD26 association, SSTR4-mediated anti-tumor effects were abrogated, leading to increased cell proliferation and motility in CD26-positive MPM cells.
(II) In addition, CD26 regulated extracellular matrix (ECM)-associated tumor cell behavior in association with integrins and periostin-ECM complex. CD9 suppressed cell invasion and migration by inhibiting the formation of CD26-α5β1 integrin complex. Moreover, expression of CD26 upregulated periostin secretion by MPM cells, leading to enhanced MPM cell migratory and invasive activity. Moreover, we showed that upregulation of periostin expression resulted from the nuclear translocation of the basic helix-loop-helix transcription factor Twist1, a process that was mediated by CD26-associated activation of Src phosphorylation.
(III) Periostin is a secreted cell adhesion protein. The N-terminal region regulates cellular functions by binding to integrins at the plasma membrane of the cells through cell adhesion domain. The C-terminal region of the protein regulates cell–matrix organization and interaction by binding such ECM proteins, leading to increased MPM cell motility. CD26 molecule in MPM plays a pivotal role in connecting ECM to intracellular signaling events associated with cell proliferation and motility.

Preclinical Proof-of-Concept (POC) Study of Anti-CD26 mAb Therapy for MPM

As described in the preceding sections, CD26/DPPIV is expressed at a high level on the surface of malignant mesothelioma cells, but not on cells

derived from normal mesothelial cells. These intriguing findings propelled our development of CD26-targeted therapy for MPM. For this purpose, we had developed a novel humanized anti-CD26 mAb, namely YS110. YS110 is a recombinant DNA-derived humanized mAb that selectively binds with high affinity to the extracellular domain of CD26. The antibody is an $IgG_1\kappa$ with a molecular weight of 144 kDa and was humanized via an *in silico* design based on the amino acid sequence of anti-human CD26 murine mAb (14D10), which inhibited tumor cell growth, migration and invasion, and enhanced survival of mouse xenograft models (Inamoto et al., 2006). YS110 is produced by fermentation in CHO mammalian cell suspension culture with the Glutamine Synthetase Expression System. *In vitro* pharmacologic evaluation of YS110 demonstrated its selective binding to human CD26 on a number of human cancer cell lines and tissues, with no apparent effect on immune activation and no inhibition of DPPIV activity, while exhibiting direct cytotoxic effect on certain human CD26-positive cancer cell lines. Moreover, our *in vitro* data indicated that YS110 induces cell lysis of MPM cells via antibody-dependent cell-mediated cytotoxicity (ADCC) in addition to its direct anti-tumor effect via cyclin-dependent kinase inhibitor (CDKI) $p27^{kip1}$ and $p21^{cip1}$ accumulation (Inamoto et al., 2007; Hayashi et al., 2016). *In vivo* experiments with mouse xenograft models involving human MPM cells demonstrated that YS110 treatment drastically inhibits tumor growth in tumor-bearing mice and reduces formation of metastases, resulting in enhanced survival (Inamoto et al., 2007; Okamoto et al., 2014; Yamamoto et al., 2014). Our data strongly suggest that YS110 may have potential clinical use as a novel cancer therapeutic agent for CD26-positive malignant mesothelioma.

FIRST-IN-HUMAN PHASE I CLINICAL TRIAL OF YS110 FOR MPM

In the POC studies using preclinical models, *in vivo* administration of 14D10 or YS110 resulted in inhibition of tumor cell growth, migration and invasion, and enhanced survival of mouse xenograft models inoculated with RCC or MPM (Inamoto et al., 2006; Inamoto et al., 2007; Okamoto et al., 2014; Yamamoto et al., 2014). In addition to our robust *in vitro* and *in vivo* data on antibody-mediated dose-dependent tumor growth inhibition, YS110 exhibited excellent safety and pharmacological profiles in non-human primate models using single and repeated increasing intravenous doses. Considering

the lack of T cell proliferation and cytokine production *in vitro*, YS110 was therefore considered not to have an agonistic nor activating effect on human CD26-positive lymphocytes. Other key safety findings were obtained from studies involving cymologus monkeys which express YS110-reactive CD26 molecules, with similar tissue distribution profiles and expression levels to human CD26. We therefore conducted the first-in-human (FIH) clinical trial of YS110 for patients with MPM and other CD26-positive solid tumors (Angevin et al., 2015).

Thirty-three heavily pre-treated patients with CD26-positive cancers including 22 malignant mesothelioma, 10 RCC and 1 urothelial carcinoma underwent YS110 administration. A total of 232 infusions (median 3 [range 1-30]) of YS110 were administered across 6 dose levels ranging from 0.1 to 6 mg/kg. Maximum tolerated dose (MTD) was not reached and 2 dose limiting toxicities (DLTs) (1 patient with grade 3 anaphylactic reaction at 1 mg/kg and 1 patient with grade 3 allergic reaction at 2 mg/kg) were reported with complete resolution following dose omission. Subsequent use of systemic steroid prophylaxis and exclusion of patients with significant allergy histories improved safety profile. No dose-dependent adverse events were observed. Blood exposure pharmacokinetics parameters (AUC and C_{max}) increased in proportion with the dose. Cytokines and immunophenotyping assays indicated CD26 target modulation with no occurrence of infectious nor autoimmune disease complications. These results demonstrated that YS110 is tolerable in human subjects.

A secondary objective of this FIH study was to evaluate the potential antitumor activity of YS110 according to RECIST 1.0 criteria (or modified RECIST criteria for mesothelioma). No objective response was achieved in any of the treated patients. However, stable disease as the best overall response was observed in 13 out of the 26 valuable patients on Day 43 of the first cycle (1 at 0.1 mg/kg, 2 at 0.4 mg/kg, 7 at 2.0 mg/kg, 1 at 4.0 mg/kg and 2 at 6.0 mg/kg). Prolonged stabilization was observed in 9 out of 13 stable disease patients who have received a total of 161 (6 to 30) infusions with a median PFS of 32 weeks (12 – 57 weeks). This FIH study conclusively demonstrated that YS110 exhibits a favorable safety profile and substantial clinical activity in heavily pretreated CD26-positive MPM patients who had previously progressed on conventional standard chemotherapies (Angevin et al., 2015).

DPPIV Enzyme Activity and Efficacy of YS110 in MPM

The FIH clinical study of YS110 revealed that an increase in YS110 infusion dose was associated with decreased serum sCD26 level, particularly in cohorts 4-6 (2.0 to 6.0mg/kg), with an approximately 80% decrease in sCD26 level (Angevin et al., 2015). Moreover, since sCD26 level reflects DPPIV enzyme activity in sera (Durinx et al., 2000), similar reduction in DPPIV enzyme activity was observed, again particularly in patients in cohorts 4-6. Although DPPIV inhibitors are clinically used as oral hypoglycemic agents (Drucker and Nauck, 2006), hypoglycemia was not observed during YS110 administration. Of note is the fact that greater than 80% inhibition of serum DPPIV activity was obtained 24 hours after oral administration of clinically available DPPIV inhibitors (drug information published by manufacturers of sitagliptin, vildagliptin, saxagliptin and *etc*.), a level of inhibition comparable to that seen in patients treated with YS110. Our current data would therefore indicate that YS110 therapy is tolerable in the clinical setting.

Recent work has demonstrated the functional role of DPPIV-mediated post-translational modification of chemokines in regulating tumor immunity through its interaction with its substrate CXCL10 (Barreira da Silva et al., 2015). Barreira de Silvia *et al*. use *in vivo* tumor-transplant models to show that DPPIV inhibition reduces tumor growth through the preservation of bioactive CXCL10 in the tumor microenvironment (TME). In the normal physiological state, CXCL10 is rapidly degraded by DPPIV, resulting in decreased recruitment and migration of $CXCR3^+$ T cells into the TME (Figure 5) (Ohnuma et al., 2015). CXCR3 has been shown to be a functional receptor for CXCL10 (Proost et al., 2001). In contrast, DPPIV inhibition enhances tumor rejection by preserving the full-length biologically active form of CXCL10, leading to increased trafficking of $CXCR3^+$ T cells into the TME (Figure 5) (Ohnuma et al., 2015). This anti-tumor response is potentiated in combination with other anti-tumor immunotherapeutic approaches including CpG adjuvant therapy, adoptive T cell transfer therapy and checkpoint blockade therapy (anti-CTLA-4 and anti-PD-1) (Barreira da Silva et al., 2015). In view of these recent findings, data from our current trial showing that serum DPPIV activity was decreased following treatment with YS110 in a dose-dependent manner would suggest that anti-tumor activity via DPPIV inhibition

may constitute yet another mechanism of action for the anti-tumor activity of YS110.

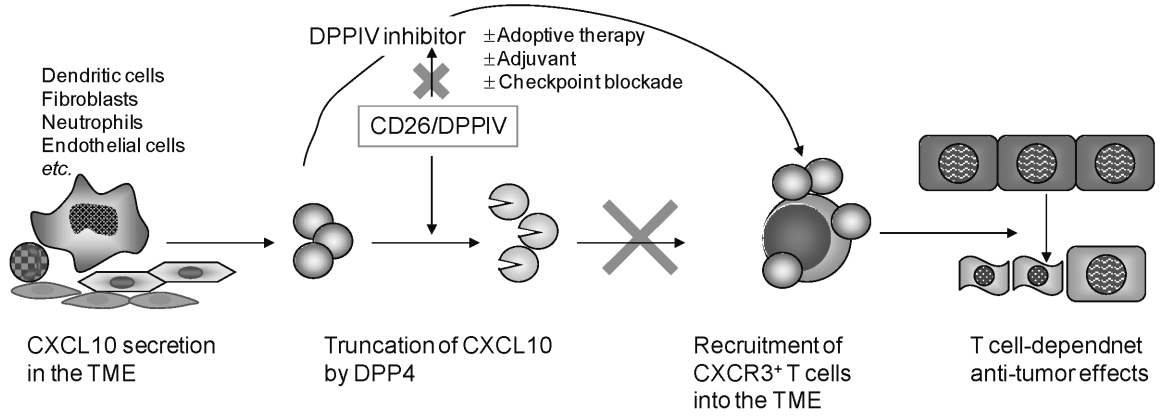

Figure 5. DPPIV inhibition suppresses truncation of its ligand CXCL10, leading to recruitment of $CXCR3^+$ T cells into tumor parenchyma.
In vivo tumor-transplant models showed that DPPIV inhibition reduced tumor growth through the preservation of bioactive CXCL10 in the tumor microenvironment (TME). In the normal physiological state, CXCL10 was rapidly degraded by CD26/DPPIV, resulting in decreased recruitment and migration of $CXCR3^+$ T cells into the tumor parenchyma. In contrast, DPPIV inhibition enhanced tumor rejection by preserving the full-length biologically active form of CXCL10, leading to increased trafficking of $CXCR3^+$ T cells into the tumor parenchyma. This anti-tumor response was potentiated in combination with other anti-tumor immunotherapeutic approaches including CpG adjuvant therapy, adoptive T cell transfer therapy and checkpoint blockade therapy such as anti-CTLA-4 and anti-PD-1.
This figure is reproduced with permission from K Ohnuma *et al.*, *Nat Immunol* 16:791-792, 2015.

MECHANISMS OF ACTION OF YS110 IN MPM

We previously showed that depletion of CD26 by RNAi results in the loss of adhesive property, suggesting that CD26 is a binding protein to the ECM (Inamoto et al., 2007). Moreover, our *in vitro* data indicate that YS110 induces cell lysis of MPM cells via ADCC in addition to its direct anti-tumor effect via CKDI $p27^{kip1}$ accumulation (Inamoto et al., 2007). More recently, we evaluated the direct anti-tumor effect of YS110 against the MPM cell lines H2452 and JMN, and investigated its effects on cell cycle and on the cell cycle regulator molecules (Hayashi et al., 2016). YS110 suppressed the proliferation of H2452 cells by approximately 20% in 48 hours of incubation. Cell cycle analysis demonstrated that the percentage of cells in G2/M phase increased by

8.0% on average following YS110 treatment; in addition, level of the cell cycle regulator $p21^{cip1}$ was increased and cyclin B1 was decreased after YS110 treatment. Inhibitory phosphorylation of both cdc2 (Tyr15) and cdc25C (Ser216) was elevated. Furthermore, activating phosphorylation of p38 MAPK (Thr180/Tyr182) and ERK1/2 (Thr202/Tyr204) was augmented following 24 hours of YS110 treatment. In addition, we investigated the synergistic effects of YS110 and the anti-tumor agent pemetrexed on selected MPM cell lines in both *in vitro* and *in vivo* studies. Pemetrexed rapidly induced CD26 expression on cell surface, and treatment with both YS110 and pemetrexed inhibited *in vivo* tumor growth accompanied by a synergistic reduction in the MIB-1 index.

We also demonstrated that treatment with YS110, which inhibited cancer cell growth, induced nuclear translocation of both cell-surface CD26 and YS110 (Yamada et al., 2009; Yamada et al., 2013). In response to YS110 treatment, CD26 was translocated into the nucleus via caveolin-dependent endocytosis, and interacted with a genomic flanking region of the *POLR2A* gene, a component of RNA polymerase II. This interaction consequently led to transcriptional repression of the *POLR2A* gene, resulting in retarded cancer cell proliferation. Furthermore, impaired nuclear transport of CD26 reversed the *POLR2A* repression induced by YS110 treatment. These findings reveal that nuclear CD26 functions in the regulation of gene expression and tumor growth, while yet another novel mechanism of action of anti-CD26 mAb therapy may involve the regulation of inducible traffic of surface CD26 molecules into the cell nucleus.

Taken together, we summarize the mechanisms of action of YS110 in MPM as follows; (i) a direct cytotoxic effect on certain human CD26-positive cancer cell lines (ADCC), (ii) a direct anti-tumor effect through the induction of cell cycle arrest by induction of $p27^{kip1}$ and $p21^{cip1}$ expression, (iii) following internalization of the CD26-YS110 complexes, an inhibition of invasion and migration of tumor cells by decreased binding to the collagen/fibronectin microenvironment matrix, and (iv) the nuclear translocation of CD26 molecules by internalization of the CD26-YS110 complexes to inhibit proliferation of MPM cells via suppression of *POLR2A* gene expression.

COMPANION DIAGNOSTICS FOR CD26-TARGETING THERAPY

The development of companion diagnostic agents to be used in conjunction with the appropriate therapeutic modalities is essential to maximize therapeutic effectiveness while minimizing associated toxicities. Detection of tumor CD26 expression is critical to determining potential eligibility for treatment with YS110, and it is also important to determine whether CD26 expression on tumors or lymphocytes is affected by anti-CD26 mAb therapy. Immunohistochemical staining of CD26 with the many anti-CD26 mAbs previously developed in our laboratory did not reveal an anti-CD26 mAb that can clearly detect the denatured CD26 molecule in formalin-fixed paraffin-embedded tissues (Dong et al., 1998; Hatano et al., 2014). Meanwhile, testing of several commercially available anti-CD26 mAbs designated as research reagents for immunohistochemical staining indicated that these mAbs could stain the denatured CD26 in formalin-fixed tissues, but not with sufficient clarity. On the other hand, our testing of commercially available anti-CD26 polyclonal antibodies (pAbs) showed that these pAbs exhibited reliable staining pattern and intensity (Amatya et al., 2011; Yamada et al., 2013). However, the disadvantage of pAbs is the potential lot-to-lot variability in staining pattern and intensity, which makes pAbs not the ideal reagents for diagnostic testing of patient specimens in the clinical setting, where consistency and uniformity are required. For this purpose, we recently developed novel anti-human CD26 mAbs that can be used as companion diagnostic reagents suitable for immunohistochemical staining of CD26 in formalin-fixed tissue sections with reliable clarity and intensity (Hatano et al., 2014). Since these mAbs display no cross-reactivity with the therapeutic humanized anti-CD26 mAb, they may be suitable for assays analyzing CD26 expression during or following treatment with the humanized anti-CD26 mAb YS110, with important implications in the clinical setting.

CONCLUSION

While the incidence of MPM continues to increase worldwide, standard chemotherapy does not lead to significant increase in survival. Our increased understanding of the biology and novel therapeutic targets of MPM will pave the way for better treatment options in the future.

Our FIH study showed that YS110 therapy is generally well-tolerated with preliminary evidence of activity in patients with advanced/refractory CD26-expresing cancers including MPM. Our findings also suggest that further clinical development of YS110 such as its use as part of combination therapies with other antineoplastic agents is warranted.

ACKNOWLEDGMENTS

This study was supported in part by a grant of the Ministry of Education, Science, Sports and Culture, Japan (K.O. and C.M.), a grant of the Ministry of Health, Labour, and Welfare, Japan (C.M.) and a Grant-in-Aid (S1311011) from the Foundation of Strategic Research Projects in Private Universities from the Ministry of Education, Culture, Sports, Science, and Technology, Japan (K.O. and C.M.).

REFERENCES

Abbott, C.A., Yu, D.M., Woollatt, E., Sutherland, G.R., McCaughan, G.W., Gorrell, M.D. (2000). Cloning, expression and chromosomal localization of a novel human dipeptidyl peptidase (DPP) IV homolog, DPP8. *FEBS J.* 267, 6140-6150.

Abdel-Rahman, O., Kelany, M. (2015). Systemic therapy options for malignant pleural mesothelioma beyond first-line therapy: a systematic review. *Expert Rev. Respir. Med*. 9, 533-549.

Alijagic, S., Moller, P., Artuc, M., Jurgovsky, K., Czarnetzki, B.M., Schadendorf, D. (1995). Dendritic cells generated from peripheral blood transfected with human tyrosinase induce specific T cell activation. *Eur. J. Immunol.* 25, 3100-3107.

Amatya, V.J., Takeshima, Y., Kushitani, K., Yamada, T., Morimoto, C., Inai, K. (2011). Overexpression of CD26/DPPIV in mesothelioma tissue and mesothelioma cell lines. *Oncol. Rep.* 26, 1369-1375.

Angevin, E., Isambert, N., Trillet-Lenoir, V.T., You, B., Alexandre, J., Zalcman, G., Viehl, P., Farace, F., Valleix, F., Podoll, T., Kuramochi, K., Miyashita, I., Hosono, O., Dang, N.H., Ohnuma, K., Yamada, T., Kaneko, Y., Morimoto, C. (2015). First-in-human phase I administration of YS110, a monoclonal antibody directed against the CD26 immunostimulatory

molecule in advanced cancer patients. *J. Clin. Oncol.* 33, supple; abstr 2519.

Aoe, K., Amatya, V.J., Fujimoto, N., Ohnuma, K., Hosono, O., Hiraki, A., Fujii, M., Yamada, T., Dang, N.H., Takeshima, Y., Inai, K., Kishimoto, T, Morimoto, C. (2012). CD26 overexpression is associated with prolonged survival and enhanced chemosensitivity in malignant pleural mesothelioma. *Clin. Cancer Res.* 18, 1447-1456.

Astoul, P., Roca, E., Galateau-Salle, F., Scherpereel, A. (2012). Malignant pleural mesothelioma: from the bench to the bedside. *Respiration* 83, 481-493.

Barreira da Silva, R., Laird, M.E., Yatim, N., Fiette, L., Ingersoll, M.A., Albert, M.L. (2015). Dipeptidylpeptidase 4 inhibition enhances lymphocyte trafficking, improving both naturally occurring tumor immunity and immunotherapy. *Nat. Immunol.* 16, 850-858.

Bauvois, B., Djavaheri-Mergny, M., Rouillard, D., Dumont, J., Wietzerbin, J. (2000). Regulation of CD26/DPPIV gene expression by interferons and retinoic acid in tumor B cells. *Oncogene* 19, 265-272.

Bjelke, J.R., Kanstrup, A.B., Rasmussen, H.B. (2006). Selectivity among dipeptidyl peptidases of the S9b family. *Cell. Mol. Biol.* 52, 3-7.

Bohm, S.K., Gum, J.R., Jr., Erickson, R.H., Hicks, J.W., Kim, Y.S. (1995). Human dipeptidyl peptidase IV gene promoter: tissue-specific regulation from a TATA-less GC-rich sequence characteristic of a housekeeping gene promoter. *Biochem. J.* 311, 835-843.

Buhling, F., Junker, U., Reinhold, D., Neubert, K., Jager, L., Ansorge, S. (1995). Functional role of CD26 on human B lymphocytes. *Immunol. Lett.* 45, 47-51.

Buhling, F., Kunz, D., Reinhold, D., Ulmer, A.J., Ernst, M., Flad, H.D., Ansorge, S. (1994). Expression and functional role of dipeptidyl peptidase IV (CD26) on human natural killer cells. *Nat. Immun*. 13, 270-279.

Chien, C.H., Huang, L.H., Chou, C.Y., Chen, Y.S., Han, Y.S., Chang, G.G., Liang, P.H., Chen, X. (2004). One site mutation disrupts dimer formation in human DPP-IV proteins. *J. Biol. Chem.* 279, 52338-52345.

Cordero, O.J., Salgado, F.J., Nogueira, M. (2009). On the origin of serum CD26 and its altered concentration in cancer patients. *Cancer Immunol. Immunother*. 58, 1723-1747.

Daddona, P.E., Kelley, W.N. (1979). Human adenosine deaminase. Stoichiometry of the adenosine deaminase-binding protein complex. *Biochim. Biophys. Acta*. 580, 302-311.

Dang, N.H., Torimoto, Y., Deusch, K., Schlossman, S.F., Morimoto, C. (1990a). Comitogenic effect of solid-phase immobilized anti-1F7 on human CD4 T cell activation via CD3 and CD2 pathways. *J. Immunol.* 144, 4092-4100.

Dang, N.H., Torimoto, Y., Schlossman, S.F., Morimoto, C. (1990b). Human CD4 helper T cell activation: functional involvement of two distinct collagen receptors, 1F7 and VLA integrin family. *J. Exp. Med.* 172, 649-652.

Dang, N.H., Torimoto, Y., Sugita, K., Daley, J.F., Schow, P., Prado, C., Schlossman, S.F., Morimoto, C. (1990c). Cell surface modulation of CD26 by anti-1F7 monoclonal antibody. Analysis of surface expression and human T cell activation. *J. Immunol.* 145, 3963-3971.

David, F., Bernard, A.M., Pierres, M., Marguet, D. (1993). Identification of serine 624, aspartic acid 702, and histidine 734 as the catalytic triad residues of mouse dipeptidyl-peptidase IV (CD26). A member of a novel family of nonclassical serine hydrolases. *J. Biol. Chem.* 268, 17247-17252.

De Meester, I., Durinx, C., Bal, G., Proost, P., Struyf, S., Goossens, F., Augustyns, K., Scharpe, S. (2000). Natural substrates of dipeptidyl peptidase IV. *Adv. Exp. Med. Biol*. 477, 67-87.

Dong, R.P., Tachibana, K., Hegen, M., Scharpe, S., Cho, D., Schlossman, S.F., Morimoto, C. (1998). Correlation of the epitopes defined by anti-CD26 mAbs and CD26 function. *Mol. Immunol.* 35, 13-21.

Drucker, D.J., Nauck, M.A. (2006). The incretin system: glucagon-like peptide-1 receptor agonists and dipeptidyl peptidase-4 inhibitors in type 2 diabetes. *Lancet* 368, 1696-1705.

Durinx, C., Lambeir, A.M., Bosmans, E., Falmagne, J.B., Berghmans, R., Haemers, A., Scharpe, S., De Meester, I. (2000). Molecular characterization of dipeptidyl peptidase activity in serum: soluble CD26/dipeptidyl peptidase IV is responsible for the release of X-Pro dipeptides. *FEBS J.* 267, 5608-5613.

Erickson, R.H., Gum, J.R., Lotterman, C.D., Hicks, J.W., Lai, R.S., Kim, Y.S. (1999). Regulation of the gene for human dipeptidyl peptidase IV by hepatocyte nuclear factor 1α. *Biochem. J.* 338, 91-97.

Erickson, R.H., Lai, R.S., Kim, Y.S. (2000a). Role of hepatocyte nuclear factor 1α and 1β in the transcriptional regulation of human dipeptidyl peptidase IV during differentiation of Caco-2 cells. *Biochem. Biophys. Res. Commun*. 270, 235-239.

Erickson, R.H., Lai, R.S., Lotterman, C.D., Kim, Y.S. (2000b). Identification of upstream stimulatory factor as an activator of the human dipeptidyl peptidase IV gene in Caco-2 cells. *Gene* 258, 77-84.

Frank, N.Y., Schatton, T., Frank, M.H. (2010). The therapeutic promise of the cancer stem cell concept. *J. Clin. Invest*. 120, 41-50.

Fujimaki, W., Takahashi, N., Ohnuma, K., Nagatsu, M., Kurosawa, H., Yoshida, S., Dang, N.H., Uchiyama, T., Morimoto, C. (2008). Comparative study of regulatory T cell function of human CD25CD4 T cells from thymocytes, cord blood, and adult peripheral blood. *Clin. Dev. Immunol.* 2008, 305859.

Fujimoto, N., Ohnuma, K., Aoe, K., Hosono, O., Yamada, T., Kishimoto, T., Morimoto, C. (2014). Clinical significance of soluble CD26 in malignant pleural mesothelioma. *PLoS ONE* 9, e115647.

Ghani, F.I., Yamazaki, H., Iwata, S., Okamoto, T., Aoe, K., Okabe, K., Mimura, Y., Fujimoto, N., Kishimoto, T., Yamada, T., Xu, C.W., Morimoto, C. (2011). Identification of cancer stem cell markers in human malignant mesothelioma cells. *Biochem. Biophys. Res. Commun*. 404, 735-742.

Haas, A.R., Sterman, D.H. (2013). Malignant pleural mesothelioma: update on treatment options with a focus on novel therapies. *Clin. Chest Med.* 34, 99-111.

Hatano, R., Ohnuma, K., Otsuka, H., Komiya, E., Taki, I., Iwata, S., Dang, N.H., Okumura, K., Morimoto, C. (2015). CD26-mediated induction of EGR2 and IL-10 as potential regulatory mechanism for CD26 costimulatory pathway. *J. Immunol*.194, 960-972.

Hatano, R., Ohnuma, K., Yamamoto, J., Dang, N.H., Morimoto, C. (2013). CD26-mediated co-stimulation in human $CD8^+$ T cells provokes effector function via pro-inflammatory cytokine production. *Immunology* 138, 165-172.

Hatano, R., Yamada, T., Matsuoka, S., Iwata, S., Yamazaki, H., Komiya, E., Okamoto, T., Dang, N.H., Ohnuma, K., Morimoto, C. (2014). Establishment of monoclonal anti-human CD26 antibodies suitable for immunostaining of formalin-fixed tissue. *Diagn. Pathol*. 9, 30.

Havre, P.A., Abe, M., Urasaki, Y., Ohnuma, K., Morimoto, C., Dang, N.H. (2008). The role of CD26/dipeptidyl peptidase IV in cancer. *Front. Biosci*. 13, 1634-1645.

Hayashi, M., Madokoro, H., Yamada, K., Nishida, H., Morimoto, C., Sakamoto, M., Yamada, T. (2016). A humanized anti-CD26 monoclonal

antibody inhibits cell growth of malignant mesothelioma via retarded G2/M cell cycle transition. *Cancer Cell Int*. 16, 35.

Hegen, M., Kameoka, J., Dong, R.P., Schlossman, S.F., Morimoto, C. (1997). Cross-linking of CD26 by antibody induces tyrosine phosphorylation and activation of mitogen-activated protein kinase. *Immunology* 90, 257-264.

Heins, J., Welker, P., Schonlein, C., Born, I., Hartrodt, B., Neubert, K., Tsuru, D., Barth, A. (1988). Mechanism of proline-specific proteinases: (I) Substrate specificity of dipeptidyl peptidase IV from pig kidney and proline-specific endopeptidase from Flavobacterium meningosepticum. *Biochim. Biophys. Acta* 954, 161-169.

Ho, L., Aytac, U., Stephens, L.C., Ohnuma, K., Mills, G.B., McKee, K.S., Neumann, C., LaPushin, R., Cabanillas, F., Abbruzzese, J.L., Morimoto, C., Dang, N.H. (2001). *In vitro* and *in vivo* antitumor effect of the anti-CD26 monoclonal antibody 1F7 on human CD30+ anaplastic large cell T-cell lymphoma Karpas 299. *Clin. Cancer Res*. 7, 2031-2040.

Hopsu-Havu, V.K., Glenner, G.G. (1966). A new dipeptide naphthylamidase hydrolyzing glycyl-prolyl-β-naphthylamide. *Histochemie. Histochemistry* 7, 197-201.

Hua, J., Davis, S.P., Hill, J.A., Yamagata, T. (2015). Diverse gene expression in human regulatory T cell subsets uncovers connection between regulatory T cell genes and suppressive function. *J. Imunol*. 195, 3642-3653.

Inamoto, T., Yamada, T., Ohnuma, K., Kina, S., Takahashi, N., Yamochi, T., Inamoto, S., Katsuoka, Y., Hosono, O., Tanaka, H., Dang, N.H., Morimoto, C. (2007). Humanized anti-CD26 monoclonal antibody as a treatment for malignant mesothelioma tumors. *Clin. Cancer Res.*13, 4191-4200.

Inamoto, T., Yamochi, T., Ohnuma, K., Iwata, S., Kina, S., Inamoto, S., Tachibana, M., Katsuoka, Y., Dang, N.H., Morimoto, C. (2006). Anti-CD26 monoclonal antibody-mediated G1-S arrest of human renal clear cell carcinoma Caki-2 is associated with retinoblastoma substrate dephosphorylation, cyclin-dependent kinase 2 reduction, $p27^{kip1}$ enhancement, and disruption of binding to the extracellular matrix. *Clin. Cancer Res.* 12, 3470-3477.

Ishii, T., Ohnuma, K., Murakami, A., Takasawa, N., Kobayashi, S., Dang, N.H., Schlossman, S.F., Morimoto, C. (2001). CD26-mediated signaling for T cell activation occurs in lipid rafts through its association with CD45RO. *Proc. Natl. Acad. Sci. USA*. 98, 12138-12143.

Iwaki-Egawa, S., Watanabe, Y., Kikuya, Y., Fujimoto, Y. (1998). Dipeptidyl peptidase IV from human serum: purification, characterization, and N-terminal amino acid sequence. J. *Biochem.* 124, 428-433.

Komiya, E., Ohnuma, K., Yamazaki, H., Hatano, R., Iwata, S., Okamoto, T., Dang, N.H., Yamada, T., Morimoto, C. (2014). CD26-mediated regulation of periostin expression contributes to migration and invasion of malignant pleural mesothelioma cells. *Biochem. Biophys. Res. Commun.* 447, 609-615.

Kondola, S., Manners, D., Nowak, A.K. (2016). Malignant pleural mesothelioma: an update on diagnosis and treatment options. *Ther. Adv. Respir. Dis*. 10, 275-288.

Maggioni, C., Barletta, G., Rijavec, E., Biello, F., Gualco, E., Grossi, F. (2016). Advances in treatment of mesothelioma. *Expert Opin. Pharmacother*. 17, 1197-1205.

Maguer-Satta, V., Besancon, R., Bachelard-Cascales, E. (2011). Concise review: neutral endopeptidase (CD10): a multifaceted environment actor in stem cells, physiological mechanisms, and cancer. *Stem Cells* 29, 389-396.

Marguet, D., Bernard, A.M., Vivier, I., Darmoul, D., Naquet, P., Pierres, M. (1992). cDNA cloning for mouse thymocyte-activating molecule. A multifunctional ecto-dipeptidyl peptidase IV (CD26) included in a subgroup of serine proteases. *J. Biol. Chem*. 267, 2200-2208.

Masuyama, J., Berman, J.S., Cruikshank, W.W., Morimoto, C., Center, D.M. (1992). Evidence for recent as well as long term activation of T cells migrating through endothelial cell monolayers *in vitro*. *J. Immunol*. 148, 1367-1374.

Morimoto, C., Schlossman, S.F. (1998). The structure and function of CD26 in the T-cell immune response. *Immunol. Rev.* 161, 55-70.

Morimoto, C., Torimoto, Y., Levinson, G., Rudd, C.E., Schrieber, M., Dang, N.H., Letvin, N.L., Schlossman, S.F. (1989). 1F7, a novel cell surface molecule, involved in helper function of CD4 cells. *J. Immunol.* 143, 3430-3439.

Morra, L., Moch, H. (2011). Periostin expression and epithelial-mesenchymal transition in cancer: a review and an update. *Virchows Arch*. 459, 465-475.

Myers, R. (2012). Asbestos-related pleural disease. *Curr. Opin. Pulm. Med*. 18, 377-381.

Nagatsu, I., Nagatsu, T., Yamamoto, T. (1968). Hydrolysis of amino acid beta-naphthylamides by aminopeptidases in human parotid salva and human serum. *Experientia* 24, 347-348.

Ogata, S., Misumi, Y., Ikehara, Y. (1989). Primary structure of rat liver dipeptidyl peptidase IV deduced from its cDNA and identification of the NH_2-terminal signal sequence as the membrane-anchoring domain. *J. Biol. Chem*. 264, 3596-3601.

Ohnuma, K., Dang, N.H., Morimoto, C. (2008a). Revisiting an old acquaintance: CD26 and its molecular mechanisms in T cell function. *Trends Immunol*. 29, 295-301.

Ohnuma, K., Hatano, R., Morimoto, C. (2015). DPP4 in anti-tumor immunity: going beyond the enzyme. *Nat. Immunol*. 16, 791-792.

Ohnuma, K., Hosono, O., Dang, N.H., Morimoto, C. (2011). Dipeptidyl peptidase in autoimmune pathophysiology. *Adv. Clin. Chem*. 53, 51-84.

Ohnuma, K., Morimoto, C. (2013). DPP4 (dipeptidyl-peptidase 4). *Atlas Genet. Cytogenet. Oncol. Haematol.* 17, 301-312.

Ohnuma, K., Munakata, Y., Ishii, T., Iwata, S., Kobayashi, S., Hosono, O., Kawasaki, H., Dang, N.H., Morimoto, C. (2001). Soluble CD26/dipeptidyl peptidase IV induces T cell proliferation through CD86 up-regulation on APCs. *J. Immunol*. 167, 6745-6755.

Ohnuma, K., Takahashi, N., Yamochi, T., Hosono, O., Dang, N.H., Morimoto, C. (2008b). Role of CD26/dipeptidyl peptidase IV in human T cell activation and function. *Front. Biosci.* 13, 2299-2310.

Ohnuma, K., Uchiyama, M., Yamochi, T., Nishibashi, K., Hosono, O., Takahashi, N., Kina, S., Tanaka, H., Lin, X., Dang, N.H., Morimoto, C. (2007). Caveolin-1 triggers T-cell activation via CD26 in association with CARMA1. *J. Biol. Chem.* 282, 10117-10131.

Ohnuma, K., Yamochi, T., Uchiyama, M., Nishibashi, K., Iwata, S., Hosono, O., Kawasaki, H., Tanaka, H., Dang, N.H., Morimoto, C. (2005). CD26 mediates dissociation of Tollip and IRAK-1 from caveolin-1 and induces upregulation of CD86 on antigen-presenting cells. *Mol. Cell. Biol.* 25, 7743-7757.

Ohnuma, K., Yamochi, T., Uchiyama, M., Nishibashi, K., Yoshikawa, N., Shimizu, N., Iwata, S., Tanaka, H., Dang, N.H., Morimoto, C. (2004). CD26 up-regulates expression of CD86 on antigen-presenting cells by means of caveolin-1. *Proc. Natl. Acad. Sci. USA*. 101, 14186-14191.

Okamoto, T., Iwata, S., Yamazaki, H., Hatano, R., Komiya, E., Dang, N.H., Ohnuma, K., Morimoto, C. (2014). CD9 Negatively Regulates CD26

expression and inhibits CD26-mediated enhancement of invasive potential of malignant mesothelioma cells. *PLoS ONE* 9, e86671.

Proost, P., Schutyser, E., Menten, P., Struyf, S., Wuyts, A., Opdenakker, G., Detheux, M., Parmentier, M., Durinx, C., Lambeir, A.M., Neyts, J., Liekens, S., Maudgal, P. C., Billiau, A., Van Damme, J. (2001). Amino-terminal truncation of CXCR3 agonists impairs receptor signaling and lymphocyte chemotaxis, while preserving antiangiogenic properties. *Blood* 98, 3554-3561.

Rasmussen, H.B., Branner, S., Wiberg, F.C., Wagtmann, N. (2003). Crystal structure of human dipeptidyl peptidase IV/CD26 in complex with a substrate analog. *Nat. Struct. Biol.* 10, 19-25.

Reya, T., Morrison, S.J., Clarke, M.F., Weissman, I.L. (2001). Stem cells, cancer, and cancer stem cells. *Nature* 414, 105-111.

Robinson, B.M. (2012). Malignant pleural mesothelioma: an epidemiological perspective. *Ann. Cardiothorac. Surg*. 1, 491-496.

Rohrborn, D., Eckel, J., Sell, H. (2014). Shedding of dipeptidyl peptidase 4 is mediated by metalloproteases and up-regulated by hypoxia in human adipocytes and smooth muscle cells. *FEBS Lett*. 588, 3870-3877.

Schramm, A., Opitz, I., Thies, S., Seifert, B., Moch, H., Weder, W., Soltermann, A. (2010). Prognostic significance of epithelial-mesenchymal transition in malignant pleural mesothelioma. *Eur. J. Cardiothorac. Surg*. 37, 566-572.

Shersher, D.D., Liptay, M.J. (2013). Multimodality treatment of pleural mesothelioma. *Surg. Oncol. Clin. N. Am.* 22, 345-355.

Stohlawetz, P., Hahn, P., Koller, M., Hauer, J., Resch, H., Smolen, J., Pietschmann, P. (1998). Immunophenotypic characteristics of monocytes in elderly subjects. *Scand. J. Imunol*. 48, 324-326.

Tanaka, T., Camerini, D., Seed, B., Torimoto, Y., Dang, N.H., Kameoka, J., Dahlberg, H.N., Schlossman, S.F., Morimoto, C. (1992). Cloning and functional expression of the T cell activation antigen CD26. *J. Immunol*. 149, 481-486.

Tanaka, T., Kameoka, J., Yaron, A., Schlossman, S.F., Morimoto, C. (1993). The costimulatory activity of the CD26 antigen requires dipeptidyl peptidase IV enzymatic activity. *Proc. Natl. Acad. Sci. USA*. 90, 4586-4590.

Thompson, M.A., Ohnuma, K., Abe, M., Morimoto, C., Dang, N.H. (2007). CD26/dipeptidyl peptidase IV as a novel therapeutic target for cancer and immune disorders. *Mini Rev. Med. Chem.* 7, 253-273.

van Meerbeeck, J.P., Damhuis, R. (2011). Facts, rumours and speculations about the mesothelioma epidemic. *Respirology* 16, 1018-1019.

van Meerbeeck, J.P., Gaafar, R., Manegold, C., Van Klaveren, R.J., Van Marck, E.A., Vincent, M., Legrand, C., Bottomley, A., Debruyne, C., Giaccone, G. (2005). Randomized phase III study of cisplatin with or without raltitrexed in patients with malignant pleural mesothelioma: an intergroup study of the European Organisation for Research and Treatment of Cancer Lung Cancer Group and the National Cancer Institute of Canada. *J. Clin. Oncol.* 23, 6881-6889.

Wang, J.C., Dick, J.E. (2005). Cancer stem cells: lessons from leukemia. *Trends Cell. Biol*. 15, 494-501.

Yamada, K., Hayashi, M., Du, W., Ohnuma, K., Sakamoto, M., Morimoto, C., Yamada, T. (2009). Localization of CD26/DPPIV in nucleus and its nuclear translocation enhanced by anti-CD26 monoclonal antibody with anti-tumor effect. *Cancer Cell Int*. 9, 17.

Yamada, K., Hayashi, M., Madokoro, H., Nishida, H., Du, W., Ohnuma, K., Sakamoto, M., Morimoto, C., Yamada, T. (2013). Nuclear localization of CD26 induced by a humanized monoclonal antibody inhibits tumor cell growth by modulating of POLR2A transcription. *PLoS ONE* 8, e62304.

Yamamoto, J., Ohnuma, K., Hatano, R., Okamoto, T., Komiya, E., Yamazaki, H., Iwata, S., Dang, N.H., Aoe, K., Kishimoto, T., Yamada, T., Morimoto, C. (2014). Regulation of somatostatin receptor 4-mediated cytostatic effects by CD26 in malignant pleural mesothelioma. *Br. J. Cancer* 110, 2232-2245.

Yamazaki, H., Naito, M., Ghani, F.I., Dang, N.H., Iwata, S., Morimoto, C. (2012). Characterization of cancer stem cell properties of CD24 and CD26-positive human malignant mesothelioma cells. *Biochem. Biophys. Res. Commun*. 419, 529-536.

Yamochi, T., Yamochi, T., Aytac, U., Sato, T., Sato, K., Ohnuma, K., McKee, K.S., Morimoto, C., Dang, N.H. (2005). Regulation of p38 phosphorylation and topoisomerase IIα expression in the B-cell lymphoma line Jiyoye by CD26/dipeptidyl peptidase IV is associated with enhanced *in vitro* and *in vivo* sensitivity to doxorubicin. *Cancer Res*. 65, 1973-1983.

Yan, W., Shao, R. (2006). Transduction of a mesenchyme-specific gene periostin into 293T cells induces cell invasive activity through epithelial-mesenchymal transformation. *J. Biol. Chem.* 281, 19700-19708.

Yaron, A., Naider, F. (1993). Proline-dependent structural and biological properties of peptides and proteins. *Crit. Rev. Biochem. Mol. Biol*. 28, 31-81.

A novel role for CD26/dipeptidyl peptidase IV as a therapeutic target

Kei Ohnuma[1], Ryo Hatano[1], Eriko Komiya[1], Haruna Otsuka[1], Takumi Itoh[1], Noriaki Iwao[2], Yutaro Kaneko[3], Taketo Yamada[4,5], Nam H. Dang[6], Chikao Morimoto[1]

[1]Department of Therapy Development and Innovation for Immune Disorders and Cancers, Graduate School of Medicine, Juntendo University, 2-1-1, Hongo, Bunkyo-ku, Tokyo 113-8421, Japan, [2]Department of Hematology, Juntendo University Shizuoka Hospital, Nagaoka 1129, Izunokuni-city, Shizuoka 410-2295, Japan, [3]Y's AC Co., Ltd., 5-3-14, Toranomon, Minato-ku, Tokyo 105-0001, Japan, [4]Department of Pathology, Keio University school of Medicine, 35 Shinanomachi, Shinjuku-ku, Tokyo 160-8582, Japan, [5]Department of Pathology, Saitama Medical University, 38 Morohongo, Moroyama-cho, Iruma-gun, Saitama 350-0459, Japan, [6]Division of Hematology/Oncology, University of Florida, 1600 SW Archer Road-Box 100278, Room MSB M410A, Gainesville, FL 32610, U.S.A.

TABLE OF CONTENTS

1. ABSTRACT

CD26 is a 110 kDa surface glycoprotein with intrinsic dipeptidyl peptidase IV activity that is expressed on numerous cell types and has a multitude of biological functions. The role of CD26 in immune regulation has been extensively characterized, with recent findings elucidating its linkage with signaling pathways and structures involved in T-lymphocyte activation as well as antigen presenting cell-T-cell interaction. In this paper, we will review emerging data on CD26-mediated immune regulation suggesting that CD26 may be an appropriate therapeutic target for the treatment of selected immune disorders as well as Middle East respiratory syndrome coronavirus. Moreover, we have had a long-standing interest in the role of CD26 in cancer biology and its suitability as a novel therapeutic target in selected neoplasms. We reported robust *in vivo* data on the anti-tumor activity of anti-CD26 monoclonal antibody in mouse xenograft models. We herein review significant novel findings and the early clinical development of a CD26-targeted therapy in selected immune disorders and cancers, advances that can lead to a more hopeful future for patients with these intractable diseases.

2. INTRODUCTION

CD26 is a 110-kDa cell surface glycoprotein with known dipeptidyl peptidase IV (DPPIV, EC3.4.1.4.5) activity in its extracellular domain (1-3), capable of cleaving amino-terminal dipeptides with either L-proline or L-alanine at the penultimate position (3). CD26 activity is dependent on the expressing cell type and the microenvironment which influence its multiple biological roles (4-7). CD26 plays an important role in immunology, autoimmunity, diabetes and cancer (8-12). Interacting directly with various other cell surface and intracellular molecules, CD26 can regulate receptor specificity and the function of various interleukins (ILs), cytokines and chemokines via its DPPIV activity (13).

In this review, we summarize our recent work on CD26/DPPIV that elucidated its suitability as a potential therapeutic target in selected immune diseases and cancers. We also discuss our current knowledge of the molecular mechanisms of CD26/DPPIV-mediated T-cell regulation, focusing particularly on CD26/DPPIV role in immune checkpoint pathways and programs associated with human immune regulation. In addition, we describe CD26/DPPIV involvement in cancer immunology.

3. IMMUNE MEDIATED DISORDERS

3.1. Chronic graft-versus-host disease

3.1.1. T cell costimulation in chronic graft-versus-host disease

Graft-versus-host disease (GVHD) is a severe complication and major cause of morbidity and mortality following allogeneic hematopoietic stem cell transplantation (alloHSCT) (14). Based on differences in clinical manifestations and

histopathology, GVHD can be divided into acute and chronic forms (14). Acute GVHD (aGVHD) and chronic GVHD (cGVHD) are traditionally diagnosed primarily by time of onset, with cGVHD occurring after day 100 of transplantation (15). However, cGVHD has distinct clinicopathologic features and is often diagnosed based on these features regardless of time of onset, being characterized by cutaneous fibrosis, involvement of exocrine glands, hepatic disease, and obliterative bronchiolitis (OB) (16, 17). OB, characterized by airway blockade, peribronchiolar and perivascular lympho-fibroproliferation and obliteration of bronchioles, is a late-stage complication of cGVHD (18). Patients diagnosed with OB have a 5-year survival rate of only 10 to 40%, compared to more than 80% of patients without OB (19, 20). Furthermore, while multiple strategies to control cGVHD involving T cell depletion from the graft or global immunosuppression have been developed, cGVHD is still a common clinical outcome in many alloHSCT patients (17, 21). In addition, immunosuppression potentially abrogates the graft-versus-leukemia (GVL) effect, associated with increased relapses following alloHSCT (22). Novel therapeutic approaches are thus needed to prevent cGVHD without eliminating the GVL effect.

GVHD is initiated when donor-derived T cells are primed by professional antigen presenting cells (APCs) to undergo clonal expansion and maturation (14). Costimulatory pathways are required to induce T cell proliferation, cytokine secretion and effector function following antigen-mediated T cell receptor activation (23), and the important role of costimulatory pathways in transplant biology has been established (24). CD26 is associated with T cell signal transduction processes as a costimulatory molecule, as well as being a marker of T cell activation (1, 25, 26). We previously showed that CD26-mediated costimulation in human CD4 T cells exerts an effect on production of T_H1 type proinflammatory cytokines such as interferon (IFN)-γ (6). Moreover, $CD26^{high}$CD4 T cells respond maximally to recall antigens with a high competence for trafficking to inflammatory tissues and for antibody synthesis by B cells (6, 26). We also showed that CD26-caveolin-1 interaction leads to activation of both CD4 T cells and APCs (27-29). More recently, we demonstrated in *in vitro* experiments that blockade of CD26-mediated T cell costimulation by soluble Fc fusion proteins containing the N-terminal domain of caveolin-1 (Cav-Ig) diminished primary and secondary proliferative responses not only to recall antigen, but also to unrelated allogeneic APC (30). Other investigators recently reported that $CD26^{high}$ T cells contain T_H17 cells, and that $CD26^{high}$ T_H17 cells are enriched in inflamed tissues including rheumatoid arthritis (RA) and inflammatory bowel diseases (IBD) (31). These accumulating data strongly suggest that CD26-mediated costimulation plays an important role in memory response to recall antigens, and that blockade of CD26 costimulation may be an effective therapeutic strategy for immune disorders including GVHD or autoimmune diseases.

3.1.2. Newly established humanized murine model of cGVHD

We previously analyzed a humanized murine aGVHD model involving mice transplanted with human adult peripheral blood lymphocytes (PBL), and showed that liver and skin were predominantly involved as target organs in this model of aGVHD, which was clearly impeded by the administration of humanized anti-CD26 monoclonal antibody (mAb) (32). Our data suggest that $CD26^+$ T cells play an effector role in this aGVHD model. However, since the mice studied in our previous work succumbed to aGVHD around 4 weeks after transplantation of human adult PBL, this early-onset model of aGVHD does not permit the assessment of longer term consequences of interventional therapies, such as their effect on the development of OB, a form of cGVHD of the lung.

In contrast to adult PBL, human umbilical cord blood (HuCB) lymphocytes have been reported to be immature, predominantly consisting of $CD45RA^+$ naïve cells (33, 34). We previously showed that, while all HuCB CD4 T cells constitutively express CD26, CD26-mediated costimulation was considerably attenuated in HuCB CD4 T cells, compared to the robust activation via CD26 costimulation of adult PBL (34). These findings provided further insights into the cellular mechanisms of immature immune response in HuCB. Based on these findings, we hypothesized that HuCB naïve CD4 T cells gradually acquire a xenogeneic response via attenuated stimulatory signaling with indolent inflammation in the target organs, leading eventually to chronic inflammatory changes. We therefore sought to develop a humanized murine pulmonary cGVHD model utilizing HuCB donor cells, and to overcome the limitations seen in the humanized murine aGVHD model such as vigorous activation of all engrafted T cells and extensive loss of B cell maturation and activation (35, 36).

We first attempted to establish a humanized murine model utilizing NOD/Shi-*scid*IL2rγ^{null} (NOG) mice as recipients and HuCB as donor cells (37). Whole CB transplant mice exhibited clinical signs/symptoms of GVHD as early as 4 weeks post-transplant, and demonstrated significantly decreased survival rate. The lung of whole CB transplant mice showed perivascular and subepithelial inflammation and fibrotic narrowing of the bronchiole. Skin of whole CB transplant mice manifested fat loss, follicular drop-out and sclerosis of the reticular dermis in the presence of apoptosis of the basilar keratinocytes while the liver exhibited portal fibrosis and cholestasis. These findings indicate that whole CB transplant mice develop pulmonary cGVDH as well as concomitant active GVHD in skin and liver. Taken together, our data demonstrate that the lung of whole CB transplant mice exhibits OB as manifestation of pulmonary cGVHD.

3.1.3. IL-26 contributes to the pathophysiology of pulmonary cGVHD

To determine the potential cellular mechanisms involved in the pathogenesis of pulmonary cGVHD, we next analyzed the composition of donor-derived human lymphocytes in the GVHD lung. Utilizing flow cytometric analysis for cell suspension isolated from the lung specimens, donor-derived human $CD3^+$ cells were found to be the predominant cell type observed in the

lung of whole CB transplant mice, comprising more than 99% of the lymphocyte population. Moreover, the human CD4 T cell subset was observed to be the predominant cell type compared to CD8 T cells in the lung of whole CB transplant mice. We next analyzed the expression profile of mRNAs of various inflammatory cytokines in human CD4 T cells isolated from the lung of whole CB transplant mice. We found that *IFNG*, *IL17A, IL21* and *IL26* were significantly increased over the course of GVHD development following whole CB transplantation, while *IL2*, *TNF* (TNF-α), *IL4*, *IL6* and *IL10* were decreased. In addition, substantial increases were seen in levels of *IFNG* and *IL26*, with *IL17A* and *IL21* remained at a low level. It has been reported that IFN-γ is produced by T_H1 cells (6), while IL-17A and IL-26 are produced by T_H17 cells (38, 39). Since both T_H1 and T_H17 cells strongly express CD26 (6, 31), we next analyzed the expression level of CD26/DPP4, finding that *DPP4* mRNA expression in human CD4 T cells infiltrating in the lung of mice with OB was significantly increased. These findings regarding mRNA expression levels were further supported by enzyme-linked immunosorbent assay (ELISA) studies examining protein levels in sera of recipient mice. To determine whether these cytokines were produced by the infiltrating human $CD26^+$CD4 T cells, we next conducted flow cytometric analyses of lymphocytes isolated from the lung of the recipient mice. Levels of human IFN-γ^+ or IL-26^+CD26^+CD4 T cells were significantly increased in whole CB transplant mice. Multicolor-staining flow cytometric studies showed that $CD26^+$CD4 T cells in the lung of whole CB transplant mice predominantly produced IL-26 rather than IFN-γ. In addition, while $CD26^+$IFN-γ^+CD4 cells exclusively expressed IL-26, $CD26^+$IL-26^+CD4 cells were predominantly IFN-γ-negative cells, and IL-$17A^+$ cells were exclusively IL-26-negative. These data suggest that $CD26^+$CD4 T cells in the lung of mice with OB express IL-26 as well as IFN-γ but do not belong to the T_H17 cell population.

To further extend the above *in vitro* results to an *in vivo* system, we analyzed the lung of murine alloreactive GVHD using human *IL26* transgenic (Tg) mice. For this purpose, we used mice carrying human *IFNG* and *IL26* transgene (190-*IFNG* Tg mice) or mice carrying human *IFNG* transgene with deleting *IL26* transcription (ΔCNS-77 Tg mice). 190-*IFNG* Tg mice exhibited production of IL-26 by CD4 T cells under T_H1- or T_H17-polarizing conditions, while expression of IL-26 was completely abrogated in ΔCNS-77 Tg mice (38). In addition, production of IFN-γ by T or NK cells was equivalent in both 190-*IFNG* Tg and ΔCNS-77 Tg mice (40). Histologic examinations of the lung of recipient NOG mice deriving from parental C57BL/6 (B6 WT) mice or ΔCNS-77 Tg mice showed peribronchial infiltration and cuffing denoting GVHD, while collagen deposits were not detected by Mallory staining, and IL-26^+ cells were not detected. On the other hand, the lung of recipient NOG mice deriving from 190-*IFNG* Tg mice showed peribronchial infiltration and cuffing denoting GVHD with collagen deposition and IL-26^+ cell infiltration. These results suggest that human IL-26, but not human IFN-γ, plays a critical role in pulmonary fibrosis associated with lung cGVHD.

3.1.4. IL-26 production via CD26-mediated T cell costimulation

To test whether human CD4 T cells produce IL-26 following CD26 costimulation, we conducted *in vitro* costimulation experiments using HuCB CD4 T cells and analyzed expression of various inflammatory cytokines. We found that levels of *IL26* and *DPP4* were significantly increased following CD26 costimulation compared with CD28 costimulation. We next conducted costimulation experiments evaluating dose and time kinetics using the CD26 costimulatory ligand Cav-Ig as well as anti-CD26 or anti-CD28 mAbs. We showed that production of IL-26 was increased following CD26 costimulation with Cav-Ig or anti-CD26 mAb in dose- and time-dependent manners, while a slight increase in IL-26 level was observed following CD28 costimulation only at higher doses of mAb and longer stimulation periods. Blocking experiments were then performed for further confirmation, showing that IL-26 production induced by Cav-Ig or anti-CD26 mAb was clearly inhibited by treatment with soluble Cav-Ig in a dose-dependent manner, while no change was observed with CD28 costimulation. These findings strongly suggest that production of IL-26 by HuCB CD4 T cells is regulated via CD26-mediated costimulation. Moreover, since the functional sequences of the N-terminal of caveolin-1 are highly conserved between human and mouse (41) allowing for the capability to bind human CD26 as a costimulatory ligand, it is conceivable that donor HuCB T cells transferred into mice were activated via CD26 costimulation triggered by murine caveolin-1. In fact, using polyclonal antibody recognizing the N-terminal of both human and murine caveolin-1, expression of caveolin-1 was detected in endothelial cells and macrophage-like cells of OB-like lesions in cGVHD lung. Taken together, CD26-mediated IL-26 production triggered by caveolin-1 is identified as a possible therapeutic target in cGVHD using HuCB NOG mice.

3.1.5. Prevention of lung cGVHD development by Cav-Ig administration

Given the role of CD26 costimulation in IL-26 production and IL-26 regulation of collagen production, we therefore sought to determine whether disruption of CD26 costimulation by a blocking reagent, Cav-Ig, prolonged survival of the recipient mice associated with a reduction in the incidence of OB. Recipients treated with Cav-Ig survived for 7 months without any clinical findings of cGVHD. Meanwhile, the survival rate of recipient mice treated with control Ig was significantly reduced, with clinical signs/symptoms of cGVHD. Human cells were engrafted similarly in both groups. Histologic examinations of the lung showed the development of OB in the control Ig cohort, while the lung of Cav-Ig recipient mice displayed normal appearances with none having positive pathology scores. These effects of Cav-Ig were also observed in other GVHD-target organs such as the skin and liver. Moreover, collagen contents in the lung were reduced in Cav-Ig administered-recipients. Taken together, the above results support the notion that Cav-Ig administration prevents the development of pulmonary cGVHD in whole CB transplant mice by decreasing the number of IL-26^+CD26^+CD4 T cells.

3.1.6. Treatment with Cav-Ig preserves GVL capability

Since GVHD and GVL effect are highly linked immune reactions (42), we evaluated the potential influence of Cav-Ig treatment on GVL effect. For this purpose, cohorts of Cav-Ig or control Ig treated recipient mice of whole CB transplant were irradiated at sublethal doses and then injected intravenously with luciferase-transfected A20 (A20-luc) cells 1 day prior to whole CB transplantation to allow for dissemination of tumor cells. The next day following transplantation, treatment with Cav-Ig or control Ig thrice a week began on day +1 until day +28. Mice inoculated with A20 cells alone all died of tumor progression within 6 weeks. Recipients treated with control Ig exhibited clinical evidence of GVHD such as weight loss and ruffled fur and died of GVHD without tumor progression in 13 weeks. In contrast, recipient mice treated with Cav-Ig displayed significantly prolonged survival without involvement of A20-luc cells. To better characterize the potency of the GVL effect, we repeated these studies with injection of A20-luc cells on day +28 after whole CB transplantation to allow for acquisition of immunosuppression by Cav-Ig treatment. Mice inoculated with A20 cells alone all died of tumor progression within 2 weeks after tumor inoculation. Recipient mice treated with control Ig demonstrated clinical evidence of GVHD such as weight loss and ruffled fur and died of GVHD without tumor progression within 13 weeks after transplantation. In contrast, recipients treated with Cav-Ig exhibited significantly prolonged survival without involvement of A20-luc cells. Collectively, these results demonstrate that Cav-Ig treatment of recipient mice of whole CB transplant was effective in reducing the symptoms of cGVHD without a concomitant loss of the GVL effect.

3.1.7. Role of CD26 in cGVHD

While the human CD26 amino acid (AA) sequence has 85% AA identity with the mouse CD26 (43), the mouse CD26 has different biologic properties from the human CD26, including the fact that the mouse CD26 is not a T cell activation marker, and does not bind to adenosine deaminase (ADA) (43, 44). Therefore, humanized murine models need to be developed to explore the role of CD26-mediated costimulation in cGVHD. With relevance as a costimulatory ligand for human CD26, human caveolin-1 has 95% AA identity with the mouse caveolin-1 (41), and the binding regions of the mouse caveolin-1 for human CD26 are well conserved. Therefore, costimulatory activation of human T cells in NOG mice can occur via CD26-caveolin-1 interaction. Moreover, the N-terminal domain is present in the outer cell surface during the antigen presenting process (27), and caveolin-1 forms homo-dimer or homo-oligomer via its N-terminal domain (41). These collective data suggest that the administered Cav-Ig binds to the N-terminal of caveolin-1 on the cell surface of APCs as well as to CD26 in T cells, leading to suppression of cGVHD in HuCB-NOG mice via blockade of CD26-caveolin-1 interaction. Conclusively, our work demonstrates that caveolin-1 blockade controls cGVHD by suppressing the immune functions of donor-derived T cells and decreasing IL-26 production. Moreover, IL-26^{+}CD26^{+}CD4 T cell infiltration appears to play a significant role in cGVHD of the lung and skin. While complete suppression of cGVHD with current interventional strategies represents a difficult challenge at the present time, our data demonstrate that control of cGVHD clinical findings can be achieved in a murine experimental system by regulating IL-26^{+}CD26^{+}CD4 T cells with Cav-Ig. Our work also suggests that Cav-Ig treatment may be a novel therapeutic approach for chronic inflammatory diseases, including RA and IBD, in which IL-26 plays an important role.

3.2. Middle East respiratory syndrome coronavirus

3.2.1. Current efforts against Middle East respiratory syndrome coronavirus

Middle East respiratory syndrome coronavirus (MERS-CoV) was first identified in a 60-year-old patient in June 2012 who presented with acute pneumonia, followed by acute respiratory distress syndrome and renal failure with a fatal outcome (45). Between 2012 and August 28, 2017, 2067 laboratory-confirmed cases of MERS-CoV infection were reported to the World Health Organization (WHO), which has notified of at least 720 deaths (around 35% fatality rate) related to MERS-CoV since September 2012 (46). Efforts to develop effective preventive and therapeutic intervention strategies are currently ongoing. Several treatment modalities have been investigated to develop effective therapies against MERS-CoV, including interferon, ribavirin, cyclosporin A, protease inhibitors, convalescent plasma and immunoglobulins. Several promising anti-MERS-CoV therapeutic agents have recently been reviewed extensively (47), while broad spectrum antiviral agents might not be sufficient to treat severe MERS-CoV patients because of its limited effective therapeutic window of opportunity (48).

An alternative approach using prophylactic regimens would be theoretically suitable to limit the spread of MERS-CoV. This scenario includes MERS-CoV vaccine and neutralizing MERS-CoV-specific mAb (48). The MERS-CoV genome encodes for 16 non-structural proteins (nsp1-16) and 4 structural proteins, the spike (S), envelope (E), membrane (M), and nucleocapsid (N) (49). The viral structural proteins, S and N, show the highest immunogenicity (50). While both S and N proteins induce T-cell responses, neutralizing antibodies are almost solely directed against the S protein, with the receptor binding domain (RBD) being the major immunodominant region (51). These great challenges have been extensively reviewed in previously published papers (48, 52).

Recent reports indicated that the spike protein S1 of MERS-CoV is required for viral entry into human host cells (53-55), using CD26/DPPIV as a functional receptor (56). Inhibiting virus entry into host cells could also be achieved by targeting the host receptor CD26/DPPIV. While inhibitors of the CD26/DPPIV enzymatic activity are used clinically to treat type 2 diabetes patients, commercially available DPPIV inhibitors would not serve this purpose since these agents have been shown not to inhibit binding of the RBD of MERS-CoV to CD26/DPPIV (57). We previously showed that human CD26 is a binding protein for ADA (58). Currently, it is known that there are two isoforms of ADA, ADA1 and ADA2 (59). ADA1 is particularly present in lymphocytes and macrophages, while ADA2 is found predominantly in the serum and other body fluids including pleural effusion (59). CD26/DPPIV binds to ADA1, but not ADA2 (58, 60, 61). The crystal structure of CD26/DPPIV and the S protein

of MERS-CoV allowed for visualization of the interacting AA in both proteins. However, our *in vitro* experiments showed that blockade of MERS-CoV binding to CD26/DPPIV by ADA1 is incomplete (62). Therefore, mAbs blocking CD26/DPPIV binding to the RBD of MERS-CoV needs to be developed.

3.2.2. CD26/DPPIV is a functional receptor for MERS-CoV entry into host cells

CD26/DPPIV, a host receptor for MERS-CoV, is conserved among different species such as bats and humans, partially explaining the large host range of MERS-CoV (63). In addition to being widely expressed in most cell types including T lymphocytes, bronchial mucosa or the brush border of proximal tubules, CD26/DPPIV exists in systemic circulation as soluble form (13). This distribution of CD26 may play a role in the systemic dissemination of MERS-CoV infection in human (64-66). Therefore, an effective therapy for MERS-CoV is needed not only to block the entry of MERS-CoV into CD26-expressing organs such as the respiratory system, kidney, liver or intestine, but also to eliminate circulating MERS-CoV. In this regard, manipulation of CD26/DPPIV levels or the development of inhibitors that target the interaction between the MERS-CoV S1 domain and its receptor may provide therapeutic opportunities to combat MERS-CoV infection. More recently, the RBD in the S protein was mapped to a 231-AA fragment of MERS-CoV S proteins (residues 358-588) (51).

3.2.3. Identification of specific anti-CD26 mAb clone for blocking MERS-CoV

We have recently mapped MERS-CoV S protein-binding regions in human CD26 molecule and demonstrated that anti-CD26 mAbs, which had been developed in our laboratory, effectively blocked the interaction between the spike protein and CD26, thereby neutralizing MERS-CoV infectivity. To determine the specific CD26 domain involved in MERS-CoV infection, we chose six different clones of anti-CD26 mAbs (4G8, 1F7, 2F9, 16D4B, 9C11, 14D10), and the humanized anti-CD26 mAb YS110, which recognize 6 distinct epitopes of the CD26 molecule (67, 68), to conduct MERS-CoV S1-Fc (S1 domain of MERS-CoV fused to the Fc region of human IgG) binding inhibition assays (62). 2F9 inhibited fully binding of MERS-CoV S1-Fc to JKT-hCD26WT (Jurkat cells transfected with full-length human CD26/DPPIV), while other anti-CD26 mAbs demonstrated certain levels of inhibition (1F7, or YS110) or no significant inhibition (4G8, 16D4B, 9C11 or 14D10). These results strongly suggest that the anti-CD26 mAb 2F9 has better therapeutic potential than recombinant MERS-CoV S1-Fc in preventing viral entry into susceptible cells, and that 1F7 or YS110 also block MERS-CoV infection.

Moreover, we have characterized the CD26 epitope involved in MERS-CoV S1-Fc binding to CD26 through the use of various CD26 mutants with deletion in the C-terminal extracellular region, since CD26 is a type II transmembrane protein (9, 29). Our biological experiments on binding regions of CD26 to MERS-CoV using mAbs showed results comparable to those obtained from crystal structure analysis (55, 69), which are summarized in a schematic diagram of human CD26 at 1-449th AAs (Figure 1). Our observations strongly suggest that the main binding regions of CD26 to MERS-CoV appear to be close to the 358th AAs recognized by 2F9, and the regions of CD26 defined by 1F7 and YS110 (248-358th AAs) are also partially involved in MERS-CoV binding.

To determine whether treatment with anti-CD26 mAbs 2F9 as well as 1F7 and YS110 could inhibit MERS-CoV infection, susceptible cells, Huh-7, were pre-incubated with various anti-CD26 mAbs prior to inoculation with the virus (62). In this experimental system, infection was almost completely blocked by 2F9 but not by control IgG or several other anti-CD26 mAbs recognizing other epitopes (4G8, 16D4B, 14D10 or 9C11). Moreover, the anti-CD26 mAbs 1F7 and YS110 considerably inhibited MERS-CoV infection of Huh-7 cells. These results demonstrate that 2F9 inhibits MERS-CoV entry, and therefore can potentially be developed as a preventive or therapeutic agent for MERS-CoV infection in the clinical setting. More importantly, the humanized anti-CD26 mAb YS110 has been evaluated in patients with CD26-expressing cancers in our recent first-in-human (FIH) phase I clinical trial (70). Since no apparent adverse effects of YS110 have been reported besides transient and tolerable injection reactions, YS110 may be an immediate therapeutic candidate for clinical use as potential treatment for MERS-CoV infection.

3.3. Psoriatic pruritus

3.3.1. CD26/DPPIV and psoriasis

Psoriasis (PSO) is one of the most common inflammatory skin diseases, found in about 1-3% of the world general population (71). For a long time, PSO had been considered as a non-pruritic dermatitis. However, within the past 30 years, a number of studies have demonstrated that approximately 60-90% of patients with PSO suffer from pruritus (71-76). Pruritus is an important symptom of PSO. Despite the fact that several studies have been undertaken to investigate the pathogenesis of pruritus in PSO, many aspects have not yet been studied (71, 77). Therefore, the pathogenesis of this symptom is far from being well-understood and, as a consequence, the therapy of pruritic psoriatic patients still remains a significant challenge for clinicians (78). It has been demonstrated that DPPIV is expressed at high levels on keratinocytes and that DPPIV inhibition suppresses keratinocyte proliferation *in vitro*, and restores partially keratinocyte differentiation *in vivo* (79). Moreover, it has been reported that DPPIV is expressed on keratinocytes and its activity is upregulated in PSO (80, 81), findings which support a potential role for DPPIV enzyme activity in the pathogenesis of PSO. While other investigators have reported a significant improvement in disease severity in PSO patients treated with a DPPIV inhibitor (82, 83), the precise mechanisms involved in DPPIV-mediated regulation of PSO have not been elucidated (84). Recent report showed that T-cell bound expression of CD26/DPPIV in psoriatic skin was explicitly present, albeit in small quantities (81). One hypothesis of potential effect of DPPIV in PSO is that T cell activation mediated by DPPIV is associated with the pathogenesis of PSO (85). Cytokines and chemokines represent the third

key player in the psoriatic chronic immune response (86). They are considered as mediators responsible for activation and recruitment of infiltrating leukocytes and therefore play a crucial role in the development and persistence of psoriatic skin lesions (87). DPPIV likely plays a pivotal role in the processing of these molecules (84). The extracellular protease domain of DPPIV (both on keratinocytes and T cells) can cleave dipeptides from the amino terminus of proteins, such as cytokines and chemokines, which are abundantly present in a chronic immune response in PSO, resulting in alterations in receptor specificity and subsequent modifications of biological activity. Taken together, it is conceivable that PSO is a disease involving the complex interplay among activated T cells, keratinocytes and cytokines, and that DPPIV has a key regulatory role in the interactions of these three disease components.

3.3.2. Elevation of sCD26 and DPPIV enzyme in sera of PSO patients

To determine whether serum soluble CD26 (sCD26) and soluble DPPIV (sDPPIV) enzyme play a role in PSO, we evaluated levels of sCD26 and sDPPIV enzyme activity in sera of patients with PSO (88). For this purpose, we performed our in-house capture assay method using anti-human CD26 mAb as a capture antibody for detecting DPPIV enzyme activity specific to sCD26 (89). Since commercially available DPPIV enzyme assay kits measure DPPIV activity in whole serum, but not in captured sCD26 molecules from the samples, it is possible that DPPIV-like peptidase activity other than that possessed by the captured sCD26 molecules was measured, leading to an overestimate of the DPPIV activity in the samples (90). Analyses of serum samples obtained from 18 healthy adult volunteers and 48 PSO patients demonstrated that serum sCD26 concentration of PSO patients was significantly higher than that of healthy adults. Moreover, serum levels of sDPPIV enzyme activity were also significantly higher in patients with PSO compared with healthy adult controls. These data suggest that DPPIV enzyme activity is increased in sera of patients with PSO, which is linked to a concomitant increase in sCD26 in the same patient population. These observations also suggest that DPPIV enzyme plays a role in the pathogenesis of PSO.

3.3.3. Increased pruritus by truncation of substance P, a ligand for CD26/DPPIV

Among various mediators of pruritus investigated in inflammatory skin diseases, substance P (SP) is a key molecule in an itch sensory nerve (91-93), consisting of 11 AA residues with dual DPPIV cleavage sites at its N-terminal position. In fact, DPPIV enzyme digests full-length SP(1-11) resulting in a truncated form of SP(5-11), an activity inhibited by the presence of the DPPIV enzyme inhibitor sitagliptin (88). Moreover, we observed that levels of SP degraded by DPPIV were increased in sera of patients with PSO. Taken together with the above data regarding an increase of sCD26/DPPIV levels in PSO patients, these results also suggest that the increase in DPPIV activity appears to play an important role in PSO by truncating SP.

We next utilized an itchy mouse model by intradermal injection (i.d.) of recombinant SP and quantified scratching behavior in mice to determine an itchy symptom. Mice treated with SP(5-11) i.d. demonstrated a significant increase in scratching behavior, compared with mice receiving control solvent or mice receiving full-length SP(1-11). On the other hand, scratching behavior in SP(1-11) i.d. mice was significantly decreased in mice treated with the DPPIV inhibitor sitagliptin. Furthermore, SP-induced scratching behavior was significantly attenuated in CD26/DPPIV knockout (CD26KO) mice compared with that observed in B6 WT mice. Our data suggest that truncated form of SP cleaved by DPPIV enzyme increases an itch sensation and that SP-induced itch sensation is attenuated by inhibition of the DPPIV activity.

To further determine that DPPIV inhibition affects pruritus, we evaluated scratching behavior utilizing an imiquimod (IMQ)-induced psoriatic itch model (94, 95). Serum levels of truncated form of SP were significantly increased in IMQ-treated mice compared with control cream-treated mice. Moreover, scratching behavior was significantly increased in IMQ-treated mice than control cream-treated mice. These data indicate that IMQ induces psoriatic itchy skin lesions in mice associated with an increase in the truncation of SP. We next analyzed the frequencies of itch scratching behavior following DPPIV inhibitor administration. IMQ-treated mice receiving sitagliptin showed significant decrease of scratching behavior compared with IMQ-treated mice receiving control solvent. Meanwhile, there was no change in scratching behavior between control cream-treated mice receiving sitagliptin or control saline, with baseline levels of scratching behavior in both cohorts. Taken together, our data suggest that treatment with the DPPIV inhibitor sitagliptin attenuates psoriatic itch sensation via a decrease in the truncated form of SP.

Previous studies have reported that serum levels of SP were decreased in patients with PSO (96-98). Meanwhile, since SP is cleaved by DPPIV enzyme and DPPIV enzyme activity is increased in PSO (88), it is important for a detailed understanding of the role of SP in PSO to precisely measure the truncated form of SP separately from full-length SP. In our recent study, we evaluated full-length SP(1-11) and truncated forms of SP and demonstrated that there was no change in the serum levels of full-length SP(1-11), SP(2-11) and SP(3-11) between PSO and healthy adult controls (88). However, we found that DPPIV enzyme activity and the truncated form of SP were significantly increased in PSO, and that the truncated form of SP(5-11) resulting from DPPIV enzyme activity is associated with an increase in itch sensation. In the IMQ-induced PSO model, the truncated form of SP was significantly increased in sera compared with control mice, and scratching behavior was decreased by administration of sitagliptin. On the other hand, there were no differences in serum levels of DPPIV enzyme activity between IMQ and control cream-treated mice. It is conceivable that the persistent existence of psoriatic skin lesions may be required for the increased serum levels of DPPIV enzyme activity seen in PSO patients, and that SP truncation may result from the increased levels of DPPIV enzyme activity in skin lesions rather than in the circulation (80, 99, 100). Our recent study has conclusively demonstrated that increase in DPPIV enzyme activity exacerbates pruritus in PSO, and that inhibition of DPPIV enzyme reduces

severity of itch scratching behavior. Moreover, our results suggest that DPPIV inhibitors are useful as therapeutic agents for pruritus including PSO.

4. CANCERS

4.1. Novel mechanism of CD26/DPPIV in cancer immunology

4.1.1. Anti-tumor effect of CXCL10-mediated CXCR3$^+$ lymphocyte via DPPIV inhibition

CD26/DPPIV regulates the activities of a number of cytokines and chemokines. However, direct *in vivo* evidence for a role for CD26 in tumor biology and its interaction with the tumor microenvironment (TME) has not yet been reported. Recent work has demonstrated clearly the interaction between DPPIV and substrate CXCL10, as well as the functional role of DPPIV-mediated post-translational modification of chemokines in regulating tumor immunity (101). Preservation of the full length, bioactive CXCL10 by DPPIV inhibition results in increased level of CXCR3$^+$ effector T cells in the TME and subsequent tumor growth reduction. CXCR3 has been shown to be a functional receptor for CXCL10 (102). Importantly, the combination of DPPIV inhibition and checkpoint blockade therapy remarkably augments the efficacy of naturally occurring and immunotherapy-based tumor immunity. These investigators therefore provide the direct evidence of DPPIV as an *in vivo* regulator of CXCL10-mediated T cell trafficking with relevance for tumor immunity and immunotherapy (Figure 2). The TME consists of numerous cell types along with the neoplastic cells. Among them are the effector lymphocytes capable of infiltrating into the tumor sites that are specifically required for anti-cancer immune response (103). CXCL10 is a chemoattractant for immune cells such as monocytes, T cells and NK cells and is secreted from a variety of cells in response to IFN-γ, including monocytes, neutrophils, eosinophils, epithelial cells, endothelial cells, fibroblasts and keratinocytes (104). CXCL10 appears to have a dual role on tumor growth, with its proliferative or anti-proliferative activity being cell-type-dependent as a result of differences in the subtype of its receptor CXCR3 (104). CXCR3 is rapidly induced on naïve T cells following activation and preferentially remains highly expressed on T_H1-type CD4$^+$ cells and CD8$^+$ cytotoxic T lymphocytes (CTL), resulting in enhancement of T cell migration to facilitate tumor immune responses (105). Although strong T_H1 and CTL responses in the TME are beneficial for tumor suppression, these responses are counterbalanced to prevent unwanted tissue damage and immunopathology by disrupting the proinflammatory loop. CXCR3$^+$ T_{reg} has been recently identified (106) , as IFN-γ signaling activates the T_H1 transcription factor *T-bet*, which in turn promotes CXCR3 expression to induce T_H1-specific T_{reg} in the inflammatory sites. Moreover, CXCR3 is a marker of CD8$^+$ IL-10-producing cells with suppressive activity in both mice and human (107). The exact factors determining whether CXCR3$^+$ effector T cells and CXCR3$^+$ regulatory lymphocytes will oppose or cooperate with each other during the tumor growth process *in vivo* remain to be elucidated.

4.1.2. Immune checkpoint mechanism via CD26/DPPIV

Although the cellular and molecular mechanisms involved in CD26-mediated T cell activation have been extensively evaluated by our group and others (4-6, 9, 13, 90), potential negative feedback mechanisms to regulate CD26-mediated activation still remain to be elucidated. Utilizing human PBL, we found that production of IL-10 by CD4$^+$ T cells is preferentially increased following CD26-mediated costimulation compared with CD28-mediated costimulation (108). IL-21 production was also greatly enhanced in the late phase of CD26 costimulation. On the other hand, production of IL-2, IL-5 or TNF-α was much lower following CD26 costimulation than CD28 costimulation. In contrast, no difference in the production of IL-17A, IFN-γ, or IL-4 was observed following CD26 or CD28-mediated costimulation. These data indicate that CD26 and CD28 costimulation of CD4$^+$ T cells results in different cytokine production profiles, with IL-10 production being preferentially enhanced following CD26 costimulation. Furthermore, we found that both the cell surface and intracellular expression of LAG3 (lymphocyte activation gene-3) was clearly enhanced with increasing doses of anti-CD26 mAb, and that CD26-induced enhancement of LAG3 was more pronounced than the effect of CD28-mediated costimulation. On the other hand, both CD26 and CD28-mediated costimulation enhanced the expression of CTLA-4 (cytotoxic T-lymphocyte-associated antigen 4) and FOXP3 (forkhead box protein P3), with no significant difference being detected between these two costimulatory pathways. In contrast with CD28 costimulation, LAP (latency associated protein) complexed with TGF-β1 was hardly induced following CD26 costimulation. We showed that all the CD4$^+$ T cells expressed LAG3 following CD26 or CD28 costimulation, and that no difference was observed in the percentage of LAG3 expressing cells, while the expression intensity of LAG3 after CD26-mediated costimulation was significantly higher than after CD28-mediated costimulation. LAG3 serves as a marker of IL-10 producing T_{reg} (109), and binds to major histocompatibility complex (MHC) class II molecules with higher affinity than CD4, leading to transduction of inhibitory signals for both T cells and APCs (110, 111). Therefore, our data strongly suggest that signaling events via CD26 may induce the development of CD4$^+$ T cells to a Type 1 regulatory T cells (Tr1)-like phenotype. By expression analysis with Western blotting and quantitative real-time polymerase chain reaction (RT-PCR) experiments and by cell functional analysis utilizing chemical inhibitors and small interfering RNA (siRNA) experiments, we showed that co-engagement of CD3 and CD26 induces preferential production of IL-10 in human CD4$^+$ T cells, mediated through NFAT (nuclear factor of activated T cells) and Raf (rapidly accelerated fibrosarcoma)-MEK (mitogen-activated protein kinase (MAPK)/extracellular signal-regulated kinase (ERK) kinase)-ERK pathways (108). High level of early growth response 2 (EGR2) is also induced following CD26 costimulation, possibly via NFAT and AP-1 (activator protein-1)-mediated signaling, and knock down of EGR2 leads to decreased IL-10 production. Taken together, these observations strongly suggest that CD26-mediated costimulation of CD4$^+$ T cells results in enhanced NFAT/AP-1-dependent EGR2 expression, which is associated with the preferential production of IL-10. Finally, we demonstrated that CD3/CD26-stimulated CD4$^+$ T cells clearly suppress

proliferative activity and effector cytokine production of bystander T cells in an IL-10-dependent manner (108). Collectively, our results above suggest that CD3/CD26 costimulation induces the development of human Tr1-like cells from $CD4^+$ T cells with high level of IL-10 production and LAG3 expression. Preclinical models showed that antibody-mediated blocking of LAG3 as potential anti-cancer therapy led to enhanced activation of antigen-specific T cells at the tumor sites and disruption of tumor growth (112). Moreover, anti-LAG3/anti-PD-1 (programmed cell death 1) antibody treatment cured most mice of established tumors that were largely resistant to single antibody treatment (112). Taken together, it is conceivable that CD26 itself may function as an inhibitory molecule of an immune checkpoint system in certain disease conditions, similar to LAG3 or PD-1.

4.2. Malignant pleural mesothelioma

4.2.1. FIH phase I clinical trial of humanized anti-CD26 mAb

Our previous work analyzing extracellular matrix (ECM) interactions and intracellular signaling events demonstrated that the malignant mesothelial cell line JMN expresses CD26 (113). Our recent in-depth studies of CD26 expression in malignant pleural mesothelioma (MPM) revealed that CD26 is preferentially expressed in MPM cells but not in normal mesothelial cells (114, 115). These intriguing findings propelled our development of CD26-targeted therapy for MPM. For this purpose, we had developed a novel humanized anti-CD26 mAb, namely YS110. YS110 is a recombinant DNA-derived humanized mAb that selectively binds with high affinity to the extracellular domain of CD26. The antibody is an $IgG_1\kappa$ with a molecular weight of 144 kDa and was humanized via an *in silico* design based on the AA sequence of anti-human CD26 murine mAb (14D10), which inhibited tumor cell growth, migration and invasion, and enhanced survival of mouse xenograft models (116). YS110 is produced by fermentation in CHO (Chinese hamster ovary) mammalian cell suspension culture with the Glutamine Synthetase Expression System. *In vitro* pharmacologic evaluation of YS110 demonstrated its selective binding to human CD26 on a number of human cancer cell lines and tissues, with no apparent effect on immune activation and no inhibition of DPPIV activity, while exhibiting direct cytotoxic effect on certain human CD26-positive cancer cell lines. Moreover, our *in vitro* data indicated that YS110 induces cell lysis of MPM cells via antibody-dependent cellular cytotoxicity (ADCC) in addition to its direct anti-tumor effect via cyclin-dependent kinase inhibitor (CDKI) $p27^{kip1}$ and $p21^{cip1}$ accumulation (68, 117). *In vivo* experiments with mouse xenograft models involving human MPM cells demonstrated that YS110 treatment drastically inhibits tumor growth in tumor-bearing mice and reduces formation of metastases, resulting in enhanced survival (68). Our data strongly suggest that YS110 may have potential clinical use as a novel cancer therapeutic agent for CD26-positive malignant mesothelioma.

In addition to our robust *in vitro* and *in vivo* data on antibody-mediated dose-dependent tumor growth inhibition, YS110 exhibited excellent safety and pharmacological profiles in non-human primate models using single and repeated increasing intravenous doses. Considering the lack of T cell proliferation and cytokine production *in vitro*, YS110 was therefore considered not to have an agonistic nor activating effect on human CD26-positive lymphocytes. Other key safety findings were obtained from studies involving cynomolgus monkeys which express YS110-reactive CD26 molecules, with similar tissue distribution profiles and expression levels to human CD26. We therefore conducted the FIH clinical trial of YS110 for patients with MPM and other CD26-positive solid tumors (70). Thirty-three heavily pre-treated patients with CD26-positive cancers including 22 malignant mesothelioma, 10 renal cell carcinoma (RCC) and 1 urothelial carcinoma underwent YS110 administration. A total of 232 infusions (median 3 (range 1-30)) of YS110 were administered across 6 dose levels ranging from 0.1. to 6.0. mg/kg. Maximum tolerated dose (MTD) was not reached and 2 dose limiting toxicities (DLTs) (1 patient with grade 3 anaphylactic reaction at 1.0. mg/kg and 1 patient with grade 3 allergic reaction at 2.0. mg/kg) were reported with complete resolution following dose omission. Subsequent use of systemic steroid prophylaxis and exclusion of patients with significant allergy histories improved safety profile. No dose-dependent adverse events were observed. Blood exposure pharmacokinetics parameters (AUC and C_{max}) increased in proportion with the dose. Cytokines and immunophenotyping assays indicated CD26 target modulation with no occurrence of infectious nor autoimmune disease complications. These results demonstrated that YS110 is tolerable in human subjects. A secondary objective of this FIH study was to evaluate the potential antitumor activity of YS110 according to RECIST 1.0. (response evaluation criteria in solid tumors) criteria (or modified RECIST criteria for mesothelioma). No objective response was achieved in any of the treated patients. However, stable disease as the best overall response was observed in 13 out of the 26 valuable patients on Day 43 of the first cycle (1 at 0.1. mg/kg, 2 at 0.4. mg/kg, 7 at 2.0. mg/kg, 1 at 4.0. mg/kg and 2 at 6.0. mg/kg). Prolonged stabilization with 26 weeks or more was observed in 7 out of 13 stable disease patients who have received a total of 143 (5 to 30 infusions/patients) infusions with a median PFS (progression-free survival) of 33 weeks (26 to 57 weeks). This FIH study conclusively demonstrated that YS110 exhibits a favorable safety profile and substantial clinical activity in heavily pretreated CD26-positive MPM patients who had previously progressed on conventional standard chemotherapies. Further clinical trial of YS110 for MPM is in progress worldwide (118).

4.2.2. DPPIV enzyme activity and efficacy of YS110

The FIH clinical study of YS110 revealed that an increase in YS110 infusion dose was associated with decreased serum sCD26 level, particularly in cohorts 4-6 (2.0. to 6.0. mg/kg), with an approximately 80% decrease in sCD26 level (70). Moreover, since sCD26 level reflects DPPIV enzyme activity in sera (119), similar reduction in DPPIV enzyme activity was observed, again particularly in patients in cohorts 4-6. Although DPPIV inhibitors are clinically used as oral hypoglycemic agents (120), hypoglycemia was not observed during YS110 administration. Of note is the fact that greater than 80% inhibition of serum DPPIV activity was obtained 24 hours after oral administration of clinically available DPPIV inhibitors (drug information published by manufacturers of sitagliptin, vildagliptin, saxagliptin and *etc.*), a level of inhibition comparable to that seen in patients treated with YS110. Our current data would therefore indicate that YS110 therapy is tolerable in the clinical setting. As

described in the previous section, recent work has demonstrated the functional role of DPPIV-mediated post-translational modification of chemokines in regulating tumor immunity through its interaction with its substrate CXCL10 (101). This anti-tumor response is potentiated in combination with other anti-tumor immunotherapeutic approaches including CpG adjuvant therapy, adoptive T cell transfer therapy and checkpoint blockade therapy (anti-CTLA-4 and anti-PD-1) (101). In view of these recent findings, data from our current trial showing that serum DPPIV activity was decreased following treatment with YS110 in a dose-dependent manner would suggest that anti-tumor activity via DPPIV inhibition may constitute yet another mechanism of action for the anti-tumor activity of YS110.

4.2.3. Mechanisms of action of YS110 for cancer treatment

We previously showed that depletion of CD26 by RNAi results in the loss of adhesive property, suggesting that CD26 is a binding protein to the ECM (68). Moreover, our observations regarding the CD26-CD9-α5β1 integrin complex suggest that CD26 regulates the interaction of MPM cells with the ECM via yet-to-be-determined integrin adhesion molecules (121). Recently, we found that expression of CD26 upregulates periostin secretion by MPM cells, leading to enhanced MPM cell migratory and invasive activity (122). Periostin is a secreted cell adhesion protein of approximately 90 kDa, which shares a homology with the insect cell adhesion molecule fasciclin 1 (FAS1) (123). We also demonstrated that the cytoplasmic region of CD26 plays a crucial role in MPM tumor biology through its linkage to somatostatin receptor 4 (SSTR4) and SHP-2 protein tyrosine phosphatase in cell membrane lipid rafts, leading to cytostatic effects in MPM cells without direct association of the ECM to CD26 by anti-CD26 mAb treatment (Figure 3) (124). In view of the findings above, we propose that CD26 forms macromolecular complexes in the cell surface of MPM by connecting periostin and ECM to intracellular signaling events (125); (i) In CD26-negative MPM cells, SSTR4 mediated inhibitory signaling to suppress cell proliferation and motility. In contrast, by locking the signaling domain of SSTR4 with CD26 association, SSTR4-mediated anti-tumor effects were abrogated, leading to increased cell proliferation and motility in CD26-positive MPM cells. (ii) In addition, CD26 regulated ECM-associated tumor cell behavior in association with integrins and periostin-ECM complex. CD9 suppressed cell invasion and migration by inhibiting the formation of CD26-α5β1 integrin complex. Moreover, expression of CD26 upregulated periostin secretion by MPM cells, leading to enhanced MPM cell migratory and invasive activity. (iii) Furthermore, periostin is a secreted cell adhesion protein. The N-terminal region regulates cellular functions by binding to integrins at the plasma membrane of the cells through cell adhesion domain. The C-terminal region of the protein regulates cell–matrix organization and interaction by binding such ECM proteins, leading to increased MPM cell motility. As a result, CD26 molecule in MPM also plays a pivotal role in connecting ECM to intracellular signaling events associated with cell proliferation and motility. It is therefore conceivable that targeting CD26 may be a novel and effective therapeutic approach for MPM.

In addition to the ECM association, our *in vitro* data indicate that YS110 induces cell lysis of MPM cells via ADCC in addition to its direct anti-tumor effect via CDKI $p27^{kip1}$ accumulation (68). More recently, we evaluated the direct anti-tumor effect of YS110 against the MPM cell lines H2452 and JMN, and investigated its effects on cell cycle and on the cell cycle regulator molecules (117). YS110 suppressed the proliferation of H2452 cells by approximately 20% in 48 hours of incubation. Cell cycle analysis demonstrated that the percentage of cells in G2/M phase increased by 8.0.% on average following YS110 treatment. In addition, level of the cell cycle regulator $p21^{cip1}$ was increased and cyclin B1 was decreased after YS110 treatment. Inhibitory phosphorylation of both cdc2 (Tyr15) and cdc25C (Ser216) was elevated. Furthermore, activating phosphorylation of p38 MAPK (Thr180/Tyr182) and ERK1/2 (Thr202/Tyr204) was augmented following 24 hours of YS110 treatment. In addition, we investigated the synergistic effects of YS110 and the anti-tumor agent pemetrexed on selected MPM cell lines in both *in vitro* and *in vivo* studies. Pemetrexed rapidly induced CD26 expression on cell surface, and treatment with both YS110 and pemetrexed inhibited *in vivo* tumor growth accompanied by a synergistic reduction in the MIB-1 index (117).

We also demonstrated that treatment with YS110, which inhibited cancer cell growth, induced nuclear translocation of both cell-surface CD26 and YS110 (126, 127). In response to YS110 treatment, CD26 was translocated into the nucleus via caveolin-dependent endocytosis, and interacted with a genomic flanking region of the *POLR2A* gene, a component of RNA polymerase II. This interaction consequently led to transcriptional repression of the *POLR2A* gene, resulting in retarded cancer cell proliferation. Furthermore, impaired nuclear transport of CD26 reversed the *POLR2A* repression induced by YS110 treatment. These findings reveal that nuclear CD26 functions in the regulation of gene expression and tumor growth, and yet another novel mechanism of action of anti-CD26 mAb therapy may involve the regulation of inducible traffic of surface CD26 molecules into the cell nucleus.

4.3. Other cancers

In contrast to our robust findings regarding the role of CD26/DPPIV on MPM, the exact role of CD26/DPPIV in other cancers remains to be elucidated, partly due to its variable expression on these tumors. In general, it is strongly expressed on some cancers, while being absent or present at low levels in others (8). Furthermore, given its multiple biological functions, including its ability to associate with several key proteins and its cleavage of a number of soluble factors to regulate their function, it is likely that the CD26/DPPIV effect on tumor biology is at least partly mediated by the effect of these biological functions on specific tumor types (128).

CD26 has also been shown to be expressed on RCC (129, 130), including the cell lines Caki-1, Caki-2, ACHN, and VMRC-RCW (116). We previously showed that anti-CD26 mAb inhibition of the Caki-2 cell line was associated with G1/S cell cycle arrest, enhanced $p27^{kip1}$ expression, down regulation of cyclin-dependent kinase 2 (CDK2) and dephosphorylation of retinoblastoma substrate (Rb) (116). We also found that anti-CD26 mAb therapy attenuated Akt activity and internalized cell surface CD26 leading to decreased CD26 binding to collagen and fibronectin. Finally, we showed that anti-CD26 mAb inhibited human RCC in a mouse xenograft model (116).

Immunofluorescence analysis revealed expression of CD26/DPPIV on peripheral blood lymphocytes of patients with B chronic lymphocytic leukemia (B-CLL), but not on peripheral B cells from normal donors (131). CD26/DPPIV could also be induced in normal B cells following treatment with IL-4, indicating that expression was regulated at the level of transcription (131). CD26/DPPIV has also been shown to be a marker for aggressive T-large granular lymphocyte (T-LGL) lymphoproliferative disorder. Our work indicated that patients with CD26-positive disease were more likely to require therapies for cytopenia and infections associated with the disease than those with CD26-negative T-LGL (132). Furthermore, CD26-related signaling may be aberrant in T-LGL as compared to T-lymphocytes from normal donors (132). Disease aggressiveness is also correlated with CD26/DPPIV expression in other subsets of T-cell malignancies including T-lymphoblastic lymphoma/acute lymphoblastic leukemia (LBL/ALL), as those with CD26-positive T-LBL/ALL had a worse clinical outcome compared to patients with CD26-negative tumors (133, 134).

JKT-hCD26WT cells resulted in a greater sensitivity to doxorubicin and etoposide compared to mock transfected cells (135-138). Jurkat cells transfected with a nonfunctional DPPIV catalytic site mutant (Ser630Ala) did not show increased doxorubicin and etoposide sensitivity, suggesting that DPPIV activity is required for chemo-sensitization. A CD26 transfectant with a mutation at the ADA binding site retains DPPIV activity and had a higher level of doxorubicin sensitivity. Surface CD26 expression and DPPIV activity are associated with increased doxorubicin sensitivity and cell cycle arrest in Jurkat cells. Also, there are differences in hyperphosphorylation and inhibition of $p34^{cdc2}$ kinase activity, phosphorylation of cdc25C, and alteration in cyclin B1 expression associated with doxorubicin sensitivity in Jurkat cell lines (136). Therefore, inhibition of CD26 increases cell survival, while increased CD26 expression is associated with decreased drug resistance. The mechanism of this decreased resistance appears to be by CD26 mediated enhanced expression of topoisomerase IIα – the target for both doxorubicin and etoposide. The increased sensitivity to doxorubicin and etoposide in CD26 expressing tumors may be important in T-cell hematologic malignancies as well as other cancers. Surface expression of CD26 increases topoisomerase IIα level in the B-cell line Jiyoye and increases doxorubicin sensitivity (139). This was demonstrated by using CD26 transfection constructs in the Jiyoye B-cell lymphoma cell line as well as by target specific siRNA inhibition of CD26 in the Karpas-299 T-cell leukemia cell line. Therefore, CD26 has effects on topoisomerase IIα and doxorubicin sensitivity in both B-cell and T-cell lines. Increased CD26/DPPIV levels are associated with increased phosphorylation of p38 and its upstream regulators – MAPK kinase (MAPKK) 3/6 and apoptosis signal-regulating kinase 1 (ASK1). Therefore, the p38 signaling pathway may be involved in the regulation of topoisomerase IIα expression. Doxorubicin treated SCID mice had increased survival in those injected with wild type CD26 compared to vector or DPPIV catalytic site mutant (Ser630Ala) injected mice. CD26/DPPIV levels may be useful predictive markers for doxorubicin treatment of cancer. CD26 level is also associated with etoposide resistance. CD26 mediated changes include hyperphosphorylation of $p34^{cdc2}$, variation in cdc25C level and phosphorylation, and changes in cyclin B1 level. Since CD26/DPPIV cleaves substrates resulting in altered function (140, 141), it is possible that CD26-associated drug sensitivity may therefore be mediated by serum-derived factors. However, our work showed that the increased doxorubicin and etoposide sensitivity of JKT-hCD26WT was independent of serum, data which suggest an effect of CD26 on cell-mediated processes, such as signal transduction, rather than serum-derived factors (137).

Pang *et al.* identified a subpopulation of $CD26^+$ cells uniformly presenting in both primary and metastatic tumors in colorectal cancer (CRC), and showed that $CD26^+$ cancer cells were associated with enhanced invasiveness and chemoresistance (142). These investigators showed that in $CD26^+$ CRC cells, mediators of epithelial to mesenchymal transition (EMT) contribute to the invasive phenotype and metastatic capacity. These results suggest that $CD26^+$ cells are cancer stem cells in CRC, and that CD26/DPPIV can be targeted for metastatic CRC therapy. Recently, other investigators demonstrated in a murine model that lung metastasis of CRC was suppressed by treatment with a DPPIV inhibitor (143). They showed a reduction of EMT markers, suggesting that the EMT status of the murine colon cancer cell line MC38 was at least in part affected by DPPIV inhibition, with a diminution in the growth of metastases. They also showed that DPPIV inhibition decreased the growth of lung metastases of colon cancer by downregulating autophagy, increasing apoptosis and arresting the cell cycle. These data therefore suggest that DPPIV inhibition may be an effective therapeutic strategy for the treatment of cancers with pulmonary metastases (143).

Yamada *et al.* comprehensively investigated gene expression profiles in surgical samples of untreated gastrointestinal stromal tumors (GIST) of the stomach and small intestine. They found that the disease-free survival of patients with CD26-positive GIST of the stomach was worse than that of patients with CD26-negative GIST (144). Moreover, the postoperative recurrence rate of CD26-negative gastric GIST cases was as low as 2.0.%. They concluded that CD26 is a significant prognostic factor of gastric GIST and may also serve as a therapeutic target (144). Meanwhile, CD26 expression was not associated with clinical outcome of small intestinal GIST.

5. SUMMARY AND PERSPECTIVES

Initially described in 1966 as an enzyme with intrinsic DPPIV activity (145), this activity was subsequently found to be identical to CD26, a 110 kDa extracellular membrane-bound glycoprotein expressed on many tissues including brain, endothelium, heart, intestine, kidney, liver, lung, skeletal muscle, pancreas, placenta, and lymphocytes (26, 146, 147). Originally characterized as a T cell differentiation antigen, CD26 is preferentially expressed on a specific population of T lymphocytes, the subset of $CD4^+CD45RO^+$ memory T cells, and is upregulated following T cell activation (15, 26). Besides being a marker of T cell activation, CD26 is also associated with T cell signal transduction processes as a costimulatory molecule (5-7). CD26 therefore has an important role in T cell biology and overall immune function, and represents a novel therapeutic target for various immune disorders (13, 52, 148-150). CD26 is also expressed on various tumors such as MPM, CRC, RCC, hepatocellular carcinoma, lung cancer, prostate cancer, GIST, thyroid cancer, and hematologic malignancies such as T-anaplastic large cell lymphoma and T-LBL/ALL (10). Moreover, in several human malignancies including CRC, chronic myeloid leukemia, gastric adenocarcinoma and MPM, CD26/DPPIV expression is reported to be a marker of cancer stem cells (142, 151-155). Given the potential role of CD26 surface expression in cancer biology, YS110 therapy may also influence tumor growth through its potential effect on the cancer stem cells of selected tumors. We recently developed novel anti-human CD26 mAbs that can be used as companion diagnostic reagents suitable for immunohistochemical staining of CD26 in formalin-fixed tissue sections with reliable clarity and intensity (155). Since these mAbs display no cross-reactivity with the therapeutic humanized anti-CD26 mAb YS110, they may be suitable for assays analyzing CD26 expression during or following treatment with YS110, with important implications in the clinical setting.

Since CD26/DPPIV has a multitude of biological functions in immune system and human tumor cells, further detailed understanding of the role of this molecule in various clinical settings may lead potentially to novel therapeutic approaches.

6. ACKNOWLEDGEMENT

This work was supported by a Grant-in-Aid (S1311011) from the Foundation of Strategic Research Projects in Private Universities from the Ministry of Education, Culture, Sports, Science, and Technology, Japan; JSPS KAKENHI Grant Number 15H04879; JSPS KAKENHI Grant Number 16H05345; JSPS KAKENHI Grant Number 26830114; a grant of the Ministry of Health, Labour, and Welfare, Japan (Grant Number 150401-01). KO, TY, NHD and CM are founding members of Y's AC Co., Ltd. YK is the CEO of of Y's AC Co., Ltd. Parts of Figures shown in Figures 1 and 2 are reproduced with permission from K Ohnuma *et al.*, *J Virol* 87: 13892-13899, 2013 (*Copyright 2013. American Society for Microbiology*), and K Ohnuma *et al.*, *Nat Immunol* 16: 791-792, 2015 (*Copyright 2015. Nature Publishing Group)*.

7. REFERENCES

1. D. A. Fox, R. E. Hussey, K. A. Fitzgerald, O. Acuto, C. Poole, L. Palley, J. F. Daley, S. F. Schlossman and E. L. Reinherz: Ta1, a novel 105 KD human T cell activation antigen defined by a monoclonal antibody. *J Immunol*, 133(3), 1250-6 (1984)

2. D. M. Nanus, D. Engelstein, G. A. Gastl, L. Gluck, M. J. Vidal, M. Morrison, C. L. Finstad, N. H. Bander and A. P. Albino: Molecular cloning of the human kidney differentiation antigen gp160: human aminopeptidase A. *Proc Natl Acad Sci U S A*, 90(15), 7069-73 (1993) doi:10.1.073/pnas.90.1.5.7.069

3. T. Tanaka, D. Camerini, B. Seed, Y. Torimoto, N. H. Dang, J. Kameoka, H. N. Dahlberg, S. F. Schlossman and C. Morimoto: Cloning and functional expression of the T cell activation antigen CD26. *J Immunol*, 149(2), 481-6 (1992)

4. I. De Meester, S. Korom, J. Van Damme and S. Scharpe: CD26, let it cut or cut it down. *Immunol Today*, 20(8), 367-75 (1999) doi:10.1.016/S0167-5699(99)01486-3

5. B. Fleischer: CD26: a surface protease involved in T-cell activation. *Immunol Today*, 15(4), 180-4 (1994) doi:10.1.016/0167-5699(94)90316-6

6. C. Morimoto and S. F. Schlossman: The structure and function of CD26 in the T-cell immune response. *Immunol Rev*, 161, 55-70 (1998) doi:10.1.111/j.1600-065X.1998.tb01571.x

7. A. von Bonin, J. Huhn and B. Fleischer: Dipeptidyl-peptidase IV/CD26 on T cells: analysis of an alternative T-cell activation pathway. *Immunol Rev*, 161, 43-53 (1998) doi:10.1.111/j.1600-065X.1998.tb01570.x

8. M. A. Thompson, K. Ohnuma, M. Abe, C. Morimoto and N. H. Dang: CD26/dipeptidyl peptidase IV as a novel therapeutic target for cancer and immune disorders. *Mini Rev Med Chem*, 7(3), 253-73 (2007) doi:10.2.174/138955707780059853

9. K. Ohnuma, N. H. Dang and C. Morimoto: Revisiting an old acquaintance: CD26 and its molecular mechanisms in T cell function. *Trends Immunol*, 29(6), 295-301 (2008) doi:10.1.016/j.it.2008.0.2.0.10

10. P. A. Havre, M. Abe, Y. Urasaki, K. Ohnuma, C. Morimoto and N. H. Dang: The role of CD26/dipeptidyl peptidase IV in cancer. *Front Biosci*, 13, 1634-45 (2008) doi:10.2.741/2787

11. P. Busek, J. Stremenova and A. Sedo: Dipeptidyl peptidase-IV enzymatic activity bearing molecules in human brain tumors--good or evil? *Front Biosci*, 13, 2319-26 (2008) doi:10.5.772/53888

12. L. Sromova, P. Busek, L. Sedova and A. Sedo: Intraindividual changes of dipeptidyl peptidase-IV in peripheral blood of patients with rheumatoid arthritis are associated with the disease activity. *BMC Musculoskelet Disord*, 16, 244 (2015) doi:10.1.186/s12891-015-0707-y

13. K. Ohnuma, N. Takahashi, T. Yamochi, O. Hosono, N. H. Dang and C. Morimoto: Role of CD26/dipeptidyl peptidase IV in human T cell activation and function. *Front Biosci*, 13, 2299-310 (2008) doi:10.2.741/2844

14. B. R. Blazar, W. J. Murphy and M. Abedi: Advances in graft-versus-host disease biology and therapy. *Nat Rev Immunol*, 12(6), 443-58 (2012) doi:10.1.038/nri3212

15. H. J. Deeg, D. Lin, W. Leisenring, M. Boeckh, C. Anasetti, F. R. Appelbaum, T. R. Chauncey, K. Doney, M. Flowers, P. Martin, R. Nash, G. Schoch, K. M. Sullivan, R. P. Witherspoon and R. Storb: Cyclosporine or cyclosporine plus methylprednisolone for prophylaxis of graft-versus-host disease: a prospective, randomized trial. *Blood*, 89(10), 3880-7 (1997)

16. A. H. Filipovich: Diagnosis and manifestations of chronic graft-versus-host disease. *Best Pract Res Clin Haematol*, 21(2), 251-7 (2008) doi:10.1.016/j.beha.2008.0.2.0.08

17. G. Socie and J. Ritz: Current issues in chronic graft-versus-host disease. *Blood*, 124(3), 374-84 (2014) doi:10.1.182/blood-2014-01-514752

18. J. W. Chien, S. Duncan, K. M. Williams and S. Z. Pavletic: Bronchiolitis obliterans syndrome after allogeneic hematopoietic stem cell transplantation-an increasingly recognized manifestation of chronic graft-versus-host disease. *Biol Blood Marrow Transplant*, 16(1 Suppl), S106-14 (2010) doi:10.1.016/j.bbmt.2009.1.1.0.02

19. A. Z. Dudek, H. Mahaseth, T. E. DeFor and D. J. Weisdorf: Bronchiolitis obliterans in chronic graft-versus-host disease: analysis of risk factors and treatment outcomes. *Biol Blood Marrow Transplant*, 9(10), 657-66 (2003) doi:10.1.016/S1083

20. C. Nakaseko, S. Ozawa, E. Sakaida, M. Sakai, Y. Kanda, K. Oshima, M. Kurokawa, S. Takahashi, J. Ooi, T. Shimizu, A. Yokota, F. Yoshiba, K. Fujimaki, H. Kanamori, R. Sakai, T. Saitoh, T. Sakura, A. Maruta, H. Sakamaki and S. Okamoto: Incidence, risk factors and outcomes of bronchiolitis obliterans after allogeneic stem cell transplantation. *Int J Hematol*, 93(3), 375-82 (2011) doi:10.1.007/s12185-011-0809-8

21. R. Zeiser and B. R. Blazar: Preclinical models of acute and chronic graft-versus-host disease: how predictive are they for a successful clinical translation? *Blood*, 127(25), 3117-26 (2016) doi:10.1.182/blood-2016-02-699082

22. R. Champlin, I. Khouri and S. Giralt: Graft-vs.-malignancy with allogeneic blood stem cell transplantation: a potential primary treatment modality. *Pediatr Transplant*, 3 Suppl 1, 52-8 (1999) doi:10.1.034/j.1399-3046.1.999.0.0054.x

23. C. E. Rudd: T-cell signaling and immunopathologies. *Semin Immunopathol*, 32(2), 91-4 (2010) doi:10.1.007/s00281-010-0203-2

24. K. A. Markey, K. P. MacDonald and G. R. Hill: The biology of graft-versus-host disease: experimental systems instructing clinical practice. *Blood*, 124(3), 354-62 (2014) doi:10.1.182/blood-2014-02-514745

25. N. H. Dang, Y. Torimoto, K. Deusch, S. F. Schlossman and C. Morimoto: Comitogenic effect of solid-phase immobilized anti-1F7 on human CD4 T cell activation via CD3 and CD2 pathways. *J Immunol*, 144(11), 4092-100 (1990)

26. C. Morimoto, Y. Torimoto, G. Levinson, C. E. Rudd, M. Schrieber, N. H. Dang, N. L. Letvin and S. F. Schlossman: 1F7, a novel cell surface molecule, involved in helper function of CD4 cells. *J Immunol*, 143(11), 3430-9 (1989)

27. K. Ohnuma, T. Yamochi, M. Uchiyama, K. Nishibashi, N. Yoshikawa, N. Shimizu, S. Iwata, H. Tanaka, N. H. Dang and C. Morimoto: CD26 up-regulates expression of CD86 on antigen-presenting cells by means of caveolin-1. *Proc Natl Acad Sci U S A*, 101(39), 14186-91 (2004) doi:10.1.073/pnas.0405266101

28. K. Ohnuma, T. Yamochi, M. Uchiyama, K. Nishibashi, S. Iwata, O. Hosono, H. Kawasaki, H. Tanaka, N. H. Dang and C. Morimoto: CD26 mediates dissociation of Tollip and IRAK-1 from caveolin-1 and induces upregulation of CD86 on antigen-

presenting cells. *Mol Cell Biol*, 25(17), 7743-57 (2005) doi:10.1.128/MCB.25.1.7.7.743-7757.2.005

29. K. Ohnuma, M. Uchiyama, T. Yamochi, K. Nishibashi, O. Hosono, N. Takahashi, S. Kina, H. Tanaka, X. Lin, N. H. Dang and C. Morimoto: Caveolin-1 triggers T-cell activation via CD26 in association with CARMA1. *J Biol Chem*, 282(13), 10117-31 (2007) doi:10.1.074/jbc.M609157200

30. K. Ohnuma, M. Uchiyama, R. Hatano, W. Takasawa, Y. Endo, N. H. Dang and C. Morimoto: Blockade of CD26-mediated T cell costimulation with soluble caveolin-1-Ig fusion protein induces anergy in CD4+T cells. *Biochem Biophys Res Commun*, 386(2), 327-32 (2009) doi:10.1.016/j.bbrc.2009.0.6.0.27

31. B. Bengsch, B. Seigel, T. Flecken, J. Wolanski, H. E. Blum and R. Thimme: Human Th17 cells express high levels of enzymatically active dipeptidylpeptidase IV (CD26). *J Immunol*, 188(11), 5438-47 (2012) doi:10.4.049/jimmunol.1103801

32. R. Hatano, K. Ohnuma, J. Yamamoto, N. H. Dang, T. Yamada and C. Morimoto: Prevention of acute graft-versus-host disease by humanized anti-CD26 monoclonal antibody. *Br J Haematol*, 162(2), 263-77 (2013) doi:10.1.111/bjh.12378

33. K. Sato, H. Nagayama and T. A. Takahashi: Aberrant CD3- and CD28-mediated signaling events in cord blood T cells are associated with dysfunctional regulation of Fas ligand-mediated cytotoxicity. *J Immunol*, 162(8), 4464-71 (1999)

34. S. Kobayashi, K. Ohnuma, M. Uchiyama, K. Iino, S. Iwata, N. H. Dang and C. Morimoto: Association of CD26 with CD45RA outside lipid rafts attenuates cord blood T-cell activation. *Blood*, 103(3), 1002-10 (2004) doi:10.1.182/blood-2003-08-2691

35. L. D. Shultz, M. A. Brehm, J. V. Garcia-Martinez and D. L. Greiner: Humanized mice for immune system investigation: progress, promise and challenges. *Nat Rev Immunol*, 12(11), 786-98 (2012) doi:10.1.038/nri3311

36. K. Tezuka, R. Xun, M. Tei, T. Ueno, M. Tanaka, N. Takenouchi and J. Fujisawa: An animal model of adult T-cell leukemia: humanized mice with HTLV-1-specific immunity. *Blood*, 123(3), 346-55 (2014) doi:10.1.182/blood-2013-06-508861

37. K. Ohnuma, R. Hatano, T. M. Aune, H. Otsuka, S. Iwata, N. H. Dang, T. Yamada and C. Morimoto: Regulation of pulmonary graft-versus-host disease by IL-26+CD26+CD4 T lymphocytes. *J Immunol*, 194(8), 3697-712 (2015) doi:10.4.049/jimmunol.1402785

38. P. L. Collins, M. A. Henderson and T. M. Aune: Lineage-specific adjacent *IFNG* and *IL26* genes share a common distal enhancer element. *Genes Immun*, 13(6), 481-8 (2012) doi:10.1.038/gene.2012.2.2

39. R. P. Donnelly, F. Sheikh, H. Dickensheets, R. Savan, H. A. Young and M. R. Walter: Interleukin-26: an IL-10-related cytokine produced by Th17 cells. *Cytokine Growth Factor Rev*, 21(5), 393-401 (2010) doi:10.1.016/j.cytogfr.2010.0.9.0.01

40. P. L. Collins, S. Chang, M. Henderson, M. Soutto, G. M. Davis, A. G. McLoed, M. J. Townsend, L. H. Glimcher, D. P. Mortlock and T. M. Aune: Distal regions of the human *IFNG* locus direct cell type-specific expression. *J Immunol*, 185(3), 1492-501 (2010) doi:10.4.049/jimmunol.1000124

41. J. A. Engelman, X. Zhang, F. Galbiati, D. Volonte, F. Sotgia, R. G. Pestell, C. Minetti, P. E. Scherer, T. Okamoto and M. P. Lisanti: Molecular genetics of the caveolin gene family: implications for human cancers, diabetes, Alzheimer disease, and muscular dystrophy. *Am J Hum Genet*, 63(6), 1578-87 (1998) doi:10.1.086/302172

42. C. J. Wu and J. Ritz: Revealing tumor immunity after hematopoietic stem cell transplantation. *Clin Cancer Res*, 15(14), 4515-7 (2009) doi:10.1.158/1078-0432.CCR-09-0873

43. D. Marguet, A. M. Bernard, I. Vivier, D. Darmoul, P. Naquet and M. Pierres: cDNA cloning for mouse thymocyte-activating molecule. A multifunctional ecto-dipeptidyl peptidase IV (CD26) included in a subgroup of serine proteases. *J Biol Chem*, 267(4), 2200-8 (1992)

44. S. Yan, D. Marguet, J. Dobers, W. Reutter and H. Fan: Deficiency of CD26 results in a change of cytokine and immunoglobulin secretion after stimulation by pokeweed mitogen. *Eur J Immunol*, 33(6), 1519-27 (2003) doi:10.1.002/eji.200323469

45. A. M. Zaki, S. van Boheemen, T. M. Bestebroer, A. D. Osterhaus and R. A. Fouchier: Isolation of a novel coronavirus from a man with pneumonia in Saudi Arabia. *N Engl J Med*, 367(19), 1814-20 (2012) doi:10.1.056/NEJMoa1211721

46. WHO Programmes and Projects. Emergencies: Middle East resipratory syndrome cornavirus (MERS-CoV).

http://www.who.int/emergencies/mers-cov/en/ (2017)

47. Y. Mo and D. Fisher: A review of treatment modalities for Middle East Respiratory Syndrome. *J Antimicrob Chemother*, 71(12), 3340-3350 (2016) doi:10.1.093/jac/dkw338

48. A. Zumla, J. F. Chan, E. I. Azhar, D. S. Hui and K. Y. Yuen: Coronaviruses - drug discovery and therapeutic options. *Nat Rev Drug Discov*, 15(5), 327-47 (2016) doi:10.1.038/nrd.2015.3.7

49. S. van Boheemen, M. de Graaf, C. Lauber, T. M. Bestebroer, V. S. Raj, A. M. Zaki, A. D. Osterhaus, B. L. Haagmans, A. E. Gorbalenya, E. J. Snijder and R. A. Fouchier: Genomic characterization of a newly discovered coronavirus associated with acute respiratory distress syndrome in humans. *MBio*, 3(6) (2012) doi:10.1.128/mBio.00473-12

50. S. Agnihothram, R. Gopal, B. L. Yount, Jr., E. F. Donaldson, V. D. Menachery, R. L. Graham, T. D. Scobey, L. E. Gralinski, M. R. Denison, M. Zambon and R. S. Baric: Evaluation of serologic and antigenic relationships between middle eastern respiratory syndrome coronavirus and other coronaviruses to develop vaccine platforms for the rapid response to emerging coronaviruses. *J Infect Dis*, 209(7), 995-1006 (2014) doi:10.1.093/infdis/jit609

51. H. Mou, V. S. Raj, F. J. van Kuppeveld, P. J. Rottier, B. L. Haagmans and B. J. Bosch: The receptor binding domain of the new Middle East respiratory syndrome coronavirus maps to a 231-residue region in the spike protein that efficiently elicits neutralizing antibodies. *J Virol*, 87(16), 9379-83 (2013) doi:10.1.128/JVI.01277-13

52. N. M. Okba, V. S. Raj and B. L. Haagmans: Middle East respiratory syndrome coronavirus vaccines: current status and novel approaches. *Curr Opin Virol*, 23, 49-58 (2017) doi:10.1.016/j.coviro.2017.0.3.0.07

53. S. Jiang, L. Lu, L. Du and A. K. Debnath: A predicted receptor-binding and critical neutralizing domain in S protein of the novel human coronavirus HCoV-EMC. *J Infect*, 66(5), 464-6 (2013) doi:10.1.016/j.jinf.2012.1.2.0.03

54. S. Gierer, S. Bertram, F. Kaup, F. Wrensch, A. Heurich, A. Kramer-Kuhl, K. Welsch, M. Winkler, B. Meyer, C. Drosten, U. Dittmer, T. von Hahn, G. Simmons, H. Hofmann and S. Pohlmann: The spike protein of the emerging betacoronavirus EMC uses a novel coronavirus receptor for entry, can be activated by TMPRSS2, and is targeted by neutralizing antibodies. *J Virol*, 87(10), 5502-11 (2013) doi:10.1.128/JVI.00128-13

55. G. Lu, Y. Hu, Q. Wang, J. Qi, F. Gao, Y. Li, Y. Zhang, W. Zhang, Y. Yuan, J. Bao, B. Zhang, Y. Shi, J. Yan and G. F. Gao: Molecular basis of binding between novel human coronavirus MERS-CoV and its receptor CD26. *Nature*, 500(7461), 227-31 (2013) doi:10.1.038/nature12328

56. V. S. Raj, H. Mou, S. L. Smits, D. H. Dekkers, M. A. Muller, R. Dijkman, D. Muth, J. A. Demmers, A. Zaki, R. A. Fouchier, V. Thiel, C. Drosten, P. J. Rottier, A. D. Osterhaus, B. J. Bosch and B. L. Haagmans: Dipeptidyl peptidase 4 is a functional receptor for the emerging human coronavirus-EMC. *Nature*, 495(7440), 251-4 (2013) doi:10.1.038/nature12005

57. L. Jiang, N. Wang, T. Zuo, X. Shi, K. M. Poon, Y. Wu, F. Gao, D. Li, R. Wang, J. Guo, L. Fu, K. Y. Yuen, B. J. Zheng, X. Wang and L. Zhang: Potent neutralization of MERS-CoV by human neutralizing monoclonal antibodies to the viral spike glycoprotein. *Sci Transl Med*, 6(234), 234ra59 (2014) doi:10.1.126/scitranslmed.3008140

58. J. Kameoka, T. Tanaka, Y. Nojima, S. F. Schlossman and C. Morimoto: Direct association of adenosine deaminase with a T cell activation antigen, CD26. *Science*, 261(5120), 466-9 (1993) doi:10.1.126/science.8101391

59. C. Gakis: Adenosine deaminase (ADA) isoenzymes ADA1 and ADA2: diagnostic and biological role. *Eur Respir J*, 9(4), 632-3 (1996) doi:10.1.183/09031936.9.6.0.9040632

60. W. A. Weihofen, J. Liu, W. Reutter, W. Saenger and H. Fan: Crystal structure of CD26/dipeptidyl-peptidase IV in complex with adenosine deaminase reveals a highly amphiphilic interface. *J Biol Chem*, 279(41), 43330-5 (2004) doi:10.1.074/jbc.M405001200

61. H. B. Rasmussen, S. Branner, F. C. Wiberg and N. Wagtmann: Crystal structure of human dipeptidyl peptidase IV/CD26 in complex with a substrate analog. *Nat Struct Biol*, 10(1), 19-25 (2003) doi:10.1.038/nsb882

62. K. Ohnuma, B. L. Haagmans, R. Hatano, V. S. Raj, H. Mou, S. Iwata, N. H. Dang, B. J. Bosch and C. Morimoto: Inhibition of Middle East respiratory syndrome coronavirus infection by anti-CD26 monoclonal antibody. *J Virol*, 87(24), 13892-9 (2013) doi:10.1.128/JVI.02448-13

63. H. A. Mohd, J. A. Al-Tawfiq and Z. A. Memish: Middle East Respiratory Syndrome Coronavirus (MERS-CoV) origin and

animal reservoir. *Virol J*, 13, 87 (2016) doi:10.1.186/s12985-016-0544-0

64. Z. A. Memish, A. I. Zumla, R. F. Al-Hakeem, A. A. Al-Rabeeah and G. M. Stephens: Family cluster of Middle East respiratory syndrome coronavirus infections. *N Engl J Med*, 368(26), 2487-94 (2013) doi:10.1.056/NEJMoa1303729

65. C. Drosten, M. Seilmaier, V. M. Corman, W. Hartmann, G. Scheible, S. Sack, W. Guggemos, R. Kallies, D. Muth, S. Junglen, M. A. Muller, W. Haas, H. Guberina, T. Rohnisch, M. Schmid-Wendtner, S. Aldabbagh, U. Dittmer, H. Gold, P. Graf, F. Bonin, A. Rambaut and C. M. Wendtner: Clinical features and virological analysis of a case of Middle East respiratory syndrome coronavirus infection. *Lancet Infect Dis*, 13(9), 745-51 (2013) doi:10.1.016/S1473-3099(13)70154-3

66. B. Guery, J. Poissy, L. el Mansouf, C. Sejourne, N. Ettahar, X. Lemaire, F. Vuotto, A. Goffard, S. Behillil, V. Enouf, V. Caro, A. Mailles, D. Che, J. C. Manuguerra, D. Mathieu, A. Fontanet, S. van der Werf and M. E.-C. s. group: Clinical features and viral diagnosis of two cases of infection with Middle East Respiratory Syndrome coronavirus: a report of nosocomial transmission. *Lancet*, 381(9885), 2265-72 (2013) doi:10.1.016/S0140-6736(13)60982-4

67. R. P. Dong, K. Tachibana, M. Hegen, S. Scharpe, D. Cho, S. F. Schlossman and C. Morimoto: Correlation of the epitopes defined by anti-CD26 mAbs and CD26 function. *Mol Immunol*, 35(1), 13-21 (1998) doi:10.1.016/S0161-5890(98)80013-8

68. T. Inamoto, T. Yamada, K. Ohnuma, S. Kina, N. Takahashi, T. Yamochi, S. Inamoto, Y. Katsuoka, O. Hosono, H. Tanaka, N. H. Dang and C. Morimoto: Humanized anti-CD26 monoclonal antibody as a treatment for malignant mesothelioma tumors. *Clin Cancer Res*, 13(14), 4191-200 (2007) doi:10.1.158/1078-0432.ccr-07-0110

69. N. Wang, X. Shi, L. Jiang, S. Zhang, D. Wang, P. Tong, D. Guo, L. Fu, Y. Cui, X. Liu, K. C. Arledge, Y. H. Chen, L. Zhang and X. Wang: Structure of MERS-CoV spike receptor-binding domain complexed with human receptor DPP4. *Cell Res*, 23(8), 986-93 (2013) doi:10.1.038/cr.2013.9.2

70. E. Angevin, N. Isambert, V. Trillet-Lenoir, B. You, J. Alexandre, G. Zalcman, P. Vielh, F. Farace, F. Valleix, T. Podoll, Y. Kuramochi, I. Miyashita, O. Hosono, N. H. Dang, K. Ohnuma, T. Yamada, Y. Kaneko and C. Morimoto: First-in-human phase 1 of YS110, a monoclonal antibody directed against CD26 in advanced CD26-expressing cancers. *Br J Cancer*, 116(9), 1126-1134 (2017) doi:10.1.038/bjc.2017.6.2

71. J. C. Szepietowski and A. Reich: Pruritus in psoriasis: An update. *Eur J Pain*, 20(1), 41-6 (2016) doi:10.1.002/ejp.768

72. G. Yosipovitch, A. Goon, J. Wee, Y. H. Chan and C. L. Goh: The prevalence and clinical characteristics of pruritus among patients with extensive psoriasis. *Br J Dermatol*, 143(5), 969-73 (2000) doi:10.1.046/j.1365-2133.2.000.0.3829.x

73. J. C. Szepietowski, A. Reich and B. Wisnicka: Pruritus and psoriasis. *Br J Dermatol*, 151(6), 1284 (2004) doi:10.1.111/j.1365-2133.2.004.0.6299.x

74. S. E. Chang, S. S. Han, H. J. Jung and J. H. Choi: Neuropeptides and their receptors in psoriatic skin in relation to pruritus. *Br J Dermatol*, 156(6), 1272-7 (2007) doi:10.1.111/j.1365-2133.2.007.0.7935.x

75. B. Amatya, G. Wennersten and K. Nordlind: Patients' perspective of pruritus in chronic plaque psoriasis: a questionnaire-based study. *J Eur Acad Dermatol Venereol*, 22(7), 822-6 (2008) doi:10.1.111/j.1468-3083.2.008.0.2591.x

76. G. Stinco, G. Trevisan, F. Piccirillo, S. Pezzetta, E. Errichetti, N. di Meo, F. Valent and P. Patrone: Pruritus in chronic plaque psoriasis: a questionnaire-based study of 230 Italian patients. *Acta Dermatovenerol Croat*, 22(2), 122-8 (2014)

77. M. Nakamura, M. Toyoda and M. Morohashi: Pruritogenic mediators in psoriasis vulgaris: comparative evaluation of itch-associated cutaneous factors. *Br J Dermatol*, 149(4), 718-30 (2003) doi:10.1.046/j.1365-2133.2.003.0.5586.x

78. A. S. Raut, R. H. Prabhu and V. B. Patravale: Psoriasis clinical implications and treatment: a review. *Crit Rev Ther Drug Carrier Syst*, 30(3), 183-216 (2013) doi:10.1.615/CritRevTherDrugCarrierSyst.2013005268

79. A. Thielitz, D. Reinhold, R. Vetter, U. Bank, M. Helmuth, R. Hartig, S. Wrenger, I. Wiswedel, U. Lendeckel, T. Kahne, K. Neubert, J. Faust, C. C. Zouboulis, S. Ansorge and H. Gollnick: Inhibitors of dipeptidyl peptidase IV and aminopeptidase N target major pathogenetic steps in acne initiation. *J Invest Dermatol*, 127(5), 1042-51 (2007) doi:10.1.038/sj.jid.5700439

80. M. Novelli, P. Savoia, M. T. Fierro, A. Verrone, P. Quaglino and M. G. Bernengo: Keratinocytes express dipeptidyl-peptidase IV (CD26) in benign and malignant skin diseases. *Br J Dermatol*, 134(6), 1052-6 (1996) doi:10.1.046/j.1365-2133.1.996.d01-900.x

81. R. G. van Lingen, P. C. van de Kerkhof, M. M. Seyger, E. M. de Jong, D. W. van Rens, M. K. Poll, P. L. Zeeuwen and P. E. van Erp: CD26/dipeptidyl-peptidase IV in psoriatic skin: upregulation and topographical changes. *Br J Dermatol*, 158(6), 1264-72 (2008) doi:10.1.111/j.1365-2133.2.008.0.8515.x

82. M. Lynch, A. M. Tobin, T. Ahern, D. O'Shea and B. Kirby: Sitagliptin for severe psoriasis. *Clin Exp Dermatol*, 39(7), 841-2 (2014) doi:10.1.111/ced.12408

83. T. Nishioka, M. Shinohara, N. Tanimoto, C. Kumagai and K. Hashimoto: Sitagliptin, a dipeptidyl peptidase-IV inhibitor, improves psoriasis. *Dermatology*, 224(1), 20-1 (2012) doi:10.1.159/000333358

84. K. Ohnuma, O. Hosono, N. H. Dang and C. Morimoto: Dipeptidyl peptidase in autoimmune pathophysiology. *Adv Clin Chem*, 53, 51-84 (2011) doi:10.1.016/B978-0-12-385855-9.0.0003-5

85. M. Diani, G. Altomare and E. Reali: T cell responses in psoriasis and psoriatic arthritis. *Autoimmun Rev*, 14(4), 286-92 (2015) doi:10.1.016/j.autrev.2014.1.1.0.12

86. J. Baliwag, D. H. Barnes and A. Johnston: Cytokines in psoriasis. *Cytokine*, 73(2), 342-50 (2015) doi:10.1.016/j.cyto.2014.1.2.0.14

87. M. P. Schon and W. H. Boehncke: Psoriasis. *N Engl J Med*, 352(18), 1899-912 (2005) doi:10.1.056/NEJMra041320

88. E. Komiya, R. Hatano, H. Otsuka, T. Itoh, H. Yamazaki, T. Yamada, N. H. Dang, M. Tominaga, Y. Suga, U. Kimura, K. Takamori, C. Morimoto and K. Ohnuma: A possible role for CD26/DPPIV enzyme activity in the regulation of psoriatic pruritus. *J Dermatol Sci*, 86(3), 212-221 (2017) doi:10.1.016/j.jdermsci.2017.0.3.0.05

89. K. Ohnuma, T. Saito, R. Hatano, O. Hosono, S. Iwata, N. H. Dang, H. Ninomiya and C. Morimoto: Comparison of two commercial ELISAs against an in-house ELISA for measuring soluble CD26 in human serum. *J Clin Lab Anal*, 29(2), 106-11 (2015) doi:10.1.002/jcla.21736

90. A. Sedo and R. Malik: Dipeptidyl peptidase IV-like molecules: homologous proteins or homologous activities? *Biochim Biophys Acta*, 1550(2), 107-16 (2001) doi:10.1.016/S0167-4838(01)00278-3

91. C. De Felipe, J. F. Herrero, J. A. O'Brien, J. A. Palmer, C. A. Doyle, A. J. Smith, J. M. Laird, C. Belmonte, F. Cervero and S. P. Hunt: Altered nociception, analgesia and aggression in mice lacking the receptor for substance P. *Nature*, 392(6674), 394-7 (1998) doi:10.1.038/32904

92. F. O. Nestle, P. Di Meglio, J. Z. Qin and B. J. Nickoloff: Skin immune sentinels in health and disease. *Nat Rev Immunol*, 9(10), 679-91 (2009) doi:10.1.038/nri2622

93. T. Akiyama and E. Carstens: Neural processing of itch. *Neuroscience*, 250, 697-714 (2013) doi:10.1.016/j.neuroscience.2013.0.7.0.35

94. L. van der Fits, S. Mourits, J. S. Voerman, M. Kant, L. Boon, J. D. Laman, F. Cornelissen, A. M. Mus, E. Florencia, E. P. Prens and E. Lubberts: Imiquimod-induced psoriasis-like skin inflammation in mice is mediated via the IL-23/IL-17 axis. *J Immunol*, 182(9), 5836-45 (2009) doi:10.4.049/jimmunol.0802999

95. K. Sakai, K. M. Sanders, M. R. Youssef, K. M. Yanushefski, L. Jensen, G. Yosipovitch and T. Akiyama: Mouse model of imiquimod-induced psoriatic itch. *Pain*, 157(11), 2536-2543 (2016) doi:10.1.097/j.pain.0000000000000674

96. C. Remrod, S. Lonne-Rahm and K. Nordlind: Study of substance P and its receptor neurokinin-1 in psoriasis and their relation to chronic stress and pruritus. *Arch Dermatol Res*, 299(2), 85-91 (2007) doi:10.1.007/s00403-007-0745-x

97. B. Amatya, K. Nordlind and C. F. Wahlgren: Responses to intradermal injections of substance P in psoriasis patients with pruritus. *Skin Pharmacol Physiol*, 23(3), 133-8 (2010) doi:10.1.159/000270385

98. T. Miyagaki, M. Sugaya, H. Suga, S. Morimura, M. Kamata, H. Ohmatsu, H. Fujita, Y. Asano, Y. Tada, T. Kadono and S. Sato: Serum soluble CD26 levels: diagnostic efficiency for atopic dermatitis, cutaneous T-cell lymphoma and psoriasis in combination with serum thymus and activation-regulated chemokine levels. *J Eur Acad Dermatol Venereol*, 27(1), 19-24 (2013) doi:10.1.111/j.1468-3083.2.011.0.4340.x

99. R. G. van Lingen, M. K. Poll, M. M. Seyger, E. M. de Jong, P. C. van de Kerkhof and P. E. van Erp: Distribution of dipeptidyl-peptidase IV on keratinocytes in the margin zone of a psoriatic lesion: a comparison with hyperproliferation and

aberrant differentiation markers. *Arch Dermatol Res*, 300(10), 561-7 (2008) doi:10.1.007/s00403-008-0862-1

100. D. J. Drucker: Enhancing incretin action for the treatment of type 2 diabetes. *Diabetes Care*, 26(10), 2929-40 (2003) doi:10.2.337/diacare.26.1.0.2.929

101. R. Barreira da Silva, M. E. Laird, N. Yatim, L. Fiette, M. A. Ingersoll and M. L. Albert: Dipeptidylpeptidase 4 inhibition enhances lymphocyte trafficking, improving both naturally occurring tumor immunity and immunotherapy. *Nat Immunol*, 16(8), 850-8 (2015) doi:10.1.038/ni.3201

102. P. Proost, E. Schutyser, P. Menten, S. Struyf, A. Wuyts, G. Opdenakker, M. Detheux, M. Parmentier, C. Durinx, A.-M. Lambeir, J. Neyts, S. Liekens, P. C. Maudgal, A. Billiau and J. Van Damme: Amino-terminal truncation of CXCR3 agonists impairs receptor signaling and lymphocyte chemotaxis, while preserving antiangiogenic properties. *Blood*, 98(13), 3554-3561 (2001) doi:10.1.182/blood.V98.1.3.3.554

103. P. van der Bruggen, C. Traversari, P. Chomez, C. Lurquin, E. De Plaen, B. Van den Eynde, A. Knuth and T. Boon: A gene encoding an antigen recognized by cytolytic T lymphocytes on a human melanoma. *Science*, 254(5038), 1643-7 (1991) doi:10.1.126/science.1840703

104. M. Liu, S. Guo and J. K. Stiles: The emerging role of CXCL10 in cancer. *Oncol Lett*, 2(4), 583-589 (2011) doi:10.3.892/ol.2011.3.00

105. J. R. Groom and A. D. Luster: CXCR3 in T cell function. *Exp Cell Res*, 317(5), 620-31 (2011) doi:10.1.016/j.yexcr.2010.1.2.0.17

106. M. A. Koch, G. Tucker-Heard, N. R. Perdue, J. R. Killebrew, K. B. Urdahl and D. J. Campbell: The transcription factor T-bet controls regulatory T cell homeostasis and function during type 1 inflammation. *Nat Immunol*, 10(6), 595-602 (2009) doi:10.1.038/ni.1731

107. Z. Shi, Y. Okuno, M. Rifa'i, A. T. Endharti, K. Akane, K. Isobe and H. Suzuki: Human CD8+CXCR3+ T cells have the same function as murine CD8+CD122+ Treg. *Eur J Immunol*, 39(8), 2106-19 (2009) doi:10.1.002/eji.200939314

108. R. Hatano, K. Ohnuma, H. Otsuka, E. Komiya, I. Taki, S. Iwata, N. H. Dang, K. Okumura and C. Morimoto: CD26-mediated induction of EGR2 and IL-10 as potential regulatory mechanism for CD26 costimulatory pathway. *J Immunol*, 194(3), 960-72 (2015) doi:10.4.049/jimmunol.1402143

109. T. Okamura, K. Fujio, M. Shibuya, S. Sumitomo, H. Shoda, S. Sakaguchi and K. Yamamoto: CD4+CD25-LAG3+ regulatory T cells controlled by the transcription factor Egr-2. *Proc Natl Acad Sci U S A*, 106(33), 13974-9 (2009) doi:10.1.073/pnas.0906872106

110. B. Huard, P. Prigent, F. Pages, D. Bruniquel and F. Triebel: T cell major histocompatibility complex class II molecules down-regulate CD4+ T cell clone responses following LAG-3 binding. *Eur J Immunol*, 26(5), 1180-6 (1996) doi:10.1.002/eji.1830260533

111. L. Macon-Lemaitre and F. Triebel: The negative regulatory function of the lymphocyte-activation gene-3 co-receptor (CD223) on human T cells. *Immunology*, 115(2), 170-8 (2005) doi:10.1.111/j.1365-2567.2.005.0.2145.x

112. L. T. Nguyen and P. S. Ohashi: Clinical blockade of PD1 and LAG3--potential mechanisms of action. *Nat Rev Immunol*, 15(1), 45-56 (2015) doi:10.1.038/nri3790

113. N. H. Dang, Y. Torimoto, S. F. Schlossman and C. Morimoto: Human CD4 helper T cell activation: functional involvement of two distinct collagen receptors, 1F7 and VLA integrin family. *J Exp Med*, 172(2), 649-52 (1990) doi:10.1.084/jem.172.2.6.4.9

114. V. J. Amatya, Y. Takeshima, K. Kushitani, T. Yamada, C. Morimoto and K. Inai: Overexpression of CD26/DPPIV in mesothelioma tissue and mesothelioma cell lines. *Oncol Rep*, 26(6), 1369-75 (2011) doi:10.3.892/or.2011.1.449

115. K. Aoe, V. J. Amatya, N. Fujimoto, K. Ohnuma, O. Hosono, A. Hiraki, M. Fujii, T. Yamada, N. H. Dang, Y. Takeshima, K. Inai, T. Kishimoto and C. Morimoto: CD26 overexpression is associated with prolonged survival and enhanced chemosensitivity in malignant pleural mesothelioma. *Clin Cancer Res*, 18(5), 1447-56 (2012) doi:10.1.158/1078-0432.CCR-11-1990

116. T. Inamoto, T. Yamochi, K. Ohnuma, S. Iwata, S. Kina, S. Inamoto, M. Tachibana, Y. Katsuoka, N. H. Dang and C. Morimoto: Anti-CD26 monoclonal antibody-mediated G1-S arrest of human renal clear cell carcinoma Caki-2 is associated with retinoblastoma substrate dephosphorylation, cyclin-dependent kinase 2 reduction, $p27^{kip1}$ enhancement, and disruption of binding

to the extracellular matrix. *Clin Cancer Res*, 12(11), 3470-7 (2006) doi:10.1.158/1078-0432.CCR-06-0361

117. M. Hayashi, H. Madokoro, K. Yamada, H. Nishida, C. Morimoto, M. Sakamoto and T. Yamada: A humanized anti-CD26 monoclonal antibody inhibits cell growth of malignant mesothelioma via retarded G2/M cell cycle transition. *Cancer Cell Int*, 16, 35 (2016) doi:10.1.186/s12935-016-0310-9

118. ClinicalTrials.gov: Clinical Study of YS110 in Patients With Malignant Pleural Mesothelioma.https://www.clinicaltrials.gov/ct2/show/NCT03177668?term=YS110&cond=Mesotheliomas+Pleural&rank=1, (2017)

119. C. Durinx, H. Neels, J. C. Van der Auwera, K. Naelaerts, S. Scharpe and I. De Meester: Reference values for plasma dipeptidyl-peptidase IV activity and their association with other laboratory parameters. *Clin Chem Lab Med*, 39(2), 155-9 (2001) doi:10.1.515/CCLM.2001.0.26

120. D. J. Drucker and M. A. Nauck: The incretin system: glucagon-like peptide-1 receptor agonists and dipeptidyl peptidase-4 inhibitors in type 2 diabetes. *Lancet*, 368(9548), 1696-705 (2006) doi:10.1.016/S0140-6736(06)69705-5

121. T. Okamoto, S. Iwata, H. Yamazaki, R. Hatano, E. Komiya, N. H. Dang, K. Ohnuma and C. Morimoto: CD9 negatively regulates CD26 expression and inhibits CD26-mediated enhancement of invasive potential of malignant mesothelioma cells. *PLoS ONE*, 9(1), e86671 (2014) doi:10.1.371/journal.pone.0086671

122. E. Komiya, K. Ohnuma, H. Yamazaki, R. Hatano, S. Iwata, T. Okamoto, N. H. Dang, T. Yamada and C. Morimoto: CD26-mediated regulation of periostin expression contributes to migration and invasion of malignant pleural mesothelioma cells. *Biochem Biophys Res Commun*, 447(4), 609-15 (2014) doi:10.1.016/j.bbrc.2014.0.4.0.37

123. L. Morra and H. Moch: Periostin expression and epithelial-mesenchymal transition in cancer: a review and an update. *Virchows Arch*, 459(5), 465-75 (2011) doi:10.1.007/s00428-011-1151-5

124. J. Yamamoto, K. Ohnuma, R. Hatano, T. Okamoto, E. Komiya, H. Yamazaki, S. Iwata, N. H. Dang, K. Aoe, T. Kishimoto, T. Yamada and C. Morimoto: Regulation of somatostatin receptor 4-mediated cytostatic effects by CD26 in malignant pleural mesothelioma. *Br J Cancer*, 110(9), 2232-45 (2014) doi:10.1.038/bjc.2014.1.51

125. K. Ohnuma, R. Hatano, H. Yamazaki, Y. Kaneko, N. H. Dang and C. Morimoto: CD26-targeted therapy: a new horizon in malignant pleural mesothelioma management. In: *Horizons in Cancer Research*. Ed S. H. Wanatabe. Nova Science Publishers, Inc., Hauppauge, NY (2017)

126. K. Yamada, M. Hayashi, W. Du, K. Ohnuma, M. Sakamoto, C. Morimoto and T. Yamada: Localization of CD26/DPPIV in nucleus and its nuclear translocation enhanced by anti-CD26 monoclonal antibody with anti-tumor effect. *Cancer Cell Int*, 9, 17 (2009) doi:10.1.186/1475-2867-9-17

127. K. Yamada, M. Hayashi, H. Madokoro, H. Nishida, W. Du, K. Ohnuma, M. Sakamoto, C. Morimoto and T. Yamada: Nuclear localization of CD26 induced by a humanized monoclonal antibody inhibits tumor cell growth by modulating of POLR2A transcription. *PLoS One*, 8(4), e62304 (2013) doi:10.1.371/journal.pone.0062304

128. P. A. Havre, M. Abe, Y. Urasaki, K. Ohnuma, C. Morimoto and N. H. Dang: CD26 expression on T cell lines increases SDF-1-alpha-mediated invasion. *Br J Cancer*, 101(6), 983-91 (2009) doi:10.1.038/sj.bjc.6605236

129. D. Droz, D. Zachar, L. Charbit, J. Gogusev, Y. Chretein and L. Iris: Expression of the human nephron differentiation molecules in renal cell carcinomas. *Am J Pathol*, 137(4), 895-905 (1990)

130. T. Stange, U. Kettmann and H. J. Holzhausen: Immunoelectron microscopic demonstration of the membrane proteases aminopeptidase N/CD13 and dipeptidyl peptidase IV/CD26 in normal and neoplastic renal parenchymal tissues and cells. *Eur J Histochem*, 44(2), 157-64 (2000)

131. B. Bauvois, I. De Meester, J. Dumont, D. Rouillard, H. X. Zhao and E. Bosmans: Constitutive expression of CD26/dipeptidylpeptidase IV on peripheral blood B lymphocytes of patients with B chronic lymphocytic leukaemia. *Br J Cancer*, 79(7-8), 1042-8 (1999) doi:10.1.038/sj.bjc.6690167

132. N. H. Dang, U. Aytac, K. Sato, S. O'Brien, J. Melenhorst, C. Morimoto, A. J. Barrett and J. J. Molldrem: T-large granular lymphocyte lymphoproliferative disorder: expression of CD26 as a marker of clinically aggressive disease and characterization of marrow inhibition. *Br J Haematol*, 121(6), 857-65 (2003) doi:10.1.046/j.1365-2141.2.003.0.4365.x

133. A. Carbone, M. Cozzi, A. Gloghini and A. Pinto: CD26/dipeptidyl peptidase IV expression in human lymphomas is restricted to CD30-positive anaplastic large cell and a subset of T-cell non-Hodgkin's lymphomas. *Hum Pathol*, 25(12), 1360-5 (1994) doi:10.1.016/0046-8177(94)90098-1

134. A. Carbone, A. Gloghini, V. Zagonel, D. Aldinucci, V. Gattei, M. Degan, S. Improta, R. Sorio, S. Monfardini and A. Pinto: The expression of CD26 and CD40 ligand is mutually exclusive in human T-cell non-Hodgkin's lymphomas/leukemias. *Blood*, 86(12), 4617-26 (1995)

135. K. Sato and N. H. Dang: CD26: a novel treatment target for T-cell lymphoid malignancies? (Review). *Int J Oncol*, 22(3), 481-97 (2003)

136. U. Aytac, F. X. Claret, L. Ho, K. Sato, K. Ohnuma, G. B. Mills, F. Cabanillas, C. Morimoto and N. H. Dang: Expression of CD26 and its associated dipeptidyl peptidase IV enzyme activity enhances sensitivity to doxorubicin-induced cell cycle arrest at the G(2)/M checkpoint. *Cancer Res*, 61(19), 7204-10 (2001)

137. U. Aytac, K. Sato, T. Yamochi, T. Yamochi, K. Ohnuma, G. B. Mills, C. Morimoto and N. H. Dang: Effect of CD26/dipeptidyl peptidase IV on Jurkat sensitivity to G2/M arrest induced by topoisomerase II inhibitors. *Br J Cancer*, 88(3), 455-62 (2003) doi:10.1.038/sj.bjc.6600791

138. K. Sato, U. Aytac, T. Yamochi, T. Yamochi, K. Ohnuma, K. S. McKee, C. Morimoto and N. H. Dang: CD26/dipeptidyl peptidase IV enhances expression of topoisomerase II α and sensitivity to apoptosis induced by topoisomerase II inhibitors. *Br J Cancer*, 89(7), 1366-74 (2003) doi:10.1.038/sj.bjc.6601253

139. T. Yamochi, T. Yamochi, U. Aytac, T. Sato, K. Sato, K. Ohnuma, K. S. McKee, C. Morimoto and N. H. Dang: Regulation of p38 phosphorylation and topoisomerase II α expression in the B-cell lymphoma line Jiyoye by CD26/dipeptidyl peptidase IV is associated with enhanced *in vitro* and *in vivo* sensitivity to doxorubicin. *Cancer Res*, 65(5), 1973-83 (2005) doi:10.1.158/0008-5472.CAN-04-2611

140. T. Oravecz, M. Pall, G. Roderiquez, M. D. Gorrell, M. Ditto, N. Y. Nguyen, R. Boykins, E. Unsworth and M. A. Norcross: Regulation of the receptor specificity and function of the chemokine RANTES (regulated on activation, normal T cell expressed and secreted) by dipeptidyl peptidase IV (CD26)-mediated cleavage. *J Exp Med*, 186(11), 1865-72 (1997) doi:10.1.084/jem.186.1.1.1.865

141. P. Proost, S. Struyf, D. Schols, G. Opdenakker, S. Sozzani, P. Allavena, A. Mantovani, K. Augustyns, G. Bal, A. Haemers, A. M. Lambeir, S. Scharpe, J. Van Damme and I. De Meester: Truncation of macrophage-derived chemokine by CD26/ dipeptidyl-peptidase IV beyond its predicted cleavage site affects chemotactic activity and CC chemokine receptor 4 interaction. *J Biol Chem*, 274(7), 3988-93 (1999) doi:10.1.074/jbc.274.7.3.9.88

142. R. Pang, W. L. Law, A. C. Chu, J. T. Poon, C. S. Lam, A. K. Chow, L. Ng, L. W. Cheung, X. R. Lan, H. Y. Lan, V. P. Tan, T. C. Yau, R. T. Poon and B. C. Wong: A subpopulation of CD26+ cancer stem cells with metastatic capacity in human colorectal cancer. *Cell Stem Cell*, 6(6), 603-15 (2010) doi:10.1.016/j.stem.2010.0.4.0.01

143. J. H. Jang, L. Baerts, Y. Waumans, I. De Meester, Y. Yamada, P. Limani, I. Gil-Bazo, W. Weder and W. Jungraithmayr: Suppression of lung metastases by the CD26/DPP4 inhibitor Vildagliptin in mice. *Clin Exp Metastasis*, 32(7), 677-87 (2015) doi:10.1.007/s10585-015-9736-z

144. U. Yamaguchi, R. Nakayama, K. Honda, H. Ichikawa, T. Hasegawa, M. Shitashige, M. Ono, A. Shoji, T. Sakuma, H. Kuwabara, Y. Shimada, M. Sasako, T. Shimoda, A. Kawai, S. Hirohashi and T. Yamada: Distinct gene expression-defined classes of gastrointestinal stromal tumor. *J Clin Oncol*, 26(25), 4100-8 (2008) doi:10.1.200/jco.2007.1.4.2.331

145. V. K. Hopsu-Havu and G. G. Glenner: A new dipeptide naphthylamidase hydrolyzing glycyl-prolyl-beta-naphthylamide. *Histochemie*, 7(3), 197-201 (1966) doi:10.1.007/BF00577838

146. C. A. Abbott, E. Baker, G. R. Sutherland and G. W. McCaughan: Genomic organization, exact localization, and tissue expression of the human CD26 (dipeptidyl peptidase IV) gene. *Immunogenetics*, 40(5), 331-8 (1994) doi:10.1.007/BF01246674

147. M. E. Morrison, S. Vijayasaradhi, D. Engelstein, A. P. Albino and A. N. Houghton: A marker for neoplastic progression of human melanocytes is a cell surface ectopeptidase. *J Exp Med*, 177(4), 1135-43 (1993) doi:10.1.084/jem.177.4.1.1.35

148. S. S. Farag, S. Srivastava, S. Messina-Graham, J. Schwartz, M. J. Robertson, R. Abonour, K. Cornetta, L. Wood, A. Secrest, R. M. Strother, D. R. Jones and H. E. Broxmeyer: *In vivo* DPP-4 inhibition to enhance engraftment of single-unit cord blood

transplants in adults with hematological malignancies. *Stem Cells Dev*, 22(7), 1007-15 (2013) doi:10.1.089/scd.2012.0.636

149. P. Proost, S. Struyf, J. Van Damme, P. Fiten, E. Ugarte-Berzal and G. Opdenakker: Chemokine isoforms and processing in inflammation and immunity. *J Autoimmun* (2017) doi:10.1.016/j.jaut.2017.0.6.0.09

150. K. Ohnuma, R. Hatano, T. Itoh, N. Iwao, N. H. Dang and C. Morimoto: Role of IL-26+CD26+CD4 T Cells in Pulmonary Chronic Graft-Versus-Host Disease and Treatment with Caveolin-1-Ig Fc Conjugate. *Crit Rev Immunol*, 36(3), 239-267 (2016) doi:10.1.615/CritRevImmunol.2016018772

151. F. I. Ghani, H. Yamazaki, S. Iwata, T. Okamoto, K. Aoe, K. Okabe, Y. Mimura, N. Fujimoto, T. Kishimoto, T. Yamada, C. W. Xu and C. Morimoto: Identification of cancer stem cell markers in human malignant mesothelioma cells. *Biochem Biophys Res Commun*, 404(2), 735-42 (2011) doi:10.1.016/j.bbrc.2010.1.2.0.54

152. H. Yamazaki, M. Naito, F. I. Ghani, N. H. Dang, S. Iwata and C. Morimoto: Characterization of cancer stem cell properties of CD24 and CD26-positive human malignant mesothelioma cells. *Biochem Biophys Res Commun*, 419(3), 529-36 (2012) doi:10.1.016/j.bbrc.2012.0.2.0.54

153. H. Herrmann, I. Sadovnik, S. Cerny-Reiterer, T. Rulicke, G. Stefanzl, M. Willmann, G. Hoermann, M. Bilban, K. Blatt, S. Herndlhofer, M. Mayerhofer, B. Streubel, W. R. Sperr, T. L. Holyoake, C. Mannhalter and P. Valent: Dipeptidylpeptidase IV (CD26) defines leukemic stem cells (LSC) in chronic myeloid leukemia. *Blood*, 123(25), 3951-62 (2014) doi:10.1.182/blood-2013-10-536078

154. S. Davies, A. Beckenkamp and A. Buffon: CD26 a cancer stem cell marker and therapeutic target. *Biomed Pharmacother*, 71, 135-8 (2015) doi:10.1.016/j.biopha.2015.0.2.0.31

155. R. Hatano, T. Yamada, S. Matsuoka, S. Iwata, H. Yamazaki, E. Komiya, T. Okamoto, N. H. Dang, K. Ohnuma and C. Morimoto: Establishment of monoclonal anti-human CD26 antibodies suitable for immunostaining of formalin-fixed tissue. *Diagn Pathol*, 9, 30-42 (2014) doi:10.1.186/1746-1596-9-30

156. K. Ohnuma, R. Hatano and C. Morimoto: DPP4 in anti-tumor immunity: going beyond the enzyme. *Nat Immunol*, 16(8), 791-2 (2015) doi:10.1.038/ni.3210

Abbreviation: AA, amino acid; ADA, adenosine deaminase; ADCC, antibody-dependent cellular cytotoxicity; aGVHD, acute graft-versus-host disease; alloHSCT, allogeneic hematopoietic stem cell transplantation; AP-1, activator protein-1; APCs, antigen presenting cells; A20-luc, luciferase-transfected A20 cell; B6 WT, parental C57BL/6 mice; Cav-Ig, soluble Fc fusion proteins containing the N-terminal domain of caveolin-1; CB, cord blood; CD26KO, CD26 knockout; cGVHD, chronic graft-versus-host disease; CRC, colorectal cancer; CTL, cytotoxic T lymphocyte; CTLA-4, cytotoxic T-lymphocyte–associated antigen 4; ΔCNS-77 Tg mice, mice carrying human *IFNG* transgene with deleting *IL26* transcription; DPPIV, dipeptidyl peptidase IV; ECM, extracellular matrix; EGR2, early growth response 2; ELISA, enzyme-linked immunosorbent assay; EMT, epithelial to mesenchymal transition; ERK, extracellular signal-regulated kinase; FIH, first-in-human; GIST, gastrointestinal stromal tumors; GVHD, graft-versus-host disease; GVL, graft-versus-leukemia; HuCB, human umbilical cord blood; IBD, inflammatory bowel diseases; i.d., intradermal injection; IFN, interferon; IL, interleukin; IMQ, imiquimod; JKT-hCD26WT, Jurkat cells transfected with full-length human CD26/DPPIV; LAG3, lymphocyte activation gene-3; LBL/ALL, lymphoblastic lymphoma/acute lymphoblastic leukemia: mAb, monoclonal antibody; MAPK, mitogen-activated protein kinase; MERS-CoV, Middle East respiratory syndrome coronavirus; MERS-CoV S1-Fc, S1 domain of MERS-CoV fused to the Fc region of human IgG; MPM, malignant pleural mesothelioma; NFAT, nuclear factor of activated T cells; NOG, NOD/Shi-*scid*IL2rγ^{null}; OB, obliterative bronchiolitis; PBL, peripheral blood lymphocyte; PD-1, programmed cell death 1; PSO, psoriasis; RA, rheumatoid arthritis; RBD, receptor binding domain; RCC, renal cell carcinoma; RECIST, response evaluation criteria in solid tumors; sCD26, soluble CD26; sDPPIV, soluble dipeptidyl peptidase IV; siRNA, small interfering RNA; SP, substance P; SSTR4, somatostatin receptor 4; Tg, transgenic; T-LGL, T-large granular lymphocyte; TME, tumor microenvironment; TNF, tumor necrosis factor; Tr1, Type 1 regulatory T cells; WHO, World Health Organization; 190-*IFNG* Tg mice, mice carrying human *IFNG* and *IL26* transgene

Key Words CD26, DPPIV, Caveolin-1, Humanized anti-CD26 monoclonal antibody, Graft-versus-host disease, Malignant pleural mesothelioma, Review

Send correspondence to: Kei Ohnuma, Department of Therapy Development and Innovation for Immune Disorders and Cancers, Graduate School of Medicine, Juntendo University, 2-1-1, Hongo, Bunkyo-ku, Tokyo 113-8421, Japan, Tel: 81-3-3868-2310, Fax: 81-3-3868-2310, E-mail: kohnuma@juntendo.ac.jp

Figure 1. Schematic diagram of human CD26 profiling the predicted contacting areas of anti-CD26 mAbs 2F9, 1F7, YS110 and MERS-CoV S1. 2F9 recognizes between 248-449th AAs including the ADA binding regions, and 1F7 or YS110 recognize between 248-358th AAs excluding the ADA binding regions. MERS-CoV contacting residues of human CD26 are indicated in stars, with available information obtained from recently published data (55, 69). TM indicates the transmembrane region of human CD26 (black box), and the extracellular domain of CD26 is located at the C-terminal residues of TM. This Figure is reprinted with permission from K Ohnuma *et al.*, *J Virol* 87: 13892-13899, 2013 (62).

Figure 2. DPP4 inhibition suppresses truncation of its ligand CXCL10, leading to recruitment of $CXCR3^+$ T cells into tumor parenchyma. Through an *in vivo* xenotransplant models, DPPIV inhibitor is found to reduce tumor growth through the preservation of bioactive CXCL10 in the tumor microenvironment (TME). In the normal physiological state, CXCL10 is rapidly degraded by CD26/DPPIV, resulting in decreased recruitment and migration of $CXCR3^+$ T cells into the tumor parenchyma. In contrast, DPPIV inhibition enhances tumor rejection by preserving the full-length biologically active form of CXCL10, leading to increased trafficking of $CXCR3^+$ T cells into the tumor parenchyma. This anti-tumor response is potentiated in combination with other anti-tumor immunotherapeutic approaches including CpG adjuvant therapy, adoptive T cell transfer therapy and checkpoint blockade therapy. This Figure is reprinted with permission from K Ohnuma *et al.*, *Nat Immunol* 16: 791-792, 2015 (156).

Figure 3. A model for cytostatic signaling mediated by SSTR4 and CD26 coassociation in MPM cells. SSTR4 molecules form homo- or oligo-dimers when stimulated by its agonists (Ago), followed by manifestation of their cytostatic effects via SHP-2 signaling **(A)**. When coassociation of SSTR4 with CD26 occurs, CD26 binds to the C-terminal region of SSTR4, which is necessary to transduce SSTR4 signaling, hence blocking the SSTR4-mediated cytostatic effects **(B)**. Meanwhile, anti-CD26 mAb ligates CD26, leading to dissociation of SSTR4 from CD26 and to recruiting lipid rafts with clustering of SSTR4 molecules **(C)**. As a result, downstream signaling of SSTR4 occurs with activation of SHP-2, leading to the observed cytostatic effects.

Running title: CD26 as therapeutic target

Figure 1

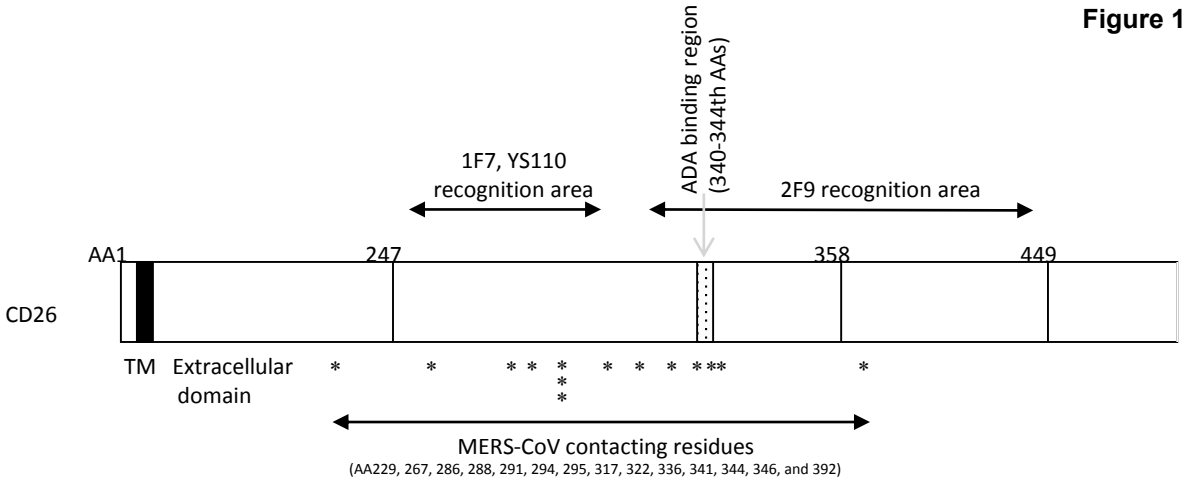

Figure 2

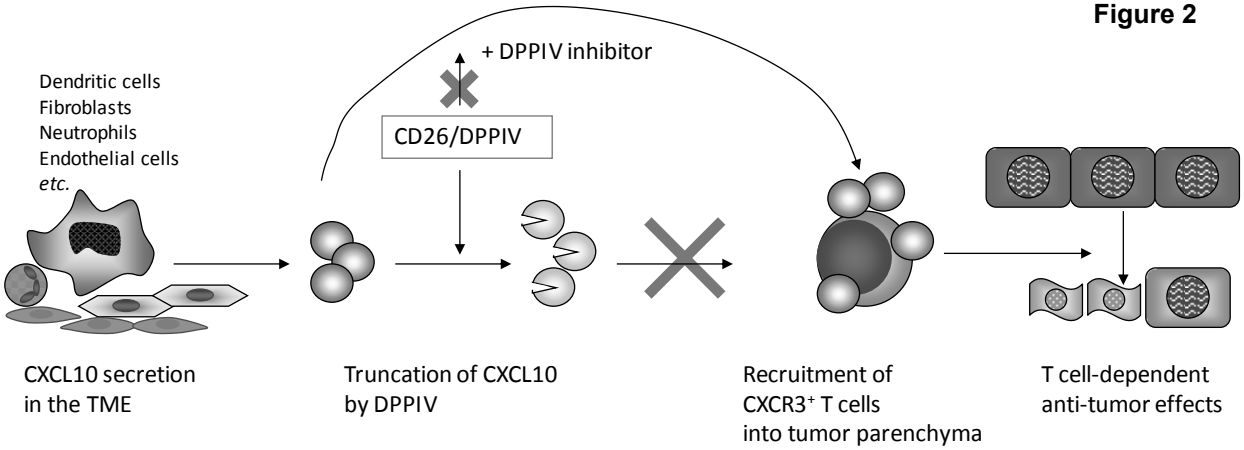

Figure 3

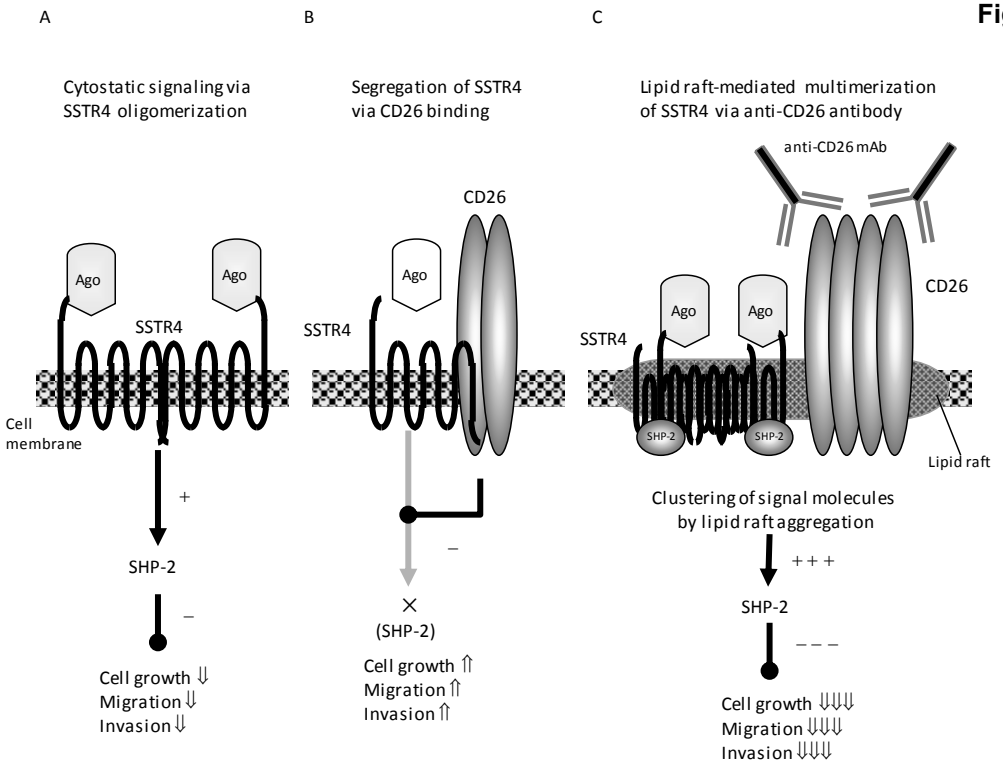

Biochemical and Biophysical Research Communications 495 (2018) 223–229

Contents lists available at ScienceDirect

Biochemical and Biophysical Research Communications

journal homepage: www.elsevier.com/locate/ybbrc

Caveolin-1, a binding protein of CD26, is essential for the anti-inflammatory effects of dipeptidyl peptidase-4 inhibitors on human and mouse macrophages

Munenori Hiromura [a, 1], Kyoko Nohtomi [a, 1], Yusaku Mori [a], Hideo Kataoka [b], Marika Sugano [c], Kei Ohnuma [d], Hirotaka Kuwata [b], Tsutomu Hirano [a, *]

[a] Department of Internal Medicine, Division of Diabetes, Metabolism, and Endocrinology, Showa University School of Medicine, 1-5-8 Hatanodai, Shinagawa-ku, 142-8555, Tokyo, Japan
[b] Department of Oral Microbiology and Immunology, School of Dentistry, Showa University, 1-5-8 Hatanodai, Shinagawa-ku, 142-8555, Tokyo, Japan
[c] Department of Periodontology, Showa University School of Dentistry, 2-1-1 Kitasenzoku Ohta-ku, 145-8515, Tokyo, Japan
[d] Department of Therapy Development and Innovation for Immune Disorders and Cancers, Graduate School of Medicine, Juntendo University, 2-1-1 Hongo, Bunkyo-ku, 113-8421, Tokyo, Japan

ARTICLE INFO

Article history:
Received 20 October 2017
Accepted 2 November 2017
Available online 4 November 2017

Keywords:
Caveolin-1
CD26
Dipeptidyl peptidase-4 inhibitor
Macrophage
Pro-inflammatory cytokine
Toll-like receptor (TLR)4

ABSTRACT

We previously reported that inhibition of dipeptidyl peptidase (DPP)-4, the catalytic site of CD26, prevents atherosclerosis in animal models through suppression of inflammation; however, the underlying molecular mechanisms have not been fully elucidated. Caveolin-1 (Cav-1), a major structural protein of caveolae located on the surface of the cellular membrane, has been reported to modulate inflammatory responses by binding to CD26 in T cells. In this study, we investigated the role of Cav-1 in the suppression of inflammation mediated by the DPP-4 inhibitor, teneligliptin, using mouse and human macrophages. Mouse peritoneal macrophages were isolated from Cav-$1^{+/+}$ and Cav-$1^{-/-}$ mice after stimulation with 3% thioglycolate. Inflammation was induced by the toll-like receptor (TLR)4 agonist, lipopolysaccharide (LPS), isolated from *Escherichia coli*. The expression of pro-inflammatory cytokines was determined using reverse transcription-polymerase chain reaction. Co-expression of Cav-1 and CD26 was detected using immunohistochemistry in both mouse and human macrophages. Teneligliptin treatment (10 nmol/L) suppressed the LPS-induced expression of interleukin (IL)-6 (70%) and tumor necrosis factor-α (37%) in peritoneal macrophages isolated from Cav-$1^{+/+}$ mice. However, teneligliptin did not have any effect on the macrophages from Cav-$1^{-/-}$ mice. In human monocyte/macrophage U937 cells, teneligliptin treatment suppressed LPS-induced expression of pro-inflammatory cytokines in a dose-dependent manner (1−10 nmol/L). These anti-inflammatory effects of teneligliptin were mimicked by gene knockdown of Cav-1 or CD26 using small interfering RNA transfection. Furthermore, neutralization of these molecules using an antibody against CD26 or Cav-1 also showed similar suppression. Teneligliptin treatment specifically inhibited TLR4 and TLR5 agonist-mediated inflammatory responses, and suppressed LPS-induced phosphorylation of IL-1 receptor-associated kinase 4, a downstream molecule of TLR4. Next, we determined whether teneligliptin could directly inhibit the physical interaction between Cav-1 and CD26 using the Biacore system. Binding of CD26 to Cav-1 protein was detected. Unexpectedly, teneligliptin also bound to Cav-1, but did not interfere with CD26-Cav-1 binding, suggesting that teneligliptin competes

Abbreviations: ANOVA, analysis of variance; Cav-1, caveolin-1; DAPI, 4′, 6-diamidino-2-phenylindole; DPP-4, dipeptidyl peptidase-4; FBS, fetal bovine serum; FITC, fluorescein isothiocyanate; GAPDH, glyceraldehyde 3-phosphate dehydrogenase; GST, glutathione *S*-transferase; IL, interleukin; IP, interferon gamma-induced protein; IRAK, IL-1 receptor-associated kinase; LPS, lipopolysaccharide; MCP, monocyte chemoattractant protein; MEM, minimum essential medium; NF-κβ, nuclear factor-kappa beta; PBS, phosphate buffered saline; PE, phycoerythrin; rhCD26, recombinant human CD26; RT-PCR, reverse transcription-polymerase chain reaction; RU, response unit; SEM, standard error of mean; siRNA, small interfering RNA; SDS, sodium dodecyl sulfate; TLR, toll-like receptor; TNF, tumor necrosis factor.

* Corresponding author. Department of Internal Medicine, Division of Diabetes, Metabolism, and Endocrinology, Showa University School of Medicine, 1-5-8 Hatanodai, Shinagawa-ku, Tokyo 142-8555, Japan.
E-mail address: hirano@med.showa-u.ac.jp (T. Hirano).
[1] Equally contributed to the paper.

https://doi.org/10.1016/j.bbrc.2017.11.016

with CD26 for binding to Cav-1. In conclusion, we demonstrated that Cav-1 is a target molecule for DPP-4 inhibitors in the suppression of TLR4-mediated inflammation in mouse and human macrophages.

1. Introduction

Dipeptidyl peptidase (DPP)-4 inhibitors are commonly used for the treatment of patients with type 2 diabetes because of their potent glucose-lowering effect, without any increase in hypoglycemia risk and body weight gain [1–3]. DPP-4, originally known as the catalytic site of the T-cell surface marker CD26, is widely expressed in most cells [4]. DPP-4 cleaves incretin hormones, such as glucose-dependent insulinotropic polypeptide and glucagon-like peptide-1 that stimulate insulin secretion in pancreatic β-cells. In addition, various peptides, which are involved in the regulation of immune and cardiovascular systems, are also cleaved by DPP-4 [5,6]. Extensive studies have been conducted to evaluate the direct vascular protective and anti-inflammatory effects of DPP-4 inhibitors. We previously reported that the DPP-4 inhibitor, vildagliptin, suppresses the progression of atherosclerosis in diabetic apolipoprotein E-null mice, and this effect is partially incretin-independent [7]. Furthermore, the direct anti-atherogenic effects of DPP-4 inhibitors on vascular cells and macrophages have been shown in vitro [7–14]. However, the underlying molecular mechanisms are not fully elucidated.

Caveolin-1 (Cav-1), a major structural protein of caveolae on the cell surface, is implicated in regulating inflammatory responses [15]. Ohnuma et al. have demonstrated an interaction between Cav-1 and CD26 in antigen-presenting cells, including T cells [16–19]. CD26 phosphorylates Cav-1 by direct binding, resulting in the activation of the nuclear factor-kappa beta (NF-κβ) pathway [17]. In addition, the enzymatic activity of CD26 is essential for its interaction with Cav-1 [19]. However, the relationship between CD26 and Cav-1 in other immune cells and the involvement of Cav-1 in the anti-inflammatory effects of DPP-4 inhibitors are yet to be determined. In the present study, we demonstrated that Cav-1 is an essential molecule for the suppression of toll-like receptor (TLR)4-induced inflammation mediated by DPP-4 inhibitors in mouse and human macrophages.

2. Materials and methods

2.1. Animal study

This study was conducted in strict accordance with the recommendations in the Guide for the Care and Use of Laboratory Animals of the National Institutes of Health (8th edition, 2011; Office of Laboratory Animal Welfare, National Institutes of Health, MD, USA). All procedures were approved by the Animal Care Committee of Showa University School of Medicine (approval number 06013). Cav-1 knockout (Cav-$1^{-/-}$) mice and their littermate controls (Cav-$1^{+/+}$) were purchased from the Jackson Laboratory (ME, USA), and kept on standard rodent chow. Six–eight-week-old female mice were intraperitoneally injected with 4 mL of 3% thioglycolate (Wako, Osaka, Japan). Four days after injection, mice were euthanized by anesthesia overdose using isoflurane. Exudate peritoneal macrophages were collected by injecting ice-cold phosphate buffered saline (PBS) into the intraperitoneal cavity. The collected cells were seeded into 3.5-cm dishes (1×10^6 cells/dish) and allowed adhesion to the dish for 1 h. The adherent cells were identified as peritoneal macrophages [20]. The cells were treated with lipopolysaccharide (LPS) (B4; Sigma-Aldrich, MO, USA) with or without the DPP-4 inhibitor (teneligliptin; gifted from Mitsubishi Tanabe Pharma, Osaka, Japan) in RPMI 1640 medium (Gibco, MA, USA) containing 10% fetal bovine serum (FBS), 100 U/mL penicillin, 100 U/mL streptomycin, and 1% minimum essential medium (MEM) non-essential amino acid solution.

2.2. Cell culture

A human monocyte/macrophage cell line, U937, was obtained from JCRB (JCRB9021; Osaka, Japan). The cells were cultured in RPMI 1640 medium containing 10% FBS. The cells were seeded into 3.5-cm dishes (1×10^6 cells/dish) and treated with LPS with or without reagents for the indicated hours. The following antibodies were used for the neutralization of target proteins: anti-CD26 antibody (H-270; sc-9153; Santa Cruz Biotechnology, TX, USA; RRID: AB_2093585), anti-Cav-1 antibody (H97; sc-7875; Santa Cruz Biotechnology; RRID: AB_2072020), and anti-Cav-1 antibody (7c8; sc-53564; Santa Cruz Biotechnology; RRID: AB_628859). TLR agonists that were used are presented in Supplemental Table 1.

2.3. Reverse transcription-polymerase chain reaction (RT-PCR)

Total RNA was isolated using RNeasy Mini Kit (Qiagen, Hilden, Germany) and used to synthesize complementary DNA using ReverTra Ace® (TOYOBO, Osaka, Japan). Real-time RT-PCR was performed using TaqMan gene expression assays and ABI 7900HT (Applied Biosystems, MA, USA). The following probe sets were used: interleukin-1β (*Il-1β*), Hs01555410_m1; *Il-6*, Hs00985639_m1 and Mm00446190_m1; tumor necrosis factor-α (*Tnf-α*), Hs01113624_g1 and Mm00443258_m1; *Nf-κβ*, Hs00765730_m1; interferon gamma-induced protein 10 (*Ip-10*), Hs00171042_m1; monocyte chemoattractant protein-1 (*Mcp-1*), Hs00234140_m1; 18S ribosomal RNA (*18s rRNA*), Hs999999901_s1; and glyceraldehyde 3-phosphate dehydrogenase (*Gapdh*), Mm03302249_g1. Expression of target gene was normalized to that of an internal control (*18s rRNA*) in U937 cells or *Gapdh* in mouse peritoneal macrophages.

2.4. Biophysical interaction analysis

In vitro protein binding was assessed using Biacore™ T100 (GE Healthcare, Buckinghamshire, England). The buffer consisted of 0.1 mol/L HEPES, 1.5 mol/L NaCl, 30 mmol/L EDTA, and 0.5% (v/v) surfactant P20. Glutathione *S*-transferase (GST)-tagged Cav-1 (Cav-1 human recombinant protein; Abnova, Taipei, Taiwan) at 5 μg/mL was immobilized on Sensor Chip CM5 (GE Healthcare) as a ligand using GST capture kit (GE Healthcare). Recombinant human CD26 (rhCD26; R&D Systems, MN, USA; 25 μg/mL), teneligliptin (100 μmol/L or 1 mmol/L), or rhCD26 (25 μg/mL) + teneligliptin (100 μmol/L or 1 mmol/L) were injected onto the sensor chip as analytes for 150 s. Glycine-HCL (10 mmol/L) was used to regenerate the immobilized sensor chip surface. Mass change on the sensor tip induced by binding between molecules was detected as response unit (RU).

2.5. Immunohistochemistry

Mouse peritoneal macrophages and U937 cells were seeded in poly-D-lysine-coated microplates and fixed with acetone-methanol (1:1) for 2 min at 23 °C. After blocking with 5% bovine serum albumin-PBS for 30 min at 4 °C, the fixed cells were incubated with primary antibodies for 1 h at 37 °C and secondary antibodies for 1 h at 37 °C. The primary antibody used for U937 cells was anti-CD26 antibody (generated by Ohnuma; 5 μg/mL; raised in rabbit) or anti-Cav-1 antibody (sc-894; Santa Cruz Biotechnology; 5 μg/mL; raised in rabbit; RRID: AB_2072042). Anti-CD26 antibody (AF954; R&D Systems; 5 μg/mL; RRID: AB_355739) or anti-Cav-1 antibody (3238; Cell Signaling Technology, MA, USA; 5 μg/mL; RRID: AB_10699017) was used for mouse peritoneal macrophages. The cells were mounted with ProLong™ Gold Antifade (Thermo Fisher Scientific, MA, USA), and images were taken with the BZ8000 microscope (KEYENCE, Osaka, Japan).

2.6. Immunoblotting

U937 cells were treated with various reagent concentrations for the indicated time periods. After incubation, the cells were washed with PBS three times and lysed using 10% sodium dodecyl sulfate (SDS). The lysates were used for protein measurement by bicinchoninic acid (Thermo Fisher Scientific), and boiled for 5 min in NuPAGE LDS Sample Buffer (3:1; Thermo Fisher Scientific). The samples (10 μg/lane) were subjected to 10% SDS-polyacrylamide gel electrophoresis, and transferred to Immobilon-P membranes (Merck Millipore, Darmstadt, Germany). The membranes were immunoblotted with antibodies against IL-1 receptor-associated kinase 4 (IRAK-4) (2H9; MAB10701; Abnova, Taipei, Taiwan; 1:500; raised in rabbit; RRID: AB_11190488), phosphorylated IRAK-4 (p-IRAK4; T345) (A8A8; MAB2538; Abnova; 1:500; raised in rabbit; RRID: AB_10555313), and β-actin (C4; sc47778; Santa Cruz Biotechnology, TX, USA; 1:200; raised in rabbit; RRID: AB_626632). The protein bands were visualized with enhanced luminal reagents (PerkinElmer, MA, USA) and quantified using FIJI software (NIH, MD, USA).

2.7. Small interfering RNA transfection

Small interfering (si)RNAs against control (sc-37007), Cav-1 (sc-29241), and CD26 (sc-42762) were obtained from Santa Cruz Biotechnology (TX, USA). Transfection was performed using X-tremeGENE siRNA transfection reagent (Roche, Basel, Switzerland) with 25 nmol/L of siRNA. The cells were used for experiments 48 h post transfection.

2.8. Cell viability

Cell viability was evaluated using CellQuanti-MTT Cell Viability Assay Kits (BioAssay Systems, CA, USA). U937 cells were seeded into 96-well plates (1×10^4 cells/well) and treated with the indicated concentrations of reagents for 22 h in 5% FBS-RPMI 1640 medium. During the last 4 h, the cells were incubated with CellQuanti-MTT reagent. Solubilization solution was added to each well, and absorbance at 570 nm was measured using infinite M200 PRO (Tecan, Männedorf, Switzerland).

2.9. Flow cytometry

Mouse peritoneal macrophages were treated with or without LPS (100 ng/mL) or teneligliptin (10 μmol/L) for 1 h, and stained with phycoerythrin (PE)-conjugated anti-CD11b antibody (Bio-Legend, CA, USA) and fluorescein isothiocyanate (FITC)-conjugated anti-CD26 antibody (Bio-Rad Laboratories, CA, USA). Fluorescence intensity was measured using BD FACSVerse™ (Becton, Dickinson and Company, NJ, USA), and data obtained were analyzed by FlowJO software (Tree Star, Inc., OR, USA).

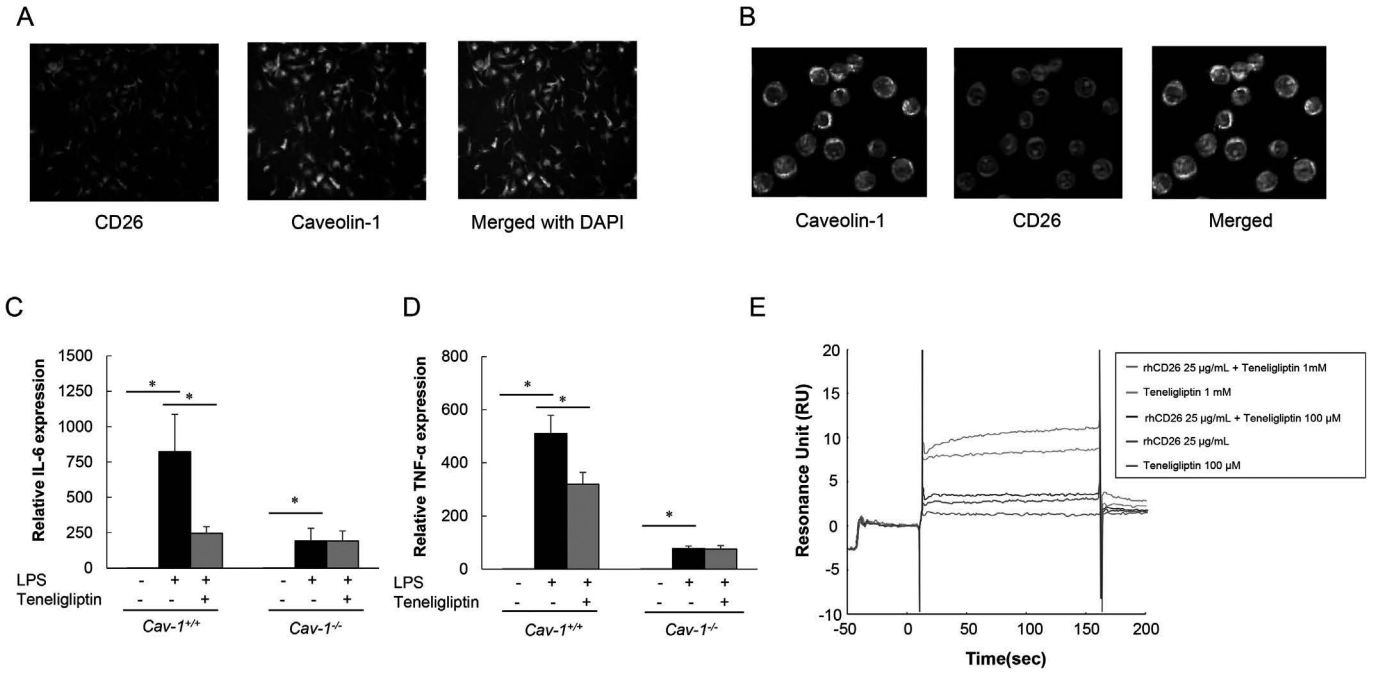

Fig. 1. The role of Cav-1 in the anti-inflammatory effects of teneligliptin. (A and B) Expression of CD26 and Cav-1 in mouse peritoneal macrophages and human U937 cells. Representative images of immunofluorescent staining of CD26 and Cav-1, and the merged images with 4′,6-diamidino-2-phenylindole (DAPI) are shown in A (mouse peritoneal macrophages) and B (human U937 cells). **(C and D)** The effects of teneligliptin on LPS-induced expression of *Il-6* and *Tnf-α* in peritoneal macrophages isolated from Cav-$1^{+/+}$ and Cav-$1^{-/-}$ mice. n = 4–6 per group. *$p < 0.05$. **(E)** Binding of rhCD26 and teneligliptin to Cav-1 protein was determined using Biacore system. The binding of protein is expressed as RU.

2.10. Statistical analysis

Values are expressed as the means ± standard error of mean (SEM). Statistical comparisons were performed by analysis of variance (ANOVA) followed by Tukey's test using JMP software (version 11; SAS Institute Inc., NC, USA). The significance level was defined as $p < 0.05$.

3. Results

3.1. Co-expression of CD26 and Cav-1 in mouse peritoneal macrophages and human U937 cells

First, we investigated whether CD26 and Cav-1 are expressed in mouse peritoneal macrophages or U937 cells. Immunofluorescent staining showed that CD26 and Cav-1 were co-expressed primarily in the cytoplasm of mouse peritoneal macrophages and U937 cells (Fig. 1A and B). In flow cytometric analysis, less than 10% of the mouse peritoneal macrophages were positive for CD26. LPS (100 ng/mL) and teneligliptin (10 μmol/L) did not affect the ratio of CD26-positive cells (Supplemental Fig. 1).

3.2. Cav-1 is involved in the anti-inflammatory effects of teneligliptin on mouse peritoneal macrophages

We evaluated whether Cav-1 is involved in the anti-inflammatory effects of teneligliptin using mouse peritoneal macrophages isolated from Cav-$1^{+/+}$ or Cav-$1^{-/-}$ mice. Treatment with LPS (100 ng/mL for 4 h), a TLR4 agonist, significantly increased *Il-6* and *Tnf-α* expression in the macrophages from Cav-$1^{+/+}$ mice, while co-treatment with teneligliptin (10 nmol/L) suppressed their expression by 70 and 37%, respectively. In Cav-$1^{-/-}$ mice, LPS treatment also increased the expression of *Il*-6 and *Tnf-α*. However, responses to LPS stimulation were lower than those observed in Cav-$1^{+/+}$ mice. Unlike that in Cav-$1^{+/+}$ mice, teneligliptin failed to suppress LPS induced expression of *Il*-6 and *Tnf-α* in Cav-$1^{-/-}$ mice (Fig. 1C and D).

3.3. Teneligliptin does not affect protein binding of CD26 and Cav-1 in vitro

A previous study using biophysical interaction analysis has shown that CD26 protein directly binds to Cav-1 protein in vitro [19]. We determined whether teneligliptin affects the interaction between CD26 and Cav-1 protein using the Biacore system, which is capable of assessing direct molecule binding by measuring mass change on the sensor chip. In this analysis, the binding of the protein was expressed as RU. Cav-1 protein was immobilized on the sensor chip as a ligand, and rhCD26 and teneligliptin were used as analytes. Administration of rhCD26 to Cav-1 protein showed elevated RU levels compared to Cav-1 protein alone. Furthermore, administration of teneligliptin (100 μmol/L or 1 mmo/L) to Cav-1 protein dose-dependently increased RU levels, indicating the direct binding of teneligliptin to Cav-1. However, co-administration of teneligliptin and rhCD26 showed higher RU levels than those observed with administration of rhCD26 or teneligliptin alone (Fig. 1 E).

3.4. Teneligliptin suppresses LPS-induced expression of pro-inflammatory molecules in U937 cells

Next, we evaluated the effects of teneligliptin on the expression

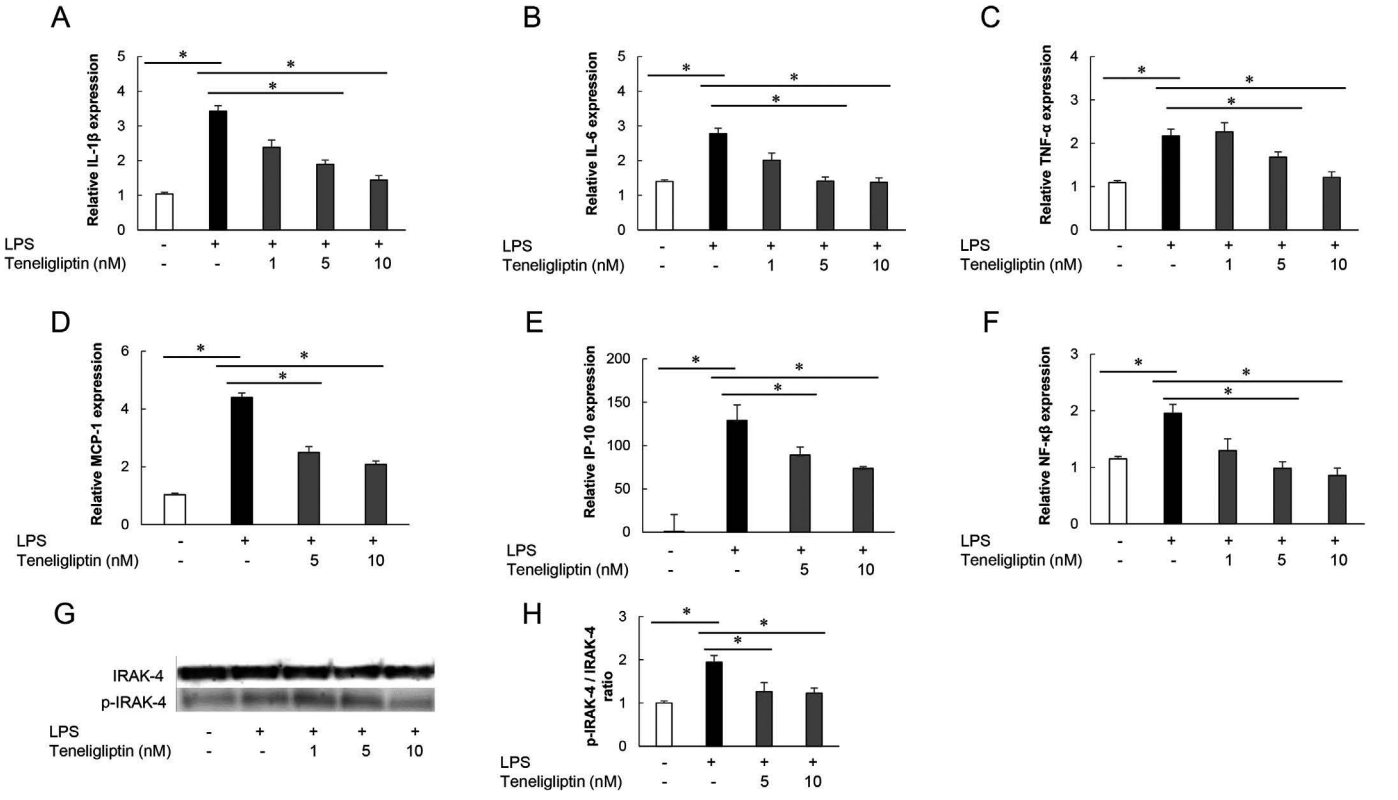

Fig. 2. The anti-inflammatory effects of teneligliptin on human macrophages. (A–F) The effect of teneligliptin on the expression of pro-inflammatory molecules in human U937 cells. Expression of *Il-1β*, *Il-6*, *Tnf-α*, *Mcp-1*, *Ip-10*, and *Nf-κβ* was measured by real-time RT-PCR. **(G)** and **(H)** The effect of teneligliptin on LPS-mediated phosphorylation of IRAK-4 in U937 cells. Representative images of immunoblot bands for phosphorylated and total IRAK-4 **(G)**. The ratio of phosphorylated IRAK-4 to total IRAK-4 **(H)**. n = 3 per group. *$p < 0.05$.

of pro-inflammatory molecules in human U937 cells. LPS treatment (10 μg/mL) increased the expression of *Il-1β*, *Il-6*, and *Tnf-α* at 6 h, and co-treatment with teneligliptin (1, 5, and 10 nmol/L) dose-dependently suppressed this increase (Fig. 2 A–C). Furthermore, teneligliptin treatment at 5 and 10 nmol/L also suppressed LPS-induced expression of *Mcp-1*, *Ip-10*, and *Nf-κβ* (Fig. 2 D–F). Consistently, teneligliptin treatment (5 and 10 nmol/L) suppressed LPS-induced phosphorylation of IRAK-4, a downstream molecule of TLR4 signaling (Fig. 2 G); however, it did not affect cell viability in the presence or absence of LPS (Supplemental Fig. 2).

Neutralization and gene knockdown of CD26 or Cav-1 suppress LPS-induced expression of pro-inflammatory molecules in U937 cells.

To obtain further insights into the role of CD26 and Cav-1 in TLR4-induced inflammatory responses, we conducted antibody neutralization and siRNA-induced gene knockdown against CD26 or Cav-1. Anti-CD26 antibody (100 ng/mL) suppressed LPS-induced expression of *Il-1β*, *Il-6*, and *Tnf-α* to the same level as that achieved by teneligliptin treatment (Fig. 3 A–C). Similarly, anti-Cav-1 polyclonal antibody (H97; 200 ng/mL), recognizing amino acids 82–178 of Cav-1, significantly suppressed LPS-induced expression of these cytokines. In contrast, anti-Cav-1 monoclonal antibody (7c8; 200 ng/mL), recognizing amino acids between residue 32 and the C-terminus of Cav-1, did not show any effect (Fig. 3 D–F). Expression of CD26 or Cav-1 was significantly decreased by siRNA transfection (Supplemental Fig. 3). Gene knockdown of CD26 and Cav-1 significantly attenuated LPS-induced expression of *Il-1β*, *Il-6*, or *Tnf-α* (Fig. 3 G–I).

3.5. The anti-inflammatory effects of teneligliptin are specific to TLR4 and TLR5 signaling pathways

Finally, we evaluated the effects of teneligliptin on inflammation induced by other TLR agonists. U937 cells were stimulated with specific agonists for TLR1–9. All agonists significantly increased the expression of *Il-1β*, *Il-6*, and *Tnf-α* (Fig. 4 A–C). Teneligliptin (5 nmol/L) suppressed the expression of these pro-inflammatory cytokines induced by LPS (TLR4 agonist) and flagellin (TLR5 agonist), but did not suppress the expression of cytokines induced by other TLR agonists.

4. Discussion

In the present study, we demonstrated that Cav-1 is a target of DPP-4 inhibitors in the suppression of inflammation in human and murine macrophages. Teneligliptin is a potent DPP-4 inhibitor that inactivates DPP-4 at a lower IC50 (0.37 nmol/L) than other DPP-4 inhibitors (IC50, 1–62 nmol/L) [21], and is wildly used for the treatment of type 2 diabetes. The anti-inflammatory effects of DPP-4 inhibitors have been shown in various immune cells of rodents and humans [8,13,14]. Consistently, teneligliptin suppressed TLR4 ligand (LPS)-induced inflammation in mouse exudate peritoneal macrophages and human U937 cells, both of which co-expressed CD26 and Cav-1. It is noteworthy that the genetic deletion of Cav-1 in macrophages reduced inflammatory responses to LPS derived from *Escherichia coli*, and that teneligliptin treatment did not suppress LPS-induced inflammation in macrophages in the absence of Cav-1.

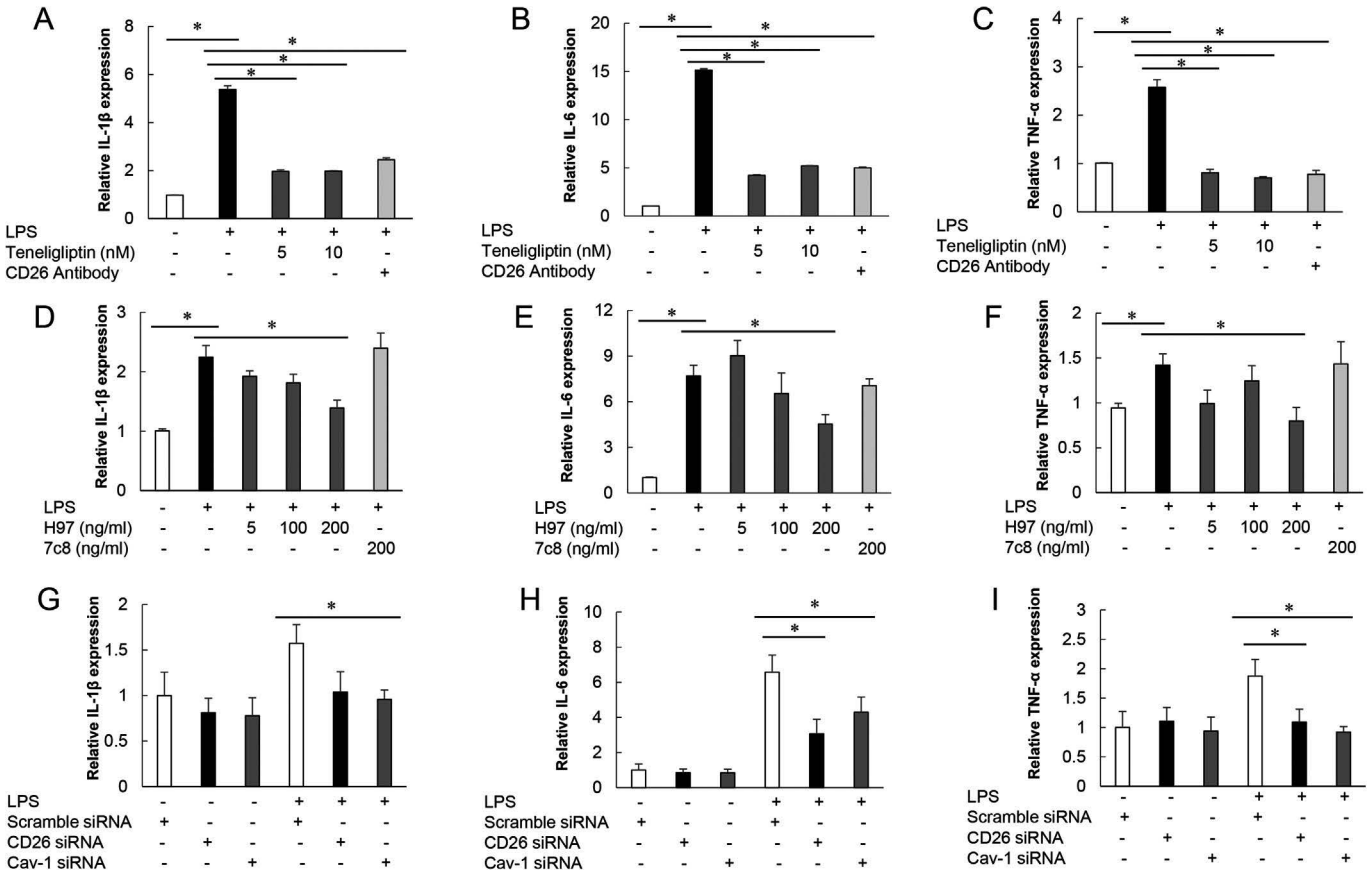

Fig. 3. The role of CD26 and Cav-1 on TLR4-induced inflammation. (A–F) The effect of neutralization by anti-CD26 or anti-Cav-1 antibody (polyclonal H97 or monoclonal 7c8) on LPS-induced expression of pro-inflammatory cytokines in U937 cells. Relative expression of *Il-1β*, *Il-6*, and *Tnf-α* to that of *18s rRNA* using anti-CD26 or anti-Cav-1 antibody is presented in A–C and D–F, respectively. n = 3–5 per group. **(G–I)** The effect of gene knockdown of CD26 or Cav-1 by siRNA transfection on LPS-induced expression of pro-inflammatory cytokines in U937 cells. n = 3–5 per group. $^{*}p < 0.05$.

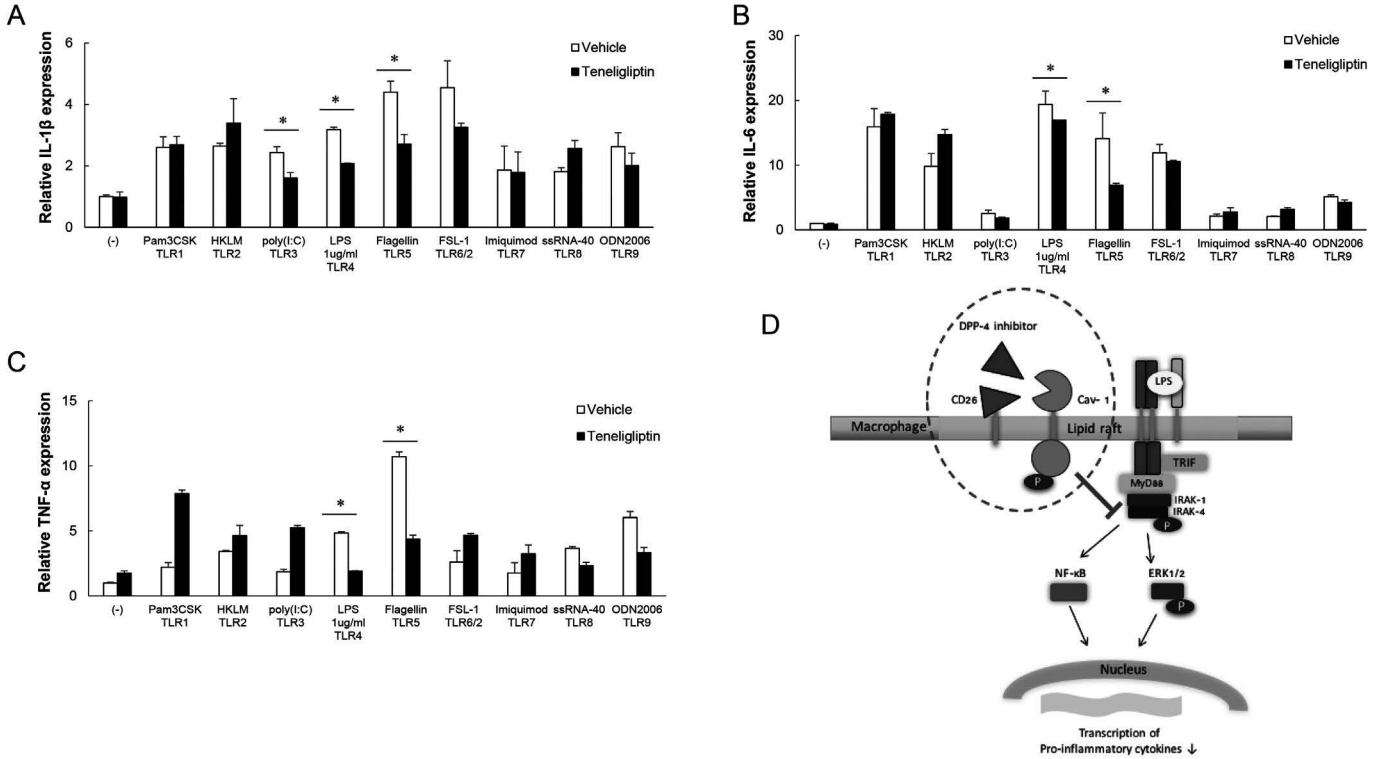

Fig. 4. TLR agonists involved in the anti-inflammatory effects of teneligliptin. (A–C) Effect of teneligliptin on the expression of pro-inflammatory cytokines (A, *Il-1β*; B, *Il-6*; C, *Tnf-α*) in U937 cells stimulated by various ligands of TLRs. The ligands of TLRs used are shown in Supplemental Table 1. n = 3 per group. *p < 0.05. **(D)** A scheme for the proposed mechanism of anti-inflammatory action of DPP-4 inhibitors in macrophages. DPP-4 inhibitors regulate the function of Cav-1 by affecting CD26 and Cav-1 interaction, resulting in the suppression of inflammatory responses via inhibiting the TLR4/IRAK-4 pathway. TRIF, TIR-domain-containing adapter-inducing interferon-β; ERK, extracellular signal-regulated kinase.

Previous studies investigating the role of Cav-1 in inflammatory responses have shown confounding results [22,23]. Cav-$1^{-/-}$ mice have been shown to be resistant to lung inflammation induced by intraperitoneal administration of LPS derived from *E. coli* via decreased NF-κβ activity [22]. In contrast, peritoneal macrophages obtained from Cav-$1^{-/-}$ mice show enhanced inflammatory responses to LPS derived from *Salmonella enterica* [23]. There is a report showing that inflammatory responses are different between LPS derived from *E. coli* and *S. enterica* and that lipid A, one of the structural components of LPS, is involved in this difference [24]. Thus, whether Cav-1 enhances or suppresses inflammatory responses may vary in different types of LPS or cells. Our data show that, in mouse macrophages, Cav-1 acts as a pro-inflammatory molecule in response to *E. coli*-derived LPS, and is a target of DPP-4 inhibitors to suppress inflammation induced by this type of LPS.

To gain further understanding about the interaction between CD26 and Cav-1, we conducted antibody neutralization and gene knockdown against CD26 and Cav-1. In human U937 cells, treatment with antibody against CD26 and siRNA transfection against Cav-1 or CD26 showed suppression in LPS-induced expression of pro-inflammatory cytokines, similar to that observed after teneligliptin treatment. However, two antibodies against Cav-1 exerted different effects: the antibody recognizing amino acids 82–178 of Cav-1 suppressed inflammatory responses to LPS, and the antibody recognizing the amino acids between residue 32 and the C-terminus of Cav-1 did not show any effect. Ohnuma et al. have demonstrated that residue 630 of CD26 (serine catalytic site having DPP-4 activity) is required to bind to Cav-1 residues 82–101 (also known as the caveolin scaffolding domain) [16]. Our findings provide further evidence that residues 82–178 of Cav-1 are essential for the inflammatory responses induced by TLR4, possibly due to their involvement in the binding of Cav-1 and CD26.

We found that teneligliptin suppress LPS-induced phosphorylation of IRAK-4 in human U937 cells. IRAK-4 has been shown to be a signaling component that is required for NF-κB activation, and is highly co-localized with Cav-1 in the caveolae of macrophages [25]. A previous study has demonstrated that Cav-1 deficiency reduces inflammatory responses to LPS by impairing IRAK-4 activity in the mouse lung [26]. Our findings indicate that suppression of IRAK-4 phosphorylation may be one of the mechanisms responsible for the anti-inflammatory effects of teneligliptin.

In conclusion, Cav-1 acts as a pro-inflammatory molecule in response to *E. coli*-derived LPS in mouse and human macrophages, and is a target of DPP-4 inhibitors to suppress TLR4-induced inflammation.

Author contribution

MH conducted in vivo and in vitro experiments, analyzed the data, and wrote the manuscript. KN conducted in vitro experiments, analyzed the data and revised the manuscript. YM analyzed the data and contributed to data interpretation and manuscript revision. HK and MS conducted in vitro experiments and contributed to data interpretation and manuscript revision. KO conducted in vitro experiments, analyzed the data, and revised the manuscript. HK contributed to data interpretation and manuscript revision. TH designed the study, and revised and finalized the manuscript. All the authors approved the final version of the manuscript for the submission.

Conflicts of interest

TH received lecture fees from MSD KK, Novartis Pharma KK,

Novo Nordisk Pharma Ltd., Sanwa Kagaku Kenkyusho Co. Ltd., Kowa Co. Ltd., Eli Lilly Japan KK, Mitsubishi Tanabe Pharma Co., and Ono Pharmaceutical Co. Ltd. All other authors declare that they have no competing interests.

Funding

This study was financially supported by MSD KK, Novartis Pharma KK, Novo Nordisk Pharma Ltd., Sanwa Kagaku Kenkyusho Co. Ltd., Kowa Co. Ltd., Eli Lilly Japan KK, and Mitsubishi Tanabe Pharma Co. However, they played no role in the design of the study, collection, analysis, and interpretation of data, or in writing the manuscript, and did not have access to data stemming from this study.

Acknowledgements

The authors would like to thank Hiroko Takeuchi for her technical assistance.

Transparency document

Transparency document related to this article can be found online at https://doi.org/10.1016/j.bbrc.2017.11.016.

Appendix A. Supplementary data

Supplementary data related to this article can be found at https://doi.org/10.1016/j.bbrc.2017.11.016.

References

[1] P. Aschner, M.S. Kipnes, J.K. Lunceford, et al., Effect of the dipeptidyl peptidase-4 inhibitor sitagliptin as monotherapy on glycemic control in patients with type 2 diabetes, Diabetes Care 29 (2006) 2632–2637.
[2] K. Nonaka, T. Kakikawa, A. Sato, et al., Efficacy and safety of sitagliptin monotherapy in Japanese patients with type 2 diabetes, Diabetes Res. Clin. Pract. 79 (2008) 291–298.
[3] T. Kadowaki, K. Kondo, Efficacy, safety and dose-response relationship of teneligliptin, a dipeptidyl peptidase-4 inhibitor, in Japanese patients with type 2 diabetes mellitus, Diabetes Obes. Metab. 15 (2013) 810–818.
[4] A. Yaron, F. Naider, Proline-dependent structural and biological properties of peptides and proteins, Crit. Rev. Biochem. Mol. Biol. 28 (1993) 31–81.
[5] J.R. Ussher, D.J. Drucker, Cardiovascular actions of incretin-based therapies, Circ. Res. 114 (2014) 1788–1803.
[6] G.P. Fadini, A. Avogaro, Cardiovascular effects of DPP-4 inhibition: beyond GLP-1, Vasc. Pharmacol. 55 (2011) 10–16.
[7] M. Terasaki, M. Nagashima, K. Nohtomi, et al., Preventive effect of dipeptidyl peptidase-4 inhibitor on atherosclerosis is mainly attributable to incretin's actions in nondiabetic and diabetic apolipoprotein E-null mice, PLoS One 13 (2013) e70933.
[8] N.N. Ta, C.A. Schuyler, Y. Li, et al., DPP-4 (CD26) inhibitor alogliptin inhibits atherosclerosis in diabetic apolipoprotein E-deficient mice, J. Cardiovasc. Pharmacol. 58 (2011) 157–166.
[9] N. Ervinna, T. Mita, E. Yasunari, et al., Anagliptin, a DPP-4 inhibitor, suppresses proliferation of vascular smooth muscles and monocyte inflammatory reaction and attenuates atherosclerosis in male apo E-deficient mice, Endocrinology 154 (2013) 1260–1270.
[10] T. Hirano, S. Yamashita, M. Takahashi, et al., Anagliptin, a dipeptidyl peptidase-4 inhibitor, decreases macrophage infiltration and suppresses atherosclerosis in aortic and coronary arteries in cholesterol-fed rabbits, Metabolism 65 (2016) 893–903.
[11] L. Liu, J. Liu, W.T. Wong, et al., Dipeptidyl peptidase 4 inhibitor sitagliptin protects endothelial function in hypertension through a glucagon-like peptide 1-dependent mechanism, Hypertension 60 (2012) 833–841.
[12] Y. Terawaki, T. Nomiyama, T. Kawanami, et al., Dipeptidyl peptidase-4 inhibitor linagliptin attenuates neointima formation after vascular injury, Cardiovasc. Diabetol. 13 (2014) 154.
[13] T. Ikeda, E. Kumagai, S. Iwata, A. Yamakawa, Soluble CD26/dipeptidyl peptidase IV enhances the transcription of IL-6 and TNF-α in THP-1 cells and monocytes, PLoS One 8 (2013) e66520.
[14] D.S. Lee, E.S. Lee, M.M. Alam, et al., Soluble DPP-4 up-regulates toll-like receptors and augments inflammatory reactions, which are ameliorated by vildagliptin or mannose-6-phosphate, Metabolism 65 (2016) 89–101.
[15] H. Feng, W. Guo, J. Han, X.A. Li, Role of caveolin-1 and caveolae signaling in endotoxemia and sepsis, Life Sci. 93 (2013) 1–6.
[16] K. Ohnuma, T. Yamochi, M. Uchiyama, et al., CD26 up-regulates expression of CD86 on antigen-presenting cells by means of caveolin-1, Proc. Natl. Acad. Sci. U. S. A. 101 (2004) 14186–14191.
[17] K. Ohnuma, T. Yamochi, M. Uchiyama, et al., CD26 mediates dissociation of Tollip and IRAK-1 from caveolin-1 and induces upregulation of CD86 on antigen-presenting cells, Mol. Cell Biol. 25 (2005) 7743–7757.
[18] K. Ohnuma, N.H. Dang, C. Morimoto, Revisiting an old acquaintance: CD26 and its molecular mechanisms in T cell function, Trends Immunol. 29 (2008) 295–301.
[19] K. Ohnuma, M. Uchiyama, T. Yamochi, et al., Caveolin-1 triggers T-cell activation via CD26 in association with CARMA1, J. Biol. Chem. 282 (2007) 10117–10131.
[20] F. de Halleux, H.S. Taper, C. Deckers, A simple procedure for identification of macrophages in peritoneal exudates, Br. J. Exp. Pathol. 54 (1973) 352–358.
[21] D. Röhrborn, N. Wronkowitz, J. Eckel, DPP4 in diabetes, front, Immunol 6 (2015) 386.
[22] S. Garrean, X.P. Gao, V. Brovkovych, et al., Caveolin-1 regulates NF-kappaB activation and lung inflammatory response to sepsis induced by lipopolysaccharide, J. Immunol. 177 (2006) 4853–4860.
[23] F.A. Medina, C.J. Almeida, E. Dew, et al., Caveolin-1-Deficient mice show defects in innate immunity and inflammatory immune response during Salmonella enterica serovar typhimurium infection, infect, Immun 74 (2006) 6665–6674.
[24] M. Muroi, K. Tanamoto, The polysaccharide portion plays an indispensable role in Salmonella lipopolysaccharide-induced activation of NF-κB through human toll-like receptor 4, Infect. Immun. 70 (2002) 6043–6047.
[25] X.M. Wang, H.P. Kim, K. Nakahira, et al., The heme oxygenase-1/carbon monoxide pathway suppresses TLR4 signaling by regulating the interaction of TLR4 with caveolin-1, J. Immunol. 182 (2009) 3809–3818.
[26] M.K. Mirza, J. Yuan, X.P. Gao, et al., Caveolin-1 deficiency dampens Toll-like receptor 4 signaling through eNOS activation, Am. J. Pathol. 176 (2010) 2344–2351.

FULL PAPER

BJC

British Journal of Cancer (2017) 116, 1126–1134 | doi: 10.1038/bjc.2017.62 BJC OPEN

Keywords: CD26; phase I; mesothelioma; immune checkpoint

First-in-human phase 1 of YS110, a monoclonal antibody directed against CD26 in advanced CD26-expressing cancers

Eric Angevin*[,1], Nicolas Isambert[2], Véronique Trillet-Lenoir[3], Benoit You[3], Jérôme Alexandre[4], Gérard Zalcman[5], Philippe Vielh[6], Françoise Farace[6], Fanny Valleix[7], Thomas Podoll[8], Yu Kuramochi[9], Itaru Miyashita[9], Osamu Hosono[10], Nam H Dang[11], Kei Ohnuma[12], Taketo Yamada[13,14], Yutaro Kaneko[15] and Chikao Morimoto[12]

*[1]Gustave Roussy, Université Paris-Saclay, Drug Development Department (DITEP), Villejuif, France; [2]Centre Georges-François Leclerc, Unité de Phases Précoces, Dijon, France; [3]Institut de Cancérologie des Hospices Civils de Lyon, CITOHL, Lyon, France; [4]Hôpital Cochin, Paris, France; [5]Centre Hospitalier Universitaire (CHU) de Caen, Centre de Recherche Clinique/Essais de phases précoces, Caen, France; [6]Gustave Roussy, Translational Research Laboratory, Villejuif, France; [7]FV Clinical subcontractor for SynteractHCR SAS, Levallois-Perret, France; [8]Y's therapeutics Inc., Redwood City, CA, USA; [9]Kissei Pharmaceutical Co., Ltd, Tokyo, Japan; [10]Department of Rheumatology and Allergy, IMSUT Hospital, The Institute of Medical Science, The University of Tokyo, Tokyo, Japan; [11]Division of Hematology/Oncology, University of Florida, Gainesville, FL, USA; [12]Department of Therapy Development and Innovation for Immune Disorders and Cancers, Graduate School of Medicine, Juntendo University, Tokyo, Japan; [13]Keio University School of Medicine, Tokyo, Japan; [14]Saitama Medical University, Saitama, Japan and [15]Y's AC Co., Ltd, Tokyo, Japan

Background: YS110 is a humanised IgG1 monoclonal antibody with high affinity to the CD26 antigen. YS110 demonstrated preclinical anti-tumour effects without significant side effects.

Methods: This FIH study was designed to determine the maximal tolerated dose (MTD) and recommended phase 2 dose (RP2D) to assess the tolerance, pharmacokinetics (PK) and pharmacodynamics profiles of YS110 and preliminary efficacy. YS110 were initially administered intravenously once every 2 weeks (Q2W) for three doses and then, based on PK data, once every week (Q1W) for five doses in patients with CD26-expressing solid tumours.

Results: Thirty-three patients (22 mesothelioma) received a median of 3 (range 1–30) YS110 infusions across six dose levels (0.1–6 mg kg^{-1}). MTD was not reached and two dose-limiting toxicities (infusion hypersensitivity reactions) led to the institution of a systemic premedication. Low-grade asthenia (30.3%), hypersensitivity (27.3%), nausea (15.2%), flushing (15.2%), chills (12.1%) and pyrexia (12.1%) were reported as ADRs. Pharmacokinetic parameters (AUC and C_{max}) increased in proportion with the dose. sCD26/DPPIV assays indicated CD26 modulation. Prolonged stable diseases were observed in 13 out of 26 evaluable patients.

Conclusions: YS110 is well tolerated up to 6 mg kg^{-1} Q1W, which has been defined as the RP2D, with encouraging prolonged disease stabilisations observed in a number of patients with advanced/refractory mesothelioma.

CD26 is a 110-kDa, type II transmembrane glycoprotein with known dipeptidyl peptidase IV (DPPIV, EC 3.4.14.5) activity in its extracellular domain and is capable of cleaving N-terminal dipeptides with either L-proline or L-alanine at the penultimate position (Torimoto *et al*, 1992; Ohnuma *et al*, 2008). CD26 activity is dependent on cell type and the microenvironment factors that

*Correspondence: Dr E Angevin; E-mail: eric.angevin@gustaveroussy.fr
This study has been previously selected for presentation at the ASCO2015 meeting.

Received 8 November 2016; revised 17 February 2017; accepted 20 February 2017; published online 14 March 2017

can influence its multiple biological roles (Havre *et al,* 2008; Ohnuma *et al,* 2011). Robust evidence from our accumulating data indicates that CD26 has an important role in T-cell biology and overall immune function (Morimoto *et al,* 1989; Tanaka *et al*, 1993; Morimoto and Schlossman, 1998; Dang *et al,* 1990a, b; Hegen *et al,* 1997; Ohnuma *et al,* 2008).

CD26 is also expressed on various tumours such as malignant pleural mesothelioma (MPM), renal cell carcinoma (RCC), colorectal cancer (CRC), hepatocellular carcinoma, lung cancer, prostate cancer, gastrointestinal stromal tumour, thyroid cancer and haematologic malignancies such as T-anaplastic large cell lymphoma, T-lymphoblastic lymphoma and T-acute lymphoblastic leukaemia (Havre *et al,* 2008).

Our previous work demonstrated that CD26 is preferentially expressed in MPM cells but not in normal mesothelial cells (Amatya *et al,* 2011), and suggested that membranous expression of CD26 is of potential importance in the treatment of MPM patients (Aoe *et al,* 2012). More recently, we demonstrated that the CD26-positive population of $CD24^{+}CD9^{+}$ MPM cells exhibits the cancer stem cell features (Ghani *et al,* 2011; Yamazaki *et al,* 2012). We also reported robust *in vivo* data on the anti-tumour activity of anti-CD26 mAb in mouse xenograft models (Ho *et al*, 2001; Inamoto *et al,* 2006, 2007; Okamoto *et al,* 2014; Yamamoto *et al,* 2014).

YS110 is a recombinant DNA-derived humanised monoclonal antibody that selectively binds with high affinity to the extracellular domain of CD26.

The antibody is an IgG1 kappa with a molecular weight of 144 kDa and was humanised via an *in silico* design based on the amino-acid sequence of anti-human CD26 murine mAb (14D10), which inhibited tumour cell growth, migration and invasion, and enhanced survival of mouse xenograft models (Inamoto *et al,* 2006). The gene of YS110 is deposited to ATCC in designated with accession No. PTA-7695. The gene is preserved in DH5α *Escherichia coli* with plasmid having insert of heavy and light chain of a humanised monoclonal antibody against human CD 26 cDNA. The strain designation is S604069. YST-pABMC 148 ($\times$ 411). YS110 is produced by fermentation in mammalian cell (Chinese hamster ovary) suspension culture with the Glutamine Synthetase Expression System. *In vitro* pharmacological evaluation of YS110 demonstrated its selective binding to human CD26 on a number of human cancer cell lines and tissues, and no evidence for immune activation and no effect on DPPIV activity, while exhibiting direct cytotoxic effect on certain human CD26-positive cancer cell lines (Inamoto *et al,* 2006). In addition to antibody-dependent cellular cytotoxicity and complement-dependent cytotoxicity (Inamoto *et al,* 2006), YS110 induces tumour cell lysis *in vitro* via alternative original mechanisms: (i) a direct anti-tumour effect through the induction of cell cycle arrest by induction of $p27^{kip1}$ expression (Inamoto *et al,* 2006, 2007), (ii) following internalisation of the CD26-YS110 complexes, an inhibition of invasion and migration of tumours cells by decreased binding to the collagen/fibronectin microenvironment matrix (Inamoto *et al,* 2006, 2007) and (iii) the nuclear translocation of CD26 molecules by internalisation of the CD26-YS110 complexes to inhibit proliferation of MPM cells via suppression of *POLR2A* gene expression (Yamada *et al,* 2013). In further studies using preclinical models, *in vivo* administration of YS110 resulted in inhibition of tumour cell growth, migration and invasion, and enhanced survival of mouse xenograft models inoculated with RCC or MPM (Inamoto, *et al,* 2007; Okamoto *et al,* 2014; Yamamoto *et al,* 2014).

In addition to our robust *in vitro* and *in vivo* data on antibody-mediated dose-dependent tumour growth inhibition, YS110 exhibited excellent safety and pharmacological profiles in non-human primate models using single and repeated increasing intravenous doses. Considering the lack of T-cell proliferation and cytokine production *in vitro*, YS110 was therefore considered not to have an agonistic nor activating effect on human CD26-positive lymphocytes.

This first-in-human phase 1 clinical trial aims to evaluate the safety, pharmacokinetic/pharmacodynamic profiles and preliminary anti-tumour effects of YS110 in patients with CD26-expressing solid tumours and, particularly, refractory malignant mesothelioma, a tumour type in which successful therapeutic advances are expected to be warranted for a long time.

MATERIALS AND METHODS

Patients. Eligible patients were 18–80 years old with locally advanced, inoperable or refractory solid tumours that were histologically documented to express the CD26 molecule. Cancer histologies included mesothelioma (pleural or peritoneal) or other solid tumours such as non-small-cell lung carcinoma, RCC or hepatocellular carcinoma. All patients were in relapse following or were refractory to prior standard therapies (regardless of the number of prior treatment lines), with a progressive evaluable/measurable disease. Other key inclusion criteria included Eastern Cooperative Oncology Group (ECOG) performance status score $\leqslant 2$, adequate bone marrow, liver and renal function; at least 4 weeks from prior surgery, chemotherapy, external radiotherapy or immunotherapy (at least 6 weeks from prior nitrosoureas). All patients provided written informed consent. This study was conducted according to the Declaration of Helsinki and was approved by an ethics committee and the French National Drug Agency.

CD26 immunohistochemistry screening. Analysis of CD26 tumour expression for pre-screening was performed centrally at Gustave Roussy by conventional immunohistochemistry performed on formalin-fixed paraffin-embedded (FFPE) archival tumour samples using a anti-human CD26 goat polyclonal antibody (AF1180, R&D Systems, Minneapolis, MN, USA) as previously described (Aoe *et al,* 2012). Briefly, all patients were pre-screened for confirmed CD26-positive expression, defined as $\geqslant$20% of the tumour cells (1+, 2+ or 3+ intensity) and verified independently by two pathologists (P Vielh and T Yamada) (Figure 1).

Study design. This first-in-human study was designed as a classical 3 + 3 dose-escalating phase 1 trial of the single agent YS110 (Supplementary Table 1). The primary objective was to determine the maximum tolerated dose (MTD) based on the occurrence of dose-limiting toxicity (DLT) and a recommended phase 2 dose (RP2D). Initially, cohorts 1–4 each planned to enrol 3, and up to 6, patients sequentially to evaluate escalating YS110 doses at 0.1, 0.4, 1 and 2 mg kg^{-1} for a total of three infusions of YS110 on days 1, 15 and 29 (one treatment cycle, Q2W). On the basis of preliminary pharmacokinetics (PK) data, the protocol was then subsequently amended to allow patients to receive a total of five infusions of YS110 on days 1, 8, 15, 22 and 29 (one treatment cycle, Q1W) at 2, 4, and 6 mg kg^{-1}. Each cohort included a 24-h monitoring period following each infusion during the first cycle for evaluation of safety, DLTs and PK. Patients who completed one cycle and demonstrated a clinical response or stable disease could receive the second cycle of YS110 treatment cycles at the same dose and dosing frequency, until disease progression or a significant observed serious adverse event (SAE). If the patient continued the treatment, the second cycle was to begin initially 4 weeks (later amended to 2 weeks) after the last infusion of the first cycle (initially Day 57; after amendment, Day 43). For the subsequent cycles, the latency period between the last administration of a cycle and the beginning of the next cycle was 2 weeks. Secondary objectives of the study were to assess the safety and tolerability

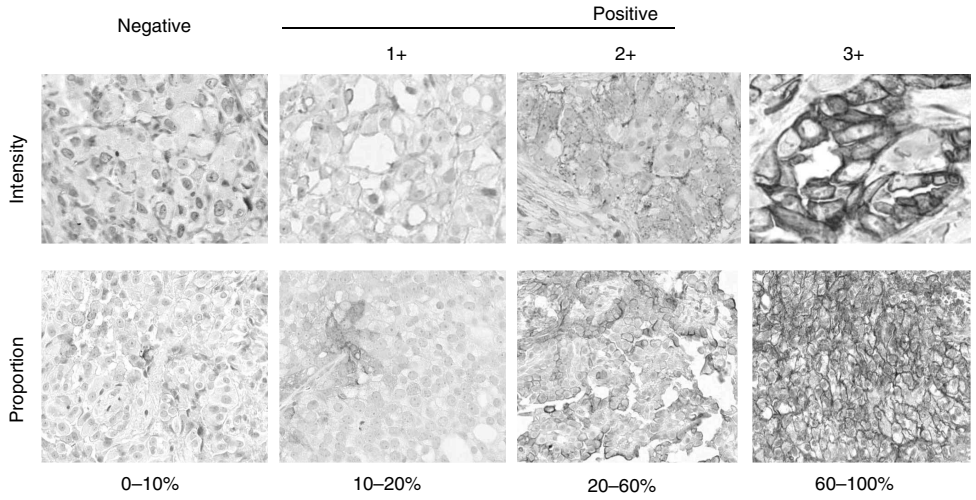

Figure 1. Evaluation of CD26 staining by immunohistochemistry in cases of mesothelioma.

profile, PK, pharmacodynamics, preliminary anti-tumour activity and to collect survival data.

Safety. All adverse events and SAEs occurring from the informed consent signature up to 30 days after the last dose were reported according to the National Cancer Institute Common Terminology Criteria for Adverse Events (CTCAE v3.0). An adverse drug reaction (ADR) was defined as an adverse event (AE) documented as possibly, probably or definitely related to the study drug or with unknown relationship to the study drug. A treatment-emergent adverse event was defined as an AE with onset on or after the first infusion. The DLT period was 2 weeks after the first YS110 infusion, whatever the dose schedule. Dose-limiting toxicities were defined as any grade $\geqslant 3$ non-haematological toxicity or a haematological toxicity of grade $\geqslant 4$. This definition was later amended to exclude reversible grade 3 infusion reactions defined as allergic reaction/hypersensitivity, fever, pain, bronchospasm, wheezing or hypoxia, occurring during the first dose infusion and resolving with a reduced infusion rate, a stop of the infusion, supportive care and/or the administration of corticosteroids (Supplementary Table S2). In case of treatment discontinuation due to reversible grade 3 infusion reactions, the patient was to be replaced with a new patient of the same cohort.

Efficacy. Preliminary clinical efficacy was evaluated by radiological and tumour marker assessments performed at screening at Day 43 of each treatment cycle, and at end of treatment until progressive disease (PD) or withdrawal of consent. Tumour response was evaluated based on RECIST 1.0 criteria and defined as partial response (PR) or PD or stable disease (SD). Partial response was defined as $\geqslant 30\%$ decrease in the sum of the longest diameter (LD) of target lesions, PD was defined as $\geqslant 20\%$ increase in the sum of the LD of target lesions and stable disease was defined as neither sufficient shrinkage to qualify for PR nor sufficient increase to qualify for PD. Patients with mesothelioma were assessed according to modified RECIST criteria.

Pharmacokinetics. Serial blood samples were obtained at pre- and post-YS110 administration at Day 1, Day 8, Day 15 and Day 29 at specified time points throughout the study. Serum levels of YS110 were analysed by ELISA by Alta Intertek (San Diego, CA, USA). The method of blood sample collection is described in Supplementary Information.

Pharmacodynamics. All treated patients with appropriate post baseline samples were evaluable for pharmacodynamics analyses on blood samples collected at days 0 (baseline), 1 (post infusion), 2, 15 (pre- and post infusion), 29 (pre- and post infusion) for immunomonitoring and soluble CD26 (sCD26)/DPPIV (sDPPIV) activity assessments.

Immunomonitoring. Immunomonitoring was performed centrally in the translational research laboratory at Institut Gustave Roussy, France (F Farace).

Immunophenotyping was performed for the monitoring of peripheral blood lymphocyte (PBL) $CD26^+$ T (i.e., $CD3^+CD4^+$, $CD3^+CD8^+$) and NK (i.e., $CD3^-CD16^{+/-}CD56^+$) subpopulations by flow cytometry using fluorochrome-conjugated commercially available specific mAbs with relevant isotypic controls (all provided from Pharmingen, San Diego, CA, USA). To ensure the specificity of the CD26 staining in blood samples collected under YS110 treatment, competition and cross-blocking experiments using the two different CD26 mAb clones 5K78 (Santa Cruz Biotechnology, Inc., Dallas, TX, USA) and M-A261 (BD Pharmingen, San Jose, CA, USA) were also performed.

Dosages of serum cytokines (i.e., interleukin 6 (IL-6), tumour necrosis factor α (TNF-α) and IL-2) were investigated by standard commercially available ELISA assays (R&D Systems).

Soluble CD26 (sCD26) and DPPIV activity assessments. Assays for soluble CD26 and DPP4 were developed in the Morimoto's Laboratory (Juntendo University, Japan) using anti-human CD26 murine mAbs that exhibit no cross-reactivity with the therapeutic humanised anti-CD26 mAb YS110 as described previously (Dong *et al*, 1998; Ohnuma *et al*, 2015a). The sampling times for sCD26 were identical to that for immunomonitoring.

Statistical analyses. Descriptive statistics were used to summarise the data. The patient sampling size was a function of the $3+3$ dose escalation schedule. The realised sample size was dependent on the number and pattern of observed DLTs. The maximum sample size was a consequence of the design's sampling requirements and the number of dose levels. In this trial with six dose levels, the maximum number of patients being exposed in each dose level was determined according to the DTL occurrence rate and confirmation of safety.

RESULTS

Screening for CD26 expression. A total of 136 patients signed an informed consent form and were screened for CD26 expression on a FFPE archival tumour tissue sample. Mesothelioma, which was previously reported as one of the CD26-expressing tumour types

was a main target indication with 60 patients screened ($n=60$, 53% were $CD26^+$ cases). Examples of CD26 immunohistochemistry and scoring are presented in Figure 1. Other tumour types screened included RCC ($n=18$, 71% $CD26^+$ cases), hepatocellular carcinoma ($n=7$, 22% $CD26^+$ cases) and various other tumour types ($n=31$, 13% $CD26^+$ cases). Overall, 56 (41%) patients were considered as $CD26^+$ with the mean percentage of CD26 expression on tumour cells of 69% (range 20–100%) in the tested samples.

Patient characteristics. Thirty-four $CD26^+$ patients (19 males and 15 females) were enroled in the study and treated at 5 investigational sites in France, with 33 patients being evaluable (19 males and 14 females). The most common tumour types were mesothelioma ($n=23$, 69.7%), RCC ($n=9$, 27.3%) and one patient had an urothelial carcinoma ($n=1$; 3.0%). All mesothelioma patients were diagnosed with the epithelioid histology and were all in advanced inoperable disease or refractory to previous line of treatment. Other tumour types were in stage III/IV Twenty-two patients were treated according to the Q2W schedule at 0.1 ($n=3$), 0.4 ($n=3$), 1 ($n=6$) and 2 mg kg^{-1} ($n=10$) and 11 according to the Q1W schedule at 2 ($n=4$), 4 ($n=3$) and 6 ($n=4$) mg kg^{-1} (Table 1). The median percentage of $CD26^+$ tumour cells in archival samples from the patients treated was 63% (range 25–100%).

Safety. Eighteen patients received at least one cycle of YS110 with three infusions per cycle and seven patients completed at least one cycle with five infusions per cycle. Nine patients did not complete the first cycle.

During the DLT observation period (i.e., 15 days following the first infusion), two DLTs were reported as serious unexpected adverse events (SUSARs) consisting of grade 3 infusion reactions (one patient at the Q2W 1 mg kg^{-1} dose level and another patient at the Q2W 2 mg kg^{-1} dose level) that completely resolved with supportive treatment, but led to permanent discontinuation of treatment. As both patients had a history of allergies, consequently, the protocol was subsequently amended to add clinically relevant allergies as a new excluding criterion, as well as the administration of a systematic steroid prophylaxis prior to each infusion to better control potential infusion reactions (chills, fever, flushing, hypotension and respiratory disorders). With these modifications, dose escalation was possible up to 6 mg kg^{-1} in four patients without DLTs. Per protocol, dose escalation was stopped at the highest level of 6 mg kg^{-1} without the MTD being achieved.

All patients had one or more AEs and 113 ADRs considered to be possibly related to YS110 were reported by 30 (90.9%) patients. The most frequently reported AEs regardless of potential relationship to YS110 were asthenia (54.5%) and aggravation of prior conditions (30.3%). Adverse effects (related or not to treatment) occurring in more than 10% of the patients are reported in Table 2 according to system organ class and preferred term. The majority of AEs were of mild (grade 1) or moderate (grade 2) severity. The most commonly reported grade $\geqslant 3$ AEs were dyspnoea (21.2%), hypersensitivity (15.2%), aggravation of prior conditions (15.2%), general physical health deterioration (12.1%) and hyperglycaemia (12.1%). Eight patients (24.2%) discontinued YS110 due to adverse events; most adverse events leading to discontinuation were considered unrelated to YS110, except for the two patients with infusion reactions considered as DLTs. Twenty-seven SAEs were reported in this study in 18 patients. Except for the two DLTs, all other SAEs, most commonly general physical health deterioration, were considered to be unrelated to YS110 but rather related to consequences of disease progression as assessed by the investigator, including the six patient deaths during the study.

No dose-dependent AEs were observed. Low-grade asthenia (30.3%), hypersensitivity (27.3%), nausea (15.2%), flushing (15.2%), chills (12.1%) and pyrexia (12.1%) were reported as ADRs.

No clinically significant abnormalities were observed in haematology and clinical chemistry laboratory parameters, as well as in ECG findings.

The main limiting toxicities in the study were infusion reactions, two being considered as DLTs leading to permanent discontinuation of treatment. Six severe hypersensitivity reactions were reported in five patients receiving a dose of 2.0 mg kg^{-1} and a severe anaphylactic reaction was reported in one patient receiving a dose of 1.0 mg kg^{-1}. These ADRs, occurring mainly at the first infusion, were reversible and manageable with curative corticosteroids and antihistaminic drugs, and further prevented by a systemic corticosteroids premedication. Overall, these ADRs that did not appear to be related either to the dose level of YS110 or to the Q2W or Q1W schedule.

Pharmacokinetics. Following single and repeat intravenous infusions of YS110, there was a trend toward decreasing clearance (CL), increasing half-life time ($T_{1/2}$) and increasing exposure (C_{max}, AUC_{0-168}, $AUC_{0-\infty}$) with increasing doses, suggesting that CL was saturating across the dose range studied. Mean volume of distribution (V_z, V_{ss}) was similar or slightly higher than human serum volume, indicative of YS110 being primarily found in serum and consistent with prior observations for monoclonal antibodies. In general, exposure increased as the dose increased. Although increases in C_{max} appeared to be dose proportional, increases in AUC_{0-168} and $AUC_{0-\infty}$ were greater than dose proportional, and this was consistent with the trend of decreasing CL with increasing doses (Table 3). In addition, YS110 PK parameters changed with repeat dosing. For doses ranging from 1 to 6 mg kg^{-1}, mean CL was ~1.1–1.6-fold higher on Day 1 (*vs* Day 29), whereas mean $T_{1/2}$ increased ~1.2–2.3-fold and exposure (AUC_{0-168}) increased ~1.3–1.8-fold on Day 29 *vs* Day 1 (Table 3).

Table 1. Baseline demographics and disease characteristics

Number of patients ($n=33$)		Schedule and dose levels (mg kg^{-1})						
Age, median (min–max) (yrs)	63 (41–76)							
ECOG PS 0/1/2 (%)	29/58/13							
Primary tumour type, *n* (%)		Q2W				Q1W		
		0.1	0.4	1	2	2	4	6
Mesothelioma (Meso)	22 (67)	3	2	2	6	3	2	4
Renal cell carcinoma (RCC)	10 (30)	—	1	4	4	—	1	—
Urothelial carcinoma (UTC)	1 (3)	—	—	—	—	1	—	—
Median number of prior therapies (min–max)	3 (1–11)							

Abbreviation: ECOG = Eastern Cooperative Oncology Group.

Table 2. Adverse events (all grades) reported by ⩾10% of patients overall in any cohort

	Dose levels (mg kg^{-1})							
Preferred term (CTCAE v3) number of patients (%)	**0.1 (*n* = 3)**	**0.4 (*n* = 3)**	**1.0 (*n* = 6)**	**2.0 (*n* = 14)**	**4.0 (*n* = 3)**	**6.0 (*n* = 4)**	**All AEs/grade 3–4 (*n* = 33)**	**All ADRs/grade3–4 (*n* = 33)**
Asthenia	3 100.0)	2 (66.7)	0 (0.0)	8 (57.1)	2 (66.7)	3 (75.0)	18 (54.5)	10 (30.3)
Condition aggravated	1 (33.3)	0 (0.0)	1 (16.7)	4 (28.6)	1 (33.3)	3 (75.0)	10 (30.3)/5 (15.2)	
Pyrexia	2 (66.7)	1 (33.3)	1 (16.7)	3 (21.4)	0 (0.0)	1 (25.0)	8 (24.2)	4 (12.1)
Chest pain	1 (33.3)	1 (33.3)	1 (16.7)	2 (14.3)	0 (0.0)	0 (0.0)	5 (15.2)	
Chills	2 (66.7)	1 (33.3)	1 (16.7)	0 (0.0)	0 (0.0)	0 (0.0)	4 (12.1)	4 (12.1)
General health deterioration	0 (0.0)	0 (0.0)	0 (0.0)	2 (14.3)	1 (33.3)	1 (25.0)	4 (12.1)/4 (12.1)	
Constipation	2 (66.7)	0 (0.0)	1 (16.7)	5 (35.7)	0 (0.0)	1 (25.0)	9 (27.3)	
Nausea	0 (0.0)	1 (33.3)	1 (16.7)	3 (21.4)	2 (66.7)	1 (25.0)	8 (24.2)	5 (15.2)
Vomiting	1 (33.3)	1 (33.3)	2 (33.3)	2 (14.3)	1 (33.3)	0 (0.0)	7 (21.2)	
Diarrhoea	0 (0.0)	2 (66.7)	1 (16.7)	1 (7.1)	0 (0.0)	1 (25.0)	5 (15.2)	
Dyspnoea	2 (66.7)	1 (33.3)	3 (50.0)	5 (35.7)	0 (0.0)	3 (75.0)	14 (42.4)/7 (21.2)	
Hyperglycaemia	0 (0.0)	0 (0.0)	1 (16.7)	3 (21.4)	2 (66.7)	2 (50.0)	8 (24.2)/4 (12.1)	
Decreased appetite	0 (0.0)	1 (33.3)	1 (16.7)	3 (21.4)	1 (33.3)	1 (25.0)	7 (21.2)	
Headache	1 (33.3)	2 (66.7)	0 (0.0)	3 (21.4)	1 (33.3)	0 (0.0)	7 (21.2)	
Flushing	0 (0.0)	0 (0.0)	0 (0.0)	1 (7.1)	2 (66.7)	3 (75.0)	6 (18.2)	5 (15.2)
Hypersensitivity	0 (0.0)	0 (0.0)	1 (16.7)	8 (57.1)	0 (0.0)	0 (0.0)	9 (27.3)/5 (15.2)	9 (27.3)/5 (15.2)
Weight decreased	0 (0.0)	1 (33.3)	0 (0.0)	5 (35.7)	0 (0.0)	0 (0.0)	6 (18.2)	

Abbreviations: ADR = adverse drug reactions; AE = adverse events; *N* = number of patients. A subject with more than one finding in a specific category was only counted once; percentages are based on the total number of subjects in each treatment group. The table is sorted by descending subject count. Infusion reactions related to YS110 treatment were further prevented by corticosteroids premedication.

Table 3. Cycle 1 pharmacokinetics parameters (mean ± s.d.) for YS110 administration

Dose (mg kg^{-1})	Dose Schedule	Day	$T_{1/2}$ (h)	C_{max} (μg ml^{-1})	AUC_{0-168} (h × μg ml^{-1})	$AUC_{0-\infty}$ (h × μg ml^{-1})	CL (ml h^{-1} kg^{-1})
0.4	Q2W	1	ND	ND	ND	ND	ND
		29	14.8 ± ND	5.85 ± ND	143 ± ND	145 ± ND	2.79 ± ND
1	Q2W	1	26.4 ± ND	22.7 ± 5.68	768 ± 73.3	692 ± ND	1.44 ± ND
		29	ND	43.5 ± 29.3	979 ± NR	ND	1.05 ± NR
2	Q2W	1	36.4 ± 12.2	39.0 ± 9.94	1710 ± 360	1810 ± 472	1.16 ± 0.245
		29	43.1 ± 12.6	40.1 ± 10.4	2080 ± 943	2280 ± 1110	1.03 ± 0.435
2	Q1W	1	24.5 ± 4.59	30.8 ± 4.20	1180 ± 243	1200 ± 251	1.72 ± 0.334
		15	31.5 ± NR	67.3 ± NR	2150 ± NR	2230 ± NR	1.22 ± NR
		29	29.8 ± NR	27.5 ± 20.1	1650 ± NR	1720 ± NR	1.33 ± NR
4	Q1W	1	46.6 ± 1.69	72.5 ± 27.1	4340 ± 1030	4740 ± 1140	0.876 ± 0.206
		15	70.4 ± NR	82.4 ± NR	6000 ± NR	7450 ± NR	0.678 ± NR
		29	76.2 ± ND	98.4 ± ND	7320 ± ND	9340 ± ND	0.547 ± ND
6	Q1W	1	67.8 ± 13.8	150 ± 22.9	10 300 ± 1800	12 800 ± 3250	0.490 ± 0.116
		15	93.7 ± 27.4	182 ± 17.2	15 700 ± 3470	22 800 ± 8250	0.393 ± 0.0793
		29	154 ± NR	205 ± 23.6	18 400 ± 4320	39 700 ± NR	0.340 ± 0.0814

Abbreviations: AUC = area under the curve; CL = clearance; ND = not determined; NR = not reported.

For the initial dose levels (0.1, 0.4, 1 and 2 mg kg^{-1}), YS110 was administered on a Q2W schedule on days 1, 15 and 29. As expected, the maximum concentrations of YS110 (C_{max}) on days 1 and 29 were proportional to the dose levels. However, calculated half-lives (1–2 days) were shorter than expected for a humanised antibody and serum concentrations were at or below detectable levels (0.4 μg ml^{-1}) by 1 week post infusion. To maintain measurable YS110 trough concentrations between doses, dosing was increased to five doses on a Q1W schedule on days 1, 8, 15, 22 and 29 for dose levels 2, 4 and 6 mg kg^{-1}. C_{max} values on day 1 were roughly proportional to dose level. Mean half-lives increased with increasing dose levels, rising significantly from day 1 to day 15 to day 29 in the 2, 4 and 6 mg kg^{-1} cohorts ($\sim$1, $\sim$2 and $\sim$3 days, respectively), and resulting in drug accumulation between the doses (Table 3).

Impact from exposure to YS110 on anti-drug antibody (ADA) response appeared to be most pronounced in the 0.4 mg kg^{-1} dose cohort. The two subjects who were ADA positive on Day 29 of Cycle 1 had notably reduced exposure relative to the one ADA negative subject. There were no ADAs detected in the higher dose groups.

Efficacy. A secondary objective of the study was to evaluate for the potential anti-tumour activity of YS110 according to RECIST 1.0 criteria (or modified RECIST criteria for mesothelioma). No objective response was observed in the treated patients. However, stable disease per RECIST criteria as the best response was observed in 13 out of the 26 evaluable patients following the first cycle of treatment, as shown in the accompanying Waterfall Plot Chart (Supplementary Figure S2). Overall median PFS was 43 days

Table 4. Time on YS110 treatment and median PFS of treated patients

Cohorts	Dose levels (mg kg^{-1})	Cancer types (*n*)	Median infusions *N* (min–max)	Median PFS days (min–max)
Q2W	0.1	Meso (3)	3 (3)	42 (41–42)
Q2W	0.4	Meso (2) RCC (1)	18 (3–20)	223 (40–273)
Q2W	1.0	Meso (2) RCC (4)	3 (1–3)	40 (28–59)
Q2W	2.0	Meso (6) RCC (4)	3 (1–27)	57 (13–399)
Q1W	2.0	Meso (3) UTC (1)	5 (1–20)	47 (5–184)
Q1W	4.0	Meso (3)	4 (3–5)	32 (22–59)
Q1W	6.0	Meso (4)	17.5 (1–30)	58 (15–258)
All	All	All	4 (1–30)	43 (5–399)

Abbreviations: Meso = malignant mesothelioma; PFS = progression-free survival duration; RCC = renal cell carcinoma; UTC = urothelial carcinoma.

(Table 4) as determined by a Kaplan–Meier Plot (Supplementary Figure S3). However, PFS of 184–399 days was observed in 7 patients (five cases of mesothelioma and two cases of RCC) out of 26 cases (mesothelioma: 19 cases, RCC: 6 cases and urinary tract carcinoma: 1 case). Table 4 summarises the median number of infusions administered and median PFS according to the different dose levels and schedule.

Pharmacodynamics

Immunomonitoring. The CD26 immunophenotyping on peripheral T and NK lymphocyte subpopulations under YS110 treatment was validated by testing two different anti-CD26 mAb clones. Indeed, in the first 12 patients tested using the M-A261 mAb (BD Pharmingen), we observed a dramatic decrease of CD26$^+$ cells consequently to YS110 administration, suggesting the lack of detection of the CD26 epitope due to YS110 binding. These results (not shown), led us to test in parallel another clone 5K78 (Santa Cruz Biotechnology) showing that CD26$^+$ cells were still detectable under YS110 treatment. The validation of this anti-CD26 mAb was ensured by competition and cross-blocking experiments using increasing dilutions of YS110 in the CD26 immunophenotyping assay demonstrating no modulation of CD26$^+$ subpopulations using the 5K78 clone in contrast to the first clone tested.

At baseline in our series of patients, the mean ± s.d. ($n = 33$) absolute values ($\times 10^6$ per ml) of lymphocytes populations were 0.94 (65.7%) ± 0.64 for CD3$^+$CD4$^+$, 0.33 (34.5%) ± 0.26 for CD3$^+$ CD8$^+$ T cells and 0.17 (8.2%) ± 0.17 for CD3$^-$CD16$^{+/-}$CD56$^+$ NK cells. The mean percentage of CD26$^+$ subpopulations in the T-CD4, T-CD8 and NK cells was 24.7%, 8.2% and 5.2%, respectively with a significant inter-patient variability. After YS110 infusions, the levels of the various PBL subpopulations decreased at day 1 and 2 (i.e., 24–48 h following YS110 infusions), with a subsequent recovery at day 15 and 29 pre-infusion samples in most patients (Supplementary Table S3). This decline in different PBL subpopulations was more frequently observed in patients who received higher doses (2, 4 and 6 mg kg^{-1}) of YS110. However, this trend was not statistically significant considering the inter-individual variations across the different dose levels.

Serum cytokines. At baseline and during YS110, no serum IL-2 production was detectable in any of the patients. Significant rise of the pro-inflammatory cytokines IL-6 and TNF-α was detected at day 1 and 2 following the first infusion of YS110 at 0.4, 1 and 2 mg kg^{-1} at various levels, including the first patient with a grade 3 infusion reactions DLT (at the Q1W 1 mg kg^{-1} dose level). Different kinetics of serum IL-6 and TNF-α production were observed in patients receiving 2 mg kg^{-1} of YS110, whereas low or undetectable levels were observed in patients receiving 4.0 and 6.0 mg kg^{-1} of YS110, likely due to the administration of systemic steroid prophylaxis.

sCD26 and DPPIV activity in sera. To determine serum levels of sCD26 protein and DPPIV enzyme activity in each cohort before and after administration of YS110, we developed an in-house ELISA assay for sCD26 and DPPIV using anti-human CD26 murine mAbs exhibiting no cross-reactivity with the therapeutic humanised anti-CD26 mAb YS110 (Dong *et al,* 1998; Ohnuma *et al,* 2015a).

As shown in Figure 2A, an increase in YS110 infusion dose was associated with decreased serum sCD26 level, particularly in the cohorts of patients treated at 2, 4 and 6 mg kg^{-1}, with ~80% decrease in sCD26 level. Moreover, as CD26 level reflects DPPIV enzyme activity in the serum, a similar reduction in DPPIV enzyme activity was observed (Figure 2B).

DISCUSSION

YS110 is the first, and currently the only CD26-directed mAb in clinical trial. This FIH study demonstrates that YS110 therapy exhibits a favourable safety profile and results in encouraging disease stabilisation in heavily pretreated CD26-positive MPM or RCC patients who had previously progressed on conventional standard therapies.

The spectrum of AEs, the most common of which were low-grade asthenia, hypersensitivity, chills, pyrexia, nausea, vomiting and headache, was similar to that previously described with humanised mAbs treatment (Scott *et al,* 2012). Two DLTs were reported as SUSARs consisting in grade 3 infusion reactions that resolved with supportive treatment. As both patients had a history of allergies, the protocol was subsequently amended to include clinically relevant allergies as a new excluding criterion, and the administration of systemic steroid prophylaxis has been implemented prior to each infusion at all cycles to better control such infusion reactions. In this study, high rate of hyperglycaemia was observed in patients in the top dose cohorts, consistent with the well-known effect of corticosteroid on glucose levels. However, hyperglycaemia resolved soon after cessation of steroid administration, whereas YS110 was detected in sera, with decreased serum DPPIV activity. Taken together, it is probable that premedicated corticosteroid, but not YS110, induces the hyperglycaemia observed in the patient cohorts receiving higher drug doses. With these new modifications, dose escalation up to 6 mg kg^{-1} was possible as in four patients in this cohort were treated without DLTs. Per protocol, 6 mg kg^{-1} was the highest dose level tested although the MTD was not achieved. The dose level of 6.0 mg kg^{-1} of YS110 was decided by study investigators to be the RP2D.

Total lymphocyte counts, as well as levels of CD26$^+$ lymphocytes, fell at Day 2 below the baseline levels. However, total lymphocyte counts recovered to reach baseline level at Day 8 and thereafter. These data indicate that YS110 administration resulted in a decrease in levels of peripheral lymphocytes including the CD26-positive lymphocyte subset soon after drug administration, and it is probable that YS110-mediated suppression of peripheral lymphocyte levels, including the CD26-positive subset, resolved by as early as Day 8. Moreover, we observed a decrease in the level of the CD26-positive subset of peripheral lymphocytes following administration of YS110 alone without steroid prophylaxis in the 0.1–2.0 mg kg^{-1} cohorts, as shown in Supplementary Table S3. Therefore, it is conceivable that YS110, but not premedication steroid, was responsible for the temporary effect on CD26-positive lymphocyte counts.

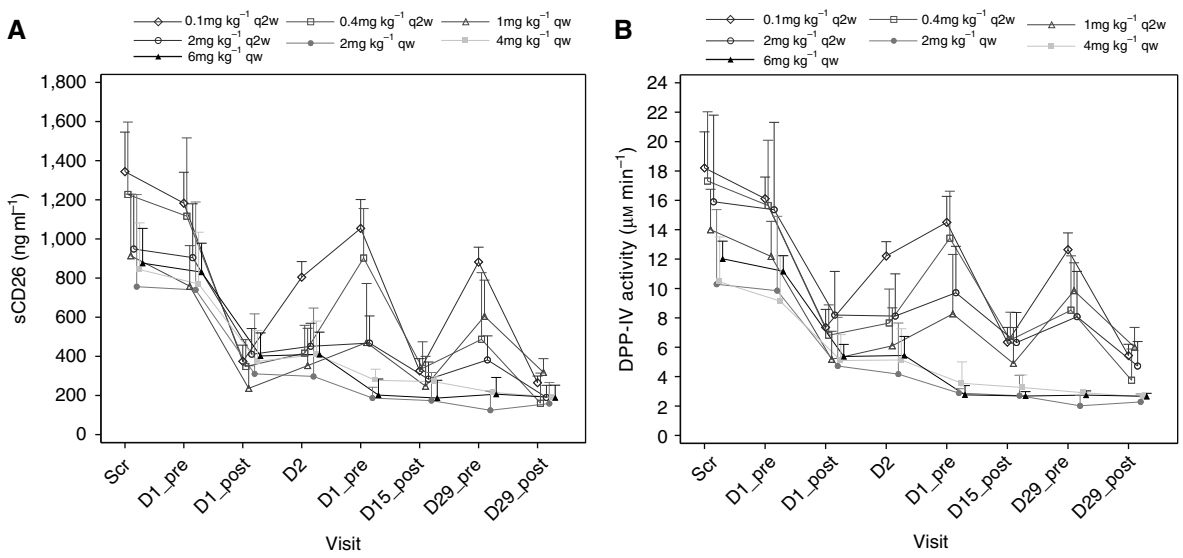

Figure 2. Changes of serum CD26/DPPIV levels following YS110 treatment: soluble CD26 (**A**) and DPPIV activity (**B**) mean ± s.d. at cycle 1 at the different dose levels.

CD26 is also present in serum and other body fluids in a truncated form as sCD26/DPPIV, and our data also indicated that DPPIV enzyme activity decreased with increasing doses of YS110 (Figure 2B). Although DPPIV inhibitors are clinically used as oral hypoglycaemia agents (Barreira da Silva *et al,* 2015), hypoglycaemia was not observed during YS110 administration. Of note is the fact that >80% inhibition of serum DPPIV activity was obtained 24 h after oral administration of clinically available DPPIV inhibitors (drug information published by each pharmaceutical company of sitagliptin, vildagliptin, saxagliptin and etc.), a level of inhibition comparable to that seen in patients treated with YS110. Our current data would therefore indicate that YS110 therapy is tolerable in the clinical setting.

The only treatment with level-one level of evidence for improving clinical outcome is the regimen consisting of a platinum doublet with an antifolate (van Meerbeeck *et al,* 2005). With this combined chemotherapy, patients with good performance status have a median overall survival of ~1 year, and a median PFS of <6 months. There is currently no standard second-line treatment with demonstrated ability to prolong survival. Importantly, patients who failed this first-line therapy have an extremely short survival (3.4 months), and are exposed to potentially life-threatening toxicities unnecessarily (Blayney *et al,* 2012). Due to the lack of efficacy of conventional therapeutic approaches, it is potentially significant that treatment with YS110 results in encouraging disease stabilisation with a median PFS of 32 weeks (26–57 weeks) in seven heavily pretreated CD26-positive patients who previously progressed on conventional therapies (Supplementary Figures S2 and S3).

Recent work has demonstrated the functional role of DPPIV-mediated posttranslational modification of chemokines in regulating tumour immunity through its interaction with its substrate CXCL10 (Ohnuma *et al,* 2015b). Preservation of the full length, bioactive CXCL10 by DPPIV inhibition using the DPPIV inhibitor sitagliptin resulted in increased level of $CXCR3^+$ effector T cells in the tumour microenvironment and subsequent tumour growth reduction (Ohnuma *et al,* 2015b). In view of these recent findings, data from our current trial showing that serum DPPIV activity was decreased following treatment with YS110 in a dose-dependent manner (Figure 2B). It would suggest that anti-tumour activity via DPPIV inhibition may constitute yet another mechanism of action for the anti-tumour activity of YS110, in addition to the mechanisms of action discussed above (Hatano *et al,* 2015).

We recently reported that CD3/CD26 costimulation induced the development of a human type 1 T_{reg} cells from $CD4^+$ T cells with high level of IL-10 production and lymphocyte activation gene 3 (LAG3) expression (Nguyen and Ohashi, 2015). Preclinical models showed that antibody-mediated blocking of LAG3 as potential anti-cancer therapy led to enhanced activation of antigen-specific T cells at the tumour sites and disruption of tumour growth (Nishikawa *et al,* 2015). Moreover, anti-LAG3/anti-PD-1 antibody treatment cured most mice of established tumours that were largely resistant to single antibody treatment (Nishikawa *et al,* 2015). Taken together, it is conceivable that CD26 itself may be a functional inhibitory molecule of an immune checkpoint system in certain disease conditions, similar to LAG3 or PD-1. In this scenario, CD26 blockade by YS110 may potentially function as an immune checkpoint blockade therapy, which can mediate anti-tumour activity in CD26-negative as well as CD26-positive cancers.

Microarray analyses of MPM cell lines treated with YS110 indicated that anti-CD26 mAb therapy resulted in the down-regulation of cytochrome *c* oxidase polypeptide I and II, and metallothione molecules that confer resistance to apoptosis or chemotherapeutic agents (Aoe *et al,* 2012). In addition, suppression of drug-resistant-related transporters, DNA repair enzyme and oncogenic protein expression was observed (Aoe *et al,* 2012). These preclinical results suggest that YS110 can function synergistically with other antineoplastic agents such as selected chemotherapeutic drugs to inhibit tumour growth.

Tumour surface expression of CD26/DPP4 may also have direct biological effects on the malignant behaviour of tumours. In several human malignancies including colorectal CRC, chronic myeloid leukaemia, gastric adenocarcinoma and MPM, CD26/DPP4 expression is reported to be a marker of cancer stem cells (Pang *et al,* 2010; Ghani *et al,* 2011; Yamazaki *et al,* 2012; Hatano *et al,* 2014; Herrmann *et al,* 2014; Davies *et al,* 2015). Given the potential role of CD26 surface expression in cancer biology, YS110 therapy may also influence tumour growth through its potential effect on the cancer stem cells of selected tumours.

In conclusion, our FIH study showed that YS110 therapy is generally well tolerated up to 6 mg kg^{-1} Q1W, which has been

defined as the RP2D and results in encouraging disease stabilisation in a number of patients with advanced/refractory CD26-expressing cancers. Our findings also suggest that further clinical development of YS110 such as its use as part of combination therapies with other antineoplastic agents is warranted.

ACKNOWLEDGEMENTS

This study was supported by Y'AC Co., Ltd, Tokyo, Japan, Kissei Pharmaceutical Co., Ltd, Tokyo, Japan and Japan Agency for Medical Research and Development (AMED).

CONFLICT OF INTEREST

Yutaro Kaneko is an employer of Y's AC Co., Ltd, Japan, Thomas Podoll is an employer of Y's Therapeutics Inc., USA, and Yu Kuramochi and Itaru Miyashita are the employees of Kissei Pharmaceutical Co., Ltd, Tokyo, Japan. Chikao Morimoto, Kei Ohnuma and Nam H Dang are stock holders of Y's AC Co., Ltd. The remaining authors declare no conflict of interest.

REFERENCES

Amatya VJ, Takeshima Y, Kushitani K, Yamada T, Morimoto C, Inai K (2011) Overexpression of CD26/DPPIV in mesothelioma tissue and mesothelioma cell lines. *Oncol Rep* **26**: 1369–1375.

Aoe K, Amatya VJ, Fujimoto N, Ohnuma K, Hosono O, Hiraki A, Fujii M, Yamada T, Dang NH, Takeshima Y, Inai K, Kishimoto T, Morimoto C (2012) CD26 overexpression is associated with prolonged survival and enhanced chemosensitivity in malignant pleural mesothelioma. *Clin Cancer Res* **18**: 1447–1456.

Barreira da Silva R, Laird ME, Yatim N, Fiette L, Ingersoll MA, Albert ML (2015) Dipeptidylpeptidase 4 inhibition enhances lymphocyte trafficking, improving both naturally occurring tumor immunity and immunotherapy. *Nat Immunol* **16**: 850–858.

Blayney JK, Ceresoli GL, Castagneto B, O'Brien ME, Hasan B, Sylvester R, Rudd R, Steele J, Busacca S, Porta C, Mutti L, O'Byrne KJ, Scullin P, Gaafar R, Baas P, Van Meerbeeck J, Fennell DA (2012) Response to chemotherapy is predictive in relation to longer overall survival in an individual patient combined-analysis with pleural mesothelioma. *Eur J Cancer* **48**: 2983–29892.

Dang NH, Torimoto Y, Deusch K, Schlossman SF, Morimoto C (1990a) Comitogenic effect of solid-phase immobilized anti-1F7 on human CD4 T cell activation via CD3 and CD2 pathways. *J Immunol* **144**: 4092–4100.

Dang NH, Torimoto Y, Sugita K, Daley JF, Schow P, Prado C, Schlossman SF, Morimoto C (1990b) Cell surface modulation of CD26 by anti-1F7 monoclonal antibody. Analysis of surface expression and human T cell activation. *J Immunol* **145**: 3963–3971.

Davies S, Beckenkamp A, Buffon A (2015) CD26 a cancer stem cell marker and therapeutic target. *Biomed Pharmacother* **71**: 135–138.

Dong RP, Tachibana K, Hegen M, Scharpe S, Cho D, Schlossman SF, Morimoto C (1998) Correlation of the epitopes defined by anti-CD26 mAbs and CD26 function. *Mol Immunol* **35**: 13–21.

Ghani FI, Yamazaki H, Iwata S, Okamoto T, Aoe K, Okabe K, Mimura Y, Fujimoto N, Kishimoto T, Yamada T, Xu CW, Morimoto C (2011) Identification of cancer stem cell markers in human malignant mesothelioma cells. *Biochem Biophys Res Commun* **404**: 735–742.

Hatano R, Yamada T, Matsuoka S, Iwata S, Yamazaki H, Komiya E, Okamoto T, Dang NH, Ohnuma K, Morimoto C (2014) Establishment of monoclonal anti-human CD26 antibodies suitable for immunostaining of formalin-fixed tissue. *Diagn Pathol* **9**: 30.

Hatano R, Ohnuma K, Otsuka H, Komiya E, Taki I, Iwata S, Dang NH, Okumura K, Morimoto C (2015) CD26-mediated induction of EGR2 and IL-10 as potential regulatory mechanism for CD26 costimulatory pathway. *J Immunol* **194**: 960–972.

Havre PA, Abe M, Urasaki Y, Ohnuma K, Morimoto C, Dang NH (2008) The role of CD26/dipeptidyl peptidase IV in cancer. *Front Biosci* **13**: 1634–1645.

Hegen M, Kameoka J, Dong RP, Schlossman SF, Morimoto C (1997) Cross-linking of CD26 by antibody induces tyrosine phosphorylation and activation of mitogen-activated protein kinase. *Immunology* **90**: 257–264.

Herrmann H, Sadovnik I, Cerny-Reiterer S, Rulicke T, Stefanzl G, Willmann M, Hoermann G, Bilban M, Blatt K, Herndlhofer S, Mayerhofer M, Streubel B, Sperr WR, Holyoake TL, Mannhalter C, Valent P (2014) Dipeptidylpeptidase IV (CD26) defines leukemic stem cells (LSC) in chronic myeloid leukemia. *Blood* **123**: 3951–3962.

Ho L, Aytac U, Stephens LC, Ohnuma K, Mills GB, McKee KS, Neumann C, LaPushin R, Cabanillas F, Abbruzzese JL, Morimoto C, Dang NH (2001) *In vitro* and *in vivo* antitumor effect of the anti-CD26 monoclonal antibody 1F7 on human CD30+ anaplastic large cell T-cell lymphoma Karpas 299. *Clin Cancer Res* **7**: 2031–2040.

Inamoto T, Yamochi T, Ohnuma K, Iwata S, Kina S, Inamoto S, Tachibana M, Katsuoka Y, Dang NH, Morimoto C (2006) Anti-CD26 monoclonal antibody-mediated G1-S arrest of human renal clear cell carcinoma Caki-2 is associated with retinoblastoma substrate dephosphorylation, cyclin-dependent kinase 2 reduction, p27kip1 enhancement, and disruption of binding to the extracellular matrix. *Clin Cancer Res* **12**: 3470–3477.

Inamoto T, Yamada T, Ohnuma K, Kina S, Takahashi N, Yamochi T, Inamoto S, Katsuoka Y, Hosono O, Tanaka H, Dang NH, Morimoto C (2007) Humanized anti-CD26 monoclonal antibody as a treatment for malignant mesothelioma tumors. *Clin Cancer Res* **13**: 4191–4200.

Morimoto C, Torimoto Y, Levinson G, Rudd CE, Schrieber M, Dang NH, Letvin NL, Schlossman SF (1989) 1F7, a novel cell surface molecule, involved in helper function of CD4 cells. *J Immunol* **143**: 3430–3439.

Morimoto C, Schlossman SF (1998) The structure and function of CD26 in the T-cell immune response. *Immunol Rev* **161**: 55–70.

Nguyen LT, Ohashi PS (2015) Clinical blockade of PD1 and LAG3–potential mechanisms of action. *Nat Rev Immunol* **15**: 45–56.

Nishikawa S, Konno M, Hamabe A, Hasegawa S, Kano Y, Fukusumi T, Satoh T, Takiguchi S, Mori M, Doki Y, Ishii H (2015) Surgically resected human tumors reveal the biological significance of the gastric cancer stem cell markers CD44 and CD26. *Oncol Lett* **9**: 2361–2367.

Ohnuma K, Dang NH, Morimoto C (2008) Revisiting an old acquaintance: CD26 and its molecular mechanisms in T cell function. *Trends Immunol* **29**: 295–301.

Ohnuma K, Hosono O, Dang NH, Morimoto C (2011) Dipeptidyl peptidase in autoimmune pathophysiology. *Adv Clin Chem* **53**: 51–84.

Ohnuma K, Saito T, Hatano R, Hosono O, Iwata S, Dang NH, Ninomiya H, Morimoto C (2015a) Comparison of two commercial ELISAs against an in-house ELISA for measuring soluble CD26 in human serum. *J Clin Lab Anal* **29**: 106–111.

Ohnuma K, Hatano R, Morimoto C (2015b) DPP4 in anti-tumor immunity: going beyond the enzyme. *Nat Immunol* **16**: 791–792.

Okamoto T, Iwata S, Yamazaki H, Hatano R, Komiya E, Dang NH, Ohnuma K, Morimoto C (2014) CD9 Negatively regulates CD26 expression and inhibits CD26-mediated enhancement of invasive potential of malignant mesothelioma cells. *PLoS ONE* **9**: e86671.

Pang R, Law WL, Chu AC, Poon JT, Lam CS, Chow AK, Ng L, Cheung LW, Lan XR, Lan HY, Tan VP, Yau TC, Poon RT, Wong BC (2010) A subpopulation of CD26+ cancer stem cells with metastatic capacity in human colorectal cancer. *Cell Stem Cell* **6**: 603–615.

Scott AM, Wolchok JD, Old LJ (2012) Antibody therapy of cancer. *Nat Rev Cancer* **12**: 278–287.

Tanaka T, Kameoka J, Yaron A, Schlossman SF, Morimoto C (1993) The costimulatory activity of the CD26 antigen requires dipeptidyl peptidase IV enzymatic activity. *Proc Natl Acad Sci USA* **90**: 4586–4590.

Torimoto Y, Dang NH, Tanaka T, Prado C, Schlossman SF, Morimoto C (1992) Biochemical characterization of CD26 (dipeptidyl peptidase IV): functional comparison of distinct epitopes recognized by various anti-CD26 monoclonal antibodies. *Mol Immunol* **29**: 183–192.

van Meerbeeck JP, Gaafar R, Manegold C, van Klaveren RJ, van Marck EA, Vincent M, Legrand C, Bottomley A, Debruyne C, Giaccone G (2005) Randomized phase III study of cisplatin with or without raltitrexed in patients with malignant pleural mesothelioma: an intergroup study of the European Organisation for Research and Treatment of Cancer Lung Cancer Group and the National Cancer Institute of Canada. *J Clin Oncol* **23**: 6881–6889.

Yamada K, Hayashi M, Madokoro H, Nishida H, Du W, Ohnuma K, Sakamoto M, Morimoto C, Yamada T (2013) Nuclear localization of CD26 induced by a humanized monoclonal antibody inhibits tumor cell growth by modulating of POLR2A transcription. *PLoS One* **8**: e62304.

Yamamoto J, Ohnuma K, Hatano R, Okamoto T, Komiya E, Yamazaki H, Iwata S, Dang NH, Aoe K, Kishimoto T, Yamada T, Morimoto C (2014) Regulation of somatostatin receptor 4-mediated cytostatic effects by CD26 in malignant pleural mesothelioma. *Br J Cancer* **110**: 2232–2245.

Yamazaki H, Naito M, Ghani FI, Dang NH, Iwata S, Morimoto C (2012) Characterization of cancer stem cell properties of CD24 and CD26-positive human malignant mesothelioma cells. *Biochem Biophys Res Commun* **419**: 529–536.

Supplementary Information accompanies this paper on British Journal of Cancer website (http://www.nature.com/bjc)

Journal of Dermatological Science 86 (2017) 212–221

Contents lists available at ScienceDirect

Journal of Dermatological Science

journal homepage: www.jdsjournal.com

A possible role for CD26/DPPIV enzyme activity in the regulation of psoriatic pruritus

Eriko Komiya[a,b], Ryo Hatano[a], Haruna Otsuka[a], Takumi Itoh[a,c], Hiroto Yamazaki[a], Taketo Yamada[d,e], Nam H. Dang[f], Mitsutoshi Tominaga[b], Yasushi Suga[g], Utako Kimura[g], Kenji Takamori[b,g], Chikao Morimoto[a], Kei Ohnuma[a,*]

[a] Department of Therapy Development and Innovation for Immune Disorders and Cancers, Graduate School of Medicine, Juntendo University, 2-1-1 Hongo, Bunkyo-ku, Tokyo 113-8421, Japan
[b] Institute for Environmental and Gender Specific Medicine, Juntendo University Graduate School of Medicine, 2-1-1 Tomioka, Urayasu, Chiba 279-0021, Japan
[c] Graduate School of Health and Sports Science, Juntendo University, 1-1 Hiragagakuendai, Inzai, Chiba 270-1695, Japan
[d] Department of Pathology, Keio University School of Medicine, 35 Shinanomachi, Shinjuku-ku, Tokyo 160-8582, Japan
[e] Department of Pathology Saitama Medical University, 38 Morohongo, Moroyama-cho, Iruma-gun, Saitama 350-0459, Japan
[f] Division of Hematology/Oncology, University of Florida, 1600 SW Archer Road- Box 100278, Room MSB M410A, Gainesville, FL 32610, USA
[g] Department of Dermatology, Juntendo University Urayasu Hospital, 2-1-1 Tomioka, Urayasu, Chiba 279-0021, Japan

ARTICLE INFO

Article history:
Received 6 October 2016
Received in revised form 22 February 2017
Accepted 8 March 2017

Keywords:
CD26/DPPIV
Substance P
Pruritus
Psoriasis

ABSTRACT

Background: Psoriasis (PSO) is one of the most common chronic inflammatory skin diseases, and pruritus affects approximately 60–90% of patients with PSO. However, the pathogenesis of pruritus in PSO remains unclear. Dipeptidyl peptidase IV (DPPIV) enzyme activity is involved in the regulation of peptide hormones, chemokines and neurotransmitters.
Objectives: Our aim is to evaluate for a potential association between DPPIV and an increased risk of pruritus, and to identify possible underlying treatment targets in affected patients.
Methods: Utilizing clinical serum samples of PSO patients and *in vivo* experimental pruritus models, we evaluated for a potential association between DPPIV and an increased risk for pruritus, and attempted to identify possible underlying treatment targets in pruritus of PSO.
Results: We first showed that levels of DPPIV enzyme activity in sera of patients with PSO were significantly increased compared to those of healthy controls. We next evaluated levels of substance-P (SP), which is a neurotransmitter for pruritus and a substrate for DPPIV enzyme. Truncated form SP cleaved by DPPIV was significantly increased in sera of PSO. In an *in vivo* pruritus model induced by SP, scratching was decreased by treatment with a DPPIV inhibitor. Moreover, DPPIV-knockout mice showed attenuation of scratching induced by SP. Finally, scratching was decreased following the administration of a DPPIV inhibitor in an imiquimod-induced PSO model. On the other hand, scratching induced by imiquimod was increased in DPPIV overexpressing-mice.
Conclusions: These results suggest that inhibition of DPPIV enzyme activity regulates pruritus in PSO.

1. Introduction

Psoriasis (PSO) is one of the most common inflammatory skin diseases, and is found in approximately 1–3% of the world general population [1]. For a long time, PSO had been considered as a non-pruritic dermatitis. However, more recently, a number of studies have demonstrated that approximately 60–90% of patients with PSO suffer from pruritus [1–6]. Although psoriatic patients consider pruritus as the most bothersome subjective sensation [5,7], effective therapy for pruritus in PSO has not been established.

Abbreviations: CD26KO, CD26/DPPIV knockout; DPPIV, dipeptidyl peptidase IV; DPPIV-Tg, CD26/DPPIV transgenic; i.d., intradermal; IMQ, imiquimod; i.p., intraperitoneal; NK-1R, nuerokinin-1 receptor; PSO, psoriasis; rsCD26(DPPIV+), recombinant soluble CD26 protein containing DPPIV enzyme activity; rsCD26 (DPPIV-), recombinant soluble CD26 with deficient DPPIV enzyme activity; sCD26, soluble CD26; sDPPIV, soluble DPPIV enzyme activity; SP, substance P.

* Corresponding author.
E-mail address: kohnuma@juntendo.ac.jp (K. Ohnuma).

http://dx.doi.org/10.1016/j.jdermsci.2017.03.005
0923-1811/

CD26 is a 110 kDa surface glycoprotein with dipeptidyl peptidase IV (DPPIV, EC 3.4.14.5) activity as a serine protease that cleaves dipeptides from the N-terminus of peptides at the penultimate position [8–10]. CD26 is also associated with T cell signal transduction processes as a costimulatory molecule, as well as being a marker of T cell activation [11,12]. We have previously reported that CD26-mediated costimulatory activity is exerted via its DPPIV enzyme activity [13]. More recently, we have shown that serum soluble CD26 (sCD26) and DPPIV enzyme activity (sDPPIV) are inversely correlated with disease activity in patients with systemic lupus erythematosus [14]. In addition, sCD26 and sDPPIV are involved in the pathogenesis of various cancers including colorectal cancer, hepatocellular carcinoma, prostate cancer and malignant mesothelioma [15–19]. Other investigators have reported that CD26/DPPIV was upregulated in psoriatic skin and that DPPIV inhibitor ameliorated psoriasis [20–23], although the biological role of CD26/DPPIV in PSO has not yet been elucidated. Meanwhile, DPPIV enzyme activity has been widely studied in metabolic and endocrine disorders, and DPPIV inhibitors have been developed as a new class of anti-diabetic drugs which act by inhibiting DPPIV, the enzyme that inactivates incretin hormone [24–26]. The potentially important role played by CD26/DPPIV in the clinical setting has led to rising interest in serum sCD26 level and sDPPIV enzyme activity in various human conditions over the past decade.

Substance P (SP) is a neuropeptide involved in afferent neuronal signal transduction [27,28]. Activation of sensory neurons in the skin causes the release of SP [29,30]. Once released, SP binds to neurokinin receptors including neurokinin-1 receptor (NK-1R) found on keratinocytes and cutaneous nerve endings, resulting in the release of additional itch mediators [29,31]. Substance P therefore appears to act to induce itch. It has been reported that the number of SP-containing nerves in the perivascular areas of pruritic psoriatic skin was increased and that expression of SP receptor in epidermis from pruritic psoriatic subjects was upregulated [3,32]. On the other hand, SP consists of 11 amino acids residues and contains the DPPIV-target sequence at its N-terminal position [33]. Previous report utilizing DPPIV deficient rat showed that circulating SP was metabolized by DPPIV enzyme [34]. However, it is not clear whether degradation of SP by DPPIV enzyme affects pruritus in patients with PSO.

In the present study, utilizing clinical serum samples of PSO patients and *in vivo* experimental pruritus models, we evaluated for a potential association between DPPIV and an increased risk for SP-induced pruritus, and attempted to identify possible underlying treatment targets in pruritus of PSO. We showed that levels of DPPIV enzyme activity in sera of patients with PSO were significantly increased compared to those of healthy controls. Moreover, truncated form SP cleaved by DPPIV was significantly increased in sera of PSO. In an *in vivo* pruritus model induced by full-length SP, scratching was decreased by treatment with a DPPIV inhibitor. Moreover, scratching was increased following injection of truncated form SP. Furthermore, DPPIV-knockout (CD26KO) mice showed attenuation of scratching induced by SP. Finally, scratching was decreased following the administration of a DPPIV inhibitor in an imiquimod (IMQ)-induced PSO model. On the other hand, scratching induced by IMQ was increased in DPPIV over-expressing transgenic (DPPIV-Tg) mice. These results suggest that inhibition of DPPIV enzyme activity regulates pruritus in PSO.

2. Materials and methods

2.1. Patients and serum collections and storage

The base cohort consisted of all PSO patients regularly seen and treated at the Juntendo Urayasu Hospital between May 2013 and October 2014. Peripheral blood samples were collected from 48 PSO patients and 18 healthy adult volunteers, using BD Vacutainer blood collection tube SSTII (BD, Franklin Lakes, NJ). Serum was obtained from 5 mL whole blood by centrifugation at $1500 \times g$ at 4 °C for 10 min, and stored at −80 °C in 500 μL aliquots. Human study protocols were approved by the Ethics Committees at the Juntendo Urayasu Hospital (Authorization Number 2013074). Informed consent was obtained from all patients. All studies on human subjects were conducted according to the principles set out in the Declaration of Helsinki.

2.2. Reagents and recombinant proteins

Recombinant full-length SP(1–11) and the DPPIV inhibitor sitagliptin were purchased from Peptide Institute (Osaka, Japan) and Sigma-Aldrich (St Louis, MO), respectively. Truncated SP(5–11) pyroglutamyl peptide was purchased from Eurofins Genomics (Ebersberg, Germany). IMQ (5% Beselna Cream) and control Absorptive cream were purchased from Mochida Pharmaceutical (Tokyo, Japan) and Nikko (Gifu, Japan), respectively. Recombinant sCD26 protein containing DPPIV enzyme activity (rsCD26(DPPIV+)) and mutant rsCD26 with deficient DPPIV enzyme activity (rsCD26(DPPIV-)) were produced according to the method described previously [13].

2.3. Animals

C57BL/6 mice were purchased from CLEA Japan (Tokyo, Japan). CD26KO ($CD26^{-/-}$) mice developed from C57BL/6 mice were kindly gifted from the laboratory of Dr. Takeshi Watanabe at Kyusyu University (Fukuoka, Japan) [35]. DPPIV-Tg mice developed from C57BL/6 mice were kindly provided from the laboratory of Dr. Chien-Te K. Tseng at University of Texas Medical Branch (Texas) [36]. These mice were bred in-house and used at 8–11 weeks of age. They were kept under controlled temperature (23–25 °C) and light (on time 8:00 A.M.–8:00 P.M.) conditions. Food and water were freely available. All experiments on animals were approved by animal ethics committee in Juntendo University (Authorization Numbers 270242 and 280038).

2.4. sCD26 concentration and DPPIV enzyme activity assay procedure

For measurement of sCD26 concentration and DPPIV enzyme activity in human samples, serum samples were removed from the −80 °C freezer and quickly thawed in a water bath at 37 °C. All samples were centrifuged $3000 \times g$ for 5 min to discard debris, and were then assayed in duplicate. An in-house sandwich ELISA for sCD26 and sDPPIV enzyme was established in our laboratory [14,37]. For evaluation of SP concentrations in human samples, the serum levels of SP and its fragments were evaluated utilizing two distinct ELISA kits, one detects SP(1–11), (2–11) and (3–11) (Substance P ELISA kit, Abcam, Cambridge, MA), and the other, SP(4–11) and (5–11) as well as SP(1–11), (2–11) and (3–11) (Substance P (Human, Rat, Mouse)-EIA kit, Phoenix Pharmaceuticals, Burlingame, CA). For measurement of DPPIV enzyme activity in murine samples, peripheral blood was harvested from tail vein at the indicated periods. After the blood samples were centrifuged to isolate sera, levels of DPPIV activity were measured utilizing DPPIV-Glo Protease Assay (Promega, Fitchburg, WI). For blood glucose analysis in murine sera, mice were put into an acrylic cage for 1 hr for acclimation and for food deprivation, followed by i.p. injection of 30 mM of sitagliptin or saline. Peripheral blood samples were harvested from tail vein, and the blood glucose concentrations were measured utilizing animal glucometer LAB Gluco (ForaCare Inc. CA) at the indicated periods.

Table 1
Demographic characteristics of cohorts.

Variable	Patients with PSO (n = 48)	Healthy Control (n = 18)
Age, years, mean ± SD (range)	49.9 ± 14.9 (19–88)	45.1 ± 10.3 (25–65)
Male/Female, n (ratio)	41/7 (5.9)	15/3 (5.0)
BMI, kg/m^2, mean ± SD (range)	26.9 ± 2.0 (19.3–42.3)	24.6 ± 1.5 (18.4–32.0)
PASI score, points, mean ± SD (range)	12.2 ± 12.0 (0.0–60.0)	N/A
Itch VAS, mm, mean ± SD (range)	29.4 ± 31.0 (0–100)	N/A
Use of Biologics[a], n (%)	13 (27.1%)	N/A
Use of Immunosuppressant[b], n (%)	2 (4.0%)	N/A

BMI, body mass index; n, number; N/A, not applicable; SD, standard deviation; PASI, psoriasis area and severity index at blood collection; PSO psoriasis; VAS, visual analogue scale at blood collection.
[a] Biologics includes anti-TNFα, anti-IL-12/23p40 and anti-IL-17A monoclonal antibody therapy.
[b] Immunosuppressant includes oral prednisolone and methotrexate.

2.5. In vitro *digestion assay for SP and amino acid sequence analysis*

Recombinant full-length SP(1–11) was incubated with rsCD26 (DPPIV+) or rsCD26(DPPIV-) at a molecular ratio of 100:1. For DPPIV inhibition experiments, 5 nmol of sitagliptin was added to the recombinant full-length SP(1–11) and rsCD26(DPPIV+) at a molecular ratio of 100:1. After incubation at 37 °C for 4 h, aliquots were transferred to PVDF membrane and subjected to N-terminal amino acid sequencing as determined by the Edman method (Toray Research Center Inc., Tokyo, Japan).

2.6. Itch murine models

For SP-induced itch murine model, mice hairs were clipped over the rostral part of the back one day before experiment. Under isoflurane anesthesia, mice received i.d. injection of full-length SP (1–11), truncated SP(5–11) or control solvent at the indicated doses, and then subjected to scratching behavior evaluation. For IMQ-induced psoriatic itch murine model, mice received a daily dose of 30 mg of IMQ or control vehicle cream on the shaved back for 5 days. On the 6th day, mice were subjected to scratching behavior evaluation as described below. On the 7th day, after macrophotographs of mice were taken, mice were sacrificed, and the skin specimens were harvested for histopathology examination.

2.7. Measurement of scratching behavior and locomotor activity

Before behavioral recording, mice (4 animals per observation) were put into an acrylic cage (19.5 × 24 × 35 cm) for at least one hour for acclimation. Subsequently, the frequency of scratch behavior of the rostral back was analyzed by the SCLABA®-Real system (NOVERTEC, Kobe, Japan) for the indicated time intervals, with observers being kept out of the experimental room. For evaluation of locomotor activities, mice were put into an acryl cage by the same method as in the scratching behavior evaluation, and were evaluated with the use of the SCLABA®-Real tracking software. Locomotor activities were measured and expressed as the total horizontal moving distance of mice during itch behavioral experiments.

2.8. Tissue histopathology

Skins from the upper back of treated mice were fixed in 10% formalin, embedded in paraffin, sectioned, mounted on slides, and stained with hematoxylin and eosin (H&E) to determine pathology. Images were captured with an Olympus digital camera DP21 attached to an Olympus BX43 microscope using CellSens software (OLYMPUS, Tokyo, Japan). Slides were evaluated by a pathologist blinded to experimental groups.

2.9. Statistics

All experiments were performed in triplicates and repeated at least 3 times. Data were expressed as mean values ± SEM (standard error of the mean), and were analyzed by two-tailed Student's *t*-test for two group comparison or by ANOVA test for multiple comparison testing followed by the Tukey-Kramer *post-hoc* test. *P* values <0.05 were considered statistically significant. Calculations were performed and graphed using GraphPad Prism 6 (GraphPad Software Inc., La Jolla, CA).

3. Results

3.1. Serum levels of sCD26 and sDPPIV enzyme are increased in patients with PSO

To determine whether sCD26 and sDPPIV enzyme play a role in PSO, we first evaluated levels of sCD26 and sDPPIV enzyme activity in sera of patients with PSO. For this purpose, peripheral blood samples were collected from healthy adult volunteers and PSO patients (regularly seen and treated at the Juntendo Urayasu Hospital). Of the 48 patients, mean (years ± S.D.) age was 49.9 (±16.9), male/female was 41/7. No patients with diabetes mellitus,

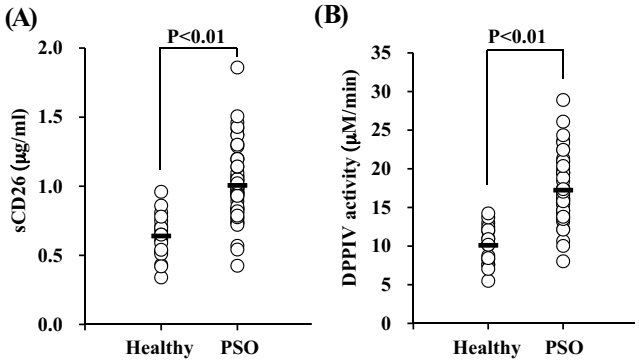

Fig. 1. Serum levels of sCD26 and DPPIV enzyme activity in patients with PSO. **(A)** Levels of sCD26 were measured in sera of PSO patients (n = 48) or healthy adult volunteers (n = 18). Levels of sCD26 in PSO patients were significantly increased as compared with healthy controls (1.02 ± 0.28 *v.s.* 0.64 ± 0.16 μg/ml; $P < 0.01$ by two-tailed Student's *t*-test). Each dot indicates individual value. The horizontal lines in the middle of scattergrams indicate each mean value. sCD26 concentration was measured using our in-house capture method as described in Materials and Methods. **(B)** Levels of sDPPIV enzyme activity were measured in sera of PSO patients (n = 48) or healthy adult volunteers (n = 18). Levels of sDPPIV enzyme activity in PSO patients were significantly increased as compared to healthy controls (17.38 ± 4.18 *v.s.* 10.17 ± 2.47 μM/min; $P < 0.01$ by two-tailed Student's *t*-test). Each dot indicates individual value. The horizontal lines in the middle of scattergrams indicate each mean value. DPPIV enzyme activity was measured using our in-house capture method as described in Materials and Methods.

hepatic or renal dysfunction were included in PSO cohort to exclude the possible influence of these conditions on serum levels of DPPIV enzyme activity [12,24]. Of the 18 healthy adult volunteers, mean (years ± S.D.) age was 45.1 (±10.3), male/female was 15/3. All healthy adult volunteers had no history of cancers and chronic diseases including diabetes mellitus, hepatic diseases, allergic diseases, HIV infection, PSO and atopic dermatitis. There was no significant difference in body mass index between PSO and control cohorts ($26.9 \pm 2.0\ kg/m^2$ *v.s.* $24.6 \pm 1.5\ kg/m^2$, $p = 0.287$ by two-tailed Student's *t*-test). Other demographic characteristics of the patients are summarized in Table 1.

As shown in Fig. 1A, serum sCD26 concentration of PSO patients was significantly higher than that of healthy adults ($1.02 \pm 0.28\ \mu g/ml$ v.s. $0.64 \pm 0.16\ \mu g/ml$). Moreover, it has been reported that DPPIV enzymatic activity was correlated with the concentration of sCD26 in normal human sera [37,38]. We therefore evaluated for potential correlation between DPPIV enzymatic activity and sCD26 level in the serum samples described above. For this purpose, we performed our in-house capture assay method using anti-human CD26 mAb as a capture antibody for detecting DPPIV enzyme activity specific to sCD26 [37]. Since commercially available DPPIV enzyme assay kits measure DPPIV activity in whole serum, but not in captured sCD26 molecules from the samples, it is possible that DPPIV-like peptidase activity other than that possessed by the captured sCD26 molecules was measured, leading to an overestimate of the DPPIV activity in the samples [39]. As shown in Fig. 1B, serum levels of sDPPIV enzyme activity were also significantly higher in patients with PSO compared with healthy adult controls ($17.38 \pm 4.18\ \mu M/min$ *v.s.* $10.17 \pm 2.47\ \mu M/min$). These data suggest that DPPIV enzyme activity is increased in sera of patients with PSO, which is linked to a concomitant increase in sCD26 in the same patient population. These observations also suggest that DPPIV enzyme plays a role in the pathogenesis of PSO.

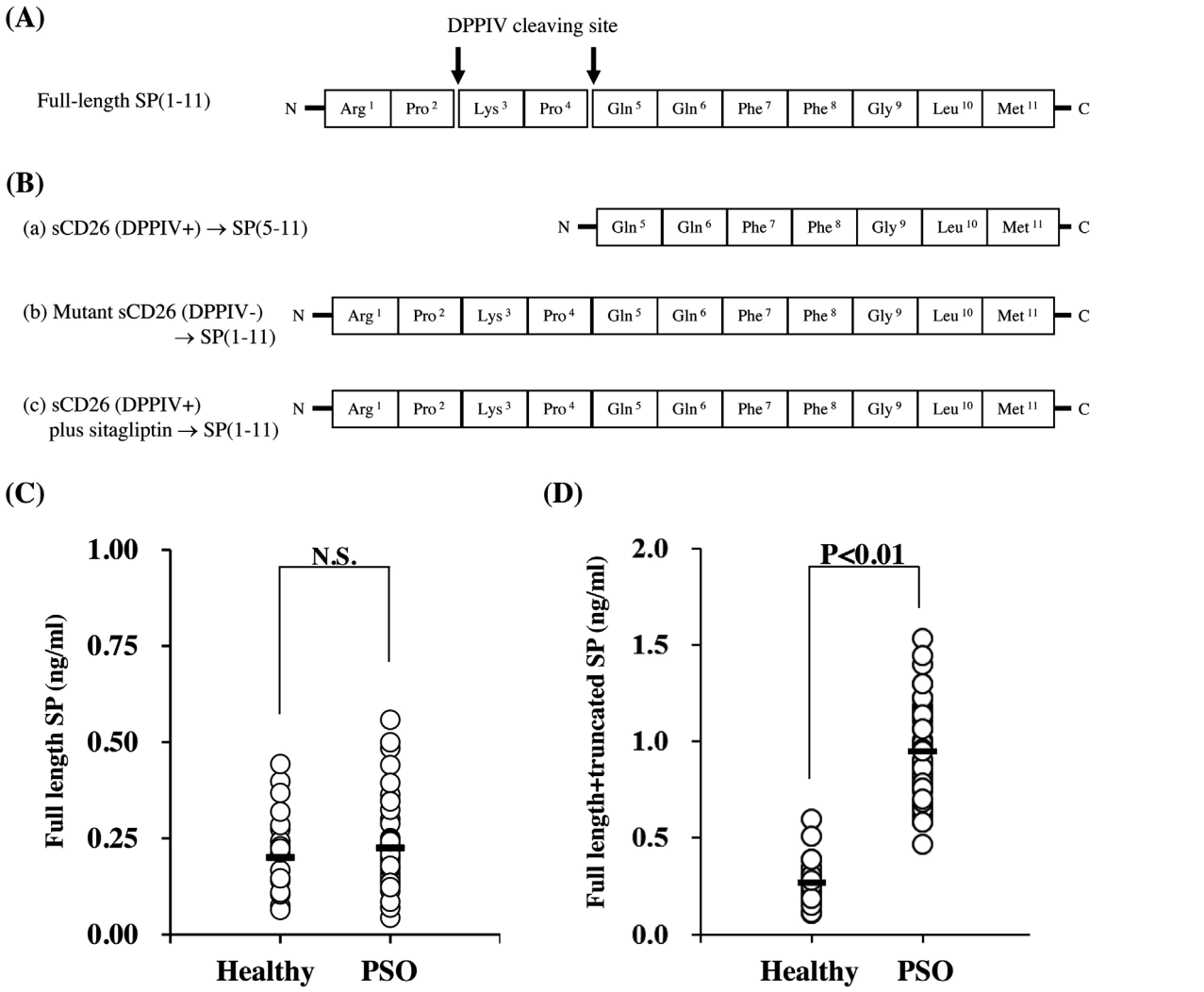

Fig. 2. *In vitro* digestion assay of substance P (SP) and serum levels of full length and truncated SP in patients with PSO. **(A)** Schematic diagram of amino acid sequence of full-length SP(1–11). Arrows indicate two DPPIV cleavage sites. **(B)** The recombinant full-length SP(1–11) was incubated with rsCD26(DPPIV +) (*panel a*) or rsCD26(DPPIV-) (*panel b*). For DPPIV inhibition experiment, sitagliptin was added to recombinant full-length SP(1–11) and rsCD26(DPPIV +) (*panel c*). After incubation at 37 °C for 4 h, aliquots were transferred to PVDF membrane and subjected to N-terminal amino acid sequencing as determined by the Edman method. The results of amino acid sequencing were shown in each right panel. **(C)** The levels of SP(1–11), (2–11), and (3–11) were measured in sera of PSO patients (n = 48) or healthy adult volunteers (n = 18). There was no significant difference in the serum levels of SP(1–11), (2–11), and (3–11) between PSO patients and healthy controls (0.23 ± 0.11 *v.s.* 0.22 ± 0.11 ng/ml; $p = 0.95$ by two-tailed Student's *t*-test). Each dot indicates individual value. The horizontal lines in the middle of scattergrams indicate each mean value. **(D)** The levels of SP(4–11) and (5–11), including SP(1–11), (2–11) and (3–11) concentrations, were measured in sera of PSO patients (n = 48) or healthy adult volunteers (n = 18). The serum levels of SP(4–11) and (5–11) including SP (1–11), (2–11) and (3–11) in PSO were significantly increased as compared to healthy controls (0.95 ± 0.25 v.s. 0.28 ± 0.13 ng/ml; $P < 0.01$ by two-tailed Student's *t*-test). Each dot indicates individual value. The horizontal lines in the middle of scattergrams indicate each mean value.

3.2. Truncated form of SP cleaved by DPPIV enzyme is increased in sera of PSO patients

It is well-known that many patients with PSO have pruritus that is generally refractory to therapy. Among various mediators of pruritus investigated in inflammatory skin diseases, SP is one of key molecules in an itch sensory nerve. While SP consists of 11 amino acids residues with dual DPPIV cleavage sites at its N-terminal position (Fig. 2A), it is unclear whether truncation of SP by DPPIV enzyme plays a role in pruritus in inflammatory skin lesions. To determine whether DPPIV enzyme cleaves full-length SP(1–11), we performed *in vitro* digestion experiments utilizing rsCD26 protein. For this purpose, recombinant full-length SP(1–11) was incubated with rsCD26 protein containing DPPIV enzyme activity (rsCD26(DPPIV+)), and an amino acid sequence analysis was performed to determine the amino acid sequence of incubated SP. Our findings indicated that rsCD26(DPPIV+) digested recombinant full-length SP(1–11), resulting in a truncated form of SP(5–11) (Fig. 2B-(a)), while rsCD26(DPPIV-) exhibited no digestive activity on SP(1–11) (Fig. 2B-(b)). On the other hand, digestion of recombinant full-length SP(1–11) by rsCD26(DPPIV +) was inhibited by the presence of the DPPIV enzyme inhibitor sitagliptin (Fig. 2B-(c)). These data indicate that native sCD26 containing DPPIV enzyme activity in sera degrades full-length SP(1–11), leading to the formation of SP(5–11).

To expand on these *in vitro* findings, we next analyzed the serum concentrations of full-length and truncated SP in patients with PSO. For this purpose, we utilized two different ELISA kits, one detects SP(1–11), (2–11) and (3–11), and the other, SP(4–11) and (5–11) as well as SP(1–11), (2–11) and (3–11). As shown in Fig. 2C, levels of SP(1–11), (2–11) and (3–11) in sera of PSO were similar to those in healthy controls (0.23 ± 0.11 ng/ml *v.s.* 0.22 ± 0.11 μg/ml). On the other hand, serum levels of SP (4–11) and (5–11) were significantly increased in patients with PSO compared with healthy controls (0.95 ± 0.25 ng/ml *v.s.* 0.28 ± 0.13 μg/ml) (Fig. 2D). Taken together with the above data, our observations suggest that levels of SP degraded by DPPIV were increased in sera of patients with PSO, and that the increase in DPPIV activity appears to play an important role in PSO by truncation of SP.

3.3. DPPIV inhibitor suppresses SP-induced pruritus

We next utilized *in vivo* models to determine whether DPPIV activity regulates pruritus induced by SP. For this purpose, we established an itchy mouse model by intradermal injection (i.d.) of full-length SP(1–11) and quantified scratching behavior in mice to determine an itchy symptom. As shown in Fig. 3A, mice treated with SP i.d. demonstrated increased scratching behavior in a dose-dependent manner of SP. Utilizing this itch model, we evaluated the effect of the DPPIV inhibitor sitagliptin on pruritus. Since we could not formally exclude the possibility that the DPPIV inhibitor induced hypoglycemia and decreased activity in treated mice, resulting in reduced scratching behavior, we measured the blood glucose levels in mice receiving sitagliptin. As shown in Fig. 3B, suppression of DPPIV enzyme activity in mice sera was clearly observed from 5 to 30 min after intraperitoneal injection (i.p.) of sitagliptin at doses of 30 mM. Meanwhile, blood glucose levels in mice treated with 30 mM of sitagliptin were similar to those in mice treated with control saline (Fig. 3C). These data suggest that *in vivo* DPPIV inhibition is observed in mice treated by i.p. sitagliptin, while mice receiving this regimen of sitagliptin did not develop hypoglycemia which might have an effect on locomotor activity. We therefore administered 30 mM of i.p. sitagliptin to SP-induced itchy model mice, and measured the frequency of scratching behavior for 1 h. Under these experimental conditions, scratching behavior in SP(1–11) i.d. mice was significantly decreased in mice treated with sitagliptin (115.9 ± 49.1 *v.s.* 13.6 ± 9.4 times/hr) (Fig. 3D). On the other hand, sitagliptin had no effect on the scratching behavior of mice treated with i.d. of control solvent (3.3 ± 3.5 *v.s.* 9.3 ± 9.5 times/h) (Fig. 3D). Meanwhile, there were no significant differences in movement length among all cohorts, indicating that the decreased scratching behavior did not result from decreased mouse activity (Fig. 3E). To further confirm that suppression of DPPIV enzyme activity decreased SP-induced pruritus, we used CD26KO mice to evaluate scratching behavior induced by SP(1–11). As shown in Fig. 3F, SP-induced scratching behavior was significantly attenuated in CD26KO mice compared with that observed in C57BL/6 wild type mice (36.5 ± 28.3 *v.s.* 97.0 ± 50.9 times/h). Meanwhile, there were no significant differences in movement length between CD26KO and wild type mice, indicating that the decreased scratching behavior did not result from decreased mouse activity (Fig. 3G). To show effects of truncated form of SP(5–11) on pruritus, an itch mouse model experiment was conducted utilizing i.d. injection of recombinant SP(5–11) peptide. As shown in Fig. 3H, mice treated with SP(5–11) i.d. demonstrated significant increase in scratching behavior (158.5 ± 29.3 times/h), compared with mice receiving control solvent (12.7 ± 9.5 times/h) or mice receiving full-length SP (1–11) (104.5 ± 30.7 times/h). Meanwhile, there were no significant differences in movement length among SP(1–11), SP(5–11)-treated and control mice, indicating that the increased scratching behavior did not result from increased mouse activity (Fig. 3I). Taken together, our data suggest that SP-induced itch sensation is attenuated by inhibition of the DPPIV activity.

3.4. DPPIV inhibitor suppresses IMQ-induced psoriatic itch

To further determine that DPPIV inhibition affects pruritus, we evaluated scratching behavior utilizing an IMQ-induced psoriatic itch model [40,41]. For this purpose, mice were treated with IMQ cream or control absorptive cream at a daily dose of 30 mg on the rostral part of the back for 5 consecutive days. As shown in Fig. 4A, mice treated with control absorptive cream showed no sign of psoriatic features (panel a), while IMQ-treated mice exhibited psoriasis-like skin including erythema, scaling and thickness (panel b). Histopathology of skin specimens obtained from IMQ-treated mice showed hyperkeratosis, acanthosis and infiltration of inflammatory cells which were compatible to those found in psoriatic skin (panel e of Fig. 4A). On the other hand, histopathology of skin specimens from control cream-treated mice showed none of these pathologic findings (panel d of Fig. 4A). We next analyzed the serum concentrations of full-length and truncated SP in IMQ-treaed mice. As shown in Fig. 4B, levels of SP(1–11), (2–11) and (3–11) in sera of IMQ-treated mice were similar to those in control cream-treated mice (0.32 ± 0.06 ng/ml *v.s.* 0.39 ± 0.01 μg/ml). On the other hand, serum levels of SP (4–11) and (5–11) were significantly increased in IMQ-treated mice compared with control cream-treated mice (0.63 ± 0.09 ng/ml *v.s.* 0.32 ± 0.08 μg/ml) (Fig. 4C). Moreover, scratching behavior was significantly increased in IMQ-treated mice than control cream-treated mice (118.7 ± 47.2 *v.s.* 26.7 ± 20.9 times/hr) (Fig. 4D). These data indicate that IMQ induces psoriatic itchy skin lesions in mice associated with an increase in the truncation of SP. Utilizing this psoriatic itch model, we analyzed the frequencies of itch scratching behaviors with DPPIV inhibitor administration. As shown in Fig. 4D, IMQ-treated mice receiving sitagliptin showed significant decrease of scratching behavior compared with IMQ-treated mice receiving control solvent (31.0 ± 16.0 *v.s.* 118.7 ± 47.2 times/hr). Meanwhile, there was no change in scratching behavior between control cream-treated mice receiving sitaglitpin or control saline (30.8 ± 17.8 *v.s.* 26.7 ± 20.9 times/hr), with baseline levels of scratching behavior in both cohorts. Moreover, there were no

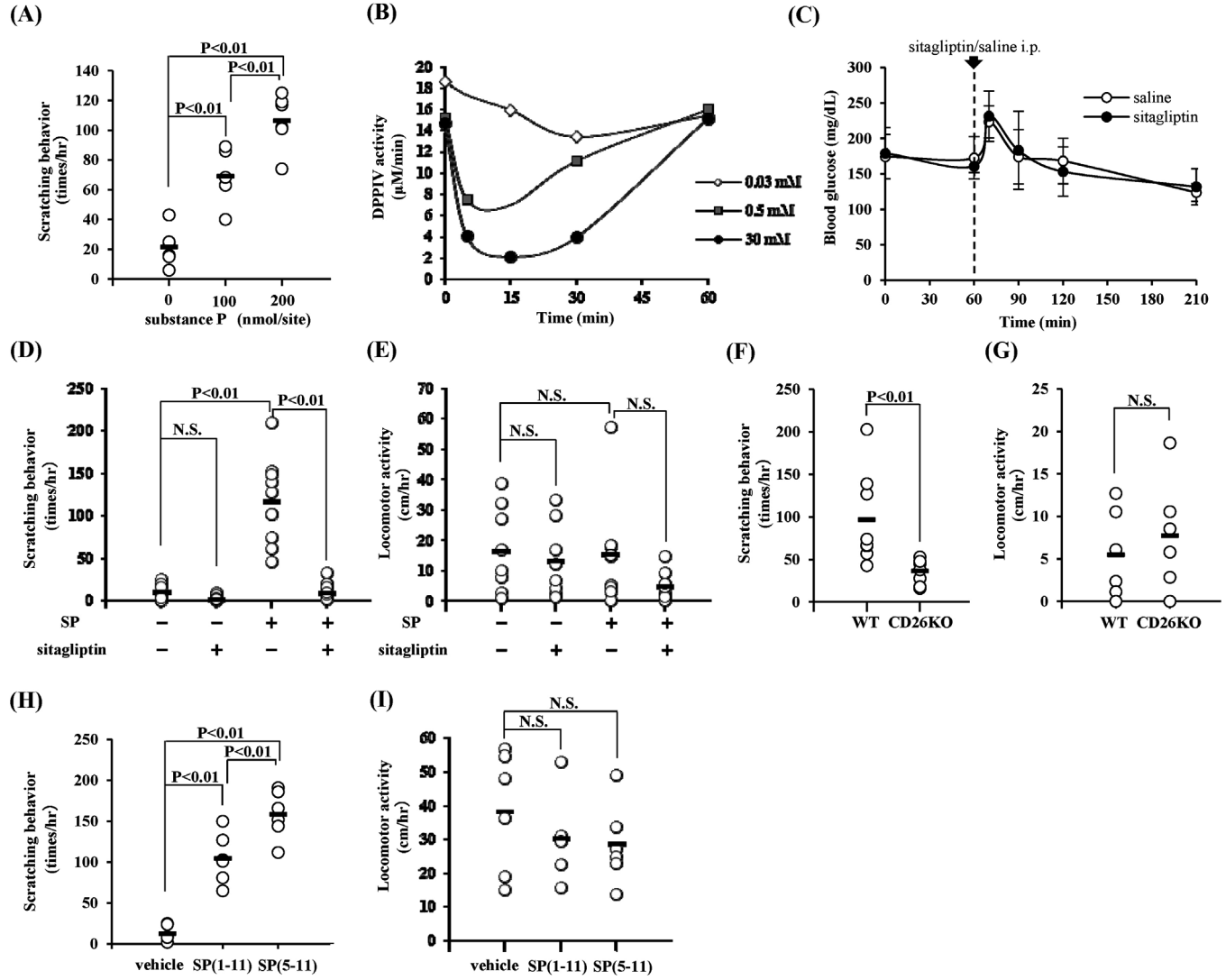

Fig. 3. Treatment with DPPIV inhibitor attenuates SP-induced pruritus. **(A)** Recombinant full-length SP(1–11) was injected at doses of 0 (saline), 100 or 200 nmol per site by i.d. into the rostral back of C57BL/6 mice. The frequency of scratching behavior was counted for 1 hr as described in Materials and Methods. Mice receiving saline exhibited scratching behavior of 21.5 ± 12.3 times/hr (n = 6). On the other hand, mice receiving 100 or 200 nmol of SP exhibited scratching behavior of 68.3 ± 17.9 or 106.3 ± 18.6 times/hr, respectively (each, n = 6), showing significant increase of scratching behavior in a dose-dependent manner of SP. Each dot indicates an individual value and the horizontal bar represents average value. **(B)** Representative plot of mean values of serum DPPIV enzyme activity in mice receiving the DPPIV inhibitor sitagliptin is shown. Sitagliptin was injected at doses of 0.03, 0.5 or 30 mM by i.p. Peripheral blood was harvested at 0, 5, 15, 30 and 60 min after injection, and levels of DPPIV enzyme activity were determined as described in Materials and Methods. Serum levels of DPPIV activity were decreased in a dose-dependent manner of sitagliptin. At 30 mM of sitagliptin, DPPIV enzyme activity in C57BL/6 mice clearly decreased to less than 20% of the value prior to administration, and lasted for at least 30 min. Similar results were observed in independent experiments (n = 6). **(C)** Blood glucose levels in mice receiving the DPPIV inhibitor sitagliptin is shown (n = 6). The blood glucose levels were measured at 0 (before 1 hr food deprivation), 60 (before 30 mM sitagliptin i.p. injection), 70, 90, 120 and 210 min. Hypoglycemia was not observed in mice treated with sitaglitpin in these experimental conditions. **(D)** Mice were treated with recombinant full-length SP(1–11) (200 nmol per site) or physiological saline by i.d. and with sitagliptin (30 mM) or saline by i.p (each, n = 10). The frequency of scratching behavior of the rostral back was counted for 1 h by the method as described in Materials and Methods. Scratching behavior was significantly increased in mice treated with 200 nmol of SP compared with control mice (115.9 ± 49.1 *v.s.* 9.3 ± 9.5 times/hr, $p < 0.01$ by ANOVA). DPPIV inhibition attenuated SP-induced itch scratching behavior (13.6 ± 9.4 times/hr, $p < 0.01$ *v.s.* saline cohorts by ANOVA), while DPPIV inhibition alone showed no significant changes in scratching behavior (3.3 ± 3.5 times/hr, *N.S.* denotes 'not significant'). Each dot indicates an individual value and the horizontal bar represents average value. **(E)** Locomotor activities of mice were measured as total horizontal moving distance during itch behavioral experiment as conducted in (D). There was no significant difference among control mice, mice receiving saline i.d. and sitagliptin i.p., mice receiving SP i.d. and saline i.p., and mice receiving SP i.d. and sitagliptin i.p. (Each, n = 10; 16.9 ± 14.1 *v.s.* 13.4 ± 12.1 *v.s.* 15.1 ± 16.2 *v.s.* 4.8 ± 4.7 cm/hr, respectively). Each dot indicates an individual value and the horizontal bar represents average value. *N.S.* denotes 'not significant' by ANOVA. **(F)** Wild type C57BL/6 (WT) and CD26 knockout (CD26KO) mice were treated with recombinant full-length SP(1–11) (200 nmol/site) by i.d. The frequency of scratching behavior was counted for 1 hr as described in Materials and Methods. The frequency of CD26KO mice scratching behavior was significantly decreased as compared to wild type mice (each, n = 8, 97.0 ± 50.9 *v.s.* 36.5 ± 23.3 times/hr, $p < 0.01$ by two-tailed Student's *t*-test). Each dot indicates an individual value and the horizontal bar represents average value. **(G)** Conducted simultaneously with itch behavior experiment as shown in (F), locomotor activities of CD26KO mice were measured as described in Materials and Methods. There was no significant difference in locomotor activity between WT and CD26KO (5.9 ± 4.1 *v.s.* 7.5 ± 2.5 cm/hr, $p = 0.535$ by two-tailed Student's *t*-test). Each dot indicates an individual value and the horizontal bar represents average value. *N.S.* denotes 'not significant'. **(H)** Mice were treated with recombinant full-length SP(1–11), truncated SP(5–11) (200 nmol per site) or control solvent (10%DMSO and 0.00625 M acetate in physiological saline) by i.d. (each, n = 6). The frequency of scratching behavior was evaluated by the same method as described in (D). Scratching behavior was significantly increased in mice treated with SP(1–11) (104.5 ± 30.7 times/hr) or SP(5–11) (158.5 ± 29.3 times/hr) than control mice (12.7 ± 9.5 time/hr) (each $p < 0.01$ by ANOVA). Moreover, scratching behavior was significantly increased in mice treated with SP(5–11) compared with mice receiving SP(1–11) ($p < 0.01$ by ANOVA). Each dot indicates an individual value and the horizontal bar represents average value. **(I)** Locomotor activities of mice were measured as total horizontal moving distance during itch behavioral experiment as conducted in (H). There was no significant difference among mice receiving control solvent, full-length SP(1–11) or truncated SP(5–11) i.d. (38.3 ± 18.0 *v.s.* 30.2 ± 12.5 *v.s.* 28.6 ± 12.0 cm/hr). Each dot indicates an individual value and the horizontal bar represents average value. *N.S.* denotes 'not significant' by ANOVA.

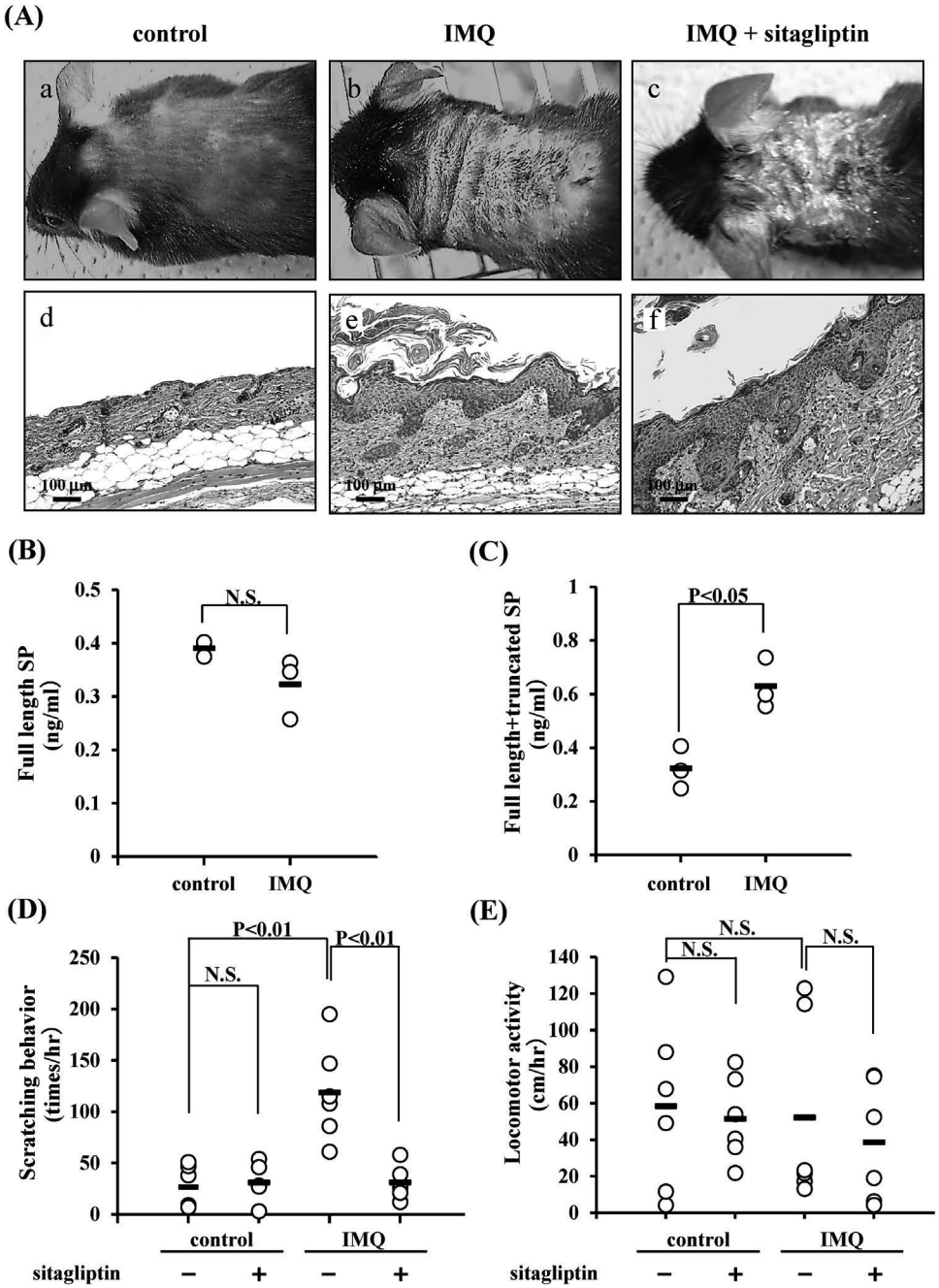

Fig. 4. DPPIV inhibitor attenuates IMQ-induced PSO derived itch. C57BL/6 mice were treated with IMQ cream or control vehicle cream at a daily dose of 30 mg on the rostral part of back for 5 days. On the 6th day, mice were treated with i.p. of sitagliptin (30 mM) or physiological saline, and then subjected to scratching behavior and locomotor activity analyses. **(A)** Representative macroscopic photographs of back skins of control cream-treated mice (*panel a*), IMQ cream-treated mice (*panel b*) or IMQ cream-treated mice receiving the DPPIV inhibitor sitagliptin (*panel c*) are shown. H&E staining histology of skin specimens obtained from each mouse is shown in *panels d, e or f*, respectively. Similar results were observed in independent experiments (n = 6). Original magnification ×100. Scale bars, 100 μm. **(B)** The levels of SP(1–11), (2–11), and (3–11) were measured in sera of IMQ or control cream-treated mice on the 6th day after treatment (each, n = 3), utilizing the same ELISA kit as conducted in Fig. 2C. There was no significant difference in the serum levels of SP(1–11), (2–11), and (3–11) between IMQ and control cream-treated mice (0.32 ± 0.06 *v.s.* 0.39 ± 0.01 ng/ml; $p = 0.11$ by two-tailed Student's *t*-test). Each dot indicates individual value. The horizontal lines in the middle of scattergrams indicate each mean value. *N.S.* denotes 'not significant'. **(C)** The levels of SP(4–11) and (5–11), including SP(1–11), (2–11) and (3–11) concentrations, were measured in sera of IMQ or control cream-treated mice on the 6th day after treatment (each, n = 3), utilizing the same ELISA kit as conducted in Fig. 2D. The serum levels of SP(4–11) and (5–11) including SP(1–11), (2–11) and (3–11) in IMQ-treated mice were significantly increased as compared with control cream-treated mice (0.63 ± 0.09 *v.s.* 0.32 ± 0.08 ng/ml; $P < 0.05$ by two-tailed Student's *t*-test). Each dot indicates individual value. The horizontal lines in the middle of scattergrams indicate each mean value. **(D)** The frequency of scratching behavior was counted for 2 hr after injection of sitagliptin or saline. Mice receiving sitagliptin showed significantly decreased IMQ-induced itch scratching behavior compared with IMQ-treated mice receiving saline (each, n = 6; 31.0 ± 16.0 *v.s.*118.7 ± 47.2 times/hr, $p < 0.01$ by ANOVA). Meanwhile, treatment with the DPPIV inhibitor alone resulted in no significant change in the frequency of scratching behavior in control cream-treated mice (each, n = 6; 30.8 ± 17.8 *v.s.* 26.7 ± 20.9, $p = 0.989$ by ANOVA). Each dot indicates an individual value and the horizontal bar represents average value. *N.S.* denotes 'not significant'. **(E)** Locomotor activities of mice were measured as total horizontal moving distance during itch behavioral experiment as conducted in (D). There was no significant difference among control cream-treated mice receiving saline or sitagliptin, and IMQ-treated mice receiving saline or sitagliptin i.p. (Each, n = 6; 58.4 ± 47.3 *v.s.* 51.4 ± 23.1 *v.s.* 52.2 ± 51.7 *v.s.* 38.7 ± 32.9 cm/hr, respectively). Each dot indicates an individual value and the horizontal bar represents average value. *N.S.* denotes 'not significant' by ANOVA.

significant differences in movement length among all cohorts, indicating that the decreased scratching behavior did not result from decreased mouse activity (Fig. 4E). In addition, there was no additional phenotypic and histologic change induced by the administration of sitagliptin (panels c and f of Fig. 4A), similar to those seen in IMQ-treated mice (panels b and e of Fig. 4A). Taken together, our data suggest that treatment with the DPPIV inhibitor sitagliptin attenuates psoriatic itch sensation via a decrease in the truncated form of SP.

3.5. Overexpression of CD26/DPPIV exaggerates IMQ-induced psoriatic itch

Finally, to further determine that DPPIV enzyme activity is associated with pruritus, we used DPPIV-Tg mice to analyze scratching behavior. As shown in Fig. 5A, DPPIV-Tg mice exhibited significant increase in DPPIV enzyme activity in sera compared with parental WT mice (177.5 ± 34.4 *v.s.* 14.9 ± 2.6 μM/min). Scratching behavior induced by IMQ cream was significantly increased in DPPIV-Tg mice than in WT mice (188.6 ± 66.2 *v.s.* 107.6 ± 45.9 times/hr) (Fig. 5B). Meanwhile, there was no change in scratching behavior between WT and DPPIV-Tg mice treated with control cream (44.9 ± 19.6 *v.s.* 40.5 ± 15.5 times/hr), with baseline levels of scratching behavior in both cohorts (Fig. 5B). Moreover, there were no significant differences in movement length between IMQ-treated WT and DPPIV-Tg mice, indicating that the observed increase in scratching behavior did not result from increased mouse activity (Fig. 5C). Taken together with the above data, our findings strongly suggest that increased DPPIV enzyme activity exaggerates psoriatic pruritus and that DPPIV may be a novel target for treatment of itch sensation in psoriasis.

4. Discussion

In the present study, we demonstrated that serum levels of DPPIV enzyme activity was significantly increased in patients with PSO, concomitant with elevation of truncated form of SP. Moreover, overexpression of DPPIV enzyme activity exaggerated itch scratching behavior in psoriatic pruritus murine model induced by IMQ cream. Furthermore, treatment with the DPPIV inhibitor sitagliptin improved itch scratching behavior in murine pruritus models induced by SP administration or IMQ cream.

Pruritus is an important symptom of PSO. Despite the fact that several studies have been undertaken to investigate the pathogenesis of pruritus in psoriasis, many aspects of this clinical manifestation have not yet been thoroughly examined [1,32]. Therefore, the pathogenesis of this symptom is far from being well-understood and, as a consequence, effective therapy for pruritus in psoriatic patients still remains a significant challenge in the clinical setting [42]. It has been shown previously that keratinocytes expressed high levels of DPPIV and that DPPIV inhibition suppressed keratinocyte proliferation *in vitro*, and partially restored keratinocyte differentiation *in vivo* [43]. It has also been reported that DPPIV activity on keratinocytes was upregulated in PSO [22,44], suggesting a potential role for DPPIV enzyme activity in the pathogenesis of PSO. While other investigators have reported a significant improvement in disease severity in patients with PSO treated with sitagliptin [21,45], the precise mechanisms involved in the effect of DPPIV inhibition on PSO have not been elucidated.

DPPIV is expressed as CD26 on T cells and DPPIV-mediated T cell activation has been demonstrated [46]. Recent report showed that the T-cell bound expression of CD26/DPPIV in psoriatic skin was explicitly present, albeit in small quantities [44]. One hypothesis regarding the potential effect of DPPIV in PSO is that T cell activation mediated by DPPIV is associated with the pathogenesis of PSO [47]. Cytokines and chemokines represent the third key player in the psoriatic chronic immune response [48], and are mediators responsible for the activation and recruitment of infiltrating leucocytes, therefore playing a crucial role in the development and persistence of psoriatic skin lesions [49]. DPPIV likely has a pivotal role in the processing of these molecules [46]. The extracellular protease domain of DPPIV (both on keratinocytes and T cells) can cleave dipeptides from the amino terminus of proteins, such as cytokines and chemokines, which are abundantly present in a chronic immune response in PSO, resulting in alterations in receptor specificity and a subsequent reduction in biological activity. Taken together, it is conceivable that in PSO, a

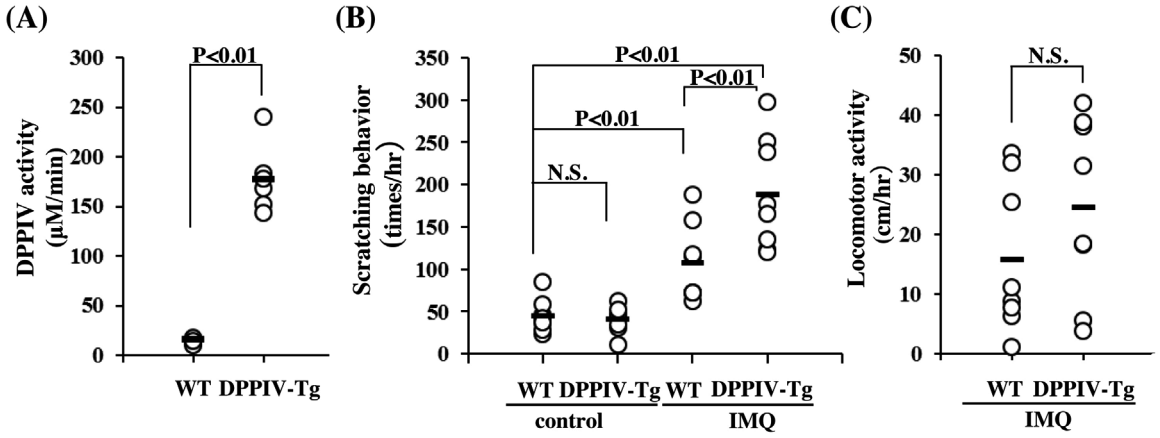

Fig. 5. Overexpression of DPPIV aggravates IMQ-induced psoriatic itch. **(A)** DPPIV enzyme activities in sera of Wild type C57BL/6 (WT) or DPPIV-Tg mice were determined as described in Materials and Methods. DPPIV-Tg mice exhibited a significant increase in DPPIV enzyme activity in sera compared with parental WT mice (each, n = 6; 177.5 ± 34.4 *v.s.* 14.9 ± 2.6 μM/min, $p < 0.01$ by Student's *t*-test). Each dot indicates an individual value and the horizontal bar represents average value. **(B)** WT and DPPIV-Tg mice were treated with IMQ cream or control vehicle cream at a daily dose of 30 mg on the rostral part of the back for 5 days (each, n = 8). Control cream-treated WT and DPPIV-Tg mice showed no significant difference in scratching behavior (44.9 ± 19.6 *v.s.* 40.5 ± 15.5 times/hr, p = 0.993 by ANOVA), while IMQ-treated WT or DPPIV-Tg mice exhibited increased scratching behavior, compared with each control cream-treated mice (44.9 ± 19.6 *v.s.* 107.6 ± 46.9 or 40.5 ± 15.5 *v.s.* 188.6 ± 66.2 times/hour, respectively; each $p < 0.01$ by ANOVA). Scratching behavior induced by IMQ-treated DPPIV-Tg mice was significantly increased compared with IMQ-treated WT mice (188.6 ± 66.2 *v.s.* 107.6 ± 46.9 times/hr, $p < 0.01$ by ANOVA). Each dot indicates an individual value and the horizontal bar represents average value. *N.S.* denotes 'not significant'. **(C)** Locomotor activities of mice were measured as total horizontal moving distance during itch behavioral experiment as conducted in (B). There was no significant difference between WT and DPPIV-Tg mice treated with IMQ cream (Each, n = 8; 15.8 ± 12.6 *v.s.* 24.6 ± 15.1 cm/hr, respectively; p = 0.228 by Student's *t*-test). Each dot indicates an individual value and the horizontal bar represents average value.

disease involving critical interplays among activated T cells, keratinocytes and cytokines, DPPIV can influence disease behavior by regulating all three components.

SP is a sensory undecapeptide of the tachykinin family distributed widely in the central and peripheral nervous systems, mediating the sensation of itch via small-diameter C fibers in the skin [50,51]. Previous studies have reported that serum levels of SP were decreased in patients with PSO [52–54]. Meanwhile, since SP is cleaved by DPPIV enzyme and DPPIV enzyme activity is increased in PSO as shown in Figs. 1 and 2, it is important for a detailed understanding of the role of SP in PSO to precisely measure the truncated form of SP separately from full-length SP. In our present study, we evaluated full-length SP(1–11) and truncated forms of SP and demonstrated that there was no change in the serum levels of full-length SP(1–11), SP(2–11) and SP(3–11) between PSO and healthy adult controls. However, we found that DPPIV enzyme activity and truncated form of SP were significantly increased in PSO, and that truncated form of SP(5–11) resulting from DPPIV enzyme activity is associated with an increase in itch sensation. In IMQ-induced PSO model, truncated form of SP was significantly increased in sera compared with control mice, and scratching behavior was decreased by administration of sitagliptin. On the other hand, there were no differences in serum levels of DPPIV enzyme activity between IMQ and control cream-treated mice (data not shown). It is conceivable that the persistent existence of psoriatic skin lesions may be required for the increased serum levels of DPPIV enzyme activity seen in PSO patients, and that SP truncation may result from the increased levels of DPPIV enzyme activity in skin lesions rather than in the circulation [22,24]. Regarding the specific receptors mediating the itch sensation of truncated SP, while SP-mediated itch has been reported to be mediated via full-length SP bound to NK-1R [29,31], future studies will be performed to determine whether truncated form of SP acts on NK-1R as an agonistic mediator or targets other pruritic receptors.

Our current study has conclusively demonstrated that increase in DPPIV enzyme activity exacerbates pruritus in PSO, and that inhibition of DPPIV enzyme reduces severity of itch scratching behavior. Moreover, our results suggest that DPPIV inhibitors are useful as therapeutic agents for pruritus including PSO. Additional studies will be conducted in the near future to better characterize and understand PSO-associated pruritus, which may lead to the development of novel effective antipruritic treatment modalities targeting the CD26/DPPIV molecule.

Conflicts-of-interest disclosure

The authors have no conflict of interest to declare.

Funding sources

This work was supported by a Grant-in-Aid (S1311011) from the Foundation of Strategic Research Projects in Private Universities from the Ministry of Education, Culture, Sports, Science, and Technology, Japan; JSPS KAKENHI Grant Number 15H04879; JSPS KAKENHI Grant Number 15K15324; JSPS KAKENHI Grant Number 16H05345; JSPS KAKENHI Grant Number 26830114; a grant of the Ministry of Health, Labour, and Welfare, Japan (Grant Number 150401-01).

Acknowledgements

The authors thank Dr. Airi Jo-Watanabe (Department of Biochemistry, Juntendo University School of Medicine), Dr. Hyeon-cheol Lee (Department of Biochemistry, Juntendo University School of Medicine), Mr. Nobuaki Takahashi (Institute for Environmental and Gender Specific Medicine, Juntendo University Graduate School of medicine), Mrs. Hiroko Madokoro (Department of Pathology, Keio University School of Medicine) and Mrs. Yuka Narita (Department of Therapy Development and Innovation for Immune Disorders and Cancers, Juntendo University Graduate School of Medicine) for excellent technical assistances and thorough discussion.

References

[1] J.C. Szepietowski, A. Reich, Pruritus in psoriasis: an update, Eur. J. Pain 20 (1) (2016) 41–46.
[2] B. Amatya, G. Wennersten, K. Nordlind, Patients' perspective of pruritus in chronic plaque psoriasis: a questionnaire-based study, J. Eur. Acad. Dermatol. Venereol. 22 (7) (2008) 822–826.
[3] S.E. Chang, S.S. Han, H.J. Jung, J.H. Choi, Neuropeptides and their receptors in psoriatic skin in relation to pruritus, Br. J. Dermatol. 156 (6) (2007) 1272–1277.
[4] G. Stinco, G. Trevisan, F. Piccirillo, S. Pezzetta, E. Errichetti, N. di Meo, F. Valent, P. Patrone, Pruritus in chronic plaque psoriasis: a questionnaire-based study of 230 Italian patients, Acta Dermatovenerol. Croat. 22 (2) (2014) 122–128.
[5] J.C. Szepietowski, A. Reich, B. Wisnicka, Pruritus and psoriasis, Br. J. Dermatol. 151 (6) (2004) 1284.
[6] G. Yosipovitch, A. Goon, J. Wee, Y.H. Chan, C.L. Goh, The prevalence and clinical characteristics of pruritus among patients with extensive psoriasis, Br. J. Dermatol. 143 (5) (2000) 969–973.
[7] A. Reich, K. Welz-Kubiak, L. Rams, Apprehension of the disease by patients suffering from psoriasis, Postepy Dermatol Alergol 31 (5) (2014) 289–293.
[8] D.A. Fox, R.E. Hussey, K.A. Fitzgerald, O. Acuto, C. Poole, L. Palley, J.F. Daley, S.F. Schlossman, E.L. Reinherz, Ta1, anovel 105 KD human T cell activation antigen defined by a monoclonal antibody, J. Immunol. 133 (3) (1984) 1250–1256.
[9] D.M. Nanus, D. Engelstein, G.A. Gastl, L. Gluck, M.J. Vidal, M. Morrison, C.L. Finstad, N.H. Bander, A.P. Albino, Molecular cloning of the human kidney differentiation antigen gp160: human aminopeptidase A, Proc. Natl. Acad. Sci. U. S. A. 90 (15) (1993) 7069–7073.
[10] T. Tanaka, D. Camerini, B. Seed, Y. Torimoto, N.H. Dang, J. Kameoka, H.N. Dahlberg, S.F. Schlossman, C. Morimoto, Cloning and functional expression of the T cell activation antigen CD26, J. Immunol. 149 (2) (1992) 481–486.
[11] C. Morimoto, S.F. Schlossman, The structure and function of CD26 in the T-cell immune response, Immunol. Rev. 161 (1998) 55–70.
[12] K. Ohnuma, N.H. Dang, C. Morimoto, Revisiting an old acquaintance: CD26 and its molecular mechanisms in T cell function, Trends Immunol. 29 (6) (2008) 295–301.
[13] T. Tanaka, J. Kameoka, A. Yaron, S.F. Schlossman, C. Morimoto, The costimulatory activity of the CD26 antigen requires dipeptidyl peptidase IV enzymatic activity, Proc. Natl. Acad. Sci. U. S. A. 90 (10) (1993) 4586–4590.
[14] H. Kobayashi, O. Hosono, T. Mimori, H. Kawasaki, N.H. Dang, H. Tanaka, C. Morimoto, Reduction of serum soluble CD26/dipeptidyl peptidase IV enzyme activity and its correlation with disease activity in systemic lupus erythematosus, J. Rheumatol. 29 (9) (2002) 1858–1866.
[15] T. Inamoto, T. Yamada, K. Ohnuma, S. Kina, N. Takahashi, T. Yamochi, S. Inamoto, Y. Katsuoka, O. Hosono, H. Tanaka, N.H. Dang, C. Morimoto, Humanized anti-CD26 monoclonal antibody as a treatment for malignant mesothelioma tumors, Clin. Cancer Res. 13 (14) (2007) 4191–4200.
[16] E. Komiya, K. Ohnuma, H. Yamazaki, R. Hatano, S. Iwata, T. Okamoto, N.H. Dang, T. Yamada, C. Morimoto, CD26-mediated regulation of periostin expression contributes to migration and invasion of malignant pleural mesothelioma cells, Biochem. Biophys. Res. Commun. 447 (4) (2014) 609–615.
[17] R. Pang, W.L. Law, A.C. Chu, J.T. Poon, C.S. Lam, A.K. Chow, L. Ng, L.W. Cheung, X. R. Lan, H.Y. Lan, V.P. Tan, T.C. Yau, R.T. Poon, B.C. Wong, A subpopulation of CD26+ cancer stem cells with metastatic capacity in human colorectal cancer, Cell Stem Cell 6 (6) (2010) 603–615.
[18] B.A. Stecca, B. Nardo, P. Chieco, A. Mazziotti, L. Bolondi, A. Cavallari, Aberrant dipeptidyl peptidase IV (DPP IV/CD26) expression in human hepatocellular carcinoma, J. Hepatol. 27 (2) (1997) 337–345.
[19] Y.X. Sun, E.A. Pedersen, Y. Shiozawa, A.M. Havens, Y. Jung, J. Wang, K.J. Pienta, R. S. Taichman, CD26/dipeptidyl peptidase IV regulates prostate cancer metastasis by degrading SDF-1/CXCL12, Clin. Exp. Metastasis 25 (7) (2008) 765–776.
[20] H. Nagai, S. Fujiwara, Y. Takahashi, C. Nishigori, Ameliorating effect of the novel dipeptidyl peptidase-4 inhibitor teneligliptin on psoriasis: a report of two cases, J. Dermatol. 42 (11) (2015) 1094–1097.
[21] T. Nishioka, M. Shinohara, N. Tanimoto, C. Kumagai, K. Hashimoto, Sitagliptin, a dipeptidyl peptidase-IV inhibitor, improves psoriasis, Dermatology 224 (1) (2012) 20–21.
[22] M. Novelli, P. Savoia, M.T. Fierro, A. Verrone, P. Quaglino, M.G. Bernengo, Keratinocytes express dipeptidyl-peptidase IV (CD26) in benign and malignant skin diseases, Br. J. Dermatol. 134 (6) (1996) 1052–1056.
[23] R.G. van Lingen, M.K. Poll, M.M. Seyger, E.M. de Jong, P.C. van de Kerkhof, P.E. van Erp, Distribution of dipeptidyl-peptidase IV on keratinocytes in the margin zone of a psoriatic lesion: a comparison with hyperproliferation and aberrant differentiation markers, Arch. Dermatol. Res. 300 (10) (2008) 561–567.
[24] D.J. Drucker, Enhancing incretin action for the treatment of type 2 diabetes, Diabetes Care 26 (10) (2003) 2929–2940.

[25] G.A. Herman, A. Bergman, C. Stevens, P. Kotey, B. Yi, P. Zhao, B. Dietrich, G. Golor, A. Schrodter, B. Keymeulen, K.C. Lasseter, M.S. Kipnes, K. Snyder, D. Hilliard, M. Tanen, C. Cilissen, M. De Smet, I. de Lepeleire, K. Van Dyck, A.Q. Wang, W. Zeng, M.J. Davies, W. Tanaka, J.J. Holst, C.F. Deacon, K.M. Gottesdiener, J.A. Wagner, Effect of single oral doses of sitagliptin, a dipeptidyl peptidase-4 inhibitor, on incretin and plasma glucose levels after an oral glucose tolerance test in patients with type 2 diabetes, J. Clin. Endocrinol. Metab. 91 (11) (2006) 4612–4619.
[26] D. Kim, L. Wang, M. Beconi, G.J. Eiermann, M.H. Fisher, H. He, G.J. Hickey, J.E. Kowalchick, B. Leiting, K. Lyons, F. Marsilio, M.E. McCann, R.A. Patel, A. Petrov, G. Scapin, S.B. Patel, R.S. Roy, J.K. Wu, M.J. Wyvratt, B.B. Zhang, L. Zhu, N.A. Thornberry, A.E. Weber, (2R)-4-oxo-4-[3-(trifluoromethyl)-5,6-dihydro[1,2,4] triazolo[4,3-a]pyrazin-7(8H)- yl]-1-(2,4,5-trifluorophenyl)butan-2-amine: a potent, orally active dipeptidyl peptidase IV inhibitor for the treatment of type 2 diabetes, J. Med. Chem. 48 (1) (2005) 141–151.
[27] C. De Felipe, J.F. Herrero, J.A. O'Brien, J.A. Palmer, C.A. Doyle, A.J. Smith, J.M. Laird, C. Belmonte, F. Cervero, S.P. Hunt, Altered nociception, analgesia and aggression in mice lacking the receptor for substance P, Nature 392 (6674) (1998) 394–397.
[28] B. Pernow, P. Substance, Pharmacol. Rev. 35 (2) (1983) 85–141.
[29] M.K. Church, Y. Okayama, S. el-Lati, Mediator secretion from human skin mast cells provoked by immunological and non-immunological stimulation, Skin Pharmacol. 4 (Suppl. 1) (1991) 15–24.
[30] A.E. Kremer, J. Feramisco, P.W. Reeh, U. Beuers, R.P. Oude Elferink, Receptors, cells and circuits involved in pruritus of systemic disorders, Biochim. Biophys. Acta 1842 (7) (2014) 869–892.
[31] M. Schmelz, R. Schmidt, A. Bickel, H.O. Handwerker, H.E. Torebjork, Specific C-receptors for itch in human skin, J. Neurosci. 17 (20) (1997) 8003–8008.
[32] M. Nakamura, M. Toyoda, M. Morohashi, Pruritogenic mediators in psoriasis vulgaris: comparative evaluation of itch-associated cutaneous factors, Br. J. Dermatol. 149 (4) (2003) 718–730.
[33] E. Heymann, R. Mentlein, Liver dipeptidyl aminopeptidase IV hydrolyzes substance P, FEBS Lett. 91 (2) (1978) 360–364.
[34] T. Karl, T. Hoffmann, R. Pabst, S. von Horsten, Extreme reduction of dipeptidyl peptidase IV activity in F344 rat substrains is associated with various behavioral differences, Physiol. Behav. 80 (1) (2003) 123–134.
[35] D. Marguet, L. Baggio, T. Kobayashi, A.M. Bernard, M. Pierres, P.F. Nielsen, U. Ribel, T. Watanabe, D.J. Drucker, N. Wagtmann, Enhanced insulin secretion and improved glucose tolerance in mice lacking CD26, Proc. Natl. Acad. Sci. U. S. A. 97 (12) (2000) 6874–6879.
[36] A.S. Agrawal, T. Garron, X. Tao, B.H. Peng, M. Wakamiya, T.S. Chan, R.B. Couch, C. T. Tseng, Generation of a transgenic mouse model of Middle East respiratory syndrome coronavirus infection and disease, J. Virol. 89 (7) (2015) 3659–3670.
[37] K. Ohnuma, T. Saito, R. Hatano, O. Hosono, S. Iwata, N.H. Dang, H. Ninomiya, C. Morimoto, Comparison of two commercial ELISAs against an in-house ELISA for measuring soluble CD26 in human serum, J. Clin. Lab. Anal. 29 (2) (2015) 106–111.
[38] T. Andrieu, V. Thibault, I. Malet, J. Laporte, B. Bauvois, H. Agut, A. Cahour, Similar increased serum dipeptidyl peptidase IV activity in chronic hepatitis C and other viral infections, J. Clin. Virol. 27 (1) (2003) 59–68.
[39] A. Sedo, R. Malik, Dipeptidyl peptidase IV-like molecules: homologous proteins or homologous activities? Biochim. Biophys. Acta 1550 (2001) 107–116.
[40] L. van der Fits, S. Mourits, J.S. Voerman, M. Kant, L. Boon, J.D. Laman, F. Cornelissen, A.M. Mus, E. Florencia, E.P. Prens, E. Lubberts, Imiquimod-induced psoriasis-like skin inflammation in mice is mediated via the IL-23/IL-17 axis, J. Immunol. 182 (9) (2009) 5836–5845.
[41] K. Sakai, K.M. Sanders, M.R. Youssef, K.M. Yanushefski, L. Jensen, G. Yosipovitch, T. Akiyama, Mouse model of imiquimod-induced psoriatic itch, Pain (2016).
[42] A.S. Raut, R.H. Prabhu, V.B. Patravale, Psoriasis clinical implications and treatment: a review, Crit. Rev. Ther. Drug Carrier Syst. 30 (3) (2013) 183–216.
[43] A. Thielitz, D. Reinhold, R. Vetter, U. Bank, M. Helmuth, R. Hartig, S. Wrenger, I. Wiswedel, U. Lendeckel, T. Kahne, K. Neubert, J. Faust, C.C. Zouboulis, S. Ansorge, H. Gollnick, Inhibitors of dipeptidyl peptidase IV and aminopeptidase N target major pathogenetic steps in acne initiation, J. Invest. Dermatol. 127 (5) (2007) 1042–1051.
[44] R.G. van Lingen, P.C. van de Kerkhof, M.M. Seyger, E.M. de Jong, D.W. van Rens, M.K. Poll, P.L. Zeeuwen, P.E. van Erp, CD26/dipeptidyl-peptidase IV in psoriatic skin: upregulation and topographical changes, Br. J. Dermatol. 158 (6) (2008) 1264–1272.
[45] M. Lynch, A.M. Tobin, T. Ahern, D. O'Shea, B. Kirby, Sitagliptin for severe psoriasis, Clin. Exp. Dermatol. 39 (7) (2014) 841–842.
[46] K. Ohnuma, O. Hosono, N.H. Dang, C. Morimoto, Dipeptidyl peptidase in autoimmune pathophysiology, Adv. Clin. Chem. 53 (2011) 51–84.
[47] M. Diani, G. Altomare, E. Reali, T cell responses in psoriasis and psoriatic arthritis, Autoimmun. Rev. 14 (4) (2015) 286–292.
[48] J. Baliwag, D.H. Barnes, A. Johnston, Cytokines in psoriasis, Cytokine 73 (2) (2015) 342–350.
[49] M.P. Schon, W.H. Boehncke, N. Psoriasis, Engl. J. Med. 352 (18) (2005) 1899–1912.
[50] F.O. Nestle, P. Di Meglio, J.Z. Qin, B.J. Nickoloff, Skin immune sentinels in health and disease, Nat. Rev. Immunol. 9 (10) (2009) 679–691.
[51] T. Akiyama, E. Carstens, Neural processing of itch, Neuroscience 250 (2013) 697–714.
[52] C. Remrod, S. Lonne-Rahm, K. Nordlind, Study of substance P and its receptor neurokinin-1 in psoriasis and their relation to chronic stress and pruritus, Arch. Dermatol. Res. 299 (2) (2007) 85–91.
[53] B. Amatya, K. Nordlind, C.F. Wahlgren, Responses to intradermal injections of substance P in psoriasis patients with pruritus, Skin Pharmacol. Physiol. 23 (3) (2010) 133–138.
[54] T. Miyagaki, M. Sugaya, H. Suga, S. Morimura, M. Kamata, H. Ohmatsu, H. Fujita, Y. Asano, Y. Tada, T. Kadono, S. Sato, Serum soluble CD26 levels: diagnostic efficiency for atopic dermatitis, cutaneous T-cell lymphoma and psoriasis in combination with serum thymus and activation-regulated chemokine levels, J. Eur. Acad. Dermatol. Venereol. 27 (1) (2013) 19–24.

Identification of senescent cell surface targetable protein DPP4

Kyoung Mi Kim,[1,4] Ji Heon Noh,[1,4] Monica Bodogai,[1] Jennifer L. Martindale,[1] Xiaoling Yang,[1] Fred E. Indig,[1] Sandip K. Basu,[2] Kei Ohnuma,[3] Chikao Morimoto,[3] Peter F. Johnson,[2] Arya Biragyn,[1] Kotb Abdelmohsen,[1] and Myriam Gorospe[1]

[1]National Institute on Aging, National Institutes of Health, Baltimore, Maryland 21224, USA; [2]National Cancer Institute, National Institutes of Health, Frederick, Maryland 21702, USA; [3]Graduate School of Medicine, Juntendo University, Tokyo 113-8421, Japan

Senescent cell accumulation in aging tissues is linked to age-associated diseases and declining function, prompting efforts to eliminate them. Mass spectrometry analysis revealed that DPP4 (dipeptidyl peptidase 4) was selectively expressed on the surface of senescent, but not proliferating, human diploid fibroblasts. Importantly, the differential presence of DPP4 allowed flow cytometry-mediated isolation of senescent cells using anti-DPP4 antibodies. Moreover, antibody-dependent cell-mediated cytotoxicity (ADCC) assays revealed that the cell surface DPP4 preferentially sensitized senescent, but not dividing, fibroblasts to cytotoxicity by natural killer cells. In sum, the selective expression of DPP4 on the surface of senescent cells enables their preferential elimination.

Supplemental material is available for this article.

Received May 24, 2017; revised version accepted August 2, 2017.

Cell senescence is a state of terminal growth arrest triggered by stress signals such as critically short telomeres, oxidative damage, oncogene activation, and hypoxia (Kuilman et al. 2010). Compared with proliferating cells, senescent cells exhibit an enlarged morphology, distinct metabolic and gene expression patterns, and increased activity of a neutral β-galactosidase (Crowe et al. 2014). They also display a senescence-associated secretory phenotype (SASP) characterized by the production and secretion of proinflammatory factors, angiogenic factors, and matrix metalloproteases that alter tissue function by promoting angiogenesis, attracting immune cells, and remodeling the extracellular matrix (Coppé et al. 2010).

Cell senescence has a range of complex effects on physiology and disease processes. Among its beneficial effects, senescent cells promote tissue morphogenesis and wound healing and suppress fibrosis and tumorigenesis in young organisms (Prieur and Peeper 2008; Muñoz-Espín et al. 2013; Storer et al. 2013; Demaria et al. 2014; Muñoz-Espín and Serrano 2014). On the other hand, extensive detrimental effects have been documented for senescent cells accumulating in tissues of older organisms, as they trigger or exacerbate age-related diseases such as cancer, cataracts, arthritis, and atherosclerosis (Baker et al. 2008, 2011; Prieur and Peeper 2008; Muñoz-Espín and Serrano 2014; van Deursen 2014).

The accumulation of senescent cells in aging tissues, as investigated in a genetic mouse model in which senescent cells were selectively eliminated, was found to promote aging-associated declines and diseases. Indeed, the removal of senescent cells from aging mouse tissues—achieved by triggering apoptotic death of cells that expressed the senescence protein p16—enhanced longevity and promoted healthy life span associated with a reduction in tumorigenesis and extended function of the renal, cardiovascular, muscular, and adipose systems (Baker et al. 2011, 2016).

With increasing evidence that senescent cells adversely influence aging-associated declines and diseases, a major goal in the field is to design interventions that recognize and eradicate senescent cells selectively. Senescent cells differ greatly from proliferating cells in the patterns of expressed proteins, including those on the cell surface that can serve as markers and therapeutic targets. Thus, we set out to identify cell surface proteins uniquely present in senescent cells. This strategy is similar to that used to eliminate cancer cells selectively (Rasmussen and Ditzel 2009). Using mass spectrometry (MS) analysis, we identified DPP4 (dipeptidyl peptidase 4; also known as CD26) as a surface protein that was strikingly more abundant in senescent cells. Importantly, senescent cells were preferentially eliminated by antibody-dependent cell-mediated cytotoxicity (ADCC), as the presence of DPP4 on their surface rendered them suitable targets for destruction by natural killer (NK) cells recognizing an anti-DPP4 antibody.

Results and Discussion

Identification of DPP4 as a novel senescent cell surface marker

To find novel surface markers selectively present on the plasma membrane of senescent cells, we used a well-characterized model of cellular senescence: proliferating WI-38 human diploid fibroblasts (HDFs; at population doubling level [PDL] 23) compared with those that had become senescent (PDL59) following extended culture. Senescent HDFs displayed a characteristic flattened and enlarged morphology and exhibited elevated senescence-associated β-galactosidase (SA-β-gal) activity, a distinctive trait of cellular senescence (Fig. 1A). Analysis of the incorporation of ^{3}H-thymidine or BrdU further indicated that senescent cells had significantly lower proliferating activity (Fig. 1A). We fractionated membrane-associated proteins and cell surface-associated proteins as described (Materials and Methods) and surveyed them by MS

[*Keywords*: CD26; cell senescence; human diploid fibroblasts]
[4]These authors contributed equally to this work.
Corresponding author: kyoungmi.kim@nih.gov
Article published online ahead of print. Article and publication date are online at http://www.genesdev.org/cgi/doi/10.1101/gad.302570.117.

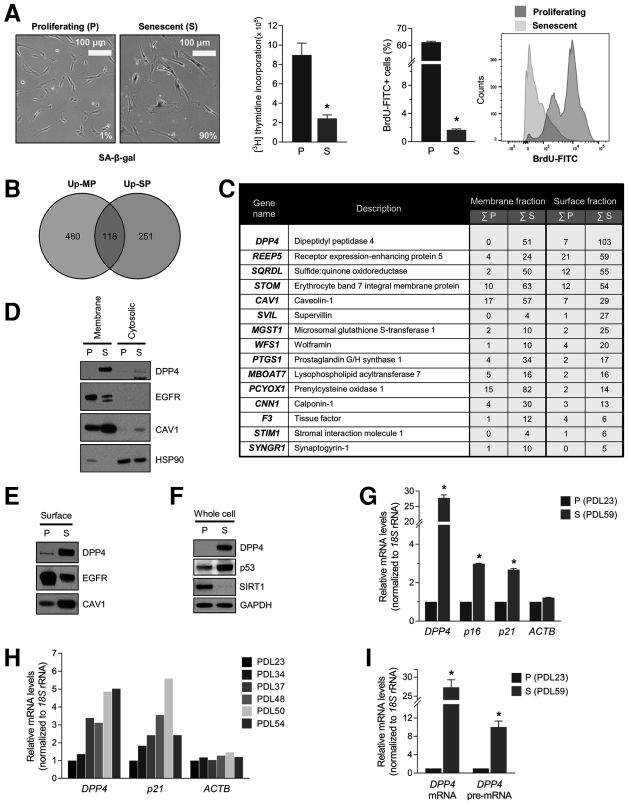

Gene name	Description	Membrane fraction ∑ P	Membrane fraction ∑ S	Surface fraction ∑ P	Surface fraction ∑ S
DPP4	Dipeptidyl peptidase 4	0	51	7	103
REEP5	Receptor expression-enhancing protein 5	4	24	21	59
SQRDL	Sulfide:quinone oxidoreductase	2	50	12	55
STOM	Erythrocyte band 7 integral membrane protein	10	63	12	54
CAV1	Caveolin-1	17	57	7	29
SVIL	Supervillin	0	4	1	27
MGST1	Microsomal glutathione S-transferase 1	2	10	2	25
WFS1	Wolframin	1	10	4	20
PTGS1	Prostaglandin G/H synthase 1	4	34	2	17
MBOAT7	Lysophospholipid acyltransferase 7	5	16	2	16
PCYOX1	Prenylcysteine oxidase 1	15	82	2	14
CNN1	Calponin-1	4	30	3	13
F3	Tissue factor	1	12	4	6
STIM1	Stromal interaction molecule 1	0	4	1	6
SYNGR1	Synaptogyrin-1	1	10	0	5

Figure 1. Identification of DPP4 as a novel senescent cell surface marker protein. (*A*, *left*) Detection of the senescent marker SA-β-gal in proliferating (P; PDL23) and senescent (S; PDL59) WI-38 HDFs; the percentages of blue cells are indicated. (*Middle*) Measurement of ^{3}H-thymidine and BrdU incorporation in proliferating and senescent WI-38 cells. (*Right*) Flow cytometry analysis of BrdU-FITC-positive proliferating and senescent cells. (*B*) Venn diagram summarizing the MS analysis; the numbers of proteins more abundant in cell membrane preparations (Up-MP; green) and cell surface preparations (Up-SP; blue) from senescent cells relative to proliferating cells are indicated. (*C*) The top 15 proteins from the intersection in *B*. The numbers indicate the sums of the PSM from two experiments. (*D–F*) Western blot analysis of DPP4 levels in membrane and cytosolic lysates (*D*), surface proteins (*E*), and whole-cell lysates (*F*). (HSP90) Cytosolic protein marker; (CAV1 and EGFR) membrane protein markers; (SIRT1) protein marker of proliferating cells; (p53) protein marker of senescent cells; (GAPDH) loading control protein. (*G–I*) Steady-state levels of *DPP4* mRNA and *DPP4* pre-mRNA quantified by RT-qPCR analysis. Total RNA was prepared from proliferating and senescent cells (*G*,*I*) or cells at PDLs between PDL23 and PDL54 (*H*). Senescent markers *p21* mRNA and *p16* mRNAs were included as positive controls, and *ACTB* mRNA was used as a negative control. mRNA levels were normalized to *18S* rRNA levels in each sample; mRNAs in PDL23 cells were set as 1 in *G–I*. The graphs in *A*, *G*, and *I* represent the means ± SEM from three independent experiments. (*) *P*-value < 0.05.

analysis (see Supplemental Table S1 for complete MS data set). We focused on the proteins that were more abundant among membrane proteins (a fraction that included endoplasmic reticulum, mitochondria, and other intracellular membrane structures) and among cell surface proteins in senescent compared with proliferating fibroblasts. Among the 118 protein candidates at the overlap of the two groups (Fig. 1B), the top 15 proteins and the PSM (peptide spectrum match) count in proliferating relative to senescent cells are listed in Figure 1C. The leading candidate on this list was DPP4 (CD26). DPP4 peptides detected by MS analysis are indicated (Supplemental Fig. S1A).

To validate these differences in DPP4 levels, we fractionated the membrane, surface-associated, and cytosolic fractions of proliferating and senescent WI-38 HDFs. Western blot analysis (Fig. 1D) revealed that DPP4 levels were robustly elevated in the membrane fraction of senescent fibroblasts but not proliferating fibroblasts or cytosolic fractions (Fig. 1D); membrane-associated proteins EGFR and Caveolin-1 (CAV1) as well as cytosolic protein HSP90 were included to monitor the cell fractionation. DPP4 was also more highly expressed on the cell surface and in whole-cell lysates (Fig. 1E,F) of senescent relative to proliferating WI-38 cells. Proteins present on the cell membrane (EGFR and CAV1), proteins showing altered levels with senescence (EGFR, CAV1, SIRT1, and p53), and a loading control (GAPDH) were also assessed.

We investigated the mechanism that led to the rise in DPP4 levels in senescent cells. RNA isolation from proliferating and senescent cells followed by RT-qPCR analysis revealed that *DPP4* mRNA was markedly higher in senescent cells (Fig. 1G); senescent markers *p16* (*CDKN2A*) mRNA and *p21* (*CDKN1A*) mRNA were also elevated (Fig. 1G). *DPP4* mRNA levels increased gradually with advancing PDLs (Fig. 1H). We quantified *DPP4* pre-mRNA levels as a surrogate measure of de novo *DPP4* mRNA transcription (Fig. 1I); the strong increase in *DPP4* pre-mRNA levels in senescent cells suggested that increased *DPP4* gene transcription was a major mechanism leading to DPP4 increase with senescence.

To test whether DPP4 increased more generally in senescent cells, we triggered senescence by exposing proliferating WI-38 and IMR-90 HDFs to ionizing radiation (IR); 10 d later, SA-β-gal activity was selectively elevated in IR-treated cells. Western blot and RT-qPCR analyses indicated that DPP4 and *DPP4* mRNA (Supplemental Fig. S1B,C) were up-regulated in IR-induced senescent HDFs, although more modestly than in HDFs undergoing replicative senescence (Fig. 1F,G). We further tested whether DPP4 levels were elevated in other models of senescence by exposing human umbilical vein endothelial cells (HUVECs) and human aortic endothelial cells (HAECs) to 4 Gy of IR to elicit senescence; 14 d later, RT-qPCR analysis revealed significantly elevated *DPP4* mRNA in senescent (IR-treated) compared with proliferating (untreated) HUVECs and HAECs (Supplemental Fig. S2A,B). Another trigger of senescence, treatment with doxorubicin (Dox), also led to a rise in *DPP4* mRNA abundance in WI-38 cells (Supplemental Fig. S2C). Moreover, oncogene-induced senescence (OIS) in mouse embryonic fibroblasts (MEFs) expressing the oncogene $HRAS^{G12V}$ via viral transduction also revealed a robust rise in DPP4 levels (Supplemental Fig. S2D). Together, these data indicate that DPP4 levels were highly and broadly elevated in senescent cells relative to proliferating cells at least in part by transcriptional induction of *DPP4* mRNA levels and that DPP4 localized on the surface of the plasma membrane.

Contribution to senescence by DPP4

Given the rise in DPP4 levels in senescent cells, we asked whether DPP4 itself might help promote cellular senescence. To test this possibility, we overexpressed DPP4 in proliferating WI-38 cells by infection with a lentivirus that expressed DPP4-Myc using control viral particles

that expressed only the Myc tag. After selection of infected cells in puromycin for 20 d, protein lysates were prepared, and Western blot analysis was used to assess senescence markers. As shown, markers p16 and p21 were elevated while SIRT1 levels declined in cells overexpressing DPP4 (Fig. 2A), supporting the notion that DPP4 promoted cell senescence. In addition, overexpression of DPP4 in WI-38 cells elevated SA-β-gal activity (Fig. 2B) and decreased ^{3}H-thymidine incorporation (Fig. 2C).

We further tested whether DPP4 contributed to eliciting senescence by silencing DPP4 in presenescent WI-38 cells (approximately PDL39–PDL45) and assessing senescence markers. As shown, the robust silencing of DPP4 by 72 h after transfection of siRNA (Supplemental Material) led to marked reductions in the levels of p53, p21, and p16 and increased SIRT1 levels, as determined by Western blot analysis (Fig. 2D). Likewise, RT-qPCR analysis revealed that the levels of senescence markers *p21* mRNA, *IL1A* mRNA, and *IL1B* mRNA were significantly reduced in the DPP4 siRNA group (Fig. 2E). Additionally, DPP4 silencing increased the number of cells in the population (Fig. 2F) and promoted incorporation of ^{3}H-thymidine and BrdU (Fig. 2G,H), further indicating that DPP4 contributed to the growth suppression characteristic of senescence. Interestingly, DPP4 silencing reduced the production of reactive oxygen species (ROS) in presenescent cells (Fig. 2I). Taken together, our results indicate that DPP4 enhances fibroblast senescence.

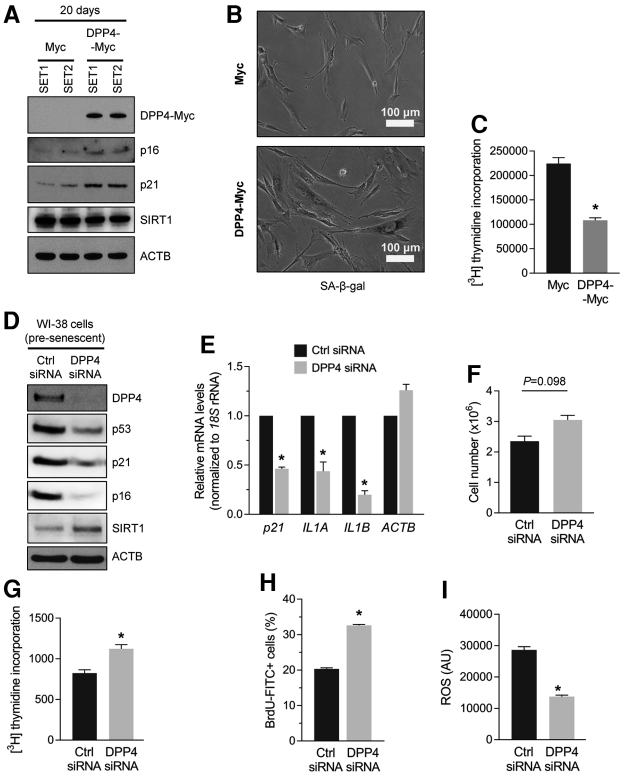

Figure 2. DPP4 contributes to the senescence program. (*A*) Proliferating WI-38 cells were infected with lentiviral particles expressing either Myc tag alone or DPP4-Myc. After 20 d of puromycin selection, cells were harvested, and whole-cell lysates were prepared for Western blot analysis to examine the levels of proteins DPP4-Myc (using anti-DPP4 antibody), p16, p21, and SIRT1 and loading control ACTB (β-Actin); endogenous DPP4 was undetectable. (*B*,*C*) Detection of the senescent marker SA-β-gal (*B*) and measurement of ^{3}H-thymidine incorporation (*C*) in the populations described in *A*. (*D–I*) Seventy-two hours after transfecting presenescent WI-38 cells (PDL39–PDL45) with control (Ctrl) siRNA or DPP4 siRNA, the levels of DPP4, p53, p21, p16, SIRT1, and ACTB in whole-cell lysates were assessed by Western blot analysis (*D*); the steady-state levels of *p21*, *IL1A*, *IL1B*, and *ACTB* mRNAs were calculated by RT-qPCR analysis and normalized to *18S* rRNA levels (*E*); cell numbers were quantified (*F*); ^{3}H-thymidine (*G*) and BrdU (*H*) incorporation was measured; and reactive oxygen species (ROS) production was measured (*I*). The graphs in *C* and *E–I* represent the means ± SEM from three independent experiments. (*) *P*-value < 0.05.

Specific selection of senescent cells using cell surface DPP4

Given that DPP4 was identified as a cell surface protein in senescent cells (Fig. 1B,C), we used confocal microscopy to further investigate this localization. Proliferating and senescent WI-38 HDFs were fixed but not permeabilized in order to detect only proteins present on the outside of the plasma membrane. As shown in Figure 3A, DPP4 signal (red) was virtually undetectable in proliferating cells but was highly abundant in senescent cultures and was found throughout the cell surface. In light of these results, we tested whether DPP4 might be a suitable selection marker for senescent cells. We used two mouse antibodies, anti-DPP4-PE and (control) mIgG-PE, to label proliferating and senescent WI-38 HDFs without fixation or permeabilization to analyze cell surface markers. Labeled samples were analyzed by flow cytometry to assess the presence of DPP4 on the cell surface. MFI (mean fluorescence intensity) analysis revealed that DPP4-labeled cells were enriched eightfold in senescent compared with proliferating WI-38 HDFs (Fig. 3B). Moreover, the number of DPP4-positive cells identified by flow cytometry analysis using DPP4-PE was only 6.05% in proliferating cells but rose to 67.9% in senescent cells (Fig. 3C). In sum, DPP4 levels are markedly elevated on the surface of senescent fibroblasts and serve as a suitable marker for the specific isolation of senescent cells.

With advancing age, senescent cells accumulate in a variety of tissues, including blood. We thus asked whether DPP4-positive cells might be detected in peripheral blood mononuclear cells (PBMCs) from three healthy young individuals (27–36 yr of age) and three healthy old individuals (78–88 yr of age) (Materials and Methods). As shown in Figure 3D, the percentage of DPP4-positive cells (as determined by flow cytometry using the DPP4-PE antibody) was higher in "old" PBMCs than in "young" PBMCs (15.5% vs. 10%). Since most DPP4 signals came from monocytes and lymphocytes, we calculated the percentages of DPP4-positive monocytes and lymphocytes and found that these percentages remained significantly higher in the old donor group than the young donor group (33% vs. 21%); see Supplemental Figure S3 for contour plots of the individual donors. To determine whether DPP4-positive cells were senescent, PBMCs from four donors (ages 27, 27, 60, and 63 yr) were labeled with DPP4-PE and sorted using anti-PE microbeads by MACS (magnetic-activated cell sorting) analysis. After isolation of RNA from the affinity-purified cells, RT-qPCR analysis was used to assess the expression of senescence markers. As shown (Fig. 3E), DPP4-positive cells in each of the four donors expressed higher levels of DPP4 and *DPP4* mRNA by Western blot and RT-qPCR analyses, respectively (to verify

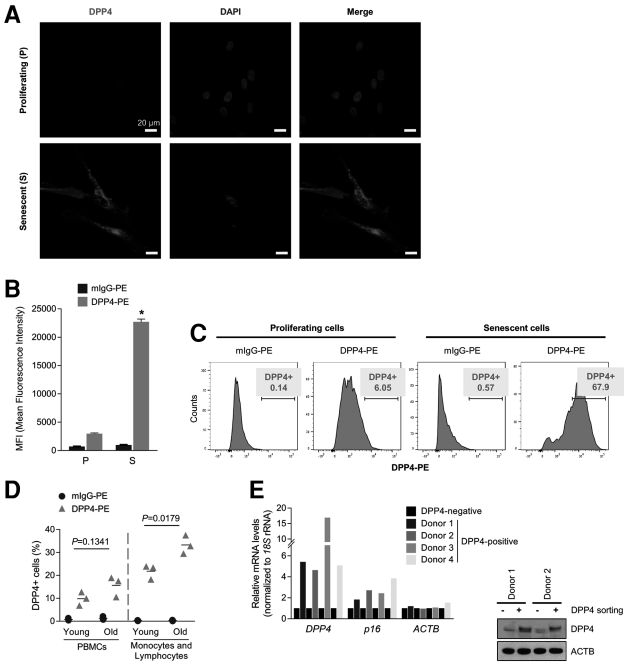

Figure 3. DPP4 is more highly expressed in senescent cells and localizes on the cell surface. (*A*) Proliferating (P) or senescent (S) WI-38 HDFs were fixed with methanol, and the endogenous DPP4 protein was detected by confocal microscopy. (*B*,*C*) WI-38 (proliferating and senescent) HDFs were harvested and incubated with either anti-DPP4-PE or control mIgG-PE antibodies. (*B*) DPP4-positive cells were analyzed by flow cytometry, and the MFI of DPP4-PE in proliferating and senescent cells was quantified. The graph represents the means ± SEM. from three independent experiments. (*) *P*-value < 0.05. (*C*) Histograms from the flow analysis representing control isotype (*left*) or DPP4 (*right*) in proliferating and senescent cells; the percentages of DPP4-PE-positive cells are indicated. The experiment shown is representative of three independent experiments. (*D*) Human peripheral blood mononuclear cells (PBMCs) obtained from young (27- to 36-yr-old) and old (78- to 88-yr-old) donors were analyzed by flow cytometry using antibodies that recognized DPP4-PE (▲) or mouse IgG-PE (•). The graph shows the percentage of DPP4-PE-positive cells. (*Left*) PBMC populations. (*Right*) Monocyte and lymphocyte populations. Each data point represents a young ($n = 3$ total) or old ($n = 3$ total) subject; horizontal lines indicate the mean values. (*E*) Human PBMCs obtained from four donors (27, 27, 60, or 63 yr old) were sorted into DPP4-positive cells and DPP4-negative cells by MACS using a DPP4-PE antibody and anti-PE microbeads. The steady-state levels of *DPP4*, *p16*, and *ACTB* mRNAs were quantified by RT-qPCR analysis after normalization to *18S* rRNA levels. Each mRNA in DPP4-negative cells was set as 1.

that the affinity pull-down was successful), and, importantly, all four samples also displayed higher levels of *p16* mRNA, which encodes the major senescence-associated protein p16. The data obtained using PBMCs further support the notion that DPP4 also serves as a surface marker for the selection of senescent cells among a heterogeneous cell population.

Selective elimination of DPP4-positive senescent cells by ADCC assay

Our initial goal was to devise a method to eliminate senescent cells selectively using a differentially expressed surface protein. Thus, after establishing that DPP4 is located on the surface of the plasma membrane of senescent cells (Figs. 1, 3), we set out to test whether we could eliminate senescent cells selectively using an antibody directed at DPP4 and the ADCC assay. Originally developed for cancer therapy, the ADCC assay uses antibodies to recognize a specific antigen on the cell surface and guide NK cells to selectively destroy the antibody-labeled cells (Weiner 2015). We carried out ADCC analysis using increasing concentrations of anti-DPP4 antibody (up to 5 μg/mL) to bind the DPP4 surface marker and thereby label proliferating and senescent WI-38 fibroblasts. We then isolated NK cells from human PBMCs and added them to the WI-38 cultures, allowing the NK cells to destroy the cells labeled by anti-DPP4 antibody. Treatment with NK cells from eight different donors in the presence of rabbit or humanized anti-DPP4 antibodies (Fig. 4A) indicated that, in every case, senescent cells exhibited stronger reductions in cell viability, as low as ~40% (as seen with "donor 8" of NK cells), compared with proliferating cells. As shown in Supplemental Figure S4, ADCC assay using a control rabbit IgG (rIgG) revealed that this antibody did not affect cell viability in proliferating or senescent cells.

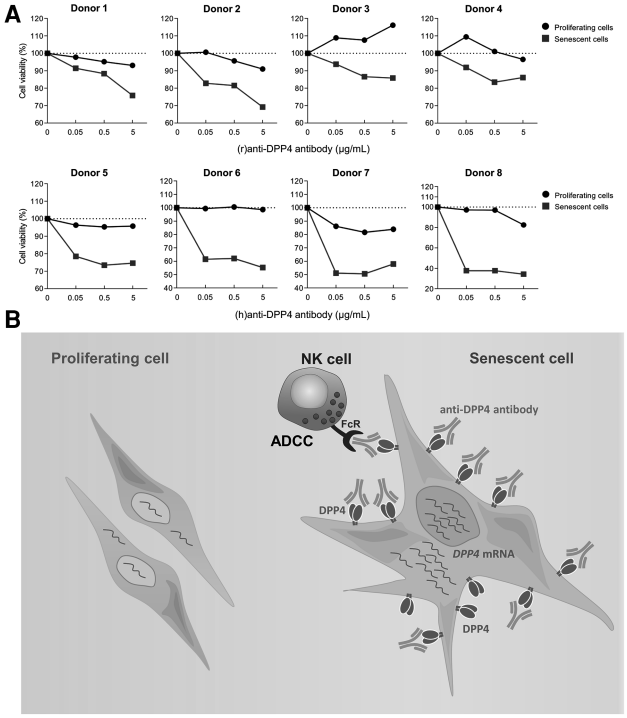

Figure 4. Eliminating DPP4-positive senescent cells by ADCC. (*A*) Proliferating and senescent WI-38 cells (5×10^4) were incubated without or with 0.05, 0.5, and 5 μg/mL anti-DPP4 antibody and either 2.5×10^5 NK cells [for rabbit (r)anti-DPP4] or 1.25×10^6 or 2.5×10^6 NK cells [for humanized (h)anti-DPP4 antibody] per well for 4 h. After removing NK cells, WI-38 cells were incubated for another 18 h, and cell viability was measured by the MTT [3-(4,5-dimethylthiazol-2-yl)-2,5-diphenyltetrazolium bromide] assay. Cell numbers were compared with those that received no anti-DPP4 antibody. Donors 1–4 were incubated with (r)anti-DPP4, and donors 5–8 were incubated with (h)anti-DPP4. (*B*) Proposed model. (*Left*) In proliferating cells, DPP4 is expressed at low levels or is undetectable. (*Right*) In senescent cells, *DPP4* mRNA levels increase transcriptionally, leading to increased production of DPP4, which localizes as a dimer on the cell surface, exposed to the extracellular space. The abundance and localization of DPP4 in senescent cells enable the selective elimination of senescent cells by ADCC.

Targeting DPP4 to eliminate senescent cells

In sum, we identified DPP4 as a protein robustly up-regulated on the plasma membrane of senescent cells. DPP4 levels increased via transcriptional induction of *DPP4* mRNA in senescent cells. Whether this increase might be mediated via transcription factors HNF and/or STAT1α in fibroblasts, as shown previously in B lymphocytes and intestinal epithelial cells (Bauvois et al. 2000; Erickson et al. 2000; D'Angelo et al. 2010), remains to be tested. We further found that senescent cells can be selectively targeted by anti-DPP4 antibodies and eliminated. Accordingly, we propose a model (Fig. 4B) in which the highly abundant DPP4 on the exposed surface of a senescent cell allows it to be recognized and eliminated by anti-DPP4 antibody-directed NK-elicited cell death. These results underscore the usefulness of targeting for selective destruction proteins differentially present on the plasma membrane of senescent cells.

DPP4 is best known as a protease that inactivates two hormones named incretins: glucose-dependent insulinotropic peptide (GIP) and glucagon-like peptide-1 (GLP-1). Incretins trigger a rapid release of insulin from pancreatic β cells after a meal; since they suppress a sudden rise in blood glucose, they are particularly beneficial in diabetes (Wu et al. 2016). Although the significance of having elevated DPP4 in senescent cells is unclear, DPP4 might influence some of the changes in glucose homeostasis that occur with aging. For example, a rise in DPP4 levels from accumulating senescent cells could contribute to the impairment of glucose metabolism that leads to hyperglycemia in the elderly. In this regard, it will be interesting to test whether DPP4 inhibitors (e.g., sitagliptin) (Scott 2017), which enhance the so-called "incretin effect" and have been used to treat diabetes, recapitulate the enhanced proliferation and suppressed senescence seen after silencing DPP4 (Fig. 2).

DPP4 and senolytic therapy

Similarly, as incretin-independent actions of DPP4 are emerging, it will be important to study whether the health benefits of DPP4 inhibitors depend partly on their impact on senescent cells irrespective of DPP4-mediated inactivation of incretins. For example, DPP4 present on the plasma membrane of lymphocytes (which we found to be elevated with age) (Fig. 3D) associates with CAV1, a membrane protein that also rises with senescence, leading to the activation of IRAK-1 and NF-κB (Ohnuma et al. 2005, 2008). Likewise, DPP4 present on the membrane of antigen-presenting cells and inflammatory cells in adipose tissue promotes inflammation independent of its effects on insulin production (Zhong et al. 2013). These actions of DPP4 as well as its interaction with extracellular matrix components such as collagen and fibronectin (Löster et al. 1995; Zhong et al. 2013) might implicate DPP4 as a factor related to SASP traits, which are modulated by NF-κB and profoundly affect extracellular matrix remodeling.

SASP has been linked to the disease-enhancing impact of senescent cells that accumulate in aging tissues, since SASP factors (cytokines, growth factors, and MMPs) perturb tissue metabolism locally and systemically. Accordingly, senescent cell elimination via genetic manipulation improved age-related pathologies (Baker et al. 2008, 2011, 2016). To achieve the same goal, several drugs called "senolytics" have been identified that selectively destroy senescent cells. Senolytics ABT737 (Yosef et al. 2016) and ABT263 (Zhu et al. 2016) were BH3 mimetic inhibitors of anti-apoptotic proteins (Bcl-xL, Bcl-2, and Bcl-w) originally developed for cancer therapy, although inhibiting Bcl-xL was found to have severe side effects. Other senolytics, such as dasatinib and quercetin (Roos et al. 2016; Zhu et al. 2016), trigger apoptosis in subsets of senescent cells, while piperlongumine appears to work best in combination with other senolytics (Wang et al. 2016). In this context, the identification of DPP4 as a targetable senescence marker can complement interventions aimed at eliminating senescent cells.

In closing, DPP4 is overexpressed in cancers such as malignant pleural mesothelioma (MPM) and renal cell and colorectal carcinoma. A recent study found that DPP4 was more highly expressed on the plasma membrane of MPM than normal mesothelioma cells (Angevin et al. 2017). Importantly, in preclinical trials, MPM tumor growth was delayed by treatment with anti-DPP4 antibody, suggesting that it was inhibitory in both cultured cells and patients. Antibody modifications such as conjugation with a toxin might enhance the cytotoxic activity of the anti-DPP4 antibody on DPP4-bearing cells. In summary, our findings have identified the cell membrane-associated protein DPP4 senescence marker as a promising target of therapeutic intervention in conditions in which it is desirable to eliminate senescent cells.

Materials and methods

Cells, cell culture, IR, and SA-β-gal assay

The source and culture of HDFs WI-38 and IMR-90, MEFs, HUVECs, and HAECs are indicated in the Supplemental Material. Proliferating WI-38 HDFs were used at PDLs ranging between PDL18 and PDL23, and senescent cells were used after additional culture (PDL47–PDL55). SA-β-gal analysis and siRNA transfections using Lipofectamine 2000 (Invitrogen) are described (Supplemental Material). Human PBMCs were isolated from participants of the Baltimore Longitudinal Study of Aging (BLSA) (Ferrucci 2008) aged 27–36 yr old (young) or 78–88 yr old (old). Proliferating WI-38 cells (approximately PDL25) and IMR-90 cells (approximately PDL25) were rendered senescent by exposure to 10 Gy of IR; cells were harvested 10 d later. Proliferating WI-38 cells were transduced with lentiviruses that expressed either DPP4-Myc or Myc (GeneCopoeia, Inc.) and selected using 1 µg/mL puromycin for 20 d before harvest.

RNA isolation, reverse transcription, and quantitative real-time PCR

Total RNA was extracted using TriPure isolation reagent (Roche), and cDNA was synthesized using random hexamers and reverse transcriptase (Invitrogen) as described (Supplemental Material). Reactions for qPCR amplification contained SYBR Green master mix (Kapa Biosystems) and were performed using an Applied Biosystems 7300 instrument. The gene-specific primers used are listed in the Supplemental Material.

Protein analysis

The preparation and analysis of cell membrane and cell surface proteins by Western blotting and MS as well as the detection of DPP4 using immunofluorescence are explained in the Supplemental Material.

Flow cytometry of WI-38 cells and PBMCs and MACS

Proliferating and senescent WI-38 cells were counted using a TC20 cell counter (Bio-Rad), washed using FACS buffer (0.5% BSA in PBS), and seeded into 96-well plates. Dead cells were stained with Zombie Aqua fixable viability kit (BioLegend); after washing, human TruStain FcX (BioLegend) was added to block the Fc receptor, and cells were labeled with DPP4-PE

(BD Biosciences) or mIgG-PE (BioLegend) for 15 min at 4°C in the dark. FACS analysis was performed on a Canto II flow cytometer (BD Biosciences) using FlowJo software (FlowJo version 10.2).

Human PBMCs were incubated with DPP4-PE (BD Biosciences) for 10 min at 4°C in the dark to label DPP4-expressing cells and then labeled with anti-PE magnetic microbeads (Miltenyi Biotec, Inc.) for 15 min at 4°C. Magnetically labeled cells were separated by MACS (Supplemental Material). Total RNA was extracted from DPP4-positive and DPP4-negative cells.

ADCC assay

Peripheral blood from participants of the BLSA (National Institute on Aging) and healthy volunteers was collected under Human Subject Protocol 2003054 and Tissue Procurement Protocol 2003-076. White blood cells were isolated by ACK lysis, and PBMCs were isolated using Ficoll (Ficoll-Paque Plus, GE Healthcare) gradients following the manufacturer's instructions. NK cells were isolated from PBMCs using a human NK cell isolation kit (Miltenyi Biotec, Inc.). Proliferating and senescent WI-38 cells growing on 24-well plates (5×10^4 cells per well) were incubated with different concentrations of control rIgG or with rabbit or humanized monoclonal antibodies recognizing 0.05, 0.5, and 5 µg/mL DPP4 for 15 min at 37°C. The isolated NK cells (2.5×10^5 cells per well for rabbit antibody and 1.25×10^6 or 2.5×10^6 for humanized antibody) were added at a ratio of 5:1 (proliferating) or 25:1 or 50:1 (senescent; NK cells:fibroblasts [proliferating or senescent]) and incubated for 4 h at 37°C. NK cells were removed by washing, fibroblasts were returned to the incubator, and, 18 h later, cell viability was analyzed using the MTT [3-(4,5-dimethylthiazol-2-yl)-2,5-diphenyltetrazolium bromide] assay (Sigma).

Acknowledgments

We thank M.K. Evans and N. Noren Hooten for providing HUVECs and HAECs. This work was supported in part by the National Institute on Aging and National Cancer Institute Intramural Research Program and the National Institutes of Health. K.O. and C.M. were supported by Grant-in-Aid (S1311011), grant 150401-01, and Japan Society for the Promotion of Science Grants-in-Aid for Scientific Research (KAKENHI) grants 15H04879, 15K15324, 16H05345, and 16K09878.

References

Angevin E, Isambert N, Trillet-Lenoir V, You B, Alexandre J, Zalcman G, Vielh P, Farace F, Valleix F, Podoll T, et al. 2017. First-in-human phase 1 of YS110, a monoclonal antibody directed against CD26 in advanced CD26-expressing cancers. *Br J Cancer* **116:** 1126–1134.

Baker DJ, Perez-Terzic C, Jin F, Pitel KS, Niederländer NJ, Jeganathan K, Yamada S, Reyes S, Rowe L, Hiddinga HJ, et al. 2008. Opposing roles for p16Ink4a and p19Arf in senescence and ageing caused by BubR1 insufficiency. *Nat Cell Biol* **10:** 825–36.

Baker DJ, Wijshake T, Tchkonia T, LeBrasseur NK, Childs BG, van de Sluis B, Kirkland JL, van Deursen JM. 2011. Clearance of p16Ink4a-positive senescent cells delays ageing-associated disorders. *Nature* **479:** 232–236.

Baker DJ, Childs BG, Durik M, Wijers ME, Sieben CJ, Zhong J, Saltness RA, Jeganathan KB, Verzosa GC, Pezeshki A, et al. 2016. Naturally occurring p16(Ink4a)-positive cells shorten healthy lifespan. *Nature* **530:** 184–189.

Bauvois B, Djavaheri-Mergny M, Rouillard D, Dumont J, Wietzerbin J. 2000. Regulation of CD26/DPPIV gene expression by interferons and retinoic acid in tumor B cells. *Oncogene* **19:** 265–272.

Coppé JP, Desprez PY, Krtolica A, Campisi J. 2010. The senescence-associated secretory phenotype: the dark side of tumor suppression. *Annu Rev Pathol* **5:** 99–118.

Crowe EP, Nacarelli T, Bitto A, Lerner C, Sell C, Torres C. 2014. Detecting senescence: methods and approaches. *Methods Mol Biol* **1170:** 425–445.

D'Angelo A, Bluteau O, Garcia-Gonzalez MA, Gresh L, Doyen A, Garbay S, Robine S, Pontoglio M. 2010. Hepatocyte nuclear factor 1α and β control terminal differentiation and cell fate commitment in the gut epithelium. *Development* **137:** 1573–1582.

Demaria M, Ohtani N, Youssef SA, Rodier F, Toussaint W, Mitchell JR, Laberge RM, Vijg J, Van Steeg H, Dollé ME, et al. 2014. An essential role for senescent cells in optimal wound healing through secretion of PDGF-AA. *Dev. Cell* **31:** 722–733.

Erickson RH, Lai RS, Kim YS. 2000. Role of hepatocyte nuclear factor 1α and 1β in the transcriptional regulation of human dipeptidyl peptidase IV during differentiation of Caco-2 cells. *Biochem Biophys Res Commun* **270:** 235–239.

Ferrucci L. 2008. The Baltimore Longitudinal Study of Aging (BLSA): a 50-year-long journey and plans for the future. *J Gerontol A Biol Sci Med Sci* **63:** 1416–1419.

Kuilman T, Michaloglou C, Mooi WJ, Peeper DS. 2010. The essence of senescence. *Genes Dev* **24:** 2463–2479.

Löster K, Zeilinger K, Schuppan D, Reutter W. 1995. The cysteine-rich region of dipeptidyl peptidase IV (CD 26) is the collagen-binding site. *Biochem Biophys Res Commun* **217:** 341–348.

Muñoz-Espin D, Serrano M. 2014. Cellular senescence: from physiology to pathology. *Nat Rev Mol Cell Biol* **15:** 482–496.

Muñoz-Espín D, Cañamero M, Maraver A, Gómez-López G, Contreras J, Murillo-Cuesta S, Rodríguez-Baeza A, Varela-Nieto I, Ruberte J, Collado M, et al. 2013. Programmed cell senescence during mammalian embryonic development. *Cell* **155:** 1104–1118.

Ohnuma K, Yamochi T, Uchiyama M, Nishibashi K, Iwata S, Hosono O, Kawasaki H, Tanaka H, Dang NH, Morimoto C. 2005. CD26 mediates dissociation of Tollip and IRAK-1 from caveolin-1 and induces upregulation of CD86 on antigen-presenting cells. *Mol Cell Biol* **25:** 7743–7757.

Ohnuma K, Dang NH, Morimoto C. 2008. Revisiting an old acquaintance: CD26 and its molecular mechanisms in T cell function. *Trends Immunol* **29:** 295–301.

Prieur A, Peeper DS. 2008. Cellular senescence in vivo: a barrier to tumorigenesis. *Curr Opin Cell Biol* **20:** 150–155.

Rasmussen N, Ditzel HJ. 2009. Scanning the cell surface proteome of cancer cells and identification of metastasis-associated proteins using a subtractive immunization strategy. *J Proteome Res* **8:** 5048–5059.

Roos CM, Zhang B, Palmer AK, Ogrodnik MB, Pirtskhalava T, Thalji NM, Hagler M, Jurk D, Smith LA, Casaclang-Verzosa G, et al. 2016. Chronic senolytic treatment alleviates established vasomotor dysfunction in aged or atherosclerotic mice. *Aging Cell* **15:** 973–977.

Scott LJ. 2017. Sitagliptin: a review in type 2 diabetes. *Drugs* **77:** 209–224.

Storer M, Mas A, Robert-Moreno A, Pecoraro M, Ortells MC, Di Giacomo V, Yosef R, Pilpel N, Krizhanovsky V, Sharpe J, Keyes WM. 2013. Senescence is a developmental mechanism that contributes to embryonic growth and patterning. *Cell* **155:** 1119–1130.

van Deursen JM. 2014. The role of senescent cells in ageing. *Nature* **509:** 439–446.

Wang Y, Chang J, Liu X, Zhang X, Zhang S, Zhang X, Zhou D, Zheng G. 2016. Discovery of piperlongumine as a potential novel lead for the development of senolytic agents. *Aging* **8:** 2915–2926.

Weiner GJ. 2015. Building better monoclonal antibody-based therapeutics. *Nat Rev Cancer* **15:** 361–370.

Wu T, Rayner CK, Horowitz M. 2016. Incretins. *Handb Exp Pharmacol* **233:** 137–171.

Yosef R, Pilpel N, Tokarsky-Amiel R, Biran A, Ovadya Y, Cohen S, Vadai E, Dassa L, Shahar E, Condiotti R, et al. 2016. Directed elimination of senescent cells by inhibition of BCL-W and BCL-XL. *Nat Commun* **7:** 11190.

Zhong J, Rao X, Deiuliis J, Braunstein Z, Narula V, Hazey J, Mikami D, Needleman B, Satoskar AR, Rajagopalan S. 2013. A potential role for dendritic cell/macrophage-expressing DPP4 in obesity-induced visceral inflammation. *Diabetes* **62:** 149–157.

Zhu Y, Tchkonia T, Fuhrmann-Stroissnigg H, Dai HM, Ling YY, Stout MB, Pirtskhalava T, Giorgadze N, Johnson KO, Giles CB, et al. 2016. Identification of a novel senolytic agent, navitoclax, targeting the Bcl-2 family of anti-apoptotic factors. *Aging Cell* **15:** 428–435.

Identification of senescent cell surface targetable protein DPP4

Kyoung Mi Kim, Ji Heon Noh, Monica Bodogai, et al.

Genes Dev. 2017, **31:** originally published online September 6, 2017
Access the most recent version at doi:10.1101/gad.302570.117

Data in Brief 15 (2017) 948–969

Contents lists available at ScienceDirect

Data in Brief

journal homepage: www.elsevier.com/locate/dib

Data Article

Gene expression microarray data from mouse cerebrum treated with rTMS for 30 days

Tetsurou Ikeda [a,b,1,*], Satoru Kobayashi [c], Chikao Morimoto [b]

[a] *Laboratory for Structural Neuropathology, RIKEN Brain Science Institute, 2-1 Hirosawa, Wako-shi, Saitama 351-0198, Japan*
[b] *Clinical Immunology, Institute of Medical Science, The University of Tokyo, 4-6-1 Shirokanedai, Minato-ku, Tokyo 108-8639, Japan*
[c] *Technical Support, Thermo Fisher Scientific K.K., 3-9 Moriya, Kanagawa-ku, Yokohama 221-0022, Japan*

ARTICLE INFO

Article history:
Received 28 June 2017
Received in revised form
12 September 2017
Accepted 12 October 2017
Available online 19 October 2017

ABSTRACT

This data article contains complementary tables related to the research article entitled, 'Effects of repetitive transcranial magnetic stimulation on ER stress-related genes and glutamate, γ-aminobutyric acid, and glycine transporter genes in mouse brain' (Ikeda et al. (2017) [1]), which showed that rTMS modulates glutamate, GABA and glycine transporters and regulates ER stress-related genes. Here we provide accompanying data collected using Affymetrix GeneChip microarrays to identify changes in gene expression in mouse cerebrum treated with rTMS for 30 days (Tables 1–10).

Specifications Table

Subject area	*Neuroscience*
More specific subject area	*Psychiatric disorders*
Type of data	*Tables*
How data was acquired	*Affymetrix GeneChip RNA microarray*

* Corresponding author.
E-mail address: ikedatetsurou@kochi-u.ac.jp (T.o.s. Ikeda).
[1] Present address: Kochi Medical School, Kochi University, Kochi, Japan.

http://dx.doi.org/10.1016/j.dib.2017.10.034

Data format	*Filtered, analysed*
Experimental factors	*Mouse brain treated with rTMS for 30 days*
Experimental features	*RNA isolation, global gene expression analyses*
Data source location	*Wako, Saitama, Japan*
Data accessibility	*Data are contained within this article*

Value of the Data

- A global gene expression analysis of mouse cerebrum treated with rTMS for 30 days.
- These data may be useful for comparison with microarray data obtained from rTMS of different durations.
- Genes identified as differentially expressed in this data set could be useful in further studies on the effects of rTMS on mouse brain.

1. Data

Affymetrix GeneChip microarray analyses of mRNA isolated from mouse cerebrum after 30 days of rTMS revealed altered expression of several genes (Tables 1–10), including glutamatergic genes (e.g., glutamate transporter), dopaminergic genes, cholinergic genes, genes of adrenergic signaling in cardiomyocytes and so on.

2. Experimental design, materials and methods

We carried out a comprehensive analysis of altered gene expression in cerebrum following chronic rTMS using a high-density oligonucleotide array (GeneChip; Affymetrix, Santa Clara, CA, USA. MG_U74Av2 probe array), as described elsewhere [2]. Using the Affymetrix algorithm [3] and multiple analysis comparison software for assessing gene expression differences, mRNAs that increased or decreased in the mouse brain following chronic rTMS relative to levels in the control mouse brain were identified. Pathway analysis was used to identify the significant pathway of the differential genes according to KEGG. And also, Gene Ontology (GO) analysis was applied to analyze the main function of the differentially expressed genes according to the gene ontology, which is the key functional classification of NCBI that can organize genes into hierarchical categories and uncover the gene regulatory network based on biological process and molecular function [4].

Using these data, we indicated that rTMS modulates glutamate, GABA and glycine transporters and regulates ER stress-related genes [1].

Table 1
Gene expression matrix after 30 days rTMS on cerebrum.

TC ID	GS	L1	C	L2	C	L3	C	L4	C	*	#	Description
93320_at	Cpt1a	0.44	I	0.15	I	0.3	I	0.17	I	4	0	carnitine palmitoyltransferase 1a, liver
93372_at	Anp32a	1.75	I	2.28	I	1.59	I	1.91	I	4	0	acidic (leucine-rich) nuclear phosphoprotein 32 family, member A
95466_at	Cotl1	2.41	I	1.11	I	2.03	I	0.83	I	4	0	coactosin-like 1 (Dictyostelium)
103012_at	Ccl21a	0.27	I	3.54	I	-1.5	D	1.6	I	3	1	chemokine (C-C motif) ligand 21A (serine); chemokine (C-C motif) ligand 21B (leucine); chemokine (C-C motif) ligand 21C (leucine); predicted gene 10591; predicted gene 13304; predicted gene 1987; predicted gene, 21541; C-C motif chemokine 21c
100307_at	Nfix	1.12	I	0.62	I	0.41	I	-0.05	NC	3	0	nuclear factor I/X
101883_s_at	Xlr3a	0.03	NC	1.16	I	0.74	I	1.79	I	3	0	X-linked lymphocyte-regulated 3A; X-linked lymphocyte-regulated 3B; X-linked lymphocyte-regulated 3C
101921_at	Rab4a	0.46	I	0.27	I	-0.01	NC	0.07	I	3	0	RAB4A, member RAS oncogene family
104175_at	Dlg4	1.09	I	1.46	I	0.41	I	1.15	NC	3	0	discs, large homolog 4 (Drosophila)
93253_at	Mapk1	-0.04	NC	0.34	I	0.34	I	0.71	I	3	0	mitogen-activated protein kinase 1
93924_f_at	Tuba3b	0.4	I	0.15	I	0.11	I	-0.09	NC	3	0	tubulin, alpha 3B
96295_at	Psat1	0.09	NC	0.11	I	0.28	I	0.44	I	3	0	phosphoserine aminotransferase 1
96590_f_at	Otud7b	0.59	NC	0.7	I	0.33	I	0.32	I	3	0	OTU domain containing 7B
99598_g_at	Gnai2	0.33	I	0.67	I	-0.1	NC	0.2	MI	3	0	guanine nucleotide binding protein (G protein), alpha inhibiting 2
102009_at	Cyfip2	0.53	I	0.21	I	-0.33	NC	-0.6	D	2	1	cytoplasmic FMR1 interacting protein 2
103275_at	Atp6v0a1	0.52	I	-1.05	D	1.2	I	-0.31	NC	2	1	ATPase, H+ transporting, lysosomal V0 subunit A1
104486_at	A2m	0.27	I	-0.91	D	0.83	I	-0.91	NC	2	1	alpha-2-macroglobulin
104564_at	Scg3	0.47	I	0.32	I	-0.49	D	-0.52	NC	2	1	secretogranin III
104643_at	Wwc1	0.72	I	0.47	I	-0.34	NC	-0.69	D	2	1	WW, C2 and coiled-coil domain containing 1
160189_at	Nudt4	-0.2	NC	-0.84	D	0.63	I	0.4	I	2	1	nudix (nucleoside diphosphate linked moiety X)-type motif 4
162138_s_at	Cbx6	0.21	I	0.27	I	-0.54	D	-0.71	NC	2	1	chromobox 6
93660_at	Camk2a	1.53	I	-0.93	D	2.09	I	-0.27	NC	2	1	calcium/calmodulin-dependent protein kinase II alpha
95301_at	S100a5	0.6	I	0.96	I	-0.86	D	-0.45	NC	2	1	S100 calcium binding protein A5
95785_s_at	Rab7	-0.36	NC	-0.91	D	0.91	I	0.4	I	2	1	RAB7, member RAS oncogene family
96583_s_at	Kif5a	-0.13	NC	-1.32	D	1.6	I	0.36	I	2	1	kinesin family member 5A
97458_at	Gnb1	0.61	I	0.8	I	-0.58	D	-0.62	NC	2	1	guanine nucleotide binding protein (G protein), beta 1
97560_at	Psap	-0.28	NC	-1.49	D	1.74	I	0.37	I	2	1	prosaposin
98457_at	Slc4a4	0.72	I	0.35	I	-0.62	NC	-0.92	D	2	1	solute carrier family 4 (anion exchanger), member 4
99458_i_at	Mark2	0.28	I	0.46	I	-0.66	D	-0.5	NC	2	1	MAP/microtubule affinity regulating kinase 2
99481_at	Atp1a2	0.86	I	0.45	I	-0.49	NC	-0.82	D	2	1	ATPase, Na+/K+ transporting, alpha 2 polypeptide
99882_at	Ids	-0.75	NC	-1.24	D	0.55	I	-0.19	MI	2	1	iduronate 2-sulfatase
100012_at	Laptm5	0.63	I	0.07	NC	0.34	MI	-0.35	NC	2	0	lysosomal-associated protein transmembrane 5
100068_at	Aldh1a1	0.21	I	0.16	I	-0.42	NC	-0.31	NC	2	0	aldehyde dehydrogenase family 1, subfamily A1

100133_at	Fyn	0.35	I	0.55	I	-0.22	NC	0.06	NC	2	0	Fyn proto-oncogene
100154_at	Tapbp	0.8	I	0.21	I	0.28	NC	-0.19	NC	2	0	TAP binding protein
100380_at	Gm10257	0.06	NC	0.26	I	-0.21	NC	0.02	I	2	0	predicted gene 10257; predicted gene 12657; H3 histone, family 3A; H3 histone, family 3B; H3 histone, family 3C; histone H3.3-like; uncharacterized LOC105242736
100494_at	Fgf1	0.48	NC	-0.23	NC	0.71	I	0.29	I	2	0	fibroblast growth factor 1
100573_f_at	Gpi1	0.35	I	0.41	I	-0.13	NC	-0.05	NC	2	0	glucose phosphate isomerase 1
100727_at	Rpl28	0.36	I	0.6	I	-0.26	NC	-0.02	NC	2	0	ribosomal protein L28
100762_at	Sema6a	2.15	I	-0.09	NC	0.39	MI	-1.7	NC	2	0	sema domain, transmembrane domain (TM), and cytoplasmic domain, (semaphorin) 6A

Gnb1, Gnai2, Dlg4 and Mapk1 are glutamatergic genes. Fyn, Camk2a and Mapk1 are cholinergic genes. Kif5a is Dopaminergic gene. Mice cerebrum stimulated by rTMS for 30days were denoted as M1 and M2, sham control were denoted as C1 and C2. N = 2. All expression ratios were converted into the $\log_2$(expression ratio) values. L1: Signal Log Ratio (M1/C1), L2: Signal Log Ratio (M2/C1), L3: Signal Log Ratio (M1/C2), L4: Signal Log Ratio (M1/C2). C1, C2 were used as a control and M1, M2 were normalized with respect to C1 and C2 to obtain expression ratios. Expression Console (EC) Ver.1.4 and Transcriptome Analysis Console (TAC) Ver.3. were used for Comparison Analysis as manufacture procedure. C means data analysis output for a Comparison Analysis illustrating Change p-values with the associated Increase (I) or Decrease (D) call. Increase calls have Change p-values closer to zero and Decrease calls have Change p-values closer to one. Finally, the Change algorithm assesses probe pair saturation, calculates a Change p-values, and assigns an (I), Marginal Increase (MI), No Change (NC), Marginal Decrease (MD), or (D) call for C. Gene with more than 2 significant difference calls was chosen. Abbreviations; TC ID: Transcript Cluster ID, GS: Gene Symbol, *: Total number of increase, #: Total number of decrease. TC ID is available for Pathway analysis.

Table 2
Gene expression matrix after 30 days rTMS on cerebrum.

TC ID	GS	L1	C	L2	C	L3	C	L4	C	*	#	Description
100774_at	Synj2bp	0.34	I	-0.15	I	-0.28	NC	-0.08	NC	2	0	synaptojanin 2 binding protein
100892_at	Ndufaf1	0.4	NC	0.31	I	0.26	NC	0.29	I	2	0	NADH dehydrogenase (ubiquinone) 1 alpha subcomplex, assembly factor 1
100992_at	Phc1	0.43	I	0.24	I	-0.07	NC	-0.28	NC	2	0	polyhomeotic-like 1 (Drosophila)
101113_at	Rhoa	0.31	I	0.16	MI	0.18	NC	-0.26	NC	2	0	ras homolog gene family, member A
101419_at	Tubb4a	0.35	I	0.51	I	-0.27	NC	-0.01	NC	2	0	tubulin, beta 4 A class IVA
101441_i_at	Itpr2	0.32	I	0.25	MI	-0.18	NC	-0.57	NC	2	0	inositol 1,4,5-triphosphate receptor 2
101467_at	S100b	0.06	NC	0.04	NC	0.53	I	0.44	I	2	0	S100 protein, beta polypeptide, neural
101510_at	Psme1	0.21	NC	0.27	I	0.08	NC	0.19	I	2	0	proteasome (prosome, macropain) activator subunit 1 (PA28 alpha)
101578_f_at	Actb	0.92	I	0.99	I	-0.4	NC	-0.47	NC	2	0	actin, beta
101587_at	Ephx1	0.9	I	0.99	I	-1.13	NC	-1.27	NC	2	0	epoxide hydrolase 1, microsomal
101855_at	Map6	0.3	I	0.15	I	-0.01	NC	-0.35	NC	2	0	microtubule-associated protein 6
101923_at	Pla2g7	0.47	I	0.42	I	-0.08	NC	-0.18	NC	2	0	phospholipase A2, group VII (platelet-activating factor acetylhydrolase, plasma)
101930_at	Nfix	0.63	I	0.34	MI	-0.11	NC	-0.34	NC	2	0	nuclear factor I/X
101960_at	Rtcb	0.24	NC	0.3	I	-0.18	NC	0.04	I	2	0	RNA 2',3'-cyclic phosphate and 5'-OH ligase
102007_at	Hccs	0.02	NC	-0.35	NC	0.41	I	0.48	I	2	0	holocytochrome c synthetase
102033_at	Tesk1	0.42	I	0.4	I	0.09	NC	-0.05	NC	2	0	testis specific protein kinase 1
102063_at	Pdpk1	0.87	I	0.2	I	-0.2	NC	-0.46	NC	2	0	3-phosphoinositide dependent protein kinase 1
102095_f_at	Spock2	0.32	I	0.18	MI	-0.53	NC	-0.73	NC	2	0	sparc/osteonectin, cwcv and kazal-like domains proteoglycan 2
102252_at	Pfdn2	0.42	I	0.24	I	-0.03	NC	-0.14	NC	2	0	prefoldin 2
102271_at	Zmiz2	0.58	I	0.54	I	-0.32	NC	-0.52	NC	2	0	zinc finger, MIZ-type containing 2
102374_at	Rcan3	0.27	NC	-0.03	NC	0.29	I	0.12	I	2	0	regulator of calcineurin 3
102384_at	Smarca2	0.42	I	0.59	I	-0.31	NC	-0.04	NC	2	0	SWI/SNF related, matrix associated, actin dependent regulator of chromatin, subfamily a, member 2
102639_at	Chst2	0.47	I	0.4	I	-0.04	NC	-0.21	NC	2	0	carbohydrate sulfotransferase 2
102691_at	Zfp385a	0.88	I	0.67	I	-0.18	NC	-0.56	NC	2	0	zinc finger protein 385A
102700_at	Tbr1	0.43	I	0.41	I	-0.37	NC	-0.43	NC	2	0	T-box brain gene 1
102752_at	Cyfip1	0.43	I	0.31	I	-0.17	NC	-0.32	NC	2	0	cytoplasmic FMR1 interacting protein 1
102787_at	Adgrg1	0.79	I	0.26	I	0.52	NC	-0.42	NC	2	0	adhesion G protein-coupled receptor G1
102815_at	Anxa11	0.28	I	0.5	I	-0.86	NC	-0.55	NC	2	0	annexin A11; predicted gene 2260; predicted gene 2274
102856_at	Sox10	0.39	I	0.45	I	-0.08	NC	-0.14	NC	2	0	SRY (sex determining region Y)-box 10
102912_at	Tnks2	0.28	I	0.34	I	-0.4	NC	-0.2	NC	2	0	tankyrase, TRF1-interacting ankyrin-related ADP-ribose polymerase 2
102942_at	Specc1	0.3	I	0.28	I	-0.35	NC	-0.43	NC	2	0	sperm antigen with calponin homology and coiled-coil domains 1
103001_at	Vegfb	0.46	MI	0.15	I	-0.13	NC	-0.02	NC	2	0	vascular endothelial growth factor B

103029_at	Pdcd4	0.76	I	0.61	I	-0.17	NC	-0.02	NC	2	0	programmed cell death 4
103040_at	Cd83	0.02	NC	0.43	I	-0.12	NC	0.11	I	2	0	CD83 antigen
103054_at	Polr2a	0.43	I	0.07	NC	0.23	I	-0.06	NC	2	0	polymerase (RNA) II (DNA directed) polypeptide A
103090_at	Uqcc1	-0.41	NC	-0.09	NC	0.21	I	0.33	I	2	0	ubiquinol-cytochrome c reductase complex assembly factor 1
103299_at	Pld4	0.88	I	0.03	NC	1.18	I	0.36	NC	2	0	phospholipase D family, member 4
103300_at	Abcb7	0.64	I	-0.12	NC	0.41	I	-0.48	NC	2	0	ATP-binding cassette, sub-family B (MDR/TAP), member 7
103305_at	Itgb4	0.83	I	2.63	I	0.51	NC	2.83	NC	2	0	integrin beta 4
103369_at	Klf13	0.77	I	0.36	I	-0.36	NC	-0.43	NC	2	0	Kruppel-like factor 13
103370_at	Lin7c	0.35	I	0.27	I	0	NC	-0.21	NC	2	0	lin-7 homolog C (C. elegans)
103404_at	Rere	0.6	I	0.19	I	0.05	NC	-0.15	NC	2	0	arginine glutamic acid dipeptide (RE) repeats
103411_at	Gna11	0.23	NC	0.48	I	0.1	NC	0.13	I	2	0	guanine nucleotide binding protein, alpha 11
103584_at	Cmip	0.32	I	0.46	I	-0.37	NC	-0.37	NC	2	0	c-Maf inducing protein

Actb, Itpr2 and Rho are oxytocin signaling pathway genes. Cyfip1and Itgb4 are actin cytoskeleton regulation genes. Pdpk1 and Pdcd4 are genes of proteoglycans in cancer. Pla2g7 amd Pld4 are ether lipid metabolism genes. Mice cerebrum stimulated by rTMS for 30days were denoted as M1 and M2, sham control were denoted as C1 and C2. N = 2. All expression ratios were converted into the $\log_2$(expression ratio) values. L1: Signal Log Ratio (M1/C1), L2: Signal Log Ratio (M2/C1), L3: Signal Log Ratio (M1/C2), L4: Signal Log Ratio (M1/C2). C1, C2 were used as a control and M1, M2 were normalized with respect to C1 and C2 to obtain expression ratios. Expression Console (EC) Ver.1.4 and Transcriptome Analysis Console (TAC) Ver.3. were used for Comparison Analysis as manufacture procedure. C means data analysis output for a Comparison Analysis illustrating Change p-values with the associated Increase (I) or Decrease (D) call. Increase calls have Change p-values closer to zero and Decrease calls have Change p-values closer to one. Finally, the Change algorithm assesses probe pair saturation, calculates a Change p-values, and assigns an (I), Marginal Increase (MI), No Change (NC), Marginal Decrease (MD), or (D) call for C. Gene with more than 2 significant difference calls was chosen. Abbreviations; TC ID: Transcript Cluster ID, GS: Gene Symbol, *: Total number of increase, #: Total number of decrease. TC ID is available for Pathway analysis.

Table 3
Gene expression matrix after 30 days rTMS on cerebrum.

TC ID	GS	L1	C	L2	C	L3	C	L4	C	*	#	Description
103611_at	Cd47	0.55	I	0.59	I	-0.22	NC	-0.18	NC	2	0	CD47 antigen (Rh-related antigen, integrin-associated signal transducer)
103613_at	Aldoart2	1.82	I	1.52	I	1.42	NC	1.55	NC	2	0	aldolase 1 A, retrogene 2
103624_at	Urm1	0.25	NC	-0.2	NC	0.54	I	0.36	I	2	0	ubiquitin related modifier 1 homolog (S. cerevisiae)
103663_at	Pomgnt1	0.35	I	0.32	I	-0.16	NC	0.07	NC	2	0	protein O-linked mannose beta 1,2-N-acetylglucosaminyltransferase
103682_at	Uri1	-0.04	NC	0.65	I	-0.23	NC	0.27	I	2	0	URI1, prefoldin-like chaperone
103748_at	Cmip	0.78	I	0.34	I	-0.03	NC	-0.27	NC	2	0	c-Maf inducing protein
103771_at	Rnf208	0.48	I	0.17	I	-0.16	NC	-0.32	NC	2	0	ring finger protein 208
104032_at	Mast3	0.6	I	0.36	I	-0.39	NC	-0.51	NC	2	0	microtubule associated serine/threonine kinase 3
104034_at	AI464131	0.63	I	0.66	I	-0.77	NC	-0.4	NC	2	0	expressed sequence AI464131
104214_at	Slc7a8	0.63	I	0.33	I	0.09	NC	0.16	NC	2	0	solute carrier family 7 (cationic amino acid transporter, y+ system).member 8
104244_at	Mark2	0.95	I	0.63	I	-0.35	NC	-0.5	NC	2	0	MAP/microtubule affinity regulating kinase 2
104250_at	Lrrc8a	0.53	I	0.12	I	-0.36	NC	-0.64	NC	2	0	leucine rich repeat containing 8A
104316_at	Gna13	0.64	I	0.59	I	-0.02	NC	-0.01	NC	2	0	guanine nucleotide binding protein, alpha 13
104352_at	Brd4	0.2	MI	0.41	I	-0.37	NC	-0.33	NC	2	0	bromodomain containing 4
104368_at	Mapre3	0.23	MI	0.56	I	-0.22	NC	-0.09	NC	2	0	microtubule-associated protein, RP/EB family, member 3
104380_at	Slc35a1	-0.23	NC	0.34	I	0.02	NC	0.7	I	2	0	solute carrier family 35 (CMP-sialic acid transporter), member 1
104409_at	Grik5	0.49	I	0.37	I	-0.16	NC	-0.25	NC	2	0	glutamate receptor, ionotropic, kainate 5 (gamma 2)
104415_at	Foxp1	0.47	I	0.2	I	-0.12	NC	-0.18	NC	2	0	forkhead box P1
104514_at	Epn1	0.3	I	0.11	I	-0.17	NC	-0.39	NC	2	0	epsin 1
104546_g_at	Csnk2a1	1.1	I	-0.1	NC	0.97	I	0.13	NC	2	0	casein kinase 2, alpha 1 polypeptide; predicted pseudogene 10031
104634_at	Lims1	0.49	NC	0.73	I	-0.16	NC	0.5	I	2	0	LIM and senescent cell antigen-like domains 1
104650_at	Ache	0.48	I	0.38	I	0.19	NC	-0.12	NC	2	0	acetylcholinesterase
104725_at	Rhoq	0.81	I	0.61	I	0.37	NC	0.02	NC	2	0	ras homolog gene family, member Q
104739_at	Tcta	0.18	NC	-0.34	NC	0.66	I	0.31	I	2	0	T cell leukemia translocation altered gene
104741_at	Zdhhc9	0.8	I	0.14	I	0.75	NC	-0.1	NC	2	0	zinc finger, DHHC domain containing 9
104747_at	Slc1a1	0.42	I	0.44	I	-0.28	NC	-0.35	NC	2	0	solute carrier family 1 (neuronal/epithelial high affinity glutamate transporter, system Xag), member 1
160111_at	Eif1ax	-0.38	NC	-0.47	NC	0.48	I	0.31	I	2	0	eukaryotic translation initiation factor 1A, X-linked
160181_at	Syp	0.37	I	0.45	I	-0.43	NC	-0.42	NC	2	0	synaptophysin
160184_at	Ergic1	0.75	I	0.12	NC	0.75	I	-0.22	NC	2	0	endoplasmic reticulum-golgi intermediate compartment (ERGIC) 1
160190_at	Syt4	0.5	I	0.68	I	-0.09	NC	-0.01	NC	2	0	synaptotagmin IV
160196_at	Smap1	0.37	I	0.42	I	-0.59	NC	-0.48	NC	2	0	small ArfGAP 1
160272_at	Cbx3	0.55	I	0.55	I	-0.41	NC	-0.13	NC	2	0	chromobox 3
160414_at	Slc38a10	0.42	I	-0.17	NC	0.28	I	-0.26	NC	2	0	solute carrier family 38, member 10
160417_at	Kif5b	0.34	I	0.7	I	-0.23	NC	0.08	NC	2	0	kinesin family member 5B

160502_at	Creg1	-0.03	NC	-0.22	NC	0.52	MI	0.14	I	2	0	cellular repressor of E1A-stimulated genes 1
160614_at	Pten	0.6	I	0.39	I	-0.13	NC	-0.36	NC	2	0	phosphatase and tensin homolog
160667_at	Evl	0.58	I	0.56	I	-0.2	NC	-0.34	NC	2	0	Ena-vasodilator stimulated phosphoprotein
160743_at	Pole3	0.41	I	-0.13	NC	0.15	I	-0.44	NC	2	0	polymerase (DNA directed), epsilon 3 (p17 subunit)
160754_at	Pygm	0.66	I	0.83	I	-0.34	NC	-0.1	NC	2	0	muscle glycogen phosphorylase
160942_at	Cbx6	0.63	I	0.23	I	-0.06	NC	-0.36	NC	2	0	chromobox 6
161015_at	Clvs1	0.11	NC	0.7	I	-0.06	NC	0.71	I	2	0	clavesin 1
161054_at	Spock1	0.62	I	0.44	I	-0.13	NC	-0.05	NC	2	0	sparc/osteonectin, cwcv and kazal-like domains proteoglycan 1
161057_at	Actr10	0.35	I	0.33	I	-0.36	NC	-0.41	NC	2	0	ARP10 actin-related protein 10

Ache is Cholinergic gene. Grik5 and Slc1a1 are Glutamatergic gene. Mice cerebrum stimulated by rTMS for 30days were denoted as M1 and M2, sham control were denoted as C1 and C2. N=2. All expression ratios were converted into the $\log_2$(expression ratio) values. L1: Signal Log Ratio (M1/C1), L2: Signal Log Ratio (M2/C1), L3: Signal Log Ratio (M1/C2), L4: Signal Log Ratio (M1/C2). C1, C2 were used as a control and M1, M2 were normalized with respect to C1 and C2 to obtain expression ratios. Expression Console (EC) Ver.1.4 and Transcriptome Analysis Console (TAC) Ver.3. were used for Comparison Analysis as manufacture procedure. C means data analysis output for a Comparison Analysis illustrating Change p-values with the associated Increase (I) or Decrease (D) call. Increase calls have Change p-values closer to zero and Decrease calls have Change p-values closer to one. Finally, the Change algorithm assesses probe pair saturation, calculates a Change p-values, and assigns an (I), Marginal Increase (MI), No Change (NC), Marginal Decrease (MD), or (D) call for C. Gene with more than 2 significant difference calls was chosen. Abbreviations; TC ID: Transcript Cluster ID, GS: Gene Symbol, *: Total number of increase, #: Total number of decrease. TC ID is available for Pathway analysis.

Table 4
Gene expression matrix after 30 days rTMS on cerebrum.

TC ID	GS	L1	C	L2	C	L3	C	L4	C	*	#	Description
161070_at	Spred2	0.28	I	0.38	I	-0.74	NC	-0.5	NC	2	0	sprouty-related, EVH1 domain containing 2
161167_r_at	Uck1	2.05	I	-0.84	NC	2.47	I	-0.66	NC	2	0	uridine-cytidine kinase 1
161371_r_at	Ptprk	1.29	NC	1.29	NC	3.1	I	2.98	I	2	0	protein tyrosine phosphatase, receptor type, K
161819_f_at	Laptm5	0.73	I	0.48	I	-0.11	NC	-0.05	NC	2	0	lysosomal-associated protein transmembrane 5
162134_r_at	2010111I01Rik	0.47	I	-0.14	NC	0.47	I	-0.47	NC	2	0	RIKEN cDNA 2010111I01 gene
162182_f_at	Kcnab2	0.54	I	0.17	I	-0.22	NC	-0.73	NC	2	0	potassium voltage-gated channel, shaker-related subfamily, beta member 2
162332_f_at	Mapre3	0.9	I	1.08	I	0.08	NC	-0.03	NC	2	0	microtubule-associated protein, RP/EB family, member 3
162499_f_at	Ube2d2a	0.48	I	0.38	I	-0.17	NC	-0.17	NC	2	0	ubiquitin-conjugating enzyme E2D 2A
92180_at	H1fx	0.42	I	0.37	I	-0.38	NC	-0.51	NC	2	0	H1 histone family, member X
92196_f_at	Sf3a2	0.37	I	0.29	I	-0.16	NC	-0.27	NC	2	0	splicing factor 3a, subunit 2
92202_g_at	Zbtb16	0.72	I	0.66	I	-0.61	NC	-0.73	NC	2	0	zinc finger and BTB domain containing 16
92227_s_at	Ctnna2	0.08	NC	0.36	I	-0.25	NC	-0.01	I	2	0	catenin (cadherin associated protein), alpha 2
92241_at	Nfic	0.68	I	0.88	I	-0.58	NC	-0.43	NC	2	0	nuclear factor I/C
92247_at	Arhgap5	0.6	I	-0.02	NC	0.31	MI	-0.43	NC	2	0	Rho GTPase activating protein 5
92350_at	Mapre1	0.82	I	0.42	I	0.09	NC	-0.44	NC	2	0	microtubule-associated protein, RP/EB family, member 1
92379_f_at	Ptprz1	0.27	MI	0.49	I	-0.55	NC	-0.2	NC	2	0	protein tyrosine phosphatase, receptor type Z, polypeptide 1
92397_at	Agap1	0.52	I	0.2	I	0.06	NC	-0.46	NC	2	0	ArfGAP with GTPase domain, ankyrin repeat and PH domain 1
92411_at	Hs1bp3	0.44	I	0.12	I	0.3	NC	-0.02	NC	2	0	HCLS1 binding protein 3
92426_at	Tspan5	0.33	I	0	NC	0.33	I	-0.14	NC	2	0	tetraspanin 5
92484_at	Hivep2	0.5	I	-0.2	NC	0.36	I	-0.45	NC	2	0	human immunodeficiency virus type I enhancer binding protein 2
92525_i_at	Nacc2	0.33	I	0.82	I	-0.03	NC	0.4	NC	2	0	nucleus accumbens associated 2, BEN and BTB (POZ) domain containing
92528_at	Adgrb1	0.37	I	0.17	I	-0.43	NC	-0.55	NC	2	0	adhesion G protein-coupled receptor B1
92586_at	Glud1	0.36	NC	0.39	I	-0.13	NC	0.24	I	2	0	glutamate dehydrogenase 1
92621_at	Pcbp2	0.43	I	0.09	I	-0.08	NC	-0.49	NC	2	0	poly(rC) binding protein 2
92659_at	Rapgef4	-0.28	NC	-0.73	NC	0.98	I	0.66	I	2	0	Rap guanine nucleotide exchange factor (GEF) 4
92678_at	Ddx25	0.22	NC	-0.07	NC	0.17	I	0.12	I	2	0	DEAD (Asp-Glu-Ala-Asp) box polypeptide 25
92795_at	Map4	0.56	I	0.5	I	-0.07	NC	-0.28	NC	2	0	microtubule-associated protein 4
92817_at	Imp3	-0.22	NC	-0.46	NC	0.23	I	-0.03	MI	2	0	IMP3, U3 small nucleolar ribonucleoprotein, homolog (yeast)
92820_at	Usp2	0.64	I	0.54	I	-0.28	NC	-0.34	NC	2	0	ubiquitin specific peptidase 2
92821_at	Usp2	0.42	I	0.29	I	-0.25	NC	-0.27	NC	2	0	ubiquitin specific peptidase 2
92838_at	Fscn1	0.73	I	0.2	NC	0.35	I	-0.16	NC	2	0	fascin homolog 1, actin bundling protein (Strongylocentrotus purpuratus)
92871_at	Sel1l	0.79	I	0.4	I	-0.19	NC	-0.36	NC	2	0	sel-1 suppressor of lin-12-like (C. elegans)
92927_at	Etv1	0.66	I	0.27	NC	0.49	I	0.26	NC	2	0	ets variant 1
92949_at	Pacsin1	0.31	I	0.33	I	-0.23	NC	-0.29	NC	2	0	protein kinase C and casein kinase substrate in neurons 1

92958_at	Foxo3	0.43	I	0.11	I	-0.44	NC	-0.54	NC	2	0	forkhead box O3
93006_at	Nfic	0.33	I	0.35	MI	-0.39	NC	-0.58	NC	2	0	nuclear factor I/C
93047_at	Nup50	0.48	I	-0.61	NC	0.81	I	-0.38	NC	2	0	nucleoporin 50
93055_at	Ankrd46	-0.16	NC	-0.14	NC	0.28	I	0.28	I	2	0	ankyrin repeat domain 46
93058_at	Eif1a	0.02	NC	0.35	I	-0.04	NC	0.26	I	2	0	eukaryotic translation initiation factor 1A
93069_at	Ube2d2a	0.04	NC	0.41	I	-0.04	NC	0.2	I	2	0	ubiquitin-conjugating enzyme E2D 2A
93129_at	Cux2	0.51	I	0.43	I	0	NC	-0.28	NC	2	0	cut-like homeobox 2
93147_f_at	Celf4	0.43	I	0.23	I	-0.2	NC	-0.39	NC	2	0	CUGBP, Elav-like family member 4
93246_at	Naa15	0.22	I	0.55	I	-0.27	NC	-0.35	NC	2	0	N(alpha)-acetyltransferase 15, NatA auxiliary subunit
93284_at	Cirbp	-0.27	NC	0.42	I	-0.02	NC	0.54	I	2	0	cold inducible RNA binding protein
93288_at	Arpc2	0.23	MI	0.44	I	-0.31	NC	-0.01	NC	2	0	actin related protein 2/3 complex, subunit 2

Kcnab2 and Pacsin1 are Synaptosome genes. Rapgef4, Arhgap5 and Ctnna2 are Leukocyte transendothelial migration genes. Mice cerebrum stimulated by rTMS for 30days were denoted as M1 and M2, sham control were denoted as C1 and C2. N=2. All expression ratios were converted into the $\log_2$(expression ratio) values. L1: Signal Log Ratio (M1/C1), L2: Signal Log Ratio (M2/C1), L3: Signal Log Ratio (M1/C2), L4: Signal Log Ratio (M1/C2). C1, C2 were used as a control and M1, M2 were normalized with respect to C1 and C2 to obtain expression ratios. Expression Console (EC) Ver.1.4 and Transcriptome Analysis Console (TAC) Ver.3. were used for Comparison Analysis as manufacture procedure. C means data analysis output for a Comparison Analysis illustrating Change p-values with the associated Increase (I) or Decrease (D) call. Increase calls have Change p-values closer to zero and Decrease calls have Change p-values closer to one. Finally, the Change algorithm assesses probe pair saturation, calculates a Change p-values, and assigns an (I), Marginal Increase (MI), No Change (NC), Marginal Decrease (MD), or (D) call for C. Gene with more than 2 significant difference calls was chosen. Abbreviations; TC ID: Transcript Cluster ID, GS: Gene Symbol, *: Total number of increase, #: Total number of decrease. TC ID is available for Pathway analysis.

Table 5
Gene expression matrix after 30 days rTMS on cerebrum.

TC ID	GS	L1	C	L2	C	L3	C	L4	C	*	#	Description
93374_at	Jph3	0.44	I	0.38	I	-0.25	NC	-0.17	NC	2	0	junctophilin 3
93382_at	Pde1b	0.61	I	0.29	I	0.04	NC	-0.27	NC	2	0	phosphodiesterase 1B, Ca2+-calmodulin dependent
93423_at	Ldoc1l	0.51	I	0.31	I	0.21	NC	-0.14	NC	2	0	leucine zipper, down-regulated in cancer 1-like
93548_at	Sec. 61b	-0.12	NC	-0.3	NC	0.29	I	0.11	I	2	0	Sec. 61 beta subunit
93645_at	Rgs7	-0.02	NC	0.53	I	-0.03	NC	0.45	I	2	0	regulator of G protein signaling 7
93659_at	Camk2a	1.66	I	-0.95	NC	1.5	I	-0.55	NC	2	0	calcium/calmodulin-dependent protein kinase II alpha
93664_at	Atp1b2	0.78	I	-0.28	NC	0.76	I	-0.15	NC	2	0	ATPase, Na+/K+ transporting, beta 2 polypeptide
93720_at	Agpat1	0.27	MI	-0.71	NC	0.51	I	-0.23	NC	2	0	1-acylglycerol-3-phosphate O-acyltransferase 1 (lysophosphatidic acid acyltransferase, alpha)
93793_at	Lasp1	0.43	I	0.28	I	-0.14	NC	-0.24	NC	2	0	LIM and SH3 protein 1
93852_at	Mef2a	0.2	I	0.25	I	-0.04	NC	-0.12	NC	2	0	myocyte enhancer factor 2A
93861_f_at	LOC105247328	0.29	I	-0.33	NC	0.56	I	-0.05	NC	2	0	MLV-related proviral Env polyprotein-like
93964_s_at	Ddx6	0.81	I	0.36	I	0.14	NC	-0.46	NC	2	0	DEAD (Asp-Glu-Ala-Asp) box polypeptide 6
93965_r_at	Ddx6	0.88	I	0.59	I	0.23	NC	-0.17	NC	2	0	DEAD (Asp-Glu-Ala-Asp) box polypeptide 6
93994_at	Chpt1	0.4	I	0.27	I	0.15	NC	0.16	NC	2	0	choline phosphotransferase 1
94057_g_at	Scd1	0.32	I	0.43	I	-0.12	NC	-0.03	NC	2	0	stearoyl-Coenzyme A desaturase 1
94077_f_at	Rpn2	0.49	MI	0.29	I	-0.13	NC	-0.27	NC	2	0	ribophorin II
94194_s_at	Hcn2	0.84	I	0.33	I	-0.23	NC	-0.61	NC	2	0	hyperpolarization-activated, cyclic nucleotide-gated K+ 2
94218_at	Tcp1	0.27	I	0.49	I	-0.05	NC	0.35	NC	2	0	t-complex protein 1
94245_at	Vimp	0.08	NC	0.26	I	0.04	NC	0.09	I	2	0	VCP-interacting membrane protein
94257_at	Rraga	0.08	NC	-0.07	NC	0.47	I	0.17	I	2	0	Ras-related GTP binding A
94335_r_at	Ina	0.45	I	0.14	I	-0.25	NC	-0.63	NC	2	0	internexin neuronal intermediate filament protein, alpha
94336_at	Otub1	0.76	I	0.43	I	0	NC	-0.55	NC	2	0	OTU domain, ubiquitin aldehyde binding 1
94353_at	Eif4ebp2	1.04	MI	-0.37	NC	0.4	I	-0.98	NC	2	0	eukaryotic translation initiation factor 4E binding protein 2
94374_at	Wdr13	0.13	NC	0.03	MI	0.06	NC	0.09	MI	2	0	WD repeat domain 13
94456_at	Set	-0.13	NC	0.77	I	-0.14	NC	0.79	I	2	0	SET nuclear oncogene
94819_f_at	Ccni	0.3	I	0.28	I	-0.4	NC	-0.28	NC	2	0	cyclin I
94832_at	Hnrnph2	0.45	NC	0.95	I	0.21	NC	0.83	I	2	0	heterogeneous nuclear ribonucleoprotein H2
94876_f_at	Gorasp2	0.29	I	0.27	I	-0.35	NC	-0.5	NC	2	0	golgi reassembly stacking protein 2
94986_at	Gng3	0.34	I	0.27	I	-0.13	NC	-0.17	NC	2	0	guanine nucleotide binding protein (G protein), gamma 3
95010_at	Traf3	0.29	I	-0.08	NC	0.31	I	-0.02	NC	2	0	TNF receptor-associated factor 3
95159_at	Gm13552	0.1	NC	0.35	I	-0.15	NC	0.22	I	2	0	predicted gene 13552; mitochondrial ribosomal protein S18B
95397_at	D430019H16Rik	0.45	I	0.28	I	0.04	NC	-0.3	NC	2	0	RIKEN cDNA D430019H16 gene
95432_f_at	Tomm70a	0.01	NC	0.35	I	-0.32	NC	0.13	MI	2	0	translocase of outer mitochondrial membrane 70 homolog A (yeast)
95447_at	Mdp1	-0.4	NC	-0.23	NC	0.43	MI	0.41	I	2	0	magnesium-dependent phosphatase 1
95468_at	Egln1	0.4	I	0.11	NC	0.26	I	0.1	NC	2	0	egl-9 family hypoxia-inducible factor 1
95530_at	Gtf2a1	0.13	NC	-0.1	NC	0.29	I	0.13	I	2	0	general transcription factor II A, 1

95721_at	Mapkapk2	0.36	I	-0.21	NC	0.6	I	-0.02	NC	2	0	MAP kinase-activated protein kinase 2
95883_at	Jade1	0.25	MI	0.54	I	-0.54	NC	-0.14	NC	2	0	jade family PHD finger 1
95927_f_at		0.55	MI	0.65	I	-0.2	NC	-0.14	NC	2	0	
96007_at	Ssr3	-0.12	NC	-0.3	NC	0.24	I	0.16	I	2	0	signal sequence receptor, gamma
96056_at	Rhoc	0.57	I	-0.23	NC	0.46	I	-0.12	NC	2	0	ras homolog gene family, member C
96065_at	Lxn	0.55	I	0.73	I	-0.43	NC	0.12	NC	2	0	latexin
96088_at	Ndrg2	0.44	I	0.48	I	-0.28	NC	-0.34	NC	2	0	N-myc downstream regulated gene 2
96102_i_at	Rad23b	-0.07	NC	0.26	I	-0.26	NC	0.12	I	2	0	RAD23b homolog (S. cerevisiae)
96186_at	Lrp10	0.58	I	-0.1	NC	0.42	I	-0.28	NC	2	0	low-density lipoprotein receptor-related protein 10

Rad23b, Sec. 61b, Vimp, Rpn2 and Ssr3 are genes of protein processing in endoplasmic reticulum. Atp1b2 and Camk2a are cAMP signaling pathway genes. Mice cerebrum stimulated by rTMS for 30days were denoted as M1 and M2, sham control were denoted as C1 and C2. N=2. All expression ratios were converted into the $\log_2$(expression ratio) values. L1: Signal Log Ratio (M1/C1), L2: Signal Log Ratio (M2/C1), L3: Signal Log Ratio (M1/C2), L4: Signal Log Ratio (M1/C2). C1, C2 were used as a control and M1, M2 were normalized with respect to C1 and C2 to obtain expression ratios. Expression Console (EC) Ver.1.4 and Transcriptome Analysis Console (TAC) Ver.3. were used for Comparison Analysis as manufacture procedure. C means data analysis output for a Comparison Analysis illustrating Change p-values with the associated Increase (I) or Decrease (D) call. Increase calls have Change p-values closer to zero and Decrease calls have Change p-values closer to one. Finally, the Change algorithm assesses probe pair saturation, calculates a Change p-values, and assigns an (I), Marginal Increase (MI), No Change (NC), Marginal Decrease (MD), or (D) call for C. Gene with more than 2 significant difference calls was chosen. Abbreviations; TC ID: Transcript Cluster ID, GS: Gene Symbol, *: Total number of increase, #: Total number of decrease. TC ID is available for Pathway analysis.

Table 6
Gene expression matrix after 30 days rTMS on cerebrum.

TC ID	GS	L1	C	L2	C	L3	C	L4	C	*	#	Description
96191_at	Arfgef1	0.59	I	0.17	I	0.24	NC	-0.28	NC	2	0	ADP-ribosylation factor guanine nucleotide-exchange factor 1 (brefeldin A-inhibited)
96211_at	Dpp8	0.38	I	-0.08	NC	0.23	MI	-0.23	NC	2	0	dipeptidylpeptidase 8
96255_at	Bnip3l	-0.01	NC	0.37	I	-0.09	NC	0.15	I	2	0	BCL2/adenovirus E1B interacting protein 3-like
96313_at	Rasgrf1	0.71	I	0.76	I	-0.25	NC	-0.19	NC	2	0	RAS protein-specific guanine nucleotide-releasing factor 1
96360_at	Arhgdia	0.33	I	0.13	I	-0.02	NC	-0.17	NC	2	0	Rho GDP dissociation inhibitor (GDI) alpha
96518_at	Wwc1	0.33	I	0.31	I	-0.34	NC	-0.5	NC	2	0	WW, C2 and coiled-coil domain containing 1
96593_at	Elk1	0.74	I	-0.53	NC	1.15	I	0.06	NC	2	0	ELK1, member of ETS oncogene family
96674_at	Tnpo3	-0.17	NC	0.57	I	-0.38	NC	0.14	I	2	0	transportin 3
96725_at	Cic	0.81	I	0.27	I	0.12	NC	-0.54	NC	2	0	capicua homolog (Drosophila)
96731_at	Ddx6	0.39	I	0.38	I	-0.09	NC	-0.34	NC	2	0	DEAD (Asp-Glu-Ala-Asp) box polypeptide 6
96741_at	Phf12	0.46	I	0.48	I	-0.46	NC	-0.17	NC	2	0	PHD finger protein 12
96784_at	Anln	-0.27	NC	-0.1	NC	0.7	I	0.32	I	2	0	anillin, actin binding protein
96811_at	Rab31	-0.01	NC	0.01	NC	0.16	I	0.04	I	2	0	RAB31, member RAS oncogene family
96813_f_at	Otud5	0.35	I	0.53	I	-0.33	NC	-0.1	NC	2	0	OTU domain containing 5
96884_at	Carhsp1	-0.1	NC	0.06	NC	0.49	I	0.51	I	2	0	calcium regulated heat stable protein 1
96920_at	Htra1	0.68	I	0.29	I	-0.24	NC	-0.62	NC	2	0	HtrA serine peptidase 1
96955_at	Atp6v0e2	0.04	NC	0.03	NC	0.17	I	-0.01	I	2	0	ATPase, H+ transporting, lysosomal V0 subunit E2
97210_at	1700037H04Rik	0.76	I	-0.13	NC	0.32	I	-0.16	NC	2	0	RIKEN cDNA 1700037H04 gene
97243_at	Slc9a3r1	0.51	I	0.39	I	-0.18	NC	-0.36	NC	2	0	solute carrier family 9 (sodium/hydrogen exchanger), member 3 regulator 1
97365_at	Coro2b	0.46	I	0.26	I	-0.17	NC	-0.36	NC	2	0	coronin, actin binding protein, 2B
97450_s_at	Aldh7a1	0.46	I	-0.07	NC	0.42	I	-0.22	NC	2	0	aldehyde dehydrogenase family 7, member A1
97487_at	Serpine2	0.32	NC	0.29	I	0.05	NC	0.1	I	2	0	serine (or cysteine) peptidase inhibitor, clade E, member 2
97530_at	Ube2i	0.01	NC	0.18	NC	0.33	I	0.36	I	2	0	ubiquitin-conjugating enzyme E2I
97536_at	Wdtc1	0.68	I	0.03	I	-0.03	NC	-0.49	NC	2	0	WD and tetratricopeptide repeats 1
97740_at	Dusp16	0.46	NC	0.53	I	0.46	NC	0.69	MI	2	0	dual specificity phosphatase 16
97770_s_at	Fam3c	0.53	I	0.63	I	-0.43	NC	-0.49	NC	2	0	family with sequence similarity 3, member C
97776_at	Drd2	0.75	I	1.11	I	0.1	NC	0.27	NC	2	0	dopamine receptor D2
97794_at	Sema7a	2.38	I	-0.83	NC	4.45	I	0.15	NC	2	0	sema domain, immunoglobulin domain (Ig), and GPI membrane anchor, (semaphorin) 7A
97841_at	Chmp2a	0.05	NC	0.37	I	-0.18	NC	0.28	I	2	0	charged multivesicular body protein 2A
97974_at	Zfpm1	0.72	I	0.2	I	0.12	NC	-0.54	NC	2	0	zinc finger protein, multitype 1
97998_at	Atn1	0.7	I	0.44	I	0.19	NC	-0.03	NC	2	0	atrophin 1
98004_at	Pkia	0.11	NC	-0.53	NC	1.12	I	0.31	I	2	0	protein kinase inhibitor, alpha
98011_at	Gabbr1	0.24	I	0.3	I	-0.21	NC	-0.23	NC	2	0	gamma-aminobutyric acid (GABA) B receptor, 1
98026_g_at	Evi2a	-0.31	NC	-0.24	NC	0.28	I	0.6	I	2	0	ecotropic viral integration site 2a

98073_at	Cux1	0.46	I	0.27	I	0.24	NC	-0.05	NC	2	0	cut-like homeobox 1
98114_at	Npc1	0.49	I	0.38	I	-0.11	NC	-0.24	NC	2	0	Niemann-Pick type C1
98127_at	Capza2	0.09	NC	0.5	I	-0.11	NC	0.22	I	2	0	capping protein (actin filament) muscle Z-line, alpha 2
98129_at	Tmsb10	0.35	I	0.25	MI	-0.41	NC	-0.72	NC	2	0	thymosin, beta 10
98141_at	Eif5b	0.34	I	0.43	I	-0.58	NC	-0.29	NC	2	0	eukaryotic translation initiation factor 5B
98150_at	Rab11b	0.27	I	0.19	I	-0.23	NC	-0.31	NC	2	0	RAB11B, member RAS oncogene family
98169_s_at	Fzd3	0.39	I	-0.49	NC	0.46	I	-0.41	NC	2	0	frizzled homolog 3 (Drosophila)
98454_at	Palm	0.4	I	0.14	MI	0	NC	-0.25	NC	2	0	paralemmin
98477_s_at	Ank3	0.57	I	0.29	I	-0.29	NC	-0.51	NC	2	0	ankyrin 3, epithelial

Arfgef1, Rab31, Rab11b, Capza2, and Chmp2a are genes of endocytosis. Mice cerebrum stimulated by rTMS for 30days were denoted as M1 and M2, sham control were denoted as C1 and C2. N=2. All expression ratios were converted into the $\log_2$(expression ratio) values. L1: Signal Log Ratio (M1/C1), L2: Signal Log Ratio (M2/C1), L3: Signal Log Ratio (M1/C2), L4: Signal Log Ratio (M1/C2). C1, C2 were used as a control and M1, M2 were normalized with respect to C1 and C2 to obtain expression ratios. Expression Console (EC) Ver.1.4 and Transcriptome Analysis Console (TAC) Ver.3. were used for Comparison Analysis as manufacture procedure. C means data analysis output for a Comparison Analysis illustrating Change p-values with the associated Increase (I) or Decrease (D) call. Increase calls have Change p-values closer to zero and Decrease calls have Change p-values closer to one. Finally, the Change algorithm assesses probe pair saturation, calculates a Change p-values, and assigns an (I), Marginal Increase (MI), No Change (NC), Marginal Decrease (MD), or (D) call for C. Gene with more than 2 significant difference calls was chosen. Abbreviations; TC ID: Transcript Cluster ID, GS: Gene Symbol, *: Total number of increase, #: Total number of decrease. TC ID is available for Pathway analysis.

Table 7
Gene expression matrix after 30 days rTMS on cerebrum.

TC ID	GS	L1	C	L2	C	L3	C	L4	C	*	#	Description
98543_at	Ctss	-0.18	NC	0.3	I	-0.03	NC	0.25	I	2	0	cathepsin S
98550_at	Set	-0.1	NC	0.46	I	-0.25	NC	0.09	I	2	0	SET nuclear oncogene
98564_f_at	Gm6654	0.39	I	0.47	I	-0.29	NC	-0.2	NC	2	0	predicted pseudogene 6654; 40S ribosomal protein S26-like; ribosomal protein S26
98588_at	Fah	-0.15	NC	-0.21	NC	0.21	I	0.58	I	2	0	fumarylacetoacetate hydrolase
98590_at	Sdc4	0.69	I	0.12	I	-0.42	NC	-0.76	NC	2	0	syndecan 4
98602_at	Rangap1	0.5	I	0.27	I	0.09	NC	-0.01	NC	2	0	RAN GTPase activating protein 1
98616_f_at	Myh7	0.64	I	0.16	I	-0.43	NC	-1.01	NC	2	0	myosin, heavy polypeptide 7, cardiac muscle, beta
98827_i_at	Kif5a	0.24	NC	-1.04	NC	1.74	I	0.33	I	2	0	kinesin family member 5 A
98866_at	Dlx6	0.92	I	1.99	I	0.7	NC	2.14	NC	2	0	distal-less homeobox 6
98925_at	Vamp2	0.91	I	0.33	NC	0.76	I	0.19	NC	2	0	vesicle-associated membrane protein 2
98993_at	Ppp2r5c	0.23	MI	0.35	I	0.08	NC	0.02	NC	2	0	protein phosphatase 2, regulatory subunit B', gamma
99023_at	Pafah1b2	-0.09	NC	-0.42	NC	0.66	I	0.26	I	2	0	platelet-activating factor acetylhydrolase, isoform 1b, subunit 2
99045_at	Eno2	0.36	I	0.34	I	-0.38	NC	-0.49	NC	2	0	enolase 2, gamma neuronal
99085_at	Usp3	0.41	NC	0.22	NC	0.65	I	0.4	I	2	0	ubiquitin specific peptidase 3
99378_f_at	H2-Q4	-0.42	NC	-0.42	NC	0.61	MI	0.53	I	2	0	histocompatibility 2, Q region locus 4
99451_at	Fam102a	0.36	I	0.16	NC	0.62	I	0.11	NC	2	0	family with sequence similarity 102, member A
99465_at	Mecp2	0.69	I	0.59	I	0.08	NC	-0.04	NC	2	0	methyl CpG binding protein 2
99504_at	St8sia3	0.38	I	0.2	MI	-0.22	NC	-0.3	NC	2	0	ST8 alpha-N-acetyl-neuraminide alpha-2,8-sialyltransferase 3
99537_at	Ruvbl1	0.03	NC	-0.28	NC	0.48	I	0.1	I	2	0	RuvB-like protein 1
99575_at	Ubqln1	0.52	NC	-0.16	NC	0.6	I	0.13	I	2	0	ubiquilin 1
99597_at	Gnai2	0.45	I	0.23	MI	-0.11	NC	-0.34	NC	2	0	guanine nucleotide binding protein (G protein), alpha inhibiting 2
99666_at	Cs	0.39	I	0.14	I	0.06	NC	-0.21	NC	2	0	citrate synthase
99893_at	Fgf13	0.07	NC	-0.57	NC	0.87	I	0.05	I	2	0	fibroblast growth factor 13

Gnai2, Kif5a and Ppp2r5c are dopaminergic synapse genes. Gnai2, Myh7 and Ppp2r5c are genes of adrenergic signaling in cardiomyocytes. Mice cerebrum stimulated by rTMS for 30days were denoted as M1 and M2, sham control were denoted as C1 and C2. N=2. All expression ratios were converted into the $\log_2$(expression ratio) values. L1: Signal Log Ratio (M1/C1), L2: Signal Log Ratio (M2/C1), L3: Signal Log Ratio (M1/C2), L4: Signal Log Ratio (M1/C2). C1, C2 were used as a control and M1, M2 were normalized with respect to C1 and C2 to obtain expression ratios. Expression Console (EC) Ver.1.4 and Transcriptome Analysis Console (TAC) Ver.3. were used for Comparison Analysis as manufacture procedure. C means data analysis output for a Comparison Analysis illustrating Change p-values with the associated Increase (I) or Decrease (D) call. Increase calls have Change p-values closer to zero and Decrease calls have Change p-values closer to one. Finally, the Change algorithm assesses probe pair saturation, calculates a Change p-values, and assigns an (I), Marginal Increase (MI), No Change (NC), Marginal Decrease (MD), or (D) call for C. Gene with more than 2 significant difference calls was chosen. Abbreviations; TC ID: Transcript Cluster ID, GS: Gene Symbol, *: Total number of increase, #: Total number of decrease. TC ID is available for Pathway analysis.

Table 8
Gene expression matrix after 30 days rTMS on cerebrum.

TC ID	GS	L1	C	L2	C	L3	C	L4	C	*	#	Description
102362_i_at	Junb	-2.26	D	-1.89	D	-1.91	D	-1.6	D	0	4	jun B proto-oncogene
102371_at	Nr4a1	-1.99	D	-1.81	D	-1.8	D	-1.72	D	0	4	nuclear receptor subfamily 4, group A, member 1
102661_at	Egr2	-1.29	D	-1.33	D	-1.7	D	-1.69	D	0	4	early growth response 2
102870_at	Dynlt1a	-0.68	D	-1.04	D	-0.62	D	-0.91	D	0	4	dynein light chain Tctex-type 1A
104598_at	Dusp1	-1.41	D	-1.38	D	-1.51	D	-1.49	D	0	4	dual specificity phosphatase 1
160172_at	Meg3	-1.61	D	-1.73	D	-0.68	D	-0.89	D	0	4	maternally expressed 3
160173_at	Meg3	-0.91	D	-1.31	D	-0.79	D	-1.15	D	0	4	maternally expressed 3
160901_at	Fos	-2.14	D	-2.01	D	-2.08	D	-1.95	D	0	4	FBJ osteosarcoma oncogene
160970_at	Odf2	-0.95	D	-1.24	D	-1.31	D	-1.54	D	0	4	outer dense fiber of sperm tails 2
161666_f_at	Gadd45b	-0.98	D	-0.99	D	-1.63	D	-1.51	D	0	4	growth arrest and DNA-damage-inducible 45 beta
96302_at	Srsf7	-0.83	D	-0.73	D	-0.82	D	-0.74	MD	0	4	serine/arginine-rich splicing factor 7
97752_at	Snhg11	-1.12	D	-0.63	D	-1.24	D	-0.71	D	0	4	small nucleolar RNA host gene 11
97890_at	Sgk1	-0.8	D	-1.04	D	-1.3	D	-1.59	D	0	4	serum/glucocorticoid regulated kinase 1
99109_at	Ier2	-0.92	D	-1.48	D	-0.87	D	-1.29	D	0	4	immediate early response 2
101058_at	Amy1	-1.11	D	-0.83	D	-1.08	MD	-0.81	NC	0	3	amylase 1, salivary
101583_at	Btg2	-0.58	D	-1.06	D	-0.6	NC	-1.04	D	0	3	B cell translocation gene 2, anti-proliferative
104410_at	Midn	-0.72	D	-0.23	NC	-1.07	D	-0.77	MD	0	3	midnolin
104639_i_at	Taf1d	-1.01	D	-0.74	D	-0.55	D	-0.63	NC	0	3	TATA box binding protein (Tbp)-associated factor, RNA polymerase I, D
160487_at	Myl4	-0.35	MD	-0.38	NC	-1.02	D	-0.96	D	0	3	myosin, light polypeptide 4
92424_at	Zfp692	-0.86	D	-0.94	D	-0.42	NC	-0.9	D	0	3	zinc finger protein 692
92542_at	Rsrp1	-1.25	D	-0.75	D	-0.96	D	-0.52	NC	0	3	arginine/serine rich protein 1
93411_at	Sema7a	-0.51	D	-0.1	NC	-1.37	D	-0.75	D	0	3	sema domain, immunoglobulin domain (Ig), and GPI membrane anchor, (semaphorin) 7A
93619_at	Per1	-0.9	D	-0.3	NC	-1.01	D	-0.8	D	0	3	period circadian clock 1
98579_at	Egr1	-0.68	D	-0.57	NC	-1.42	D	-1.04	D	0	3	early growth response 1
99347_f_at	Eml5	-0.92	D	-1.48	D	-0.97	NC	-1.44	D	0	3	echinoderm microtubule associated protein like 5
100002_at	Itih3	0.54	I	0.22	NC	-0.65	D	-0.82	D	1	2	inter-alpha trypsin inhibitor, heavy chain 3
100592_at	Ghitm	-0.56	D	-1.06	D	0.52	I	-0.01	NC	1	2	growth hormone inducible transmembrane protein
100599_at	Atf4	-0.82	D	-0.58	D	-0.27	NC	-0.01	MI	1	2	activating transcription factor 4
162457_f_at	Hba-a1	0.7	I	-1.46	D	-0.12	NC	-2.33	D	1	2	hemoglobin alpha, adult chain 1; hemoglobin alpha, adult chain 2
93722_at	Ensa	-0.46	MD	-0.83	D	0.38	I	-0.03	NC	1	2	endosulfine alpha
93909_f_at	Noct	-0.61	D	-0.84	D	0.35	I	0.08	NC	1	2	nocturnin
94781_at	Hba-a1	0.35	I	-1.71	D	-0.38	NC	-2.42	D	1	2	hemoglobin alpha, adult chain 1
97263_s_at	Csnk1d	-0.65	D	-1.23	D	0.13	I	-0.4	NC	1	2	casein kinase 1, delta
99009_at	Nnt	0.77	I	-0.6	D	-0.1	NC	-1.56	D	1	2	nicotinamide nucleotide transhydrogenase
99095_at	Max	-0.62	D	0.36	NC	-0.98	D	0.01	I	1	2	Max protein
100050_at	Id1	-0.75	D	-0.55	NC	-0.64	D	-0.49	NC	0	2	inhibitor of DNA binding 1

Table 8 (*continued*)

TC ID	GS	L1	C	L2	C	L3	C	L4	C	*	#	Description
100064_f_at	Gja1	0.23	NC	-0.09	NC	-0.62	D	-0.7	D	0	2	gap junction protein, alpha 1
100348_at	Gm40022	-0.82	D	-0.93	MD	-1.22	NC	-1.12	NC	0	2	predicted gene, 40022
100482_at	Zfp598	-0.42	D	-0.81	D	-0.33	NC	-0.64	NC	0	2	zinc finger protein 598
100536_at	Mobp	-0.11	NC	-0.22	NC	-0.72	D	-0.66	D	0	2	myelin-associated oligodendrocytic basic protein
100611_at	Lyz2	0.32	NC	-1.04	D	0.06	NC	-1.05	D	0	2	lysozyme 2
101482_at	Ppp1cc	0.08	NC	-0.04	NC	-0.59	D	-0.77	D	0	2	protein phosphatase 1, catalytic subunit, gamma isoform
101580_at	Cox7b	-0.62	D	-0.43	NC	-0.71	D	-0.43	NC	0	2	cytochrome c oxidase subunit VIIb
101596_at	C78859	-0.96	MD	-0.8	MD	-0.66	NC	-0.91	NC	0	2	expressed sequence C78859
101740_at	Adra1a	-0.04	NC	-2.3	D	-1.47	NC	-4.05	D	0	2	adrenergic receptor, alpha 1a

Atf4, Adra1a, Myl4 and Ppp1cc are genes of adrenergic signaling in cardiomyocytes. Fos, Max, Atf4, Dusp1, Gadd45b and Nr4a1 are genes of MAPK signaling pathway. Fos, Atf4 and Ppp1cc are Dopaminergic genes. Csnk1d, Id1 and Ppp1cc are genes of hippo signaling pathway. Csnk1d and Per1 are circadian rhythm genes. Mice cerebrum stimulated by rTMS for 30days were denoted as M1 and M2, sham control were denoted as C1 and C2. N = 2. All expression ratios were converted into the $\log_2$(expression ratio) values. L1: Signal Log Ratio (M1/C1), L2: Signal Log Ratio (M2/C1), L3: Signal Log Ratio (M1/C2), L4: Signal Log Ratio (M1/C2). C1, C2 were used as a control and M1, M2 were normalized with respect to C1 and C2 to obtain expression ratios. Expression Console (EC) Ver.1.4 and Transcriptome Analysis Console (TAC) Ver.3. were used for Comparison Analysis as manufacture procedure. C means data analysis output for a Comparison Analysis illustrating Change p-values with the associated Increase (I) or Decrease (D) call. Increase calls have Change p-values closer to zero and Decrease calls have Change p-values closer to one. Finally, the Change algorithm assesses probe pair saturation, calculates a Change p-values, and assigns an (I), Marginal Increase (MI), No Change (NC), Marginal Decrease (MD), or (D) call for C. Gene with more than 2 significant difference calls was chosen. Abbreviations; TC ID: Transcript Cluster ID, GS: Gene Symbol, *: Total number of increase, #: Total number of decrease. TC ID is available for Pathway analysis.

Table 9
Gene expression matrix after 30 days rTMS on cerebrum.

TC ID	GS	L1	C	L2	C	L3	C	L4	C	*	#	Description
101869_s_at	Hbb-b1	0.03	NC	-1.76	D	-0.05	NC	-1.94	D	0	2	hemoglobin, beta adult major chain; hemoglobin, beta adult minor chain; hemoglobin, beta adult s chain; hemoglobin, beta adult t chain
101936_at	Clk4	-0.63	D	-0.73	D	-0.4	NC	-0.3	NC	0	2	CDC like kinase 4
101962_at	Ddx17	-0.73	D	-0.35	NC	-0.58	D	-0.19	NC	0	2	DEAD (Asp-Glu-Ala-Asp) box polypeptide 17
102255_at	Osmr	0.04	NC	-1.08	MD	-3.48	NC	-3.02	MD	0	2	oncostatin M receptor
102431_at	Mapt	-0.01	NC	-0.04	NC	-0.61	D	-0.6	D	0	2	microtubule-associated protein tau
102574_at	Fgf11	2.96	NC	-1.26	D	3.35	NC	-0.77	D	0	2	fibroblast growth factor 11
102779_at	Gadd45b	-1.04	D	-1.15	D	-0.64	NC	-0.62	NC	0	2	growth arrest and DNA-damage-inducible 45 beta
102781_at	Ccnl2	-0.78	D	-0.93	D	-0.72	NC	-0.79	NC	0	2	cyclin L2
103253_at	Lin7b	-0.46	D	-0.39	NC	-0.64	D	-0.56	NC	0	2	lin-7 homolog B (C. elegans)
103427_at	Fbxl3	-0.67	D	-0.63	D	-0.2	NC	-0.39	NC	0	2	F-box and leucine-rich repeat protein 3
103448_at	S100a8	2.13	NC	-2.11	D	1.42	NC	-2.74	D	0	2	S100 calcium binding protein A8 (calgranulin A)
103460_at	Ddit4	-0.34	NC	-0.5	NC	-1.1	D	-1.48	D	0	2	DNA-damage-inducible transcript 4
103534_at	Hbb-b2	0.17	NC	-1.63	D	-0.09	NC	-2.34	D	0	2	hemoglobin, beta adult minor chain
103811_at	Invs	-0.58	NC	-1.39	D	-1.34	NC	-2	D	0	2	inversin
103863_at	Sft2d1	-0.41	D	-0.66	D	-0.18	NC	-0.29	NC	0	2	SFT2 domain containing 1
103990_at	Fosb	0.08	NC	-1.24	D	-0.3	NC	-1.35	D	0	2	FBJ osteosarcoma oncogene B
104155_f_at	Atf3	-1.59	D	-2.13	D	-0.47	NC	-1.05	NC	0	2	activating transcription factor 3
104578_f_at	Actn1	0.08	NC	-0.05	NC	-0.69	D	-0.86	D	0	2	actinin, alpha 1
104640_f_at	Taf1d	-0.02	NC	-0.47	NC	-0.68	D	-0.97	D	0	2	TATA box binding protein (Tbp)-associated factor, RNA polymerase I, D
104701_at	Bhlhe40	-0.38	NC	-0.42	NC	-0.87	D	-0.9	D	0	2	basic helix-loop-helix family, member e40
160140_at	Tbce	-1.09	D	-0.66	NC	-0.92	D	-0.82	NC	0	2	tubulin-specific chaperone E
160182_at	Srsf6	-0.6	D	-0.7	D	-0.45	NC	-0.56	NC	0	2	serine/arginine-rich splicing factor 6
160316_at	AI503316	-0.89	D	-1.11	D	-0.01	NC	-0.74	NC	0	2	expressed sequence AI503316; heterogeneous nuclear ribonucleoprotein U
160407_at	Actr1a	-1.42	D	-2.18	D	-0.11	NC	-0.68	NC	0	2	ARP1 actin-related protein 1 A, centractin alpha
160547_s_at	Txnip	-0.6	NC	-1.07	D	-0.7	NC	-1.28	D	0	2	thioredoxin interacting protein
160564_at	Lcn2	-0.8	NC	-3.16	D	-0.92	NC	-3.84	D	0	2	lipocalin 2
160791_at	Luc7l3	-0.9	D	-0.14	NC	-1.26	D	-0.37	NC	0	2	LUC7-like 3 (S. cerevisiae)
160894_at	Cebpd	-0.15	NC	-1.06	D	-0.34	NC	-1.37	D	0	2	CCAAT/enhancer binding protein (C/EBP), delta
161462_r_at	6820431F20Rik	-1.44	NC	-2.05	D	-1.53	NC	-2.36	D	0	2	cadherin 11 pseudogene; predicted gene, 21811
162093_at	Yars	-0.87	D	-0.94	D	-0.07	NC	-0.35	NC	0	2	tyrosyl-tRNA synthetase
162399_f_at	Atxn2	-0.14	NC	-0.23	NC	-0.94	D	-1.23	D	0	2	ataxin 2
162424_f_at	Ddx17	-0.58	D	-0.11	NC	-0.86	D	-0.23	NC	0	2	DEAD (Asp-Glu-Ala-Asp) box polypeptide 17
162459_f_at	Col6a1	-0.11	NC	-0.78	NC	-3.33	D	-4.01	D	0	2	collagen, type VI, alpha 1
92211_at	Bod1l	-0.56	D	-0.69	D	-0.56	NC	-0.5	NC	0	2	biorientation of chromosomes in cell division 1-like

Table 9 (*continued*)

TC ID	GS	L1	C	L2	C	L3	C	L4	C	*	#	Description
92233_at	Paxbp1	-0.62	D	-0.93	D	-0.61	NC	-0.68	NC	0	2	PAX3 and PAX7 binding protein 1
92523_at	Kcnj6	0.42	NC	-1.73	D	1.6	NC	-1.02	MD	0	2	potassium inwardly-rectifying channel, subfamily J, member 6
92636_f_at	Gm10177	-0.34	D	-0.09	NC	-0.52	D	-0.23	NC	0	2	predicted gene 10177; predicted gene, 17756; predicted gene 4184; protein transport protein Sec. 61 subunit gamma; protein transport protein Sec. 61 subunit gamma-like; SEC. 61, gamma subunit
92642_at	Car2	-0.42	MD	-0.37	NC	-0.88	D	-0.72	NC	0	2	carbonic anhydrase 2
92665_f_at	3830403N18Rik	-3.41	D	-3.56	NC	-3.93	D	-4.21	NC	0	2	RIKEN cDNA 3830403N18 gene; X-linked lymphocyte-regulated
92751_i_at	Wnt10b	0.49	NC	-1.75	D	-2.13	NC	-4.2	D	0	2	wingless-type MMTV integration site family, member 10B
92768_s_at	Alas2	-0.01	NC	-1.89	D	-0.66	NC	-2.71	D	0	2	aminolevulinic acid synthase 2, erythroid

Ddit4, Col6a1, Fgf11 and Osmr genes of PI3K-AKT signaling pathway. Fbxl3 and Bhlhe40 are circadian rhythm genes. Mice cerebrum stimulated by rTMS for 30days were denoted as M1 and M2, sham control were denoted as C1 and C2. N=2. All expression ratios were converted into the $\log_2$(expression ratio) values. L1: Signal Log Ratio (M1/C1), L2: Signal Log Ratio (M2/C1), L3: Signal Log Ratio (M1/C2), L4: Signal Log Ratio (M1/C2). C1, C2 were used as a control and M1, M2 were normalized with respect to C1 and C2 to obtain expression ratios. Expression Console (EC) Ver.1.4 and Transcriptome Analysis Console (TAC) Ver.3. were used for Comparison Analysis as manufacture procedure. C means data analysis output for a Comparison Analysis illustrating Change p-values with the associated Increase (I) or Decrease (D) call. Increase calls have Change p-values closer to zero and Decrease calls have Change p-values closer to one. Finally, the Change algorithm assesses probe pair saturation, calculates a Change p-values, and assigns an (I), Marginal Increase (MI), No Change (NC), Marginal Decrease (MD), or (D) call for C. Gene with more than 2 significant difference calls was chosen. Abbreviations; TC ID: Transcript Cluster ID, GS: Gene Symbol, *: Total number of increase, #: Total number of decrease. TC ID is available for Pathway analysis.

Table 10
Gene expression matrix after 30 days rTMS on cerebrum.

TC ID	GS	L1	C	L2	C	L3	C	L4	C	*	#	Description
92777_at	Cyr61	-1.09	NC	-1.87	D	-1.21	NC	-2.36	D	0	2	cysteine rich protein 61
92787_at	Ankrd10	-0.66	D	-1	D	-0.31	NC	-0.69	NC	0	2	ankyrin repeat domain 10
92802_s_at	Plp1	-0.61	D	-0.99	D	0.03	NC	-0.42	NC	0	2	proteolipid protein (myelin) 1
92945_at	Gria2	-0.45	NC	-0.06	NC	-0.96	D	-0.82	D	0	2	glutamate receptor, ionotropic, AMPA2 (alpha 2)
93009_at	Gstm2	-2	D	-4.19	D	-0.85	NC	-2.44	NC	0	2	glutathione S-transferase, mu 2
93126_at	Ckb	-0.01	NC	-0.12	NC	-0.53	D	-0.56	D	0	2	creatine kinase, brain
93274_at	Clk1	-1.11	D	-1.04	D	-0.6	NC	-0.46	NC	0	2	CDC-like kinase 1
93285_at	Dusp6	-0.48	NC	-0.52	NC	-0.58	D	-0.83	D	0	2	dual specificity phosphatase 6
93353_at	Lum	-0.93	D	-0.76	D	0.22	NC	0.25	NC	0	2	lumican
93390_g_at	Prom1	0.11	NC	0.05	NC	-1.44	D	-1.09	D	0	2	prominin 1
93478_at	Dnajc21	-0.14	NC	-0.07	NC	-1.02	MD	-1.39	D	0	2	DnaJ (Hsp40) homolog, subfamily C, member 21
93486_at	Slc27a1	0.53	NC	-0.65	D	-0.4	NC	-1.46	D	0	2	solute carrier family 27 (fatty acid transporter), member 1
93615_at	Pbx3	0.26	NC	0.07	NC	-0.63	D	-0.94	D	0	2	pre B cell leukemia homeobox 3
93666_at	Lmo2	-0.51	D	-0.72	D	0.08	NC	-0.23	NC	0	2	LIM domain only 2
93773_f_at	Zranb2	-0.71	D	-0.4	NC	-0.61	D	-0.41	NC	0	2	zinc finger, RAN-binding domain containing 2
93985_at	Tiparp	-1.11	D	-0.46	NC	-0.74	D	-0.79	NC	0	2	TCDD-inducible poly(ADP-ribose) polymerase
94155_at	Rgs4	-0.56	MD	-0.96	D	0.49	NC	-0.31	NC	0	2	regulator of G-protein signaling 4
94192_at	Gdap10	-0.41	NC	-1.15	D	-0.66	NC	-1.24	D	0	2	ganglioside-induced differentiation-associated-protein 10
94349_at	Khdc1b	-2.59	NC	-4.38	D	0.41	NC	-1.57	D	0	2	KH domain containing 1B
94379_at	Kif1b	-1.4	NC	-1.71	D	-1.62	NC	-2.65	D	0	2	kinesin family member 1B
94395_at	Fubp1	-0.48	NC	-0.78	D	-0.99	D	-1.05	NC	0	2	far upstream element (FUSE) binding protein 1
94460_at	Stk38	-0.43	D	-0.79	D	-0.04	NC	-0.37	NC	0	2	serine/threonine kinase 38
94516_f_at	Penk	0.16	NC	0.02	NC	-0.78	D	-0.89	D	0	2	preproenkephalin
94689_at	Gm39971	-0.03	NC	-0.48	NC	-1.5	D	-2	D	0	2	predicted gene, 39971
95001_at	Akap8	-0.88	D	-1	MD	-0.62	NC	-0.84	NC	0	2	A kinase (PRKA) anchor protein 8
95081_at	Exosc8	-1.38	D	-1.39	D	-0.8	NC	-0.95	NC	0	2	exosome component 8
95134_at	Mid1ip1	-0.92	D	-0.8	D	-0.3	NC	-0.2	NC	0	2	Mid1 interacting protein 1 (gastrulation specific G12-like (zebrafish))
95339_r_at	Mmp12	-2.02	MD	-4.34	D	-1.71	NC	-4.09	NC	0	2	matrix metallopeptidase 12
95418_at	Rasl11b	0.02	NC	-0.09	NC	-0.76	D	-0.85	D	0	2	RAS-like, family 11, member B
95674_r_at	Basp1	-0.37	D	-0.21	NC	-0.51	D	-0.3	NC	0	2	brain abundant, membrane attached signal protein 1
95694_at	Top1	-0.2	NC	-0.4	NC	-0.56	D	-0.63	D	0	2	topoisomerase (DNA) I
96464_at	Plxnb2	-0.41	NC	-1.64	D	0.19	NC	-0.78	MD	0	2	plexin B2
96672_at	Hopx	-0.45	D	-0.64	D	-0.29	NC	-0.52	NC	0	2	HOP homeobox
96785_at	Kank3	-0.55	D	-0.33	NC	-1.08	D	-0.92	NC	0	2	KN motif and ankyrin repeat domains 3
96912_s_at	Ctla2a	-0.8	D	-1.02	D	-0.38	NC	-0.77	NC	0	2	cytotoxic T lymphocyte-associated protein 2 alpha; cytotoxic T lymphocyte-associated protein 2 beta

Table 10 (*continued*)

TC ID	GS	L1	C	L2	C	L3	C	L4	C	*	#	Description
96961_at	Pcgf2	-0.35	NC	-1.18	D	-0.08	NC	-0.74	D	0	2	polycomb group ring finger 2
97142_at	DXErtd242e	-1.93	D	-2.25	D	-2.93	NC	-3.23	NC	0	2	DNA segment, Chr X, ERATO Doi 242, expressed
97358_at	Adgrl1	0.02	NC	0.08	NC	-0.66	D	-0.5	MD	0	2	adhesion G protein-coupled receptor L1
97759_at	Kcnma1	-0.15	NC	-0.06	NC	-0.87	D	-0.65	D	0	2	potassium large conductance calcium-activated channel, subfamily M, alpha member 1
98474_r_at	Tnfaip6	-1.14	D	-0.3	NC	-1.1	MD	0.04	NC	0	2	tumor necrosis factor alpha induced protein 6
98475_at	Matn2	-0.17	NC	-0.29	NC	-0.76	D	-1.16	D	0	2	matrilin 2
99089_at	Mal	-0.28	NC	-0.61	NC	-0.92	D	-1.12	D	0	2	myelin and lymphocyte protein, T cell differentiation protein
99622_at	Klf4	-0.81	NC	-0.52	NC	-2.7	D	-2.56	D	0	2	Kruppel-like factor 4 (gut)
99830_at	Kalrn	-0.16	NC	0.04	NC	-0.89	D	-0.69	D	0	2	kalirin, RhoGEF kinase

Lmo2, Pbx3 and Prom1 are genes of transcriptional misregulation in cancer. Mice cerebrum stimulated by rTMS for 30days were denoted as M1 and M2, sham control were denoted as C1 and C2. N=2. All expression ratios were converted into the $\log_2$(expression ratio) values. L1: Signal Log Ratio (M1/C1), L2: Signal Log Ratio (M2/C1), L3: Signal Log Ratio (M1/C2), L4: Signal Log Ratio (M1/C2). C1, C2 were used as a control and M1, M2 were normalized with respect to C1 and C2 to obtain expression ratios. Expression Console (EC) Ver.1.4 and Transcriptome Analysis Console (TAC) Ver.3. were used for Comparison Analysis as manufacture procedure. C means data analysis output for a Comparison Analysis illustrating Change p-values with the associated Increase (I) or Decrease (D) call. Increase calls have Change p-values closer to zero and Decrease calls have Change p-values closer to one. Finally, the Change algorithm assesses probe pair saturation, calculates a Change p-values, and assigns an (I), Marginal Increase (MI), No Change (NC), Marginal Decrease (MD), or (D) call for C. Gene with more than 2 significant difference calls was chosen. Abbreviations; TC ID: Transcript Cluster ID, GS: Gene Symbol, *: Total number of increase, #: Total number of decrease. TC ID is available for Pathway analysis.

Acknowledgements

This work was partly supported by a grant from the Japanese Society for the Promotion of Science (Grant no.17109011). Furthermore, this work was supported by the Global COE Program 'Center of Education and Research for the Advanced Genome-Based Medicine-For personalized medicine and the control of worldwide infectious disease' and MEXT Japan. The authors would like to thank Enago for the English language review. The authors would like to thank Mr. Masaru Kurosawa and Dr. Nobuyuki Nukina for the support for the experiment.

Transparency document. Supporting information

Transparency data associated with this article can be found in the online version at http://dx.doi.org/10.1016/j.dib.2017.10.034.

References

[1] T. Ikeda, W. Kobayashi and C. Morimoto, Effects of repetitive transcranial magnetic stimulation on ER stress-related genes and glutamate, γ-aminobutyric acid, and glycine transporter genes in mouse brain. Submitted.
[2] S. Kotliarova, N.R. Jana, N. Sakamoto, M. Kurosawa, H. Miyazaki, M. Nekooki, H. Doi, Y. Machida, H.K. Wong, T. Suzuki, C. Uchikawa, Y. Kotliarov, K. Uchida, Y. Nagao, U. Nagaoka, A. Tamaoka, K. Oyanagi, F. Oyama, N. Nukina, Decreased expression of hypothalamic neuropeptides in Huntington disease transgenic mice with expanded polyglutamine-EGFP fluorescent aggregates, J. Neurochem. 93 (2005) 641–653.
[3] R.J. Lipshutz, S.P. Fodor, T.R. Gingeras, D.J. Lockhart, High density synthetic oligonucleotide arrays, Nat. Genet. 21 (1999) 20–24.
[4] The Gene Ontology (GO) Project in 2006, Nucleic Acids Res. 34 (2006) (2006) D322–D326.

Current Cancer Therapy Reviews, 2017, *13*, 76-88

REVIEW ARTICLE

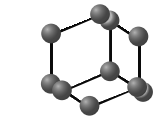

Current and Emerging Therapy for Malignant Pleural Mesothelioma: Focus on CD26/Dipeptidyl Peptidase IV as a Therapeutic Target

Bently P. Doonan[1], Kei Ohnuma[2], Long H. Dang[1], Chikao Morimoto[2] and Nam H. Dang[1,*]

[1]*University of Florida, Gainesville, FL, USA;* [2]*Juntendo University, Tokyo, Japan*

Abstract: ***Background*:** Malignant mesothelioma is a largely incurable disease that is refractory to current therapies. CD26 is a multifunctional cell surface protein involved in autoimmune disease, diabetes, and cancer. It has a role in T cell function, extracellular protein modification, as a prognostic factor for cancer, and as a therapeutic target for malignant mesothelioma. New treatment strategies are urgently needed for malignant pleural mesothelioma (MPM), and CD26-targeted therapy represents a novel approach.

***Outline*:** In this review, the most current and up-to-date literature available was reviewed and the current state of malignant mesothelioma treatment is described. Throughout the review the need for new therapeutic approaches is highlighted in the shortcomings of current therapy. CD26 is a target that is fit to take on these shortcomings. In this review we discuss the structure and function of CD26, its role in malignant mesothelioma and the future of anti-CD26 therapy as a versatile immunotherapeutic option.

***Conclusion*:** This review highlights the areas of most promise in treating MPM, these include immune checkpoint blockade, passive immunization, and based on our recently published data, targeting of CD26 with its specific mAb. Finally we describe how the anti-CD26 mAb YS110 was recently evaluated in the first-in-human phase I clinical trial, showing prolonged disease stabilization and a favorable side effect profile. Through better understanding of CD26, new pathways to treating and potentially curing malignant mesothelioma may be discovered.

ARTICLE HISTORY

Received: April 26, 2017
Revised: August 01, 2017
Accepted: August 24, 2017

DOI:
10.2174/1573394713666170907160734

Keywords: Asbestos, CD26, dipeptidyl peptidase IV, immunotherapy, Malignant Pleural Mesothelioma, YS110.

1. INTRODUCTION

The human leukocyte surface antigen CD26 is an active cell surface peptidase that is structurally identical to dipeptidyl peptidase IV (DPPIV), able to cleave N-terminal dipeptides from peptides with terminal L-alanine or L-proline residues (1-4). It is composed of 766 amino acids, the majority of which comprise the extracellular domain of the protein where a peptidase catalytic site is found and where important ligand binding sites for adenosine deaminase (ADA) and fibronectin are located [1-4]. The remainder of the protein structure includes a short 6-peptide cytoplasmic domain and a 23-peptide transmembrane region [4]. Through this peptidase activity CD26/DPPIV has significant effects on enhancing cellular response to external stimuli, effects on glucose homeostasis,

*Address correspondence to this author at the Division of Hematology/Oncology, University of Florida, P.O. Box 100278, Gainesville FL 326100278, USA; Tel: (352) 273-7832; Fax: (352) 273-5006; E-mail: nam.dang@medicine.ufl.edu

1875-6301/17 $58.00+.00

T cell stimulation and activation, and the biological behavior of selected human neoplasms. CD26 has relatively widespread expression on leukocytes, fibroblasts, mesothelium, endothelial, epithelial cells, and can be found in kidney, intestine, prostate, pancreas, and liver cells [5]. Since its discovery in 1966 by Hopsu-Havu and Glenner, CD26/DPPIV has been the focus of vigorous study in its pluripotent role in glucose homeostasis, inflammation, and more recently in tumorigenesis and as a therapeutic target in cancer [6]. The various immunomodulatory effects of CD26 have been previously summarized by our group and recently revisited and expanded by Klemann *et al*. [7, 8]. These works summarize the numerous substrates for DPPIV/CD26 and their far-reaching roles in autoimmune diseases such as multiple sclerosis, asthma, arthritis, and inflammatory bowel disease [7-9]. Likewise, CD26 involvement in malignancy has been extensively reviewed and characterized, including its potential role in terms of its role as a tumor suppressor, cancer biomarker, and therapeutic target [6, 10-14]. Additionally CD26 has been described as a marker for so-called cancer stem cells (CSCs) which have been a highly sought after targets in chemo-immunotherapy approaches [15]. Given the preponderance of evidence for CD26 involvement in various malignancies, as well as its role in immune activation and the biology of cancer stem cells, CD26 represents an ideal immunotherapeutic target; including for the aggressive, almost always fatal cancer malignant pleural mesothelioma (MPM).

Malignant pleural mesothelioma (MPM) is an aggressive and fatal disease. Over the past 60 years, since its acceptance as an independent oncological process, the incidence of MPM has continued to rise [16]. MPM is almost exclusively a direct result of exposure to asbestos [17]. Chronic pleural inflammation, ionizing radiation, and SV40 virus have been proposed as alternative exposures that can result in MPM, but these account for less than 20% of all cases [17]. Asbestos, a term for naturally occurring families of minerals that separate into thin fibers, has been used for greater than 5000 years for its high tensile strength and fire resistant properties [18]. It wasn't until the 1960s that the direct correlation between asbestos exposure and cancer development was validated and accepted [19]. Since that time, the WHO and International Agency for research in cancer have defined asbestos as a class I carcinogen responsible for both lung cancer and malignant pleural mesothelioma [18]. Inhaled asbestos fibers end up in the pleura, induce cytotoxic effects, and cause DNA damage and chronic inflammation [20]. This process is constant and smoldering for the next 20-60 years prior to the development of MPM. This long period of latency and protracted asymptomatic period explains the delayed peak in MPM cases and the increasing incidence over the past 40 years [21]. For example, in the US the peak in asbestos consumption occurred in the early 1970s, and its manufacturing was banned in the late 1980s, with total consumption and exposure risk being significantly reduced by the late 1990s; but the peak in MPM diagnoses of roughly 2,500-3,000 cases did not occur until about 2002 [22]. The expected plateau effect for MPM diagnoses for most industrialized nations that have banned the use of asbestos are expected to occur between 2015 and 2030, but countries like Russia, China, Brazil, and India continue to both mine and use asbestos at an alarming rate [23]. China has become the worlds largest asbestos-consuming country, has little to no reporting mechanism of its MPM rates, and will likely experience a surge in MPM diagnoses in the future [24]. With this predictable man-made epidemic looming on the horizon, new strategies are required for treating this aggressive disease as current strategies show limited efficacy, poor survival benefit, and have significant morbidity associated with them [18]. In this review, we will discuss the current state of malignant mesothelioma treatment and some of the burgeoning therapies currently in clinical trials. We will also highlight the work done on CD26 expression in MPM, its potential as a biomarker, and its functional role in MPM survival, invasion, and migration. Finally, we will review the ongoing clinical development of an anti-CD26 monoclonal antibody in malignant mesothelioma and its potential far-reaching implications as a novel immunotherapeutic agent.

2. CURRENT THERAPIES

If left untreated, MPM has an average life expectancy of 8 months and a 5-year mortality of greater than 95% [24]. Our best efforts with multimodal therapy may extend this outcome by mere months, further emphasizing the extreme need for improved therapies. Current therapeutic strategies

Table 1. Principal characteristics and benefit of current therapies for MPM.

First Line Therapy	Overall Survival (Months)	Improvement *vs*. SOC	Study Features/ Limitations	References
None	8	n/a	Na/	Zhang *et al.* Ann Transl Med 2015
Cisplatin + pemetrexed (SOC)	16.1	0	225 pts, newly diagnosed MPM, ECOG 0-2	Zalcman *et al.* Lancet 2016
SOC + bevacizumab	18.8	2.7	223 pts, newly diagnosed MPM, ECOG 0-2	Zalcman *et al.* Lancet 2016
SOC + EPP	21.9	5.8	54 pts, stage I to III MPM, otherwise healthy, ECOG 0-1	Krug *et al.* J clin oncol 2009
EPP + IMRT	14.2	None	63 pts, able to tolerate EPP, minimal comorbidities	Rice *et al.* Ann thorac surg 2007
EPP + SOC + hemithoracic RT	29.1	13	42 pts, ECOG 0-1, T1-3 N0-2 (33 pts who entered study could not tolerate all phases of therapy)	Krug *et al.* J clin oncol 2009
PD + SOC + IMPRINT	20.2	4.4	70 pts, retrospective study over 30 years, high karnofsky score	Shaikh *et al.* J of thoracic oncol 2017
CRS-207 + SOC	8.5*	N/A	38 pts, treatment naïve, ECOG 0-1	Jahan *et al.* J of thoracic oncol 2016

Second Line Therapy	Overall Survival (Months)	Improvement *vs*. Historic Chemo	Study Features/ Limitations	Reference
Tremelimumab + SOC	10.7	2.0	29 pts, ECOG 0-1, primarily epithelioid histology	Calabro *et al.* Lancet Respir Med 2015 MESOT-TREM-2012

Abbreviations: MPM (Malignant Pleural Mesothelioma), ECOG (Eastern Cooperative Oncology Group Performance Status), SOC (Standard of Care), pts (patients), EPP (Extrapleural Pneumonectomy), PD (Pleurectomy with Decortication), IMRT (Intensity-modulated Radiation Therapy), CRS-207 (live, attenuated, double-deleted listeria monocytogenes engineered to express tumor-associated antigen mesothelin).* (progression free survival, overall survival goal not met to date).

for MPM include surgery, radiation, chemotherapy, and more recently targeted therapy and immunotherapy [25-31]. Table **1** summarizes the mainstays of treatment and the benefit of traditional therapies over systemic chemotherapy. The roles of surgery and radiation as part of MPM treatment are rife with controversy, with these modalities showing limited benefit in patients with advanced disease.

2.1. Multimodal (Surgical Resection, Radiotherapy, and Chemotherapy)

Surgical intervention is difficult to perform, since achieving negative margins when extracting thin areas of pleura is difficult to accomplish and is associated with a significant level of risk, requiring a high level of familiarity and expertise with the procedure [32]. Two main surgical interventions are currently in use, pleurectomy/decortication (P/D) and Extrapleural Pneumonectomy (EPP) [29]. As illustrated in the MARS trial, EPP, an invasive aggressive debulking procedure showed no benefit when added to chemotherapy/radiation, being associated with a worse median survival when compared with no surgical intervention, and may actually cause harm [33, 34]. However, it is important to note that this study, like many involving MPM, is extremely underpowered and involved only 19 individuals re-

ceiving EPP [34]. With the high morbidity and required technical expertise, this procedure has therefore fallen out of favor except in those patient fortunate enough to be diagnosed at an early-localized stage.

P/D is being evaluated currently in the MARS2 trial to evaluate the role of surgery in MPM therapy, aside from its value in diagnostic biopsy [32]. In a similar vein, radiotherapy has been used in combination with chemotherapy and surgery as part of a trimodal therapeutic approach, or following surgery to prevent tumor seeding of thoracoscopy or thoracotomy scars. Trimodal therapy involves chemotherapy followed by EPP or P/D and intensity modulated radiotherapy as combination treatment for MPM. Results from small trimodal clinical trials suggest that, in certain patient populations, this aggressive multipronged attack may improve overall survival by up to 6 months *vs.* standard of care (SOC) [35]. However, this treatment option is only valuable to those MPM patients with limited burden of disease, excellent performance status, and epitheliod histology [36]. While surgery and radiotherapy may have some role to play in specific MPM cases, the mainstay of treatment for the past 20 years has been systemic chemotherapy.

2.2. Systemic Chemotherapy in Malignant Mesothelioma (SOC)

For a prolonged period of time, there was no consensus as to the optimum systemic chemotherapy used for MPM due to the limited randomized clinical trial data to support one strategy over another. It is important to mention that systemic chemotherapy for MPM is palliative in nature and has been the only intervention to show modest improvement in overall survival [27, 37]. This situation changed in 2003 following the availability of the results of the EMPHACIS phase III trial, which showed the superiority of the combination of cisplatin and pemetrexed over cisplatin alone, which was the most commonly used first line chemotherapy at the time [38, 39]. In this study, median survival was improved from 9.3 to 12.1 months [39]. These data led to the formal approval of the pemetrexed/cisplatin combination as the new SOC for MPM, a development which has not changed in the decade plus since it was first described [37]. Additional studies have validated the use of a different antifolate, raltitrexed, with cisplatin as an appropriate alternative regimen if pemetrexed is not well-tolerated [40]. Many clinicians also substitute carboplatin for cisplatin to reduce toxicity with little clinical difference in outcomes and without formal FDA approval [41]. Meanwhile, the recently published MAPS study demonstrated the clinical benefit of adding bevacizumab to SOC which resulted in an additional 2.7 month survival benefit though not without risks as the bevacizumab arm had higher reported adverse events across multiple subgroups and significant increases in grade 3-4 arterial and venous thromboembolic events [42]. However, even with this increase in median survival from the addition of bevacizumab plus SOC, MPM typically recurs as an incurable disease, necessitating the development of effective second line therapeutic options. Unlike the case with first line therapy, there is currently no established SOC therapy for disease recurrence or progression following initial management. The most common second line chemotherapy options include the vinca alkaloid vinorelbine, the anti-nucleoside analog gemcitabine, and the re-administration of single agent pemetrexed, which have shown the most promise in terms of tolerability but have failed to improve overall survival [27, 43]. In view of these shortcomings of currently available therapies, novel treatment strategies including targeted strategies and immunotherapy have been explored as both adjunctive and independent options for systemic therapy of MPM.

2.3. Targeted Therapies and Immunotherapy in Malignant Mesothelioma

Given the overwhelming lack of second line options in MPM and the large percentage of patients diagnosed with advanced disease that is not amenable to aggressive multimodal approaches, there has been a focus on targeted therapies with biological agents over the last 10 years, albeit with mostly disappointing results. Targeting various tyrosine kinases and the process of angiogenesis, as well as representing various forms of immunotherapy, these therapies can be broadly subcategorized into small molecule inhibitors, angiogenesis inhibitors, histone deacetylase (HDAC) inhibitors, and gene mutation targeting. The small molecule inhibitors include multitargeting receptor tyrosine kinase inhibitors (mTKIs), selective tyrosine kinase inhibitors (sTKIs), and

proteasome inhibitors. These molecules have garnered much focus in the oncologic world with broad applications in both solid and liquid tumors [44-47]. Unfortunately, phase I and phase II clinical trials involving the mTKIs sorafenib, sunitinib, pazopanib, and desatinib showed either limited anti-mesothelioma activity, the inability to induce remission, and/or unacceptable toxicity [48-52]. These receptor tyrosine kinase inhibitors broadly target EGFR, VEGFR, PDGFR, and C-kit to exert their anticancer effects. While these self-signaling molecules are upregulated in MPM, they do not appear vital to its propagation and are not MPM specific, which likely contributes to the limited efficacy of these drugs. Interestingly, the process of angiogenesis has only been successfully targeted by the monoclonal antibody bevacizumab and not by the above mentioned mTKIs which target VEGFR, or by the biologic agent thalidomide which primarily works through angiogenesis inhibition [53, 54]. Thalidomide was tested in clinical trials as both adjunct to standard of care treatment and as maintenance therapy for MPM patients previously treated with platinum based chemotherapy. The results of these studies showed no benefit to thalidomide as adjunct and no improvement in overall survival (OS) *vs* supportive care alone as maintenance therapy [27, 54]. Guazelli *et al*., recently summarized active phase I and phase II clinical trials and highlight that many studies have looked at targeting the EGFR or VEGR pathway with little success to show for it up to this point, this review expertly highlights the current clinical trials that are ongoing from Clincaltrials.gov [53]. Since EGFR expression is upregulated in the majority of MPM, selective tyrosine kinase inhibitors like erlotinib and gefitinib should theoretically exhibit increased activity against MPM. Unfortunately, similar to the mTKIs, results from phase II clinical trials were disappointing. Limited efficacy and marked resistance to these sTKIs was observed even in the presence of detectable EGFR expression on MPM tumors [55-57]. Similar results to these were seen with the proteasome inhibitor bortezomib, which has been approved for use in multiple myeloma and is currently in clinical trials for multiple other cancers including non-small cell lung cancer and metastatic breast cancer [58]. In two different clinical trials bortezomib failed to show objective response as monotherapy and failed to provide significant OS survival or disease progression benefit when combined with SOC [59].

HDAC inhibitors, specifically vorinostat, which modify and limit deacetylation of histone and block access genes that are overused by cancer cells for progression and division, showed promising results in early clinical trials [60]. These results prompted the large-scale VANTAGE-014 phase III double blind, randomized placebo control study using vorinostat monotherapy as either second- or third-line therapy for MPM [61]. Results reported in the Lancet in 2015 of this large well designed and well executed study (660 patients enrolled) showed no benefit to vorinostat over placebo in terms of overall survival [61]. Gene mutations have been a hallmark of targeted cancer therapy, but few highly conserved gene mutations in MPM have been identified, and studies involving those found and targeted have failed to result in clinically significant efficacy. The most common mutations observed through molecular genetic analysis of patient MPM samples include BAP1, PTEN/PI3K, CDKN2A/ARF, and NF2 [62-65]. Of these, NF2 has been identified in 40% of MPM and results in inactivation of a protein called Merlin which is involved in cell adhesion and motility. Of potential therapeutic value is the fact that Merlin loss increases cell sensitivity to focal adhesion kinase (FAK) inhibitors [66]. Initial research showed FAK inhibitors, specifically defactinib, along with their MPM cytotoxic effect reduced so called cancer stem cell populations in MPM with potential for more durable prolonged response *vs* SOC [66]. These results prompted a large phase II COMMAND study which enrolled 372 patients to receive defactinib plus SOC *vs* placebo plus SOC control arm as first line therapy for MPM [67]. Unfortunately as is often the case in MPM clinical trials, the study was stopped during recruitment when no difference in defactinib *vs* placebo were observed, even when subdivided to those patients with identifiable merlin loss [68].

Immunotherapy has been on the forefront of cancer therapy for the past 20 years and recent successes in immune checkpoint inhibition, tumor escape mechanism targeting, passive immunotherapy, and dendritic cell vaccines have pushed the field further with ever broadening application [69-71]. Recent advances in immunotherapy and current clinical trials in MPM are well summarized by

Thapa *et al*., [72]. In their review of current immunologic strategies, the failures of targeting MPM with single agent immunotherapy warrants the use of combination strategies to improve efficacy [72]. One of the more successful pathways of immunotherapy described in their work and others is the use of immune checkpoint inhibition as a novel target in MPM [72]. An example of immune checkpoint inhibition is the strategy of targeting and blocking CTLA-4. CTLA-4 is a cell surface co-factor expressed on the surface of T cells that acts as an inhibitory cofactor for CD80 and CD86 [73]. CTLA-4 competes with CD28 for binding with CD80/86 and when bound sends an inhibitor signal to antigen presenting cells to decrease the inflammatory response and diminish cell activation. This process allows CTLA-4 to protect surrounding cells and the system as a whole from uncontrolled immune stimulation [74]. Tumor cells, including malignant mesothelioma, express increased level of CTLA-4 as a means of blocking anti-tumor immune responses [74]. Inhibition of CTLA-4, or so-called checkpoint inhibition, therefore can restore the anti-tumor immune response, resulting in T cells recognition and attack of tumors that had previously been undetected. In a recent review, Guazelli *et al.* have summarized the role of CTLA-4 targeting in MPM [75]. They and others point out monoclonal antibodies (mAb) directed against CTLA-4 have shown impressive results in melanoma and have been tested in early clinical trials with MPM [75]. The CTLA-4 mAb Tremelimumab has been investigated in the MESOT-TREM-2008, and MESOT-TREM-2012 phase II clinical trials in patients with chemotherapy-resistant MPM [28, 75, 76]. In these studies, Tremelimumab treatment resulted in a disease control rate of 31% when administered every 3 months, and a control rate of 52% when given every 4 weeks, a regimen that led to improved efficacy in other cancers [75-77]. Furthermore, with the shorter dosing time, median OS was improved to 10.7 months compared to historical averages of 8.7 months with second line chemo [77]. These early results have led to an ongoing study comparing Tremelimumab monotherapy *vs* placebo control. Additionally, combination immunotherapies, CTLA-4 blockade combined with anti-PD-L1 therapy is under active investigation and was recently presented at ASCO 2016 with the combination of Tremelimumab and durvalumab [75]. Like CTLA-4, programmed death ligand 1 (PD-L1) is overexpressed in MPM, particularly the sarcomatoid type, and exerts an inhibitory effect on T cells to suppress the anti-tumor immune response [77]. Binding PD-L1 with ligand specific mAbs therefore blocks this tumor escape mechanism, potentially resulting in greater susceptibility of MPM to immune destruction. In the recent KEYNOTE-028 phase I clinical trial, the PD-1 mAb pembrolizumab was tested in a 25 patient cohort and showed an impressive overall disease control rate of 76% [73, 78]. This has prompted larger phase II investigation to further explore the anti-MPM activity of pembrolizumab [73].

Additional passive immunotherapy strategies in MPM have focused on targeting the tumor-associated antigen Mesothelin. Mesothelin expression is increased in MPM and likely plays a role in cell adhesion and invasion [79, 80]. Strategies focusing on mesothelin targeting have involved the mAb Amatuximab, anti-mesothelin vaccine CRS-207, and the mAb-toxin fusion protein called SS1P [79]. Amatuximab is a chimeric anti-mesothelin mAb that was tested in a phase II multicenter trial of 89 MPM patients in combination with SOC (pemetrexed/cisplatin) *vs* SOC alone, with improved OS in the Amatuximab-containing arm [81]. The anti-mesothelin vaccine CRS-207 is a live, attenuated, derivative of listeria monocytogenes that expressed the mesothelin Ag and activates both innate and adaptive immunity [82]. The synergistic effects of CRS-207 and SOC chemotherapy was tested in a phase I trial of 38 MPM patients which showed encouraging anti-tumor immunity, with a progression free survival of 8.5 months [82]. Encouraging results from this study has led to a large multicenter phase III clinical trial that is currently recruiting. Similarly, the recombinant anti-mesothelin and truncated pseudomonas exotoxin SS1P has shown significant anti-tumor activity and tolerability in a phase I clinical trial [83]. Finally, adoptive transfer of *ex vivo* stimulated dendritic cells, so called dendritic cell vaccination has recently shown activity in MPM. In a trial of 10 patients with MPM, cyclophosphamide was given to reduce activity of T regulatory cells prior to infusion of dendritic cells pulsed with autologous tumor lysate [84]. Results of this small study showed radiographic disease control in 8/10 patients and an impressive OS of greater than 2

years in 7/10 patients [84]. This technique will likely be expanded and further investigated in future years.

3. POTENTIAL APPROACH TO TARGETING CD26 IN MPM

As discussed above, treatment for MPM beyond first line therapy is still unsatisfactory due to limited efficacy, and novel therapeutic approaches are urgently needed for this patient population. While immunotherapy approaches appear promising with encouraging efficacy in multiple small studies, the observed benefit is still relatively short lasting and typically limited to only a few months. Additionally some concerns that arise with all studies involving immunotherapy include utilizing progression free survival (PFS) *vs* OS as an overall marker of drug efficacy or combining drugs that lack single-agent activity. In a recent study published in the Journal of Clinical Oncology, Tan *et al.* performed a meta-analysis of trials with results posted on ClinicalTrials.gov where they found a majority of studies showing significant benefit on PFS but not on OS [85]. They highlight the need for studies to look at both PFS and OS and to not use one as a surrogate marker for the other [85]. In separate commentary, Gyawali and Prasad illustrate that multiple trials over the past decade where multiple drugs without proven single-agent efficacy were added together as a novel treatment and showed PFS but rarely showed an effect on OS [86]. They pose in additional manuscript that by combining multiple therapies to extent PFS we run the risk of subjecting patients to unnecessary side effects and risks for little benefit [87]. These compelling examples shed light on the grain of salt mentality that is needed when evaluating the efficacy of immunotherapy. Unfortunately, as is usually the case, most of these trials and analysis did not include studies involving MPM. Given the small treatment arms and aggressive nature of MPM small gains in PFS may indicate improvement in OS but the low power of these studies makes statistical extrapolation difficult and with such a short OS window for these patients even small gains should be looked at as possible treatment strategies. There studies confirm and support the need for improved targeting in diseases like MPM and stresses the importance of single-agent efficacy in therapy design before a drug is pushed forward through clinical trials and towards FDA approval. Thus, an ideal target in MPM would be one that is highly expressed by malignant mesothelioma cells but absent from normal mesothelioma, and plays a role in tumor proliferation or invasiveness. In addition, therapy specifically targeting this antigen should work in concert with chemotherapy to enhance treatment efficacy without increasing side effect burden, have strong activity as a single agent, and improve both PFS and OS in MPM patients. All these characteristics can be found potentially in the surface antigen CD26.

3.1. CD26 Expression and Function in MPM

CD26 is a multifunctional cell surface receptor with roles in immune regulation, T cell activation, and malignant potential of various cancers. CD26 is highly expressed in MPM and was originally identified as a potential target by our group [88, 89]. Our initial work demonstrated that targeting CD26 with anti-CD26 mAb resulted in *in vitro* growth inhibition of MPM cell line [89]. Subsequently, we showed high CD26 expression on various human MPM types including localized MPM, well-differentiated papillary MPM, and diffuse MPM but not on adenomatoid tumors or reactive mesothelioma cells [88]. Complementing our earlier *in vitro* work, we also demonstrated for the first time the potential for targeting CD26 in MPM with anti-CD26 mAb in an *in vivo* NOD-SCID mouse model of MPM. This initial evaluation for CD26 expression on a small sample population of MPM tissues was then further expanded in a follow-up paper which demonstrated overexpression of CD26 in MPM in more than 120 different MPM surgical samples including epitheliod mesothelioma, biphasic mesothelioma, and sarcomatoid mesothelioma as well as 8 different mesothelioma cell lines [90]. Interestingly, the more aggressive sarcomatoid mesothelioma samples had reduced cell surface CD26 expression but retained cytoplasmic CD26 expression. This work suggested that the morphology of the mesothelioma cell type, which has been used as a prognostic factor in the disease, correlated with CD26 expression and that loss of membranous CD26 was associated with the more aggressive spindle shaped sarcomatoid mesothelioma, raising the possibility that the loss of CD26 in these cells represented an epithelial to mesenchymal transition for MPM potentially responsible for the difficulty in treating and poorer

outcome associated with sarcomatoid MPM [90]. We subsequently showed that CD26 surface expression was associated with improved survival in MPM patients that received chemotherapy and potentially contributed to mesothelioma chemosensitivity [91]. We also demonstrated through *in vitro* investigation that CD26 was associated with enhanced proliferative activity of MPM and through downstream gene activation, CD26 upregulated mechanisms that increased chemotherapy sensitivity [91]. Given the increased surface expression of CD26 in favorable MPM phenotypes, soluble CD26 (sCD26) was investigated as potential biomarker for MPM. We showed in a recent preclinical model of MPM that sCD26 levels were higher in patients with the favorable epitheliod phenotype than those with the aggressive sarcomatoid subtype and through therapeutic monitoring, reduction in sCD26 may indicate progression of disease [92]. Whether sCD26 can be used in high-risk patients, those with previous significant asbestos exposure or those residents of asbestos mining communities, as a screening tool for early detection of disease remains to be determined. Additionally, CD26 expression was identified and characterized as a marker for so called cancer stem cells (CSC) in MPM and was found to be co-expressed with the CSC marker CD24 [93]. In this study we used shRNA knockdown of CD24 and CD26 to determine the effects of gene silencing in the MPM cell line Meso-1 [93]. We showed that through silencing of CD26 but not CD24 MPM cellular invasion was reduced and MPM showed reduced proliferation [93]. Gene knockout of CD26 additionally caused an reduction in the cancer cell signaling molecules IGFBP7, IGFBP3, Wnt5A, and IL7R [93]. These studies also showed CD26 played a role in asymmetric cell division and invasion potential in MPM cell lines [93]. These collective works clearly validated CD26 as a surface receptor upregulated in MPM with various roles in cell proliferation, invasion, and chemosensitivity, while loss of expression correlated with progression of MPM to a more aggressive treatment-resistant phenotype.

These studies on CD26 expression in MPM were subsequently followed by our work evaluating molecular mechanisms for CD26 role in cellular invasiveness. We showed that CD26 promotes invasiveness through the formation of CD26-α5β1 integrin molecular complexes that interact with various cell surface and endothelium receptors and stimulate extra-cellular matrix metalloproteinases [94]. In addition, the short 6 amino acid cytoplasmic region of CD26 plays a crucial role in MPM migration and invasion through upregulation of periostin [95]. We demonstrated that the lipid raft platforms clustered around CD26, indirect activation and phosphorylation of the proto-oncogene Src occurred resulting in nuclear translocation of the transcription factor Twist1 [95]. Through this mechanism, periostin production is increased, associated with an enhancement in the migratory potential and invasiveness of MPM, contributing to both progression of disease and metastases. CD26 therefore represents a targetable MPM specific molecule with a direct role in the invasiveness and metastatic potential of MPM.

3.2. CD26 Targeting in Malignant Mesothelioma

As mentioned above, proof-of-concept studies using preclinical MPM models demonstrate that targeting CD26 with its specific mAbs is a viable anti-cancer therapeutic approach. Treatment of MPM cell lines with the humanized anti-CD26 mAB, YS110 resulted in $p27^{kip1}$ accumulation leading to cytotoxicity in both *in vitro* and *in vivo* models [88]. Binding of YS110 also had a direct role in regulating binding to extra-cellular matrix proteins, biphasic antitumor immunity through immune activation and direct cytotoxicity, as well as inhibition of distant metastases [88]. In addition, anti-CD26 mAB enhanced nuclear translocation of CD26 with downstream effects resulting in mesothelioma growth suppression [96, 97]. Cellular localization analysis revealed that YS110 caused an increase in transport *via* caveolin-dependent endocytosis and accumulation of CD26 to the nucleus of MPM resulting in suppression of POLR2 gene expression and subsequent growth suppression of MPM cells, while highlighting a secondary anti-tumor mechanism of anti-CD26 mABs [96, 97]. Meanwhile, a recently published paper demonstrated that YS110 caused retarded G2/M cell cycle progression through inhibition of phosphorylation of cdc2 and cdc25C and activation of ERK1/2 [98]. Importantly, a synergistic effect between YS110 and the first line anti-MPM chemotherapeutic agent pemetrexed was observed, as the combination of YS110 and pemetrexed showed superior anti-tumor activity associated with combinatorial G1/S and G2/M cell cycle tran-

sition inhibition than either agent alone in a mouse xenograft model of MPM [98].

These encouraging preclinical results along with our increased understanding of the novel molecular mechanisms involved in CD26 targeting in cancer cells led to the first-in-human phase I study of YS110 in CD26 expressing cancer cells. This recently published study involved 33 patients with CD26+ tumors (22 of whom had heavily pretreated MPM) treated with a standard 3+3 escalation scheme with escalating doses of YS110 [99]. YS110 was generally well tolerated even to doses of 6mg/kg weekly, with maximal tolerated dose not reached and only 2 patients reporting grade 3 or higher anaphylactic or allergic reactions, which entirely resolved with supportive treatment and dose omission [99]. When the study was subsequently amended to add clinically relevant allergies as a new exclusion criterion and to allow for the administration of a systemic steroid prophylaxis prior to each infusion to better control infusions reactions, the safety profile was even further improved with treatment doses being escalated to 6mg/kg without dose limiting toxicities. While there was a transient decrease in total peripheral lymphocyte counts and CD26+ lymphocyte subsets following antibody administration, there was no observed autoimmune or infectious disease occurrences [99]. Furthermore, in this first-in-human phase I study, prolonged disease stabilization was observed in a significant number of patients that received YS110 [99, 100]. Thirteen of 26 evaluable patients treated with YS110 had stable disease as the best response for an overall median PFS of 43 days, while 7 patients (including five cases of mesothelioma) experienced prolonged PFS of 184-399 days [99, 100]. Taken together, data from both preclinical studies as well as the recently completed first-in-human phase I clinical trial indicate that additional testing of YS110, which may represent a major breakthrough in the treatment of MPM, in future clinical trials as either single agent therapy or as part of combination therapies with other anti-neoplastic agents, would be warranted.

CONCLUSION

MPM is an ongoing oncological concern. With continued mining and use of asbestos globally in developing countries and major industrialized nations like China and Russia, MPM cases will predictably increase in the coming decades. When found, treatment strategies include combination surgery, radiation, and chemotherapy; although few patients are diagnosed in time to benefit from definitive surgery, with systemic chemotherapy being thus left for many patients as their only option. While beneficial at reducing symptoms, systemic chemotherapy with pemetrexed and cisplatin (SOC) fails to provide curative benefit for most MPM patients and only extends overall survival by a matter of months. The addition of novel biologic agents such as bevacizumab to standard of care will likely provide modest survival benefit but has yet to become the approved standard. For most patients with MPM, following initial systemic therapy, disease commonly relapses with progression and metastases. Over the past 20 years, many chemo- and immunotherapeutics have been evaluated as potential treatments for MPM with limited benefit. Novel immunotherapy strategies including passive immunotherapy, mesothelin targeting, and checkpoint inhibition targeting have recently shown promise in small phase I and II studies. In this review, we highlight the need for novel therapeutic approaches in MPM and discuss the potential of CD26 as a new molecular target. CD26 is highly expressed in MPM with limited expression in normal mesothelial cells. Unlike other immunotherapeutic targets, CD26 has a direct role in progression, invasion, metastasis, and cancer-stem cell proliferation in MPM. Our recently completed first-in-human phase I clinical trial involving the anti-CD26 mAb YS110 suggests that successful targeting of CD26 may lead potentially to improved disease control and prolonged overall survival with limited toxic side effects in malignant mesothelioma. The successful development of a CD26-targeted approach will enhance the treatment armamentarium available against MPM as we prepare for this predictive epidemic.

LIST OF ABBREVIATIONS

DPPIV	=	Dipeptidyl Peptidase IV
MPM	=	Malignant Pleural Mesothelioma
mAb	=	Monoclonal Antibody
SOC	=	Standard of Care

CSC = Cancer Stem Cells

OS = Overall Survival

CONSENT FOR PUBLICATION

Not applicable.

CONFLICT OF INTEREST

Nam H. Dang, Chikao Morimoto, and Kei Ohnuma are stockholders of Y's AC Co, Ltd.

ACKNOWLEDGEMENTS

Declared none.

REFERENCES

[1] Ohnuma K, Dang NH, Morimoto C. Revisiting an old acquaintance: CD26 and its molecular mechanisms in T cell function. Trends Immunol 2008; 29(6): 295-301.

[2] Boonacker E, Van Noorden CJ. The multifunctional or moonlighting protein CD26/DPPIV. Eur J Cell Biol 2003; 82(2): 53-73.

[3] Hosono O, Ohnuma K, Dang NH, Morimoto C. CD26: A key molecule in immune regulation and autoimmune diseases. Mod Rheumatol 2003; 13(3): 199-204.

[4] Matteucci E, Giampietro O. Dipeptidyl peptidase-4 (CD26): Knowing the function before inhibiting the enzyme. Curr Med Chem 2009; 16(23): 2943-51.

[5] Mortier A, Gouwy M, Van Damme J, Proost P, Struyf S. CD26/dipeptidylpeptidase IV-chemokine interactions: Double-edged regulation of inflammation and tumor biology. J Leukoc Biol 2016; 99(6): 955-69.

[6] Cordero OJ, Salgado FJ, Nogueira M. On the origin of serum CD26 and its altered concentration in cancer patients. Cancer Immunol Immunother 2009; 58(11): 1723-47.

[7] Ohnuma K, Takahashi N, Yamochi T, Hosono O, Dang NH, Morimoto C. Role of CD26/dipeptidyl peptidase IV in human T cell activation and function. Front Biosci 2008; 13: 2299-310.

[8] Klemann C, Wagner L, Stephan M, Von Hörsten S. Cut to the chase: A review of CD26/dipeptidyl peptidase-4 (DPP4)'S entanglement in the immune system. Clin Exp Immunol 2016; 185(1): 1-21.

[9] Ohnuma K, Inoue H, Uchiyama M, *et al*. T-cell activation *via* CD26 and caveolin-1 in rheumatoid synovium. Mod Rheumatol 2006; 16(1): 3-13.

[10] Dang NH, Morimoto C. CD26: An expanding role in immune regulation and cancer. Histol Histopathol 2002; 17(4): 1213-26.

[11] Dang NH, Aytac U, Sato K, *et al*. T-large granular lymphocyte lymphoproliferative disorder: Expression of CD26 as a marker of clinically aggressive disease and characterization of marrow inhibition. Br J Haematol 2003; 121(6): 857-65.

[12] Havre PA, Abe M, Urasaki Y, Ohnuma K, Morimoto C, Dang NH. The role of CD26/dipeptidyl peptidase IV in cancer. Front Biosci 2008; 13: 1634-45.

[13] Lam CS, Cheung AH, Wong SK, *et al*. Prognostic significance of CD26 in patients with colorectal cancer. PLoS One 2014; 9(5): e98582.

[14] Ho L, Aytac U, Stephens LC, *et al*. *In vitro* and *in vivo* antitumor effect of the anti-CD26 monoclonal antibody 1F7 on human CD30+ anaplastic large cell T-cell lymphoma Karpas 299. Clin Cancer Res 2001; 7(7): 2031-40.

[15] Davies S, Beckenkamp A, Buffon A. CD26 a cancer stem cell marker and therapeutic target. Biomed Pharmacother 2015; 71: 135-8.

[16] Ai J, Stevenson JP. Current issues in malignant pleural mesothelioma evaluation and management. Oncologist 2014; 19(9): 975-84.

[17] Robinson BM. Malignant pleural mesothelioma: An epidemiological perspective. Ann Cardiothorac Surg 2012; 1(4): 491-6.

[18] Røe OD, Stella GM. Malignant pleural mesothelioma: History, controversy and future of a manmade epidemic. Eur Respir Rev 2015; 24(135): 115-31.

[19] Riva MA, Carnevale F, Sironi VA, De Vito G, Cesana G. Mesothelioma and asbestos, fifty years of evidence: Chris Wagner and the contribution of the Italian occupational medicine community. Med Lav 2010; 101(6): 409-15.

[20] Bononi A, Napolitano A, Pass HI, Yang H, Carbone M. Latest developments in our understanding of the pathogenesis of mesothelioma and the design of targeted therapies. Expert Rev Respir Med 2015; 9(5): 633-54.

[21] Pasdar EA, Smits M, Stapelberg M, *et al*. Characterisation of mesothelioma-initiating cells and their susceptibility to anti-cancer agents. PLoS One 2015; 10(5): e0119549.

[22] Price B, Ware A. Time trend of mesothelioma incidence in the United States and projection of future cases: An update based on SEER data for 1973 through 2005. Crit Rev Toxicol 2009; 39(7): 576-88.

[23] Markowitz S. Asbestos-related lung cancer and malignant mesothelioma of the pleura: Selected current issues. Semin Respir Crit Care Med 2015; 36(3): 334-46.

[24] Zhang W, Wu X, Wu L, Zhao X. Advances in the diagnosis, treatment and prognosis of malignant pleural mesothelioma. Ann Transl Med 2015; 3(13): 182.

[25] Adusumilli PS. Translational immunotherapeutics: Chemoimmunotherapy for malignant pleural mesothelioma. Cancer 2014; 120(21): 3268-71.

[26] Blomberg C, Nilsson J, Holgersson G, *et al*. Randomized trials of systemic medically-treated malignant

mesothelioma: A systematic review. Anticancer Res 2015; 35(5): 2493-501.

[27] Buikhuisen WA, Hiddinga BI, Baas P, van Meerbeeck JP. Second line therapy in malignant pleural mesothelioma: A systematic review. Lung Cancer 2015; 89(3): 223-31.

[28] Calabrò L, Maio M. Immune checkpoint blockade in malignant mesothelioma. Semin Oncol 2015; 42(3): 418-22.

[29] Cao C, Akhunji Z, Fu B, *et al*. Surgical management of malignant pleural mesothelioma: An update of clinical evidence. Semin Thorac Cardiovasc Surg 2015; 27(1): 6-8.

[30] Christoph DC, Eberhardt WE. Systemic treatment of malignant pleural mesothelioma: New agents in clinical trials raise hope of relevant improvements. Curr Opin Oncol 2014; 26(2): 171-81.

[31] Jing XQ, Zhou L, Sun XD, Yu JM, Meng X. Pemetrexed maintenance therapy following bevacizumab-containing first-line chemotherapy in advanced malignant pleural mesothelioma: A case report and literatures review. Medicine (Baltimore) 2016; 95(14): e3351.

[32] Bertoglio P, Waller DA. The role of thoracic surgery in the management of mesothelioma: An expert opinion on the limited evidence. Expert Rev Respir Med 2016; 10(6): 663-72.

[33] Treasure T, Waller D, Tan C, *et al*. The mesothelioma and radical surgery randomized controlled trial: The mars feasibility study. J Thorac Oncol 2009; 4(10): 1254-8.

[34] Treasure T, Lang-Lazdunski L, Waller D, *et al*. Extrapleural pneumonectomy versus no extra-pleural pneumonectomy for patients with malignant pleural mesothelioma: Clinical outcomes of the Mesothelioma and Radical Surgery (MARS) randomised feasibility study. Lancet Oncol 2011; 12(8): 763-72.

[35] Thieke C, Nicolay NH, Sterzing F, *et al*. Long-term results in malignant pleural mesothelioma treated with neoadjuvant chemotherapy, extrapleural pneumonectomy and intensity-modulated radiotherapy. Radiat Oncol 2015; 10: 267.

[36] Federico R, Adolfo F, Giuseppe M, *et al*. Phase II trial of neoadjuvant pemetrexed plus cisplatin followed by surgery and radiation in the treatment of pleural mesothelioma. BMC Cancer 2013; 13: 22.

[37] Kondola S, Manners D, Nowak AK. Malignant pleural mesothelioma: An update on diagnosis and treatment options. Ther Adv Respir Dis 2016; 10(3): 275-88.

[38] Reck M, Gatzemeier U. Pemetrexed-cisplatin combination in mesothelioma. Expert Rev Anticancer Ther 2005; 5(2): 231-7.

[39] Vogelzang NJ, Rusthoven JJ, Symanowski J, *et al*. Phase III study of pemetrexed in combination with cisplatin versus cisplatin alone in patients with malignant pleural mesothelioma. J Clin Oncol 2003; 21(14): 2636-44.

[40] van Meerbeeck JP, Gaafar R, Manegold C, *et al*. Randomized phase III study of cisplatin with or without raltitrexed in patients with malignant pleural mesothelioma: An intergroup study of the European Organisation for Research and Treatment of Cancer Lung Cancer Group and the National Cancer Institute of Canada. J Clin Oncol 2005; 23(28): 6881-9.

[41] Habib EE, Fahmy ES. Chemotherapy management of malignant pleural mesothelioma: A phase II study comparing two popular chemotherapy regimens. Clin Transl Oncol 2013; 15(11): 965-8.

[42] Zalcman G, Mazieres J, Margery J, *et al*. Bevacizumab for newly diagnosed pleural mesothelioma in the Mesothelioma Avastin Cisplatin Pemetrexed Study (MAPS): A randomised, controlled, open-label, phase 3 trial. Lancet 2016; 387(10026): 1405-14.

[43] Abdel-Rahman O, Kelany M. Systemic therapy options for malignant pleural mesothelioma beyond first-line therapy: A systematic review. Expert Rev Respir Med 2015; 9(5): 533-49.

[44] Hall RD, Le TM, Haggstrom DE, Gentzler RD. Angiogenesis inhibition as a therapeutic strategy in Non-Small Cell Lung Cancer (NSCLC). Transl Lung Cancer Res 2015; 4(5): 515-23.

[45] Kim SH, Park WS, Joung JY, Seo HK, Lee KH, Chung J. Systemic treatments for metastatic renal cell carcinoma: 10-year experience of immunotherapy and targeted therapy. Cancer Res Treat 2016; 48(3): 1092-101.

[46] Cella D, Beaumont JL. Pazopanib in the treatment of advanced renal cell carcinoma. Ther Adv Urol 2016; 8(1): 61-9.

[47] Siddiqi T, Rosen ST. Novel biologic agents for non-Hodgkin lymphoma and chronic lymphocytic leukemia-part 2: Adoptive cellular immunotherapy, small-molecule inhibitors, and immunomodulation. Oncology (Williston Park) 2015; 29(4): 299-308.

[48] Dubey S, Jänne PA, Krug L, *et al*. A phase II study of sorafenib in malignant mesothelioma: Results of cancer and leukemia group B 30307. J Thorac Oncol 2010; 5(10): 1655-61.

[49] Camidge DR, Blais N, Jonker DJ, *et al*. Sunitinib combined with pemetrexed and cisplatin: Results of a phase I dose-escalation and pharmacokinetic study in patients with advanced solid malignancies, with an expanded cohort in non-small cell lung cancer and mesothelioma. Cancer Chemother Pharmacol 2013; 71(2): 307-19.

[50] Laurie SA, Gupta A, Chu Q, *et al*. Brief report: A phase II study of sunitinib in malignant pleural mesothelioma. The NCIC Clinical Trials Group. J Thorac Oncol 2011; 6(11): 1950-4.

[51] Dudek AZ, Pang H, Kratzke RA, *et al*. Phase II study of dasatinib in patients with previously treated malignant mesothelioma (cancer and leukemia group B 30601): A brief report. J Thorac Oncol 2012; 7(4): 755-9.

[52] Mathy A, Baas P, Dalesio O, van Zandwijk N. Limited efficacy of imatinib mesylate in malignant meso-

thelioma: A phase II trial. Lung Cancer 2005; 50(1): 83-6.

[53] Guazzelli A, Bakker E, Tian K, Demonacos C, Krstic-Demonacos M, Mutti L. Promising investigational drug candidates in phase I and phase II clinical trials for mesothelioma. Expert Opin Investig Drugs 2017: 26(8): 933-944.

[54] Buikhuisen WA, Burgers JA, Vincent AD, *et al*. Thalidomide versus active supportive care for maintenance in patients with malignant mesothelioma after first-line chemotherapy (NVALT 5): An open-label, multicentre, randomised phase 3 study. Lancet Oncol 2013; 14(6): 543-51.

[55] Govindan R, Kratzke RA, Herndon JE, *et al*. Gefitinib in patients with malignant mesothelioma: A phase II study by the cancer and leukemia group B. Clin Cancer Res 2005; 11(6): 2300-4.

[56] Garland LL, Rankin C, Gandara DR, *et al*. Phase II study of erlotinib in patients with malignant pleural mesothelioma: A southwest oncology group study. J Clin Oncol 2007; 25(17): 2406-13.

[57] Jackman DM, Kindler HL, Yeap BY, *et al*. Erlotinib plus bevacizumab in previously treated patients with malignant pleural mesothelioma. Cancer 2008; 113(4): 808-14.

[58] O'Brien ME, Gaafar RM, Popat S, *et al*. Phase II study of first-line bortezomib and cisplatin in malignant pleural mesothelioma and prospective validation of progression free survival rate as a primary endpoint for mesothelioma clinical trials (European Organisation for research and treatment of cancer 08052). Eur J Cancer 2013; 49(13): 2815-22.

[59] Tada Y, Suzuki T, Shimada H, Hiroshima K, Tatsumi K, Tagawa M. Molecular-targeted therapy for malignant mesothelioma. Pleura 2015; 2: 1-11.

[60] Paik PK, Krug LM. Histone deacetylase inhibitors in malignant pleural mesothelioma: Preclinical rationale and clinical trials. J Thorac Oncol 2010; 5(2): 275-9.

[61] Krug LM, Kindler HL, Calvert H, *et al*. Vorinostat in patients with advanced malignant pleural mesothelioma who have progressed on previous chemotherapy (VANTAGE-014): A phase 3, double-blind, randomised, placebo-controlled trial. Lancet Oncol 2015; 16(4): 447-56.

[62] McMillan R, Zauderer M, Bott M, Ladanyi M. Important recent insights into the genetics and biology of malignant pleural mesothelioma. Ann Cardiothorac Surg 2012; 1(4): 462-5.

[63] de Assis LV, Locatelli J, Isoldi MC. The role of key genes and pathways involved in the tumorigenesis of malignant mesothelioma. Biochim Biophys Acta 2014; 1845(2): 232-47.

[64] Lo Iacono M, Monica V, Righi L, *et al*. Targeted next-generation sequencing of cancer genes in advanced stage malignant pleural mesothelioma: A retrospective study. J Thorac Oncol 2015; 10(3): 492-9.

[65] Jean D, Daubriac J, Le Pimpec-Barthes F, Galateau-Salle F, Jaurand MC. Molecular changes in mesothelioma with an impact on prognosis and treatment. Arch Pathol Lab Med 2012; 136(3): 277-93.

[66] Shapiro IM, Kolev VN, Vidal CM, *et al*. Merlin deficiency predicts FAK inhibitor sensitivity: A synthetic lethal relationship. Sci Transl Med 2014; 6(237): 237ra68.

[67] Fennell DA, Baas P, Kindler HL, *et al*. COMMAND: A phase II randomized, double-blind, placebo-controlled, multicenter study of defactinib as maintenance therapy in subjects with malignant pleural mesothelioma that has not progressed on at least four cycles of pemetrexed/platinum therapy. J Clin Oncol 2014; 32: 15.

[68] Verastem Stops Enrollment Due to Futility in the COMMAND Study of *VS*-6063 for the Treatment of Malignant Pleural Mesothelioma [press release]. 2015; http://www.businesswire.com/news/home/20150928005465/en/Verastem-Stops-Enrollment-Due-Futility-COMMAND-Study

[69] Maggioni C, Barletta G, Rijavec E, Biello F, Gualco E, Grossi F. Advances in treatment of mesothelioma. Expert Opin Pharmacother 2016: 17(9): 1197-205.

[70] Hassan R, Schweizer C, Lu KF, *et al*. Inhibition of mesothelin-CA-125 interaction in patients with mesothelioma by the anti-mesothelin monoclonal antibody MORAb-009: Implications for cancer therapy. Lung Cancer 2010; 68(3): 455-9.

[71] Calabrò L, Maio M. Immune checkpoint blockade in malignant mesothelioma: A novel therapeutic strategy against a deadly disease? Oncoimmunology 2014; 3(1): e27482.

[72] Thapa B, Watkins DN, John T. Immunotherapy for malignant mesothelioma: Reality check. Expert Rev Anticancer Ther 2016; 6: 1-10.

[73] Ceresoli GL, Bonomi M, Sauta MG. Immune checkpoint inhibitors in malignant pleural mesothelioma: Promises and challenges. Expert Rev Anticancer Ther 2016; 16(7): 673-5.

[74] Roncella S, Laurent S, Fontana V, *et al*. CTLA-4 in mesothelioma patients: Tissue expression, body fluid levels and possible relevance as a prognostic factor. Cancer Immunol Immunother 2016; 65(8): 909-17.

[75] Guazzelli A, Bakker E, Krstic-Demonacos M, Lisanti MP, Sotgia F, Mutti L. Anti-CTLA-4 therapy for malignant mesothelioma. Immunotherapy 2017; 9(3): 273-80.

[76] Calabrò L, Morra A, Fonsatti E, *et al*. Efficacy and safety of an intensified schedule of tremelimumab for chemotherapy-resistant malignant mesothelioma: An open-label, single-arm, phase 2 study. Lancet Respir Med 2015; 3(4): 301-9.

[77] Marcq E, Pauwels P, van Meerbeeck JP, Smits EL. Targeting immune checkpoints: New opportunity for mesothelioma treatment? Cancer Treat Rev 2015; 41(10): 914-24.

[78] Alley EW, Molife LR, Santoro A, *et al*. Abstract CT103: Clinical safety and efficacy of pembrolizumab (MK-3475) in patients with malignant pleural

mesothelioma: Preliminary results from KEYNOTE-028. Cancer Res 2015; 75(15 Suppl): CT103.

[79] Remon J, Reguart N, Corral J, Lianes P. Malignant pleural mesothelioma: New hope in the horizon with novel therapeutic strategies. Cancer Treat Rev 2015; 41(1): 27-34.

[80] Servais EL, Colovos C, Rodriguez L, *et al*. Mesothelin overexpression promotes mesothelioma cell invasion and MMP-9 secretion in an orthotopic mouse model and in epithelioid pleural mesothelioma patients. Clin Cancer Res 2012; 18(9): 2478-89.

[81] Hassan R, Kindler HL, Jahan T, *et al*. Phase II clinical trial of amatuximab, a chimeric antimesothelin antibody with pemetrexed and cisplatin in advanced unresectable pleural mesothelioma. Clin Cancer Res 2014; 20(23): 5927-36.

[82] Jahan T, Hassan R, Alley E, *et al*. 208O_PR: CRS-207 with chemotherapy (chemo) in malignant pleural mesothelioma (MPM): Results from a phase 1b trial. J Thorac Oncol 2016; 11(4 Suppl): S156.

[83] Hassan R, Sharon E, Thomas A, *et al*. Phase 1 study of the antimesothelin immunotoxin SS1P in combination with pemetrexed and cisplatin for front-line therapy of pleural mesothelioma and correlation of tumor response with serum mesothelin, megakaryocyte potentiating factor, and cancer antigen 125. Cancer 2014; 120(21): 3311-9.

[84] Cornelissen R, Hegmans JP, Maat AP, *et al*. Extended tumor control after dendritic cell vaccination with low-dose cyclophosphamide as adjuvant treatment in patients with malignant pleural mesothelioma. Am J Respir Crit Care Med 2016; 193(9): 1023-31.

[85] Tan A, Porcher R, Crequit P, Ravaud P, Dechartres A. Differences in treatment effect size between overall survival and progression-free survival in immunotherapy trials: A meta-epidemiologic study of trials with results posted at ClinicalTrials.gov. J Clin Oncol 2017; 35(15): 1686-94.

[86] Gyawali B, Prasad V. Drugs that lack single-agent activity: Are they worth pursuing in combination? Nat Rev Clin Oncol 2017; 14(4): 193-4.

[87] Gyawali B, Prasad V. Combining drugs and extending treatment: A PFS end point is not sufficient. Nat Rev Clin Oncol 2017; 14(9): 521-522.

[88] Inamoto T, Yamada T, Ohnuma K, *et al*. Humanized anti-CD26 monoclonal antibody as a treatment for malignant mesothelioma tumors. Clin Cancer Res 2007; 13(14): 4191-200.

[89] Dang NH, Torimoto Y, Schlossman SF, Morimoto C. Human CD4 helper T cell activation: Functional involvement of two distinct collagen receptors, 1F7 and VLA integrin family. J Exp Med 1990; 172(2): 649-52.

[90] Amatya VJ, Takeshima Y, Kushitani K, Yamada T, Morimoto C, Inai K. Overexpression of CD26/DPPIV in mesothelioma tissue and mesothelioma cell lines. Oncol Rep 2011; 26(6): 1369-75.

[91] Aoe K, Amatya VJ, Fujimoto N, *et al*. CD26 overexpression is associated with prolonged survival and enhanced chemosensitivity in malignant pleural mesothelioma. Clin Cancer Res 2012; 18(5): 1447-56.

[92] Fujimoto N, Ohnuma K, Aoe K, *et al*. Clinical significance of soluble CD26 in malignant pleural mesothelioma. PLoS One 2014; 9(12): e115647.

[93] Yamazaki H, Naito M, Ghani FI, Dang NH, Iwata S, Morimoto C. Characterization of cancer stem cell properties of CD24 and CD26-positive human malignant mesothelioma cells. Biochem Biophys Res Commun 2012; 419(3): 529-36.

[94] Okamoto T, Iwata S, Yamazaki H, *et al*. CD9 negatively regulates CD26 expression and inhibits CD26-mediated enhancement of invasive potential of malignant mesothelioma cells. PLoS One 2014; 9(1): e86671.

[95] Komiya E, Ohnuma K, Yamazaki H, *et al*. CD26-mediated regulation of periostin expression contributes to migration and invasion of malignant pleural mesothelioma cells. Biochem Biophys Res Commun 2014; 447(4): 609-15.

[96] Yamada K, Hayashi M, Du W, *et al*. Localization of CD26/DPPIV in nucleus and its nuclear translocation enhanced by anti-CD26 monoclonal antibody with anti-tumor effect. Cancer Cell Int 2009; 9: 17.

[97] Yamada K, Hayashi M, Madokoro H, *et al*. Nuclear localization of CD26 induced by a humanized monoclonal antibody inhibits tumor cell growth by modulating of POLR2A transcription. PLoS One 2013; 8(4): e62304.

[98] Hayashi M, Madokoro H, Yamada K, *et al*. A humanized anti-CD26 monoclonal antibody inhibits cell growth of malignant mesothelioma *via* retarded G2/M cell cycle transition. Cancer Cell Int 2016; 16: 35.

[99] Angevin E, Isambert N, Trillet-Lenoir V, *et al*. First-in-human phase 1 of YS110, a monoclonal antibody directed against CD26 in advanced CD26-expressing cancers. Br J Cancer 2017; 116: 1926.

[100] Nakano T, Kuribayashi K, Mikami K. Possible new therapeutic agents for malignant pleural mesothelioma: Anti-CD26 monoclonal antibody and naftopidil. Expert Rev Anticancer Ther 2016; 8: 1-3.

Pancreas Fat and β Cell Mass in Humans With and Without Diabetes: An Analysis in the Japanese Population

Rie Murakami,[1] Yoshifumi Saisho,[1] Yuusuke Watanabe,[1] Jun Inaishi,[1] Tami Tsuchiya,[1] Kinsei Kou,[1,2] Seiji Sato,[1,3] Minoru Kitago,[4] Yuko Kitagawa,[4] Taketo Yamada,[5,6] and Hiroshi Itoh[1]

[1]Department of Internal Medicine, Keio University School of Medicine, Tokyo 160-8582, Japan; [2]Department of Internal Medicine, Hiratsuka City Hospital, Kanagawa 254-0065, Japan; [3]Shinseikai Sato Hospital, Fukushima 965-0877, Japan; [4]Department of Surgery, Keio University School of Medicine, Tokyo 160-8582, Japan; [5]Department of Pathology, Keio University School of Medicine, Tokyo 160-8582, Japan; and [6]Department of Pathology, Saitama Medical University, Saitama 350-0495, Japan

Context: The mechanisms by which β cell mass is reduced in patients with type 2 diabetes remain unclear. It has been postulated that ectopic fat deposits in the pancreas induce β cell apoptosis, leading to the development of diabetes.

Objective: The aim of this study was to clarify the effects of intrapancreatic fat on β and α cell mass in humans with and without diabetes.

Design and Subjects: Using our tissue database, pancreas sections of 72 Japanese nondiabetic (NDM) autopsy cases and 50 diabetic and 49 age- and body mass index (BMI)–matched NDM patients who underwent pancreatic surgery were analyzed. In addition to histological grading, intrapancreatic fat area (IPFA) was quantified as fractional intralobular, but not interlobular, fat area to the whole pancreas area.

Results: Although IPFA was positively correlated with age and BMI, there was no significant difference in IPFA between cases with and without diabetes. Moreover, no association was found between IPFA and either β or α cell area, or glycated hemoglobin.

Conclusion: These findings suggest that pancreatic fat deposits have little effect on β cell mass and the development of diabetes in humans. (***J Clin Endocrinol Metab*** **102: 3251–3260, 2017)**

Type 2 diabetes (T2DM) is characterized by a deficit of β cell mass (1–4). Although it has been reported that the deficit of β cell mass in patients with T2DM is attributable to an increase in β cell apoptosis (1), the mechanisms that cause β cell apoptosis remain uncertain.

Obesity is an established risk factor for T2DM (5, 6). When fat supply exceeds the capacity of subcutaneous fat storage, spilled-over fat leads to ectopic fat deposits in not only visceral adipose tissue, but also various organs, including the pancreas (7, 8). It has been reported that fatty acids induce β cell apoptosis in *in vitro* and *in vivo* studies of rodents (9, 10), the so-called lipotoxicity hypothesis. In Zucker Diabetic Fatty rats, β cell dysfunction and apoptosis were accompanied by excess lipid accumulation in islets, suggesting that excess lipid accumulation in the pancreas induces β cell apoptosis (9, 10).

However, conflicting results regarding the relationship between pancreatic fat content and β cell function or dysglycemia have been shown in human studies (7, 11–13). Although pancreatic fat content measured by magnetic resonance imaging or magnetic resonance spectrometry (MRS) has been shown to correlate with β

ISSN Print 0021-972X ISSN Online 1945-7197
Printed in USA

Received 7 April 2017. Accepted 31 May 2017.
First Published Online 14 June 2017

Abbreviations: ACA, α cell area; BCA, β cell area; BMI, body mass index; CT, computed tomography; DM, diabetic; HbA1c, glycated hemoglobin; IPFA, intrapancreatic fat area; IQR, interquartile range; MRS, magnetic resonance spectrometry; NDM, nondiabetic; SD, standard deviation; T2DM, type 2 diabetes.

cell function and/or dysglycemia (14–16), we have previously reported no significant difference in pancreatic fat content measured by computed tomography (CT) imaging between subjects with and without T2DM (17).

One of the major reasons for this inconsistency may be the difficulty of measurement of pancreatic fat content. Because the pancreas is surrounded by fat tissue in the retroperitoneal space, it is difficult to precisely exclude the fat outside the pancreas. Although attempts to improve the accuracy of pancreatic fat measurement using imaging tools have been made (14, 18, 19), it remains impossible to completely distinguish interlobular fat (*i.e.*, fat outside the pancreas) from intralobular fat of the pancreas due to the intricate lobular structure of the pancreas. Moreover, in contrast to the liver, in which fat is diffusely distributed within hepatocytes, pancreatic fat is mainly present in adipocytes within the pancreas (20), and thereby the distribution of fat is not homogeneous within the pancreas, which accounts for the difficulty of assessment of pancreatic fat content by imaging methods.

In view of these limitations of imaging studies, we conducted a histological evaluation of intrapancreatic fat content using pancreas samples from 72 autopsy cases and 50 patients with and 49 without diabetes who underwent pancreatic surgery in an attempt to gain more insight into the relationship between pancreatic fat and β cell mass and diabetes.

Research Design and Methods

Subjects

This study was approved by the Ethics Committee of the Keio University School of Medicine. The cases have been reported in our prior studies (3, 21). For autopsy cases, specimens of pancreas obtained at autopsy were acquired with the permission of the bereaved families. For patients who underwent pancreatic surgery, written informed consent was obtained from each patient, whereas it was waived for patients who had discontinued hospital visits at the time of study enrollment (n = 40).

A total of 72 autopsy cases without diabetes [nondiabetic (NDM)-1 group] and 99 patients who underwent pancreatic surgery [50 diabetic (DM) patients and 49 patients without diabetes (NDM-2 group)] were included in this study. The characteristics of the cases, which have been previously reported (3, 21), are summarized in Table 1. All subjects were Japanese.

Autopsy cases

Potential cases were first identified by retrospective analysis of the Keio University autopsy database. To be included, cases were required to have (1) been aged 20 to 69 years, (2) had a full autopsy within 24 hours of death, (3) medical information prior to death, (4) no history of diabetes, pancreatitis, pancreatic tumor, or pancreatic surgery, (5) no use of glucocorticoids, and (6) pancreatic tissue stored that was of adequate size and quality. Cases were excluded if pancreatic tissue had undergone autolysis.

Surgical cases

As previously described (3), subjects who underwent pancreatic surgery and whose resected pancreas sample contained adequate normal pancreas for histological analysis were included in the study. Of these, 41 patients had been diagnosed with T2DM before the diagnosis of pancreatic tumors, and eight patients were diagnosed with pancreatic cancer and diabetes at the same time. There was no case of type 1 diabetes or case in which glutamic acid decarboxylase antibody was positive.

Glycemic markers

In autopsy cases, glycated hemoglobin (HbA1c) measured within 1 year prior to death was obtained from the medical records (21). In patients who underwent pancreatic surgery, information including HbA1c, casual plasma glucose, and serum C-peptide immunoreactivity levels was obtained from the medical records, as previously described (3). HbA1c was measured by high-performance liquid chromatography and expressed as National Glycohemoglobin Standardization Program and International Federation of Clinical Chemistry values. Serum C-peptide immunoreactivity was measured by chemiluminescent enzyme immunoassay.

Table 1. Characteristics of Subjects

		Autopsy Cases	Surgical Cases	
	Total	NDM-1	NDM-2	DM
N	171	72	50	49
Sex (male/female)	107/64	46/26	26/24	35/14
Age (y)	58 ± 15	47 ± 12	64 ± 14	67 ± 9
Height (m)	1.63 ± 0.09	1.65 ± 0.09	1.61 ± 0.08	1.63 ± 0.09
Weight (kg)	61.9 ± 14.3	66.2 ± 16.7	58.6 ± 10.5	58.9 ± 12.2
BMI (kg/m^2)	23.0 ± 4.1	24.1 ± 5.0	22.5 ± 2.7	21.9 ± 3.5
Casual plasma glucose (mmol/L)[a]	6.4 ± 2.1	5.2 ± 1.0	6.2 ± 1.2	8.3 ± 2.5
HbA1c (%)[a]	6.3 ± 1.6	5.3 ± 0.7	5.6 ± 0.5	7.8 ± 1.6
HbA1c (mmol/mol)[a]	45 ± 17	34 ± 7	38 ± 6	61 ± 18
Pancreas head/body or tail (n)	27/144	7/65	6/44	14/35

Data are expressed as mean ± SD. Note that NDM-2 and DM groups were matched for age and BMI, as previously reported (3).

[a] Casual plasma glucose and HbA1c levels were measured in 169 cases and 132 cases, respectively.

Pancreatic tissue processing

The pancreas was fixed in formaldehyde and then embedded in paraffin for subsequent analysis. Autopsy specimens were sampled from the body or tail portion of the pancreas, except for seven specimens sampled from the head of the pancreas. Seventy-nine and 20 surgical specimens were sampled from the body or tail portion and the head portion, respectively. Five-micrometer sections were cut from the tumor-free region and stained for light microscopy as follows: (1) with hematoxylin-eosin, (2) for insulin (peroxidase staining) with hematoxylin, (3) for glucagon with hematoxylin, (4) for insulin and Ki67 for assessment of β cell replication, and (5) for insulin and single-stranded DNA or cleaved poly(adenosine 5′-diphosphate-ribose) polymerase-1 for assessment of β cell apoptosis, as previously described (3, 21).

Morphometric analysis

As previously described (3, 21, 22), to quantify fractional β cell area (BCA), the entire pancreatic section was imaged at ×200 magnification (×20 objective) using a Mirax Scan and Mirax Viewer (Carl Zeiss MicroImaging GmbH, Göttingen, Germany). The ratio of BCA to total pancreas area was digitally measured using Image Pro Plus software (Media Cybernetics, Silver Springs, MD). Likewise, the ratio of α cell area (ACA) to total pancreas area was also digitally measured, and the ratio of ACA to BCA was determined in each case. Intraobserver coefficient of variance (computed in five cases studied on five occasions) and interobserver variance were approximately 7% and 12%, respectively (3, 21). All measurements were conducted twice, and the mean of the two measurements was used.

To conduct further morphometric analysis, scattered β cells, insulin-positive duct cells, and β cell replication were quantified in randomly selected areas of the pancreas that contained more than 100 islets in each case, using a Mirax Viewer (Carl Zeiss MicroImaging GmbH). Scattered β cells were defined as a cluster of three or fewer β cells in acinar tissue, and the density of scattered β cells was determined as the number of scattered β cells/pancreas area (mm^2). Likewise, the density of islets and individual islet size were also determined in the same area. Insulin-positive duct cells were also counted and expressed as the number of insulin-positive duct cells/pancreas area (mm^2). The frequency of β cell replication was expressed as the percentage of islets.

Assessment of intrapancreatic fat content

Intrapancreatic fat content was graded based on histological evaluation [none (–) to severe (+++)] (Fig. 1). Because pancreatic fat is extracted during specimen dehydration, intrapancreatic fat appears as lobulated spaces within the pancreas lobes. These intrapancreatic adipocytes were confirmed by perilipin staining (antiperilipin A antibody-carboxyterminal end; ab61682, Abcam, Cambridge, United Kingdom). These intrapancreatic fat areas (IPFAs) were also quantified using Image Pro Plus software (Media Cybernetics). Only pancreatic fat within parenchymal tissue (*i.e.*, intralobular fat), but not interlobular fat (*i.e.*, fat outside the pancreas), was measured as IPFA. Thus, IPFA was calculated as a fraction of total pancreatic area.

Statistical analysis

Data are presented as mean ± standard deviation (SD) in the text and tables unless otherwise indicated. Non-normally distributed data are presented as median and interquartile range (IQR). Mann-Whitney *U* test was used to assess differences between two groups, and comparisons among the three groups were performed by Kruskal-Wallis test. Spearman correlation analysis was carried out for correlation analysis. Multivariate analysis was used to adjust for confounding factors such as age and body mass index (BMI). All analyses were performed using the Statistical Package for the Social Sciences (version 23; SPSS, Chicago, IL), and $P < 0.05$ was considered statistically significant.

Results

Intrapancreatic fat content in subjects with and without diabetes

Intrapancreatic adipocytes were diffusely distributed within the pancreatic lobes, and as the number of adipocytes increased, they formed clusters, which were readily distinguishable from other structures such as vessels, ducts, and interlobular adipocytes (Fig. 1). Adipocytes were not observed within the islets. Histological grade of intrapancreatic fat content was closely correlated with IPFA (Table 2). IPFA varied among subjects (median, 0.51%; IQR, 0.17% to 1.27%). There was no difference in IPFA between samples from the head portion of the pancreas (n = 27) and those from the body or

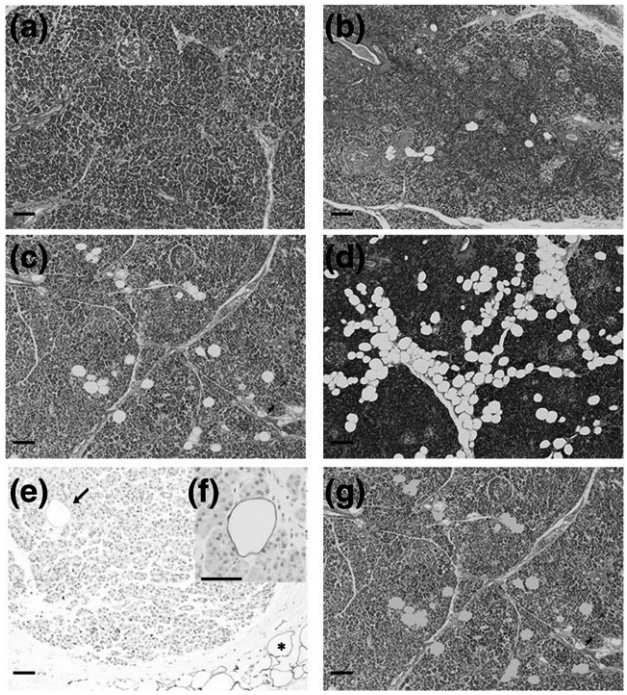

Figure 1. (a–d) Representative photomicrographs of histological grades of intrapancreatic fat content. (a) Grade (–). (b) Grade (+). (c) Grade (++). (d) Grade (+++). (e) Intrapancreatic adipocytes were confirmed by perilipin staining (brown). Interlobular pancreatic adipocytes are indicated by asterisk. (f) Higher magnification (×40 objective) of intrapancreatic adipocyte. (g) IPFA was carefully quantified as a fraction of IPFA (shown in orange), but not interlobular fat area, to the total pancreas area. Scale bar = 100 μm.

Table 2. Characteristics of Subjects According to Histological Grade of Intrapancreatic Fat Content

Intrapancreatic Fat Content	(–)	(+)	(++) to (+++)	P^a
N (%)	33 (19)	80 (47)	58 (34)	
Sex (male/female)	24/9	46/34	37/21	0.31
Age (y)	54 ± 15	56 ± 16	61 ± 13	0.04
Height (m)	1.64 ± 0.09	1.63 ± 0.09	1.63 ± 0.09	0.82
Weight (kg)	60.0 ± 13.4	60.1 ± 11.5	65.7 ± 17.5	0.04
BMI (kg/m^2)	21.9 ± 3.3	22.4 ± 3.2	24.5 ± 5.1	<0.01
DM (%)	39	19	36	0.08
Casual plasma glucose (mmol/L)[b]	6.6 ± 2.3	6.2 ± 2.1	6.7 ± 1.9	0.28
HbA1c (%)[b]	6.7 ± 1.8	6.1 ± 1.5	6.4 ± 1.4	0.22
HbA1c (mmol/mol)[b]	50 ± 20	43 ± 17	46 ± 15	0.22
IPFA (%)	0.07 (0.04–0.17)	0.40 (0.19–0.66)	1.82 (0.97–2.66)	<0.01

Data are expressed as mean ± SD or median (IQR).

[a] *P* for Kruskal-Wallis test or χ^2 test among three groups.

[b] Casual plasma glucose and HbA1c levels were measured in 169 and 132 cases, respectively.

tail portion of the pancreas (n = 144; median, 0.50%; IQR, 0.17% to 1.09% vs median, 0.52%; IQR, 0.17% to 1.31%; $P = 0.61$) [Supplemental Fig. 2(a)]. There was no difference in IPFA between autopsy cases (NDM-1) and surgical cases (NDM-2) (median, 0.45%; IQR, 0.12% to 1.20% vs median, 0.51%; IQR, 0.26 to 0.99; $P = 0.39$) [Fig. 2(a)]. Although we previously reported a significant reduction in BCA in patients with diabetes compared with age- and BMI-matched patients without diabetes (NDM-2) (1.48% ± 1.08% vs 0.80% ± 0.54%, $P < 0.001$) (3),

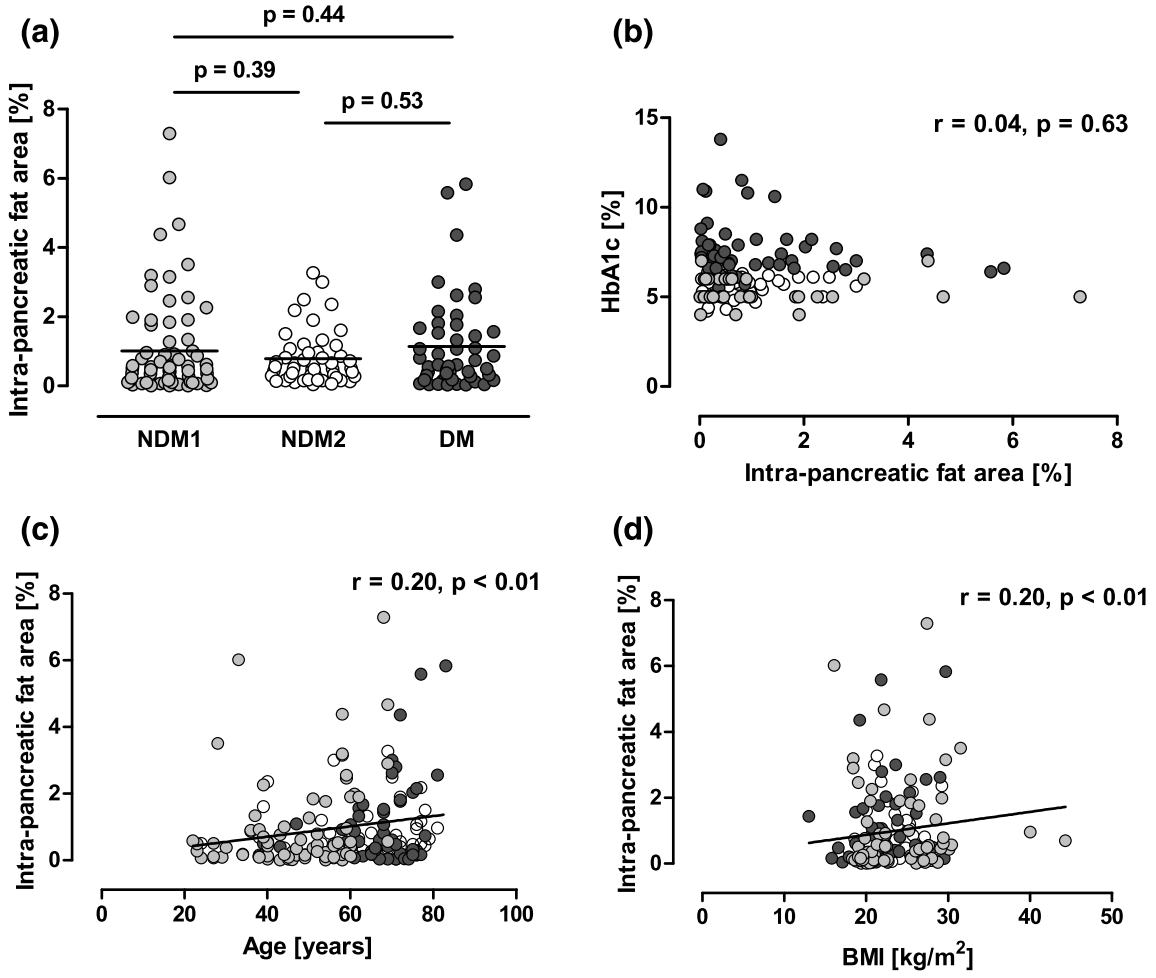

Figure 2. (a) IPFA in autopsy cases without diabetes (NDM-1), surgical cases with diabetes (DM), and surgical cases without diabetes matched for age and BMI (NDM-2). (b–d) Correlations between IPFA and (b) HbA1c, (c) age, and (d) BMI. Light-gray circles show autopsy cases. Dark-gray and white circles show surgical cases with and without diabetes, respectively.

there was no difference in IPFA between the two groups (median, 0.51%; IQR, 0.04% to 3.27% vs median, 0.61%; IQR, 0.03% to 5.83%; $P = 0.53$) [Fig. 2(a)]. In view of the fact that there was no significant difference in intrapancreatic fat content either between autopsy and surgical cases or between cases with and without diabetes, we conducted subsequent analyses in the combined cases as well as within each group.

Factors associated with intrapancreatic fat content

Characteristics of the subjects according to the histological grade of intrapancreatic fat content are shown in Table 2 and Supplemental Table 1 for surgical cases. Histological grade of intrapancreatic fat content was associated with age and BMI, but not with HbA1c or plasma glucose level. As well as histological grade, IPFA was significantly correlated with age and BMI in the total cases (both $r = 0.20$, $P < 0.01$) [Fig. 2(c) and 2(d)], but not with HbA1c [Fig. 2(b)]. In surgical cases, the duration of obesity as well as current BMI, but not maximum BMI, tended to associate with intrapancreatic fat content ($P = 0.07$ and 0.66, respectively) (Supplemental Table 1). The results were not markedly changed when the analysis was conducted only in the DM group (Supplemental Table 2). There was no significant correlation between IPFA and casual plasma glucose or serum C-peptide immunoreactivity level (Supplemental Table 2; Supplemental Fig. 1).

Relationships between intrapancreatic fat content and BCA, ACA, and islet morphology

There was no difference in either BCA or ACA among the groups according to the histological grade of intrapancreatic fat content [Fig. 3(a) and 3(b)], and there was no significant correlation between IPFA and BCA or ACA ($r = 0.05$, $P = 0.56$ and $r = -0.12$, $P = 0.12$) [Fig. 3(f) and 3(g)]. ACA/BCA ratio was also not associated with histological grade or IPFA [Fig. 3(c) and 3(i)]. When the NDM-1, NDM-2, and DM groups were analyzed separately (Supplemental Table 2), BCA and ACA were positively correlated with IPFA in the DM group ($r = 0.30$, $P = 0.04$ and $r = 0.30$, $P = 0.04$, respectively), and ACA was negatively correlated with IPFA in the NDM-1 group ($r = -0.28$, $P = 0.02$). However, the significant correlations were attenuated after adjustment for age and BMI (Supplemental Table 2).

Difference in mean islet size was also statistically significant among the histological grading groups ($P = 0.03$) [Fig. 3(e)], but no association between IPFA and mean islet size was detected ($r = 0.00$, $P = 0.99$) [Fig. 3(j)]. These results were not changed when the analyses were conducted in each group separately (*i.e.*, NDM-1, NDM-2, and DM groups) (Supplemental Table 2). There was no association between IPFA and islet density ($r = -0.10$, $P = 0.21$) [Fig. 3(i)].

Relationships between intrapancreatic fat content and markers of β cell turnover

Intrapancreatic fat content assessed as histological grade or IPFA was not associated with either frequency of β cell replication, insulin-positive duct cells, or scattered β cells (Fig. 4). No β cell apoptosis was observed in these cases, as previously reported (3, 21).

Discussion

The current study, applying histological evaluation of intrapancreatic fat content, showed the following: (1) There was no significant difference in intrapancreatic fat content between subjects with and without diabetes. (2) No association between intrapancreatic fat content and β cell mass, islet morphology, or markers of β cell turnover was observed. (3) There was no correlation between intrapancreatic fat content and HbA1c level. (4) Intrapancreatic fat content increased with age and obesity in humans.

T2DM is characterized by a deficit of β cells, presumably due to an increase in β cell apoptosis (1). However, the mechanisms by which β cell apoptosis increases in patients with T2DM remain unclear. A longitudinal cohort in the UK Prospective Diabetes Study suggested that β cell dysfunction begins over 10 years before the onset of T2DM (23). Reduced β cell mass in patients with prediabetes has also been reported (1, 24, 25), suggesting that β cell loss occurs even before the onset of T2DM.

Ectopic fat deposits are a hallmark of metabolic syndrome and T2DM (8, 26). Rodent studies have suggested the possibility that ectopic fat deposits in the pancreas induce β cell apoptosis and the development of hyperglycemia (9, 10), the so-called lipotoxicity hypothesis. Since then, the association between pancreas fat content and β cell function or glucose tolerance status has been actively investigated (7, 11–13).

Tushuizen *et al.* (14) first reported, using MRS, that pancreatic fat content was increased in patients with T2DM, and pancreatic fat content was negatively associated with β cell function in NDM subjects. However, the small sample size (12 with T2DM, 24 without diabetes) with an almost significant difference in BMI between the two groups has been pointed out as a limitation of that study (27). We have previously reported, using CT scan images of over 2000 subjects, that there was no significant difference in pancreas fat content between age-, sex-, and BMI-matched subjects with and without T2DM (17).

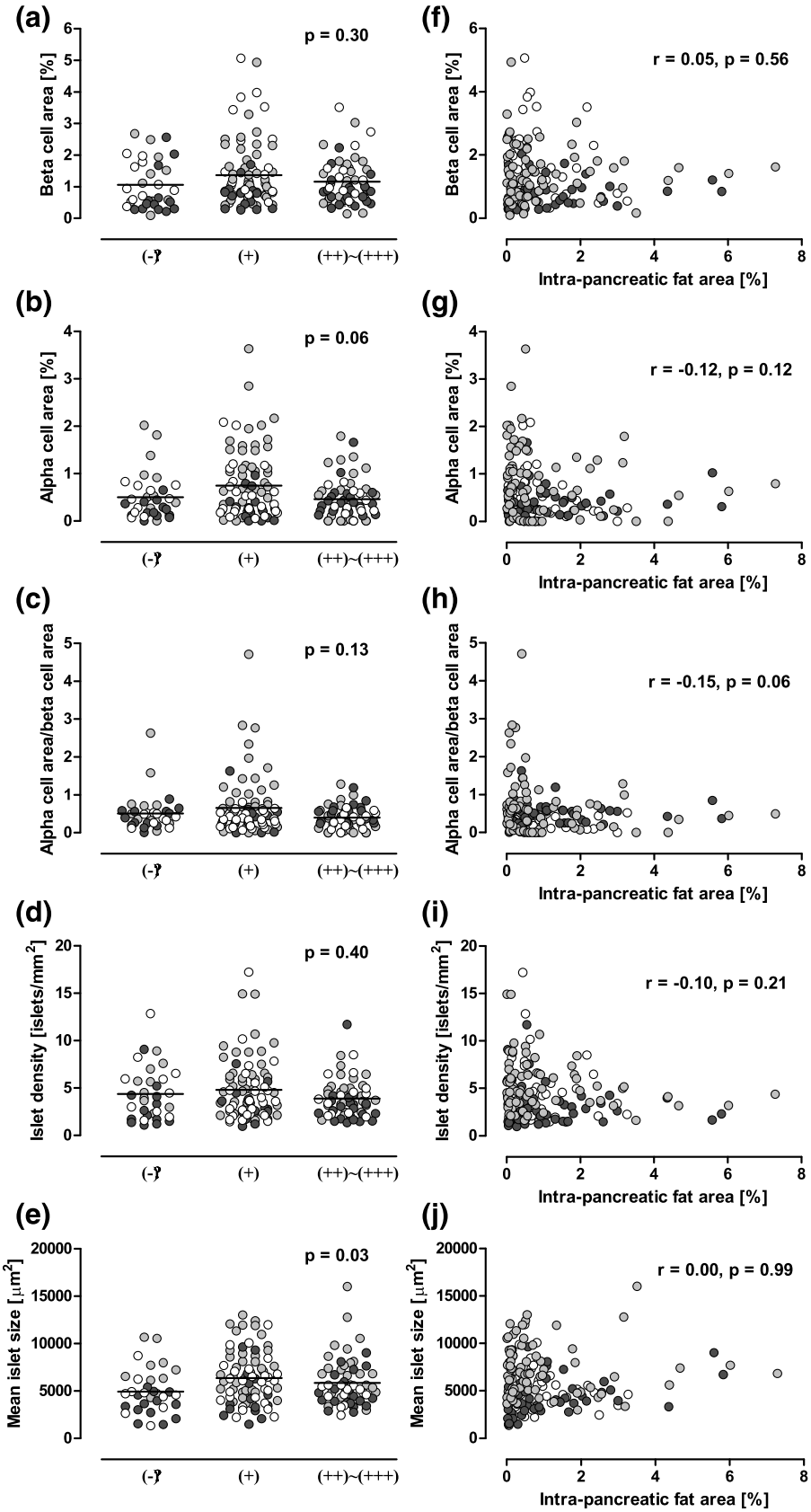

Figure 3. (a–e) Comparisons among groups according to histological grade of intrapancreatic fat content: (a) BCA, (b) ACA, (c) ACA/BCA ratio, (d) islet density, and (e) mean islet size. (f–j) Correlations between IPFA and (f) BCA, (g) ACA, (h) ACA/BCA ratio, (i) islet density, and (j) mean islet size. Light-gray circles show autopsy cases. Dark-gray and white circles show surgical cases with and without diabetes, respectively.

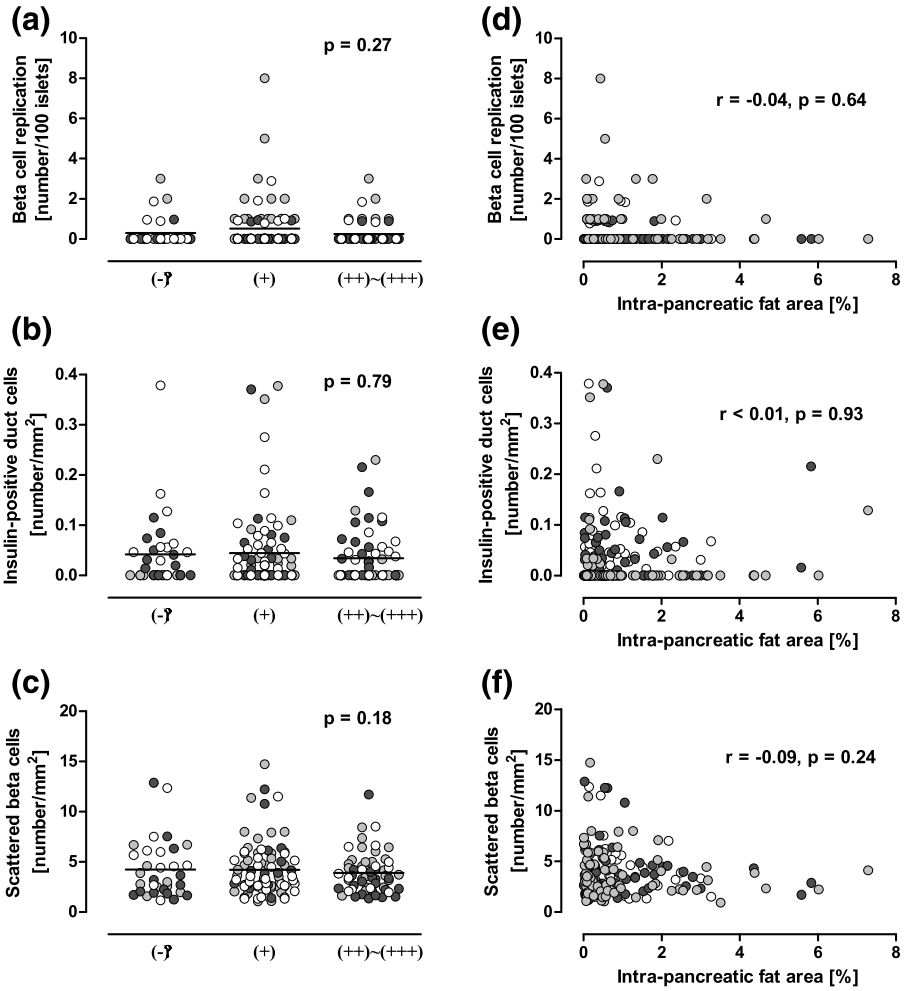

Figure 4. (a–c) Comparisons among three groups according to histological grade of intrapancreatic fat content: frequency of (a) β cell replication, (b) insulin-positive duct cells, and (c) scattered β cells. (d–f) Correlations between IPFA and frequency of (d) β cell replication, (e) insulin-positive duct cells, and (f) scattered β cells. Light-gray circles show autopsy cases. Dark-gray and white circles show surgical cases with and without diabetes, respectively.

Furthermore, these inconsistent results of imaging studies may be in part due to difficulties in accurate measurement of pancreatic fat (11). The pancreas is surrounded by fat in the retroperitoneal space and consists of an intricate lobular structure, making it inevitably difficult to distinguish intrapancreatic fat from fat outside the pancreas. In this study, to overcome these limitations of imaging studies, by conducting histological assessment of intrapancreatic fat content, we reported that there was no relationship between intrapancreatic fat content and β cell mass or dysglycemia in humans.

Our findings are also in line with prior histological studies assessing pancreas fat in subjects with diabetes, which have shown no difference in pancreatic fat content in subjects with and without T2DM (17, 20, 28, 29). Our study applied quantification of intrapancreatic fat content in a relatively large number of subjects with a wide range of age and BMI, and we believe our findings are more objective and robust compared with those of these prior histological studies. Our conclusion that there is no association between intrapancreatic fat content and diabetes is also supported by the finding of no association between intrapancreatic fat content and β cell mass.

Recent rodent studies have suggested that dedifferentiation of β cells and conversion from β to α cells is one of the mechanisms of β cell loss in T2DM (30), although histological studies in humans have suggested that β cell dedifferentiation has only a minor role, and presumably β cell apoptosis is a major cause of β cell loss in patients with T2DM (31), in line with the observation of reduced islet size in patients with T2DM (3, 32, 33). In this study, we found no significant relationship between IPFA and either BCA or ACA/BCA ratio, suggesting that intrapancreatic fat content is unlikely to be associated with this intriguing possibility.

Recently, several studies showing no association between pancreatic fat and T2DM have also been published. Begovatz *et al.* (18) conducted an assessment of intrapancreatic fat by magnetic resonance imaging/MRS in 56 subjects with and without dysglycemia. In that

study, they measured intrapancreatic fat carefully after excluding the fat outside the pancreas and found no association between intrapancreatic fat content and β cell function or dysglycemia (18). Yamazaki *et al.* (34) conducted a longitudinal study showing that pancreatic fat assessed by CT imaging was not associated with the development of T2DM independently of obesity. Moreover, whereas it has been reported that the improvement of dysglycemia by a very low-calorie diet in adults with T2DM was associated with improvement of pancreatic fat content (35), Gow *et al.* (36) did not find such an association between pancreatic fat and improvement of hyperglycemia during treatment with a very low-calorie diet in young people with T2DM. Taking these results together, to date, there is no concrete evidence for a causal association of pancreatic fat with the development of diabetes. Further studies to improve the accuracy of intrapancreatic fat measurement *in vivo* in humans are warranted. Also, because intra- and interlobular pancreatic fat content are both increased with aging and obesity, future studies should be carefully conducted to exclude these important confounders.

As with other studies, our study was not free from limitations. First, we assessed intrapancreatic fat in a section of the pancreas. Intrapancreatic fat content may differ among different portions of the pancreas. However, it has been reported that the proportion of fat content did not differ among the head, body, and tail portions of the pancreas (37, 38), and we found no significant difference in IPFA between samples from the head of the pancreas and those from the body or tail of the pancreas [Supplemental Fig. 2(a)]. Also, the results did not change when the analyses were conducted using only samples from the body or tail of the pancreas (n = 144, data not shown). It should also be noted that β cell mass was assessed as fractional BCA in a section of the pancreas, although it is widely used as a measure of β cell mass, as discussed previously (3, 21). Nonetheless, it should be kept in mind that the individual values may not be truly representative for any particular pancreas, although we believe that the overall conclusions are valid because of the large number of subjects studied. Whereas increased pancreatic fat infiltration has been reported in patients with pancreatic ductal adenocarcinoma (39), we found no significant difference in IPFA between patients with and without pancreatic cancer (median, 0.57%; IQR, 0.33% to 1.14% vs median, 0.56%; IQR, 0.20% to 1.35%; $P = 0.94$) [Supplemental Fig. 2(b)]. Second, the histological measurement of fat was indirect, because fat is removed during tissue processing and section staining. However, the morphological features of adipocytes were readily identified, and we also confirmed the presence of adipocytes in the pancreas by perilipin staining (Fig. 1). We also assessed the intrapancreatic fat content using a grading system and confirmed consistent results between the two methods. Although we did not assess lipid content within islets, close correlations among IPFA, pancreatic triacylglycerol content (20), and islet triacylglycerol content (9) have been reported in rodent models. Thus, it is reasonable to assume that IPFA reflects islet triglyceride content. Third, we could not assess β cell function in most of the subjects. Thus, although we found no association between IPFA and BCA, we cannot exclude the possibility that IPFA is associated with β cell dysfunction. However, the absence of association between IPFA and HbA1c, C-peptide immunoreactivity, or presence of diabetes suggests that the effect of IPFA on β cell function is, if any, modest. Although we could not exclude the possibility that patients with pancreatic diabetes, but not T2DM, were included in this study, we found no significant difference in IPFA between subjects with duration of diabetes ≤3 years (n = 23) and those with duration of diabetes >3 years (n = 26; median, 0.61%; IQR, 0.17% to 1.53% vs median, 0.59%; IQR, 0.26% to 1.71%; $P = 0.41$). Finally, this study included only Japanese subjects. We have reported that there was no significant correlation between β cell mass and BMI in Japanese subjects with and without T2DM (3, 21), suggesting that the adaptive increase in β cell mass in response to obesity is minimal in the Japanese population. Thus, our findings may not be applicable to other ethnicities, and future studies including multiple ethnic groups are needed.

In conclusion, there was no correlation between intrapancreatic fat content and β cell mass or turnover, or dysglycemia. These findings suggest that ectopic fat deposits in the pancreas may not be responsible for the development of diabetes in humans.

Acknowledgments

We thank Yuko Madokoro, Department of Pathology, Keio University School of Medicine, for technical assistance and Wendy Gray for editing the manuscript.

Address all correspondence and requests for reprints to: Yoshifumi Saisho, MD, PhD, Department of Internal Medicine, Keio University School of Medicine, 35 Shinanomachi, Shinjuku-ku, Tokyo 160-8582, Japan. E-mail: ysaisho@keio.jp.

This study was supported by funding from the Japan Diabetes Foundation, Keio Gijuku Academic Development Funds, and Japan Society for the Promotion of Science Grants-in-Aid for Scientific Research (JSPS KAKENHI) Grant Number JP15K09399 (to Y.S.).

Author contributions: Y.S. designed and performed the research. R.M., J.I., and K.K. contributed to the data analysis. R.M., Y.S., Y.W., J.I., T.T., K.K., S.S., M.K., Y.K., T.Y., and H.I.

contributed to the discussion and reviewed and edited the manuscript. Y.S. is the guarantor of this work and, as such, had full access to all the data in the study and takes responsibility for the integrity of the data and the accuracy of the data analysis.

Disclosure Summary: The authors have nothing to disclose.

References

1. Butler AE, Janson J, Bonner-Weir S, Ritzel R, Rizza RA, Butler PC. Beta-cell deficit and increased beta-cell apoptosis in humans with type 2 diabetes. *Diabetes*. 2003;**52**(1):102–110.
2. Rahier J, Guiot Y, Goebbels RM, Sempoux C, Henquin JC. Pancreatic beta-cell mass in European subjects with type 2 diabetes. *Diabetes Obes Metab*. 2008;**10**(Suppl 4):32–42.
3. Inaishi J, Saisho Y, Sato S, Kou K, Murakami R, Watanabe Y, Kitago M, Kitagawa Y, Yamada T, Itoh H. Effects of obesity and diabetes on alpha- and beta-cell mass in surgically resected human pancreas. *J Clin Endocrinol Metab*. 2016;**101**(7):2874–2882.
4. Saisho Y. β-cell dysfunction: its critical role in prevention and management of type 2 diabetes. *World J Diabetes*. 2015;**6**(1): 109–124.
5. Guh DP, Zhang W, Bansback N, Amarsi Z, Birmingham CL, Anis AH. The incidence of co-morbidities related to obesity and overweight: a systematic review and meta-analysis. *BMC Public Health*. 2009;**9**:88.
6. Hu Y, Bhupathiraju SN, de Koning L, Hu FB. Duration of obesity and overweight and risk of type 2 diabetes among US women. *Obesity (Silver Spring)*. 2014;**22**(10):2267–2273.
7. van Raalte DH, van der Zijl NJ, Diamant M. Pancreatic steatosis in humans: cause or marker of lipotoxicity? *Curr Opin Clin Nutr Metab Care*. 2010;**13**(4):478–485.
8. Sattar N, Gill JM. Type 2 diabetes as a disease of ectopic fat? *BMC Med*. 2014;**12**:123.
9. Lee Y, Lingvay I, Szczepaniak LS, Ravazzola M, Orci L, Unger RH. Pancreatic steatosis: harbinger of type 2 diabetes in obese rodents. *Int J Obes*. 2010;**34**(2):396–400.
10. Lee Y, Hirose H, Ohneda M, Johnson JH, McGarry JD, Unger RH. Beta-cell lipotoxicity in the pathogenesis of non-insulin-dependent diabetes mellitus of obese rats: impairment in adipocyte-beta-cell relationships. *Proc Natl Acad Sci USA*. 1994;**91**(23): 10878–10882.
11. Saisho Y. Pancreas volume and fat deposition in diabetes and normal physiology: consideration of the interplay between endocrine and exocrine pancreas. *Rev Diabet Stud*. 2016;**13**(2-3): 132–147.
12. Pezzilli R, Calculli L. Pancreatic steatosis: is it related to either obesity or diabetes mellitus? *World J Diabetes*. 2014;**5**(4):415–419.
13. Smits MM, van Geenen EJM. The clinical significance of pancreatic steatosis. *Nat Rev Gastroenterol Hepatol*. 2011;**8**(3):169–177.
14. Tushuizen ME, Bunck MC, Pouwels PJ, Bontemps S, van Waesberghe JH, Schindhelm RK, Mari A, Heine RJ, Diamant M. Pancreatic fat content and beta-cell function in men with and without type 2 diabetes. *Diabetes Care*. 2007;**30**(11):2916–2921.
15. Szczepaniak LS, Victor RG, Mathur R, Nelson MD, Szczepaniak EW, Tyer N, Chen I, Unger RH, Bergman RN, Lingvay I. Pancreatic steatosis and its relationship to β-cell dysfunction in humans: racial and ethnic variations. *Diabetes Care*. 2012;**35**(11):2377–2383.
16. Heni M, Machann J, Staiger H, Schwenzer NF, Peter A, Schick F, Claussen CD, Stefan N, Häring H-U, Fritsche A. Pancreatic fat is negatively associated with insulin secretion in individuals with impaired fasting glucose and/or impaired glucose tolerance: a nuclear magnetic resonance study. *Diabetes Metab Res Rev*. 2010; **26**(3):200–205.
17. Saisho Y, Butler AE, Meier JJ, Monchamp T, Allen-Auerbach M, Rizza RA, Butler PC. Pancreas volumes in humans from birth to age one hundred taking into account sex, obesity, and presence of type-2 diabetes. *Clin Anat*. 2007;**20**(8):933–942.
18. Begovatz P, Koliaki C, Weber K, Strassburger K, Nowotny B, Nowotny P, Müssig K, Bunke J, Pacini G, Szendrödi J, Roden M. Pancreatic adipose tissue infiltration, parenchymal steatosis and beta cell function in humans. *Diabetologia*. 2015;**58**(7):1646–1655.
19. Lingvay I, Esser V, Legendre JL, Price AL, Wertz KM, Adams-Huet B, Zhang S, Unger RH, Szczepaniak LS. Noninvasive quantification of pancreatic fat in humans. *J Clin Endocrinol Metab*. 2009;**94**(10): 4070–4076.
20. Pinnick KE, Collins SC, Londos C, Gauguier D, Clark A, Fielding BA. Pancreatic ectopic fat is characterized by adipocyte infiltration and altered lipid composition. *Obesity (Silver Spring)*. 2008;**16**(3): 522–530.
21. Kou K, Saisho Y, Satoh S, Yamada T, Itoh H. Change in β-cell mass in Japanese nondiabetic obese individuals. *J Clin Endocrinol Metab*. 2013;**98**(9):3724–3730.
22. Saisho Y, Butler AE, Manesso E, Elashoff D, Rizza RA, Butler PC. β-cell mass and turnover in humans: effects of obesity and aging. *Diabetes Care*. 2013;**36**(1):111–117.
23. U.K. Prospective Diabetes Study Group. U.K. prospective diabetes study 16. Overview of 6 years' therapy of type II diabetes: a progressive disease. *Diabetes*. 1995;**44**(11):1249–1258.
24. Meier JJ, Breuer TG, Bonadonna RC, Tannapfel A, Uhl W, Schmidt WE, Schrader H, Menge BA. Pancreatic diabetes manifests when beta cell area declines by approximately 65% in humans. *Diabetologia*. 2012;**55**(5):1346–1354.
25. Yoneda S, Uno S, Iwahashi H, Fujita Y, Yoshikawa A, Kozawa J, Okita K, Takiuchi D, Eguchi H, Nagano H, Imagawa A, Shimomura I. Predominance of β-cell neogenesis rather than replication in humans with an impaired glucose tolerance and newly diagnosed diabetes. *J Clin Endocrinol Metab*. 2013;**98**(5): 2053–2061.
26. Kusminski CM, Shetty S, Orci L, Unger RH, Scherer PE. Diabetes and apoptosis: lipotoxicity. *Apoptosis*. 2009;**14**(12):1484–1495.
27. Saisho Y, Butler AE, Butler PC 2008 Pancreatic fat content and beta-cell function in men with and without type 2 diabetes: response to Tushuizen et al. *Diabetes Care*. 2008;**31**(5):e38–e39.
28. Olsen TS. Lipomatosis of the pancreas in autopsy material and its relation to age and overweight. *Acta Pathol Microbiol Scand [A]*. 1978;**86A**(5):367–373.
29. Clark A, Wells CA, Buley ID, Cruickshank JK, Vanhegan RI, Matthews DR, Cooper GJ, Holman RR, Turner RC. Islet amyloid, increased A-cells, reduced B-cells and exocrine fibrosis: quantitative changes in the pancreas in type 2 diabetes. *Diabetes Res*. 1988;**9**(4):151–159.
30. Talchai C, Xuan S, Lin HV, Sussel L, Accili D. Pancreatic β cell dedifferentiation as a mechanism of diabetic β cell failure. *Cell*. 2012;**150**(6):1223–1234.
31. Butler AE, Dhawan S, Hoang J, Cory M, Zeng K, Fritsch H, Meier JJ, Rizza RA, Butler PC. Beta-cell deficit in obese type 2 diabetes, a minor role of beta-cell dedifferentiation and degranulation. *J Clin Endocrinol Metab*. 2016;**101**(2):523–532.
32. Sato S, Saisho Y, Inaishi J, Kou K, Murakami R, Yamada T, Itoh H. Effects of glucocorticoid treatment on beta- and alpha-cell mass in Japanese adults with and without diabetes. *Diabetes*. 2015;**64**(8): 2915–2927.
33. Westermark P, Wilander E. The influence of amyloid deposits on the islet volume in maturity onset diabetes mellitus. *Diabetologia*. 1978;**15**(5):417–421.
34. Yamazaki H, Tsuboya T, Katanuma A, Kodama Y, Tauchi S, Dohke M, Maguchi H. Lack of independent association between fatty pancreas and incidence of type 2 diabetes mellitus: 5-year Japanese cohort study. *Diabetes Care*. 2016;**39**(10):1677–1683.
35. Lim EL, Hollingsworth KG, Aribisala BS, Chen MJ, Mathers JC, Taylor R. Reversal of type 2 diabetes: normalisation of beta cell function in association with decreased pancreas and liver triacylglycerol. *Diabetologia*. 2011;**54**(10):2506–2514.
36. Gow ML, Baur LA, Johnson NA, Cowell CT, Garnett SP. Reversal of type 2 diabetes in youth who adhere to a very-low-energy diet: a pilot study. *Diabetologia*. 2017;**60**(3):406–415.

37. Li J, Xie Y, Yuan F, Song B, Tang C. Noninvasive quantification of pancreatic fat in healthy male population using chemical shift magnetic resonance imaging: effect of aging on pancreatic fat content. *Pancreas*. 2011;**40**(2):295–299.
38. Idilman IS, Tuzun A, Savas B, Elhan AH, Celik A, Idilman R, Karcaaltincaba M. Quantification of liver, pancreas, kidney, and vertebral body MRI-PDFF in non-alcoholic fatty liver disease. *Abdom Imaging*. 2015;**40**(6):1512–1519.
39. Hori M, Takahashi M, Hiraoka N, Yamaji T, Mutoh M, Ishigamori R, Furuta K, Okusaka T, Shimada K, Kosuge T, Kanai Y, Nakagama H. Association of pancreatic fatty infiltration with pancreatic ductal adenocarcinoma. *Clin Transl Gastroenterol*. 2014;**5**:e53.

Biochemical and Biophysical Research Communications 493 (2017) 514–520

Contents lists available at ScienceDirect

Biochemical and Biophysical Research Communications

journal homepage: www.elsevier.com/locate/ybbrc

A novel phenylphthalimide derivative, pegylated TC11, improves pharmacokinetic properties and induces apoptosis of high-risk myeloma cells via G2/M cell-cycle arrest

Shuji Aida [a], Masashi Hozumi [a], Daiju Ichikawa [a], Kazuki Iida [a], Yuko Yonemura [b], Noriko Tabata [b], Taketo Yamada [c], Maiko Matsushita [a], Takeshi Sugai [d], Hiroshi Yanagawa [a, b], Yutaka Hattori [a, *]

[a] Clinical Physiology & Therapeutics, Keio University Faculty of Pharmacy, Tokyo, Japan
[b] IDAC Theranostics Inc., Tokyo, Japan
[c] Department of Pathology, Saitama Medical University, Saitama, Japan
[d] Organic and Biocatalytic Chemistry, Keio University Faculty of Pharmacy, Tokyo, Japan

ARTICLE INFO

Article history:
Received 29 August 2017
Accepted 31 August 2017
Available online 1 September 2017

Keywords:
Multiple myeloma
Pegylation of low molecule compounds
Phenylphthalimide derivative
G2/M arrest
Celebron

ABSTRACT

Despite the development of new drugs for multiple myeloma (MM), the prognosis of MM patients with high-risk cytogenetic abnormalities such as t (4; 14) and del17p remains poor. We reported that a novel phenylphthalimide derivative, TC11, induced apoptosis of MM cells *in vitro* and *in vivo*, and TC11 directly bound to α-tubulin and nucleophosmin-1 (NPM1). However, TC11 showed low water solubility and poor pharmacokinetic properties. Here we synthesized a water-soluble TC11-derivative, PEG(E)-TC11, in which HOEtO-TC11 is pegylated with PEG through an ester bond, and we examined its anti-myeloma activity. We observed that PEG(E)-TC11 and its hydrolyzed product, HOEtO-TC11, induced G2/M arrest and the apoptosis of MM cells. Intraperitoneal administration of PEG(E)-TC11 to xenografted mice revealed improved pharmacokinetic properties and significantly delayed tumor growth. TC11 and its derivatives did not bind to cereblon (CRBN), which is a responsible molecule for thalidomide-induced teratogenicity. These results suggest that PEG(E)-TC11 is a good candidate drug for treating high-risk MM.

1. Introduction

Multiple myeloma (MM) is a hematological malignancy that is characterized by the proliferation of malignant plasma cells. MM comprises 13% of hematological malignancies, and it is the second most frequent after malignant lymphoma [1]. MM usually occurs in elderly individuals, and the patients show symptoms such as anemia, nephropathy, bone lytic lesions, hypercalcemia, and amyloidosis [2].

Recent advances in the treatment of MM using newly developed drugs have significantly improved the prognosis of MM patients. For example, immunomodulatory drugs (IMiDs) such as thalidomide, lenalidomide, and pomalidomide and proteasome inhibitors including bortezomib, carfilzomib and ixazomib play central roles in MM treatment [3–5]. However, IMiDs have substantial limitations when they are used to treat MM [6,7]. For example, thalidomide has a high level of teratogenicity, and newborn infants whose mothers have taken thalidomide have suffered from phocomelia [8]. A second problem is that IMiDs show only limited effects against the MM of patients with high-risk chromosomal abnormalities such as t (4; 14) and del17p (deletion of *TP53* gene). The MM patients with these cytogenetic abnormalities showed significantly shorter survival than those with a normal karyotype [9]. Thus, the drug design of novel IMiDs that are non-teratogenic as well as highly effective for high-risk MM cells is strongly desired.

IMiDs are multifunctional compounds, and their molecular mechanisms have not been fully elucidated. It was reported that IMiDs directly bind to cereblon (CRBN), a component of E3 ubiquitin ligase complex, and the IMiDs induced teratogenicity and showed antitumor effects [10–13]. A proteome analysis revealed various CRBN substrates, and it was reported that the degradation

* Corresponding author. Division of Clinical Physiology and Therapeutics, Keio University Faculty of Pharmacy, 1-5-30 Shiba-koen, Minato-ku, Tokyo 105-8512, Japan.
E-mail address: hattori-yt@pha.keio.ac.jp (Y. Hattori).

http://dx.doi.org/10.1016/j.bbrc.2017.08.159
0006-291X/

of IKZF1 (ikaros) and IKZF3 (aiolos) by IMiDs are important for the induction of apoptosis of MM cells [14]. More recently, Eichner et al. reported that IMiDs inhibited CRBN chaperone function and abrogated cell surface CD147-MCT1 expression [15]. This effect by IMiDs was closely related to teratogenicity. Taken together, these findings indicate that CRBN mediates biological actions of IMiDs, and that various downstream CRBN substrates demonstrate multifunctional effects of IMiDs.

We reported that a novel phenylphthalimide derivative, 2-(2,6-diisopropylphenyl)-5-amino-1H-isoindole-1,3-dione (TC11) induced the apoptosis of high-risk MM cells *in vivo* and *in vitro* and inhibited the differentiation of osteoclasts. We also demonstrated that TC11 directly bound to α-tubulin and the protein nucleophosmin-1 (NPM1) by an *in vitro* virus (IVV) method [16,17]. A major drawback of TC11 was its low water solubility, which hampered its absorption into blood and limited its antitumor effects when it was intraperitoneally administered in tumor-bearing mice.

In the present study, we attempted to improve the solubility of TC11 in water by linking TC11 with polyethylene glycol (PEG) through an ester bond, and we designated the resulting derivative PEG(E)-TC11. We found that PEG(E)-TC11 was very efficiently absorbed into the bloodstream and showed significantly high maximum blood concentrations compared to TC11.

PEG(E)-TC11 effectively inhibited the growth of MM cell xenografts in SCID mice. Our histopathological observations of xenografted mice administered PEG(E)-TC11 showed the apoptosis of MM cells. To elucidate the mechanisms underlying the ability of PEG(E)-TC11 to induce the apoptosis of MM cells with high-risk cytogenetic abnormalities, we also examined the effects of PEG(E)-TC11 on cell-cycle regulation.

2. Materials & methods

2.1. Synthesis of compounds, PEG(E)-TC11 and hydroxyethoxy-TC11

PEG(E)-TC11 was synthesized from 4-hydroxyphthalic acid by the following six steps. Nitration of 4-hydroxyphthalic acid by guanidine nitrate in 85% sulfuric acid at 0°−5 °C for 3 h afforded a mixture of 5-nitro- and 3-nitro-4-hydroxyphthalic acids with the ratio of 1 to 1 at 96% yield (step 1), which was then refluxed in dehydrated toluene containing P_2O_5 at 100 °C overnight to give a mixture of 5-nitro- and 3-nitro-4-hydroxyphthalic acid anhydrides at the ratio of 1 to 0.6 in 51% yield (step 2).

Nitrophthalimide derivatives were obtained by refluxing a mixture of 5-nitro- and 3-nitrophthalic acid anhydrides and 2,6-diisopropylaniline in acetic acid at 140 °C overnight at 96% yield (step 3), and separated from each other by silica gel column chromatography. Reaction of the isolated 5-nitrophthalimide derivative with ethylene bromohydrin in DMF at 110 °C overnight yielded 4-hydroxyethoxy-5-nitrophthalimide derivative at 81% yield (step 4), which was pegylated with mPEG11-COOH with a molecular weight of 550 (step 5) followed by catalytic hydrogenation to finally give PEG(E)-TC11 (step 6). Hydroxyethoxy-TC11 (HOEtO-TC11) was also obtainable by the catalytic hydrogenation of 4-hydroxyethoxy-5-nitrophthalimide derivative prepared in step 4. The chemical structures of synthetic compounds were confirmed by ^{1}H NMR spectroscopy and mass spectrometry.

2.2. Cell lines

The human MM cell lines KMM1, KMS11, KMS21, KMS27, KMS28, and KMS34 were established and provided by Dr. T. Ohtuki (Kawasaki Medical University, Kurashiki, Japan). The human MM cell line MUM24 was established in our laboratory [18]. All cell lines were cultured in RPMI1640 medium (Sigma-Aldrich, St. Louis, MO) containing 10% fetal bovine serum (FBS) (Gibco, Grand Island, NY) and 1% Pen-Strep (Gibco) at 37 °C and 5% CO_2.

2.3. High-performance liquid chromatography (HPLC)

PEG(E)-TC11 was mixed with 10% FBS containing RPMI1640 medium at 37 °C, and 2, 6, 12, 24 or 48 h later, samples were collected and refined by solid phase extraction (Sep-Pak®, Waters, Milford, MA), and liquate out 1 mL of acetonitrile. All samples were analyzed by high-performance liquid chromatography (HPLC). The Inertsil ODS-3 column (GL Science, Tokyo) was used. The mobile phases were acetonitrile and distilled water (50:50). The flow rate was 0.7 ml/min. The compounds were detected by fluorescence. The excitation wavelength was 380 nm, and the fluorescence wavelength was 530 nm.

2.4. Cell viability assay

MM cells (2×10^4 cells per well) were seeded in 96-well plates and incubated with various concentrations (0−30 μM) of TC11, PEG(E)-TC11, or HOEtO-TC11 at 37 °C for 48 h. The cell viability was assessed by a Cell Proliferation Kit I (MTT) (Roche Diagnostics, Indianapolis, IN) according to the manufacturer's handling instructions.

2.5. Apoptosis detection assay

KMS34 cells (8×10^5 per well) were seeded in six-well plates and incubated with 10 μM of TC11 or PEG(E)-TC11 at 37 °C for 24, 48, or 72 h. The cells were then collected and stained with FITC-labeled Annexin-V and propidium iodide (PI) (Biovision, Milpitas, CA). A flow cytometry analysis was performed with a BD LSR II system (BD Biosciences, San Jose, CA).

2.6. Cell-cycle assay

KMS34 cells (8×10^5 per well) were seeded in six-well plates and incubated with 3 μM of TC11, PEG(E)-TC11, or HOEtO-TC11 at 37 °C for 12, 24, or 36 h. The cells were then collected and fixed in 70% ethanol, and incubated at 4 °C overnight. The cells were suspended in phosphate-buffered saline (PBS) plus 0.1 mg/mL RNaseA and incubated at room temperature for 30 min. After incubation, the cells were stained by PI in the dark for 30 min. The cells were then analyzed by a FACSCalibur (BD Biosciences).

2.7. In vivo tumor growth assay

The *in vivo* tumor growth assay was performed as described with several modifications [19]. Briefly, 3×10^7 KMS11 cells were subcutaneously inoculated into 5-week-old male ICR/SCID mice (Clea Japan, Tokyo). When the plasmacytoma reached 50 mm^3, the intraperitoneal injections of drugs were started: 186 μmol/kg of TC11 or PEG(E)-TC11 dissolved in 10% DMSO (Sigma-Aldrich)/1% Tween80 (Sigma-Aldrich)/saline (Otsuka Pharmaceuticals, Tokyo), or saline. Drugs or control (10% DMSO/1% Tween80/saline, or saline) was injected intraperitoneally twice every 3 days for 14 days. The tumor volume was calculated as width × length^2 × 0.52 [20].

2.8. Histopathologic assay

The histopathologic analysis was performed as described [19]. After 14-day treatment with PEG(E)-TC11 or control, the mice were sacrificed and the isolated plasmacytoma were fixed with 10% formalin and embedded in paraffin. Plasmacytomas were sliced at

5 μm and stained with hematoxylin and eosin (H.E.). Anti-human cleaved PARP (Asp214) polyclonal antibody (Cell Signaling Technology Japan, Tokyo), anti-cleaved caspase-3 (Asp175) polyclonal antibody (Cell Signaling Technology Japan) were used for immunohistochemistry.

2.9. Pharmacokinetics study

To evaluate the pharmacokinetics after the intraperitoneal injection of TC11 or PEG(E)-TC11 in 5-week-old male ICR mice (Clea Japan), we extracted peripheral blood from the tail veins using heparin-coated hematocrit tubes (Terumo, Tokyo). Peripheral blood samples were centrifuged immediately at 3400 *g* for 15 min at 4 °C. Ten μL of plasma and standard were refined by solid phase extraction (Sep-Pak®) and liquated out with 1 mL acetonitrile and analyzed by HPLC.

2.10. Surface plasmon resonance analysis

We performed a surface plasmon resonance (SPR) analysis with a Biacore 3000 system (GE Healthcare, Buckinghamshire, UK) to determine the binding kinetics of drugs to CRBN. All experiments were performed at 25 °C using TBS buffer (25 mM Tris-HCl, pH 7.4, 137 mM NaCl, 3 mM KCl). CRBN was immobilized onto the sensor chip NTA (GE Healthcare). To determine the dissociation constants, we injected three different concentrations of TC11, PEG(E)-TC11, HOEtO-TC11, thalidomide and lenalidomide (Santa Cruz Biotechnology, Santa Cruz, CA). The injection periods for association and dissociation were 300 s. The binding data were analyzed with 1:1 binding with the mass transfer model using the BIA evaluation software, ver. 4.1 (Biacore).

2.11. Statistical analysis

We performed a one-way analysis of variance (ANOVA) followed by the Tukey test for unpaired results to evaluate differences between more than two groups. Differences were considered to be significant when p-values <0.05 were obtained. All statistical analyses were conducted using the IBM SPSS Statistics program, ver. 23 (IBM, Armonk, NY).

3. Results

3.1. The pegylation of TC11 increased the water solubility

To examine the water solubility of pegylated TC11, we measured the saturated concentrations of TC11 and PEG(E)-TC11 in 100 mM Tris-HCl (pH 7.5) by HPLC. Although TC11 showed a low saturated concentration (2 mg/100 mL), PEG(E)-TC11 saturated with an approx. 4500 times higher concentration (8894 mg/100 mL).

The chemical structure of PEG(E)-TC11 is shown in Fig. 1A. When PEG(E)-TC11 was dissolved in RPMI1640 medium containing 10% FBS, PEG branches were immediately excised from TC11. Consequently, HOEtO-TC11 was produced (Fig. 1B), which we hypothesized would show biological activities after the hydrolysis of PEG(E)-TC11 in blood. A time-course increase in the HOEtO-TC11 concentration was observed when PEG(E)-TC11 was incubated with 10% FBS containing RPMI1640 medium (Fig. 1C). These results suggested that PEG(E)-TC11 was probably hydrolyzed and converted into HOEtO-TC11 by serum esterase.

3.2. PEG(E)-TC11 inhibited cell proliferation and induced the apoptosis of MM cells with high-risk cytogenetic abnormalities

To examine whether PEG(E)-TC11 inhibits the proliferation of MM cells, we performed an MTT assay using eight MM cell lines including those with high-risk cytogenetic abnormalities. PEG(E)-TC11 inhibited the proliferation of all eight MM cell lines in a dose-dependent manner regardless of the existence of cytogenetic change (Fig. 2A). Since PEG(E)-TC11 was immediately hydrolyzed to HOEtO-TC11, we also examined the growth inhibitory activity of HOEtO-TC11, and we found that HOEtO-TC11 also significantly inhibited all of the MM cell lines. Very interestingly, water-soluble PEG(E)-TC11 and HOEtO-TC11 much more potently inhibited the proliferation of MM cells compared to TC11 against the KMM1, KMS11, KMS21, KMS34, and MUM24 cells. The exact reason for the superior growth inhibition by their water-soluble forms has not been elucidated.

We examined whether PEG(E)-TC11 induced the apoptosis of MM cells. We performed Annexin V/PI staining of MUM24 cells. The treatment of MM cells with 10 μM of PEG(E)-TC11 or TC11 increased in the annexin V+/PI- and annexin V+/PI + fractions in a time-dependent manner (Fig. 2B).

3.3. PEG(E)-TC11 also inhibited cell proliferation in vivo in KMS11-xenografted mice

We next evaluated the anti-myeloma effect of PEG(E)-TC11 and TC11 *in vivo* using KMS11-xenografted mice. KMS11 cells have high-risk cytogenetic abnormalities including t (4; 14) and del17p. PEG(E)-TC11 and TC11 were administered intraperitoneally to the xenografted mice (186 μmol/kg) for 14 days. The PEG(E)-TC11- and TC11-treated mice showed significantly reduced tumor growth compared to the control mice (Fig. 3A). Neither compound resulted in serious systemic toxicity such as significant weight loss or abnormal behavior. PEG(E)-TC11 tended to reveal more potent tumor growth inhibition than TC11, although the difference was not significant. In one of the PEG(E)-TC11-treated mice, the skin xenografted tumor completely disappeared. These results suggest that PEG(E)-TC11 also has more potent antitumor activity *in vivo* than TC11, which is probably due to the change of pharmacokinetics in the mice by the increased water solubility.

In our histopathological examination of PEG(E)-TC11 treated xenografts, the hematoxylin-eosin staining revealed the aggregation of nuclei in the PEG(E)-TC11 treated mice. The immunohistochemical staining revealed that PARP- and cleaved-caspase3-positive cells were increased in the PEG(E)-TC11 treated mice. These results indicated that PEG(E)-TC11 exhibited antitumor activity via apoptosis *in vivo* (Fig. 3B).

3.4. PEG(E)-TC11 showed higher blood concentrations in mice compared to TC11

To evaluate the pharmacokinetics of PEG(E)-TC11, we examined the plasma concentrations of PEG(E)-TC11 and those of TC11 in ICR mice over time after a single injection of 186 μmol/kg PEG(E)-TC11 or TC11. The results demonstrated that the PEG modification of TC11 significantly increased the peak blood concentration (Cmax) from 2.6 to 24.4 μM and extended the elimination half-life (t1/2) from 1.4 to 2.2 h (Fig. 3C). These results suggested that the pegylation of water-insoluble TC11 increased the absorption from the peritoneal cavity to the blood, resulting in an increase in the Cmax value. We also speculated that the above-mentioned alteration of pharmacokinetics led to the increased tumor growth inhibition by PEG(E)-TC11 compared to TC11.

3.5. PEG(E)-TC11 induced G2/M cell-cycle arrest in MM cells

To investigate the mechanisms of induction of MM cell death, we performed a cell-cycle analysis by flow cytometry. Three μM of

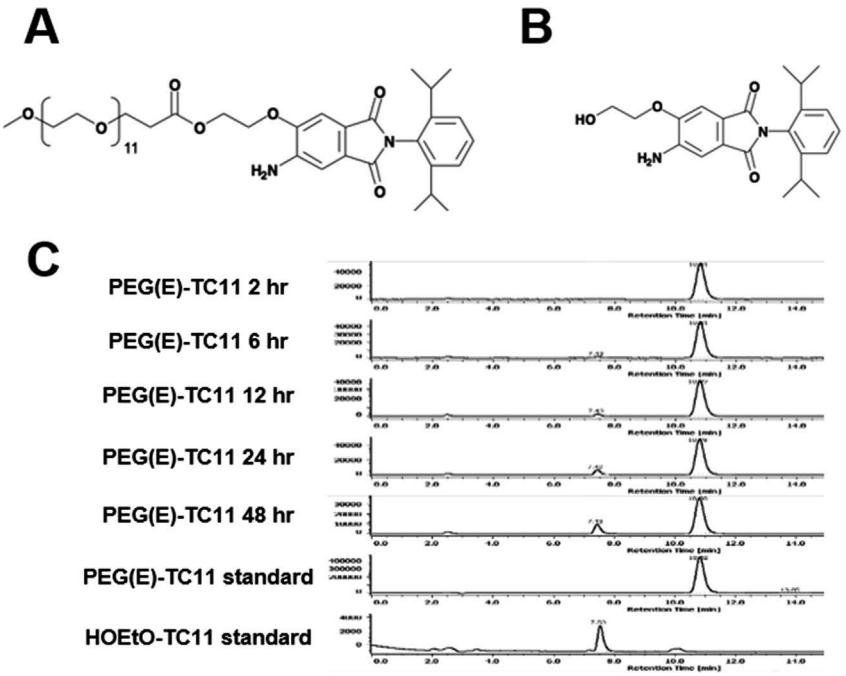

Fig. 1. The chemical structures of the TC11 derivatives. The chemical structures of PEG(E)-TC11 (**A**) and HOEtO-TC11 (**B**). The HPLC chromatogram of PEG(E)-TC11 and its hydrolyzed product HOEtO-TC11 (**C**). The peak of PEG(E)-TC11 and HOEtO-TC11 appeared in approx. 10.9 min and 7.5 min, respectively.

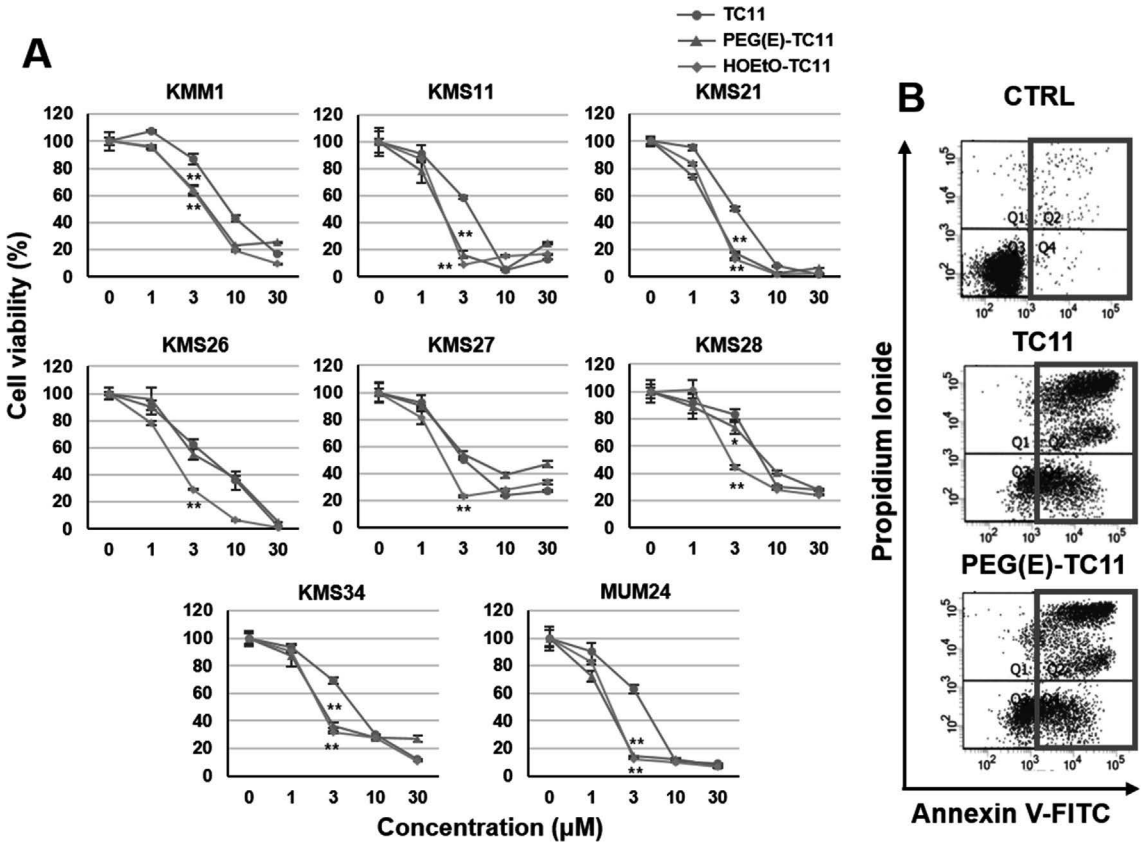

Fig. 2. The anti-myeloma effect of PEG(E)-TC11 *in vitro*. A: Human myeloma cell lines KMM1, KMS11, KMS21, KMS26, KMS27, KMS28, KMS34, and MUM24 were incubated with the indicated concentrations of the drugs for 48 h. The viable cell numbers were determined by MTT assay. Values are mean ± SD, n = 3. *p < 0.05, **p < 0.01 (Tukey test vs. TC11). **B:** Flow cytometry analysis of apoptotic cells. MUM24 was incubated with 10 μM of TC11 or PEG(E)-TC11 for 48 h, and the cells were then stained with FITC-labeled Annexin-V and PI and analyzed with a BD LSR II system.

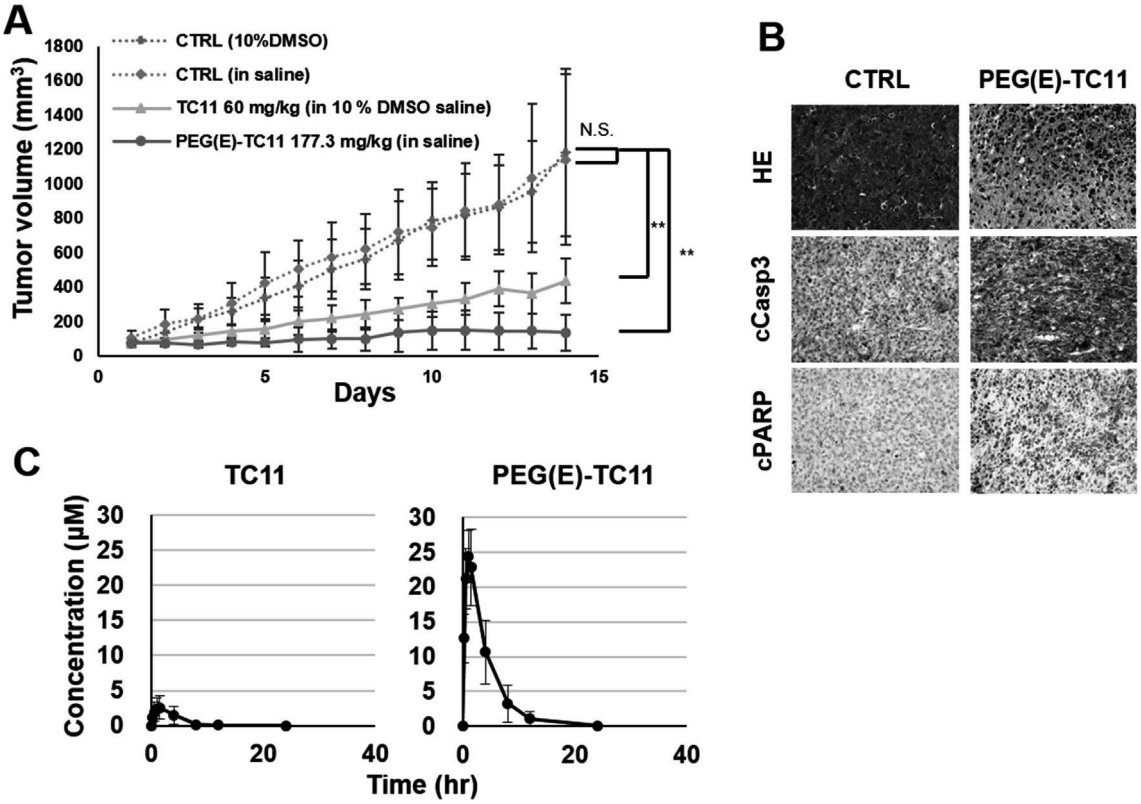

Fig. 3. The anti-myeloma effect of PEG(E)-TC11 *in vivo*. A: The growth curve of plasmacytoma. KMS11-inoculated mice were treated with 186 μmol/kg of TC11 or PEG(E)-TC11 twice every 3 days for 2 weeks. After observation, the mice were sacrificed and isolated plasmacytomas were fixed with 10% formalin. Values are mean ± SD, n = 6–7. $^{**}p < 0.01$ (Tukey test vs. control [Saline]). **B:** Histopathological examination of the KMS11-derived plasmacytomas. The plasmacytomas were sliced and stained with H.E., anti-human cleaved PARP (Asp214) polyclonal antibody and anti-cleaved caspase-3 (Asp175) polyclonal antibody. **C:** Pharmacokinetics study of TC11 and PEG(E)-TC11. Plasma concentrations of TC11 or HOEtO-TC11 in mice after a single injection of 186 μM/kg of TC11 or HOEt-TC11 were determined by HPLC.

PEG(E)-TC11 and TC11 both significantly induced cell-cycle arrest in a time-dependent manner. After 1-day drug exposure, the G2/M fractions were 18.8% in the control, 60.40% in the TC11 treatment, and 68.40% in the PEG(E)-TC11 treatment (Fig. 4A).

3.6. Anti-myeloma effects of PEG(E)-TC11 and TC11 are independent of the CRBN pathway

It was reported that IMiDs were known to induce cytotoxicity and teratogenicity via their binding to CRBN. It is important to determine whether or not PEG(E)-TC11 binds to CRBN, and to address this question, we performed the SPR assay. As shown in Fig. 4B, PEG(E)-TC11, TC11 and HOEtO-TC11 did not bind to CRBN, whereas thalidomide and lenalidomide directly bound to CRBN with high affinities; their binding affinities (K_D) were 5.66×10^{-7} and 3.65×10^{-6} M, respectively. These results indicated that TC11 and its derivatives did not interact with CRBN. The treatments with PEG(E)-TC11, HOEtO-TC11, and TC11 resulted in the growth inhibition of MM cells independently from CRBN binding (Fig. 4B).

3.7. Discussion

Various drugs have been developed to treat MM. In particular, IMiDs are effective for relapsed and refractory MM patients and have extended the survival rate of untreated patients [3,5]. However, IMiDs have two substantial limitations; their teratogenicity and limited effects against high-risk MM patients [6,21].

We reported that a novel phthalimide derivative, TC11, induced the apoptosis of high-risk MM cells *in vitro* and *in vivo* [16,17]. One of the major drawbacks of TC11 for further preclinical development is its low water solubility, and to overcome this problem, we synthesized pegylated TC11, which shows much higher water saturated concentrations compared to TC11.

Pegylation is commonly used for increasing water solubility and changing pharmacokinetic parameters. It has been used for improving the bioavailability and extending the blood retention time of water-insoluble drugs such as camptothecin, paclitaxel, and interferon [22–24]. Generally, pegylation is expected to increase the maximum blood concentration (Cmax) value and to elongate the elimination half-life (t1/2). For example, the Cmax and t1/2 of interferon-gamma (IFN-γ) are 3411 pg/ml and 0.9 h, and those of pegylated-IFN-γ are 567,297 pg/ml and 29.1 h, respectively [25].

In the present study, the pegylation of TC11 resulted in an eightfold-higher Cmax, probably due to the increase of absorption from the peritoneal cavity to the bloodstream. However, the elongation of t1/2 by TC11 pegylation was only 1.8-fold. Considering the ester-binding structure between PEG and TC11, we suspect that the immediate hydrolyzation and dissociation of a PEG branch from TC11 is a cause of the limited elongation of t1/2. It was reported that carboxylesterase activity is much higher in mouse plasma compared to human plasma [26]. We therefore suspect that PEG(E)-TC11 was immediately hydrolyzed to HOEtO-TC11 by carboxylesterase in the blood.

We examined whether the modification of chemical structure by pegylation would alter the antitumor activity of TC11. As shown in Fig. 2A, PEG(E)-TC11 and its hydrolyzate HOEtO-TC11 both significantly inhibited the growth of all eight MM cell lines [16]. In our earlier study, we identified α-tubulin and NPM1 as TC11-

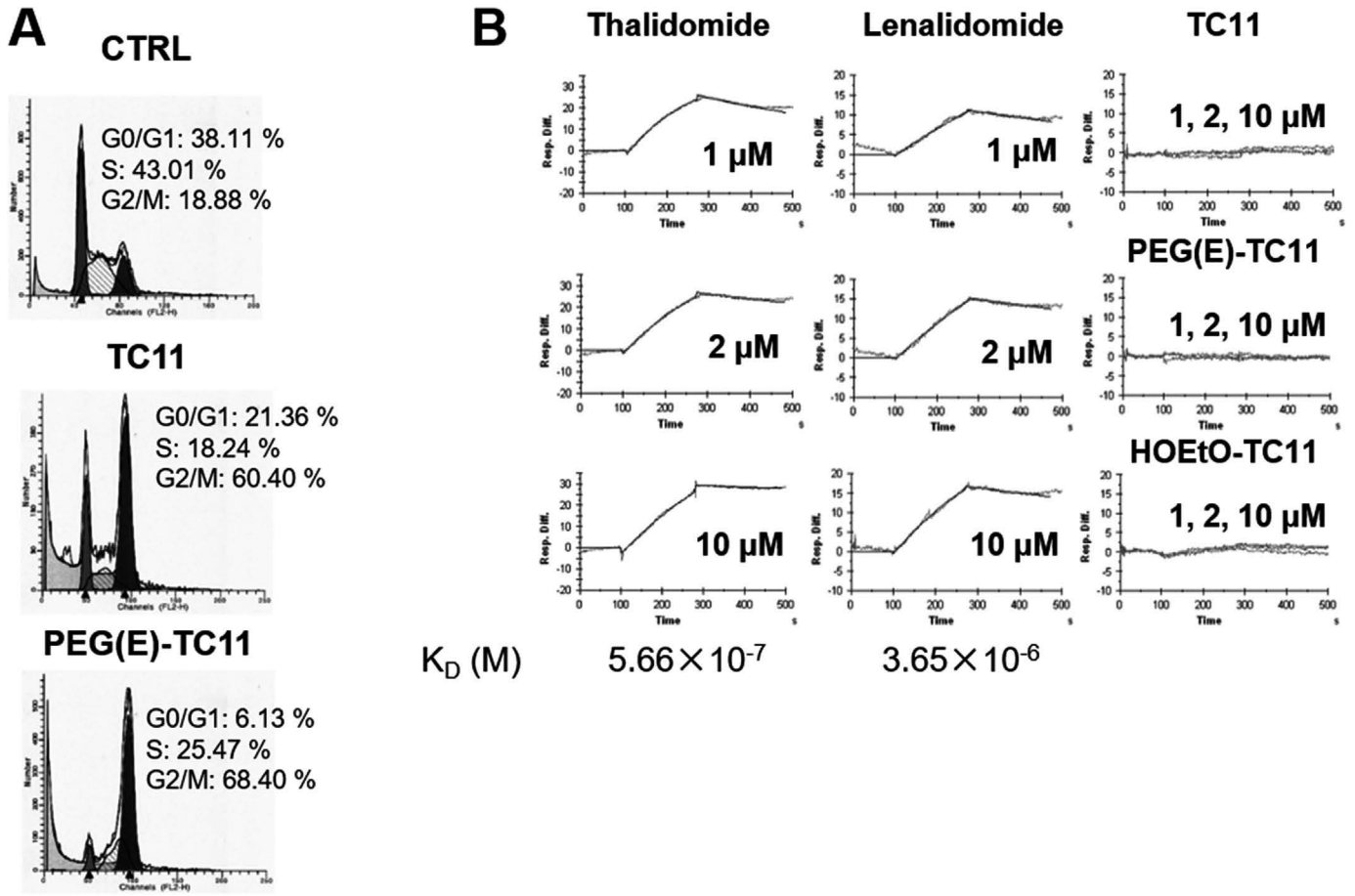

Fig. 4. PEG(E)-TC11 and TC11 induced G2/M arrest in a CRBN-independent manner. A: Cell-cycle analysis of PEG(E)-TC11-, TC11- and HOEtO-TC11-treated cells. KMS34 cells were incubated with 3 μM of TC11, PEG(E)-TC11 or HOEtO-TC11 for 24 h; the cells were then fixed with 70% EtOH and labeled with PI and analyzed by a FACSCalibur. **B:** The SPR analysis of the ability of TC11 and its derivatives to bind to CRBN. CRBN was immobilized onto the sensor chip NTA followed by SPR analysis. *Left panels*, the affinity of thalidomide to CRBN; *middle panels*, the affinity of lenalidomide; *right panels*, the affinity of TC11 and its derivatives.

binding proteins that are involved in cell-cycle regulation [17]. As shown in Fig. 4A, PEG(E)-TC11 and HOEtO-TC11 more clearly induced G2/M arrest compared to TC11. The reason why PEG(E)-TC11 and HOEtO-TC11 induced cell-cycle arrest more potently than TC11 is not clear.

We also confirmed the anti-myeloma effect of PEG(E)-TC11 *in vivo* using xenografts of KMS11 cells which harbored cytogenetic abnormalities such as t (4; 14) translocation and del17p. In the PEG(E)-TC11-injected mice, the KMS11 xenografts proliferated more slowly compared to those in the TC11-treated mice, although the difference in the growth inhibition between PEG(E)-TC11 and TC11 was not statistically significant. We speculate that the potentiated growth inhibition of PEG(E)-TC11 is brought about by the alteration of pharmacokinetics as described earlier.

Deletion of the *TP53* tumor suppressor gene is one of the representative high-risk cytogenetic abnormalities in MM and other hematological malignancies [9]. TP53 plays a central role in the G1/S checkpoint of the cell cycle [27]. Drugs used to treat MM such as lenalidomide induced apoptosis via G1/S arrest [28,29]. However, MM cells with deletion of *TP53* gene did not reveal G1/S arrest by treatment with lenalidomide (data not shown). To the contrary, TC11 and its derivatives induced G2/M arrest independent of TP53 function. We thus consider TC11 and its derivatives effective for high-risk MM with deletion of *TP53* gene.

In 2010, it was reported that IMiDs directly bound to CRBN, which mediated teratogenicity as well as antitumor effects [10–12]. In the present study, we determined the binding dissociation constants (K_D) of PEG(E)-TC11 and TC11 to CRBN by an SPR analysis. Thalidomide and lenalidomide bound to CRBN with high affinity, whereas TC11 and its derivatives did not bind to CRBN at any concentration. Ito et al. reported that the knock-down of CRBN gene abrogated thalidomide-induced teratogenicity in zebrafish embryos [12]. If CRBN is a responsible molecule for thalidomide-induced teratogenicity, TC11 and its derivatives are expected to be safe compounds lacking CRBN-mediated teratogenicity.

In conclusion, our present findings demonstrated that a novel pegylated phenylphthalimide derivative, PEG(E)-TC11, has anti-myeloma effect for MM that has high-risk cytogenetic abnormalities *in vitro* and *in vivo*. In addition, PEG(E)-TC11 improved the pharmacological properties of TC11 such as absorption from the peritoneal cavity to the bloodstream. PEG(E)-TC11 inhibited cell growth via G2/M arrest in a CRBN-independent manner. Thus, PEG(E)-TC11 should be considered as a candidate compound for overcoming high-risk MM.

Acknowledgements

We thank Dr. Takemi Ohtsuki for the gift of MM cell lines and Yuka Masaharu for her helpful scientific assistance. This work was supported in part by a Grant-in-Aid for Scientific Research and a grant from the Private University Strategic Research Base Development Program of the Ministry of Education, Culture, Sports,

Science and Technology (MEXT) of Japan, International Myeloma Foundation Japan's Grants, Japanese Society of Myeloma (JSM) Research Award, and Keio Gijuku Academic Development Funds.

Transparency document

Transparency document related to this article can be found online at http://dx.doi.org/10.1016/j.bbrc.2017.08.159.

References

[1] M.A. Dimopoulos, E. Terpos, Multiple myeloma, Ann. Oncol. 21 (Suppl 7) (2010) 143–150 vii.
[2] A. Palumbo, K. Anderson, Multiple myeloma, N. Eng. J. Med. 364 (2011) 1046–1060.
[3] P.G. Richardson, E. Blood, C.S. Mitsiades, et al., A randomized phase 2 study of lenalidomide therapy for patients with relapsed or relapsed and refractory multiple myeloma, Blood 108 (2006) 3458–3464.
[4] M.V. Mateos, J.M. Hernandez, M.T. Hernandez, et al., Bortezomib plus melphalan and prednisone in elderly untreated patients with multiple myeloma: results of a multicenter phase 1/2 study, Blood 108 (2006) 2165–2172.
[5] M.A. Dimopoulos, A. Anagnostopoulos, D. Weber, Treatment of plasma cell dyscrasias with thalidomide and its derivatives, J. Clin. Oncol. 21 (2003) 4444–4454.
[6] H. Avet-Loiseau, J. Soulier, J.P. Fermand, et al., Impact of high-risk cytogenetics and prior therapy on outcomes in patients with advanced relapsed or refractory multiple myeloma treated with lenalidomide plus dexamethasone, Leukemia 24 (2010) 623–628.
[7] H. Chang, A. Jiang, C. Qi, et al., Impact of genomic aberrations including chromosome 1 abnormalities on the outcome of patients with relapsed or refractory multiple myeloma treated with lenalidomide and dexamethasone, Leuk. Lymphoma 51 (2010) 2084–2091.
[8] Y. Hattori, T. Iguchi, Thalidomide for the treatment of multiple myeloma, Congenit. Anom. (Kyoto) 44 (2004) 125–136.
[9] S.Z. Usmani, P. Rodriguez-Otero, M. Bhutani, et al., Defining and treating high-risk multiple myeloma, Leukemia 29 (2015) 2119–2125.
[10] J. Kronke, N.D. Udeshi, A. Narla, et al., Lenalidomide causes selective degradation of IKZF1 and IKZF3 in multiple myeloma cells, Science 343 (2014) 301–305.
[11] J. Kronke, E.C. Fink, P.W. Hollenbach, et al., Lenalidomide induces ubiquitination and degradation of CK1alpha in del(5q) MDS, Nature 523 (2015) 183–188.
[12] T. Ito, H. Ando, T. Suzuki, et al., Identification of a primary target of thalidomide teratogenicity, Science 327 (2010) 1345–1350.
[13] E.S. Fischer, K. Bohm, J.R. Lydeard, et al., Structure of the DDB1-CRBN E3 ubiquitin ligase in complex with thalidomide, Nature 512 (2014) 49–53.
[14] C.C. Bjorklund, L. Lu, J. Kang, et al., Rate of CRL4(CRBN) substrate Ikaros and Aiolos degradation underlies differential activity of lenalidomide and pomalidomide in multiple myeloma cells by regulation of c-Myc and IRF4, Blood Cancer J. 5 (2015) e354.
[15] R. Eichner, M. Heider, V. Fernandez-Saiz, et al., Immunomodulatory drugs disrupt the cereblon-CD147-MCT1 axis to exert antitumor activity and teratogenicity, Nat. Med. 22 (2016) 735–743.
[16] H. Shiheido, F. Terada, N. Tabata, et al., A phthalimide derivative that inhibits centrosomal clustering is effective on multiple myeloma, PLoS One 7 (2012) e38878.
[17] M. Matsushita, Y. Ozaki, Y. Hasegawa, et al., A novel phthalimide derivative, TC11, has preclinical effects on high-risk myeloma cells and osteoclasts, PLoS One 10 (2015) e0116135.
[18] Y. Hattori, W. Du, T. Yamada, et al., A myeloma cell line established from a patient refractory to thalidomide therapy revealed high-risk cytogenetic abnormalities and produced vascular endothelial growth factor, Blood Cancer J. 3 (2013) e115.
[19] W. Du, Y. Hattori, T. Yamada, et al., NK4, an antagonist of hepatocyte growth factor (HGF), inhibits growth of multiple myeloma cells: molecular targeting of angiogenic growth factor, Blood 109 (2007) 3042–3049.
[20] D. Tomioka, N. Maehara, K. Kuba, et al., Inhibition of growth, invasion, and metastasis of human pancreatic carcinoma cells by NK4 in an orthotopic mouse model, Cancer Res. 61 (2001) 7518–7524.
[21] U. Klein, A. Jauch, T. Hielscher, et al., Chromosomal aberrations +1q21 and del(17p13) predict survival in patients with recurrent multiple myeloma treated with lenalidomide and dexamethasone, Cancer 117 (2011) 2136–2144.
[22] R.B. Greenwald, Y.H. Choe, J. McGuire, et al., Effective drug delivery by PEGylated drug conjugates, Adv. Drug Deliv. Rev. 55 (2003) 217–250.
[23] J.S. Choi, B.W. Jo, Enhanced paclitaxel bioavailability after oral administration of pegylated paclitaxel prodrug for oral delivery in rats, Int. J. Pharm. 280 (2004) 221–227.
[24] J.H. Hoofnagle, L.B. Seeff, Peginterferon and ribavirin for chronic hepatitis C, N. Eng. J. Med. 355 (2006) 2444–2451.
[25] C.M. Fam, S.P. Eisenberg, S.J. Carlson, et al., PEGylation improves the pharmacokinetic properties and ability of interferon gamma to inhibit growth of a human tumor xenograft in athymic mice, J. Interferon Cytokine Res. 34 (2014) 759–768.
[26] T. Satoh, M. Hosokawa, Structure, function and regulation of carboxylesterases, Chem. Biol. Interact. 162 (2006) 195–211.
[27] S.J. Kuerbitz, B.S. Plunkett, W.V. Walsh, et al., Wild-type p53 is a cell cycle checkpoint determinant following irradiation, Proc. Natl. Acad. Sci. U. S. A. 89 (1992) 7491–7495.
[28] A.K. Gandhi, J. Kang, L. Capone, et al., Dexamethasone synergizes with lenalidomide to inhibit multiple myeloma tumor growth, but reduces lenalidomide-induced immunomodulation of T and NK cell function, Curr. Cancer Drug Targets 10 (2010) 155–167.
[29] D. Verhelle, L.G. Corral, K. Wong, et al., Lenalidomide and CC-4047 inhibit the proliferation of malignant B cells while expanding normal CD34+ progenitor cells, Cancer Res. 67 (2007) 746–755.

Utility of Survivin, BAP1, and Ki-67 immunohistochemistry in distinguishing epithelioid mesothelioma from reactive mesothelial hyperplasia

KEI KUSHITANI[1], VISHWA JEET AMATYA[1], AMANY SAYED MAWAS[2], RUI SUZUKI[1], YOSHIHIRO MIYATA[3], MORIHITO OKADA[3], KOUKI INAI[1], TAKUMI KISHIMOTO[4] and YUKIO TAKESHIMA[1]

[1]Department of Pathology, Institute of Biomedical and Health Sciences, Hiroshima University, Hiroshima 734-8551, Japan; [2]Department of Pathology and Clinical Pathology, Faculty of Veterinary Medicine, South Valley University, Qena 83523, Egypt; [3]Department of Surgical Oncology, Research Center for Radiation Casualty Medicine, Research Institute for Radiation Biology and Medicine, Hiroshima University, Hiroshima 734-8551; [4]Department of Internal Medicine, Okayama Rosai Hospital, Okayama 702-8055, Japan

Received June 30, 2017; Accepted November 20, 2017

DOI: 10.3892/ol.2018.7765

Abstract. Histological distinction between epithelioid mesothelioma (EM) and reactive mesothelial hyperplasia (RMH) can be challenging. The aim of this study was to assess the diagnostic utility of Survivin, Ki-67, and loss of BRCA1-associated protein 1 (BAP1) expressions in distinguishing EM from RMH using immunohistochemistry. Formalin-fixed, paraffin-embedded specimens from 78 cases of EM and 80 cases of RMH were immunohistochemically examined for Survivin, BAP1, and Ki-67. In addition, receiver operating characteristic curve analyses were performed to establish the cut-off values for Survivin and Ki-67 labelling indices. Survivin (cut-off value: 5%) had 67.7% sensitivity and 100% specificity, while Ki-67 (cut-off value: 10%) had 85.1% sensitivity and 87.5% specificity, and BAP1 had 66.2% sensitivity and 100% specificity for the differentiation of EM from RMH. Among the combinations of two markers, the combination of Survivin and BAP1 (Survivin-positive and/or BAP1-loss finding) had the highest diagnostic accuracy (sensitivity: 89.8%; specificity: 100%; accuracy: 95.3%). We recommend using the combination of Survivin and BAP1 to distinguish EM from RMH.

Introduction

Malignant mesothelioma (MM) is a relatively rare but highly aggressive malignant neoplasm arising from mesothelial cells of the pleura, peritoneum, pericardium, and tunica vaginalis. It is well-correlated with occupational and environmental asbestos exposure. (1,2) The incidence of MM has increased in many countries; (3) in Japan, mortality due to MM has increased since the 1990s, and is predicted to peak in the 2030s (4).

Epithelioid mesothelioma (EM) must be differentiated from reactive mesothelial hyperplasia (RMH), which is a non-neoplastic condition frequently caused by pleuritis, peritonitis, or serosal invasion of other cancers. Due to the close resemblance of EM to RMH, differentiation by routine histological observation alone can be challenging.

Various established and novel immunohistochemical markers have been utilized to distinguish EM from other malignancies (5-8) and RMH (6,9-17) Multiple potential immunohistochemical markers, including Ki-67, desmin, epithelial membrane antigen (EMA), p53, glucose transporter 1, insulin-like growth factor 2 messenger RNA binding protein-3 and BRCA1-associated protein 1 (BAP1) have been evaluated. However, despite the use of these immunohistochemical markers, the distinction between EM and RMH remains challenging in some cases.

Recently, detection of *p16 (CDKN2A)* homozygous deletion (*p16* HD) using fluorescence *in situ* hybridization (FISH) has been used to differentiate MM from RMH, with 100% specificity. However, the sensitivity of this marker for pleural EM varies between 45 and 86%, while its sensitivity for peritoneal EM ranges from 14 to 41% in different laboratories (10,18-20). In our unpublished experience, *p16* HD (detected by FISH) was present in 63.2% (12/19) of EM cases, but absent in all RMH cases (0/20). Although the detection of *p16* HD using FISH may be considered highly specific, its sensitivity in differentiating EM from RMH is not very high. In addition, FISH analysis cannot be applied in all cases or in all pathology laboratories, given its high cost and stringent experimental requirements.

We recently reported that phorbol 12-myristate-13-acetate-induced protein-1 (PMAIP-1; Noxa) and baculoviral IAP repeat-containing 5 (BIRC5; Survivin) mRNA expression levels are significantly higher in EM than in non-neoplastic pleural tissue, and discussed the utility of anti-Noxa antibody

Correspondence to: Professor Yukio Takeshima, Department of Pathology, Institute of Biomedical and Health Sciences, Hiroshima University, 1-2-3 Kasumi, Minami-ku, Hiroshima 734-8551, Japan
E-mail: ykotake@hiroshima-u.ac.jp

Key words: BAP1, immunohistochemistry, Ki-67, mesothelioma, reactive mesothelial hyperplasia, survivin

for the distinction between EM and RMH (21). However, the utility of Survivin IHC for the differentiation of benign and malignant mesothelial proliferation has not yet been assessed.

Here, we studied the utility of Survivin and Ki-67 expressions along with the loss of BAP1 expression in distinguishing benign from malignant mesothelial proliferation.

Materials and methods

Patients and histological samples. We used formalin-fixed, paraffin-embedded (FFPE) specimens from 78 patients with a definite histological diagnosis of EM who had undergone thoracoscopic pleural biopsy, pleurectomy/decortication, extrapleural pneumonectomy, or autopsy between 2000 and 2016. FFPE histological samples from surgical specimens obtained from 80 patients with a histological diagnosis of RMH were obtained via thoracoscopic biopsy, laparoscopic biopsy, or surgical resection between 2005 and 2016. These samples were retrieved from the archives of the Department of Pathology at Hiroshima University (Hiroshima, Japan). Each of the tumour specimens was independently reviewed by three pathologists (K.K., V.J.A, and Y.T.), and all cases of mesothelioma were diagnosed according to currently accepted World Health Organization Histological Criteria (6,22).

The tissue samples were retrieved from the archive of the Department of Pathology at Hiroshima University's Institute of Biomedical and Health Sciences. The collection of tissue specimens for this study was carried out in accordance with the 'Ethics Guidelines for Human Genome/Gene Research' enacted by the Japanese Government. Ethical approval was obtained from the institutional ethics review committee (Hiroshima University E-974). All experimental procedures were in accordance with the with ethical guidelines.

Immunohistochemical procedures. Immunohistochemical staining of sections from the FFPE tissue samples was performed using Ventana BenchMark GX (Roche Diagnostics, Basel, Switzerland). In brief, after deparaffinization using EZ-Prep (Roche Diagnostics) and antigen retrieval using Cell Conditioning 1 buffer at 95˚C for 32 min, sections were incubated with primary antibodies. The primary antibodies were anti-Survivin (cat. no. AF886, polyclonal, dilution of 1:200; R&D systems, Minneapolis, MN, USA), anti-BAP1 (C-4, dilution of 1:50; Santa Cruz Biotechnology, Inc., Dallas, TX, USA), and anti-Ki-67 (MIB-1, dilution of 1:25; Dako, Glostrup, Denmark). Incubation with secondary antibodies and detection was performed using the Ventana UltraView Universal DAB Detection kit.

Nuclear staining of Survivin, BAP1, and Ki-67 in EM or RMH cells with the same or higher intensity than internal positive controls was regarded as positive staining. Negative staining of BAP1 was defined as completely absent nuclear staining in the target cells in the presence of a positive internal control such as lymphocytes or stromal cells. Although some cases had weak cytoplasmic positivity for Survivin and BAP1, we have not included cases with only cytoplasmic positivity for Survivin and BAP1 for evaluation in this study. Immunoreactivity of Survivin and Ki-67 was evaluated using a labelling index (% of positive cells) in the 'hot spot' exhibiting the highest number of positive cells compared to the rest of the lesion. We evaluated at least 100 (maximum 500) EM or RMH cells in high power fields (x400). Counting of labelling indices of Survivin and Ki-67 was performed by three pathologists (K.K., V.J.A, and Y.T.) independently; the mean of three numbers was then calculated.

Statistical analysis. Receiver operating characteristic (ROC) curve analysis was performed to establish the cut-off values for the Survivin and Ki-67 labelling indices. The cut-off points were determined based on the Youden index. All statistical analyses were performed using EZR (Saitama Medical Center, Jichi Medical University, Saitama, Japan), a graphical user interface for R (The R Foundation for Statistical Computing, Vienna, Austria). More precisely, it is a modified version of R commander designed to add statistical functions frequently used in biostatistics (23).

Sensitivity, specificity, positive predictive values, negative predictive values, and diagnostic accuracies were calculated for each marker and combinations of two markers.

Results

Survivin expression and cut-off value. Representative immunohistochemical staining images for EM and RMH are shown in Fig. 1. Survivin expression was significantly higher in EM than in RMH. The mean of the Survivin labelling indices in EM [mean, 9.3; range, 0-24.5, standard deviation (SD), 6.5] was significantly higher than that in RMH (mean, 1.2; range, 0-4.0, SD, 1.2) (t-test, P-value <0.001). Distributions of the Survivin labelling indices in EM and RMH are shown in Fig. 2A.

The cut-off value for the Survivin IHC assay led by the result of ROC analysis was 4.000 (Fig. 2B). Based on the ROC analysis, and in consideration of convenience in practical pathological diagnosis, we set the cut-off value for the Survivin IHC assay at 5%. Immunoreactivity of Survivin was classified as negative (positivity of less than 5% of the mesothelioma cells or non-neoplastic mesothelial cells) or positive (positivity of over 5% of the mesothelioma or mesothelial cells).

Forty-two of 62 (67.7%) EM cases were positive for Survivin. In contrast, none of the RMH cases were positive for Survivin (Table I).

Ki-67 expression and cut-off value. Representative immunohistochemical staining images for EM and RMH are shown in Fig. 3. Ki-67 expression was also significantly higher in EM than in RMH. The mean of the Ki-67 labelling indices in EM (mean, 32.6; range, 1.0-90.0; SD, 22.1) was significantly higher than that in RMH (mean, 3.5; range, 0-20.0, SD, 4.2) (t-test, P-value <0.001). Distributions of the Ki-67 labelling indices in EM and RMH are shown in Fig. 4A.

The cut-off value for the Ki-67 IHC assay led by the result of ROC analysis was 10.333 (Fig. 4B). Based on the ROC analysis, and in consideration of convenience in practical pathological diagnosis, we set the cut-off value for the Ki-67 IHC assay at 10%. Immunoreactivity of Ki-67 was classified as negative (positivity of less than 10% of the mesothelioma cells or non-neoplastic mesothelial cells) or positive (positivity of over 10% of the mesothelioma or mesothelial cells).

Fifty-seven of 67 (85.1%) EM cases and 7 of 56 (12.5%) RMH cases were positive for Ki-67 (Table I).

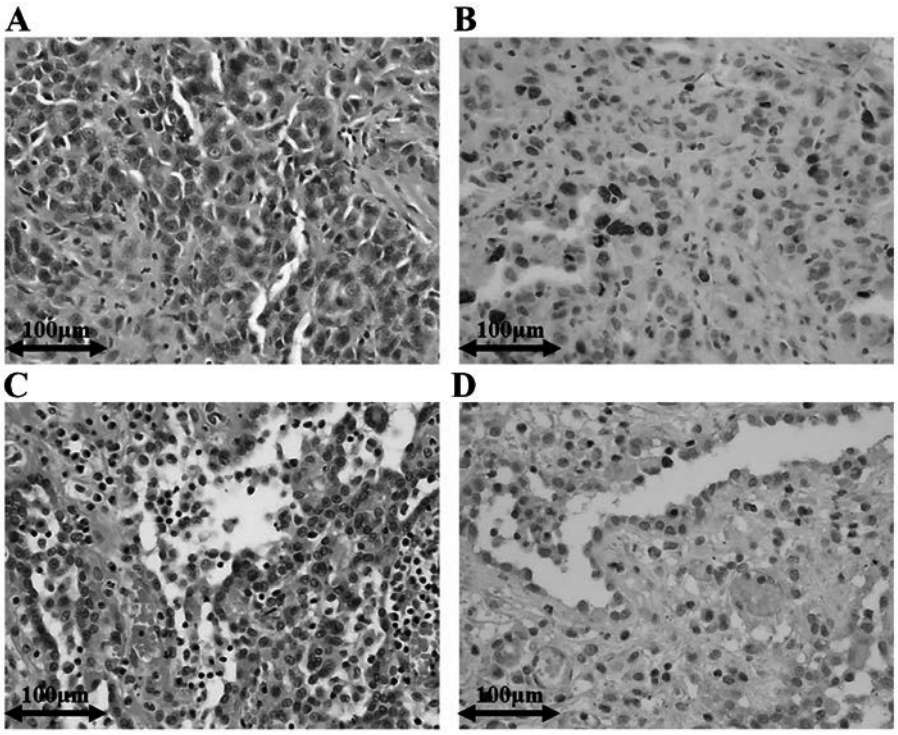

Figure 1. Representative histological images of Survivin IHC. (A) EM with H&E staining. (B) Survivin IHC in EM; labelling index, 18.1. (C) RMH with H&E stain. (D) Survivin IHC in RMH; labelling index, 1.3. IHC, immunohistochemistry; EM, epithelioid mesothelioma; RMH, reactive mesothelial hyperplasia; H&E, haematoxylin and eosin.

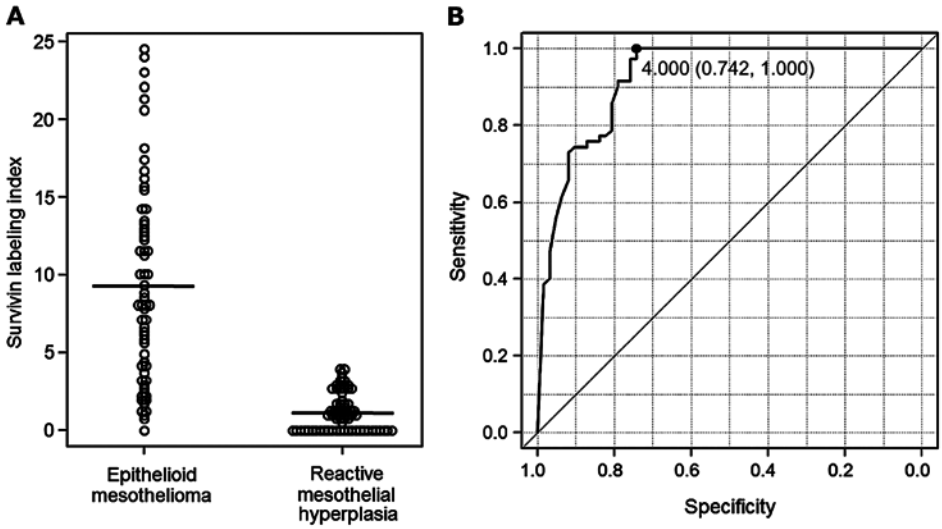

Figure 2. (A) Distribution of Survivin labelling index in epithelioid mesothelioma and reactive mesothelial hyperplasia. The horizontal line in the dot chart shows the mean. (B) ROC analysis. ROC curve was estimated using Survivin labelling index. Cut-off value based on the Youden index is also shown. ROC, receiver operating characteristic.

BAP1 expression. Loss of nuclear BAP1 expression was observed in 49 of 74 (66.2%) cases of EM (Table I). Almost all cases without BAP1 expression had a homogenous expression loss pattern. No heterogeneous loss patterns were observed. In contrast, nuclear BAP1 expression was preserved in all 78 RMH cases (Table I). Representative immunohistochemical staining images for EM and RMH are shown in Fig. 5.

Utilities of each marker and combinations of two markers. The sensitivity and specificity of each marker and combinations of two markers for the distinction between EM and RMH are shown in Table II. Among three single markers and six combination patterns of two markers, 'Survivin-positive and/or BAP1-loss' finding showed the highest diagnostic accuracy (95.3%).

Discussion

Accurate histopathological differentiation between MM and RMH is extremely important, not only for clinical management, but also for the appropriate operation of the public

Table I. Immunohistochemical findings of Survivin, Ki-67, and BAP1 in epithelioid mesothelioma and reactive mesothelial hyperplasia.

Immunohistochemical data	Epithelioid mesothelioma			Reactive mesothelial hyperplasia		
	n (%)	Negative	Positive	n (%)	Negative	Positive
Survivin expression	42/62 (67.7)	20	42	0/70	70	0
Ki-67 expression	57/67 (85.1)	10	57	7/56 (12.5)	49	7
BAP1-loss	49/74 (66.2)	25	49	0/78	78	0

BAP1, BRCA1-associated protein 1.

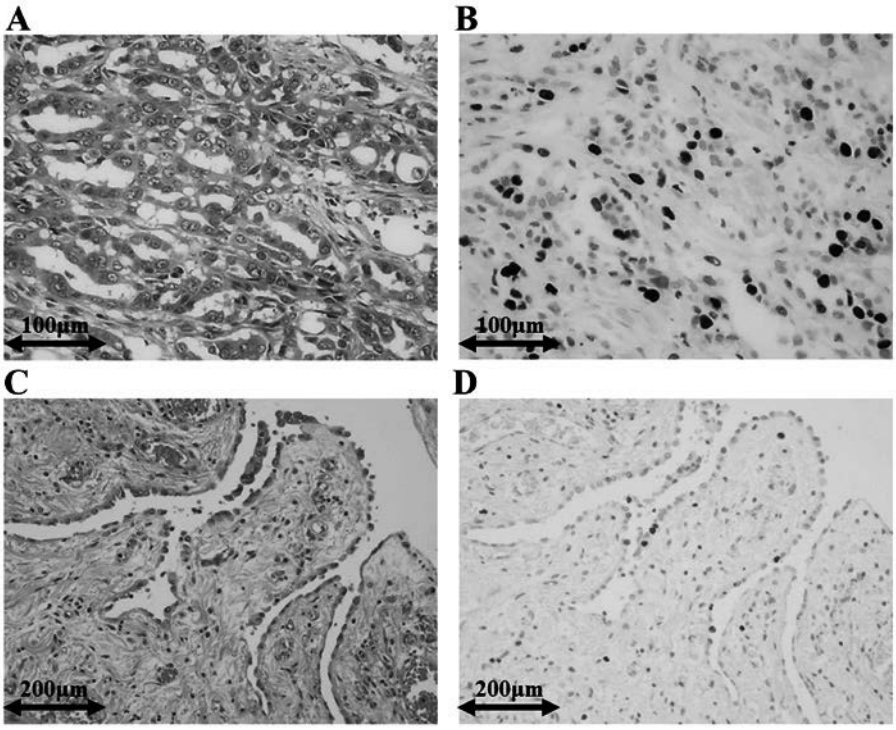

Figure 3. Representative histological images of Ki-67 IHC. (A) EM with H&E stain. (B) Ki-67 IHC in EM; labelling index, 35.0. (C) RMH with H&E stain. (D) Ki-67 IHC in RMH; labelling index, 8.7. IHC, immunohistochemistry; EM, epithelioid mesothelioma; RMH, reactive mesothelial hyperplasia; H&E, haematoxylin and eosin.

compensation system for victims of environmental and occupational asbestos exposure and their dependents. To obtain a better marker for EM, we evaluated the diagnostic utilities of Survivin, BAP1, and Ki-67 in differentiating EM from RMH. We found that the sensitivity and specificity of the nuclear Survivin labelling index following the use of a properly determined cut-off value was appropriate in distinguishing EM from RMH. The utility of Survivin IHC for the differentiation between benign and malignant mesothelial proliferation has not been reported to date. To the best of our knowledge, this is the first report evaluating the utility of Survivin IHC in differentiating EM from RMH.

Survivin is the smallest member of the inhibitor of apoptosis (IAP) family, and is expressed highly in most human foetal tissues and cancers. However, it is completely absent in terminally-differentiated tissues. Survivin functions as a regulator of both cell division and apoptosis. The function of Survivin differs according to cellular localization. Cytosolic Survivin is believed to function as an apoptotic suppressor, while nuclear Survivin is postulated to regulate cell division (24). Overexpression of Survivin is associated with tumour progression and poor prognosis in many types of human malignancies, including MM (25,26). In fact, several reports indicate that Survivin is a promising marker for the diagnosis of malignant pleural effusion (27). Survivin has also been reported to be associated with anti-tumour activity and outcomes of chemotherapy in MM, and is a new therapeutic target for the treatment of MM (28-30).

While the Survivin labelling indices of the EM cases in our study were similar to those reported by Meerang *et al* (25), they were significantly lower than those reported by Hmeljak *et al* (median, 67; mean, 63; range, 9.7-94.9; SD, 20.8) (26). This discrepancy in Survivin expression may be due to differences in staining technique, source of antibodies used for analysis,

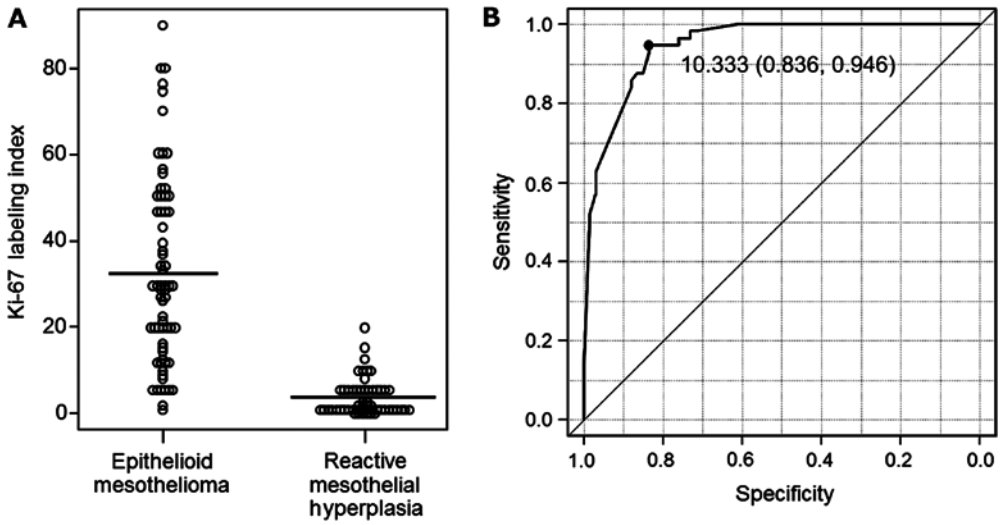

Figure 4. (A) Distributions of Ki-67 labelling index in epithelioid mesothelioma and reactive mesothelial hyperplasia. The horizontal line in the dot chart shows the mean. (B) ROC analysis. ROC curve was estimated using Ki-67 labelling index. Cut-off value based on the Youden index is also shown. ROC, receiver operating characteristic.

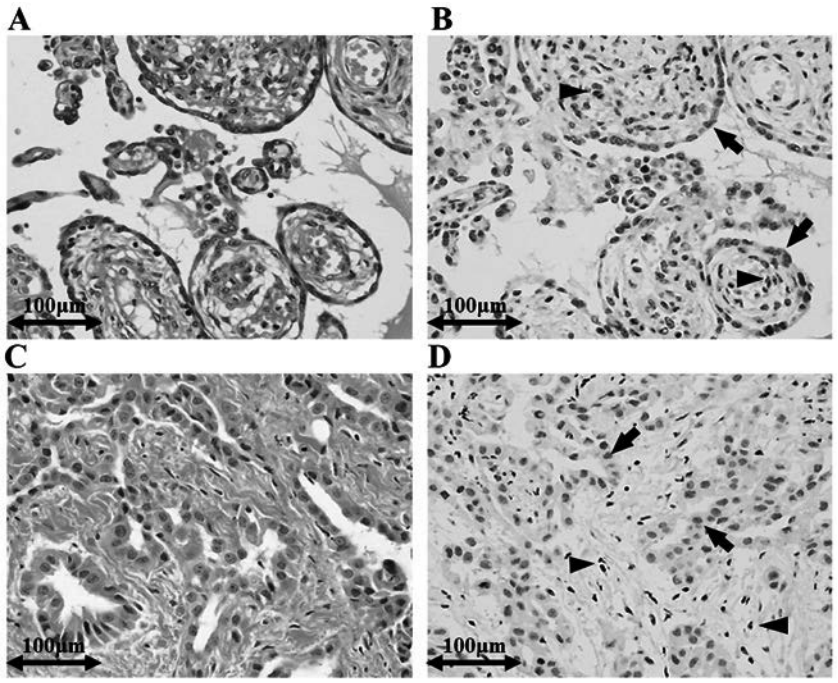

Figure 5. Representative histological images of BAP1 IHC. (A) RMH with H&E stain. (B) BAP1 IHC in RMH. Nuclear staining of the mesothelial cells (arrows) demonstrated the same intensity as that of internal positive controls (arrowheads; stromal cells). (C) EM with H&E stain. (D) BAP1 IHC in EM. Nuclear staining was not observed in tumour cells (loss of expression). Strong nuclear staining was observed in internal positive controls (arrowheads; stromal cells). IHC, immunohistochemistry; EM, epithelioid mesothelioma; RMH, reactive mesothelial hyperplasia; H&E, haematoxylin and eosin; BAP1, BRCA1-associated protein 1.

and the quantification technique. In our study, we used fully automated immunohistochemical staining utilising equipment from Roche for reproducible results. We also used commercially available antibodies from reputable sources and evaluated nuclear reactivity alone. Evaluation of nuclear reactivity was reproducible and was independently confirmed by 3 pathologists.

Several studies have determined that germline mutations in the gene for *BAP1* predispose individuals to developing various tumours, including MM, cutaneous melanocytic tumours, uveal melanoma, lung adenocarcinoma, and meningioma (31). These studies suggest that germline mutations in *BAP1* result in a 'tumour predisposition syndrome' linking BAP1 to many other cancers. Somatic mutations in the *BAP1* gene have also been relatively frequently reported in MMs, uveal melanomas, and renal cell carcinomas (31). BAP1 is encoded by the *BAP1* gene, which is located on the short arm of chromosome 3 (3p21). BAP1 is a deubiquitinase targeting histones and the host cell factor-1 transcriptional co-factor, and plays a role in transcriptional regulation, chromatin modulation, cell cycle

Table II. Sensitivity, specificity, PPVs, NPVs and diagnostic accuracies of each marker and combinations of two markers for the differential diagnosis between epithelioid mesothelioma and reactive mesothelial hyperplasia.

Immunohistochemical findings	Sensitivity (%)	Specificity (%)	PPV (%)	NPV (%)	Accuracy (%)
Survivin-positive	67.7	100.0	100.0	77.8	84.8
BAP1-loss	66.2	100.0	100.0	75.7	83.6
Ki-67-positive	85.1	87.5	89.1	83.1	86.2
Survivin-positive and/or BAP1-loss	89.8	100.0	100.0	92	95.3
Both Survivin-positive and BAP1-loss	39.0	100	100.0	65.7	71.9
Survivin-positive and/or Ki-67-positive	91.1	86.3	87.9	89.8	88.8
Both Survivin-positive and Ki-67-positive	66.1	100.0	100.0	72.9	82.2
BAP1-loss and/or Ki-67-positive	96.9	92.1	94.3	95.9	94.8
Both BAP1-loss and Ki-67-positive	53.8	100	100.0	64.3	74.8

PPV, positive predictive values; NPV, negative predictive values; BAP1, BRCA1-associated protein 1.

regulation, and DNA repair (31,32). Several different alterations in the *BAP1* gene have been described, including large deletions of exons leading to loss of the N-terminal region, or to premature protein termination, focal deletions, frameshift mutations due to insertions or deletions, splice site mutations, and base substitutions leading to nonsense and missense mutations. Frameshift mutations and missense and nonsense substitutions are the most common sequence alterations. Truncating mutations frequently result in loss of the nuclear localization signal and/or the C-terminal protein-binding domain, while missense mutations interfere with the ubiquitin hydrolase function of BAP1 (31). As the detection of these alterations in *BAP1* has been made possible in recent years using immunohistochemistry (IHC), immunohistochemical detection of BAP1 loss has also been reported to be useful in distinguishing MM from RMH. However, the sensitivity of this assay in differentiating MM from RMH does not exceed 70% (10-13). Several studies indicate that the loss of nuclear BAP1 expression as assessed by IHC is closely correlated with genetic alterations in BAP1 (33-35).

In the present study, the frequency of BAP1 loss in EM was 66.2% (49/74), similar to those found in previous reports (10-13). Recently, Hida *et al* reported a focal heterogeneous BAP1 staining pattern in mesothelioma cases (10). However, in our study, almost all EM cases had either a uniform positive staining pattern or completely negative staining for BAP1. There were some EM cases that appeared to have focal staining for BAP1; however, careful observation of these cases under high power magnification confirmed that these focal positive cells were in fact inflammatory cells infiltrating into the mesothelioma or stromal cells. We classified such cases as cases with no loss of BAP1 expression. This may be the reason for the observed heterogeneous BAP1 staining pattern in mesothelioma. However, other reasons, such as differences in staining techniques and improper processing of the tumour, may also contribute to apparent differences between studies.

The specificity of a Survivin labelling index of over 5% and a loss of BAP1 expression was 100%. However, sensitivity of Survivin labelling index (67.7%) and loss of BAP1 expression (66.2%) alone are not sufficient for differential diagnosis. Although diagnostic accuracies of Survivin (84.8%) and BAP1 (83.6%) as single markers were inferior to that of EMA (95.5%), (21) the diagnostic accuracy of the combination of Survivin and BAP1 (Survivin-positive and/or BAP1-loss) was 95.3%, which was almost similar to EMA. Recently, Shinozaki-Ushiku *et al* proposed using a combination of BAP1 and enhancer of zeste homolog 2 (EZH2) expression to differentiate between MM from RMH; the sensitivity of this combination was 90%, while the specificity was absolute (36). The sensitivity (89.8%) and specificity (100%) of the combination of Survivin and BAP1 IHC in this study was comparable to those of previous reports (36).

A positive correlation between nuclear Survivin and Ki-67 labelling indices was previously reported by Meerang *et al* (25). We observed a similar correlation between Survivin and Ki-67 labelling indices in our study (data not shown). Although this correlation was present in both EM and RMH, it was more conspicuous in EM. Ki-67 protein is present during all active phases of the cell cycle (G1, S, G2, and mitosis), but is absent in resting cells (G0). Therefore, Ki-67 is well known as a so-called 'proliferation marker', and the Ki-67 labelling index is often correlated with the clinical course of cancer (37,38). On the other hand, nuclear Survivin plays important roles in the regulation of mitosis. Survivin expression is found to be dominant only in the G2/M phase, and Survivin is known to localize to components of the mitotic spindle during the metaphase and anaphase of mitosis (39,40). Therefore, both nuclear Survivin and Ki-67 may be considered proliferation markers. We can thus explain both the high expression of Survivin and Ki-67 in EM compared to RMH, and the positive correlation between the nuclear Survivin and Ki-67 labelling indices.

Although various studies have reported the usefulness of Ki-67 IHC in differentiating EM from RMH, (14-17) it is not routinely utilized for the confirmation of mesothelioma due to its low sensitivity and specificity.

The sensitivity, specificity, and diagnostic accuracy of Ki-67 (85.1, 87.5, and 86.2%, respectively) in this study were almost the same or slightly higher compared with previous reports (14,15,17). These values were relatively high but not sufficient for differential diagnosis by single marker. However, the diagnostic accuracy

of the combination of Ki-67 and BAP1 was 94.8%, which was almost the same as that of the combination of Survivin and BAP1.

We evaluated the utility of Survivin, BAP1, and Ki-67 IHC in distinguishing EM from RMH. Based on our results, 'Survivin-positive and/or BAP1-loss' finding strongly suggest EM, therefore we recommend the use of a combination of Survivin and BAP1. In addition, further evaluation of the Ki-67 labelling index may be useful for accurate differential diagnosis.

Acknowledgements

The authors would like to thank the Technical Centre of Hiroshima University for technical assistance. This study was funded in part by the Japanese Ministry of Health, Labour, and Welfare.

References

1. Robinson BW, Musk AW and Lake RA: Malignant mesothelioma. Lancet 366: 397-408, 2005.
2. Roggli VL, Sharma A, Butnor KJ, Sporn T and Vollmer RT: Malignant mesothelioma and occupational exposure to asbestos: A clinicopathological correlation of 1445 cases. Ultrastruct Pathol 26: 55-65, 2002.
3. Delgermaa V, Takahashi K, Park EK, Le GV, Hara T and Sorahan T: Global mesothelioma deaths reported to the World Health Organization between 1994 and 2008. Bull World Health Organ 89: 716-724, 2011.
4. Murayama T, Takahashi K, Natori Y and Kurumatani N: Estimation of future mortality from pleural malignant mesothelioma in Japan based on an age-cohort model. Am J Ind Med 49: 1-7, 2006.
5. Churg A, Roggli V, Galateau-Salle F, Cagle PhT, Gibbs AR, Hasleton PhS, Henderson DW, Vignaud JM, Inai K, Praet M, *et al*: Tumours of the pleura. In: WHO Classification of Tumours of the Lung, Pleura, Thymus and Heart. Travis WD, Brambilla E, Burke AP, Marx A and Nicholson AG (eds). IARC Press, Lyon, pp153-181, 2015.
6. Husain AN, Colby T, Ordonez N, Krausz T, Attanoos R, Beasley MB, Borczuk AC, Butnor K, Cagle PT, Chirieac LR, *et al*: Guidelines for pathologic diagnosis of malignant mesothelioma: 2012 update of the consensus statement from the International Mesothelioma Interest Group. Arch Pathol Lab Med 137: 647-667, 2013.
7. Ordóñez NG: Application of immunohistochemistry in the diagnosis of epithelioid mesothelioma: A review and update. Hum Pathol 44: 1-19, 2013.
8. Kushitani K, Amatya VJ, Okada Y, Katayama Y, Mawas AS, Miyata Y, Okada M, Inai K, Kishimoto T and Takeshima Y: Utility and pitfall of immunohistochemistry in the differential diagnosis between epithelioid mesothelioma and poorly differentiated lung squamous cell carcinoma. Histopathology 70: 375-384, 2017.
9. Minato H, Kurose N, Fukushima M, Nojima T, Usuda K, Sagawa M, Sakuma T, Ooi A, Matsumoto I, Oda M, *et al*: Comparative immunohistochemical analysis of IMP3, GLUT1, EMA, CD146, and desmin for distinguishing malignant mesothelioma from reactive mesothelial cells. Am J Clin Pathol 141: 85-93, 2014.
10. Hida T, Hamasaki M, Matsumoto S, Sato A, Tsujimura T, Kawahara K, Iwasaki A, Okamoto T, Oda Y, Honda H and Nabeshima K: BAP1 immunohistochemistry and p16 FISH results in combination provide higher confidence in malignant pleural mesothelioma diagnosis: ROC analysis of the two tests. Pathol Int 66: 563-570, 2016.
11. Hwang HC, Sheffield BS, Rodriguez S, Thompson K, Tse CH, Gown AM and Churg A: Utility of BAP1 immunohistochemistry and p16 (CDKN2A) FISH in the diagnosis of malignant mesothelioma in effusion cytology specimens. Am J Surg Pathol 40: 120-126, 2016.
12. McGregor SM, Dunning R, Hyjek E, Vigneswaran W, Husain AN and Krausz T: BAP1 facilitates diagnostic objectivity, classification, and prognostication in malignant pleural mesothelioma. Hum Pathol 46: 1670-1678, 2015.
13. Cigognetti M, Lonardi S, Fisogni S, Balzarini P, Pellegrini V, Tironi A, Bercich L, Bugatti M, Rossi G, Murer B, *et al*: BAP1 (BRCA1-associated protein 1) is a highly specific marker for differentiating mesothelioma from reactive mesothelial proliferations. Mod Pathol 28: 1043-1057, 2015.
14. Kimura F, Okayasu I, Kakinuma H, Satoh Y, Kuwao S, Saegusa M and Watanabe J: Differential diagnosis of reactive mesothelial cells and malignant mesothelioma cells using the cell proliferation markers minichromosome maintenance protein 7, geminin, topoisomerase II alpha and Ki-67. Acta Cytol 57: 384-390, 2013.
15. Kimura F, Kawamura J, Watanabe J, Kamoshida S, Kawai K, Okayasu I and Kuwao S: Significance of cell proliferation markers (Minichromosome maintenance protein 7, topoisomerase IIalpha and Ki-67) in cavital fluid cytology: Can we differentiate reactive mesothelial cells from malignant cells? Diagn Cytopathol 38: 161-167, 2010.
16. Hasteh F, Lin GY, Weidner N and Michael CW: The use of immunohistochemistry to distinguish reactive mesothelial cells from malignant mesothelioma in cytologic effusions. Cancer Cytopathol 118: 90-96, 2010.
17. Taheri ZM, Mehrafza M, Mohammadi F, Khoddami M, Bahadori M and Masjedi MR: The diagnostic value of Ki-67 and repp86 in distinguishing between benign and malignant mesothelial proliferations. Arch Pathol Lab Med 132: 694-697, 2008.
18. Churg A, Sheffield BS and Galateau-Salle F: New markers for separating benign from malignant mesothelial proliferations: Are we there yet? Arch Pathol Lab Med 140: 318-321, 2016.
19. Hiroshima K, Wu D, Hasegawa M, Koh E, Sekine Y, Ozaki D, Yusa T, Walts AE, Marchevsky AM, Nabeshima K, *et al*: Cytologic differential diagnosis of malignant mesothelioma and reactive mesothelial cells with fish analysis of p16. Diagn Cytopathol 44: 591-598, 2016.
20. Walts AE, Hiroshima K, McGregor SM, Wu D, Husain AN and Marchevsky AM: BAP1 immunostain and CDKN2A (p16) FISH analysis: Clinical applicability for the diagnosis of malignant mesothelioma in effusions. Diagn Cytopathol 44: 599-606, 2016.
21. Kushitani K, Amatya VJ, Mawas AS, Miyata Y, Okada M and Takeshima Y: Use of anti-noxa antibody for differential diagnosis between epithelioid mesothelioma and reactive mesothelial hyperplasia. Pathobiology 83: 33-40, 2016.
22. Travis WD, Brambilla E, Nicholson AG, Yatabe Y, Austin JHM, Beasley MB, Chirieac LR, Dacic S, Duhig E, Flieder DB, *et al*: The 2015 World Health Organization Classification of Lung Tumors: Impact of genetic, clinical and radiologic advances since the 2004 classification. J Thorac Oncol 10: 1243-1260, 2015.
23. Kanda Y: Investigation of the freely available easy-to-use software 'EZR' for medical statistics. Bone Marrow Transplant 48: 452-458, 2013.
24. Garg H, Suri P, Gupta JC, Talwar GP and Dubey S: Survivin: A unique target for tumor therapy. Cancer Cell Int 16: 49, 2016.
25. Meerang M, Bérard K, Friess M, Bitanihirwe BK, Soltermann A, Vrugt B, Felley-Bosco E, Bueno R, Richards WG, Seifert B, *et al*: Low merlin expression and high survivin labeling index are indicators for poor prognosis in patients with malignant pleural mesothelioma. Mol Oncol 10: 1255-1265, 2016.
26. Hmeljak J, Erčulj N, Dolžan V, Pižem J, Kern I, Kovač V, Cemažar M and Cör A: Is survivin expression prognostic or predictive in malignant pleural mesothelioma? Virchows Arch 462: 315-321, 2013.
27. Chen S, Wang Y, An L, Fei ZT and Li T: The diagnostic value of survivin in malignant pleural effusion: A meta-analysis. Clin Chim Acta 441: 142-147, 2015.
28. Bertino P, Panigada M, Soprana E, Bianchi V, Bertilaccio S, Sanvito F, Rose AH, Yang H, Gaudino G, Hoffmann PR, *et al*: Fowlpox-based survivin vaccination for malignant mesothelioma therapy. Int J Cancer 133: 612-623, 2013.
29. De Cesare M, Cominetti D, Doldi V, Lopergolo A, Deraco M, Gandellini P, Friedlander S, Landesman Y, Kauffman MG, Shacham S, *et al*: Anti-tumor activity of selective inhibitors of XPO1/CRM1-mediated nuclear export in diffuse malignant peritoneal mesothelioma: The role of survivin. Oncotarget 6: 13119-13132, 2015.
30. Goričar K, Kovač V, Franko A, Dodič-Fikfak M and Dolžan V: Serum survivin levels and outcome of chemotherapy in patients with malignant mesothelioma. Dis Markers 2015: 316739, 2015.
31. Murali R, Wiesner T and Scolyer RA: Tumours associated with BAP1 mutations. Pathology 45: 116-126, 2013.
32. Scheuermann JC, de Ayala Alonso AG, Oktaba K, Ly-Hartig N, McGinty RK, Fraterman S, Wilm M, Muir TW and Müller J: Histone H2A deubiquitinase activity of the Polycomb repressive complex PR-DUB. Nature 465: 243-247, 2010.

33. Bott M, Brevet M, Taylor BS, Shimizu S, Ito T, Wang L, Creaney J, Lake RA, Zakowski MF, Reva B, *et al*: The nuclear deubiquitinase BAP1 is commonly inactivated by somatic mutations and 3p21.1 losses in malignant pleural mesothelioma. Nat Genet 43: 668-672, 2011.
34. Testa JR, Cheung M, Pei J, Below JE, Tan Y, Sementino E, Cox NJ, Dogan AU, Pass HI, Trusa S, *et al*: Germline BAP1 mutations predispose to malignant mesothelioma. Nat Genet 43: 1022-1025, 2011.
35. Yoshikawa Y, Sato A, Tsujimura T, Emi M, Morinaga T, Fukuoka K, Yamada S, Murakami A, Kondo N, Matsumoto S, *et al*: Frequent inactivation of the BAP1 gene in epithelioid-type malignant mesothelioma. Cancer Sci 103: 868-874, 2012.
36. Shinozaki-Ushiku A, Ushiku T, Morita S, Anraku M, Nakajima J and Fukayama M: Diagnostic utility of BAP1 and EZH2 expression in malignant mesothelioma. Histopathology 70: 722-733, 2017.
37. Scholzen T and Gerdes J: The Ki-67 protein: From the known and the unknown. J Cell Physiol 182: 311-322, 2000.
38. Brown DC and Gatter KC: Monoclonal antibody Ki-67: Its use in histopathology. Histopathology 17: 489-503, 1990.
39. Altieri DC: Validating survivin as a cancer therapeutic target. Nat Rev Cancer 3: 46-54, 2003.
40. Kim JY, Chung JY, Lee SG, Kim YJ, Park JE, Yoo KS, Yoo YH, Park YC, Kim BG and Kim JM: Nuclear interaction of Smac/DIABLO with survivin at G2/M arrest prompts docetaxel-induced apoptosis in DU145 prostate cancer cells. Biochem Biophys Res Commun 350: 949-954, 2006.

Lung Cancer 115 (2018) 103–108

Contents lists available at ScienceDirect

Lung Cancer

journal homepage: www.elsevier.com/locate/lungcan

A phase I trial of afatinib and bevacizumab in chemo-naïve patients with advanced non-small-cell lung cancer harboring EGFR mutations: Okayama Lung Cancer Study Group Trial 1404

Takashi Ninomiya[a,*], Naoyuki Nogami[b], Toshiyuki Kozuki[b], Daijiro Harada[b], Toshio Kubo[a,c], Kadoaki Ohashi[d], Shoichi Kuyama[e], Kenichiro Kudo[e], Akihiro Bessho[f], Nobuaki Fukamatsu[f], Nobukazu Fujimoto[g], Keisuke Aoe[h], Takuo Shibayama[i], Keisuke Sugimoto[j], Nagio Takigawa[k], Katsuyuki Hotta[l], Katsuyuki Kiura[a]

[a] *Department of Respiratory Medicine and Allergy, Okayama University Hospital, 2-5-1, Shikata-cho, Okayama, Japan*
[b] *Department of Thoracic Oncology and Medicine, National Hospital Organization, Shikoku Cancer Center, 160, Minamiumemoto-ko, Matsuyama, Japan*
[c] *Center for Oncology, Okayama University Hospital, 2-5-1, Shikata-cho, Okayama, Japan*
[d] *Department of Hematology, Oncology and Respiratory Medicine, Okayama University Graduate School of Medicine, Dentistry and Pharmaceutical Sciences, 2-5-1, Shikata-cho, Okayama, Japan*
[e] *Department of Respiratory Medicine, Iwakuni Clinical Center, 1-1-1, Atago-cho, Iwakuni, Japan*
[f] *Department of Respiratory Medicine, Japanese Red Cross Okayama Hospital, 2-1-1, Aoe, Okayama, Japan*
[g] *Department of Medical Oncology, Okayama Rosai Hospital, 1-10-25, Chikkomidorimachi, Okayama, Japan*
[h] *Department of Medical Oncology, National Hospital Organization, Yamaguchi-Ube Medical Center, 685, Higashikiwa, Ube, Japan*
[i] *Department of Respiratory Medicine, National Hospital Organization, Okayama Medical Center, 1711-1, Tamasu, Okayama, Japan*
[j] *Department of Respiratory Medicine, Japanese Red Cross Kobe Hospital, 1-3-1, Wakihamakaigann-dori, Chuo-ku, Kobe, Japan*
[k] *Department of General Internal Medicine 4, Kawasaki Medical School, 2-6-1, Nakasange, Okayama, Japan*
[l] *Center for Innovative Clinical Medicine, Okayama University Hospital, 2-5-1, Shikata-cho, Okayama, Japan*

ARTICLE INFO

Keywords:
Non-small-cell lung cancer
EGFR
Bevacizumab
Afatinib
EGFR-TKI
Phase Ib

ABSTRACT

Objective: In advanced epidermal growth factor receptor (EGFR)-mutant non-small-cell lung cancer (NSCLC), treatment with afatinib, a second-generation EGFR-tyrosine kinase inhibitor (TKI), confers a significant survival benefit over platinum-based chemotherapy. The first-generation EGFR-TKIs gefitinib and erlotinib in combination with bevacizumab have improved progression-free survival. We hypothesized that the combination of afatinib with bevacizumab would further improve efficacy, and conducted a phase I trial to test this hypothesis.
Materials and methods: Untreated patients with advanced EGFR-mutant NSCLC were enrolled. The primary endpoint was safety. Two doses of afatinib, 40 mg/day (level 0) and 30 mg/day (level −1), were evaluated in combination with 15 mg/kg bevacizumab every 3 weeks. Optimal dosing was determined by dose-limiting toxicity (DLT), with the concentration at which ≤4 of 12 patients experienced toxicity considered the recommended dose.
Results: Nineteen patients were enrolled (level 0:5, level −1:14). Three of the five patients at level 0 experienced a DLT, which indicated that this dose was unfeasible. Three patients at level −1 developed a DLT of grade 3 non-hematological toxicity, which was soon resolved. Grade 3 or worse adverse events were experienced by all five patients at dose level 0 (diarrhea in 2, skin rash in 1, hypoxia in 1, and paronychia in 1), and by three patients at level −1 (diarrhea in 2 and anorexia in 1). Among 16 evaluable patients, 1 had a complete response, 12 had partial responses, and 0 had progressive disease.
Conclusion: Afatinib plus bevacizumab (level −1) was well tolerated and showed evidence of favorable disease control. This combination therapy may represent a potent therapeutic option for patients with EGFR-mutant NSCLC.

* Corresponding author at: Department of Respiratory Medicine and Allergy, Okayama University Hospital, 2-5-1, Shikata-cho, Okayama, 700-8558, Japan.
E-mail address: tninomiya5@okayama-u.ac.jp (T. Ninomiya).

https://doi.org/10.1016/j.lungcan.2017.11.025
Received 12 October 2017; Received in revised form 22 November 2017; Accepted 27 November 2017
0169-5002/

1. Introduction

Lung cancer is a leading cause of death worldwide. The major pathological subtype of lung cancer is non-small-cell lung cancer (NSCLC); in some NSCLCs, activating mutations in the epidermal growth factor receptor (EGFR) gene have been reported [1]. In this subgroup of patients, an EGFR-tyrosine kinase inhibitor (EGFR-TKI) was found to prolong progression-free survival (PFS) compared with standard platinum-based chemotherapy [2–7]. While the median overall survival (OS) of this patient subgroup reaches almost 2 years with EGFR-TKI treatment, this is still insufficient. To prolong PFS and OS, more effective treatments are needed.

Afatinib, a second-generation EGFR-TKI, is an irreversible inhibitor of the ErbB family that is expected to inhibit tumors with activating EGFR mutations more strongly than are reversible EGFR-TKIs. Our preclinical study revealed that afatinib prolonged survival compared with gefitinib in an *egfr*-driven mouse lung cancer model [8]. In a clinical study, afatinib significantly improved outcomes in treatment-naïve patients with NSCLC harboring EGFR mutations compared with gefitinib [9]. In a combined analysis of phase III studies comparing afatinib with platinum-based chemotherapy, afatinib significantly prolonged both PFS and OS [10], while first-generation EGFR-TKIs (gefitinib or erlotinib) prolonged PFS but not OS [2,3]. Thus, second-generation EGFR-TKIs are suggested to achieve better outcomes than those of first-generation inhibitors.

Vascular endothelial growth factor (VEGF)-A, by binding to the VEGF receptor (VEGFR)-2, promotes angiogenesis in the tumor microenvironment and indirectly promotes tumor growth. We previously described the synergistic effects of afatinib and bevacizumab, a recombinant monoclonal antibody targeting VEGF-A [8]. In our preclinical study, the combination of bevacizumab with afatinib was more effective than afatinib alone in a xenograft model of NSCLC cells harboring EGFR mutations. Clinically, we and another group have already shown favorable PFS with acceptable toxicity profiles for combination therapy consisting of bevacizumab and first-generation EGFR-TKIs in untreated EGFR-mutant tumors [11–13]. The median PFSs of patients treated with erlotinib/bevacizumab therapy and gefitinib/bevacizumab therapy were 16.0 months and 14.4 months, respectively. However, combination therapy of bevacizumab with the second-generation EGFR-TKI afatinib had not been evaluated clinically.

Against this background, we hypothesized that the combination of bevacizumab with afatinib would yield improved efficacy. As the first step to test this hypothesis, we initiated a phase I trial of this combination therapy in chemo-naïve patients with advanced NSCLC harboring EGFR mutations.

2. Materials and methods

2.1. Study design

This open-label, phase I study was conducted in 16 institutions in Japan (UMIN000015944). The study protocol was approved by the institutional review boards of each participating center. Written informed consent was obtained from each patient prior to the study. This study was performed in accordance with the Declaration of Helsinki and all relevant Japanese laws and regulations.

The aim of this study was to evaluate the feasibility and recommended dose of combination therapy in chemo-naïve patients with advanced NSCLC harboring EGFR mutations. The primary outcome measure was dose-limiting toxicity (DLT). Secondary outcome measures were the objective response rate, PFS, OS, and specific toxicity.

2.2. Patients

Those patients who met the following criteria were eligible: histologically or cytologically confirmed stage IIIB/IV or postoperative recurrent non-squamous NSCLC with activating EGFR mutations (either exon 19 deletion or Leu858Arg), age $\geq$20 years, Eastern Cooperative Oncology Group performance status of 0 or 1, adequate organ function, and life expectancy of 3 months or more. Those who received previous EGFR-TKI therapy or radiation therapy for lung tumors were excluded. Tumor samples were screened by PCR-based hypersensitive EGFR mutation testing in local laboratories, according to standard testing practices.

Major exclusion criteria included confirmation of the Thr790Met mutation, presence of symptomatic brain metastasis or leptomeningeal carcinomatosis, history or presence of hemoptysis, bloody sputum or a coagulation disorder, tumor invading or abutting major blood vessels, tumor cavitation, or coexisting or previous interstitial lung disease.

2.3. Treatment regimen

Six patients were first scheduled to receive 40 mg afatinib daily plus 15 mg/kg intravenous bevacizumab repeated at 3-week intervals (level 0) until disease progression or unacceptable toxicity was observed. If no more than two patients experienced DLT, an additional six patients were treated at the same dose. If no more than two patients experienced DLT in both sets (a rate or DLT < 33.3%), we concluded this dose schedule to be feasible and planned a subsequent phase II trial. Otherwise, we repeated the same treatment of 30 mg/day afatinib and 15 mg/kg bevacizumab (level −1). If four or fewer patients experienced DLT (a rate of DLT < 33.3%), this level was recommended; if not, further investigation of this combination therapy was not pursued.

2.4. Safety and efficacy assessment

Severity of toxicity was assessed according to the Common Terminology Criteria for Adverse Events v 4.0. Although all treatment courses were analyzed to determine the DLT and maximum tolerated dose, the decision to lower the dose level was based on toxicity during the first 28 days from initiation of the combination therapy. A DLT was defined as any of the following adverse drug reactions: grade 4 hematological toxicity, grade 4 hypertension, grade 3 or worse non-hematological toxicity other than hypertension, grade 2 non-hematological toxicity lasting $\geq$7 days despite supportive care, grade 2 or worse left ventricular function or renal function, grade 1 or worse pneumonitis, or inability to receive the second course of bevacizumab due to bevacizumab toxicity.

Antitumor activity was assessed radiologically (by computed tomography or magnetic resonance imaging) every 2 months. All responses were defined according to the criteria of RECIST 1.1. If a patient had a documented complete response (CR) or partial response (PR), a confirmatory evaluation was performed after 4 weeks. Disease control was defined as the best tumor response among CR, PR, and stable disease (SD) that had been confirmed and sustained for at least 6 weeks. The response rate (RR) was defined as the number of patients with the best tumor response (CR or PR) among all patients with measurable lesions. OS was defined as the time from the date of registration to death from any cause. PFS was defined as the time from the date of registration to the date of the detection of progressive disease or of death from any cause. OS and PFS were assessed by the Kaplan-Meier method.

3. Results

3.1. Patient characteristics

From December 2014 to July 2016, 19 patients were enrolled, of whom 5 were treated at dose level 0 and 14 at dose level −1. The clinical characteristics of all patients are listed in Table 1. Three patients were withdrawn for toxicity (Fig. 1).

Table 1
Patient characteristics by dose level.

Characteristics	All patients (n = 19)	Level 0 (n = 5)	Level −1 (n = 14)
Age (years)			
Median	67.0	65.0	67.5
Range	40–76	42–68	40–76
Sex			
Male	10	3	7
Female	9	2	7
ECOG performance status			
0	10	4	6
1	9	1	8
Histology			
Adenocarcinoma	19	5	14
Disease status			
IV	9	3	6
Postoperative recurrence	10	2	8
EGFR mutation			
Exon 19 deletion	8	2	6
Exon 21 L858R	11	3	8
Brain metastasis			
Positive	9	2	7
Negative	10	3	7

Dose level 0: afatinib (40 mg once daily) plus bevacizumab (15 mg/kg intravenously repeated at 3-week intervals). Dose level −1: afatinib (30 mg once daily) plus bevacizumab (15 mg/kg intravenously repeated at 3-week intervals).
ECOG, Eastern Cooperative Oncology Group.

3.2. DLTs

Three of five patients at dose level 0 experienced DLTs: grade 3 diarrhea (n = 2) and hypoxia (n = 1); thus, we concluded that this dose level was unfeasible. At level −1, 3 of 14 patients developed DLTs: grade 3 diarrhea (n = 2) and anorexia (n = 1). Although we originally planned to enroll only 12 patients in level −1, 14 patients were ultimately included due to the timing of patient enrollment. The rate of DLT was 60% at dose level 0 and 21.4% at dose level −1. The maximum tolerated/recommended dose was determined to be 30 mg afatinib once daily with 15 mg/kg of bevacizumab repeated at 3-week intervals. All DLTs resolved soon after discontinuation of afatinib. Four patients who experienced DLT of grade 3 diarrhea reduced their dosage of afatinib and resumed treatment after recovering. Those patients who experienced hypoxia or anorexia stopped therapy, based on the investigator's decision and the patients' requests, respectively.

Table 2
Adverse events.

Adverse Event	n (%)	
	Any Grade	Grade 3[b]
Dose level 0 (n = 5)		
Diarrhea	5 (100)	2 (40)[a]
Rash acneiform	4 (80)	1 (20)
Paronychia	4 (80)	1 (20)
Hypertension	3 (60)	0
AST/ALT increase	2 (40)	0
Hypoxia	1 (20)	1 (20)[a]
Fatigue	1 (20)	0
Bleeding	1 (20)	0
Mucositis oral	1 (20)	0
Proteinuria	1 (20)	0
Dose level −1 (n = 14)		
Rash acneiform	13 (93)	1 (7)
Diarrhea	12 (86)	2 (14)[a]
Paronychia	7 (50)	0
Nausea/Vomiting	4 (29)	0
Hypertension	4 (29)	0
Proteinuria	4 (29)	0
Anorexia	3 (21)	1 (7)[a]
Mucositis Oral	3 (21)	1 (7)
Fatigue	3 (21)	0
Bleeding	1 (7)	0

Dose level 0: afatinib (40 mg once daily) plus bevacizumab (15 mg/kg intravenously repeated at 3-week intervals). Dose level −1: afatinib (30 mg once daily) plus bevacizumab (15 mg/kg intravenously repeated at 3-week intervals).
AST/ALT, aspartate aminotransferase/alanine aminotransferase ratio.
[a] DLTs comprised grade 3 diarrhea (n = 4), hypoxia (n = 1), and anorexia (n = 1).
[b] There were no grade 4 or 5 adverse events.

3.3. Adverse events

The frequent (> 25%) adverse events were acneiform rash, diarrhea, paronychia, hypertension, and proteinuria. The main grade 3 toxicities are listed in Table 2. All patients at dose level 0 and 4 of 14 patients (29%) at level −1 had grade 3 toxicities. There were no grade 4 or 5 toxicities. Three patients at level 0 and five patients at level −1 required dose reductions for toxicity. Three patients at level 0 and one patient at level −1 discontinued the protocol therapy for toxicity, and two patients at level −1 discontinued for anorexia (Fig. 1).

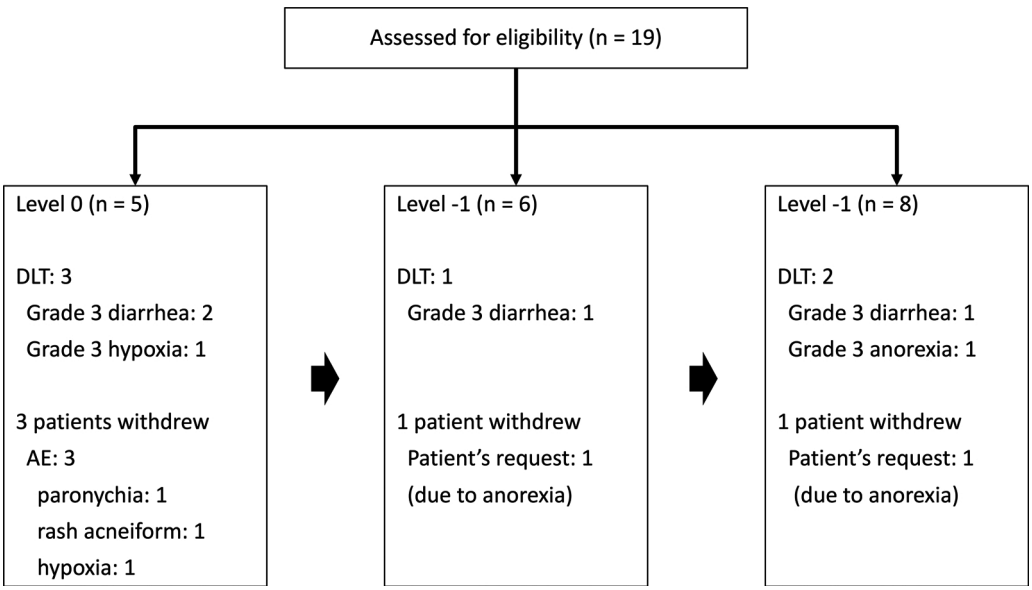

Fig. 1. Flow chart showing the study progression. Abbreviations: DLT, dose limiting toxicity; AE, adverse event.

Table 3
Response and disease control rates.

	No. of Patients (n = 16)	%
Response		
Complete response	1	6.3
Partial response	12	75.0
Stable disease	3	18.8
Progressive disease	0	0
Response rate (95% CI)	13	81.3 (62.1–100)
Disease control rate	16	100

A total of 16 patients who had measurable lesions were evaluated (Level 0, n = 4, Level −1, n = 12).
Disease control implies complete response, partial response, and stable disease. CI, confidence interval.

3.4. Treatment activity

Of 19 patients, 16 had baseline measurable lesions. Of these 16 patients, 1 had a confirmed CR and 12 a PR for an overall RR of 81.3% (95% confidence interval: 62.1–100%) in our intent-to-treat analysis (Table 3). There was no disease progression in any of the patients, and the disease control rate (DCR, summation percentage of CR, PR, and SD) was 100%. A waterfall plot for the 15 response-evaluable patients with at least one follow-up scan is presented in Fig. 2A. The treatment duration, treatment dose, and dose reduction or discontinuation of afatinib due to toxicity for each patient are shown in Fig. 2B. No disease progression has been reported at this time (median follow-up: 104 [range: 41–536] days).

4. Discussion

This is the first trial to assess the combination of a second-generation EGFR-TKI with an angiogenesis inhibitor. In the dose level 0 group, the rate of DLT was 60%, and the two patients without DLT required dose reductions for toxicity. Therefore, this dose level was not considered feasible. In the dose level −1 group, the rate of DLT was 21.4%, which met the primary end point. Of the 14 patients at this level, 7 were able to continue therapy at this dose, and we concluded that this does should be investigated further.

The most frequent toxicity was rash acneiform (17/19 patients), followed by diarrhea (16/19 patients). Specifically, diarrhea rapidly increased around day 10–14, when it reached grade 3, and was considered a DLT, although the toxicity immediately resolved after cessation of afatinib. The other grade 3 toxicities also resolved immediately. The bevacizumab toxicities noted were bleeding, hypertension, and proteinuria, but all were grade 1 or 2.

The LUX-Lung 3 (LL3) study was a large, prospective, randomized trial comparing afatinib with cisplatin-based chemotherapy for patients with advanced EGFR mutant NSCLC [6]. Included in this trial was a cohort of 54 Japanese patients treated with afatinib alone. Within this group, adverse events included diarrhea (100%), rash acneiform (100%), nail effects (92.6%), and stomatitis (92.6%) [14]. Time to first onset of diarrhea was within 14 days after starting afatinib for most patients. In terms of grade 3 toxicities, diarrhea occurred in 22.2%, rash acneiform in 20.4%, nail effects in 25.9%, and stomatitis in 7.4%, respectively. These safety profiles were generally consistent with that of our dose level −1. Adverse events leading to dose reduction occurred in 75.9% in the LL3 study. Here, dose level 0 was deemed too toxic, with all patients requiring either a dose reduction or discontinuation of therapy.

In a phase II trial comparing bevacizumab and erlotinib combination therapy with erlotinib monotherapy (JO25567), more grade 3 or worse adverse events were reported in the combination therapy group (91% vs 53%) [11]. In a similar phase II trial examining the use of bevacizumab and gefitinib combination therapy (OLCSG1001), grade 2 or worse rash was seen in 15% of patients [12], compared to only 2–5% for gefitinib monotherapy [2,3,15]. Taken together, these studies show that toxicities caused by EGFR-TKIs are exacerbated by the addition of bevacizumab. In this trial, afatinib-associated toxicities were also expected to worsen with the addition of bevacizumab, necessitating a lower recommended afatinib dose of 30 mg/day.

Like the LL3 trial, the LUX-Lung 6 (LL6) trial was also a large, prospective, randomized trial that compared afatinib with cisplatin-based chemotherapy for patients with advanced EGFR mutant NSCLC. The LL3 study was conducted globally and included Japanese patients, while the LL6 study was limited to patients in China, Thailand, and South Korea [6,7]. In a post hoc analysis of LL3 and LL6, afatinib trough plasma concentrations after treatment at the 40 mg dose were found to be higher on day 22 in patients whose doses were subsequently reduced to 30 mg due to toxicity, compared with those who remained on the 40 mg dose, with similar plasma concentrations observed in both groups on day 43 [16]. Furthermore, total treatment time tended to be longer in patients requiring a dose reduction compared to those maintained at the same dose, with similar PFS times in each group. This tolerability-guided dose adjustment of afatinib is thought to have played an important role in determining patient outcomes, allowing patients to maintain adequate plasma concentrations and continue effective therapy. In the LL3 study, Japanese patients were more likely to require a dose reduction (to 30 mg or 20 mg) due to adverse events than the overall study population (75.9% vs. 57.2%, respectively). Nevertheless, the median PFS was similar to that observed in the overall population (13.8 months vs. 11.1 months, respectively) [14]. In the present study evaluating afatinib combined with bevacizumab, the recommended afatinib dose (30 mg/day) should yield adequate plasma concentrations in all patients.

In two different phase II trials assessing the use of erlotinib alone or in combination with bevacizumab, the overall RR and DCR were 69% and 100%, respectively for the JO25567 trial [11], compared with 78% and 92%, respectively, for the BELIEF trial [13]. In the OLCSG1001 phase II trial of bevacizumab alone or combined with gefitinib, the overall RR and DCR were 73.8% and 97.6%, respectively [12]. The finding that almost no patients showed early refractory responses might be a feature of these combination therapies of EGFR-TKIs and bevacizumab. The overall RR of 81.3% and DCR of 100% in the present trial indicates that the combination therapy we evaluated might also have this effect. The PFS and OS data are still immature.

The current study had several limitations. Although toxicities were evaluated using the pre-defined criteria set forth in the protocol, the follow-up time may have been too short, as no disease progression was observed. Furthermore, the scope of this trial was limited, assessing only a small number of patients from a handful of institutes in a single country. Observation gathered over a longer period of time, as well as in a larger cohort of patients, will be necessary, particularly for side effects such as paronychia, hypertension, renal toxicity, thrombosis, and bleeding, as these would be more common during prolonged therapy. To that end, we have just initiated a larger randomized trial comparing the combination of afatinib and bevacizumab with afatinib alone (UMIN000027432). In this trial, 100 patients (50 patients per group) will be enrolled, enabling better assessment of the safety and efficacy of these treatments over longer treatment times, and across a larger number of patients.

In summary, the combination therapy of bevacizumab with afatinib, at doses of 30 mg/day afatinib and 15 mg/kg bevacizumab, was feasible and potentially effective.

Contributors

All authors contributed to the protocol writing. TN, TK, and KH also took part in the trial design and set-up. TN, TK, and KH participated in the sample size calculation. NN, DH, KO, SK, AB, NF, KA, TS, NT, KS, KK, and NF contributed to the subject enrollment.

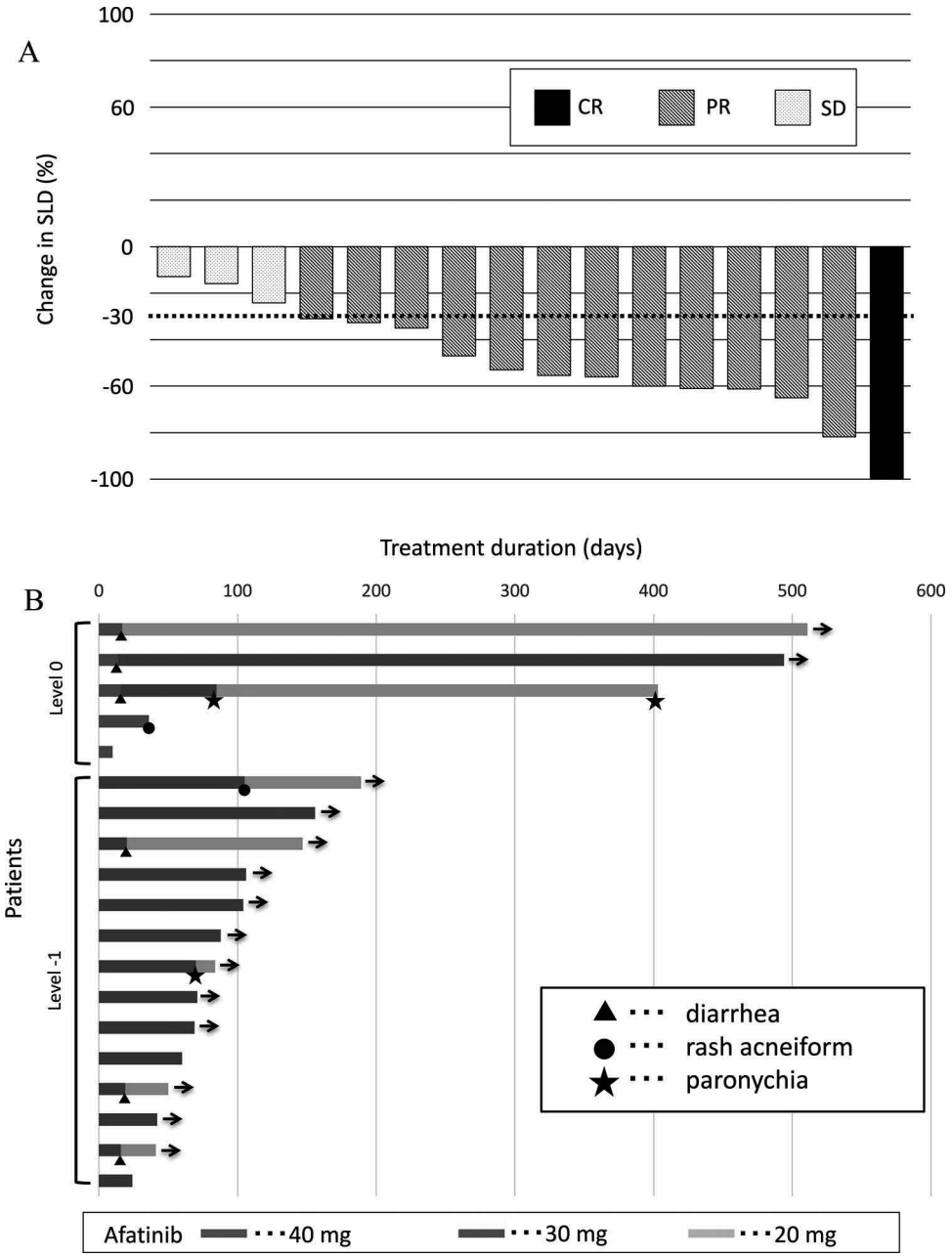

Fig. 2. A. Waterfall plot for the patients with measurable lesions. Abbreviations: SLDsum of the longest diameters; CRcomplete response; PRpartial response; SDstable disease. B. Swimmer plot for all patients.

Trial sponsorship and financing information

This research received no specific grant from any funding agency in the public, commercial, or not-for-profit sectors.

Conflict of interest

TN received honoraria outside the current work from MSD, Boehringer–Ingelheim, and Chugai Pharmaceutical. NN received honoraria outside the current work from AstraZeneca, Ono Pharmaceutical, Astellas, Taiho Pharmaceutical, Eli Lilly Japan, Pfizer Inc. Japan, Boehringer–Ingelheim, and Chugai Pharmaceutical. TK received honoraria outside the current work from AstraZeneca, Ono Pharmaceutical, BMS, Kyowa Hakko Kirin, Eli Lilly Japan, Pfizer Inc. Japan, Boehringer–Ingelheim, and Chugai Pharmaceutical. TK has also received research funding outside the current work from AstraZeneca, Ono Pharmaceutical, BMS, Eli Lilly Japan, MSD, and Chugai Pharmaceutical. DH received honoraria outside the current work from Ono Pharmaceutical, BMS, Kyowa Hakko Kirin and Yakult Honsha Co. Ltd. KO has received a research grant from Novartis Pharmaceuticals Japan. SK received honoraria outside the current work from Ono Pharmaceutical, BMS, Eli Lilly Japan, Boehringer–Ingelheim, Meiji Seika Pharma Co., and Chugai Pharmaceutical. AB received honoraria outside the current work from AstraZeneca, Novartis, Eli Lilly Japan, Taiho Pharmaceutical, Pfizer Inc. Japan and Chugai Pharmaceutical. AB has also received research funding outside the current work from AstraZeneca and Amgen. NF received honoraria outside the current work from KISSEI Co. Ltd. KA received honoraria outside the current work from AstraZeneca, Eli Lilly Japan, Ono Pharmaceutical, and BMS. NT has received honoraria outside the current work from Eli Lilly Japan, AstraZeneca, Daiichi–Sankyo Pharmaceutical, Chugai Pharmaceutical, Taiho Pharmaceutical, Pfizer Inc. Japan, Boehringer–Ingelheim, and Ono Pharmaceutical, and research funding from AstraZeneca, Pfizer Inc. Japan, Kyowa Hakko Kirin, Eli Lilly Japan, Chugai Pharmaceutical, Nippon Kayaku Co. Ltd, Taiho Pharmaceutical, Takeda Pharmaceutical Co. Ltd,

Boehringer–Ingelheim, and Ono Pharmaceutical. KH received honoraria outside the current work from AstraZeneca, Ono Pharmaceutical, Astellas, Novartis, BMS, MSD, Eli Lilly Japan, Daiichi–Sankyo Pharmaceutical, Boehringer–Ingelheim, Nihon Kayaku, Taiho Pharmaceutical, and Chugai Pharmaceutical. KH has also received research funding outside the current work from AstraZeneca, Boehringer–Ingelheim, Ono Pharmaceutical, Astellas, Novartis, BMS, Eli Lilly Japan, MSD, and Chugai Pharmaceutical. KK has received honoraria from Eli Lilly Japan, Nihon Kayaku, AstraZeneca, Daiichi-Sankyo Pharmaceutical, Chugai Pharmaceutical, Taiho Pharmaceutical, and Sanofi-Aventis. All of the other authors declare no conflicts of interest regarding this study.

Acknowledgements

The authors wish to acknowledge and thank the coordinators and all the other investigators who contributed to this study as independent data-monitoring committee members, including Drs. Yoshiko Ogata, Makoto Sakugawa (Japanese Red Cross Okayama Hospital), Tomoko Yamagishi, Sae Wada (Okayama Rosai Hospital), Daisuke Minami, Takamasa Nakasuka (Okayama Medical Center), Daisuke Nojima (Iwakuni Medical Center), Nobuaki Ochi (Kawasaki Medical School General Medical Center), Yusuke Hata, Hirohisa Kano (Okayama University Hospital), Yosuke Toyota (Fukuyama Medical Center), Mikio Kataoka, and Masafumi Fujii. This study has been conducted with support from the Center for Innovative Clinical Medicine, Okayama University Hospital.

References

[1] T.J. Lynch, D.W. Bell, R. Sordella, S. Gurubhagavatula, R.A. Okimoto, B.W. Brannigan, P.L. Harris, S.M. Haserlat, J.G. Supko, F.G. Haluska, D.N. Louis, D.C. Christiani, J. Settleman, D.A. Haber, Activating mutations in the epidermal growth factor receptor underlying responsiveness of non-small-cell lung cancer to gefitinib, N. Engl. J. Med. 350 (2004) 2129–2139, http://dx.doi.org/10.1056/NEJMoa040938.

[2] M. Maemondo, A. Inoue, K. Kobayashi, S. Sugawara, S. Oizumi, H. Isobe, A. Gemma, M. Harada, H. Yoshizawa, I. Kinoshita, Y. Fujita, S. Okinaga, H. Hirano, K. Yoshimori, T. Harada, T. Ogura, M. Ando, H. Miyazawa, T. Tanaka, Y. Saijo, K. Hagiwara, S. Morita, T. Nukiwa, North-East Japan Study Group, Gefitinib or chemotherapy for non-small-cell lung cancer with mutated EGFR, N. Engl. J. Med. 362 (2010) 2380–2388, http://dx.doi.org/10.1056/NEJMoa0909530.

[3] T. Mitsudomi, S. Morita, Y. Yatabe, S. Negoro, I. Okamoto, J. Tsurutani, T. Seto, M. Satouchi, H. Tada, T. Hirashima, K. Asami, N. Katakami, M. Takada, H. Yoshioka, K. Shibata, S. Kudoh, E. Shimizu, H. Saito, S. Toyooka, K. Nakagawa, M. Fukuoka, West Japan Oncology Group, Gefitinib versus cisplatin plus docetaxel in patients with non-small-cell lung cancer harbouring mutations of the epidermal growth factor receptor (WJTOG3405): an open label, randomised phase 3 trial, Lancet Oncol. 11 (2010) 121–128, http://dx.doi.org/10.1016/S1470-2045(09)70364-X.

[4] C. Zhou, Y.-L. Wu, G. Chen, J. Feng, X.-Q. Liu, C. Wang, S. Zhang, J. Wang, S. Zhou, S. Ren, S. Lu, L. Zhang, C. Hu, C. Hu, Y. Luo, L. Chen, M. Ye, J. Huang, X. Zhi, Y. Zhang, Q. Xiu, J. Ma, L. Zhang, C. You, Erlotinib versus chemotherapy as first-line treatment for patients with advanced EGFR mutation-positive non-small-cell lung cancer (OPTIMAL, CTONG-0802): a multicentre, open-label, randomised, phase 3 study, Lancet Oncol. 12 (2011) 735–742, http://dx.doi.org/10.1016/S1470-2045(11)70184-X.

[5] R. Rosell, E. Carcereny, R. Gervais, A. Vergnenegre, B. Massuti, E. Felip, R. Palmero, R. Garcia-Gomez, C. Pallares, J.M. Sanchez, R. Porta, M. Cobo, P. Garrido, F. Longo, T. Moran, A. Insa, F. De Marinis, R. Corre, I. Bover, A. Illiano, E. Dansin, J. de Castro, M. Milella, N. Reguart, G. Altavilla, U. Jimenez, M. Provencio, M.A. Moreno, J. Terrasa, J. Muñoz-Langa, J. Valdivia, D. Isla, M. Domine, O. Molinier, J. Mazieres, N. Baize, R. Garcia-Campelo, G. Robinet, D. Rodriguez-Abreu, G. Lopez-Vivanco, V. Gebbia, L. Ferrera-Delgado, P. Bombaron, R. Bernabe, A. Bearz, A. Artal, E. Cortesi, C. Rolfo, M. Sanchez-Ronco, A. Drozdowskyj, C. Queralt, I. de Aguirre, J.L. Ramirez, J.J. Sanchez, M.A. Molina, M. Taron, L. Paz-Ares, Spanish Lung Cancer Group in collaboration with Groupe Français de Pneumo-Cancérologie, Associazione Italiana Oncologia Toracica, Erlotinib versus standard chemotherapy as first-line treatment for European patients with advanced EGFR mutation-positive non-small-cell lung cancer (EURTAC): a multicentre, open-label, randomised phase 3 trial, Lancet Oncol. 13 (2012) 239–246, http://dx.doi.org/10.1016/S1470-2045(11)70393-X.

[6] L.V. Sequist, J.C.-H. Yang, N. Yamamoto, K. O'Byrne, V. Hirsh, T. Mok, S.L. Geater, S. Orlov, C.-M. Tsai, M. Boyer, W.-C. Su, J. Bennouna, T. Kato, V. Gorbunova, K.H. Lee, R. Shah, D. Massey, V. Zazulina, M. Shahidi, M. Schuler, Phase III study of afatinib or cisplatin plus pemetrexed in patients with metastatic lung adenocarcinoma with *EGFR* mutations, J. Clin. Oncol. 31 (2013) 3327–3334, http://dx.doi.org/10.1200/JCO.2012.44.2806.

[7] Y.-L. Wu, C. Zhou, C.-P. Hu, J. Feng, S. Lu, Y. Huang, W. Li, M. Hou, J.H. Shi, K.Y. Lee, C.-R. Xu, D. Massey, M. Kim, Y. Shi, S.L. Geater, Afatinib versus cisplatin plus gemcitabine for first-line treatment of Asian patients with advanced non-small-cell lung cancer harbouring EGFR mutations (LUX-Lung 6): an open-label, randomised phase 3 trial, Lancet Oncol. 15 (2014) 213–222, http://dx.doi.org/10.1016/S1470-2045(13)70604-1.

[8] T. Ninomiya, N. Takigawa, E. Ichihara, N. Ochi, T. Murakami, Y. Honda, T. Kubo, D. Minami, K. Kudo, M. Tanimoto, K. Kiura, Afatinib prolongs survival compared with gefitinib in an epidermal growth factor receptor-driven lung cancer model, Mol. Cancer Ther. 12 (2013) 589–597, http://dx.doi.org/10.1158/1535-7163.MCT-12-0885.

[9] K. Park, E.-H. Tan, K. O'Byrne, L. Zhang, M. Boyer, T. Mok, V. Hirsh, J.C.-H. Yang, K.H. Lee, S. Lu, Y. Shi, S.-W. Kim, J. Laskin, D.-W. Kim, C.D. Arvis, K. Kölbeck, S.A. Laurie, C.-M. Tsai, M. Shahidi, M. Kim, D. Massey, V. Zazulina, L. Paz-Ares, Afatinib versus gefitinib as first-line treatment of patients with EGFR mutation-positive non-small-cell lung cancer (LUX-Lung 7): a phase 2B, open-label, randomised controlled trial, Lancet Oncol. 17 (2016) 577–589, http://dx.doi.org/10.1016/S1470-2045(16)30033-X.

[10] J.C.-H. Yang, Y.-L. Wu, M. Schuler, M. Sebastian, S. Popat, N. Yamamoto, C. Zhou, C.-P. Hu, K. O'Byrne, J. Feng, S. Lu, Y. Huang, S.L. Geater, K.Y. Lee, C.-M. Tsai, V. Gorbunova, V. Hirsh, J. Bennouna, S. Orlov, T. Mok, M. Boyer, W.-C. Su, K.H. Lee, T. Kato, D. Massey, M. Shahidi, V. Zazulina, L.V. Sequist, Afatinib versus cisplatin-based chemotherapy for EGFR mutation-positive lung adenocarcinoma (LUX-Lung 3 and LUX-Lung 6): analysis of overall survival data from two randomised, phase 3 trials, Lancet Oncol. 16 (2015) 141–151, http://dx.doi.org/10.1016/S1470-2045(14)71173-8.

[11] T. Seto, T. Kato, M. Nishio, K. Goto, S. Atagi, Y. Hosomi, N. Yamamoto, T. Hida, M. Maemondo, K. Nakagawa, S. Nagase, I. Okamoto, T. Yamanaka, K. Tajima, R. Harada, M. Fukuoka, N. Yamamoto, Erlotinib alone or with bevacizumab as first-line therapy in patients with advanced non-squamous non-small-cell lung cancer harbouring EGFR mutations (JO25567): an open-label, randomised, multicentre, phase 2 study, Lancet Oncol. 15 (2014) 1236–1244, http://dx.doi.org/10.1016/S1470-2045(14)70381-X.

[12] E. Ichihara, K. Hotta, N. Nogami, S. Kuyama, D. Kishino, M. Fujii, T. Kozuki, M. Tabata, D. Harada, K. Chikamori, K. Aoe, H. Ueoka, S. Hosokawa, A. Bessho, A. Hisamoto-Sato, T. Kubo, I. Oze, N. Takigawa, M. Tanimoto, K. Kiura, Phase II trial of gefitinib in combination with bevacizumab as first-line therapy for advanced non–small cell lung cancer with activating EGFR gene mutations: the Okayama Lung Cancer Study Group Trial 1001, J. Thorac Oncol. 10 (2015) 486–491, http://dx.doi.org/10.1097/JTO.0000000000000434.

[13] R. Rosell, U. Dafni, E. Felip, A. Curioni-Fontecedro, O. Gautschi, S. Peters, B. Massutí, R. Palmero, S.P. Aix, E. Carcereny, M. Früh, M. Pless, S. Popat, A. Kotsakis, S. Cuffe, P. Bidoli, A. Favaretto, P. Froesch, N. Reguart, J. Puente, L. Coate, F. Barlesi, D. Rauch, M. Thomas, C. Camps, J. Gómez-Codina, M. Majem, R. Porta, R. Shah, E. Hanrahan, R. Kammler, B. Ruepp, M. Rabaglio, M. Kassapian, N. Karachaliou, R. Tam, D.S. Shames, M.A. Molina-Vila, R.A. Stahel, B.E.L.I.E.F. collaborative group, Erlotinib and bevacizumab in patients with advanced non-small-cell lung cancer and activating EGFR mutations (BELIEF): an international, multicentre, single-arm, phase 2 trial, Lancet Respir. Med. 5 (2017) 435–444, http://dx.doi.org/10.1016/S2213-2600(17)30129-7.

[14] T. Kato, H. Yoshioka, I. Okamoto, A. Yokoyama, T. Hida, T. Seto, K. Kiura, D. Massey, Y. Seki, N. Yamamoto, Afatinib versus cisplatin plus pemetrexed in Japanese patients with advanced non-small cell lung cancer harboring activating EGFR mutations: subgroup analysis of LUX-lung 3, Cancer Sci. 106 (2015) 1202–1211, http://dx.doi.org/10.1111/cas.12723.

[15] T.S. Mok, Y.-L. Wu, S. Thongprasert, C.-H. Yang, D.-T. Chu, N. Saijo, P. Sunpaweravong, B. Han, B. Margono, Y. Ichinose, Y. Nishiwaki, Y. Ohe, J.-J. Yang, B. Chewaskulyong, H. Jiang, E.L. Duffield, C.L. Watkins, A.A. Armour, M. Fukuoka, Gefitinib or carboplatin–paclitaxel in pulmonary adenocarcinoma, N. Engl. J. Med. 361 (2009) 947–957, http://dx.doi.org/10.1056/NEJMoa0810699.

[16] J.C.-H. Yang, L.V. Sequist, C. Zhou, M. Schuler, S.L. Geater, T. Mok, C.-P. Hu, N. Yamamoto, J. Feng, K. O'Byrne, S. Lu, V. Hirsh, Y. Huang, M. Sebastian, I. Okamoto, N. Dickgreber, R. Shah, A. Märten, D. Massey, S. Wind, Y.-L. Wu, Effect of dose adjustment on the safety and efficacy of afatinib for EGFR mutation-positive lung adenocarcinoma: post hoc analyses of the randomized LUX-Lung 3 and 6 trials, Ann. Oncol. 27 (2016) 2103–2110, http://dx.doi.org/10.1093/annonc/mdw322.

Sato et al. Oncogenesis (2018)7:11
DOI 10.1038/s41389-017-0017-3

Oncogenesis

ARTICLE Open Access

Therapeutic potential of targeting S100A11 in malignant pleural mesothelioma

Hiroki Sato[1], Masakiyo Sakaguchi[2], Hiromasa Yamamoto[1], Shuta Tomida[3], Keisuke Aoe[4,5], Kazuhiko Shien[1], Takahiro Yoshioka[6], Kei Namba[1], Hidejiro Torigoe[1], Junichi Soh[1], Kazunori Tsukuda[1], Hiroyuki Tao[5,7], Kazunori Okabe[5,7], Shinichiro Miyoshi[1], Harvey I. Pass[8] and Shinichi Toyooka[1,6]

Abstract

Malignant pleural mesothelioma (MPM) is an aggressive tumor with an unfavorable prognosis. The standard therapeutic approaches are limited to surgery, chemotherapy, and radiotherapy. Because the consequent clinical outcome is often unsatisfactory, a different approach in MPM treatment is required. S100A11, a Ca^{2+}-binding small protein with two EF-hands, is frequently upregulated in various human cancers. Interestingly, it has been found that intracellular and extracellular S100A11 have different functions in cell viability. In this study, we focused on the impact of extracellular S100A11 in MPM and explored the therapeutic potential of an S100A11-targeting strategy. We examined the secretion level of S100A11 in various kinds of cell lines by enzyme-linked immunosorbent assay. Among them, six out of seven MPM cell lines actively secreted S100A11, whereas normal mesothelial cell lines did not secrete it. To investigate the role of secreted S100A11 in MPM, we inhibited its function by neutralizing S100A11 with an anti-S100A11 antibody. Interestingly, the antibody significantly inhibited the proliferation of S100A11-secreting MPM cells in vitro and in vivo. Microarray analysis revealed that several pathways including genes involved in cell proliferation were negatively enriched in the antibody-treated cell lines. In addition, we examined the secretion level of S100A11 in various types of pleural effusions. We found that the secretion of S100A11 was significantly higher in MPM pleural effusions, compared to others, suggesting the possibility for the use of S100A11 as a biomarker. In conclusion, our results indicate that extracellular S100A11 plays important roles in MPM and may be a therapeutic target in S100A11-secreting MPM.

Introduction

Malignant pleural mesothelioma (MPM) is a highly invasive and aggressive tumor that develops in the mesothelial lining of the pleura. The median survival of patients with MPM from the time of diagnosis is usually less than 1 year[1,2]. While surgical resection is the treatment of first choice for early-stage disease, recurrence of the disease often makes the prognosis poorer. In addition, most MPM cases are of advanced-stage disease, for which the benefits of a standard chemotherapeutic regimen with cisplatin and pemetrexed are very limited. These considerations demand the development of novel therapeutic strategies for MPM.

Proteins of the S100 family are small molecules (ranging from 9 to 14 kDa) with two EF-hands and in humans, the family is composed of 20 different members (S100A1–S100A16, S100β, S100G, S100P, and S100Z). This group of proteins modulates a variety of cellular processes, including cell proliferation, differentiation, and intracellular signaling by functioning both as intracellular Ca^{2+} sensors and as extracellular factors[3–5].

S100A11, also called S100C or calgizzarin, was cloned from chicken gizzard in 1991[6]. We previously reported that S100A11 has two ambivalent functions in the cells.

Correspondence: Shinichi Toyooka (toyooka@md.okayama-u.ac.jp)
[1]Department of General Thoracic Surgery and Breast and Endocrinological Surgery, Okayama University Graduate School of Medicine, Dentistry and Pharmaceutical Sciences, Okayama, Japan
[2]Department of Cell Biology, Okayama University Graduate School of Medicine, Dentistry and Pharmaceutical Sciences, Okayama, Japan
Full list of author information is available at the end of the article

Namely, in the cytoplasmic compartment, S100A11 inhibits the growth of normal human keratinocytes in response to high Ca^{2+} or transforming growth factor β[7,8]. Contrarily, the binding of extracellular S100A11 to the receptor for advanced glycation end products (RAGE) enhances the production of epidermal growth factor family proteins, resulting in growth stimulation[5,9]. Based on these findings, we have studied the biological activity of S100A11 by focusing both on intracellular and extracellular S100A11. As for the function of intracellular S100A11, we have shown that the intracellular S100A11–ANXA2 complex helps plasma membrane repair, which was critical for survival and metastasis, in metastatic breast cancer cell line[10]. Additionally, it is reported that intracellular S100A11 promotes pseudopodial actin dynamics, which plays a critical role in tumor metastasis and the suppression of S100A11 results in inhibition of cell migration and invasion, and the reversion of Epithelial to mesenchymal transition (EMT) in various metastatic cell lines[11]. Regarding extracellular S100A11, we have recently reported that, in mesothelioma cells, S100A11 dimerizes in the peroxisome after transportation of monomeric S100A11 through the interaction with PEX14, an essential component of peroxisomal import machinery, and actively secreted[12]. However, despite advances in the understanding of the biological activity and mechanisms of this protein, little is known about its therapeutic or diagnostic potential. In this study, we investigated the relationship between extracellular S100A11 and MPM, and explored the possibility of an intervention in S100A11 function for MPM treatment and diagnosis.

Results

Secretion levels of S100A11 in malignant cell lines and overexpression of S100A11 in MPM

We first examined the secretion level of S100A11 in the culture media of various cell lines by enzyme-linked immunosorbent assay (ELISA). Seven MPM, 2 normal mesothelial, 12 lung cancer, 3 gastric cancer, 3 colorectal cancer, and 3 breast cancer cell lines were used for this analysis, and the result is shown in Fig. 1a. We detected increased levels of S100A11 in cancer cells with various secretion levels. Of interest, there was the marked difference in S100A11 secretion between MPM cells and normal cells. All examined MPM cell lines except for MSTO-211H commonly secreted S100A11, whereas no secretion was observed in normal mesothelial cell lines. MPM cell lines were classified into three categories based on the secretion level of S100A11: High (YUMC44, H290, and H28), Low (HP-1, H2452, and H2052), and None (MSTO-211H). To investigate the correlation between S100A11 secretion and protein expression, protein expression levels of S100A11 in MPM and normal mesothelial cell lines were determined by western blot analysis. S100A11 was significantly overexpressed in MPM cell lines, compared to normal mesothelial cell lines (Fig. 1b). To confirm the same phenomenon in clinical MPM specimens, three histological subtypes of MPM tissues, epithelioid, sarcomatoid, and biphasic type, were obtained from the patients who underwent surgery at the Okayama University Hospital and then studied for S100A11 expression. We also prepared the paraffin blocks filled with H2452 and MeT-5A cells to use as a positive and negative control, respectively. Immunohistochemistry demonstrated that S100A11 was mainly localized in the cytoplasm or nucleus and was strongly positive in MPM cells, but not in surrounding normal lung cells. Representative images are shown in Fig. 1c. Taken together, these results suggest that S100A11 is aberrantly overexpressed in MPM at both cultured cells and clinical samples and secreted from MPM cells.

Inhibition of the amount of extracellular S100A11 in MPM cells

Next, we examined the involvement of extracellular S100A11 in the growth regulation of MPM cells. As shown in Fig. 2a, MTT assay revealed that administration of the purified S100A11 recombinant protein to the cultures promoted cellular proliferation of MPM cell lines (H2452 and H2052) in a dose-dependent manner up to the point of 100 ng/ml. The growth induction stimulated by extracellular foreign S100A11 at the concentration of 1000 ng/ml was almost equal in H2452 cells or tended to little bit decline in H2052 cells when compared to those at the concentration of 100 ng/ml. While the highest concentration (10,000 ng/ml) commonly worked as growth inhibition in the both cell lines. These results provided us an optimal concentration of extracellular S100A11 (100 ng/ml) in growth stimulation of MPM cells. To inhibit the function of secreted S100A11, we used an anti-S100A11 antibody (Proteintech Group), which has been previously reported as a neutralizing antibody for S100A11[13]. Similarly, we confirmed that the screened antibody decreased the quantity of S100A11 in the cell culture media (Fig. 2b). The effect was continued for about 48 h and then expired at later time point, probably due to the consumption of the antibody life. We also confirmed that moues control IgG had no effect on cell growth of MPM cell lines (H2052 and H2452, data not shown). Based on these results, the anti-S100A11 antibody was administered on day 1 and day 3 in culture system. We found that cellular growth of "Low" cells (H2452 and H2052) was both highly suppressed by an anti-S100A11 antibody with a final concentration of 100 ng/ml in culture media (Fig. 2c, top). On the other hand, in "High" cells (H290 and H28), the same concentration of the anti-S100A11 antibody did not show any appreciable effect on their cell

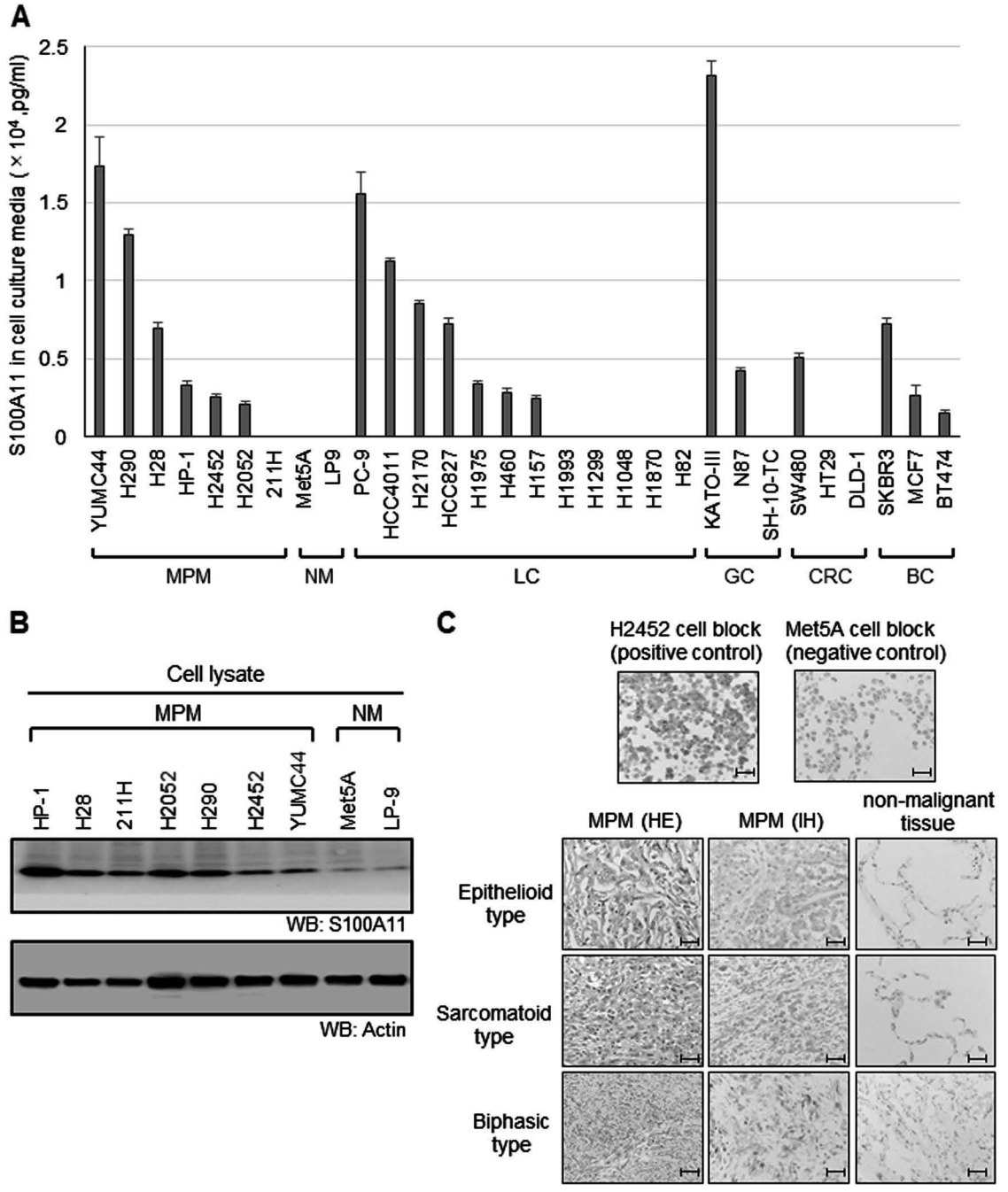

Fig. 1 High secretion and overexpression of S100A11 in MPM. a Concentration of secreted S100A11 in the culture media of various cell lines, as determined by ELISA. The secretion level of S100A11 in all MPM cell lines, except for 211H, is higher than that of NM. 211H MSTO-211H, NM normal mesothelial cell, LC lung cancer, GC gastric cancer, CRC colorectal cancer, BC breast cancer. **b** Protein level of S100A11 was higher in MPM cell lines, compared to NM. NM normal mesothelial cell. **c** Immunohistochemical analysis of S100A11 in surgically resected tissues from patients with MPM. The representative images of three MPM subtypes are shown. The pictures on the left show hematoxylin–eosin (HE)-stained images corresponding to the S100A11-stained images in the middle. Scale bars, 50 μm (positive and negative control) and 100 μm (clinical samples)

growth. Facing to the issue, we increased the antibody dose up to 1 μg/ml. The higher dose gave suppression of cell growth even in these cell lines (Fig. 2c, bottom). As for "None" cells (MSTO-211H), the antibody did not affect the cell growth, regardless of dose (Fig. 2c). To further evaluate the effect of anti-S100A11 antibody on the migration and invasion of MPM, we performed a Boyden chamber assay. Microscopy images of the Boyden

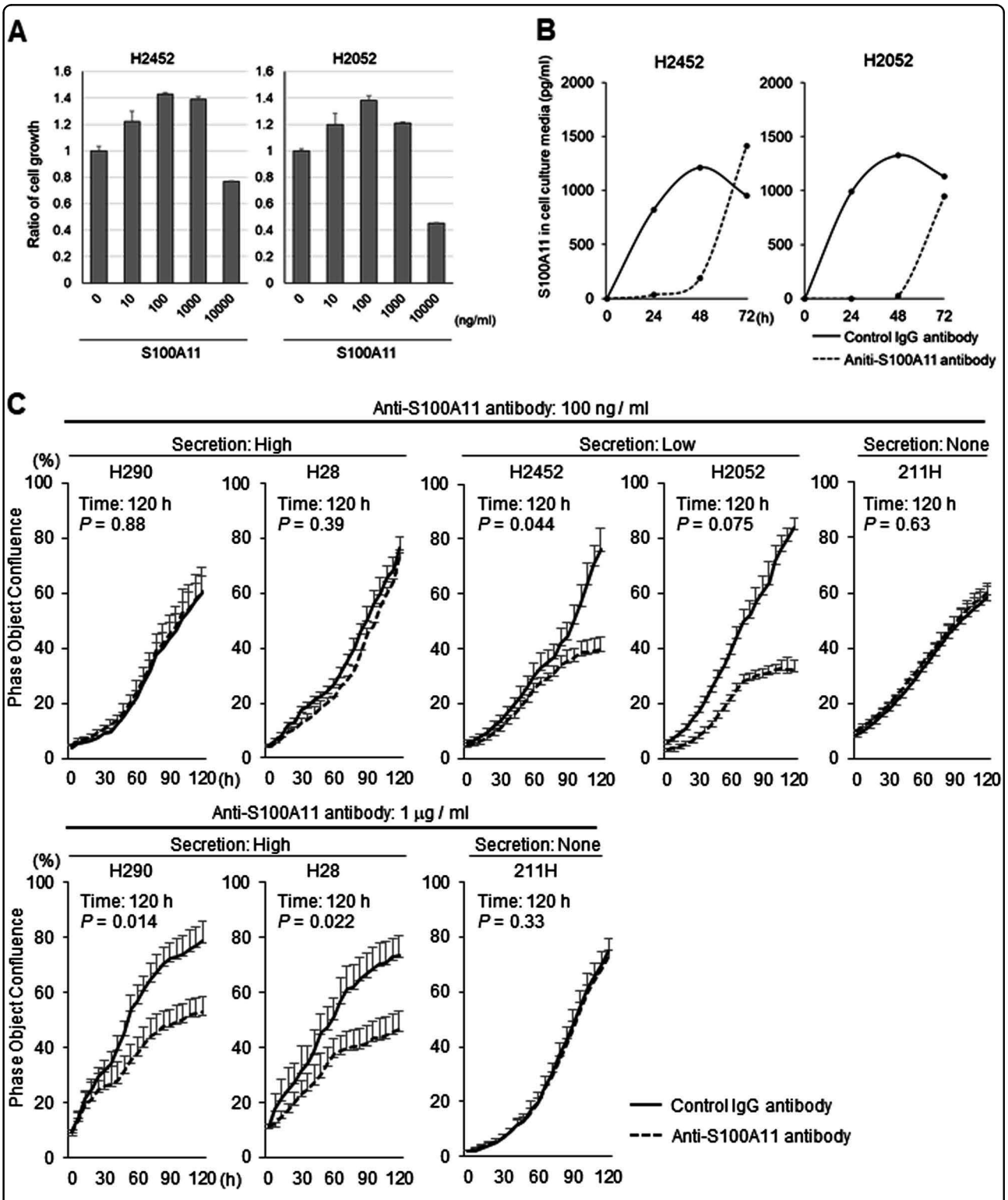

Fig. 2 Suppression of MPM cell growth through neutralization of extracellular S100A11. a Effect of S100A11 recombinant protein on cell growth. Cells were treated or not treated with the foreign S100A11 protein at the indicated concentrations for 48 h. MTT assay was used for the following growth evaluation. **b** Effect of an anti-S100A11 antibody on the concentration of S100A11 in cell culture media. The antibody was added to the culture media of MPM cells (H2452 and H2052) at time 0. The concentration of S100A11 was significantly lower in the anti-S100A11 antibody-treated group, indicating that the specific antibody can neutralize secreted S100A11. **c** Effect of neutralization of extracellular S100A11 on cell growth in MPM cells. An anti-S100A11 antibody significantly inhibited cell growth in H2052, H2452, H290, and H28 cells (100 ng/ml antibody for H2052 and H2452 and 1 μg/ml for H290 and H28, respectively)

chamber assay are shown in Supplementary Fig. S1A and S1B. Migration and invasion were significantly suppressed in MPM cells treated with the antibody. To confirm the used antibody specificity, we tried to assess whether replenishing foreign S100A11 protein in the culture could cancel the antibody-mediated anticancer behaviors in vitro. As shown in Supplementary Fig. S1A–C, we found that this procedure effectively enfeebled cancer preventive benefits of the antibody in all the three experimental contexts, migration, invasion, and growth of MPM cell lines (H2452 and H2052).

There is a close relationship between cellular growth and cell cycle condition. This prompted us to examine whether cell cycle can be affected by the extracellular S100A11. Cyclins D and B were reliable good makers for cell cycle G1/S-phase and G2/M-phase, respectively, so that we investigated the expression levels of them after stimulation of the cells with 100 ng/ml of S100A11. By the western blot analysis approach, we found that Cyclin D but not Cyclin B was significantly induced with time dependency after the addition of S100A11 in MPM cultures (H2452 and H2052) (Fig. S1D). In addition, we found that anti-apoptotic Bcl-2 protein was significantly elevated with a similar manner to those of Cyclin D in both H2452 and H2052 cells (Fig. S1D). These results suggest that the secreted S100A11 positively regulates not only cell cycle, especially in a specific activation of the G1 phase and following G1/S transition through an induction of Cyclin D, but also survival via induction of Bcl-2.

The alteration of downstream signaling affected by the anti-S100A11 antibody and the S100A11 recombinant protein

To gain insight into the intracellular signaling events induced by the neutralization of extracellular S100A11, we investigated the key molecules regarding to cancer progression. MPM cells were cultured with the anti-S100A11 antibody (1 μg/ml), S100A11 recombinant protein (100 ng/ml), or mouse control IgG (1 μg/ml). Lysates were extracted every 6 h and subjected to western blot analysis (Supplementary Fig. S2). As a result, we found that the treatment with the anti-S100A11 antibody significantly suppressed the constitutive phosphorylation of endogenous STAT3 in H2452 and H2052 cells. Unexpectedly, in cases of AKT and MAPK, both phosphorylation status were commonly upregulated temporary at once at 6 h and then tended to be gradually suppressed with a time-dependent manner (Supplementary Fig. S2A). This may be possibly explained by compensation of the STAT3 downregulation. Next as a converse experiment, we stimulated the cells with extra recombinant S100A11 under the absence of the antibody in culture. The addition of S100A11 recombinant protein in turn activated the downstream proteins, STAT3, AKT, and MAPK (Supplementary Fig. S2B). To further specify the central pathway related to the extracellular S100A11-induced proliferation of MPM cells, we tried to inhibit the intracellular activations of STAT3, MEK, and PI3K and assessed the following cellular proliferations. Unexpectedly, we found that either Stattic: STAT3 inhibitor, Trametinib: MEK inhibitor, or Taselisib: PI3K inhibitor, effectively suppressed the S100A11-stimulated cellular proliferation with a similar inhibitory degree, suggesting that these molecules play a crucial role in cellular growth and they cooperatively function toward same way regarding growth upregulation under the downstream of RAGE upon S100A11 binding (Supplementary Fig. S2D). Taken together, these results strongly suggest that the secreted S100A11 plays a critical role on MPM progression through upregulation of cell growth, motility, and invasion with an autocrine manner and the extracellular S100A11 is becoming a prominent molecule for therapeutic target of the MPM progression.

An anti-S100A11 antibody inhibits the tumorigenic potential in a mouse xenograft model of MPM

We investigated the antitumor effect of the validated anti-S100A11 neutralizing antibody on the MPM in a xenograft mouse model, using H2452 and H290 cells. We subcutaneously injected tumor cells and the anti-S100A11 antibody, and evaluated the effect of the antibody on the tumorigenic potential. As shown in Fig. 3a, b, the tumor growth in the antibody-administered group was significantly suppressed, compared to those of the control group.

Microarray analysis of H2052 and H2452 cells treated with an S100A11 neutralizing antibody

To reveal the mechanisms involved in the anticancer activity induced by neutralization of extracellular S100A11, we carried out gene expression microarray analysis. The details of the expression profile studies are reported in Supplementary Table S1. Clustering analysis based on the transcripts showed a clear distinction between the cell lines treated or untreated with the antibody (Fig. 4). Next, a gene set enrichment analysis (GSEA) was performed to clarify the groups of genes affected by anti-S100A11 antibody administration. We found that several pathways, including genes involved in cell proliferation (HALLMARK_MITOTIC_SPINDLE), (HALLMARK_P53_PATHWAY 1), (HALLMARK_PI3K_AKT_MTOR_SIGNALING), and (HALLMARK_KRAS_SIGNALING_DN), and a subgroup of genes related to protein secretion (HALLMARK_-PROTEIN_SECRETION) were negatively enriched in the antibody-treated cell lines (Table 1). These results are consistent with our in vitro and in vivo data.

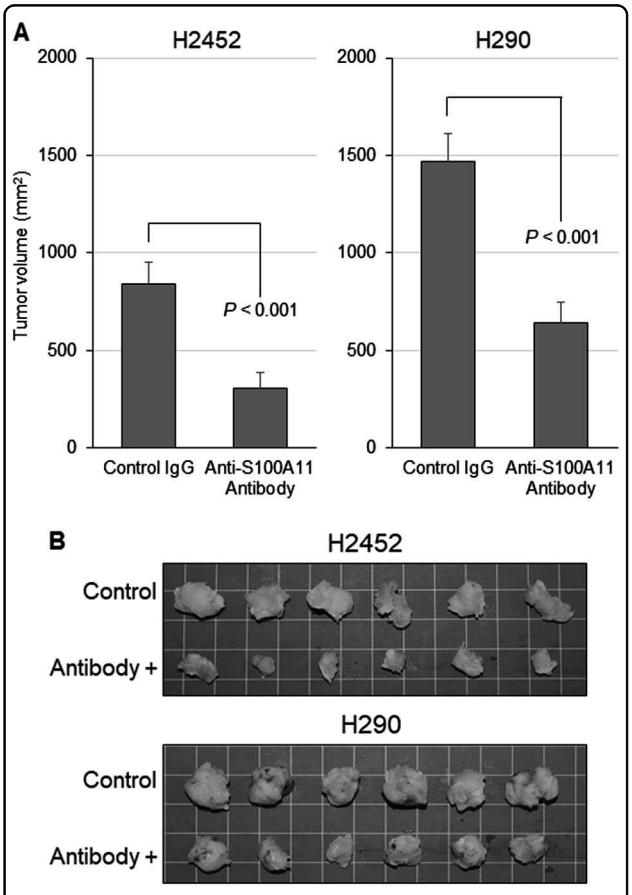

Fig. 3 Negative effect of the treatment with an anti-S100A11 antibody on MPM tumor growth in vivo. a The mean volume of the subcutaneous xenograft tumors was calculated for six tumors in each group. The anti-S100A11 antibody significantly inhibits the tumorigenic potential in mouse xenografts of H2452 and H290 cells. **b** Appearance of the tumors at the time of sacrifice after treatment with control IgG or anti-S100A11 antibody. Tumors in the upper side of the photo were treated with mouse IgG control and tumors in the lower side were treated with an anti-S100A11 antibody

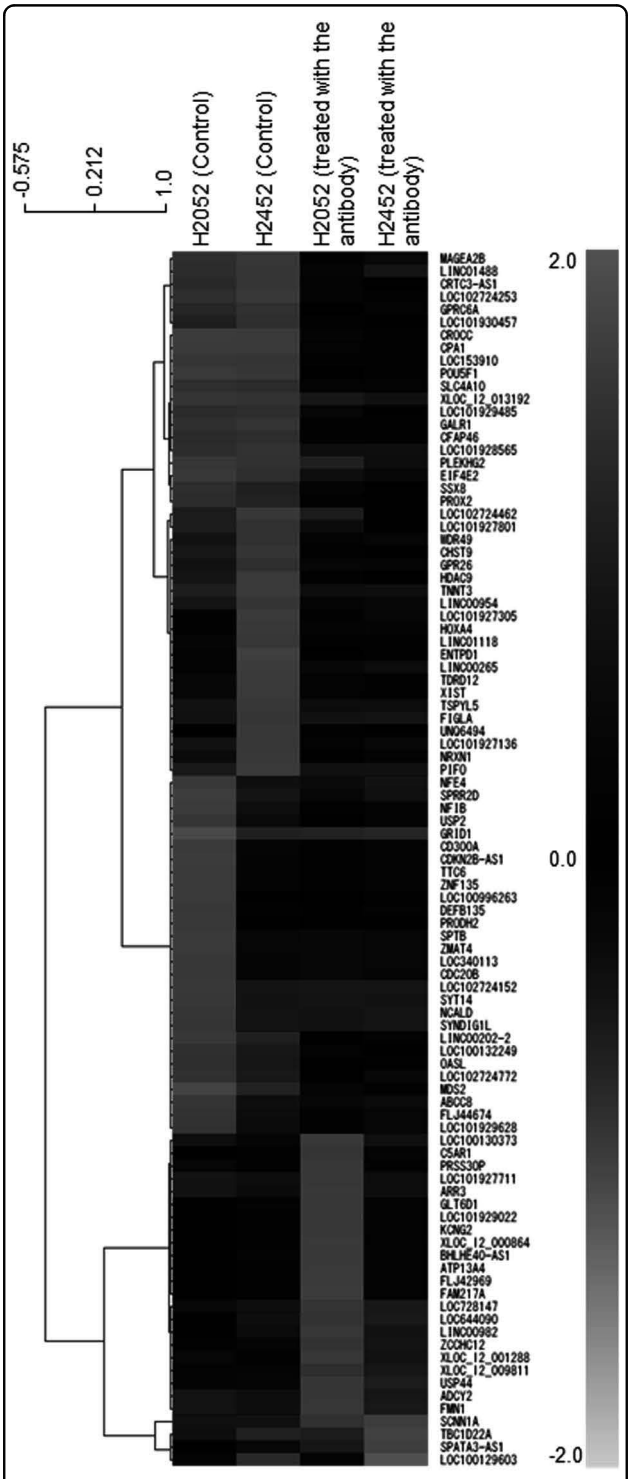

Fig. 4 Global gene expression changes upon treatment with an anti-S100A11 antibody Clustering and heatmap of MPM cell lines are shown. Paired comparison analysis based on 50,739 probes indicated 2222 differentially expressed transcripts between antibody-treated MPM cell lines and parental MPM cell lines (H2052 and H2452). Clustering using Pearson correlation and average linkage was based on these transcripts. The color bar represents the expression values after log2 transformation

Function of RAGE as a receptor for S100A11

To explore the function of RAGE as a receptor for S100A11 in MPM, we first confirmed the positive expression of RAGE in MPM cell lines by western blot analysis (Fig. 5a). To prevent the intrinsic RAGE activation caused by ligand binding, we used sRAGE, which acts as decoy to compete with S100A11, the ligand for the cellular RAGE, and examined a series of effector molecules regarding to RAGE downstream signaling. MPM cells were treated or not treated with S100A11 recombinant protein (100 ng/ml) under the presence or absence of sRAGE (1 μg/ml). Twenty-four hours later, the treated-cell lysates were prepared and then subjected to western blot analysis. We found that blockage of RAGE signaling suppressed the phosphorylation of STAT3 and MAPK induced by S100A11 stimulation (Fig. 5b). Additionally,

Table 1 Enriched pathways in the parental and antibody-treated cell lines

	ES	FDR *q*-val
GSEA pathway (parental cell line, $n = 2$)		
HALLMARK_PANCREAS_BETA_CELLS	0.83	0.274
HALLMARK_REACTIVE_OXIGEN_SPECIES_PATHWAY	0.6	0.274
HALLMARK_COAGULATION	0.52	1.000
HALLMARK_PEROXISOME	0.51	0.995
HALLMARK_MYC_TARGETS_V2	0.44	0.926
HALLMARK_GLYCOLYSIS	0.42	0.722
GSEA pathway (anti-S100A11 antibody-treated cell line, $n = 2$)		
HALLMARK_PI3K_AKT_MTOR_SIGNALING	−0.56	0.819
HALLMARK_PROTEIN_SECRETION	−0.47	0.47
HALLMARK_KRAS_SIGNALING_DN	−0.47	0.811
HALLMARK_MYOGENESIS	−0.47	0.87
HALLMARK_MITOTIC_SPINDLE	−0.33	0.887
HALLMARK_P53_PATHWAY	−0.35	0.409

ES enriched score, *FDR* false discovery rate

MTT assays revealed that sRAGE mitigated growth promotion in both H2452 and H2052 cells, indicating that S100A11–RAGE axis plays a pivotal role in MPM progression in response to the secreted extracellular S100A11 (Fig. 5c).

Secretion levels of S100A11 in pleural effusions

To explore the possibility of using S100A11 as a useful marker for diagnosis of MPM, we examined the secretion levels of S100A11 in several types of pleural effusions. We obtained pleural effusions from 29 MPM patients (biphasic type: $n = 10$, epithelioid type: $n = 15$, sarcomatoid type: $n = 4$), 11 benign asbestosis (BA) patients, and 12 patients who underwent thoracic surgery at the Okayama University Hospital and the National Hospital Organization Yamaguchi-Ube Medical Center (Ube, Yamaguchi, Japan). Postoperative pleural effusions were obtained from lung cancer ($n = 10$) or pulmonary cyst ($n = 2$) patients after postoperative day 2. The concentration of S100A11 was measured by ELISA. As shown in Fig. 6, the level of S100A11 was remarkably elevated in pleural effusion obtained from MPM patients when compared to that obtained from BA patients as a benchmark ($P = 0.014$). Furthermore, we found that the secretion level of S100A11 was significantly higher in pleural effusion from BA patients than that from postoperative patients ($P = 0.041$).

Discussion

In this study, we found that extracellular S100A11, via RAGE, has a critical role in tumor progression of MPM. The blockage of extracellular S100A11 with a neutralizing antibody inhibited the cell proliferation, migration, and invasion of MPM cells. Additionally, in a mouse xenograft model, tumorigenesis of MPM cells was markedly inhibited by an anti-S100A11 antibody. These results suggest that extracellular S100A11 is a potential therapeutic target for MPM. Interestingly, we found that protein expression levels of S100A11 are not correlated with secretion levels in various cells lines, suggesting that intracellular increasing in stock level of S100A11 protein is not essential factor for its secretory mechanism. In fact, MSTO-211H showed no secretion of S100A11 even though plenty of S100A11 protein was stored in cells. To clarify the reason of this discrepancy at the molecular level, further comprehensive investigation with focusing on secretory pathways of leaderless proteins is indispensable.

One of the interesting features of S100A11 is to possess different functions depending on its location and on different cell types, as we reported previously[9]. Accumulating evidence indicates that S100A11 expression is upregulated in various cancers and promote cancer development[14–17]. However, this is not common in all cancer species, for example, low expression of S100A11 in bladder cancers is associated with poor survival in the patients[18]. Therefore, S100A11 might act sometimes as an oncogene, and sometimes as a suppressor gene, and have a key role in the progression of malignant tumors based on the balance of its ambivalent effect, which may be different depending on cancer types. When considering the use of this protein for treatment, the targeting of intracellular S100A11 would require the unitarily control of its two different functions. Thus, it is more convenient to focus on extracellular S100A11 for developing new therapeutic strategies for MPM.

RAGE, which was first identified as a RAGE, is known to bind different ligands, such as amyloid-beta peptide, HMGB1 (amphoterin), and some members of the S100 family, including S100A11[19–21]. We found that RAGE-positive MPM cells constitutively express and secrete S100A11, the S100A11–RAGE axis is greatly involved in sustained phosphorylation of downstream effector molecules, STAT3, MAPK, and PI3K–AKT, and the blockage of S100A11–RAGE connection using either sRAGE or S100A11 neutralizing antibody effectively inhibits cell growth of MPM cells. For the S100A11-mediated growth upregulation, Cyclin D and Bcl-2 might be critically relevant. How are these molecules induced under the RAGE activation? One hint may come from the Fig. S2D. The S100A11-induced Cyclin D but not Bcl-2 was significantly downregulated by the STAT3, MEK and PI3K

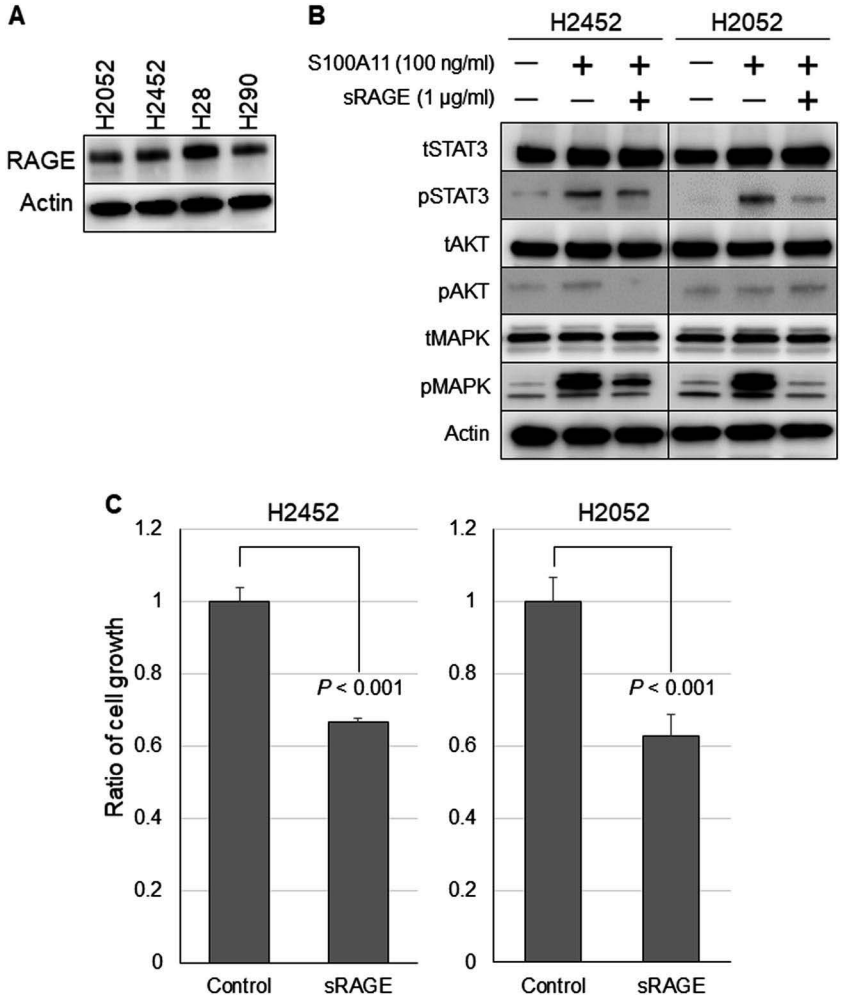

Fig. 5 Secreted S100A11 exerts its important role in the proliferation of MPM cells via RAGE. a RAGE protein expression in MPM cells. **b** Inhibition of RAGE signaling through sRAGE significantly suppressed the phosphorylation of STAT3 and MAPK induced by S100A11 recombinant protein. **c** The effect of sRAGE on the growth of MPM cells examined by MTT assay. Cell proliferation was significantly inhibited by sRAGE

inhibitors, suggesting that the molecules regarding pathways coordinately regulate Cyclin D expression after the RAGE activation upon S100A11 binding. Through this study, we hence strongly recognized a significant role of secreted S100A11 in mesothelioma progression.

In our experiments, growth inhibitory effect of sRAGE was limited and insufficient in comparison with the that of anti-S100A11 antibody, indicating that an additional S100A11 receptor, such as CD36, might activate survival or proliferative pathways in the cells[9,22]. Moreover, RAGE has been shown to have many distinct biological functions. For instance, van Zoelen and colleagues[23] demonstrated that RAGE signaling contributed to an effective antibacterial defense during *Escherichia coli* infection (inhibition of bacterial outgrowth and dissemination), and RAGE deficiency resulted in enhanced organ injuries due to liver necrosis. Thus, the adverse effects due to the inhibition of RAGE signaling are still unclear and as a therapeutic target for MPM, it seems more convenient to inhibit extracellular S100A11 than RAGE at present.

Although "High" cells (H290 and H28) displayed resistance to the S100A11 antibody at lower concentration (100 ng/ml), the effect of S100A11 antibody was shown when much higher concentration of it (1 μg/ml) was used. Thus, the secretion of S100A11 in MPM cells was prerequisite for the antibody approach and measurement of the secretion level of S100A11 was quite important index to predict an effectiveness of the S100A11 antibody. We hence examined the secretion level of S100A11 in pleural effusion. The concentration of S100A11 in MPM pleural effusions was significantly higher than that in pleural effusions of BA and postoperative patients, though the amount of secreted S100A11 is high in pleural effusions from both patients with MPM and BA. Generally, BA is

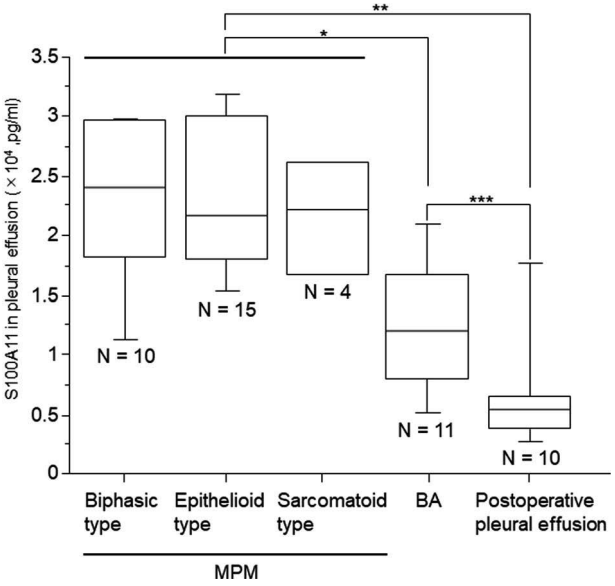

Fig. 6 Secretion levels of S100A11 in pleural effusions, as determined by ELISA. Significant differences among the different types of pleural effusion were observed (*: MPM vs BA, $P = 0.014$, **: MPM vs postoperative pleural effusion, $P < 0.001$, ***: BA vs postoperative pleural effusion, $P = 0.041$)

not regarded as a precancerous lesion of mesothelioma. Taking it into account, we consider that MPM cells actively secrete S100A11 in pleural effusion. These results suggest that S100A11 can be not only a therapeutic target but also an early diagnosis marker. In addition, it is of note mentioning that the concentration of S100A11 in the pleural effusions of patients with BA was significantly higher than that of postoperative patients. The association between high expression of proteins of the S100 protein family and inflammatory diseases has been reported[24–27]; this along with our results suggest that S100A11 may be involved in chronic inflammation.

In conclusion, we showed that extracellular S100A11 plays an important role in MPM progression and neutralization of extracellular S100A11 directly linked to marked suppression of MPM developments in vitro and in vivo. Our results suggest that extracellular S100A11 can be a novel, selective and effective therapeutic target in S100A11-secreting MPM, since normal cells displayed no secretion phenotype of S100A11.

Materials and methods

Cell lines and reagents

We used seven human MPM cell lines [NCI-H28 (H28), NCI-H290 (H290), NCI-H2052 (H2052), NCI-H2452 (H2452), HP-1, YUMC44, and MSTO-211H], two human normal mesothelial cell lines (MeT-5A and LP-9), 10 human lung cancer cell lines [HCC827, PC-9, HCC4011, NCI-H1975 (H1975), NCI-H1993 (H1993), NCI-H1299 (H1299), NCI-H460 (H460), NCI-H2170 (H2170), NCI-H157 (H157), and NCI-H82 (H82)], two human extrapulmonary small-cell cancer cell lines [NCI-H1048 (H1048) and NCI-H1870 (H1870)], three gastric cancer cell lines [KATO III, NCI-N87 (N87), and SH-10-TC], three colorectal cancer cell lines (SW480, HT29, and DLD-1), and three breast cancer cell lines (MCF-7, BT474, and SK-BR-3). Two MPM cell lines (HP-1 and H2452) were established by one of the authors (H.I.P.)[28]. Three MPM cell lines (H28, H290, and H2052 obtained in 2002), two lung cancer cell lines (HCC4011 and H82 obtained in 2008), and two extrapulmonary small-cell cancer cell lines (H1048 and H1870 obtained in 2008) were kindly gifted by Dr. Adi F. Gazdar (Hamon Center for Therapeutic Oncology Research and Department of Pathology, University of Texas Southwestern Medical Center at Dallas, Dallas, TX, USA)[29]. YUMC44 cell line was established by one of the authors (H.Y.)[30]. MSTO-211H, MeT-5A, N87 cell lines, seven lung cancer cell lines (HCC827, H1975, H1993, H1299, H460, H2170, and H157), three breast cancer cell lines (MCF-7, BT474, and SK-BR-3), and three colorectal cancer cell lines (Sw480, HT29, and DLD-1) were purchased from the American Type Culture Collection (Manassas, VA, USA). Two gastric cancer cell lines (KATO III and SH-10-TC) were obtained from the Cell Resource Center for Biomedical Research Institute of Development Aging and Cancer, Tohoku University (Sendai, Miyagi, Japan). LP-9 cell line was purchased from the Coriell Cell Repository (Camden, NJ, USA). PC-9 cell line was purchased from Riken Cell Bank (Tsukuba, Ibaragi, Japan). The cell lines within 30 passages were used in this study and the cumulative culture length was less than 6 months. For cell lines with long-term preservation in liquid nitrogen, DNA fingerprinting analysis by short tandem repeat profiling (the PowerPlex 1.2 System, Promega) was performed for the cell authentication. All the cell lines, except for LP-9 and breast cancer cell lines, were maintained in RPMI-1640 medium (Sigma–Aldrich, St Louis, MO, USA, Product No. R8758) supplemented with 10% fetal bovine serum (FBS). The three breast cancer cell lines were cultured in Dulbecco's modified Eagle's medium (Sigma–Aldrich, Product No. D6429) with 10% FBS. LP-9 was cultured in Ham's F12 medium (Sigma–Aldrich, Product No. N4888)/Medium 199 (Sigma–Aldrich, Product No. M7653) (1:1 mixture) with 10% FBS, 2 mM L-glutamine (Thermo Fisher Scientific, Waltham, MA, USA, catalog #25030-081), 1.7 nM epidermal growth factor (Sigma–Aldrich, Product No. E9644), and 1100 nM hydrocortisone (Sigma–Aldrich, Product No. H0888). All the cell lines were grown in a humidified incubator with 5% CO_2 at 37°C and routinely tested for mycoplasma by Venor GeM OneStep kit (Minerva Biolabs, Berlin, Germany, Product No. 11-8050). Soluble receptor for

advanced glycation end products (RAGE) Fc chimera (sRAGE) (R&D Systems, Minneapolis, MN, USA, accession #Q15109), static (Abcam, Cambridge, MA, USA, ab120952), trametinib (GSK-1120212) (LC Laboratories, Woburn, MA, USA, catalog #T-8132), Taselisib (GDC-0032) (Selleckchem, Houston, TX, USA, catalog #S7103), and the mouse IgG-isotype control (Abcam, ab37355) were obtained from the designated sources. S100A11 recombinant protein was prepared as described previously[5].

Determination of the concentration of S100A11 by ELISA

The concentration of S100A11 was measured using the CircuLex S100A11 ELISA Kit (Circulex, Nagano, Japan, Code No. CY-8063) according to the manufacturer's protocol. The standard curve for the ELISA was obtained using various concentrations of recombinant human S100A11. Samples were diluted 5- to 10-fold. The absorbance was measured at the dual wavelengths of 450/540 nm using the Flex Station 3 microplate reader (Sunnyvale, CA, USA) and the concentration of S100A11 (in pg/ml) was calculated according to the standard curve.

Western blot analysis

The detailed protocol has been described previously[31]. The primary antibodies used for western blot analyses were as follows: EGFR (catalog #4267), phospho- (p-) EGFR (Tyr1068) (#3777), Stat3 (#12640), p-Stat3 (Tyr705) (#9145), Akt (#9272), p-Akt (Ser473) (#4060), p44/p42 MAPK (#9102), p-p44 / p42 MAPK (#9101), Cyclin B1 (#4138), Cyclin D1 (#2922), Bcl-2 (#2872) (Cell Signaling Technology, Danvers, MA, USA), S100A11 (Medical & Biological Laboratories, Nagoya, Japan, catalog #CY-M1037), and β-actin (used as a loading control) (Merck Millipore, Billerica, MA, USA, catalog # MAB1501). The following secondary antibodies were used: goat anti-rabbit (catalog #sc-2030) or anti-mouse (catalog #sc-2031) immunoglobulin G (IgG)-conjugated horseradish peroxidase (Santa Cruz Biotechnology, Dallas, TX, USA). To detect specific signals, the membranes were examined using the ECL Prime Western Blotting Detection System (GE Healthcare, Amersham, UK, Code No. RPN2235) and LAS-3000 imager (Fujifilm, Tokyo, Japan).

Immunohistochemical analysis of clinical samples

MPM tissues were obtained from patients who underwent surgery at the Okayama University Hospital, in Okayama City, Japan. The experimental protocol was approved by the Institutional Review Board/Ethical Committee of the Okayama University Graduate School of Medicine, Dentistry and Pharmaceutical Sciences and Okayama University Hospital (Permit Number: 1508-027) and informed consent, including publication of patient photos, was obtained from all the patients. Tissue samples were fixed in 10% formaldehyde and embedded in paraffin. The immunohistochemical (IHC) staining for S100A11 was performed using an S100A11 primary antibody (R&D Systems, accession #P31949). The detailed protocol for the IHC staining has been described previously[32].

Cell proliferation assays

To examine the effect of the anti-S100A11 antibody (Proteintech Group, Chicago, IL, USA, catalog #10237-1-AP) on cell proliferation, the IncuCyte Zoom Live Cell Imaging System (Essen Biosciences, Ann Arbor, Michigan, USA) was used. In brief, 1.0×10^4 cells were seeded into each well of a 24-well plate. After 24 h of incubation, the plates were placed in the Incucyte Zoom system. Images were taken every 6 h for the indicated amount of time. The percent of confluence over time was calculated using the Incucyte Zoom software. For experiments testing the effect of sRAGE on cell proliferation, the thiazolyl blue tetrazolium bromide (MTT) (Sigma–Aldrich, catalog #M2128) dye reduction method was used, as described previously[33].

Cell migration and invasion assays

Cell migration and invasion were analyzed using a Boyden chamber assay. The cells were cultured with an antibody (100 ng/ml) for 24–48 h (for migration assays) or 48–72 h (for invasion assays). The detailed protocol has been described previously[34].

Xenograft model

The protocol was approved by the Animal Care and Use Committee of Okayama University (Permit Number: OKU-2016205). Six-week-old NOD/SCID female mice were purchased from Charles River Laboratories (Yokohama, Kanagawa, Japan). To evaluate the effect of the anti-S100A11 neutralizing antibody, mice were randomly divided into two groups: an antibody-administered group and a control group ($n = 3$ for each group). Each cell line (5×10^6 cells) suspended in 200 µL RPMI-1640 media and Matrigel Basement Membrane Matrix (Corning, NY, USA, catalog #354234) was subcutaneously injected into the backs of the mice either with 1 µg/ml anti-S100A11 antibody (proteintech Group) or mouse IgG-isotype control (two tumors per mouse). The injection was repeated five times every 3 days. Four weeks after the first injection, the mice were sacrificed and the tumors were harvested, measured, and photographed. The tumor volume was calculated using the empirical formula $V = 1/2 \times [(\text{shortest diameter})^2 \times (\text{the longest diameter})]$. No randomization and no blinding was performed. Sample size estimates were based on our previous experience.

Microarray and GSEA

Before and after treatment of H2052 and H2452 cells with the anti-S100A11 antibody (Proteintech Group), total RNAs were extracted from cell lines using an RNeasy Mini Kit (Qiagen, Venlo, the Netherlands, catalog #74104). Purified total RNA samples were hybridized on the Human Whole Genome DNA Microarray system (SurePrint G3 Human 8x60K ver. 2.0, Agilent Technologies, Santa Clara, CA) to obtain the altered gene expression profile. The fold change in the expression of individual genes was calculated and genes with fold changes exceeding 2-fold or below 2-fold were considered up- and downregulated, respectively (Supplementary Table S1). The specific enrichment of gene sets was further analyzed using the GSEA software (GSEA ver. 2.0) downloaded from the GSEA Website (http://software.broadinstitute.org/gsea/index.jsp).

Statistical analyses

All in vitro experiments were performed at least three times. Data are expressed as the mean±standard deviation. All data were analyzed using the JMP® 9.0.0 software for Windows (SAS Institute, Inc., Cary, NC, USA). The Student's *t*-tests was used to compare means of continuous scores between two independent groups. Otherwise, the Mann–Whitney *U*-test was used. An *F*-test to compare variances was performed, if necessary. All statistical tests were two-sided, and probability values less than 0.05 indicated statistically significant differences.

Acknowledgements

The authors thank Dr. Takehiro Matsubara (Biobank, Okayama University Graduate School of Medicine, Dentistry and Pharmaceutical Sciences, Okayama, Japan) and Ms. Fumiko Isobe (Department of General Thoracic Surgery and Breast and Endocrinological Surgery, Okayama University Graduate School of Medicine, Dentistry and Pharmaceutical Sciences, Okayama, Japan) for their technical supports. This study was supported by a Management Expenses Grants.

Author details

[1]Department of General Thoracic Surgery and Breast and Endocrinological Surgery, Okayama University Graduate School of Medicine, Dentistry and Pharmaceutical Sciences, Okayama, Japan. [2]Department of Cell Biology, Okayama University Graduate School of Medicine, Dentistry and Pharmaceutical Sciences, Okayama, Japan. [3]Department of Bioinformatics, Okayama University Graduate School of Medicine, Dentistry and Pharmaceutical Sciences, Okayama, Japan. [4]Department of Medical Oncology, National Hospital Organization Yamaguchi-Ube Medical Center, Ube, Yamaguchi, Japan. [5]Department of Clinical Research, National Hospital Organization Yamaguchi-Ube Medical Center, Ube, Yamaguchi, Japan. [6]Department of Clinical Genomic Medicine, Okayama University Graduate School of Medicine, Dentistry and Pharmaceutical Sciences, Okayama, Japan. [7]Department of Thoracic Surgery, National Hospital Organization Yamaguchi-Ube Medical Center, Ube, Yamaguchi, Japan. [8]Department of Cardiothoracic Surgery, New York University Langone Medical Center, New York, NY, USA

Conflict of interest

The authors declare that they have no competing interests.

Supplementary Information: The online version of this article (https://doi.org/10.1038/s41389-017-0017-3) contains supplementary material.

Received: 27 June 2017 Accepted: 21 September 2017
Published online: 24 January 2018

References

1. Milano, M. T. & Zhang, H. Malignant pleural mesothelioma: a population-based study of survival. *J. Thorac. Oncol.* **5**, 1841–1848 (2010).
2. Robinson, B. W. & Lake, R. A. Advances in malignant mesothelioma. *N. Engl. J. Med.* **353**, 1591–1603 (2005).
3. Bresnick, A. R., Weber, D. J. & Zimmer, D. B. S100 proteins in cancer. *Nat. Rev. Cancer* **15**, 96–109 (2015).
4. Donato, R. S100: a multigenic family of calcium-modulated proteins of the EF-hand type with intracellular and extracellular functional roles. *Int. J. Biochem. Cell. Biol.* **33**, 637–668 (2001).
5. Sakaguchi, M. et al. S100A11, an dual mediator for growth regulation of human keratinocytes. *Mol. Biol. Cell.* **19**, 78–85 (2008).
6. Todoroki, H., Kobayashi, R., Watanabe, M., Minami, H. & Hidaka, H. Purification, characterization, and partial sequence analysis of a newly identified EF-hand type 13-kDa Ca(2+)-binding protein from smooth muscle and non-muscle tissues. *J. Biol. Chem.* **266**, 18668–18673 (1991).
7. Sakaguchi, M. et al. S100C/A11 is a key mediator of Ca(2+)-induced growth inhibition of human epidermal keratinocytes. *J. Cell. Biol.* **163**, 825–835 (2003).
8. Sakaguchi, M. et al. Truncation of annexin A1 is a regulatory lever for linking epidermal growth factor signaling with cytosolic phospholipase A2 in normal and malignant squamous epithelial cells. *J. Biol. Chem.* **282**, 35679–35686 (2007).
9. Sakaguchi, M. & Huh, N. H. S100A11, a dual growth regulator of epidermal keratinocytes. *Amino Acids* **41**, 797–807 (2011).
10. Jaiswal, J. K. et al. S100A11 is required for efficient plasma membrane repair and survival of invasive cancer cells. *Nat. Commun.* **5**, 3795 (2014).
11. Shankar, J. et al. Pseudopodial actin dynamics control epithelial-mesenchymal transition in metastatic cancer cells. *Cancer Res.* **70**, 3780–3790 (2010).
12. Saho, S. et al. Active secretion of dimerized S100A11 induced by the peroxisome in mesothelioma cells. *Cancer Microenviron.* **9**, 93–105 (2016).
13. Fan, C. et al. S100A11 mediates hypoxia-induced mitogenic factor (HIMF)-induced smooth muscle cell migration, vesicular exocytosis, and nuclear activation. *Mol. Cell. Proteom.* **10**(M110), 000901 (2011).
14. Anania, M. C. et al. S100A11 overexpression contributes to the malignant phenotype of papillary thyroid carcinoma. *J. Clin. Endocrinol. Metab.* **98**, E1591–E1600 (2013).
15. Hao, J. et al. Selective expression of S100A11 in lung cancer and its role in regulating proliferation of adenocarcinomas cells. *Mol. Cell. Biochem.* **359**, 323–332 (2012).
16. Ohuchida, K. et al. S100A11, a putative tumor suppressor gene, is overexpressed in pancreatic carcinogenesis. *Clin. Cancer Res.* **12**, 5417–5422 (2006).
17. Oue, N. et al. Gene expression profile of gastric carcinoma: identification of genes and tags potentially involved in invasion, metastasis, and carcinogenesis by serial analysis of gene expression. *Cancer Res.* **64**, 2397–2405 (2004).
18. Memon, A. A. et al. Down-regulation of S100C is associated with bladder cancer progression and poor survival. *Clin. Cancer Res.* **11**, 606–611 (2005).
19. Hori, O. et al. The receptor for advanced glycation end products (RAGE) is a cellular binding site for amphoterin. Mediation of neurite outgrowth and co-expression of rage and amphoterin in the developing nervous system. *J. Biol. Chem.* **270**, 25752–25761 (1995).
20. Rauvala, H. & Rouhiainen, A. RAGE as a receptor of HMGB1 (Amphoterin): roles in health and disease. *Curr. Mol. Med.* **7**, 725–734 (2007).
21. Yan, S. D. et al. RAGE and amyloid-beta peptide neurotoxicity in Alzheimer's disease. *Nature* **382**, 685–691 (1996).
22. Cecil, D. L. et al. Inflammation-induced chondrocyte hypertrophy is driven by receptor for advanced glycation end products. *J. Immunol.* **175**, 8296–8302 (2005).

23. van Zoelen, M. A. et al. Receptor for advanced glycation end products facilitates host defense during Escherichia coli-induced abdominal sepsis in mice. *J. Infect. Dis.* **200**, 765–773 (2009).
24. Algermissen, B., Sitzmann, J., LeMotte, P. & Czarnetzki, B. Differential expression of CRABP II, psoriasin and cytokeratin 1 mRNA in human skin diseases. *Arch. Dermatol. Res.* **288**, 426–430 (1996).
25. Hirono, K. et al. Expression of myeloid-related protein-8 and -14 in patients with acute Kawasaki disease. *J. Am. Coll. Cardiol.* **48**, 1257–1264 (2006).
26. Hofmann, M. A. et al. RAGE mediates a novel proinflammatory axis: a central cell surface receptor for S100/calgranulin polypeptides. *Cell* **97**, 889–901 (1999).
27. Sorg, C. The calcium binding proteins MRP8 and MRP14 in acute and chronic inflammation. *Behring Inst. Mitt.* **91**, 126–137 (1992).
28. Pass, H. I. et al. Characteristics of nine newly derived mesothelioma cell lines. *Ann. Thorac. Surg.* **59**, 835–844 (1995).
29. Phelps, R. M. et al. NCI-Navy Medical Oncology Branch cell line data base. *J. Cell. Biochem. Suppl.* **24**, 32–91 (1996).
30. Suzawa, K. et al. Establishment and molecular characterization of cell lines from Japanese patients with malignant pleural mesothelioma. *Oncol. Lett.* **11**, 705–712 (2016).
31. Shien, K. et al. Knockdown of the epidermal growth factor receptor gene to investigate its therapeutic potential for the treatment of non-small-cell lung cancers. *Clin. Lung Cancer* **13**, 488–493 (2012).
32. Shien, K. et al. Prognostic impact of cancer stem cell-related markers in non-small cell lung cancer patients treated with induction chemoradiotherapy. *Lung Cancer* **77**, 162–167 (2012).
33. Sato, H. et al. Targeting the miR-200c/LIN28B axis in acquired EGFR-TKI resistance non-small cell lung cancer cells harboring EMT features. *Sci. Rep.* **7**, 40847 (2017).
34. Tanaka, N. et al. Frequent methylation and oncogenic role of microRNA-34b/c in small-cell lung cancer. *Lung Cancer* **76**, 32–38 (2012).

BRIEF REPORT

A Phase II Study of Trastuzumab Emtansine in HER2-Positive Non–Small Cell Lung Cancer

Katsuyuki Hotta, MD, PhD, MPH,[a,b,*] Keisuke Aoe, MD, PhD,[c] Toshiyuki Kozuki, MD, PhD,[d] Kadoaki Ohashi, MD, PhD,[a] Kiichiro Ninomiya, MD,[a] Eiki Ichihara, MD, PhD,[a] Toshio Kubo, MD, PhD,[a] Takashi Ninomiya, MD, PhD,[a] Kenichi Chikamori, MD, PhD,[c] Daijiro Harada, MD, PhD,[d] Naoyuki Nogami, MD, PhD,[d] Taizo Hirata, MD, PhD,[a] Shiro Hinotsu, MD, PhD,[b] Shinichi Toyooka, MD, PhD,[e] Katsuyuki Kiura, MD, PhD[a]

[a]*Department of Respiratory Medicine, Okayama University Hospital, Okayama, Japan*
[b]*Center of Innovative Clinical Medicine, Okayama University Hospital, Okayama, Japan*
[c]*Department of Medical Oncology, National Hospital Organization Yamaguchi-Ube Medical Center, Ube, Japan*
[d]*Department of Thoracic Oncology, National Hospital Organization Shikoku Cancer Center, Matsuyama, Japan*
[e]*General Thoracic Surgery and Breast and Endocrinological Surgery, Okayama University Graduate School of Medicine, Okayama, Japan*

Received 10 September 2017; revised 26 October 2017; accepted 31 October 2017
Available online - 4 December 2017

ABSTRACT

Trastuzumab emtansine (T-DM1), an anti–erb-b2 receptor tyrosine kinase 2 (HER2) antibody-drug conjugate, has been shown to significantly improve survival in HER2-positive breast cancer. We report a phase II trial of T-DM1 monotherapy in relapsed NSCLC with documented HER2 positivity (an immunohistochemistry [IHC] score of 3+, both an IHC score of 2+ and fluorescence in situ hybridization positivity, or exon 20 mutation). This study was terminated early because of limited efficacy. The demographic characteristics in the 15 assessable patients were as follows: median age, 67 years; male sex, 47%; performance status of 0 to 1, 80%; HER2 status IHC 3+, 33%; HER status IHC 2+/fluorescence in situ hybridization–positive, 20%; and exon 20 mutation, 47%. The median number of delivered cycles was 3 (range 1–11). One patient achieved a partial response with an objective response rate of 6.7% (90% confidence interval: 0.2–32.0). With a median follow-up time of 9.2 months, the median progression-free survival time and median survival time were 2.0 and 10.9 months, respectively. Grade 3 or 4 adverse events included thrombocytopenia (40%) and hepatotoxicity (20%) without any treatment-related deaths. T-DM1 had a limited efficacy for HER2-positive NSCLC in our cohort. Applying the concept of precision medicine to tumors appears challenging; thus, additional molecular approaches are warranted.

Keywords: Non–small cell lung cancer; HER2; trastuzumab emtansine; precision medicine

Introduction

Recent driver oncogene–based precision therapy has dramatically changed the treatment strategy for NSCLC, representatively targeting *EGFR* and ALK receptor tyrosine kinase gene (*ALK*) aberrations. However, outcomes in other lung cancers remain poor even with standard chemotherapy.[1,2] Consequently, further development of novel oncogenes and corresponding targeted therapeutic agents is warranted.

***Corresponding author.**

Disclosure: Dr. Hotta has received honoraria outside the current work from AstraZeneca, Ono Pharmaceutical, Astellas, Novartis, Bristol-Myers Squibb, Merck Sharp Dohme, Eli Lilly Japan, Daiichi-Sankyo Pharmaceutical, Boehringer-Ingelheim, Nihon Kayaku, Taiho Pharmaceutical, and Chugai Pharmaceutical. Dr. Hotta also has received research funding outside the current work from AstraZeneca, Boehringer-Ingelheim, Ono Pharmaceutical, Astellas, Novartis, Bristol-Myers Squib, Eli Lilly Japan, Merck Sharp Dohme, and Chugai Pharmaceutical. Dr. Ohashi has received a research grant from Novartis Pharmaceuticals Japan. Dr. Katsuyuki Kiura has received honoraria from Eli Lilly Japan, Nihon Kayaku, AstraZeneca, Daiichi-Sankyo Pharmaceutical, Chugai Pharmaceutical, Taiho Pharmaceutical, and Sanofi-Aventis. The remaining authors declare no conflict of interest.

Trial Registration: A Study of Trastuzumab Emtansine in Patients with HER2-Positive, Recurrent Metastatic Non-Small Cell Lung Cancer. UMIN000017709.

Address for correspondence: Katsuyuki Hotta, MD, PhD, MPH, Center for Innovative Clinical Medicine, Okayama University Hospital, 2-5-1, Shikata-cho, Okayama 700 8558, Japan. E-mail: khotta@okayama-u.ac.jp

ISSN: 1556-0864

https://doi.org/10.1016/j.jtho.2017.10.032

In addition, erb-b2 receptor tyrosine kinase 2 (HER2) aberrations have been detected, accounting for 4.7% to 10% of NSCLC in terms of grade 3+ HER2 immunohistochemistry (IHC) expression.[3] Additionally, the large epidemiological studies have identified tumors with positive HER2 fluorescence in situ hybridization (FISH) in 1.7% and HER2-mutant tumors in 3.6%.[4]

Trastuzumab emtansine (T-DM1) is a novel antibody-drug conjugate that uses trastuzumab, an anti-HER2 antibody, to deliver the maytansinoid antimicrotubule agent DM1, which binds to microtubules in a manner similar to that of vinca alkaloids.[5] T-DM1 has been shown to confer a survival benefit over the standard regimen applied in HER2-positive, relapsed breast cancer.[6]

As for NSCLC, the Calu 3 lung carcinoma cell line (HER2-IHC 3+) showed preclinically dose-dependent inhibition of cell growth after T-DM1 treatment.[5] Moreover, lung tumors with erb-b2 receptor tyrosine kinase 2 gene (*HER2*) insertion mutations in exon 20, a confirmed driver oncogene, showed dramatic shrinkage with HER2-targeted therapy.[7] These studies suggested that T-DM1 might be effective against both HER2-positive lung and breast cancers.

However, few prospective studies of HER2-targeted therapy for lung cancer have been conducted, prompting us to launch this phase II trial.

Methods

Study Population and Intervention

Patients who met the eligibility criteria, including HER2 positivity,[8] were enrolled for registration at three institutes in Japan: Yamaguchi-Ube Medical Centre, Shikoku Cancer Centre, and Okayama University Hospital. T-DM1 was kindly provided by Chugai Pharmaceuticals. Patients had to have had one or more lines of prior chemotherapy. Written informed consent was obtained from all patients before applying the study procedures. This study was approved by the institutional review boards.

Patients received T-DM1 intravenously, at a dose of 3.6 mg/kg over 90 minutes on day 1 of each 21-day cycle until the disease progressed or unmanageable toxic effects developed, as similar to the protocol for breast cancer.[6]

HER2 Tests

HER2 status was assessed in the laboratory (SRL, Tokyo, Japan) by using tumor formalin-fixed, paraffin-embedded archived tissues; no cytologic specimens were allowed, but biopsy or surgical specimens were. The level of HER2 protein expression was determined by IHC by using the Ventana I-VIEW PATHWAY anti–HER-2/neu (4B5) (Roche, Basel, Switzerland).[9] IHC scores of 3+ and 2+ were considered strongly and weakly positive, respectively.[9] FISH assays were also performed using the PathVysion HER-2 DNA probe kit (Vysis/Abbott Laboratories, Downers Grove, IL) to ascertain negativity or positivity according to a cutoff value of 2.0 (of the median ratio of HER2 to chromosome 17 copy numbers). We conducted a separate validation study to review the IHC and FISH specimens to define their positivity (unpublished data, Hotta K, 2017). Mutation analysis was performed by direct sequencing at a central laboratory (Genetic Labo, Japan) to detect known mutations (M774_A775insAYVM, A775_G776insYVMA, G776L insC, G776V insC, and P780_Y781insGSP).[4]

Finally, in this trial, HER2 was defined as positive in the presence of an IHC score of 3+, an IHC score of 2+ and FISH positivity, or an exon 20 insertion mutation.

Statistical Analysis

The primary end point was the objective response rate (ORR), which was centrally confirmed by three independent board members with the Response Evaluation Criteria in Solid Tumors (version 1.1) every 6 weeks. Secondary outcome end points included safety, overall survival, and progression-free survival (PFS). We considered the lower limit of interest to be 10%.[10] Assuming that a 20% or more increase in historical data in ORR would be clinically meaningful, we needed 30 patients with a one-sided α of 0.05 and 1-β of 0.8, considering a 10% dropout rate, according to the Simon minimax design. We also planned to conduct an interim analysis after the first 15 patients had been registered; early study termination would be considered if the ORR was obtained in no more than one patient. The confidence interval (CI) of the ORR was calculated with a confidence coefficient of two-tailed 90% and 95%.

Regarding the efficacy analysis, waterfall and swimmer plots were also produced. The PFS and overall survival times were calculated from the date of registration to the first documented date of disease progression and date of death, respectively, by the Kaplan-Meier method. Statistical analyses were conducted with STATA software (version 14.0, StataCorp LP, College Station, TX).

Results

Patients

This study was terminated early because of the limited efficacy, which did not satisfy the criteria in the interim analysis; this led to only 16 of the 30 patients planned being registered between September 2015 and November 2016. Among them, 15 were considered assessable for further analysis: one patient was excluded because of a protocol deviation in the registration process. The patients' characteristics are listed in Table 1. Regarding HER2 status, 33% of cases were scored IHC 3+, 20% were scored IHC 2+/FISH positive, and 47% showed the

mutations. All 15 patients were followed up sufficiently to allow assessment of the primary end point.

Treatment Delivery

The treatment delivery is summarized in Table 2. The median delivered number of cycles to each patient was 3 (Table 2). Four patients (27%) required dose reduction during the second cycle or later because of adverse events (AEs) (see Table 2). Treatment was ultimately discontinued in all patients, mainly on account of disease progression (see Table 2).

ORR and Survival

A partial response was centrally confirmed in a female patient with a HER2-mutant tumor (Table 3). Thus, the ORR (the primary end point) was 6.7% (90% CI: 0.2%–32.0%, 95% CI: 0.3%–27.9%), whereas seven patients (46.7%) each had stable disease and progressive disease (Fig. 1*A*). When patients were stratified by type of HER2 aberration, no tumor shrinkage was seen in the subgroup with an IHC score of 3+ or IHC 2+/FISH-positive tumors (n = 8) (Fig. 1*B* and Table 3). With a median follow-up time of 9.2 months, the median PFS time was 2.0 months (90% CI: 1.2–4.0, 95% CI: 1.4–4.0), whereas the median survival time was 10.9 months (90% CI: 2.3–, 95% CI: 4.4–12.0) (Fig. 2*A* and *B*).

Table 1. Patient Characteristics (N = 15)

Characteristic	Value
Median age (range), y	67 (45-77)
Sex	
Male/female	7 (47%)/8 (53%)
Smoking status	
Never/ever	10 (67%)/5 (33%)
ECOG PS	
0	2 (13%)
1	10 (67%)
2	3 (20%)
Adenocarcinoma histologic type	15 (100%)
Stage IV/recurrence[a]	9 (60%)/6 (40%)
HER2 positivity	
IHC 3+	5 (33%)
IHC 2+/FISH-positive	3 (20%)
Exon 20 mutations	7 (47%)
A775_G776insYVMA	5 (33%)
P780_Y781insGSP	1 (7%)
G776VinsC	1 (7%)
Other driver oncogenes	
EGFR	2 (13%)[b]
EML4-ALK	0
Median No. of prior chemotherapy regimens (range)	4 (1-7)

[a]Postoperative recurrence.
[b]Exon 19 deletion and exon 21 point mutation in one patient each.
ECOG, Eastern Cooperative Oncology Group; PS, performance status; HER2, erb-b2 receptor tyrosine kinase 2; IHC, immunohistochemistry; FISH, fluorescence in situ hybridization; EML4, echinoderm microtubule-associated protein-like 4 gene; ALK, anaplastic lymphoma kinase.

Table 2. Treatment Delivery (N = 15)

Characteristic	Value
Total no. of treatment cycles, median (range)	3 (1-11)
Cycles received	
≥4 cycles	6 patients (40%)
3 cycles	2 patients (13%)
2 cycles	5 patients (33%)
1 cycle	2 patients (13%)
No. of patients with dose reduction	4 (27%)
Reasons for dose reduction	
Thrombocytopenia	2 patients
AST elevation	1 patient
Infusion reaction	1 patient
No. of patients who discontinued treatment	15 (100%)
Reasons for discontinuation of treatment	
Disease progression	12
Adverse events[a]	2
Attending doctor's discretion	1

[a]Interstitial pneumonia (grade 2) and prolonged thrombocytopenia (grade 3) in one patient each.
AST, aspartate transaminase.

Safety

All grade 3 to 4 AEs are listed in Table 4. Almost all of the AEs were known ones, primarily thrombocytopenia (n = 6 [40%]) and hepatotoxicity (n = 3 [20%]). Among the 15 patients, there was no case of treatment-related death.

Grade 3 acute renal failure with a serum creatinine level of 3.08 mg/dL developed in one patient. The AE was

Table 3. Objective Response

	CR	PR	Stable Disease	PD
Overall cohort (N = 15)	0	1 (6.7%)	7 (46.7%)	7 (46.7%)
Subgroups by HER2 aberration pattern				
IHC/FISH-positive (n = 8)	0	0	3 (37.5%)	5 (62.5%)
Mutant-positive (n = 7)	0	1 (14.3%)	4 (57.1%)	2 (28.6%)
A775_G776insYVMA (n = 5)	0	1	3	1
G776VinsC (n = 1)	0	0	0	1
P780_Y781insGSP (n = 1)	0	0	1	0

Note: The objective response rate (i.e., the primary end point) was centrally confirmed by three independent extramural review board members and evaluated according to the Response Evaluation Criteria in Solid Tumors (version 1.1) every 6 weeks.
CR, complete response; PR, partial response; PD, progressive disease; HER2, erb-b2 receptor tyrosine kinase 2 IHC, immunohistochemistry; FISH, fluorescence in situ hybridization.

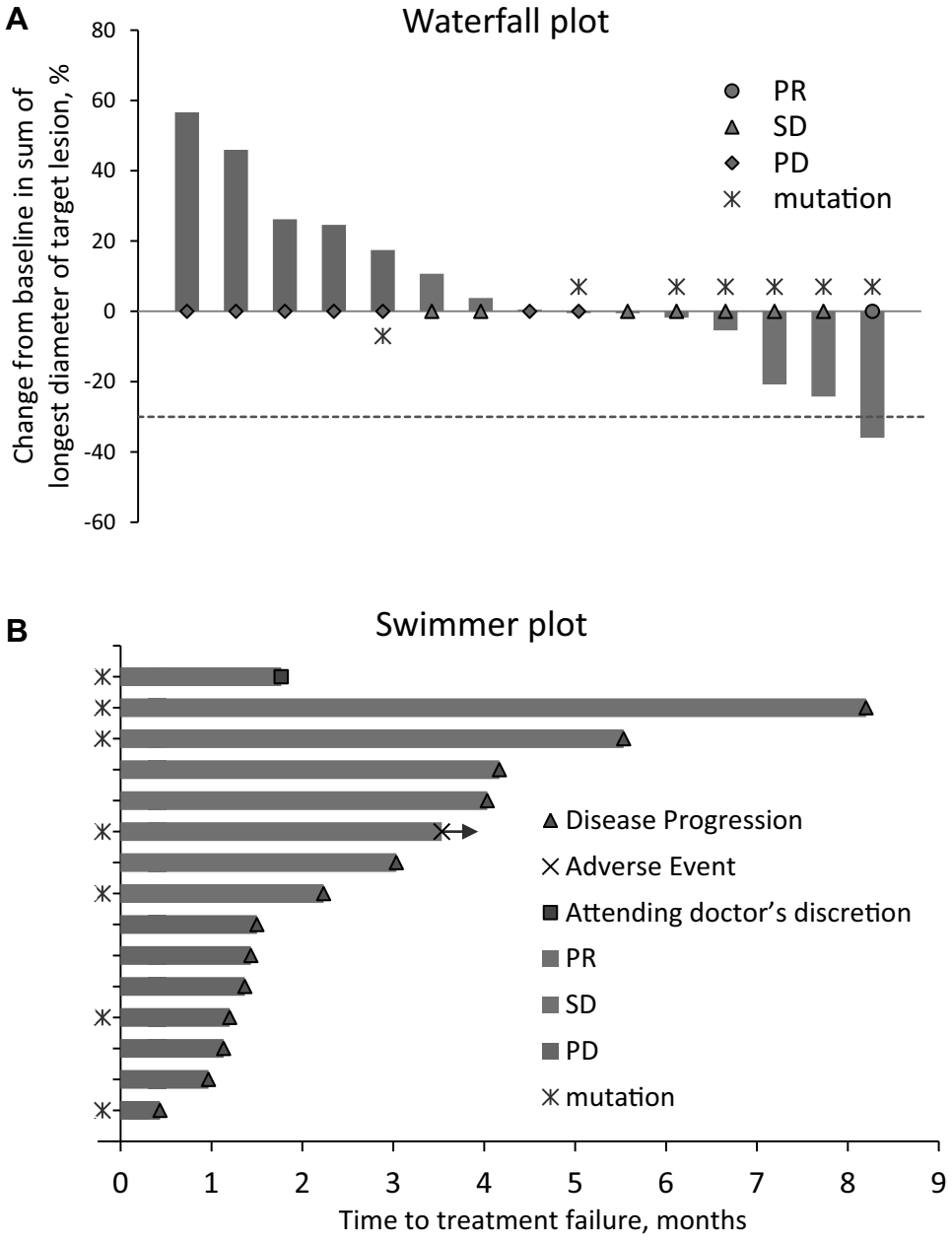

Figure 1. Objective response rate (N = 15). Waterfall plot (*A*) and swimmer plot (*B*). In the case of one responder, the attending physician judged progressive disease (PD) at an earlier time in the treatment course than did the independent radiologic review committee. PR, partial response.

recovered to grade 0 within 1 week during provision of appropriate supportive care. Interstitial pneumonia was observed in one patient (grade 2) during the fifth cycle, as detected by computed tomography. No further examination with bronchoscopy was performed in this case and the AE was resolved shortly thereafter without any steroid or oxygen therapy but just discontinuation of T-DM1.

Discussion

In this study, 1 of 15 patients (6.7%) responded to T-DM1, which did not meet the primary end point (see Table 3). The median PFS and median survival times were 2.0 and 10.9 months, respectively. The AE profiles were almost the same as those obtained in trials for approval for use in breast cancer.[6]

The investigational agent did not show high efficacy in this study (see Table 3 and Fig. 1), which is similar to the results of the very recent trials investigating HER2-targeted therapy in lung cancer (Supplementary Table 1). In particular, IHC 3+ or IHC 2+/FISH-positive tumors were rarely responsive to the investigational agent in this study (see Fig. 1 and Table 3). Although the precise reason remains unknown, it could be

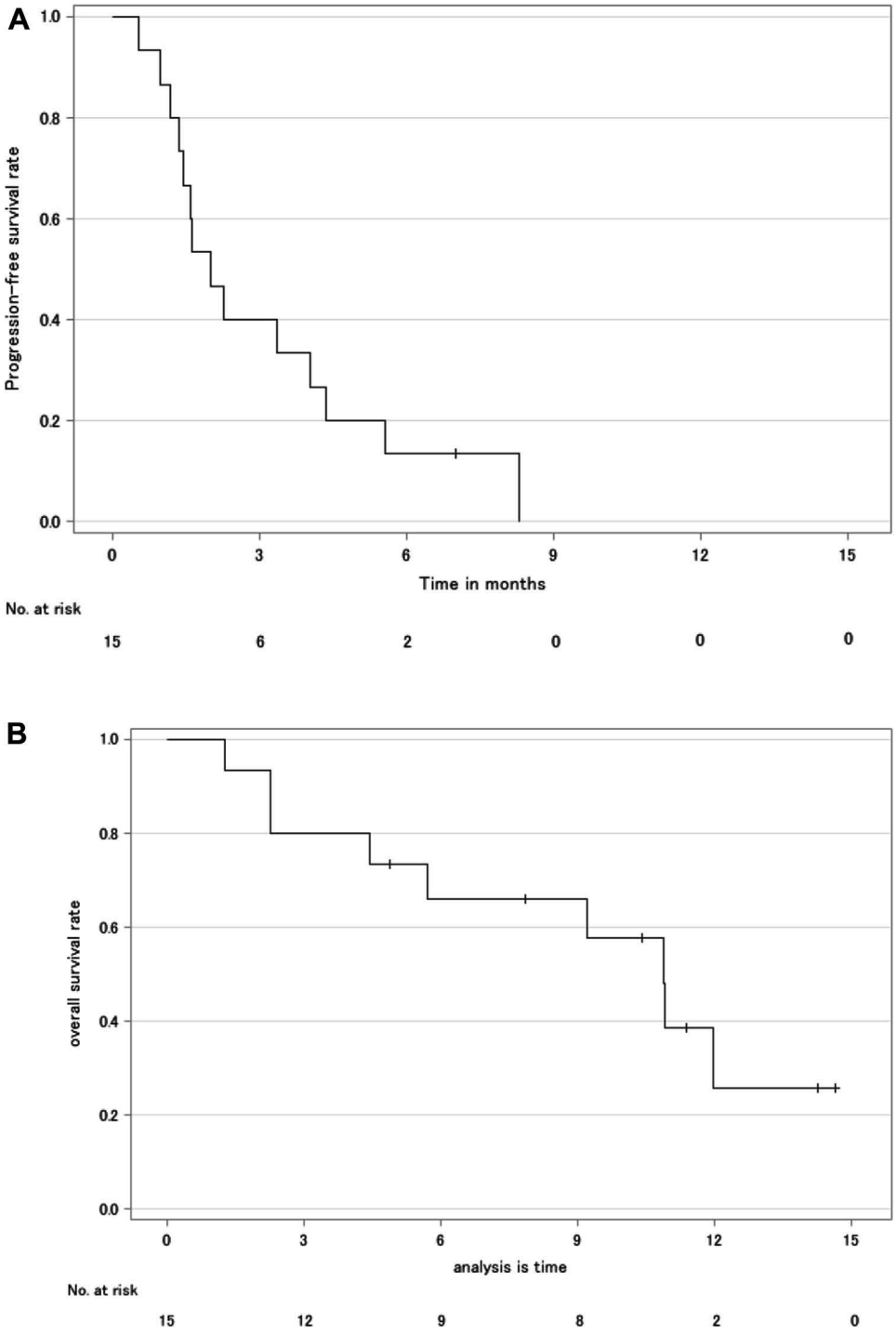

Figure 2. Survival (N = 15). Progression-free survival (*A*) and overall survival (*B*).

attributable to tumor heterogeneity, which was detected in 30% of the NSCLC cases.[11] It may be that only strongly HER2-immunostained cells were killed in the tumors after exposure to T-DM1, whereas the weakly stained cells might have escaped cell death and continued to grow. Unfortunately, we did not obtain or analyze tumor specimens at the time of disease progression. Further molecular analyses are warranted to elucidate the mechanisms underlying these tumors.

Another reason for the low sensitivity could be molecularly inappropriate patient selection. We might have overestimated HER2 IHC positivity because in the present study, we used the scoring system for IHC status that is applied to gastric cancer, which is less strict than

Table 4. Grade 3 to 4 Adverse Events

Category	Grade 3	Grade 4	Grades 3-4
Thrombocytopenia	5 (33%)	1 (7%)	6 (40%)
Hypokalemia	1 (7%)	0 (0%)	1 (7%)
Hyperuricemia	0 (0%)	1 (7%)	1 (7%)
AST/ALT level increase	1 (7%)	0 (0%)	1 (7%)
γ-GTP level increase	1 (7%)	0 (0%)	1 (7%)
LFT result abnormality	1 (7%)	0 (0%)	1 (7%)
Decreased appetite	1 (7%)	0 (0%)	1 (7%)
Nausea	1 (7%)	0 (0%)	1 (7%)
Acute renal failure	1 (7%)	0 (0%)	1 (7%)
Gingivitis	1 (7%)	0 (0%)	1 (7%)
Lung infection	1 (7%)	0 (0%)	1 (7%)

Note: No treatment-related deaths were observed.
ALT, Alanine transaminase; AST, aspartate transaminase; LFT, liver function test; γ-GTP, γ-glutamyltransferase.

that used for breast cancer.[9] Furthermore, the sensitivity of HER2-targeted agents was dependent on the IHC staining intensity.[12]

Regarding HER2-mutant tumors, we designed this study to limit the types of mutations to those confirmed as driver oncogenes in previous reports[4] but did not exclude tumors with co-mutation in the phosphatidylinositol-4,5-bisphosphate 3-kinase catalytic subunit alpha gene (*PIK3CA*); such mutation was reported as a potential intrinsic resistance mechanism, possibly leading to the low sensitivity.

The current study had several limitations. First, it used a single-arm design, and various potential biases could not be eliminated. Additionally, the study comprised a small number of patients recruited from only a few institutes in one country, thus lowering the likelihood of confirmative results. The relationship between type of HER2 mutations and efficacy also remains unknown. Our study results should be interpreted together with those of relevant previous studies (see Supplementary Table 1).

In conclusion, T-DM1 showed limited efficacy against HER2-positive NSCLCs in our cohort. It seems that the concept of precision medicine is difficult to apply to tumors. Additional molecular approaches are warranted for precision medicine in the treatment of HER2-positive tumors.

Acknowledgments

This research was supported by a specific grant from the Japan Agency for Medical Research and Development, which is funded by the Japanese government. No additional external funding was received for this study. The investigational agent was kindly provided by Chugai Pharmaceuticals. All of the authors contributed to the writing of the study protocol. Kadoaki Ohashi, Katsuyuki Hotta, Taizo Hirata, Kiichiro Ninomiya, and Katsuyuki Kiura also participated in the trial design and setup. Kadoaki Ohashi, Katsuyuki Hotta, Kiichiro Ninomiya, and Katsuyuki Kiura calculated the required sample size.

Appendix

The contributing members of the HER2-CS Group are as follows:

Steering Committee: K. Hotta, K. Ohashi, K. Ninomiya, T. Hirata, S. Hinotsu, S. Toyooka, and K. Kiura.

Advisers on the *HER2* aberration analysis: H. Yanai (Okayama University Hospital) and M. Takata (Kyoto University).

Independent Data and Safety Monitoring Committee: T. Kato (Kanagawa Cancer Center), J. Sasaki (Kitazato University), and N. Ebi (Iizuka Hospital).

Drug supplier: Chugai Pharmaceutical Co. Ltd.

Study site investigators: K. Hotta, K. Ohashi, K. Ninomiya, M. Tabata, A. Sato, E. Ichihara, T. Kubo, T. Ninomiya, T. Hirata, D. Minami, Y. Kato, H. Higo, G. Makimoto, Y. Toyota, N. Oda, M. Nakanishi, T. Tamura, H. Kayatani, K. Kudo, K. Nishii, S. Senoo, H. Kano, H. Watanabe, T. Ando, T. Nakasuka, N. Hara, J. Itano, H. Nakashima, S. Toyooka, and K. Kiura (Okayama University Hospital): K. Aoe, K. Chikamori, K. Oishi, T. Maeda, D. Kishino, R. Okamoto, H. Ueoka, and H. Kamei (Yamaguchi-Ube Medical Center); and T. Kozuki, D. Harada, A. Nishioka, Y. Minemoto, and N. Nogami (Shikoku Cancer Center Hospital).

This study was conducted with dedicated support from the following persons:

HER2-CS Group: S. Harita, G. Ikeda, M. Yasugi, E. Kurimoto, K. Nakano, and K. Gemba (Chugoku Central Hospital); T. Moritaka and K. Inoue (Ehime Prefectural Central Hospital); S. Miyoshi, N. Hamaguchi, R. Ito, and Y. Sano (Ehime University Hospital); I. Takata and A. Mitani (Fukuyama City Hospital); N. Ishikawa, T. Nishisaka, H. Shoda, A. Nishida, K. Hamai, and S. Tamamoto (Hiroshima Prefectural Hospital); M. Yamasaki (Hiroshima Red Cross Hospital and Atomic-bomb Survivors Hospital); K. Fujitaka, T. Masuda, S. Miyamoto, and N. Hattori (Hiroshima University Hospital); K. Sugimoto, S. Fujii, and Y. Ueda (Japanese Red Cross Kobe Hospital); A. Bessho, S. Hosokawa, Y. Sakugawa, N. Fukamatsu, and K. Ogata (Japanese Red Cross Okayama Hospital); T. Murakami (Japanese Red Cross Society Himeji Hospital); Y. Ueda (Kagawa Prefectural Central Hospital); S. Bandoh and N. Kanaji (Kagawa University Hospital); N. Takigawa, H. Yamane, N. Ochi, and Y. Honda (Kawasaki Hospital); M. Oka and M. Kittaka (Kawasaki Medical School Hospital); T. Kubota and A. Yokoyama (Kochi Medical School Hospital]); H. Yoshioka, T. Tanaka, T. Yokoyama, and E. Sato (Kurashiki Central Hospital); Y. Shiota and N. Horita (Kure Kyosai Hospital); T. Kanematsu (Matsuyama Red Cross

Hospital); Y. Awaya, A. Nakamasu, and Y. Sano (Miyoshi Central Hospital); I. Murakami (NHO Higashi-Hiroshima Medical Center); S. Kuyama, K. Kudo, T. Tamura, T. Umeno, and D. Morichika (NHO Iwakuni Medical Center); T. Shibayama, K. Fujiwara, and Sato K (NHO Okayama Medical Center); K. Nishii (Okayama Health Foundation Hospital); Fujimoto N, Fuchimoto Y, and T. Kishimoto (Okayama Rosai Hospital); H. Kawai and K. Watanabe (Okayama Saiseikai General Hospital); K. Tokumo (Onomichi General Hospital); T. Murakami (Onomichi Municipal Hospital); T. Isobe and Y. Tsubata (Shimane University School of Medicine); M. Inoue (Shimonoseki City Hospital); H. Ichikawa (Takamatsu Hospital); Y. Nishioka, M. Hanibuchi, and H. Goto (Tokushima University Hospital); T. Sumikawa (Tottori Prefectural Central Hospital); M. Kodani, H. Suyama, H. Makino, Y. Ueda, N. Kinoshita, and E. Shimizu (Tottori University Hospital); H. Obata and H. Ikegami (Yamaguchi-ken Saiseikai Shimonoseki General Hospital); and Y. Kunihiro, T. Kobayashi, K. Ueda, M. Hayashi, M. Kamiya, and J. Murakami (Yamaguchi University Hospital).

LC-SCRUM group: S. Matsumoto and K. Goto.

Center for Innovative Clinical Medicine, Okayama University Hospital: K. Miyake, K. Ueda, H. Okuda, N. Kondoh, M. Fukata, S. Kuroda, S. Sugihara, M. Nakabayashi, N. Hiramatsu, S. Hinotsu, K. Zama, W. Ishii, Y. Ohe, C. Harada, M. Yoshida, K. Kamikawa, J. Sakurai, and K. Shikata.

Supplementary Data

Note: To access the supplementary material accompanying this article, visit the online version of the *Journal of Thoracic Oncology* at www.jto.org and at https://doi.org/10.1016/j.jtho.2017.10.032.

References

1. Hotta K, Fujiwara Y, Matsuo K, et al. Recent improvement in the survival of patients with advanced non-small-cell lung cancer enrolled into phase III trials of first-line systemic chemotherapy. *Cancer*. 2007;109:939–948.
2. Hotta K, Matsuo K, Ueoka H, Kiura K, Tabata M, Tanimoto M. Addition of platinum compounds to a new agent in patients with advanced non-small-cell lung cancer: a literature based meta-analysis of randomised trials. *Ann Oncol*. 2004;15:1782–1789.
3. Kuyama S, Hotta K, Tabata M, et al. Impact of HER2 gene and protein status on the treatment outcome of cisplatin-based chemoradiotherapy for locally advanced non-small cell lung cancer. *J Thorac Oncol*. 2008;3:477–482.
4. Mazières J, Peters S, Lepage B, et al. Lung cancer that harbors an HER2 mutation: epidemiologic characteristics and therapeutic perspectives. *J Clin Oncol*. 2013;31:1997–2003.
5. Lewis Phillips GD, Li G, Dugger DL, et al. Targeting HER2-positive breast cancer with trastuzumab-DM1, an antibody-cytotoxic drug conjugate. *Cancer Res*. 2008;68:9280–9290.
6. Verma S, Miles D, Gianni L, et al. Trastuzumab emtansine for HER2-positive advanced breast cancer. *New Engl J Med*. 2012;367:1783–1791.
7. Perera SA, Li D, Shimamura T, et al. HER2YVMA drives rapid development of adenosquamous lung tumors in mice that are sensitive to BIBW2992 and rapamycin combination therapy. *Proc Nat Acad Sci U S A*. 2009;106:474–479.
8. Ohashi K, Hotta K, Hirata T, et al. Trastuzumab emtansine in HER2+ recurrent metastatic non-small-cell lung cancer: study protocol. *Clin Lung Cancer*. 2017;18:92–95.
9. Bang YJ, Van Cutsem E, Feyereislova A, et al. Trastuzumab in combination with chemotherapy versus chemotherapy alone for treatment of HER2-positive advanced gastric or gastro-oesophageal junction cancer (ToGA): a phase 3, open-label, randomised controlled trial. *Lancet*. 2010;376:687–697.
10. Shepherd FA, Dancey J, Ramlau R, et al. Prospective randomized trial of docetaxel versus best supportive care in patients with non-small-cell lung cancer previously treated with platinum-based chemotherapy. *J Clin Oncol*. 2000;18:2095–2103.
11. Kobyakov DS, Avdalyan AM, Klimachev VV, Lazarev AF, Lushnikova EL, Nepomnyaschikh LM. Non-small cell lung cancer: HER2 oncogene status. *Arkh Patol*. 2015;77(2):3–9 [in Russian].
12. Stinchcombe T, Stahel RA, Bubendorf L, et al. Efficacy, safety, and biomarker results of trastuzumab emtansine (T-DM1) in patients (pts) with previously treated HER2-overexpressing locally advanced or metastatic non-small cell lung cancer (mNSCLC) [abstract]. *J Clin Oncol*. 2017;35(suppl):8509.

Original Article

Anamorelin (ONO-7643) for the Treatment of Patients With Non–Small Cell Lung Cancer and Cachexia: Results From a Randomized, Double-Blind, Placebo-Controlled, Multicenter Study of Japanese Patients (ONO-7643-04)

Nobuyuki Katakami, MD[1]; Junji Uchino, MD[2,3]; Takuma Yokoyama, MD[4]; Tateaki Naito, MD[5]; Masashi Kondo, MD[6,7]; Kouzo Yamada, MD[8]; Hiromoto Kitajima, MD[9]; Kozo Yoshimori, MD[10]; Kazuhiro Sato, MD[11]; Hiroshi Saito, MD[12]; Keisuke Aoe, MD[13]; Tetsuya Tsuji, MD[14]; Yuichi Takiguchi, MD[15]; Koichi Takayama, MD[2]; Naoyuki Komura, MS[16]; Toru Takiguchi, MS [16]; and Kenji Eguchi, MD[17]

BACKGROUND: Cachexia, described as weight loss (mainly in lean body mass [LBM]) and anorexia, is common in patients with advanced cancer. This study examined the efficacy and safety of anamorelin (ONO-7643), a novel selective ghrelin receptor agonist, in Japanese cancer patients with cachexia. **METHODS:** This double-blind clinical trial (ONO-7643-04) enrolled 174 patients with unresectable stage III/IV non–small cell lung cancer (NSCLC) and cachexia in Japan. Patients were randomized to daily oral anamorelin (100 mg) or a placebo for 12 weeks. The primary endpoint was the change from the baseline LBM (measured with dual-energy x-ray absorptiometry) over 12 weeks. The secondary endpoints were changes in appetite, body weight, quality of life, handgrip strength (HGS), and 6-minute walk test (6MWT) results. **RESULTS:** The least squares mean change (plus or minus the standard error) in LBM from the baseline over 12 weeks was 1.38 ± 0.18 and -0.17 ± 0.17 kg in the anamorelin and placebo groups, respectively ($P < .0001$). Changes from the baseline in LBM, body weight, and anorexia symptoms showed significant differences between the 2 treatment groups at all time points. Anamorelin increased prealbumin at weeks 3 and 9. No changes in HGS or 6MWT were detected between the groups. Twelve weeks' treatment with anamorelin was safe and well tolerated in NSCLC patients. **CONCLUSIONS:** Anamorelin significantly increased LBM and improved anorexia symptoms and the nutritional state, but not motor function, in Japanese patients with advanced NSCLC. Because no effective treatment for cancer cachexia is currently available, anamorelin can be a beneficial treatment option. ***Cancer* 2017;000:000–000.** © *2017 American Cancer Society.*

KEYWORDS: anamorelin (ONO-7643), cachexia, lean body mass, non–small cell lung cancer, randomized controlled trial.

INTRODUCTION

Cachexia is commonly related to many clinically important conditions, such as anorexia, inflammation, and degradation of skeletal muscle protein, in which muscle wasting plays a key role. Cachexia is frequently observed in patients with cancer (50%-80%) and leads to approximately 20% of deaths among cancer patients.[1-5] Moreover, cancer cachexia not only is associated with higher rates of toxicity from chemotherapeutic drugs[6] but also leads to a poor prognosis as well as reduced quality of life (QOL).[7]

Cancer cachexia cannot be completely reversed with conventional nutritional support,[8] and there are limited pharmacological therapies useful for the management of cachexia.

Corresponding author: Nobuyuki Katakami, MD, Division of Integrated Oncology, Institute of Biomedical Research and Innovation, 2-2 Minatojima Minamimachi, Chuo-Ku, Hyogo 650-0047, Japan; nkatakami@kcho.jp

[1]Division of Integrated Oncology, Institute of Biomedical Research and Innovation, Kobe, Japan; [2]Department of Pulmonary Medicine, Kyoto Prefectural University of Medicine, Kyoto, Japan; [3]Department of Respiratory Medicine, Fukuoka University School of Medicine, Fukuoka, Japan; [4]Department of Respiratory Medicine, Kyorin University Hospital, Mitaka, Japan; [5]Division of Thoracic Oncology, Shizuoka Cancer Center, Shizuoka, Japan; [6]Department of Respiratory Medicine Graduate School of Medicine, Nagoya University, Nagoya, Japan; [7]Department of Respiratory Medicine, Fujita Health University, Toyoake, Japan; [8]Department of Thoracic Oncology, Kanagawa Cancer Center, Yokohama, Japan; [9]Department of Respiratory Medicine, National Hospital Organization Shikoku Cancer Center, Matsuyama, Japan; [10]Department of Clinical Oncology, Japan Anti-Tuberculosis Association, Fukujuji Hospital, Kiyose, Japan; [11]Department of Respiratory Medicine, Nagaoka Red Cross Hospital, Nagaoka, Japan; [12]Department of Respiratory Medicine, Aichi Cancer Center Aichi Hopital, Aichi, Japan; [13]Department of Medical Oncology, National Hospital Organization Yamaguchi-Ube Medical Center, Ube, Japan; [14]Department of Rehabilitation Medicine, Keio University School of Medicine, Tokyo, Japan; [15]Department of Medical Oncology, Graduate School of Medicine, Chiba University, Chiba, Japan; [16]Ono Pharmaceutical Co, Ltd, Osaka, Japan; [17]Health Science on Supportive Medicine for Intractable Diseases, Teikyo University School of Medicine, Tokyo, Japan

See editorial on pages 000-000, this issue.

The clinical trial registration was JapicCTI-142451 (http://www.clinicaltrials.jp/user/search/directCteDetail.jsp?clinicalTrialId=14228).

We thank all the patients as well as the caregivers, investigators, and onsite staff who contributed to this clinical trial.

Additional supporting information may be found in the online version of this article.

DOI: 10.1002/cncr.31128, **Received:** June 19, 2017; **Revised:** September 8, 2017; **Accepted:** September 14, 2017, **Published online** Month 00, 2017 in Wiley Online Library (wileyonlinelibrary.com)

Ghrelin, a peptide hormone produced by ghrelin-producing endocrine cells in the gut, acts as a regulator of hunger, which is also involved in the regulation of food intake.[9-11] Furthermore, ghrelin induces the secretion of growth hormone and thereby acts as a growth hormone secretagogue.[12,13]

Anamorelin (ONO-7643) is an orally active, high-affinity, selective agonist of the ghrelin receptor.[14,15] Previous phase 1 and 2 trials have demonstrated the safety and efficacy of anamorelin treatment for increasing body weight, lean body mass (LBM), and food intake.[16-18] Two multinational phase 3 clinical studies in patients with advanced non–small cell lung cancer (NSCLC) and cachexia reported that anamorelin administration for 12 weeks increased LBM and body weight and substantially improved the symptoms of anorexia/cachexia.[19]

A randomized, double-blind, phase 2 trial investigated 50 and 100 mg of anamorelin versus a placebo in Japanese patients with NSCLC and cachexia; treatment with 100 mg of anamorelin in that study demonstrated improvements in LBM, body weight, appetite, and QOL with no tolerability issues.[20] Therefore, in the current study, 100 mg of anamorelin was selected to confirm its action in increasing LBM in Japanese patients with NSCLC and cachexia.

MATERIALS AND METHODS

Study Design

We conducted a multicenter (43 sites in Japan), randomized, double-blind, placebo-controlled trial that comprised an observation/run-in period of 2 weeks, a treatment period of 12 weeks, and a follow-up period of 4 weeks. Visits during the treatment period were planned at weeks 0, (baseline/randomization), 1, 3, 6, 9, and 12. All procedures followed during this study were in accordance with the spirit of the Declaration of Helsinki, the study protocol, the standards specified under the Pharmaceutical Affairs Act of Japan (article 80, paragraph 2 and article 14, paragraph 3), and Good Clinical Practice (effective as of April 1, 1997; Japanese Ministry of Health and Welfare Ordinance No. 28). Ethics committee approval for the study was obtained from each center.

Patients

This study included patients with stage III or IV NSCLC who were not to undergo an operation, were 20 years old or older, had involuntary weight loss $\geq 5\%$ within the last 6 months, had anorexia, had 2 or more applicable symptoms (fatigue, malaise, reduced overall muscular strength, and arm muscle circumference [in centimeters] $<$ 10th percentile), and had more than 1 of the following conditions: albumin level < 3.2 g/dL, C-reactive protein level > 5.0 mg/L, hemoglobin level < 12 g/dL, Eastern Cooperative Oncology Group (ECOG) performance status (PS) of 0 to 2, and estimated life expectancy ≥ 4 months. Anorexia, malaise, fatigue, and reduced muscular strength needed to be grade 1 or higher according to the National Cancer Institute's Common Terminology Criteria for Adverse Events (version 4.0). The following formula was used to ascertain the arm muscle circumference:

Arm muscle circumference (cm) = Arm circumference (cm) $-$ 3.14 $\times$ Triceps skinfold thickness (mm)/10.

Patients were excluded if they had known symptomatic brain metastases or uncontrolled diabetes. Written informed consent was obtained from each patient. All eligible patients were randomized by a centralized allocation center and were further stratified by the enrollment site and reductions in weight during the last 6 months (5%-10% and $>$10%). The randomization methodology used a randomization table and sealed envelopes to randomize the patients.

Interventions and Concomitant Therapies

After enrollment, patients were randomly assigned to either 100 mg of anamorelin or a placebo once daily throughout the therapy period. In this study, patients were enrolled regardless of their treatment history with chemotherapy for NSCLC, but they were prohibited from newly taking epidermal growth factor receptor tyrosine kinase inhibitors during the treatment period because of their possible effect on the QOL assessment.

During the study period, radiotherapy (other than palliative radiation therapy for bone metastases or radiation therapy for metastases in the brain), general corticosteroids, growth hormone formulations, medroxyprogesterone, megestrol acetate, Chinese herbal drugs, antiarrhythmic drugs, antitumor anthracyclines, inhibitors and inducers of cytochrome P450 3A4, and other experimental treatments were not permitted.

Efficacy Assessments

The primary endpoint of the trial was the mean change in LBM (estimated by dual-energy x-ray absorptiometry [DEXA]) from the baseline over the 12-week treatment period. The secondary endpoints of the study were changes in the body weight, body composition (ascertained by DEXA), appetite, Cancer Fatigue Scale (CFS) score, ECOG PS, Karnofsky Performance Scale (KPS) score, handgrip strength (HGS), Quality-of-Life Questionnaire for Cancer Patients Treated With Anticancer

Drugs (QOL-ACD) score, 6-minute walk test (6MWT) results, and serum biomarkers. The LBM and other body composition–related variables, ECOG PS, KPS, HGS, 6MWT, and serum biomarkers were determined at the baseline and in weeks 3, 6, 9, and 12. The body weight, QOL-ACD score, and CFS score were determined at the baseline and in weeks 1, 3, 6, 9, and 12. In addition, the efficacy parameters were recorded after treatment discontinuation.

Body composition was determined via DEXA with either the GE Lunar system (GE, Wauwatosa, Wisconsin) or the Hologic system (Hologic, Bedford, Massachusetts). DEXA was used to assess the LBM, fat mass, bone mineral content, and overall body mass by means of standardized methods. A grip dynamometer (Tracker Freedom Wireless Grip; JTECH Medical, Midvale, Utah) was used for the measurement of HGS.

The QOL-ACD (see online supporting information) is a self-rated measure assessing the condition of a patient during the last few days according to a 1 to 5 scale, and it is composed of 4 domains (functional, physical, mental, and psychosocial) and a global face scale developed as a generic questionnaire for assessing QOL in Japanese cancer patients receiving chemotherapy.[21] The CFS is a self-rated scale evaluating current fatigue in cancer patients, and it has 3 dimensions (physical fatigue, affective fatigue, and cognitive fatigue). The scale is composed of 15 items scored on a 1 to 5 scale for a maximum score of 60, with higher scores indicating more severe fatigue. ECOG PS and KPS were used to quantify the PS of the patients. After a $\geq$ 12-hour fast, blood samples were collected for the estimation of insulin-like growth factor 1 (IGF-1), insulin-like growth factor-binding protein 3 (IGFBP-3), and prealbumin. Laboratory tests were performed at each study site.

Safety

The safety parameters included the vital signs, electrocardiography (centrally assessed) with all 12 leads, status of the tumor (evaluated by investigators using Response Evaluation Criteria in Solid Tumors [RECIST] guidelines), clinical laboratory tests, and adverse events (AEs). AEs were reported with the National Cancer Institute's Common Terminology Criteria for Adverse Events (version 4.0), and they were classified according to the system organ class/preferred term.

Statistical Analysis

Analyses were performed according to the predetermined study protocol and statistical analysis plan. The full analysis set (FAS) was used for the analysis of all efficacy variables. The FAS comprised all eligible patients who had undergone a minimum of 1 efficacy assessment after the initiation of the study drug. The safety analysis set was used for the analysis of safety data and comprised all patients who had received the study drug at least once.

The findings of a phase 2 trial (ONO-7643-03), in which the mean difference in LBM (according to DEXA) between 100 mg of anamorelin and the placebo was 0.89 ± 1.94 kg, were used to determine the sample size for this study.[20] At least 76 patients were required in each treatment arm to reject the null hypothesis at $P < .05$ and a power of 80%. Under the assumption that approximately 10% of the patients would withdraw/drop out of the study, a total of 170 patients (85 patients per group) were to be enrolled. Descriptive statistics were used to summarize the baseline parameters. An analysis of covariance for repeated measurement data, using the study arm, time point, and prior reductions in weight (5%-10% and $>$10%) as fixed factors and the baseline value as a covariate, was used to analyze efficacy parameters. The difference in the least squares mean from the initiation of treatment to a specific point of time was determined for both groups. The least squares mean differences between patients who received anamorelin and those who received the placebo were determined with 95% confidence intervals (CIs). A study arm–point of time interaction was incorporated for the assessment of secondary endpoints (differences in the body mass composition, QOL-ACD score, CFS score, body weight, KPS, serum biomarkers, HGS, and 6MWT results). Descriptive statistics were used to assess safety parameters and are reported as numbers and percentages of patients. The total incidence of AEs and adverse drug reactions (ADRs) was compared between the study groups with the chi-square test. There was no adjustment for the multiplicity of statistical testing, and an imputation method was not used for missing data.

RESULTS

Patients

A total of 174 patients were enrolled in this study from May 2014 to October 2015. Ninety of these 174 patients were randomized to the placebo group, and 84 were randomized to the 100-mg anamorelin group (Fig. 1). One patient did not receive treatment. One patient treated with 100 mg of anamorelin failed to meet the inclusion criteria and hence was excluded from the FAS. The FAS comprised 172 patients, with 90 and 82 in the placebo

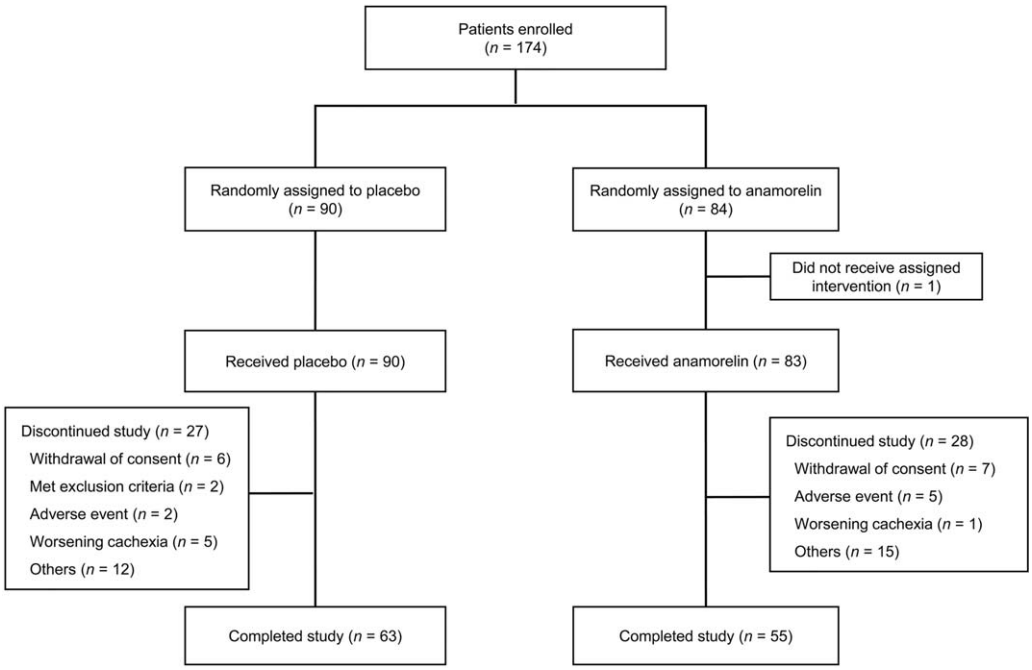

Figure 1. Enrollment and outcomes.

and anamorelin groups, respectively. There were 11 deaths in the placebo group and 5 deaths in the anamorelin group. AEs led to treatment discontinuation in 2 patients from the placebo group and in 5 patients from the anamorelin group. The baseline characteristics of the 2 groups were similar (Table 1).

LBM

As shown in Figure 2, the increase in LBM over 12 weeks was found to be significantly larger in the anamorelin-treated patients versus the placebo-treated patients, with least squares means and standard errors of 1.38 ± 0.18 and -0.17 ± 0.17 kg, respectively. Overall, the change in the anamorelin-treated patients versus the placebo-treated patients was 1.56 kg (95% CI, 1.11-2.00 kg; $P < .0001$). At week 3 and thereafter, a significant difference ($P < .0001$) in the LBM gain in comparison with the baseline was noted between the treatment groups.

Body Weight

In comparison with the placebo, anamorelin induced a significant weight gain (Fig. 2), which is in agreement with anamorelin's mechanism of action and the LBM gain. The body weight gain was evident at week 1 of treatment and continued thereafter.

Other Body Composition Parameters

In comparison with the placebo, anamorelin significantly increased other body composition parameters, including the total body mass, fat mass, appendicular LBM (arms and legs), and trunk LBM (Supporting Table 1 [see online supporting information]).

QOL-ACD

Throughout the study period from week 1, the anamorelin-treated patients showed significant improvements in comparison with the placebo-treated patients in the QOL-ACD scores for items 7 to 11 ("physical condition"), item 8 ("Did you have a good appetite?"), item 9 ("Did you enjoy your meals?"), and item 11 ("Did you lose any weight?"; Fig. 3A-D). The efficacy of anamorelin was not definite in other domains.

Other Secondary Endpoints

The effects of 100 mg of anamorelin on CFS, HGS, and 6MWT are shown in Figure 2 and Supporting Table 2 (see online supporting information). There were marginal effects on CFS, HGS, and 6MWT. In comparison with the placebo group, the anamorelin group showed significant increases in the serum IGF-1, IGFBP-3, and prealbumin levels (Fig. 4A-C).

TABLE 1. Demographics and Baseline Characteristics of the Patients

Parameter	Placebo (n = 90)	Anamorelin (n = 84)
Sex, No. (%)		
Male	57 (63.3)	59 (70.2)
Female	33 (36.7)	25 (29.8)
Age, mean ± SD, y	67.2 ± 7.9	67.6 ± 9.9
Weight, mean ± SD, kg	49.73 ± 8.32	52.23 ± 9.43
BMI, mean ± SD, kg/m^2	19.27 ± 2.31	19.81 ± 2.60
Weight loss, No. (%)		
5-10	52 (57.8)	50 (60.2)
>10	38 (42.2)	33 (39.8)
Missing	-	1
Body composition (DEXA), mean ± SD, kg		
LBM	37.06 ± 6.34	38.88 ± 7.06
Body fat	10.68 ± 4.21	11.29 ± 5.04
BMC	1.90 ± 0.56	2.06 ± 0.57
Total body mass	49.63 ± 8.61	52.23 ± 9.73
Grip strength, mean ± SD, kg		
Dominant hand	26.70 ± 8.01	27.87 ± 9.35
Nondominant hand	25.12 ± 7.01	26.41 ± 8.30
6-min walk distance, mean ± SD, m	375.7 ± 88.4	379.6 ± 89.6
QOL-ACD, mean ± SD	70.9 ± 13.0	74.9 ± 13.0
Cancer Fatigue Scale, mean ± SD	23.8 ± 9.7	24.4 ± 9.7
ECOG PS, No. (%)		
0	13 (14.4)	9 (10.8)
1	65 (72.2)	64 (77.1)
2	12 (13.3)	10 (12.0)
Missing	-	1
NSCLC type per histological criteria, No. (%)		
Adenocarcinoma	71 (78.9)	67 (79.8)
Squamous cell	16 (17.8)	14 (16.7)
Other	1 (1.1)	2 (2.4)
Unknown	2 (2.2)	1 (1.2)
Disease stage		
IIIA	1 (1.1)	3 (3.6)
IIIB	11 (12.2)	6 (7.1)
IV	60 (66.7)	49 (58.3)
Recurrence	18 (20.0)	26 (31.0)
Time from diagnosis to starting study drug, mean ± SD, d	609.4 ± 741.7	768.7 ± 698.0
Previous history of chemotherapy (No. of times), No. (%)		
0	2 (2.2)	2 (2.4)
1	31 (34.4)	20 (23.8)
2	18 (20.0)	19 (22.6)
≥3	39 (43.3)	43 (51.2)
Concomitant cancer therapy, No. (%)		
Chemotherapy	70 (77.8)	64 (76.2)
EGFR TKI	29 (32.2)	23 (27.7)
Radiation	6 (6.7)	7 (8.3)
Supportive care	19 (21.1)	18 (21.7)
Missing	-	1

Abbreviations: BMC, bone mineral content; BMI, body mass index; DEXA, dual-energy x-ray absorptiometry; ECOG, Eastern Cooperative Oncology Group; EGFR, epidermal growth factor receptor; LBM, lean body mass; NSCLC, non–small cell lung cancer; PS, performance status; QOL-ACD, Quality-of-Life Questionnaire for Cancer Patients Treated With Anticancer Drugs (Kurihara Group Questionnaire); SD, standard deviation; TKI, tyrosine kinase inhibitor.

Safety

On the basis of the RECIST criteria, a complete response and a partial response were observed in 1 (1.5%) and 3 patients (4.5%), respectively, in the anamorelin-treated group and in 0 (0.0%) and 2 patients (2.7%), respectively, in the placebo group. Stable disease was observed in 21 (31.3%) and 22 patients (29.7%) in the anamorelin-treated and placebo groups, respectively. Thirty-eight of the anamorelin-treated patients (56.4%) showed progressive disease, whereas 47 patients (63.5%) in the placebo group did. Non–complete response/non–progressive disease cases were observed for 4 (6.0%) and 3 patients (4.1%) in the anamorelin-treated and placebo groups, respectively. The median survival times were found to be similar for the 2 groups (8.08 months [95% CI, 5.98-11.56 months] for anamorelin and 8.21 months [95% CI, 6.67-12.39 months] for the placebo; hazard ratio, 1.17 [95% CI, 0.82-1.67]; $P = .3762$).

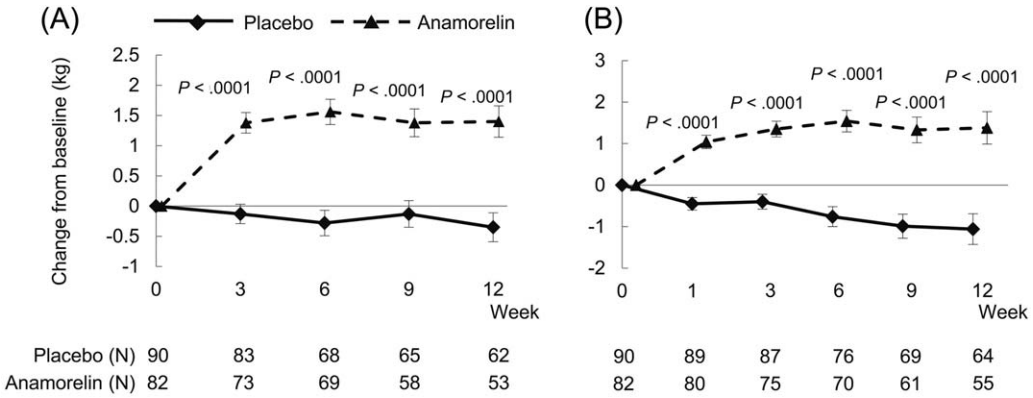

(C)

	Placebo (n = 90)	Anamorelin (n = 82)	P-value
Primary endpoint[a]			
Lean body mass (kg)	−0.17 ± 0.17	1.38 ± 0.18	<.0001
Secondary endpoints[a]			
Body weight (kg)	−0.50 ± 0.19	1.06 ± 0.20	<.0001
Appetite[b]	0.3 ± 0.1	0.7 ± 0.1	.0005
Cancer Fatigue Scale	1.4 ± 0.7	1.7 ± 0.7	.7170
Handgrip strength (kg)	−0.60 ± 0.28	0.05 ± 0.30	.0854
6-min walk distance (m)	11.7 ± 7.2	11.7 ± 7.8	.9987

[a]Least squares mean ± standard error for change from baseline over 12 weeks.
[b]Appetite was evaluated with QOL-ACD item 8 "Did you have a good appetite?"

Figure 2. Time-course changes for the anamorelin and placebo groups in (A) lean body mass and (B) body weight and (C) changes in primary and secondary efficacy measures from the baseline over 12 weeks. QOL-ACD indicates Quality-of-Life Questionnaire for Cancer Patients Treated With Anticancer Drugs.

Table 2 summarizes the overall incidences of AEs and ADRs. The frequency of AEs was found to be similar in the anamorelin group and the placebo group. On the other hand, the anamorelin group reported a significantly higher number of ADRs in comparison with the placebo group; however, all the ADRs were grade 3 or lower. The most common ADRs were first-degree atrioventricular block and rash, which were followed by increased γ-glutamyltransferase and diabetes mellitus. All these events were grade 1 or 2 except for 1 case of rash.

DISCUSSION

The current study demonstrated that anamorelin significantly improved LBM and body weight in Japanese patients with NSCLC and cachexia in comparison with a placebo. Significant improvements in LBM and body weight were observed in the anamorelin group at the early time points of week 3 and week 1, respectively, in comparison with the placebo group, and they were sustained thereafter during the 12-week study period.

The National Comprehensive Cancer Network clinical guidelines for the management of anorexia/cachexia define the primary treatment goals as promoting weight gain/stabilization and relieving symptoms of anorexia.[22] Similarly, the clinical practice guidelines on cancer cachexia given by the European Palliative Care Research Collaborative specify that the treatment goals for cachexia should be a reversal of the loss of body weight and muscle mass and that the minimum objective must be the maintenance of body weight and the prevention of further body weight loss.[23] The results of the current study satisfy the treatment goals in these guidelines.

As for appetite, a considerable increase was reported in the anamorelin group versus the placebo group as early as week 1, and it was subsequently sustained throughout the study period. The increased level of prealbumin, a nutritional state marker, suggested increased food intake. Decreases in appetite and food intake are considered to be the main underlying causes for the worsening of the physical and psychological status in cancer patients.[24] Anorexia leads to QOL deterioration in cancer patients[25] and is also a prognostic factor.[26] Therefore, oncologists should consider ensuring sufficient energy and protein intake for all cancer patients.[27]

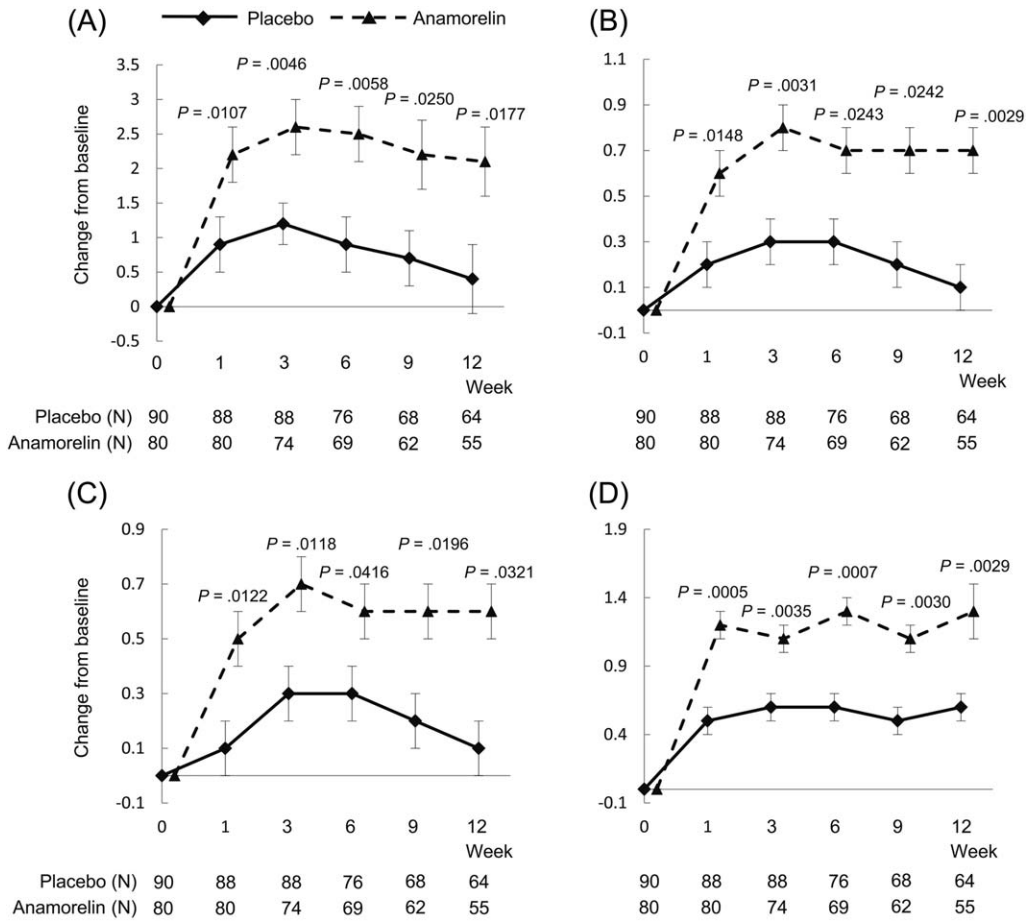

Figure 3. Time-course changes for the anamorelin and placebo groups in the QOL-ACD scores for (A) items 7 to 11 ("physical condition"), (B) item 8 ("Did you have a good appetite?"), (C) item 9 ("Did you enjoy your meals?"), and (D) item 11 ("Did you lose any weight?"). QOL-ACD indicates Quality-of-Life Questionnaire for Cancer Patients Treated With Anticancer Drugs.

Under the present conditions, where there are no effective treatment methods for cancer cachexia, anamorelin may have great clinical significance by preventing weight loss and ameliorating anorexia.

In contrast, in the assessment of motor function, including HGS and 6MWT results, no improvement was observed after anamorelin administration. Previous researchers have suggested that patients who are affected by long-term illness and systemic inflammation may display an unusual association between muscle mass and muscular strength.[28-30] Furthermore, the most suitable measure for muscle strength in advanced cancer patients is unidentified. The 6MWT measurements may have been affected by respiratory insufficiency in patients with NSCLC. The cause of cachexia is multifactorial, and pharmacological treatment alone may not be able to bring about a complete reversal of all features of the syndrome (especially improvements in motor function). Therefore, it is expected that a multimodal treatment combining medicine, exercise, and nutrition may improve the condition and symptoms of cachexia, including motor function.

In general, patients in the 2 treatment groups showed similar overall survival times and tumor responses as assessed by RECIST, and this indicated that the therapy had no effect on the progression of the disease. In addition, patient characteristics such as the disease stage and previous use of chemotherapy and prevailing factors that affect the prognosis were similar between the 2 treatment arms.

In comparison with patients receiving the placebo, the frequency of ADRs was significantly higher in patients receiving anamorelin; however, most deaths and treatment discontinuations were caused by disease progression and not by the study drugs. In comparison with the placebo-treated patients, first-degree atrioventricular

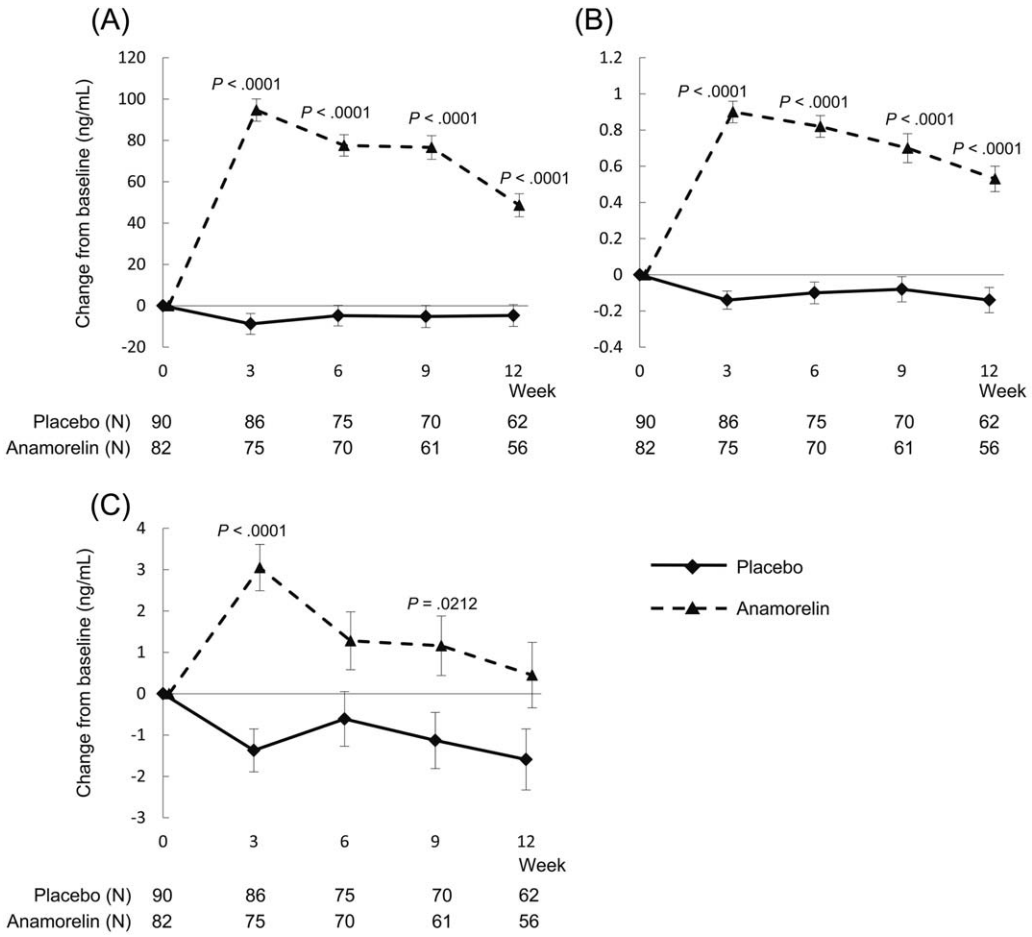

Figure 4. Time-course changes for the anamorelin and placebo groups in (A) insulin-like growth factor 1, (B) insulin-like growth factor-binding protein 3, and (C) prealbumin.

block and rash occurred at rates $\geq$ 5%, and they had a higher incidence in the anamorelin-treated patients. However, all first-degree atrioventricular block cases were grade 1, and only 1 case of rash was grade 3; this suggests no major risk. The frequencies of these ADRs were observed to be higher in the current study versus the multinational phase 3 studies.[19] The frequent electrocardiogram measurements might have caused the higher incidence of first-degree atrioventricular block. Although no apparent cause of rash has been identified, we think that there is a possibility that this might have been influenced by chemotherapy applied during the study. In agreement with previous studies,[19,20] increases in blood glucose levels were more frequently observed with anamorelin treatment; this was, however, controllable. The changes in glucose homeostasis might have been caused by effects of IGF-1 and growth hormone on glucose metabolism or by a possible effect of the reversal of cancer anorexia/cachexia syndrome. These findings suggest that anamorelin is safe and well tolerated in Japanese cancer patients with cachexia.

The current research had some shortcomings. First, we could not confirm the efficacy of anamorelin by functional measures of HGS and 6MWT. Second, its efficacy for fatigue was not confirmed. The lack of a treatment effect observed for CFS may have arisen because fatigue associated with cancer is a problematic manifestation to ameliorate in patients with advanced cancer and particularly in patients with more symptomatic disease.[31,32] This is partly due to the multiple and complex causes of fatigue, including chemotherapy, anemia, nutritional issues, and pain.[33]

The efficacy of anamorelin in the current study for increasing LBM and body weight and improving anorexia symptoms and the nutritional state with no improvement in motor function is consistent with the recent results of 2 multinational phase 3 studies with anamorelin.[19]

TABLE 2. Safety

	Placebo (n = 90)	Anamorelin (n = 83)
AEs, No. (%)	73 (81.1)	74 (89.2)
AEs		
Difference vs placebo, % (95% CI)		8.0 (–2.4, 18.5)
P		.1390
SAEs, No. (%)	8 (8.9)	16 (19.3)
Discontinuations due to AEs, No. (%)	2 (2.2)	3 (3.6)
ADRs, No. (%)	20 (22.2)	34 (41.0)
ADRs		
Difference vs placebo, % (95% CI)		18.7 (5.1, 32.4)
P		.0079
Serious ADRs, No. (%)	0 (0.0)	2 (2.4)
Discontinuations due to ADRs, No. (%)	1 (1.1)	2 (2.4)
Deaths, No. (%)	11 (12.2)	5 (6.0)
ADRs by grade, No. (%)		
1/2	18 (20.0)	28 (33.7)
3	2 (2.2)	6 (7.2)
ADRs in > 2% of patients, No. (%)		
First-degree atrioventricular block	0 (0.0)	5 (6.0)
Tachycardia	0 (0.0)	2 (2.4)
Edema	0 (0.0)	2 (2.4)
Peripheral edema	0 (0.0)	2 (2.4)
Pyrexia	0 (0.0)	2 (2.4)
γ-Glutamyltransferase increase	1 (1.1)	3 (3.6)
Glycosylated hemoglobin increase	1 (1.1)	2 (2.4)
Diabetes mellitus	0 (0.0)	3 (3.6)
Hyperglycemia	1 (1.1)	2 (2.4)
Headache	1 (1.1)	2 (2.4)
Rash	1 (1.1)	5 (6.0)
Hypertension	0 (0.0)	2 (2.4)
Hot flush	0 (0.0)	2 (2.4)

Abbreviations: ADR, adverse drug reaction; AE, adverse event; CI, confidence interval; SAE, severe adverse event.

Although anamorelin cannot improve motor function or survival, it may be of great importance for alleviating anorexia, a highly unmet medical need, to help patients with advanced cancer to enjoy their meals and thereby achieve better QOL.

On the basis of our findings, once daily administration of 100 mg of anamorelin showed favorable results for LBM gains in Japanese patients with NSCLC and cachexia; hence 100 mg could be the desired dose for such patients. Anamorelin therapy was associated with augmentation of IGF-1 and IGFBP-3 levels, and this suggests an increase in the synthesis of proteins that can have direct growth effects on skeletal muscle. Moreover, anamorelin was associated with favorable improvements in appetite and increases in prealbumin, and this indicates an improved nutritional status. Even though the incidences of ADRs and treatment discontinuations due to AEs were higher in the anamorelin group, most of the treatment discontinuations were associated with the progression of disease and not with anamorelin. The efficacy of anamorelin to improve LBM and anorexia was thus confirmed in Japanese patients with NSCLC and cachexia. Because no effective treatment for cancer cachexia is currently available, anamorelin can be one of the beneficial treatment options.

FUNDING SUPPORT

The study sponsor, Ono Pharmaceutical Co, Ltd (Osaka, Japan), was involved in the study design, provision of study materials, data collection and interpretation, and writing of the report.

CONFLICT OF INTEREST DISCLOSURES

Nobuyuki Katakami reports personal fees from AstraZeneca, Eli Lilly, Pfizer, Boehringer Ingelheim, Ono, Taiho, and Novartis Pharma KK and grants from MSD, Astellas, AstraZeneca, Eisai, Amgen, Shionogi, Daiichi Sankyo, Chugai, Eli Lilly, Boehringer Ingelheim, Bristol-Myers Squibb, Maruishi, and Merck Serono outside the submitted work. Tateaki Naito reports personal fees from Ono during the conduct of the study. Masashi Kondo reports personal fees from Ono, Chugai, Pfizer, Novartis, Eli Lilly, Taiho, and AstraZeneca and grants from Eli Lilly outside the submitted work. Hiroshi Saito reports personal fees from Ono during the conduct of the study; grants from Taiho and Merck Serono outside the submitted work; and personal fees from Pfizer, AstraZeneca, and Kyowa Hakko Kirin outside the submitted work. Yuichi Takiguchi reports grants and personal fees from Ono, AstraZeneca, Taiho, Nippon Boehringer Ingelheim, and Chugai outside the submitted work. Koichi Takayama reports personal fees from Ono during the conduct of the study and personal fees from AstraZeneca, Eli Lilly,

Chugai, and Ono outside the submitted work. Naoyuki Komura and Toru Takiguchi are employees of Ono. Kenji Eguchi reports grants from Ono outside the submitted work.

AUTHOR CONTRIBUTIONS

Nobuyuki Katakami: Conception and design, acquisition of data, data analysis and interpretation, manuscript writing, and final approval of manuscript. **Junji Uchino**: Acquisition of data, manuscript writing, and final approval of manuscript. **Takuma Yokoyama**: Acquisition of data, manuscript writing, and final approval of manuscript. **Tateaki Naito**: Acquisition of data, manuscript writing, and final approval of manuscript. **Masashi Kondo**: Acquisition of data, manuscript writing, and final approval of manuscript. **Kouzo Yamada**: Acquisition of data, manuscript writing, and final approval of manuscript. **Hiromoto Kitajima**: Acquisition of data, manuscript writing, and final approval of manuscript. **Kozo Yoshimori**: Acquisition of data, manuscript writing, and final approval of manuscript. **Kazuhiro Sato**: Acquisition of data, manuscript writing, and final approval of manuscript. **Hiroshi Saito**: Conception and design, acquisition of data, data analysis and interpretation, manuscript writing, and final approval of manuscript. **Keisuke Aoe**: Conception and design, acquisition of data, data analysis and interpretation, manuscript writing, and final approval of manuscript. **Tetsuya Tsuji**: Conception and design, data analysis and interpretation, manuscript writing, and final approval of manuscript. **Yuichi Takiguchi**: Conception and design, acquisition of data, data analysis and interpretation, manuscript writing, and final approval of manuscript. **Koichi Takayama**: Conception and design, data analysis and interpretation, manuscript writing, and final approval of manuscript. **Naoyuki Komura**: Conception and design, data analysis and interpretation, manuscript writing, and final approval of manuscript. **Toru Takiguchi**: Conception and design, data analysis and interpretation, manuscript writing, and final approval of manuscript. **Kenji Eguchi**: Conception and design, data analysis and interpretation, manuscript writing, and final approval of manuscript.

REFERENCES

1. Bruera E. ABC of palliative care. Anorexia, cachexia, and nutrition. *BMJ.* 1997;315:1219-1222.
2. Dewys WD, Begg C, Lavin PT, et al. Prognostic effect of weight loss prior to chemotherapy in cancer patients. Eastern Cooperative Oncology Group. *Am J Med.* 1980;69:491-497.
3. Reuben DB, Mor V, Hiris J. Clinical symptoms and length of survival in patients with terminal cancer. *Arch Intern Med.* 1988;148: 1586-1591.
4. von Haehling S, Anker SD. Treatment of cachexia: an overview of recent developments. *J Am Med Dir Assoc.* 2014;15:866-872.
5. von Haehling S, Anker SD. Prevalence, incidence and clinical impact of cachexia: facts and numbers—update 2014. *J Cachexia Sarcopenia Muscle.* 2014;5:261-263.
6. Fearon K, Arends J, Baracos V. Understanding the mechanisms and treatment options in cancer cachexia. *Nat Rev Clin Oncol.* 2013;10: 90-99.
7. von Haehling S, Anker SD. Cachexia as a major underestimated and unmet medical need: facts and numbers. *J Cachexia Sarcopenia Muscle.* 2010;1:1-5.
8. Fearon K, Strasser F, Anker SD, et al. Definition and classification of cancer cachexia: an international consensus. *Lancet Oncol.* 2011; 12:489-495.
9. Neary NM, Small CJ, Wren AM, et al. Ghrelin increases energy intake in cancer patients with impaired appetite: acute, randomized, placebo-controlled trial. *J Clin Endocrinol Metab.* 2004;89:2832-2836.
10. Wren AM, Seal LJ, Cohen MA, et al. Ghrelin enhances appetite and increases food intake in humans. *J Clin Endocrinol Metab.* 2001;86: 5992.
11. Akamizu T, Takaya K, Irako T, et al. Pharmacokinetics, safety, and endocrine and appetite effects of ghrelin administration in young healthy subjects. *Eur J Endocrinol.* 2004;150:447-455.
12. Kojima M, Hosoda H, Date Y, Nakazato M, Matsuo H, Kangawa K. Ghrelin is a growth-hormone–releasing acylated peptide from stomach. *Nature.* 1999;402:656-660.
13. Smith RG, Cheng K, Schoen WR, et al. A nonpeptidyl growth hormone secretagogue. *Science.* 1993;260:1640-1643.
14. Currow DC, Abernethy AP. Anamorelin hydrochloride in the treatment of cancer anorexia-cachexia syndrome. *Future Oncol.* 2014;10: 789-802.
15. Zhang H, Garcia JM. Anamorelin hydrochloride for the treatment of cancer-anorexia-cachexia in NSCLC. *Expert Opin Pharmacother.* 2015;16:1245-1253.
16. Garcia JM, Friend J, Allen S. Therapeutic potential of anamorelin, a novel, oral ghrelin mimetic, in patients with cancer-related cachexia: a multicenter, randomized, double-blind, crossover, pilot study. *Support Care Cancer.* 2013;21:129-137.
17. Garcia JM, Polvino WJ. Effect on body weight and safety of RC-1291, a novel, orally available ghrelin mimetic and growth hormone secretagogue: results of a phase I, randomized, placebo-controlled, multiple-dose study in healthy volunteers. *Oncologist.* 2007;12:594-600.
18. Garcia JM, Polvino WJ. Pharmacodynamic hormonal effects of anamorelin, a novel oral ghrelin mimetic and growth hormone secretagogue in healthy volunteers. *Growth Horm IGF Res.* 2009;19:267-273.
19. Temel JS, Abernethy AP, Currow DC, et al. Anamorelin in patients with non–small-cell lung cancer and cachexia (ROMANA 1 and ROMANA 2): results from two randomised, double-blind, phase 3 trials. *Lancet Oncol.* 2016;17:519-531.
20. Takayama K, Katakami N, Yokoyama T, et al. Anamorelin (ONO-7643) in Japanese patients with non–small cell lung cancer and cachexia: results of a randomized phase 2 trial. *Support Care Cancer.* 2016;24:3495-3505.
21. Matsumoto T, Ohashi Y, Morita S, et al. The Quality of Life Questionnaire for Cancer Patients Treated With Anticancer Drugs (QOL-ACD): validity and reliability in Japanese patients with advanced non–small-cell lung cancer. *Qual Life Res.* 2002;11:483-493.
22. National Comprehensive Cancer Network. NCCN clinical practice guidelines in oncology: palliative care. http://www.nccn.org/professionals/physician_gls/f_guidelines.asp. Accessed December 28, 2016.
23. Radbruch L, Elsner F, Trottenberg P, Strasser F, Fearon K. Clinical Practice Guidelines on Cancer Cachexia in Advanced Cancer Patients With a Focus on Refractory Cachexia. Aachen, Germany: European Palliative Care Research Collaborative; 2010.
24. Piil K, Juhler M, Jakobsen J, Jarden M. Controlled rehabilitative and supportive care intervention trials in patients with high-grade gliomas and their caregivers: a systematic review. *BMJ Support Palliat Care.* 2016;6:27-34.
25. Takayama K, Atagi S, Imamura F, et al. Quality of life and survival survey of cancer cachexia in advanced non–small cell lung cancer patients—Japan nutrition and QOL survey in patients with advanced non–small cell lung cancer study. *Support Care Cancer.* 2016;24: 3473-3480.
26. Quinten C, Coens C, Mauer M, et al. Baseline quality of life as a prognostic indicator of survival: a meta-analysis of individual patient data from EORTC clinical trials. *Lancet Oncol.* 2009;10:865-871.
27. Aapro M, Arends J, Bozzetti F, et al. Early recognition of malnutrition and cachexia in the cancer patient: a position paper of a European School of Oncology task force. *Ann Oncol.* 2014;25:1492-1499.
28. Chen L, Nelson DR, Zhao Y, Cui Z, Johnston JA. Relationship between muscle mass and muscle strength, and the impact of comorbidities: a population-based, cross-sectional study of older adults in the United States. *BMC Geriatr.* 2013;13:74.

29. Dobs AS, Boccia RV, Croot CC, et al. Effects of enobosarm on muscle wasting and physical function in patients with cancer: a double-blind, randomised controlled phase 2 trial. *Lancet Oncol.* 2013;14:335-345.
30. Park SW, Goodpaster BH, Strotmeyer ES, et al. Decreased muscle strength and quality in older adults with type 2 diabetes: the Health, Aging, and Body Composition Study. *Diabetes.* 2006;55:1813-1818.
31. Jean-Pierre P, Morrow GR, Roscoe JA, et al. A phase 3 randomized, placebo-controlled, double-blind, clinical trial of the effect of modafinil on cancer-related fatigue among 631 patients receiving chemotherapy: a University of Rochester Cancer Center Community Clinical Oncology Program Research Base study. *Cancer.* 2010;116:3513-3520.
32. Minton O, Berger A, Barsevick A, et al. Cancer-related fatigue and its impact on functioning. *Cancer.* 2013;119(suppl 11):2124-2130.
33. Neefjes EC, van der Vorst MJ, Blauwhoff-Buskermolen S, Verheul HM. Aiming for a better understanding and management of cancer-related fatigue. *Oncologist.* 2013;18:1135-1143.

Histopathology 2016 DOI: 10.1111/his.13073

Utility and pitfalls of immunohistochemistry in the differential diagnosis between epithelioid mesothelioma and poorly differentiated lung squamous cell carcinoma

Kei Kushitani,[1] Vishwa J Amatya,[1] Yasuko Okada,[2] Yuya Katayama,[2] Amany S Mawas,[1,3] Yoshihiro Miyata,[4] Morihito Okada,[4] Kouki Inai,[1,5] Takumi Kishimoto[6] & Yukio Takeshima[1]

[1]*Department of Pathology, Institute of Biomedical and Health Sciences, Hiroshima University, Hiroshima, Japan,* [2]*Faculty of Medicine, Hiroshima University, Hiroshima, Japan,* [3]*Department of Pathology and Clinical Pathology, Faculty of Veterinary Medicine, South Valley University, Qena, Egypt,* [4]*Department of Surgical Oncology, Research Centre for Radiation Casualty Medicine, Research Institute for Radiation Biology and Medicine, Hiroshima University, Hiroshima, Japan,* [5]*Pathologic Diagnostic Centre, Inc., Hiroshima, Japan, and* [6]*Department of Internal Medicine, Okayama Rosai Hospital, Okayama, Japan*

Date of submission 30 June 2016
Accepted for publication 30 August 2016
Published online *Article Accepted* 2 September 2016

Kushitani K, Amatya V J, Okada Y, Katayama Y, Mawas A S, Miyata Y, Okada M, Inai K, Kishimoto T & Takeshima Y

(2016) *Histopathology*. DOI: 10.1111/his.13073

Utility and pitfalls of immunohistochemistry in the differential diagnosis between epithelioid mesothelioma and poorly differentiated lung squamous cell carcinoma

Aims: The aims of this study were to clarify the usefulness of immunohistochemistry in the differential diagnosis of epithelioid mesothelioma with a solid growth pattern [solid epithelioid mesothelioma (SEM)] and poorly differentiated squamous cell carcinoma (PDSCC), and to confirm the validity of a specific type of antibody panel. Additionally, we aimed to clarify the pitfalls of immunohistochemical analyses.

Methods and results: Formalin-fixed paraffin-embedded specimens from 36 cases of SEM and 38 cases of PDSCC were immunohistochemically examined for calretinin, podoplanin (D2-40), Wilms' tumour gene product (WT1), cytokeratin (CK) 5/6, p40, p63, carcinoembryonic antigen (CEA), epithelial-related antigen (MOC31), claudin-4, thyroid transcription factor-1 (TTF-1), and napsin A. WT1 showed the highest diagnostic accuracy (85.1%) as a mesothelial marker, and CEA, p40 and claudin-4 showed higher diagnostic accuracies (95.9%, 94.6%, and 93.2%, respectively) as carcinoma markers. Calretinin (diagnostic accuracy: 75.7%), D2-40 (diagnostic accuracy: 67.6%), CK5/6 (diagnostic accuracy: 63.5%), TTF-1 (diagnostic accuracy: 55.4%) and napsin A (diagnostic accuracy: 52.7%) could not differentiate between SEM and PDSCC. Among these markers, the combination of calretinin and WT1 showed the highest diagnostic accuracy (86.5%) as a positive marker, and the combination of p40 and CEA showed the highest diagnostic accuracy (97.3%) as a negative marker. The combination of CEA and claudin-4 also showed relatively high diagnostic accuracy (94.6%) as a negative marker.

Conclusions: We recommend the combination of WT1 and calretinin as a positive maker, and the combination of CEA and claudin-4 as a negative marker, for differential diagnoses of SEM and PDSCC.

Keywords: calretinin, carcinoembryonic antigen, claudin-4, immunohistochemistry, mesothelioma, p40, squamous cell carcinoma, WT1 protein

Introduction

Malignant mesothelioma (MM) is a rare, aggressive malignant neoplasm that most commonly arises from

Address for correspondence: Yukio Takeshima, MD, PhD, 1-2-3 Kasumi, Minami-ku, Hiroshima 734-8551, Japan. e-mail: ykotake@hiroshima-u.ac.jp

pleural mesothelial cells. MM is correlated with occupational and environmental asbestos exposure.[1–5] As the incidence of MM has increased in many countries, pathologists encounter this disease frequently. In Japan, the death toll from MM has been increasing since the 1990s, and it is predicted to peak in the 2030s.[6]

A diffuse pleurotropic growth pattern is characteristic of MM.[7,8] However, a number of non-mesotheliomatous neoplasms showing diffuse pleurotropic growth patterns (described as 'pseudomesotheliomatous growth') have been reported, and most of these tumours are peripheral lung carcinomas.[9–13] Although the majority of pseudomesotheliomatous lung carcinomas are adenocarcinomas (ACs), a few pseudomesotheliomatous pulmonary squamous cell carcinoma (SCC) cases have also been reported.[14] Lately, the incidence of peripheral-type pulmonary SCC, but not central SCC, has been increasing.[15,16] Thus, the chance of encountering 'pseudomesotheliomatous' SCCs might increase. Additionally, MM may occur as a localized mass similar to peripheral lung cancer and other pleural tumours; it is then classified as 'localized MM' according to the new World Health Organization (WHO) classification.[7] Therefore, the histopathological differential diagnosis of MM and SCC will become crucial in the future.

Malignant mesotheliomas are divided into three major histological subtypes: epithelioid, sarcomatoid, and biphasic. Among these, epithelioid mesothelioma (EM) shows a wide range of histological and cytological patterns, such as papillary, tubular, solid, clear cell, deciduoid, rhabdoid, and pleomorphic.[17] Poorly differentiated SCC (PDSCC) shows a nested, sheet-like or cord-like histological pattern, and lacks obvious keratinization and/or intercellular bridges in some parts of or throughout the tumour.[18] Therefore, the differential diagnosis between EM showing a solid histological pattern [solid EM (SEM)] and PDSCC can be challenging with conventional light microscopy (haematoxylin and eosin-stained specimen) alone.

The role of immunohistochemistry in distinguishing pleural EM from pulmonary AC has received much attention. Currently, many immunohistochemical markers are available for distinguishing pleural EM from pulmonary AC. Among these, calretinin, cytokeratin (CK) 5/6, podoplanin (D2-40) and Wilms' tumour gene product (WT1) are regarded as the best positive markers for EM, and carcinoembryonic antigen (CEA), MOC31 [epithelial-related antigen (ERA)], Ber-EP4, BG-8, thyroid transcription factor-1 (TTF)-1, and napsin A are regarded as the best positive markers for lung AC.[19–22]

However, there are only a few reports on the immunohistochemical differential diagnosis of EM and lung SCC. Ordonez *et al.* have reported the immunohistochemical analyses of 30 EMs showing a solid pattern and 30 pulmonary non-keratinizing SCCs, and have recommended the combination of two positive (WT1 and calretinin/mesothelin) and two negative (p63 and ERA) markers for differentiating EM from lung SCC.[23]

Here, we examined 11 commercially available immunohistochemical markers in histological specimens of SEM and PDSCC obtained from Japanese cases. We aimed to evaluate the usefulness of immunohistochemistry in differentiating SEM from PDSCC, and to recommend the best antibody panel for use in pathological laboratories, after considering the pitfalls of immunohistochemical analyses.

Materials and methods

PATIENTS AND HISTOLOGICAL SAMPLES

We used formalin-fixed paraffin-embedded (FFPE) specimens from 36 patients with a definite histological diagnosis of SEM who had undergone pleural biopsy, pleurectomy/decortication, extrapleural pneumonectomy or autopsy between 2000 and 2014.

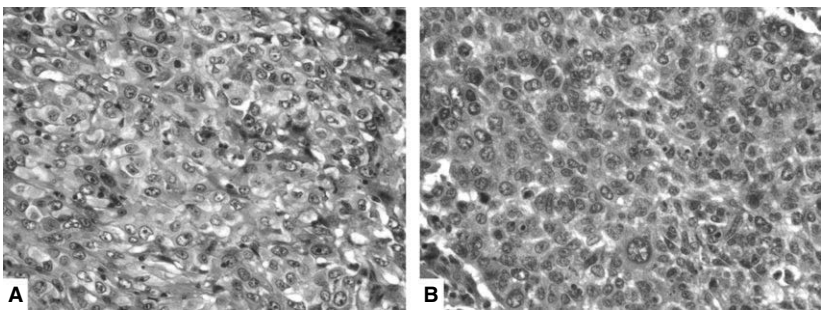

Figure 1. Representative histological images of solid epithelioid mesothelioma and poorly differentiated squamous cell carcinoma. (**A**) Solid epithelioid mesothelioma. (**B**) Poorly differentiated squamous cell carcinoma.

SEM was defined as 'EM consisting of mainly solid, sheet-like or cord-like proliferations of cuboidal or polygonal epithelioid cells' (Figure 1A). All SEM cases used in this study were comprehensively diagnosed according to a combination of clinical history (e.g. occupational asbestos exposure), radiographic examination (e.g. diffuse pleurotropic growth pattern, lack of intrapulmonary mass, or the presence of pleural plaques), and histopathological findings. In all cases, we performed immunohistochemical investigation with 15–20 markers, including the 11 markers examined in this study.

Formalin-fixed paraffin-embedded histological samples of the surgical specimens from 38 patients with a histological diagnosis of primary pulmonary PDSCC were obtained by surgical resection (wedge resection, segmentectomy, lobectomy, or pneumonectomy) from 2000 to 2014. PDSCC included keratinizing SCC with minimal squamous differentiation (keratinization and/or intercellular bridge) and non-keratinizing SCC, as defined in the WHO 2015 criteria (Figure 1B).[24] The samples were collected from the archives of the Department of Pathology at Hiroshima University. Among 38 PDSCCs that we examined, 34 were of the peripheral type, and four were of the central type. Ten cases showed invasion to the visceral pleura but not right through and exposed on the surface of the pleura, seven cases showed focal invasion to the parietal pleura or chest wall, and 21 cases were intrapulmonary lesions without pleural invasion. There was no case showing diffuse pleurotropic growth.

Each tumour specimen was reviewed by three pathologists (K.K., V.J.A., and Y.T.); all of the cases were rediagnosed on the basis of the currently accepted histological criteria.[17,18]

This study was performed in accordance with the Ethics Guidelines for Human Genome/Gene Research enacted by the Japanese government for the collection of tissue specimens, and was approved by the institutional ethics review committee (Hiroshima University E-48).

IMMUNOHISTOCHEMICAL PROCEDURES

Immunohistochemical staining of sections from the FFPE tissue samples was performed with Ventana BenchMark GX (Roche Diagnostics, Basel, Switzerland), by use of the Ventana ultraView Universal DAB Detection Kit; the staining procedure is based on the indirect biotin-free system. Protocols involving heat induction-based or protease digestion-based antigen retrieval were performed as recommended by the manufacturer, with some modifications. Table 1 shows the list of primary antibodies, clones, sources, and antibody dilutions.

Table 1. Primary antibodies used in this study

Marker	Clone	Manufacturer	Dilution	Location of evaluation
Calretinin	SP65	Ventana	Prediluted	Nucleus
Podoplanin	D2-40	Nichirei Bioscience	Prediluted	Membrane
WT1	6F-H2	Ventana	Prediluted	Nucleus
CK5/6	D5/16 B4	Dako	1:25	Membrane and/or cytoplasm
p40	BC28	Biocare Medical	1:100	Nucleus
p63	DAK-p63	Dako	1:25	Nucleus
CEA	COL-1	Nichirei Bioscience	Prediluted	Membrane and/or cytoplasm
ERA	MOC31	Dako	1:25	Membrane
Claudin-4	3E2C1	Life Technologies	1:100	Membrane
TTF-1	SPT24	Nichirei Bioscience	Prediluted	Nucleus
Napsin A	MRQ-60	Ventana	Prediluted	Cytoplasm

CEA, carcinoembryonic antigen; CK, cytokeratin; ERA, epithelial-related antigen; TTF-1, thyroid transcription factor-1; WT1, Wilms' tumour gene product.

Immunoreactivity was scored as either negative (no immunostaining) or positive. Cells showing nuclear staining for calretinin, WT1, p40, p63, and TTF-1, membranous staining for podoplanin, ERA, and claudin-4, cytoplasmic staining for napsin A or membranous and/or cytoplasmic staining for CK5/6 and CEA were regarded as 'positive'. The immunoreactivity grade was semiquantified as follows: 0, 0% positive cells or trace staining; 1+, 1–10% positive cells; 2+, 11–50% positive cells; and 3+, >51% positive cells.

EVALUATION OF UTILITY OF EACH MARKER AND COMBINATIONS OF TWO MARKERS

Sensitivity, specificity, positive predictive values (PPVs), negative predictive values (NPVs) and diagnostic accuracies were calculated for each marker and combination of two markers.

Results

IMMUNOREACTIVITY OF ANTIBODIES FOR SEM AND PDSCC

The detection rates of each antibody in SEM and PDSCC are shown in Table 2. Representative immunohistochemical staining images for SEM and PDSCC are shown in Figures 2 and 3, respectively. The staining pattern for each antibody for the two tumour types is described in the following paragraphs.

CALRETININ

Thirty-three of 36 SEMs (91.7%) and 15 of 38 PDSCCs (39.5%) were positive for calretinin. In SEMs, immunoreactivity was generally strong and diffuse (grade 3+). In contrast, in PDSCCs, the staining grade was distributed from 1+ to 3+ approximately equally.

D2-40

Thirty-five of 36 SEMs (97.2%) and 23 of 28 PDSCCs (60.5%) were positive for D2-40. In the majority of SEMs, immunoreactivity was strong and diffuse (grade 3+), whereas the majority of PDSCCs showed a focal or multifocal positive pattern (grade 1+/2+).

WT1

Twenty-six of 36 SEMs (72.2%) were positive for WT1, with most of them showing grade 3+, whereas only one PDSCC (2.6%) was focally positive (grade 1+) for WT1.

CK5/6

Twenty-six of 36 (72.2%) of SEMs and 37 of 38 (97.4%) of PDSCCs were positive for CK5/6. For both tumours, the majority of cases showed diffuse and strong immunoreactivity (grade 3+).

P40

Only two SEMs (5.6%) were positive for p40, and staining was observed in an extremely confined area (grade 1+). In contrast, 36 of 38 PDSCCs (94.7%) were positive for p40, and most cases showed diffuse and strong immunoreactivity (grade 3+).

Table 2. Immunohistochemical findings for solid epithelioid mesothelioma (SEM) and poorly differentiated squamous cell carcinoma (PDSCC) for various antibodies

		SEM staining grade					PDSCC staining grade			
Marker	SEM, *n* (%)	0	1+	2+	3+	PDSCC, *n* (%)	0	1+	2+	3+
Calretinin	33/36 (91.7)	3	0	2	31	15/38 (39.5)	23	7	4	4
D2-40	35/36 (97.2)	1	3	2	30	23/38 (60.5)	15	5	12	6
WT1	26/36 (72.2)	10	5	3	18	1/38 (2.6)	37	1	0	0
CK5/6	26/36 (72.2)	10	5	6	15	37/38 (97.4)	1	2	6	29
p40	2/36 (5.6)	34	2	0	0	36/38 (94.7)	2	0	4	32
p63	6/36 (16.7)	30	5	0	1	37/38 (97.4)	1	1	2	34
CEA	0/36 (0)	36	0	0	0	35/38 (92.1)	3	14	13	8
ERA	12/36 (33.3)	24	8	3	1	34/38 (89.5)	4	5	11	18
Claudin-4	2/36 (5.6)	34	2	0	0	35/38 (92.1)	3	3	17	15
TTF-1	0/36 (0)	36	0	0	0	5/38 (13.2)	33	5	0	0
Napsin A	0/36 (0)	36	0	0	0	3/38 (7.9)	35	3	0	0

CEA, carcinoembryonic antigen; CK, cytokeratin; ERA, epithelial-related antigen; TTF-1, thyroid transcription factor-1; WT1, Wilms' tumour gene product.
The grade of immunoreactivity was semiquantified as follows: 0, 0% positive cells or trace staining; 1+, 1–10% positive cells; 2+, 11–50% positive cells; 3+, >51% positive cells.

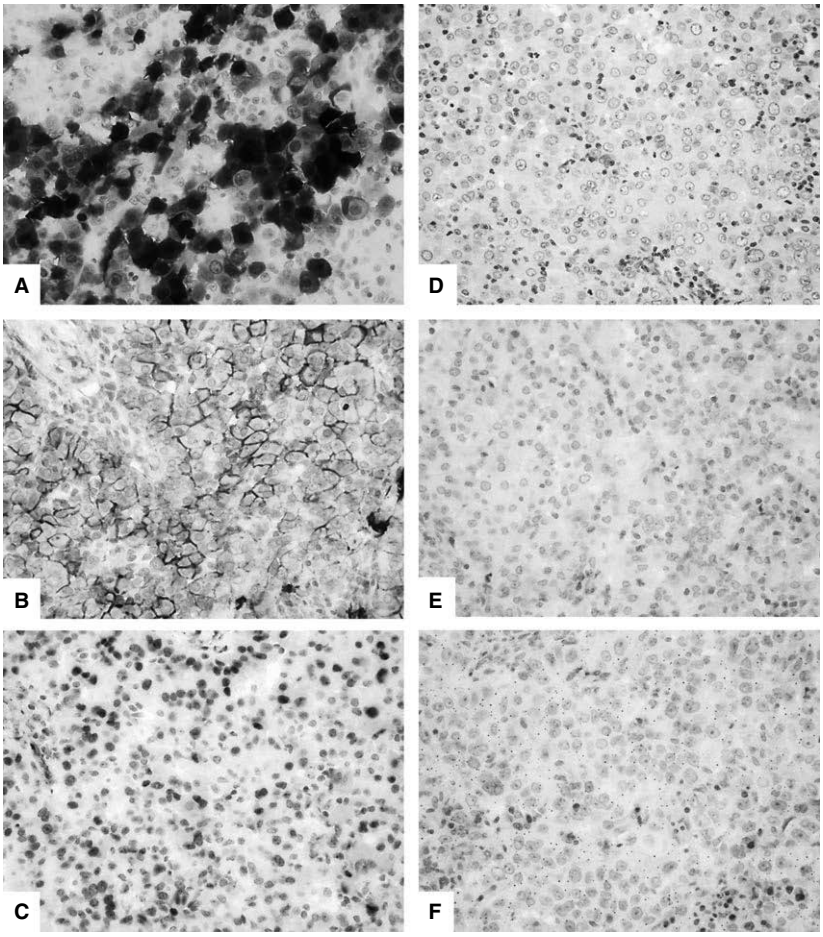

Figure 2. Representative immunohistochemical staining panel for solid epithelioid mesothelioma. The mesothelioma cells showed positivity for calretinin (nuclear) (**A**), D2-40 (membranous) (**B**), and Wilms' tumour gene product (nuclear) (**C**), but were negative for carcinoembryonic antigen (**D**), p40 (**E**), and claudin-4 (**F**).

P63

Six of 36 SEMs (16.7%) were positive for p63, and most of them showed staining in an extremely confined area (grade 1+). However, one SEM showed diffuse and strong immunoreactivity (grade 3+). In contrast, 37 of 38 PDSCCs (97.4%) were positive for p63, and most of them showed diffuse and strong immunoreactivity (grade 3+).

CEA

None of the SEMs were positive CEA. In contrast, 92.1% of PDSCCs were positive for CEA. However, in the majority of the CEA-positive PDSCCs, staining was limited to ≤50% of the tumour cells (grades 1+ and 2+).

ERA

Approximately 33.3% of SEMs and 89.5% of PDSCCs were positive for ERA. In the majority of the ERA-positive SEMs, staining was limited to ≤50% of the tumour cells (grades 1+ and 2+). In contrast, approximately half of the ERA-positive PDSCCs showed diffuse and strong immunoreactivity (grade 3+).

CLAUDIN-4

Only two SEMs (5.6%) were positive for claudin-4, and staining was observed in an extremely confined area (grade 1+). In contrast, 35 of 38 PDSCCs (92.1%) were positive for claudin-4, and, in most of them, staining was observed in ≥10% of the tumour cells (grade 2+ or 3+).

TTF-1 AND NAPSIN A

None of the SEMs were positive for TTF-1 or napsin A; five PDSCCs that were positive for TTF-1 and three PDSCCs that were positive for napsin A showed focal immunoreactivity (grade 1+).

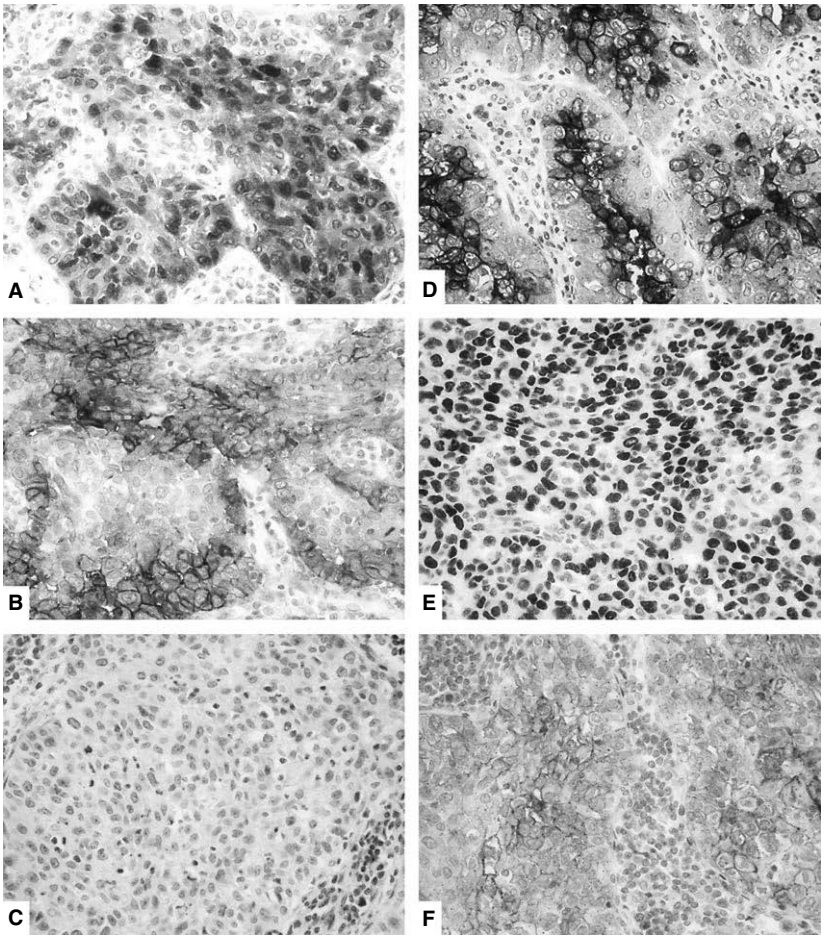

Figure 3. Representative immunohistochemical staining panel for poorly differentiated squamous cell carcinoma. The carcinoma cells were positive for calretinin (nuclear) (**A**), D2-40 (membranous) (**B**), carcinoembryonic antigen (cytoplasmic) (**D**), p40 (nuclear) (**E**), and claudin-4 (membranous) (**F**), but negative for Wilms' tumour gene product (**C**).

SENSITIVITY, SPECIFICITY, PPVS, NPVS AND DIAGNOSTIC ACCURACIES OF EACH ANTIBODY FOR DIFFERENTIAL DIAGNOSIS BETWEEN SEM AND PDSCC

The sensitivity, specificity, PPVs, NPVs and diagnostic accuracies of each marker and combination of two markers for the differential diagnosis between SEM and PDSCC are shown in Tables 3–5.

For SEM, WT1 as a positive marker and p40, p63, CEA and claudin-4 as negative markers showed relatively high diagnostic accuracy (>80%). Among the 11 antibodies evaluated, that for CEA showed the highest sensitivity, NPV and diagnostic accuracy (Table 3).

Among the combinations of two markers, the combination of calretinin and WT1 (both calretinin positivity and WT1 positivity) showed the highest specificity, PPV and diagnostic accuracy as a positive marker (Table 4), and the combination of p40 and CEA (both p40 negativity and CEA negativity) showed the highest specificity, PPV and diagnostic accuracy as a negative marker (Table 5).

Discussion

Here, we used various commercially available markers to differentiate SEM with a solid growth pattern from PDSCC showing minimal or no keratinization, and attempted to identify the best antibody panel for differentiating SEM and PDSCC, with their pitfalls in interpretation. We found that WT1 had the highest diagnostic accuracy as a positive marker, and that CEA, p40, p63 and claudin-4 showed high diagnostic accuracies as negative markers (>90%).

Wilms' tumour gene product encodes a zinc-finger transcription factor that controls the expression of many growth factors and their receptors.[25] Nuclear immunoreactivity for WT1 has been reported in 43–100% of EMs,[20–22,26] whereas it is negligibly expressed in pulmonary ACs and SCCs.[20,21,23,27] In

Table 3. Sensitivity, specificity, positive predictive values (PPVs), negative predictive values (NPVs) and diagnostic accuracies of each antibody for the differential diagnosis between solid epithelioid mesothelioma and non-keratinizing squamous cell carcinoma

Immunohistochemical findings	Sensitivity (%)	Specificity (%)	PPV (%)	NPV (%)	Diagnostic accuracy (%)
Calretinin-positive	91.7	60.5	68.8	88.5	75.7
D2-40-positive	97.2	39.5	60.3	93.8	67.6
WT1-positive	72.2	97.4	96.3	78.7	85.1
CK5/6-positive	72.2	2.6	41.3	9.1	36.5
p40-negative	94.4	94.7	94.4	94.7	94.6
p63-negative	83.3	97.4	96.8	86.0	90.5
CEA-negative	100	92.1	92.3	100	95.9
ERA-negative	66.7	89.5	85.7	73.9	78.4
Claudin-4-negative	94.4	92.1	91.9	94.6	93.2
TTF-1-negative	100	13.2	52.2	100	55.4
Napsin A-negative	100	7.9	50.7	100	52.7

CEA, carcinoembryonic antigen; CK, cytokeratin; WT1, TTF-1, thyroid transcription factor-1; Wilms' tumour gene product.

Table 4. Sensitivity, specificity, positive predictive values (PPVs), negative predictive values (NPVs) and diagnostic accuracies of combinations of two positive markers for the differential diagnosis between solid epithelioid mesothelioma and non-keratinizing squamous cell carcinoma

Combination of two markers	Sensitivity (%)	Specificity (%)	PPV	NPV	Diagnostic accuracy
Calretinin-positive and D2-40-positive	88.9	73.7	76.2	87.5	81.1
Calretinin-positive or D2-40-positive	100	26.3	56.3	100	62.2
Calretinin-positive and WT1-positive	72.2	100	100	79.2	86.5
Calretinin-positive or WT1-positive	91.7	57.9	67.3	88	74.3
D2-40-positive and WT1-positive	72.2	97.4	96.3	78.7	85.1
D2-40-positive or WT1-positive	97.2	39.5	60.3	93.8	67.6

WT1, Wilms' tumour gene product.

this study, although the sensitivity of WT1 (72.2%) was the lowest among the positive markers, its high specificity (97.4%) and the fact that it showed the highest diagnostic accuracy (85.1%) among three positive markers (calretinin, D2-40, and WT1) for differentiating SEM from PDSCC led us to consider WT1 as the best positive marker. Previously, Ordonez *et al.* had reported WT1 positivity in 93% (28 of 30 cases) of the EMs studied.[23] In this study, 72.2% of EMs tested positive for WT1, which is lower than the positivity percentage reported by Ordonez *et al.* Differences in the source of the primary antibody or staining system might explain this discrepancy. The positivity rate for WT1 in SEMs in this study was similar to that observed in our previous studies on EMs with a tubulopapillary pattern,[20,21] indicating that the WT1 positivity rate is not different between tubulopapillary and solid EMs. Additionally, we

Table 5. Sensitivity, specificity, positive predictive values (PPVs), negative predictive values (NPVs) and diagnostic accuracies of combinations of two negative markers for the differential diagnosis between solid epithelioid mesothelioma and non-keratinizing squamous cell carcinoma

Combination of two markers	Sensitivity (%)	Specificity (%)	PPV (%)	NPV (%)	Diagnostic accuracy (%)
p40-negative and CEA-negative	94.4	100	100	95	97.3
p40-negative or CEA-negative	100	86.8	87.8	100	93.2
p40-negative and claudin-4-negative	91.7	100	100	92.7	95.9
p40-negative or claudin-4-negative	100	86.8	87.8	100	93.2
CEA-negative and claudin-4-negative	94.4	94.7	94.4	94.7	94.6
CEA-negative or claudin-4-negative	100	89.5	90	100	94.6

CEA, carcinoembryonic antigen.

detected positivity in the endothelium of blood vessels in the same sections of SEM, which excludes the possibility of false-negative results.

Calretinin is a 29-kDa, calcium-binding protein involved in calcium signalling, and is strongly expressed in the neurons of the retina and sensory pathways.[28,29] Immunoreactivity for calretinin has been reported in 55–100% of EM cases.[22] In this study, calretinin showed relatively high sensitivity (91.7%) as a positive marker for SEM. However, the specificity (60.5%) and diagnostic accuracy (75.7%) were not sufficiently high, although the distribution of the reactive grade in PDSCC was lower than that in EM. Therefore, the utility of calretinin for differentiation between SEM and PDSCC is limited. However, the combination of calretinin and WT1 antibodies would be helpful for elevating the low sensitivity of WT1 (72.2%) for practical application and detection of mesothelial origin. D2-40 is not useful for differentiating SEM from PDSCC; although D2-40 showed the highest sensitivity (97.2%) as a positive marker for SEM, its specificity (39.5%) and diagnostic accuracy (67.6%) were the lowest among the three positive markers for mesothelioma (calretinin, D2-40, and WT1).

p40 (ΔNp63), a non-transactivating isoform of p63, is a squamous/basal-type biomarker.[30] p63 and p40 are expressed in most SCCs, but are rarely expressed in EMs; p40 shows higher sensitivity and specificity than p63.[30,31] In addition, Bishop *et al.* reported that p63 was expressed in various proportions of ACs and large-cell lymphomas, and p40 showed much higher specificity for SCC.[32] In this study, both p40 and p63 showed high sensitivity, specificity, and diagnostic accuracy, but the sensitivity and diagnostic accuracy of p40 were higher than those of p63, suggesting that p40 is a useful negative marker for distinguishing SEM from PDSCC. However, a small number of EMs showed positivity for p40 and/or p63 (most cases were graded as 1+); this phenomenon must be kept in mind when p40 is used in practical pathological diagnosis.

Claudin-4 is a major component of tight junctions, and is widely expressed in most epithelial and carcinoma cells.[33–35] Membranous immunoreactivity for claudin-4 has been reported in 88–100% of carcinomas of various origins and in 0–29% of EMs.[33,34,36,37] Therefore, claudin-4 is considered to be a useful immunohistochemical marker for distinguishing EM from various carcinomas. In this study, claudin-4 showed high sensitivity (94.4%), specificity (92.1%), and diagnostic accuracy (93.2%), implying that claudin-4 is a useful negative marker for distinguishing SEM from PDSCC.

Carcinoembryonic antigen was the first accepted immunohistochemical marker for differentiating EM from lung AC;[38] because of its high sensitivity and specificity, it is still considered to be one of the best markers.[39] Ordonez reported that CEA is also useful for differentiating EM from lung SCC.[23] In this study, CEA showed the best sensitivity (100%) and diagnostic accuracy (95.9%) among all 11 evaluated markers, suggesting that CEA is the best negative marker for distinguishing SEM from PDSCC.

Ordnez *et al.* and the IMIG2012 update recommend MOC31 (ERA) as a negative marker (positivity rate: EM, 2–10%; SCC, 97–100%).[17,23] However, on the basis of the results of the present study, we cannot recommend the use of MOC31 as a negative maker

(positivity rate: EM, 33.3; SCC, 89.5). This discrepancy may be attributable to the different clones of antibodies and differences in the antigen detection systems used.

The IMIG2012 guideline recommended consideration of two mesothelial and two carcinoma markers, on the basis of morphology at initial workup,[17] and the new WHO classification recommends calretinin, CK5/6, WT1 and D2-40 as the best mesothelial markers.[7] However, the choice of markers for differentiating SEM from poorly differentiated non-small cell carcinoma requires attention. Calretinin, D2-40 and CK5/6 are useful mesothelial markers for differentiating EM from AC. However, these markers are not useful for distinguishing SEM from PDSCC, because of their low sensitivity or specificity. Therefore, when two of these three markers are chosen as mesothelial markers, there is some possibility of misdiagnosing PDSCC as SEM. Similarly, although TTF-1 and napsin A are useful carcinoma markers for differentiating EM from pulmonary AC, they are not useful for differentiating EM from SCC. Therefore, the use of TTF-1 and napsin A as carcinoma markers may also lead to misdiagnosis of PDSCC as SEM.

In this study, the combination of calretinin and WT1 showed the highest diagnostic accuracy as a positive marker panel, and the combination of p40 and CEA showed the highest diagnostic accuracy (97.3%) as a negative marker panel. From these results, the combination of calretinin, WT1, p40 and CEA seems to be the best immunohistochemical marker panel for distinguishing SEM from PDSCC. However, when p40 is chosen as one of the carcinoma markers, there is some possibility of misdiagnosing solid AC as SEM, because p40 is rarely expressed in AC.[30–32] In contrast, claudin-4 is widely expressed in both AC and SCC,[33–35] and the diagnostic accuracy of the combination of CEA and claudin-4 (94.6%) was comparable to that of p40 and CEA (97.3%). On the basis of these considerations, claudin-4 should be used as a carcinoma marker instead of p40, in the histopathological differential diagnosis of pleural tumours consisting of solid, sheet-like or cord-like proliferations of epithelioid cells, which require differentiation from PDSCC or solid AC.

In conclusion, we conducted immunohistochemical analyses for differentiating SEM from PDSCC, using 11 commercially available antibodies. On the basis of our results, we recommend the use of a combination of WT1 and calretinin as a positive maker, and a combination of CEA and claudin-4 as a negative marker, to overcome the weaknesses of the individual markers to some extent. In the future, there should be an emphasis on the identification and utilization of new markers, especially mesothelial-specific positive markers.

Conflicts of interest

The authors have no conflicts of interest to declare.

Author contributions

K. Inai, T. Kishimoto and Y. Takeshima designed the research study. K. Kushitani, Y. Miyata, M. Okada and Y. Takeshima contributed to the collection of cases. K. Kushitani, Y. Okada and Y. Katayama performed the research. K. Kushitani wrote the first draft of the manuscript. V. J. Amatya, A. S. Mawas and Y. Takeshima contributed to the final approval of the manuscript.

Acknowledgements

The authors thank the Technical Centre, Hiroshima University, for technical assistance, and thank Editage (www.editage.jp) for English-language editing. This study was funded in part by the Japanese Ministry of Health, Labour and Welfare.

References

1. Gemba K, Fujimoto N, Aoe K *et al.* Treatment and survival analyses of malignant mesothelioma in Japan. *Acta Oncol.* 2013; **52**; 803–808.
2. Gemba K, Fujimoto N, Kato K *et al.* National survey of malignant mesothelioma and asbestos exposure in Japan. *Cancer Sci.* 2012; **103**; 483–490.
3. Prazakova S, Thomas PS, Sandrini A, Yates DH. Asbestos and the lung in the 21st century: an update. *Clin. Respir. J.* 2014; **8**; 1–10.
4. Robinson BW, Musk AW, Lake RA. Malignant mesothelioma. *Lancet* 2005; **366**; 397–408.
5. Roggli VL, Sharma A, Butnor KJ, Sporn T, Vollmer RT. Malignant mesothelioma and occupational exposure to asbestos: a clinicopathological correlation of 1445 cases. *Ultrastruct. Pathol.* 2002; **26**; 55–65.
6. Murayama T, Takahashi K, Natori Y, Kurumatani N. Estimation of future mortality from pleural malignant mesothelioma in Japan based on an age-cohort model. *Am. J. Ind. Med.* 2006; **49**; 1–7.
7. Galateau-Salle F, Churg A, Roggli V *et al.* Tumours of the pleura. In Travis WD, Brambilla E, Burke AP, Marx A, Nicholson AG eds. *World Health Organization classification of tumours of the lung, pleura, thymus and heart*. Lyon: IARC Press, 2015; 153–181.
8. Churg A, Cagle P, Roggli V. *Tumors of the serosal membranes*. Washington, DC: American Registry of Pathology, 2006; 147.

9. Harwood TR, Gracey DR, Yokoo H. Pseudomesotheliomatous carcinoma of the lung. A variant of peripheral lung cancer. *Am. J. Clin. Pathol.* 1976; **65**; 159–167.
10. Koss MN, Fleming M, Przygodzki RM, Sherrod A, Travis W, Hochholzer L. Adenocarcinoma simulating mesothelioma: a clinicopathologic and immunohistochemical study of 29 cases. *Ann. Diagn. Pathol.* 1998; **2**; 93–102.
11. Mayall FG, Gibbs AR. 'Pleural' and pulmonary carcinosarcomas. *J. Pathol.* 1992; **167**; 305–311.
12. Oka K, Otani S, Yoshimura T *et al.* Mucin-negative pseudomesotheliomatous adenocarcinoma of the lung: report of three cases. *Acta Oncol.* 1999; **38**; 1119–1121.
13. Shah IA, Salvatore JR, Kummet T, Gani OS, Wheeler LA. Pseudomesotheliomatous carcinoma involving pleura and peritoneum: a clinicopathologic and immunohistochemical study of three cases. *Ann. Diagn. Pathol.* 1999; **3**; 148–159.
14. Attanoos RL, Gibbs AR. 'Pseudomesotheliomatous' carcinomas of the pleura: a 10-year analysis of cases from the Environmental Lung Disease Research Group, Cardiff. *Histopathology* 2003; **43**; 444–452.
15. Funai K, Yokose T, Ishii G *et al.* Clinicopathologic characteristics of peripheral squamous cell carcinoma of the lung. *Am. J. Surg. Pathol.* 2003; **27**; 978–984.
16. Sakurai H, Asamura H, Watanabe S, Suzuki K, Tsuchiya R. Clinicopathologic features of peripheral squamous cell carcinoma of the lung. *Ann. Thorac. Surg.* 2004; **78**; 222–227.
17. Husain AN, Colby T, Ordonez N *et al.* Guidelines for pathologic diagnosis of malignant mesothelioma: 2012 update of the consensus statement from the International Mesothelioma Interest Group. *Arch. Pathol. Lab. Med.* 2013; **137**; 647–667.
18. Travis WD, Brambilla E, Nicholson AG *et al.* The 2015 World Health Organization classification of lung tumors: impact of genetic, clinical and radiologic advances since the 2004 classification. *J. Thorac. Oncol.* 2015; **10**; 1243–1260.
19. Galateau-Salle F, Churg A, Roggli V, Travis WD; World Health Organization Committee for Tumors of the Pleura. The 2015 World Health Organization classification of tumors of the pleura: advances since the 2004 classification. *J. Thorac. Oncol.* 2016; **11**; 142–154.
20. Kushitani K, Takeshima Y, Amatya VJ, Furonaka O, Sakatani A, Inai K. Immunohistochemical marker panels for distinguishing between epithelioid mesothelioma and lung adenocarcinoma. *Pathol. Int.* 2007; **57**; 190–199.
21. Amatya VJ, Takeshima Y, Kohno H *et al.* Caveolin-1 is a novel immunohistochemical marker to differentiate epithelioid mesothelioma from lung adenocarcinoma. *Histopathology* 2009; **55**; 10–19.
22. Ordonez NG. Application of immunohistochemistry in the diagnosis of epithelioid mesothelioma: a review and update. *Hum. Pathol.* 2013; **44**; 1–19.
23. Ordonez NG. The diagnostic utility of immunohistochemistry in distinguishing between epithelioid mesotheliomas and squamous carcinomas of the lung: a comparative study. *Mod. Pathol.* 2006; **19**; 417–428.
24. Tsao M-S, Brambilla E, Nicholson AG *et al.* Squamous cell carcinoma. In Travis WD, Brambilla E, Burke AP, Marx A, Nicholson AG eds. *World Health Organization classification of tumours of the lung, pleura, thymus and heart*. Lyon: IARC Press, 2015; 51–55.
25. Hohenstein P, Hastie ND. The many facets of the Wilms' tumour gene, WT1. *Hum. Mol. Genet.* 2006; **15**(Spec. No. 2); R196–R201.
26. Takeshima Y, Amatya VJ, Kushitani K, Inai K. A useful antibody panel for differential diagnosis between peritoneal mesothelioma and ovarian serous carcinoma in Japanese cases. *Am. J. Clin. Pathol.* 2008; **130**; 771–779.
27. Ordonez NG. The immunohistochemical diagnosis of mesothelioma: a comparative study of epithelioid mesothelioma and lung adenocarcinoma. *Am. J. Surg. Pathol.* 2003; **27**; 1031–1051.
28. Rogers JH. Calretinin: a gene for a novel calcium-binding protein expressed principally in neurons. *J. Cell Biol.* 1987; **105**; 1343–1353.
29. Doglioni C, Dei Tos AP, Laurino L *et al.* Calretinin: a novel immunocytochemical marker for mesothelioma. *Am. J. Surg. Pathol.* 1996; **20**; 1037–1046.
30. Pelosi G, Rossi G, Cavazza A *et al.* Deltanp63 (p40) distribution inside lung cancer: a driver biomarker approach to tumor characterization. *Int. J. Surg. Pathol.* 2013; **21**; 229–239.
31. Tatsumori T, Tsuta K, Masai K *et al.* P40 is the best marker for diagnosing pulmonary squamous cell carcinoma: comparison with p63, cytokeratin 5/6, desmocollin-3, and SOX2. *Appl. Immunohistochem. Mol. Morphol.* 2014; **22**; 377–382.
32. Bishop JA, Teruya-Feldstein J, Westra WH, Pelosi G, Travis WD, Rekhtman N. P40 (DeltaNp63) is superior to p63 for the diagnosis of pulmonary squamous cell carcinoma. *Mod. Pathol.* 2012; **25**; 405–415.
33. Facchetti F, Lonardi S, Gentili F *et al.* Claudin 4 identifies a wide spectrum of epithelial neoplasms and represents a very useful marker for carcinoma versus mesothelioma diagnosis in pleural and peritoneal biopsies and effusions. *Virchows Arch.* 2007; **451**; 669–680.
34. Soini Y, Kinnula V, Kahlos K, Paakko P. Claudins in differential diagnosis between mesothelioma and metastatic adenocarcinoma of the pleura. *J. Clin. Pathol.* 2006; **59**; 250–254.
35. Lodi C, Szabo E, Holczbauer A *et al.* Claudin-4 differentiates biliary tract cancers from hepatocellular carcinomas. *Mod. Pathol.* 2006; **19**; 460–469.
36. Lonardi S, Manera C, Marucci R, Santoro A, Lorenzi L, Facchetti F. Usefulness of claudin 4 in the cytological diagnosis of serosal effusions. *Diagn. Cytopathol.* 2011; **39**; 313–317.
37. Ordonez NG. Value of claudin-4 immunostaining in the diagnosis of mesothelioma. *Am. J. Clin. Pathol.* 2013; **139**; 611–619.
38. Wang NS, Huang SN, Gold P. Absence of carcinoembryonic antigen-like material in mesothelioma: an immunohistochemical differentiation from other lung cancers. *Cancer* 1979; **44**; 937–943.
39. Ordonez NG. What are the current best immunohistochemical markers for the diagnosis of epithelioid mesothelioma? A review and update *Hum. Pathol.* 2007; **38**; 1–16.

Modern Pathology (2017), 1–10

MUC4, a novel immunohistochemical marker identified by gene expression profiling, differentiates pleural sarcomatoid mesothelioma from lung sarcomatoid carcinoma

Vishwa Jeet Amatya[1], Kei Kushitani[1], Amany Sayed Mawas[1,2], Yoshihiro Miyata[3], Morihito Okada[3], Takumi Kishimoto[4], Kouki Inai[1,5] and Yukio Takeshima[1]

[1]Department of Pathology, Hiroshima University Graduate School of Biomedical and Health Sciences, Hiroshima, Japan; [2]Department of Pathology and Clinical Pathology, South Valley University, Qena, Egypt; [3]Department of Surgical Oncology, Research Institute for Radiation Biology and Medicine, Hiroshima University, Hiroshima, Japan; [4]Department of Internal Medicine, Okayama Rosai Hospital, Okayama, Japan and [5]Pathologic Diagnostic Center, Inc., Hiroshima, Japan

Sarcomatoid mesothelioma, a histological subtype of malignant pleural mesothelioma, is a very aggressive tumor with a poor prognosis. Histological diagnosis of sarcomatoid mesothelioma largely depends on the histomorphological feature of spindled tumor cells with immunohistochemical reactivity to cytokeratins. Diagnosis also requires clinico-radiological and/or macroscopic evidence of an extrapulmonary location to differentiate it from lung sarcomatoid carcinoma. Although there are promising immunohistochemical antibody panels to differentiate mesothelioma from lung carcinoma, a consensus on the immunohistochemical markers that distinguish sarcomatoid mesothelioma from lung sarcomatoid carcinoma has not been reached and requires further study. We performed whole gene expression analysis of formalin-fixed paraffin-embedded tissue from sarcomatoid mesothelioma and lung sarcomatoid carcinoma and observed significant differences in the expression of MUC4 and other genes between sarcomatoid mesothelioma and lung sarcomatoid carcinoma. Immunohistochemistry demonstrated that MUC4 was expressed in the spindled tumor cells of lung sarcomatoid carcinoma (21/29, 72%) but was not expressed in any sarcomatoid mesothelioma (0/31, 0%). To differentiate sarcomatoid mesothelioma from lung sarcomatoid carcinoma, negative MUC4 expression showed 100% sensitivity and 72% specificity and accuracy rate of 87%, which is higher than immunohistochemical markers such as calretinin, D2-40 and Claudin-4. Therefore, we recommend to include MUC4 as a novel and useful negative immunohistochemical marker for differentiating sarcomatoid mesothelioma from lung sarcomatoid carcinoma.
Modern Pathology advance online publication, 27 January 2017; doi:10.1038/modpathol.2016.181

Malignant pleural mesothelioma, a highly aggressive tumor with a poor prognosis, is strongly associated with asbestos exposure; its incidence is increasing in Japan and Western countries and is expected to increase in developing countries.[1] It is histologically classified into three subtypes: epithelioid, biphasic, and sarcomatoid mesothelioma.[2] The International Mesothelioma Interest Group (IMIG) has published guidelines for the differential diagnosis of epithelioid mesothelioma from lung adenocarcinoma and squamous cell carcinoma using immunohistochemical antibody panels of mesothelioma markers (calretinin, D2-40, WT1, cytokeratin 5/6), lung adenocarcinoma markers (CEA, TTF-1, Napsin-A, MOC-31, BerEP4, BG8, B72.3) and lung squamous carcinoma markers (p63, p40, MOC-31, Ber-EP4, cytokeratin 5/6).[3]

However, a consensus on the immunohistochemical markers that differentiate sarcomatoid mesothelioma from lung sarcomatoid carcinoma

Correspondence: Dr Y Takeshima, MD, PhD, Department of Pathology, Hiroshima University Graduate School of Biomedical and Health Sciences, 1-2-3 Kasumi, Minami-ku, Hiroshima 734-8551, Japan.
E-mail: ykotake@hiroshima-u.ac.jp
Received 15 June 2016; revised 3 September 2016; accepted 6 September 2016; published online 26 January 2017

has not been reached and requires further study. The histological diagnosis of sarcomatoid mesothelioma largely depends on the histomorphological feature of spindled tumor cells supported by immunohistochemical cytokeratin reactivity; it also requires clinico-radiological and/or macroscopic evidence of an extrapulmonary location. The immunohistochemical markers for lung adenocarcinoma and squamous carcinoma are not useful for diagnosing lung sarcomatoid carcinoma. To date, D2-40 and calretinin are two commonly used positive mesothelial markers expressed in sarcomatoid mesothelioma.[4–7] However, without convincing calretinin and D2-40 positivity, it is difficult to differentiate sarcomatoid mesothelioma from sarcomatoid carcinoma. In previous reports, including ours, high D2-40 sensitivity has been reported to differentiate sarcomatoid mesothelioma from lung sarcomatoid carcinoma; however, D2-40 specificity is not perfect.[6,7] Therefore, the clinico-radiological identification of tumor location at the extrapulmonary site remains essential to differentiate between these two diseases.

In recent decades, gene expression profiling has been used in many cancers to identify the pathways involved in malignant transformation and to identify novel candidate diagnostic and prognostic markers. We have recently reported the application of gene expression analysis to identify novel markers differentiating epithelioid mesothelioma from reactive mesothelial hyperplasia by PCR array.[8] Although gene expression analysis requires specimens with a high proportion of tumor cells containing good quality RNA, we successfully analyzed the RNA extracted from formalin-fixed paraffin-embedded samples.

The aim of this study was to perform gene expression analysis on spindled tumor cells dissected from formalin-fixed paraffin-embedded tissue of sarcomatoid mesothelioma and lung sarcomatoid carcinoma. Our gene expression microarray data identified several novel genes that are differentially expressed between sarcomatoid mesothelioma and lung sarcomatoid carcinoma, and of these, we validated MUC4 as a novel and useful negative immunohistochemical marker differentiating sarcomatoid mesothelioma from lung sarcomatoid carcinoma.

Materials and methods

Formalin-Fixed Paraffin-Embedded Tissue Samples

Sarcomatoid mesothelioma and lung sarcomatoid carcinoma cases were retrieved from surgical pathology archives of our department during 2005–2014. The clinical details were also reviewed from the patient record files. The location of tumor was confirmed by reviewing clinical information (especially chest computed tomography findings to confirm the tumor localization), gross findings and reviewing histological sections stained with H&E and Elastica van Gieson. All lung sarcomatoid carcinoma cases in this study were located in the pulmonary parenchyma, which was confirmed by radiological, thoracoscopic and operative findings. None of the lung sarcomatoid carcinoma showed diffuse pleurotropic growth pattern described as 'pseudomesotheliomatous growth'. Sarcomatoid mesothelioma was located in extrapulmonary site showing dominant pleurotrophic growth pattern without obvious tumor mass in lung parenchyma. Pathological diagnosis of each case was confirmed by histological findings and immunohistochemical marker panel recommended by Guidelines for Pathologic Diagnosis of Malignant Mesothelioma-2012 Update of the Consensus Statement from the International Mesothelioma Interest Group[3] and current 2015 WHO histological classification of tumours of the lung, pleura, thymus and heart.[9] Sarcomatoid mesothelioma is characterized by a proliferation of spindle cells arranged in fascicles or having a haphazard distribution involving adjacent adipose tissue, parietal pleura or lung parenchyma.[9] Lung sarcomatoid carcinoma is a poorly differentiated non-small cell lung carcinoma that contains a component of sarcoma or sarcoma-like (spindle and/or giant cell) differentiation. Lung sarcomatoid carcinoma is a group of five types of carcinomas based on specific histological criteria and described as giant cell carcinoma, pleomorphic carcinoma, carcinosarcoma, spindle cell carcinoma and pulmonary blastoma. Of these, spindle cell carcinoma and pleomorphic carcinoma with predominant spindle cell component requires the differentiation from sarcomatoid mesothelioma. The number of patients who were diagnosed as sarcomatoid mesothelioma and lung sarcomatoid carcinoma after surgical resection and/or autopsy examination in Hiroshima University Hospital during 2005–2014 were 35 and 34 respectively, suggesting similar frequencies of their incidence. Localization of four cases of sarcomatoid mesothelioma and five cases of lung sarcomoid carcinoma could not be confirmed and thus were excluded from this study. Finally, 31 cases of sarcomatoid mesothelioma and 29 cases of lung sarcomatoid carcinoma were analyzed in the present study. Sarcomatoid mesothelioma included 25 cases of pure sarcomatoid growth (pure sarcomatoid mesothelioma) and 6 cases of biphasic mesothelioma showing predominantly sarcomatoid growth. Lung sarcomatoid carcinoma included 5 cases of spindle cell carcinoma and 24 of pleomorphic carcinoma with predominant spindle cell carcinoma component. Minor foci of squamous cell carcinoma and adenocarcinoma component were present in 5 and 19 cases of pleomorphic carcinoma. Carcinosarcoma, giant cell carcinoma and pulmonary blastema were not included in this study.

The anonymized (unlinkable) tissue samples were provided by the Department of Pathology for gene expression analysis and immunohistochemical

study. This study is in accordance with the Ethics Guidelines for Human Genome/Gene Research enacted by the Japanese Government for the collection of tissue specimens and was approved by the institutional ethics review committee (Hiroshima University E-48).

Gene Expression Analysis

Formalin-fixed paraffin-embedded sections from six cases of sarcomatoid mesothelioma and six cases of lung sarcomatoid carcinoma were used for gene expression analysis. RNA extraction for gene expression analysis was performed from the spindled tumor cells of these cases. Five 10-μm-thick formalin-fixed paraffin-embedded tissue sections containing >90% spindled tumor tissue were processed for total RNA extraction using the Maxwell 16 LEV RNA FFPE Purification Kit (Promega, Tokyo, Japan) according to the manufacturer's protocol. After deparaffinization and lysis with proteinase K treatment, the samples were treated with a DNase cocktail for 15 min at room temperature, followed by RNA purification using a MAXWELL 16 instrument according to the manufacturer's protocol (Promega).

RNA quality was analyzed with an RNA StdSens Analysis kit using an Experion automated electrophoresis system (Bio-Rad Laboratories, Hercules, CA, USA). RNA quantity was estimated with a Qubit RNA HS Kit using a Qubit Fluorometer 2.0 (Molecular Probes/Life Technologies, Carlsbad, CA, USA). The Almac Xcel Array GeneChip (Affymetrix, Santa Clara, CA, USA) contains probe sets of >97 000 transcripts and was used to analyze gene expression profiles. Total RNA was amplified and labeled with a 3′ IVT Labeling Kit (Affymetrix) before hybridization onto the GeneChip. Briefly, 100 ng total RNA was amplified with a SensationPlus FFPE Amplification Kit (Affymetrix) to generate 30 μg of SenseRNA according to the manufacturer's protocol. Twenty-five micrograms of SenseRNA was labeled with a 3′ IVT Labeling Kit (Affymetrix) and hybridized to a Almac Xcel Array GeneChip (Affymetrix) at 45 °C for 16 h using a GeneChip Hybridization Oven 645 (Affymetrix). The hybridized GeneChip was washed, stained using GeneChip Fluidic Station 450 (Affymetrix) and scanned with a GeneChip Scanner 3000 7G (Affymetrix) using the GeneChip Operating Software (Affymetrix). The data were analyzed using the Gene Expression Console Software (Affymetrix), and further statistical analyses were performed using the Subio Software Platform (Subio, Amami-shi, Japan) to calculate plot graphs, fold change of expression and hierarchical clustering.

Validation of Gene Expression Analysis

The same 12 cases of sarcomatoid mesothelioma and lung sarcomatoid carcinoma that were analyzed for gene expression profiling were used to validate the microarray expression data. The relative mRNA expression of *MUC4*, a highly expressed gene in lung sarcomatoid carcinoma, and *IGF2*, highly expressed in sarcomatoid mesothelioma, was assessed with SYBR Green-based real-time RT-PCR using GAPDH as a control. A total of 100 ng RNA was used for mRNA expression with a one-step SYBR Green RT-PCR Kit (Takara-Bio, Tokyo, Japan) using a MX3000P real-time PCR thermal cycler (Stratagene, Agilent Technologies, Tokyo, Japan). The primer pairs used were *MUC4*-F: CAGGCCACCAACTTCA TCG; *MUC4*-R: ACACGGATTGCGTCGTGAG; *IGF2*-F: GTGGCATCGTTGAGGAGTG; *IGF2*-R: CACGTCC CTCTCGGACTTG; *GAPDH*-F: ACAACTTTGGTATC GTGGAAGG; and *GAPDH*-R: GCCATCACGCCA CAGTTTC. Data analysis was performed using the δδCT method for relative quantification. Briefly, threshold cycles (CT) for *GAPDH* (reference) and *MUC4*, *IGF2* (samples) were determined in triplicate. The relative expression (rI) was calculated using the formula: $rI = 2^{-(CT\ sample - CT\ normal)}$.

Immunohistochemistry

Immunohistochemistry was performed using 3-μm tissue sections from the best representative formalin-fixed paraffin-embedded sarcomatoid mesothelioma and lung sarcomatoid carcinoma tissue blocks. All of the immunohistochemical staining was performed with a Benchmark GX automated immunohistochemical station (Ventana, Roche Diagnostics, Tokyo, Japan) using the ultraView Universal DAB Detection Kit (Ventana, Roche Diagnostic, Tokyo, Japan). The antigen retrieval methods and antibodies used in this study are summarized in Table 1. Immunoreactivity was scored as negative (0, no immunostaining) or positive. Positive immunoreactivity was graded as +1 for up to 10% of tumor cells showing positive immunostaining, +2 for >10–50% of the tumor cells, and +3 for >50% of the tumor cells. Only spindled tumor cells from sarcomatoid mesothelioma and lung sarcomatoid carcinoma were evaluated for the immunoreactivity of various markers. Statistical analyses were performed using Fisher's exact test. Sensitivity, specificity, positive predictive value, negative predictive value and accuracy rate were calculated using a simple 2 × 2 table.

Results

Differential Gene Expression and Validation in Sarcomatoid Mesothelioma and Lung Sarcomatoid Carcinoma

Out of the 97 000 analyzable transcripts on the Almac Xcel Array GeneChip, 2099 statistically significant mRNA transcripts were differentially expressed between sarcomatoid mesothelioma and lung sarcomatoid carcinoma by a more than a two-fold difference (Figure 1, plot graph). The

Table 1 List of antibodies with their clone, commercial source and reaction conditions

Antibody to	*Clone*	*Provider*	*Dilution*	*Antigen retrieval*
MUC4	8G7	Santa Cruz Biotechnology	× 25	CC1, 60 min
Calretinin	SP65	Ventana	Prediluted	CC1, 30 min
Podoplanin	D2-40	Nichirei	Prediluted	CC1, 60 min
WT1	6F-H2	Dako	× 25	CC1, 60 min
Pancytokeratin	AE1/AE3	Ventana	Prediluted	Protease 8 min
Cytokeratin	CAM5.2	Ventana	Prediluted	Protease 8 min
p40	BC28	Biocare Medical	× 50	CC1, 60 min
TTF-1	SP141	Ventana	Prediluted	CC1, 60 min
Claudin-4	3E2C1	Life Technologies	× 50	CC1, 60 min

Abbreviation: CC1, cell conditioning buffer 1 (Tris-based buffer, pH 8.5 from Ventana).

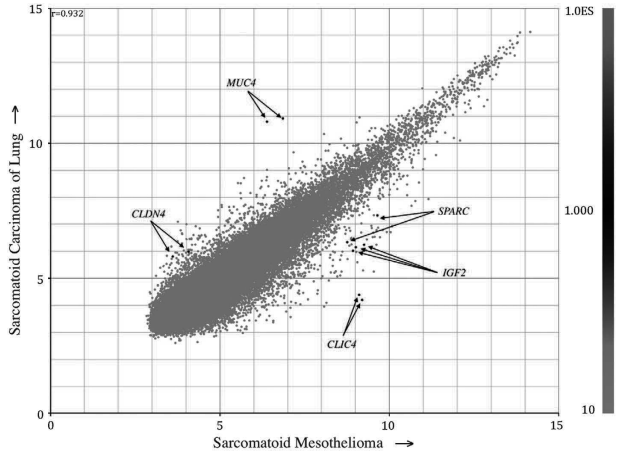

Figure 1 Scatter plot of raw data from the microarray experiments demonstrating MUC4 and CLDN4 with lower expression and IGF2, CLIC4 and SPARC4 with higher expression in sarcomatoid mesothelioma compared with that of lung sarcomatoid carcinoma.

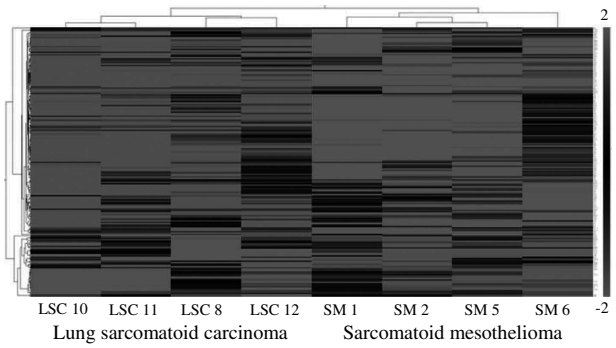

Figure 2 The hierarchical clustering of RNA transcripts with more than five-fold differential expression between sarcomatoid mesothelioma and lung sarcomatoid carcinoma revealed 156 upregulated mRNA transcripts, including *IGF2*, *MEG3*, *CLIC4* and *SPARC*, in sarcomatoid mesothelioma and 46 upregulated mRNA transcripts, including *MUC4* and *Claudin4*, in lung sarcomatoid carcinoma.

hierarchical clustering of mRNAs with more than a five-fold difference in expression revealed 156 upregulated mRNA transcripts, including *IGF2*, *MEG3*, *CLIC4* and *SPARC*, in sarcomatoid mesothelioma and 46 upregulated mRNA transcripts, including *MUC4* and *Claudin4*, in lung sarcomatoid carcinoma (Figure 2, hierarchical clustering; Supplementary Table S1). The mRNA expression hits were validated by real-time RT-PCR of *MUC4* and *IGF2*. *MUC4* mRNA expression was negligible in all six sarcomatoid mesothelioma, and the expression was observed in five of the six lung sarcomatoid carcinoma samples. *IGF2* mRNA was expressed in all of the sarcomatoid mesothelioma samples, although it was also expressed in three of the six lung sarcomatoid carcinoma samples (detailed data not shown).

Immunohistochemical Profiles of Sarcomatoid Mesothelioma and Lung Sarcomatoid Carcinoma

The percentage of positivity and immunohistochemical score for MUC4, mesothelioma markers (calretinin, D2-40, WT1) and lung carcinoma markers (TTF-1, p40, Claudin-4) along with the cytokeratins AE1/AE3 and CAM5.2 are shown in Table 2.

MUC4 Expression

MUC4 expression was observed in the cytoplasm of tumor cells, and the positivity of spindled tumor cells alone was evaluated. MUC4 was also observed in the surrounding normal lung tissue, particularly in bronchial tissue, and was considered an internal positive marker. It was expressed in spindled tumor cells of 21 lung sarcomatoid carcinoma (21/29, 72%; Figure 3b) but none in sarcomatoid mesothelioma (0/31, 0%; Figure 4b). In addition to spindled tumor cells of lung sarcomatoid carcinoma, MUC4 was also expressed in the non-small cell carcinoma component consisting of adenocarcinoma or squamous cell carcinoma in pleomorphic carcinoma. Among lung sarcomatoid carcinoma, 3 cases showed expression in $>50\%$ of tumor cells, 9 cases in 10–50% of tumor cells and 9 cases in $<10\%$ of tumor cells. Out of the 21 lung sarcomatoid carcinoma cases with MUC4

Table 2 Potential immunohistochemical markers for sarcomatoid mesothelioma and lung sarcomatoid carcinoma

	Sarcomatoid mesothelioma						*Lung sarcomatoid carcinoma*							
			Immunohistochemical score[a]						*Immunohistochemical score*[a]					
Antibody	*Positive cases*	*(%)*	*0*	*1+*	*2+*	*3+*	*Positive cases*	*(%)*	*0*	*1+*	*2+*	*3+*	P-*value*[b]	P-*value*[c]
MUC4	0/31	0	31	0	0	0	21/29	72	8	9	9	3	< 0.01	< 0.01
Calretinin	23/31	74	8	7	11	5	13/29	45	16	5	6	2	< 0.05	< 0.05
D2-40	22/31	71	9	9	12	1	9/29	31	20	9	0	0	< 0.01	< 0.01
WT1	6/31	19	25	5	1	0	1/29	3	28	1	0	0	NS	NS
AE1/AE3	29/31	94	2	2	8	19	29/29	100	0	5	2	22	NS	NS
CAM5.2	28/31	90	3	1	8	19	28/29	97	1	6	5	17	NS	NS
TTF-1	0/31	0	31	0	0	0	15/29	52	14	0	4	11	< 0.01	< 0.01
p40	2/31	7	29	2	0	0	6/29	21	23	0	3	3	NS	NS
Claudin-4	0/31	0	31	0	0	0	13/29	45	16	4	5	4	< 0.01	< 0.01

Abbreviations: NA, not available; NS, not significant; TTF-1, thyroid transcription factor; WT1, Wilms' tumor gene product.
[a]Calculated by Fisher's exact test of the positive rate between two groups.
[b]Calculated by the Mann–Whitney *U*-test of reactivity scores of the markers between two groups.
[c]Immunohistochemical score was semiquantified as follows: 0: 0%; 1+: 1–10%; 2+: 11–50%; 3+: >51% of spindled tumor cells.

expression, p40 expression was observed only in 3 cases, TTF-1 in 12 cases and Claudin-4 in 10 cases. Of the nine lung sarcomatoid carcinoma cases without MUC4 expression, p40 expression was observed in three cases, TTF-1 in three cases and Claudin-4 in three cases.

Calretinin, D2-40 and WT1

Calretinin was expressed in the nucleus and cytoplasm of spindled tumor cells of 23 (74%) sarcomatoid mesothelioma and 13 (45%) lung sarcomatoid carcinoma samples, and D2-40 was expressed in the spindled tumor cells of 21 (71%) sarcomatoid mesothelioma and 9 (31%) lung sarcomatoid carcinoma. The immunohistochemical scoring pattern for calretinin expression was not different between sarcomatoid mesothelioma and lung sarcomatoid carcinoma. However, the immunohistochemical scoring pattern for D2-40 expression showed a higher score in sarcomatoid mesothelioma than in lung sarcomatoid carcinoma. WT1 nuclear expression was present in only 6 (19%) sarcomatoid mesothelioma and 1 (3%) lung sarcomatoid carcinoma, revealing it to be a poor immunohistochemical marker to differentiate sarcomatoid mesothelioma from lung sarcomatoid carcinoma.

TTF-1, p40, Claudin-4

Nuclear expression of TTF-1 and P40 was observed in 15 (52%) and 6 (21%) cases of lung sarcomatoid carcinoma, respectively. TTF-1 expression was not observed in sarcomatoid mesothelioma, but p40 expression was observed in 2 (7%) sarcomatoid mesothelioma cases. TTF-1 and/or p40 immunoreactivity was present in 19 of the 29 (66%) cases of lung sarcomatoid carcinoma and 2 of the 31 (7%) cases of sarcomatoid mesothelioma. Claudin-4 and/or TTF-1/p40 immunoreactivity was present in 25 of the 29 (86%) of lung sarcomatoid carcinoma and 2 of the 31 (7%) cases of sarcomatoid mesothelioma. However, p40 expression in sarcomatoid mesothelioma was focal and heterogeneous with an immunohistochemical score of 1.

Cytokeratins, AE1/AE3, CAM5.2

Cytokeratin AE1/AE3 and CAM5.2 expression was present in >90% of both lung sarcomatoid carcinoma and sarcomatoid mesothelioma samples. The majority of sarcomatoid mesothelioma and lung sarcomatoid carcinoma cases showed the expression of both cytokeratins, and the remaining two lung sarcomatoid carcinoma cases and one sarcomatoid mesothelioma case expressed at least one of the two cytokeratins.

Sensitivity and Specificity of Each Marker to Differentially Diagnose Sarcomatoid Mesothelioma and Lung Sarcomatoid Carcinoma

The sensitivity, specificity, positive predictive value, negative predictive value and accuracy rate of each marker differentiating sarcomatoid mesothelioma from lung sarcomatoid carcinoma are shown in Table 3. The negative expression of the carcinoma markers TTF-1 and Claudin-4 showed 100% sensitivity, whereas p40 showed 94%; however, their specificity was restricted around or below 50%. The positive expression of calretinin showed 74% sensitivity and 55% specificity, and D2-40 showed 71% sensitivity and 69% specificity. Although WT1 showed the highest specificity of 97%, its sensitivity

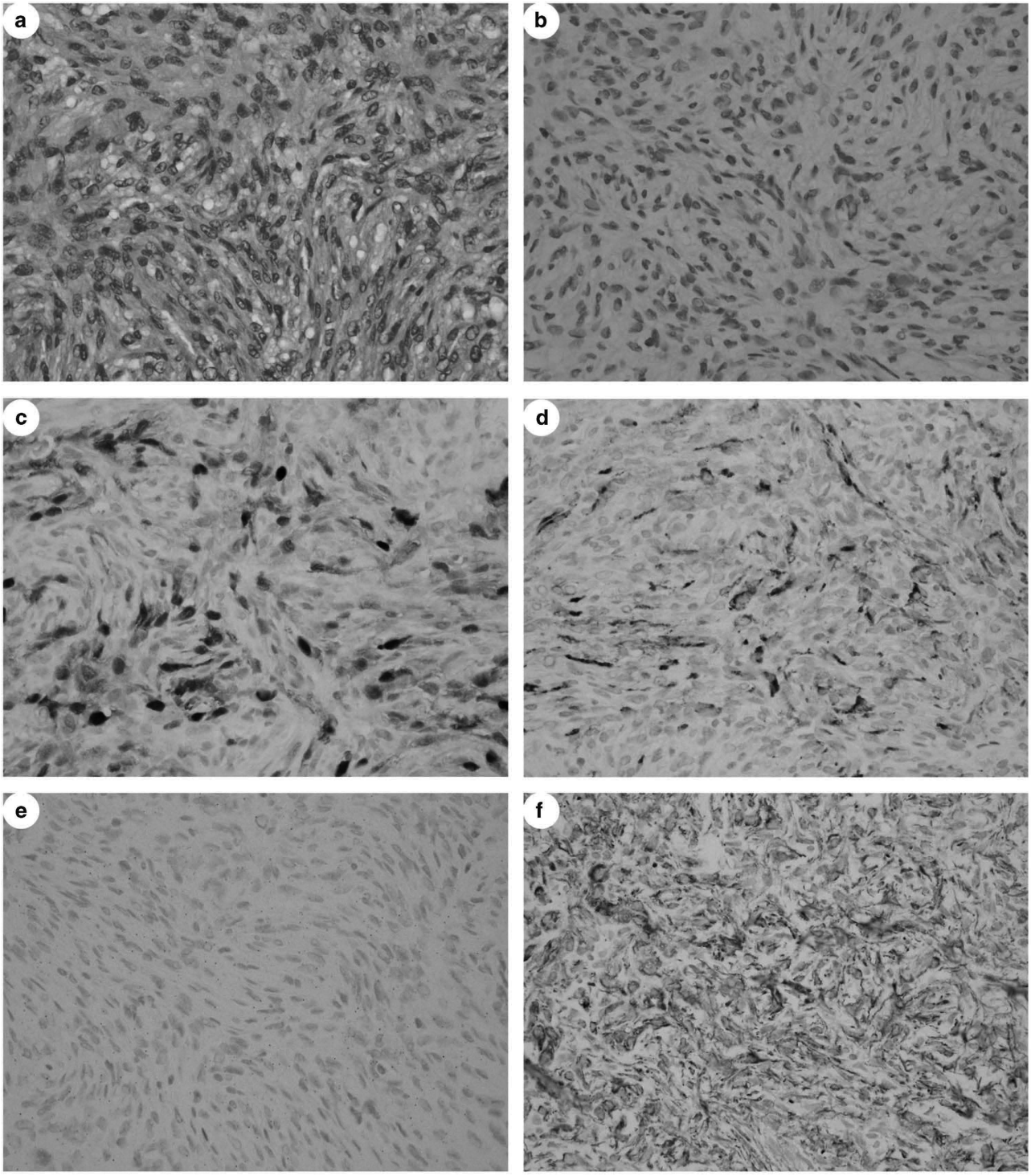

Figure 3 Representative pictures of immunohistochemical expression of MUC4 (**b**), Calretinin (**c**), D2-40 (**d**), Claudin-4 (**e**) and AE1/AE3 (**f**) from sarcomatoid mesothelioma (**a**). None of the sarcomatoid mesotheliomas showed immunohistochemical MUC4 expression.

was $<20\%$. AE1/AE3 and CAM5.2 showed high 94 and 90% sensitivities and near 0% specificity. In comparison to all of these known immunohistochemical markers, negative expression of MUC4 showed 100% sensitivity and 72% specificity, making the accuracy rate of 87%, the highest among these immunohistochemical markers.

Value of Immunohistochemical Marker Panel to Differentially Diagnosis Sarcomatoid Mesothelioma and Lung Sarcomatoid Carcinoma

MUC4 showed the highest sensitivity and specificity among the immunohistochemical markers for differentiatiation of sarcomatoid mesothelioma from lung

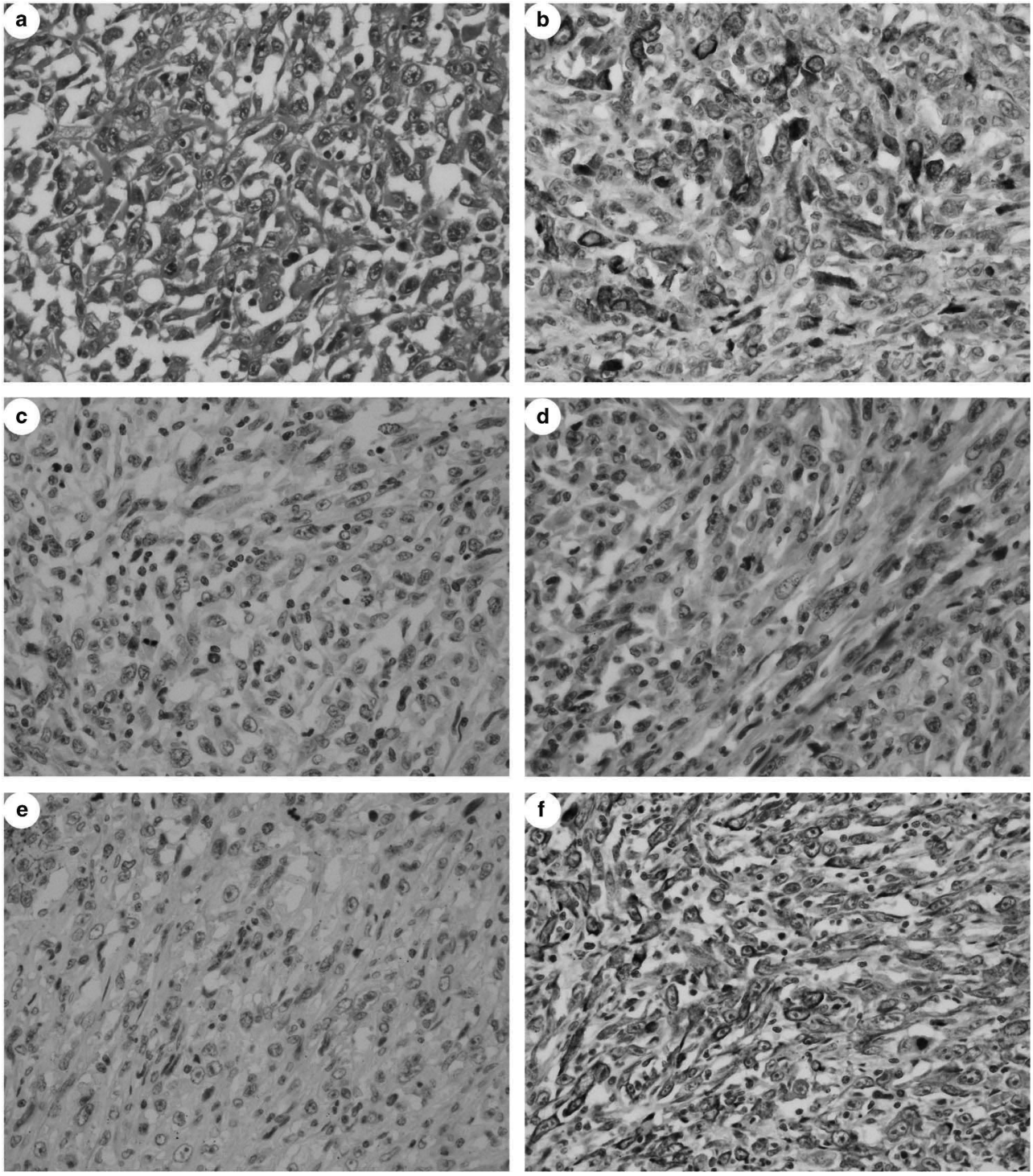

Figure 4 Representative pictures of immunohistochemical MUC4 expression (**b**), Calretinin (**c**), D2-40 (**d**), Claudin-4 (**e**) and AE1/AE3 (**f**) of lung sarcomatoid carcinoma (**a**). Twenty-one of the 29 (72%) lung sarcomatoid carcinomas exhibited cytoplasmic expression of MUC4.

sarcomatoid carcinoma. However, the specificity was 72%. Therefore, a combination of various markers was considered. Various combinations of immunohistochemical markers are shown in Table 4. Among the negative immunohistochemical markers, combination of MUC4, TTF-1 and p40 was observed in 26 of the 29 lung sarcomatoid carcinoma cases (90% specificity) and 2 of the 31sarcomatoid mesothelioma cases (93% sensitivity). Combination of MUC4 and Claudin-4 expression was found in 24 of the 29 lung sarcomatoid carcinoma cases (83% specificity) and none of the sarcomatoid

Table 3 Sensitivity, specificity, PPV, NPV and accuracy rate of each antibody to differentially diagnose sarcomatoid mesothelioma from lung sarcomatoid carcinoma

Findings	*Sensitivity (%)*	*Specificity (%)*	*PPV (%)*	*NPV (%)*	*Accuracy rate (%)*	P-*value*
MUC4 (−)	100	72	80	100	87	< 0.01
Calretinin (+)	74	55	64	67	65	< 0.05
D2-40 (+)	71	69	71	69	70	< 0.01
WT1 (+)	19	97	86	53	57	NS
AE1/AE3 (+)	94	0	50	0	48	NS
CAM5.2 (+)	90	3	50	25	48	NS
TTF-1 (−)	100	52	69	100	77	< 0.01
p40 (−)	94	21	56	75	58	NS
Claudin-4 (−)	100	45	66	100	73	< 0.01

Abbreviations: NPV, negative predictive value; NS, not significant; PPV, positive predictive value.

Table 4 Sensitivity, specificity, PPV, NPV and accuracy rate of two or more markers to differentially diagnose sarcomatoid mesothelioma from lung sarcomatoid carcinoma

Immunohistochemical markers	*Sensitivity (%)*	*Specificity (%)*	*PPV (%)*	*NPV (%)*	*Accuracy rate (%)*	P-*value*
p40 (−)/TTF-1 (−)	94	66	74	91	80	< 0.01
Claudin-4 (−)/TTF-1 (−)/p40 (−)	94	90	91	93	92	< 0.01
Claudin-4 (−)/TTF-1 (−)	100	83	86	100	92	< 0.01
MUC4 (−)/TTF-1 (−)/p40 (−)	94	93	94	93	93	< 0.01
MUC4 (−)/Claudin-4 (−)	100	83	86	100	92	< 0.01
MUC4 (−)/TTF-1 (−)/Claudin-4 (−)	100	90	91	100	95	< 0.01
MUC4 (−)/TTF-1 (−)/p40 (−)/Claudin-4 (−)	94	97	97	93	95	< 0.01

Abbreviations: NPV, negative predictive value; PPV, positive predictive value.

mesothelioma cases (100% sensitivity). The combination of MUC4, TTF-1 and Claudin-4 was observed in 26 of the 29 lung sarcomatoid carcinoma cases (90% specificity) and 0 of the 31 sarcomatoid mesothelioma cases (100% sensitivity).

Discussion

Sarcomatoid mesothelioma has the histomorphological feature of spindled tumor cells and resembles many tumors with spindled cells, including true sarcoma or sarcomatoid carcinomas. The immunohistochemical reactivity to cytokeratin remains critical to differentiate it from true sarcomas. However, differentiating sarcomatoid mesothelioma from lung sarcomatoid carcinoma is challenging, as the histomorphological and immunohistochemical characteristics are extremely similar. For this reason, clinical and/or gross evidence of an extrapulmonary location is indispensable for its diagnosis. Although the mesothelioma markers calretinin and D2-40 have been utilized to differentiate sarcomatoid mesothelioma from lung sarcomatoid carcinoma, they are not absolute, as their sensitivity and specificity are not sufficiently high. Although we previously reported the sensitivity of calretinin (78%) and D2-40 (87%), specificity was not high for calretinin (41%) and D2-40 (74%).[7] Our past and present data on calretinin and D2-40 were similar to reports by Ordonez *et al*[4] and Padgett *et al*.[6] Considering the low specificity of calretinin, D2-40 is considered the single most important immunohistochemical marker for its differentiation. However, in our practical experience, it is still very difficult to interpret the reactivity of D2-40 in these tumors, particularly in cases showing prominent fibro-collagenous proliferation.

TTF-1, a lung adenocarcinoma marker, and p40, a squamous cell carcinoma marker, have emerged as useful markers for non-small cell lung carcinoma[10,11] and are thus supposed to be expressed in pleomorphic lung carcinoma. TTF-1 might be identified as a novel marker differentiating pleomorphic carcinoma from sarcomatoid mesothelioma because of its low expression in sarcomatoid mesothelioma. However, in this study, despite their specificity of 100 or 94%, the sensitivity of TTF-1 (51%) and p40 (21%) are not good to distinguish sarcomatoid mesothelioma and lung sarcomatoid carcinoma. Though p40 expression is good marker of squamous cell carcinoma, it has been also reported in a few mesothelioma cases.[12] In this study too, we observed p40 expression in two sarcomatoid mesothelioma cases but very focal and heterogeneous, unlike its expression in squamous cell carcinoma. Claudin-4, which is reported to be a very reliable universal carcinoma marker differentiating epithelioid mesothelioma from various carcinomas,[13,14] showed limited value in lung sarcomatoid carcinoma cases. In this study, only half of lung sarcomatoid

carcinoma expressed Claudin-4, and its punctate expression in the cytoplasm of spindled cells of lung sarcomatoid carcinoma resembled that of the punctate expression in the cytoplasm of sarcomatoid mesothelioma. TTF-1, p40 and Claudin-4 expression can be reliable markers for pleomorphic carcinomas with a prominent carcinoma component, such as adenocarcinoma or squamous cell carcinoma.

In this study, we analyzed all of the genes expressed in sarcomatoid mesothelioma and lung sarcomatoid carcinoma with the aim of identifying novel markers for their differential diagnosis. Although frozen tissue yields better and less degradable RNA for gene expression analysis, we preferred formalin-fixed paraffin-embedded tissue samples because they included the microscopically identifiable spindle cell tumor tissue. For this analysis, we have to amplify the small amount of RNA extracted from the formalin-fixed paraffin-embedded tissue before hybridization to the GeneChip. The Almac Xcel GeneChip from Affymetrix, which we used here, has been reported to produce identical results to the GeneChip using RNA derived from frozen tissue samples. In addition, it contains proprietary Almac-sequenced data and filtered public data for biomarker discovery and the validation of oncogene-related transcripts for a much higher detection rate in degraded samples.

From the differential expression analysis, a more than five-fold expression change in *IGF2*, *CLIC4* and *SPARC* was observed in sarcomatoid mesothelioma, and IGF2 expression was validated by real-time RT-PCR. We did not uncover significant differential expression of IGF2 between sarcomatoid mesothelioma and lung sarcomatoid carcinoma (data not shown). The discrepancy between the microarray data and real-time RT-PCR data can be explained because *IGF2* mRNA expression on a microarray chip is the relative expression between both lung sarcomatoid carcinoma and sarcomatoid mesothelioma but in a different quantity. We later investigated the immunohistochemical expression IGF2, CLIC4 and SPARC proteins in sarcomatoid mesothelioma and lung sarcomatoid carcinoma. However, there was no significant differential expression of these proteins between lung sarcomatoid carcinoma and sarcomatoid mesothelioma, limiting their applicability as an immunohistochemical positive marker of sarcomatoid mesothelioma.

In contrast, microarray gene expression analysis showed increased expression of *MUC4* in lung sarcomatoid carcinoma compared with that of sarcomatoid mesothelioma, and we found negligible *MUC4* mRNA expression in sarcomatoid mesothelioma at the mRNA level. MUC4 stands for member of mucin protein of high molecular weight glycoprotein.[15] It is expressed in various normal epithelium of the respiratory tract, particularly in the trachea and bronchi[16] and in the epithelium of the digestive and urogenital tracts.[17] MUC4 expression has been reported in various human carcinomas, including pancreatic,[18] breast[19] and lung adenocarcinoma.[20] Llinares *et al*[21] reported the diagnostic value of MUC4 expression in distinguishing epithelioid mesothelioma and lung adenocarcinoma. They found that MUC4 was expressed in 0 of the 41 epithelioid mesotheliomas and in 32 of the 35 (91%) lung adenocarcinoma. To our knowledge, this report has not been validated by other laboratories, as the antibody to MUC4 was not commercially available in the past. We observed MUC4 expression in lung adenocarcinoma and lung squamous cell carcinoma and observed no expression in epithelioid mesothelioma using a commercially available anti-MUC4 antibody. The current study is the first report to describe MUC4 expression in lung sarcomatoid carcinoma and no MUC4 expression in sarcomatoid mesothelioma. We observed a high specificity (72%) and absolute sensitivity (100%) for negative MUC4 expression to differentiate sarcomatoid mesothelioma from lung sarcomatoid carcinoma, with an accuracy rate of 87%. These values are far better than any previously identified immunohistochemical markers differentiating sarcomatoid mesothelioma from lung sarcomatoid carcinoma.

The sensitivity of MUC4 expression as a negative marker was the highest of the immunohistochemical markers in this study. Lung sarcomatoid carcinoma cases showing MUC4 expression (21 cases) also demonstrated co-expression of TTF-1 in 12 cases, Claudin-4 in 10 cases and p40 in 3 cases. Furthermore, lung sarcomatoid carcinoma cases without MUC4 expression showed TTF-1 expression in three cases, p40 in three cases and Claudin-4 in three cases. Therefore, MUC4 expression has better additional value of the immunohistochemical markers for the differential diagnosis of sarcomatoid mesothelioma from lung sarcomatoid carcinoma. The sensitivity of these markers can be improved by combining two or more, and the addition of TTF-1 and Claudin-4 to MUC4 expression improved the accuracy rate up to 95% for the differential diagnosis of sarcomatoid mesothelioma from lung sarcomatoid carcinoma.

In conclusion, we identified a novel immunohistochemical marker MUC4 that differentiates sarcomatoid mesothelioma from lung sarcomatoid carcinoma by applying whole gene expression analysis. The combination of MUC4 with TTF-1/p40 and Claudin-4 improved the sensitivity and specificity for differential diagnosis. Therefore, we propose including MUC4 as an additional negative marker to the immunohistochemical marker panel to differentiate sarcomatoid mesothelioma from lung sarcomatoid carcinoma.

Acknowledgments

We thank Ms Naomi Fukuhara for her administrative assistance. This work was supported in part by the

Japan Society for the Promotion of Science, Grants-in-Aid Scientific Research No. JP26460452 (YT) from the Ministry of Education, Science, Sports and Culture. Part of this study was performed at the Analysis Center of Life Science, Hiroshima University.

Disclosure/conflict of interest

The authors declare no conflict of interest.

References

1 Delgermaa V, Takahashi K, Park EK, *et al.* Global mesothelioma deaths reported to the World Health Organization between 1994 and 2008. Bull World Health Organ 2011;89:716–724, 24A–24C.
2 Roggli V, Churg A, Chirieac LR, *et al.* Sarcomatoid, desmoplastic, and biphasic mesothelioma. In: Travis WD, Brambilla E, Burke S, *et al.* (eds). WHO Classification of Tumours of the Lung, Pleura, Thymus, and Heart. IARC: Lyon, France, 2015, pp 165–168.
3 Husain AN, Colby T, Ordonez N, *et al.* Guidelines for pathologic diagnosis of malignant mesothelioma: 2012 update of the consensus statement from the International Mesothelioma Interest Group. Arch Pathol Lab Med 2013;137:647–667.
4 Ordonez NG. D2-40 and podoplanin are highly specific and sensitive immunohistochemical markers of epithelioid malignant mesothelioma. Hum Pathol 2005;36:372–380.
5 Chu AY, Litzky LA, Pasha TL, *et al.* Utility of D2-40, a novel mesothelial marker, in the diagnosis of malignant mesothelioma. Mod Pathol 2005;18:105–110.
6 Padgett DM, Cathro HP, Wick MR, *et al.* Podoplanin is a better immunohistochemical marker for sarcomatoid mesothelioma than calretinin. Am J Surg Pathol 2008;32:123–127.
7 Takeshima Y, Amatya VJ, Kushitani K, *et al.* Value of immunohistochemistry in the differential diagnosis of pleural sarcomatoid mesothelioma from lung sarcomatoid carcinoma. Histopathology 2009;54:667–676.
8 Kushitani K, Amatya VJ, Mawas AS, *et al.* Use of anti-Noxa antibody for differential diagnosis between epithelioid mesothelioma and reactive mesothelial hyperplasia. Pathobiology 2016;83:33–40.
9 Kerr KM, Pelosi G, Austin JHM, *et al.* Pleomorphic, spindle cell, and giant cell carcinoma. In: Travis WD, Brambilla E, Burke AP, *et al.* (eds). WHO Classification of Tumours of the Lung, Pleura, Thymus and Heart, 4th edn. IARC: Lyon, France, 2015, pp 88–90.
10 Travis WD, Noguchi M, Yatabe Y, *et al.* Adenocarcinomal. In: Travis WD, Brambilla E, Burke AP, *et al.* (eds). WHO Classification of Tumours of the Lung, Pleura, Thymus and Heart, 4th edn. IARC: Lyon, France, 2015, pp 26–37.
11 Tsao M-S, Brambilla E, Nicholson AG, *et al.* Squamous cell carcinoma. In: Travis WD, Brambilla E, Burke AP, *et al.* (eds). WHO Classification of Tumours of the Lung, Pleura, Thymus and Heart, 4th edn. IARC: Lyon, France, 2015, pp 51–55.
12 Tatsumori T, Tsuta K, Masai K, *et al.* p40 is the best marker for diagnosing pulmonary squamous cell carcinoma: comparison with p63, cytokeratin 5/6, desmocollin-3, and sox2. Appl Immunohistochem Mol Morphol 2014;22:377–382.
13 Ordonez NG. Value of claudin-4 immunostaining in the diagnosis of mesothelioma. Am J Clin Pathol 2013;139:611–619.
14 Facchetti F, Lonardi S, Gentili F, *et al.* Claudin 4 identifies a wide spectrum of epithelial neoplasms and represents a very useful marker for carcinoma versus mesothelioma diagnosis in pleural and peritoneal biopsies and effusions. Virchows Arch 2007;451:669–680.
15 Chaturvedi P, Singh AP, Batra SK. Structure, evolution, and biology of the MUC4 mucin. FASEB J 2008;22:966–981.
16 Copin MC, Devisme L, Buisine MP, *et al.* From normal respiratory mucosa to epidermoid carcinoma: expression of human mucin genes. Int J Cancer 2000;86:162–168.
17 Audie JP, Janin A, Porchet N, *et al.* Expression of human mucin genes in respiratory, digestive, and reproductive tracts ascertained by in situ hybridization. J Histochem Cytochem 1993;41:1479–1485.
18 Moniaux N, Chaturvedi P, Varshney GC, *et al.* Human MUC4 mucin induces ultra-structural changes and tumorigenicity in pancreatic cancer cells. Br J Cancer 2007;97:345–357.
19 Rakha EA, Boyce RW, Abd El-Rehim D, *et al.* Expression of mucins (MUC1, MUC2, MUC3, MUC4, MUC5AC and MUC6) and their prognostic significance in human breast cancer. Mod Pathol 2005;18:1295–1304.
20 Kwon KY, Ro JY, Singhal N, *et al.* MUC4 expression in non-small cell lung carcinomas: relationship to tumor histology and patient survival. Arch Pathol Lab Med 2007;131:593–598.
21 Llinares K, Escande F, Aubert S, *et al.* Diagnostic value of MUC4 immunostaining in distinguishing epithelial mesothelioma and lung adenocarcinoma. Mod Pathol 2004;17:150–157.

Supplementary Information accompanies the paper on Modern Pathology website (http://www.nature.com/modpathol)

Identification of DAB2 and Intelectin-1 as Novel Positive Immunohistochemical Markers of Epithelioid Mesothelioma by Transcriptome Microarray Analysis for its Differentiation From Pulmonary Adenocarcinoma

Masatsugu Kuraoka, MD,†‡ Vishwa J. Amatya, MBBS, PhD,* Kei Kushitani, MD, PhD,* Amany S. Mawas, MVSc,*§ Yoshihiro Miyata, MD, PhD,‖ Morihito Okada, MD, PhD,‖ Takumi Kishimoto, MD, PhD,¶ Kouki Inai, MD, PhD,*# Takashi Nishisaka, MD, PhD,† Taijiro Sueda, MD, PhD,‡ and Yukio Takeshima, MD, PhD**

Abstract: As there are currently no absolute immunohistochemical positive markers for the definite diagnosis of malignant epithelioid mesothelioma, the identification of additional "positive" markers that may facilitate this diagnosis becomes of clinical importance. Therefore, the aim of this study was to identify novel positive markers of malignant mesothelioma. Whole genome gene expression analysis was performed using RNA extracted from formalin-fixed paraffin-embedded tissue sections of epithelioid mesothelioma and pulmonary adenocarcinoma. Gene expression analysis revealed that disabled homolog 2 (DAB2) and Intelectin-1 had significantly higher expression in epithelioid mesothelioma compared with that in pulmonary adenocarcinoma. The increased mRNA expression of DAB2 and Intelectin-1 was validated by reverse transcriptase polymerase chain reaction of RNA from tumor tissue and protein expression was validated by Western blotting of 5 mesothelioma cell lines. The utility of DAB2 and Intelectin-1 in the differential diagnosis of epithelioid mesothelioma and pulmonary adenocarcinoma was examined by an immunohistochemical study of 75 cases of epithelioid mesothelioma and 67 cases of pulmonary adenocarcinoma. The positive rates of DAB2 and Intelectin-1 expression in epithelioid mesothelioma were 80.0% and 76.0%, respectively, and 3.0% and 0%, respectively, in pulmonary adenocarcinoma. Immunohistochemically, the sensitivity and specificity of DAB2 was 80% and 97% and those of Intelectin-1 were 76% and 100% for differentiation of epithelioid mesothelioma from pulmonary adenocarcinoma. In conclusion, DAB2 and Intelectin-1 are newly identified positive markers of mesothelioma and have potential to be included in future immunohistochemical marker panels for differentiation of epithelioid mesothelioma from pulmonary adenocarcinoma.

Key Words: DAB2, Intelectin-1, gene expression analysis, immunohistochemistry, epithelioid mesothelioma, pulmonary adenocarcinoma

(*Am J Surg Pathol* 2017;00:000–000)

Malignant mesothelioma is a rare and fatal malignant tumor.[1] In Japan, the mesothelioma death rate is increasing, approaching 1500 deaths in 2015, increased from 500 in 1995 according to Vital Statistics data published by the Ministry of Health, Labour and Welfare, Japan.[2] Similarly, the death rate due to mesothelioma is increasing globally, including the UK and Ireland,[3] the United States and other developing countries.[4] Asbestos exposure is the main risk factor for malignant pleural mesothelioma, including both occupational and environmental exposure. The time interval between first exposure to asbestos and diagnosis of mesothelioma is speculated to range from 20 to 50 years. Apart from the relatively long time it takes for asbestos to cause disease, delayed onset of symptoms can contribute to late-stage diagnosis and by then, the cancer spreads into the thoracic cavity and is more difficult to treat. Therefore, accurate diagnosis of mesothelioma is essential for its correct management.

A common site of origin of malignant mesothelioma is the pleura followed by other tissues including the peritoneum, pericardium, and tunica vaginalis. Malignant

From the Departments of *Pathology; ‡Surgery, Institute of Biomedical and Health Sciences; ‖Department of Surgical Oncology, Research Institute for Radiation Biology and Medicine, Hiroshima University; †Department of Clinical Research and Laboratory, Hiroshima Prefectural Hospital; #Pathologic Diagnostic Center Inc., Hiroshima, Japan; ¶Department of Internal Medicine, Okayama Rosai Hospital, Okayama, Japan; and §Department of Pathology and Clinical Pathology, South Valley University, Qena, Egypt.

Part of this study was performed at the Analysis Center of Life Science, Hiroshima University.

Conflicts of Interest and Source of Funding: T.K., K.I., and Y.T. has received grant from the Japanese Ministry of Health, Labour and Welfare Organization. The authors have disclosed that they have no significant relationships with, or financial interest in, any commercial companies pertaining to this article.

Correspondence: Yukio Takeshima, MD, PhD, Department of Pathology, Hiroshima University Institute of Biomedical and Health Sciences, Hiroshima University, 1-2-3 Kasumi, Minami-ku, Hiroshima 734-8551, Japan (e-mail: ykotake@hiroshima-u.ac.jp).

Supplemental Digital Content is available for this article. Direct URL citations appear in the printed text and are provided in the HTML and PDF versions of this article on the journal's Website, www.ajsp.com.

mesothelioma is classified into 3 major histologic subtypes: epithelioid, sarcomatoid, and biphasic as described in the 2015 World Health Organization (WHO) histologic classification of tumors of lung and pleura, 2015.[5] Epithelioid mesothelioma, which constitutes more than 60% of all mesothelioma, is the most common histologic subtype, and has a relatively better prognosis than sarcomatoid or biphasic mesothelioma. Epithelioid mesothelioma shows various histologic patterns including tubulopapillary, micropapillary, acinar, adenomatoid, and solid. As epithelioid mesothelioma closely resembles other malignant tumors showing pseudomesotheliomatous growth patterns, such as those of primarily lung carcinoma, breast carcinoma, and cancer that affects the lining of internal organs, the diagnosis of malignant mesothelioma is challenging, both histopathologically and clinically. Currently, the final diagnosis of malignant mesothelioma requires thorough reviewing of clinico-radiologic and pathologic findings (gross examination and histologic findings in tissue samples) with adequate immunohistochemical and/or genetic analyses. As an immunohistochemical marker with absolute sensitivity and specificity is not yet available, the search for additional novel immunohistochemical markers is critical.

The aim of this study was to identify novel positive immunohistochemical markers by analysis of whole gene expression data using microarray gene chips. We performed gene expression analysis on epithelioid cells dissected from formalin-fixed paraffin-embedded (FFPE) tissue of epithelioid mesothelioma and pulmonary adenocarcinoma and identified several novel genes that are differentially expressed between epithelioid mesothelioma and pulmonary adenocarcinoma. Of these, we identified disabled homolog 2 (DAB2) and Intelectin-1 as potential novel positive immunohistochemical markers of epithelioid mesothelioma for differentiation from pulmonary adenocarcinoma.

MATERIALS AND METHODS

Patients and Histologic Samples

The materials included in this study were obtained from the archives of the Department of Pathology, Hiroshima University. The study group consisted of 75 patients with epithelioid mesothelioma who had undergone thoracoscopic pleural biopsy, pleurectomy/decortication, extrapleural pneumonectomy, or autopsy between 2000 and 2016. Between 2005 and 2016, 67 pulmonary adenocarcinoma cases were also obtained by thoracoscopic surgical segmentectomy or lobectomy of lung harboring adenocarcinoma. All microscopic slides were reviewed and reclassified using the current WHO histologic classification of tumors of lung and pleura, 2015[6] by 4 pathologists (M.K., K.K., V.J.A., and Y.T.). Pathologic diagnosis of each case was confirmed by histologic findings and an immunohistochemical marker panel recommended by Guidelines for Pathologic Diagnosis of Malignant Mesothelioma: 2012 Update of the Consensus Statement from the International Mesothelioma Interest Group (IMIG)[7] and current 2015 WHO histologic classification of tumors of the lung, pleura, thymus, and heart.[6]

Anonymized tissue samples were provided by the Department of Pathology for gene expression and immunohistochemical analysis. This study was carried out in accordance with the Ethics Guidelines for Human Genome/Gene Research enacted by the Japanese Government for the collection of tissue specimens and was approved by the institutional ethics review committee (Hiroshima University E-974).

Gene Expression Analysis

Identification of Genes With Marked Difference Between Epithelioid Mesothelioma and Pulmonary Adenocarcinoma

FFPE sections from 6 epithelioid mesothelioma cases and 6 pulmonary adenocarcinoma cases were used for gene expression analysis. RNA extraction for gene expression analysis was performed from papillary or solid growth of tumor cells in each specimen. Five 10 μm thick FFPE tumor tissue sections, each approximately 1 cm in diameter, were processed for total RNA extraction using the Maxwell RSC RNA FFPE Kit (Promega KK, Tokyo, Japan) according to the manufacturer's protocol. Briefly, after deparaffinization and lysis with proteinase K, the samples were treated with DNase I for 15 minutes at room temperature. Following this, RNA purification was carried out according to the manufacturer's protocol using a Maxwell RSC automation instrument (Promega KK). RNA quality check and quantification was performed as described previously[8] and RNA with an absorbance ratio of ≥ 1.9 between 260 and 280 nm was used for microarray analysis. The Human Transcriptome 2.0 GeneChip Array (Affymetrix, Santa Clara, CA) containing gene transcript sets of 44,699 protein coding and 22,829 nonprotein coding clusters was used to analyze gene expression profiles. Total RNA was amplified and labeled with a 3′ IVT Labeling Kit (Affymetrix) before hybridization onto the GeneChip. Briefly, 100 ng total RNA was amplified with GeneChip 3′ IVT Pico kit (Affymetrix) to generate 30 μg of SenseRNA according to the manufacturer's protocol. SenseRNA (25 μg) was labeled with a 3′ IVT Labeling Kit (Affymetrix) and hybridized to a Human Transcriptome 2.0 GeneChip (Affymetrix) as described previously.[8] The data were analyzed using the Gene Expression Console Software (Affymetrix), and further statistical analyses were performed using the Subio Software Platform (Subio, Amami-shi, Japan) to plot graphs and for fold change of expression and hierarchical clustering.

Validation of Gene Expression Analysis

Real-time Reverse Transcriptase Polymerase Chain Reaction

The same 6 cases of epithelioid mesothelioma and pulmonary adenocarcinoma that were analyzed for gene expression profiling were used to validate the microarray

expression data by mRNA expression. The relative mRNA expression of DAB2 and Intelectin-1 was assessed with SYBR Green-based real-time reverse transcriptase polymerase chain reaction (RT-PCR) using GAPDH as a control. A total of 100 ng of RNA was used for mRNA expression with a VeryQuest SYBR Green 1-step RT-PCR Master Mix (Affymetrix) using a Stratagene Mx3000P qPCR System (Agilent Technologies, Santa Clara, CA). The primer pairs used for amplification of DAB2 and Intelectin-1 were DAB2-F: GTA GAA ACA AGT GCA ACC AAT GG, DAB2-R: GCC TTT GAA CCT TGC TAA GAG A, ITLN1-F: ACG TGC CCA ATA AGT CCC C, ITLN1-R: CCG TTG TCA GTC CAA CAC TTT C. Primers for GAPDH were GAPDH-F: ACA ACT TTG GTA TCG TGG AAG G, GAPDH-R: GCC ATC ACG CCA CAG TTT C. Data analysis was performed using the δδCT method for relative quantification. Briefly, threshold cycles (CT) for GAPDH (control) and DAB2 and Intelectin-1 (samples) were determined in triplicate. The relative expression (r_I) was calculated using the formula: $r_I = 2^{-(\text{CT sample} - \text{CT normal})}$.

Western Blotting

Total proteins were extracted from 5 commercially available mesothelioma cell lines (ACC-MESO-1, CRL-5915, ACC-MESO-4, CRL-5946, HMMME) using cell lysis protein extraction reagent (Cell-LyEX1 kit, TOYO B-Net, Tokyo, Japan). Approximately 25 μg of protein was subjected to electrophoresis on a Novex 10% Bis-Tris gel using a Bolt mini gel tank (Thermo Fisher Scientific, Yokohama, Japan). The proteins were then transferred to a Hybond-P PVDF membrane (GE Healthcare, Buckinghamshire, UK) using a Mini Blot Module (Thermo Fisher Scientific). After treating with blocking buffer, the transfer membrane was incubated with anti-DAB2 antibody (1:2000 rabbit polyclonal, catalog #HPA028888; Sigma-Aldrich, St. Louis, MO), anti-Human Intelectin-1 (1:2000, mouse monoclonal 3G9; Immuno-Biological Laboratories, Gunma, Japan) overnight at 4°C. This was followed by streptavidin-labeled anti-mouse or anti-rabbit secondary antibodies (Cell Signaling Technology, Tokyo, Japan) and Immunostar LD (Wako Pure Chemicals, Tokyo, Japan) as a chemiluminescent detection reagent. Anti-GAPDH antibody (rabbit polyclonal, Santa Cruz Biotechnology, CA) was used as control. The blot membrane was captured by scanning with C-DiGit Blot Scanner (LI-COR) for detection of proteins of interest.

Immunohistochemical Procedures and Evaluation of Expression of DAB2 and Intelectin-1

Immunohistochemistry was performed using 3 μm tissue sections prepared from the best representative FFPE blocks of epithelioid mesothelioma and pulmonary adenocarcinoma cases. Immunohistochemical staining was performed using the Ventana Benchmark GX automated immunohistochemical station (Roche Diagnostics, Tokyo, Japan). Cell Condition buffer #1 at 95°C for 32 minutes (Roche Diagnostics) was used for antigen retrieval. The sections were then incubated with primary antibodies to calretinin (rabbit monoclonal, SP65, prediluted; Roche Diagnostics), podoplanin (mouse monoclonal, D2-40, Prediluted; Nichirei Bioscience, Tokyo, Japan), Wilms' tumor gene product (WT1) (mouse monoclonal, 6F-H12, 1:25; Dako, Glostrup, Denmark), DAB2 (rabbit polyclonal, catalog #HPA028888, 1:200; Sigma-Aldrich), and Intelectin-1 (mouse monoclonal, 3G9, 1:1000; Immuno-Biological Laboratories). Incubation with the secondary antibody and detection was performed with Ventana ultraView Universal DAB Detection Kit.

Immunoreactivity was scored as either negative (no immunostaining) or positive. Cells showing nuclear staining for calretinin and WT1, cytoplasmic staining for DAB2 and Intelectin-1, or membranous staining for podoplanin (clone: D2-40) were recorded as "positive." Positive immunoreactivity was further scored as 1+ for up to 10% of tumor cells showing positive immunostaining, 2+ for 10% to 50% positive tumor cells, and 3+ for >50% positive tumor cells. Statistical analyses were performed using the Fisher exact test. Sensitivity, specificity, positive predictive value, negative predictive value, and accuracy rate were calculated using a simple 2 × 2 table.

RESULTS

Differential Gene Expression and Validation in Epithelioid Mesothelioma and Pulmonary Adenocarcinoma

Of the 44,699 protein coding and 22,829 nonprotein coding transcripts on the Human Transcriptome 2.0 GeneChip Array, 902 statistically significant mRNA transcripts were differentially expressed, with a greater than 1.3-fold difference, between epithelioid mesothelioma and pulmonary adenocarcinoma (Fig. 1). Hierarchical clustering of 426 protein coding mRNA transcripts revealed 197 upregulated mRNA transcripts in epithelioid mesothelioma, including CALB2, WT1, DAB2, and Intelectin-1, and 229 upregulated mRNA transcripts in pulmonary adenocarcinoma, including CEACAM6 and NAPSA (Fig. 2; Supplementary Table S1, Supplemental Digital Content 1, http://links.lww.com/PAS/A504).

Real-time RT-PCR showed relative mRNA expression of DAB2 and Intelectin-1 was significantly higher in epithelioid mesothelioma than that in pulmonary adenocarcinoma (data not shown). Western blot analysis showed DAB2 and Intelectin-1 protein expression in all 5 commercially available mesothelioma cells lines with an electrophoretic band of 80 kDa with DAB2 and 1 or 2 electrophoretic bands in the range of 30 to 40 kDa with the Intelectin-1 antibody (Fig. 3).

Immunohistochemical Expression Profiles in Epithelioid Mesothelioma and Pulmonary Adenocarcinoma

The expression of positive mesothelioma markers are summarized in Table 1 and the representative images for DAB2 and Intelectin-1 expression in epithelioid mesothelioma and pulmonary adenocarcinoma are pre-

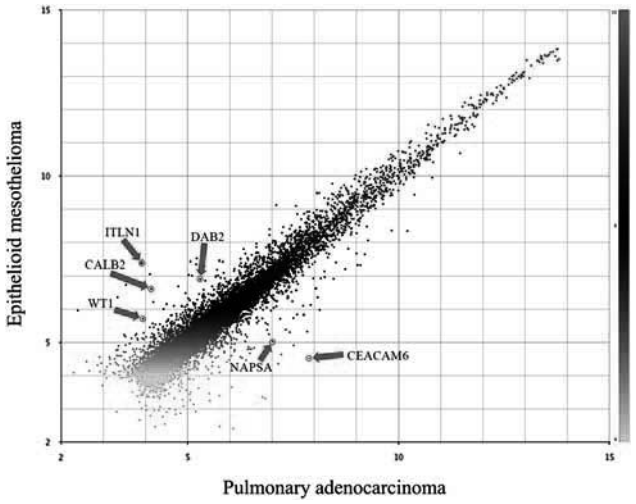

FIGURE 1. Scatter plot diagram showing differential expression of various genes between epithelioid mesothelioma and pulmonary adenocarcinoma. Note, DAB2 and Intelectin-1 locate toward the epithelioid mesothelioma, in addition to previously known mesothelioma positive markers, CALB2 (calretinin) and WT1, while NAPSA (Napsin-A) and CEACAM6 (major gene for CEA), positive pulmonary adenocarcinoma markers, locate towards pulmonary adenocarcinoma.

sented in Figures 4 and 5, respectively. The staining pattern for each marker in 2 tumor types is described in the following sections.

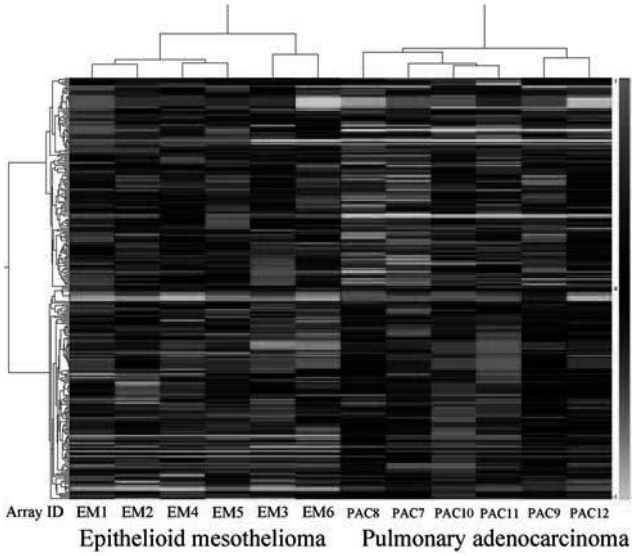

FIGURE 2. Supervised hierarchical clustering of differentially expressed genes between epithelioid mesothelioma and pulmonary adenocarcinoma. The hierarchical clustering of 426 protein coding mRNA transcripts revealed 197 upregulated mRNA transcripts in epithelioid mesothelioma and 229 upregulated mRNA transcripts in pulmonary adenocarcinoma. See detailed data in Supplementary Table S1 (Supplemental Digital Content 1, http://links.lww.com/PAS/A504).

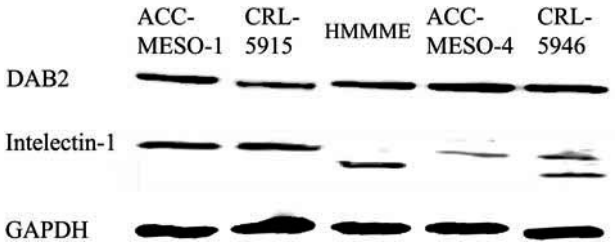

FIGURE 3. Western blot showing DAB2 and Intelectin-1 expression in mesothelioma cell lines. DAB2 expression is present in all 5 mesothelioma cell lines as a single band; however, Intelectin-1 expression is present as either a single or double band.

DAB2 and Intelectin-1 Expression

The expression of DAB2 and Intelectin-1 was localized in the cytoplasm of tumor cells in epithelioid mesothelioma cases. Positive DAB2 expression was observed in 60 of 75 epithelioid mesotheliomas (80.0%) and 2 of 67 pulmonary adenocarcinomas (3.0%). In half of epithelioid mesotheliomas, DAB2 immunoreactivity was generally strong and diffuse (score 3+). In contrast, pulmonary adenocarcinomas showing DAB2 expression was focal (score 1+). In addition, DAB2 expression in alveolar macrophages in pulmonary adenocarcinomas was a helpful internal positive control. Positive Intelectin-1 expression was observed in 57 of 75 epithelioid mesotheliomas (76.0%), with most of them showing score 3+, whereas none of the 67 pulmonary adenocarcinomas were positive for Intelectin-1.

Calretinin, D2-40, and WT1 Expression

Positive calretinin expression was recorded for 74 of 75 epithelioid mesotheliomas (98.7%) and 17 of 67 pulmonary adenocarcinomas (25.4%). In epithelioid mesotheliomas, immunoreactivity was generally strong and diffuse (score 3+). In contrast, staining score in pulmonary adenocarcinomas was 1+ and 2+. There were no score 3+ cases in pulmonary adenocarcinomas. Positive D2-40 expression was observed in 71 of 75 epithelioid mesotheliomas (94.7%), with most of them showing score 3+, whereas only 7 pulmonary adenocarcinomas (10.4%) were focally positive (score 1+ and 2+) for D2-40. Positive WT1 expression was recorded in 62 of 75 epithelioid mesotheliomas (82.7%), whereas none of 67 pulmonary adenocarcinomas (0%) were positive for WT1.

Sensitivity and Specificity of Each Marker for Differential Diagnosis of Epithelioid Mesothelioma and Pulmonary Adenocarcinoma

The sensitivity and specificity of each marker for the differential diagnosis between epithelioid mesothelioma and pulmonary adenocarcinoma are shown in Table 2. Sensitivity of Intelectin-1 (76%) was lowest among 5 positive markers; however, its specificity (100%) was absolute. Sensitivity (80.0%) and specificity (97.0%) of

TABLE 1. Immunohistochemical Findings for Epithelioid Mesothelioma and Pulmonary Adenocarcinoma

	Epithelioid Mesothelioma					Pulmonary Adenocarcinoma				
		Immunoreactivity Score*					Immunoreactivity Score*			
Marker	n/N (%)	0	1+	2+	3+	n/N (%)	0	1+	2+	3+
DAB2	60/75 (80.0)	15	12	18	30	2/67 (3.0)	65	2	0	0
Intelectin-1	57/75 (76.0)	18	17	4	36	0/67 (0)	67	0	0	0
Calretinin	74/75 (98.7)	1	7	2	65	17/67 (25.4)	50	10	7	0
Podoplanin (D2-40)	71/75 (94.7)	4	5	6	60	7/67 (10.4)	60	5	2	0
WT1	62/75 (82.7)	13	18	7	37	0/67 (0)	67	0	0	0

*0, negative; 1+, <10% positive; 2+, 10% to 50% positive; 3+, 50% < positive.

DAB2 were nearly those of WT1. Specificity of calretinin (74.6%) was lowest among 5 markers.

DISCUSSION

Pathologically, the role of immunohistochemistry in distinguishing pleural epithelioid mesothelioma from pulmonary adenocarcinoma has received much attention especially in the last 20 years. Currently, there are many immunohistochemical markers available for distinguishing epithelioid mesothelioma from pulmonary adenocarcinoma. Among these, calretinin, cytokeratin 5/6, podoplanin (D2-40), and WT1 are the preferred positive markers for epithelioid mesothelioma. Carcinoembryonic antigen (CEA), MOC31 (epithelial-related antigen), Ber-EP4, BG-8, thyroid transcription factor-1, claudin-4, and napsin-A are the preferred positive markers for pulmonary adenocarcinoma. The IMIG 2012 guidelines recommended the consideration of 2 mesothelial and 2 carcinoma markers, based on morphology at initial observation.[7] In practice, immunohistochemical examination, most laboratories use calretinin, D2-40, and WT1 for diagnosis of epithelioid mesothelioma. However, pathologists must interpret the results of staining by these markers carefully, as specificity of calretinin (74.6% in this study, 90% to 95% in IMIG 2012 guidelines) and D2-40 (88.9% in this study, up to 85% in IMIG 2012 guidelines) is not absolute; additionally, WT1 shows low sensitivity (82.7% in this study, approximately 90% to 100% in IMIG 2012 guidelines). Therefore, novel positive immunohistochemical markers, other than calretinin, D2-40, or WT1, are necessary for increasing the accuracy of epithelioid mesothelioma diagnosis.

Recent development of molecular techniques enabled gene expression analysis from RNA extracted from archival FFPE tumor tissues using GeneChip technology. This method is very useful to find new diagnostic markers, especially in rare tumors, including malignant mesothelioma. We have recently reported the identification of a novel marker, MUC4, for differentiating pleural sarcomatoid mesothelioma from pulmonary sarcomatoid carcinoma by analyzing gene expression data from a gene chip microarray.[8] In this study, we performed gene expression microarray analysis of 6 cases of mesothelioma and 6 cases of pulmonary adenocarcinoma to identify differentially expressed gene products in epithelioid mesothelioma and pulmonary adenocarcinoma. We found that the expression of DAB2 and Intelectin-1 in epithelioid mesothelioma was significantly higher than that in pulmonary adenocarcinoma and this was validated by real-time RT-PCR analysis of mRNA extracted from the same tissue source and Western blot analysis of proteins extracted from mesothelioma cell lines. Immunohistochemical analysis showed that expression of DAB2 and Intelectin-1 in epithelioid mesotheliomas was significantly higher than that in pulmonary adenocarcinomas. These novel positive mesothelial markers, DAB2 and/or Intelectin-1, contribute in accurate mesothelioma diagnosis, in addition to known positive markers (calretinin, D2-40, and WT1). In the present study, we analyzed gene expression analysis of only 6 cases of epithelioid mesothelioma and 6 cases of pulmonary adenocarcinoma, and found many differentially expressed genes mentioned in Supplementary Table S1 (Supplemental Digital Content 1, http://links.lww.com/PAS/A504). As the analysis of substantially larger number will make these findings more credible, we plan to include more cases in the future.

DAB2, a mitogen-responsive phosphoprotein, is expressed in normal ovarian epithelial cells, but is downregulated or absent from ovarian carcinoma cell lines, suggesting its role as a tumor suppressor.[9] Decreased DAB2 expression has been reported in various human cancers, including esophageal,[10] lung,[11] ovarian,[9] prostate,[12] and breast[13] cancers. DAB2 downregulation in these cancers were reported partly due to miRNA targeting DAB2[10,14] or promoter hypermethylation.[13,15] However, the biological significance or expression of DAB2 has not yet been reported in malignant mesothelioma. In the present study, we found increased expression of DAB2 in epithelioid mesothelioma compared with that in pulmonary adenocarcinoma by gene expression microarray analysis. We also confirmed this increased expression of DAB2 in epithelioid mesothelioma by real-time RT-PCR and western blot. From the differential analysis of DAB2 expression between epithelioid mesothelioma and pulmonary adenocarcinoma by immunohistochemical study, we found higher sensitivity and specificity in epithelioid mesothelioma of >80%. In 2 of the 67 cases of pulmonary adenocarcinoma, DAB2 expression was identified in tumor cells but with a low immunoreactivity score. DAB2 expression in pulmonary adenocarcinomas was present in inflammatory cell infiltration, mainly macrophages; therefore, precaution must be taken by the physician

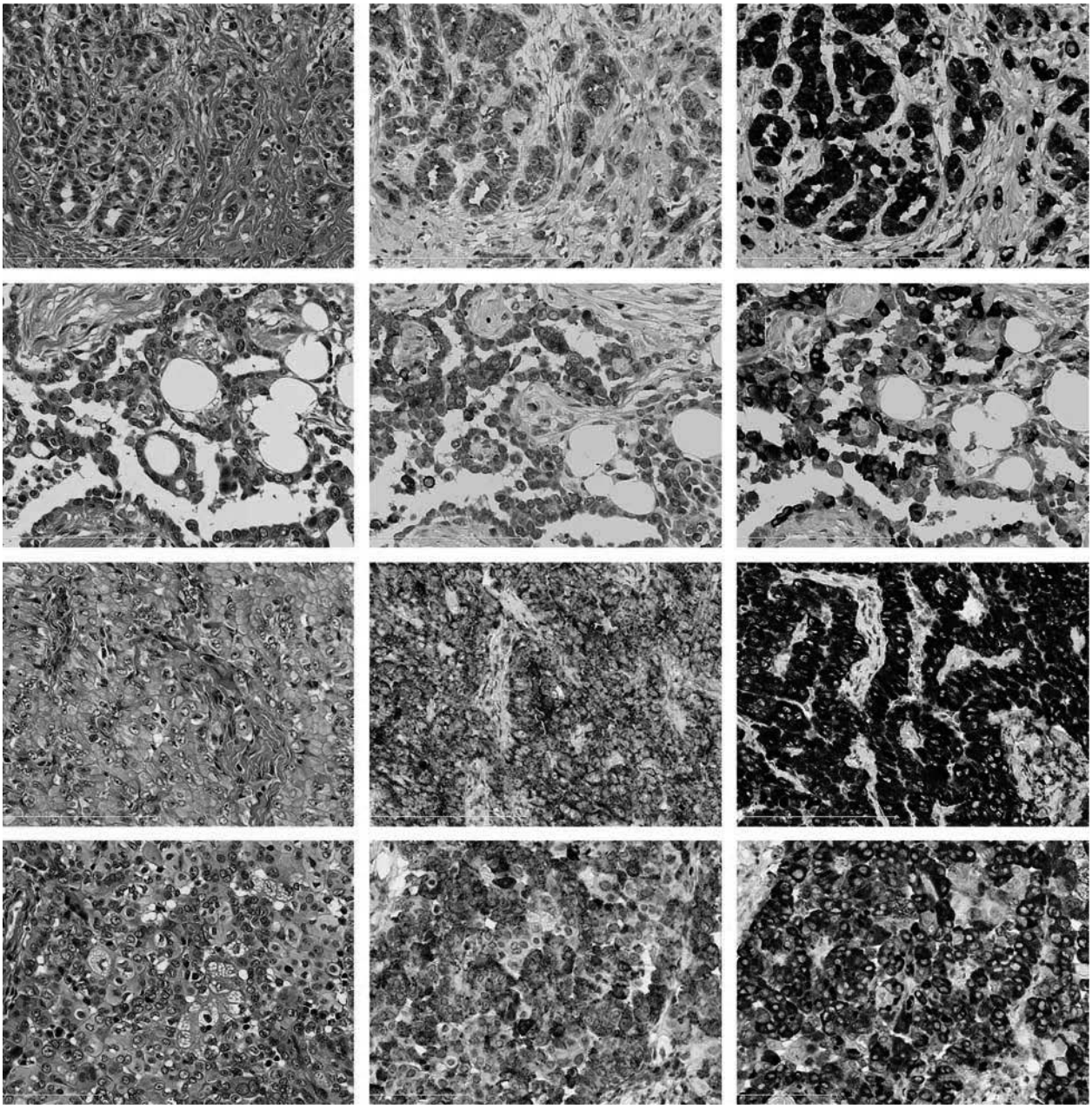

FIGURE 4. DAB2 and Intelectin-1 expression in epithelioid mesothelioma. Various histomorphologic patterns of epithelioid mesothelioma showing prominent expression of DAB2 (middle column) and Intelectin-1 (right column). Each row shows epithelioid mesothelioma with corresponding DAB2 and Intelectin-1 immunohistochemistry.

when interpreting pulmonary adenocarcinoma results for DAB2 expression.

Human Intelectin-1, also known as omentin, is a galactose-binding lectin that is usually expressed in the heart and small intestine as a host defense lectin that binds to bacterial galactofuranose.[16] Intelectin-1 is mainly expressed in the intestinal goblet cells and omentum, and occasionally in the thymus, bronchus, heart, liver, kidney collecting tubule cells, bladder umbrella, and mesothelial cells.[17] Recently, the overexpression of Intelectin-1 in human malignant pleural mesothelioma and its secretion into pleural effusions indicated toward it being a potential biomarker.[17,18] It was reported that Intelectin-1 was not expressed in various cancers, except in some mucus-producing adenocarcinomas.[19] In the present study, we observed high expression of Intelectin-1 mRNA in epithelioid mesothelioma, definite expression of Intelectin-1 in mesothelioma cell lines by western blot analysis, and in 57 of 75 mesothelioma tissue samples by immunohistochemical analysis. In addition, we also found Intelectin-1 expression in non-neoplastic mesothelial lining cells and goblet cells in bronchi and bronchioles

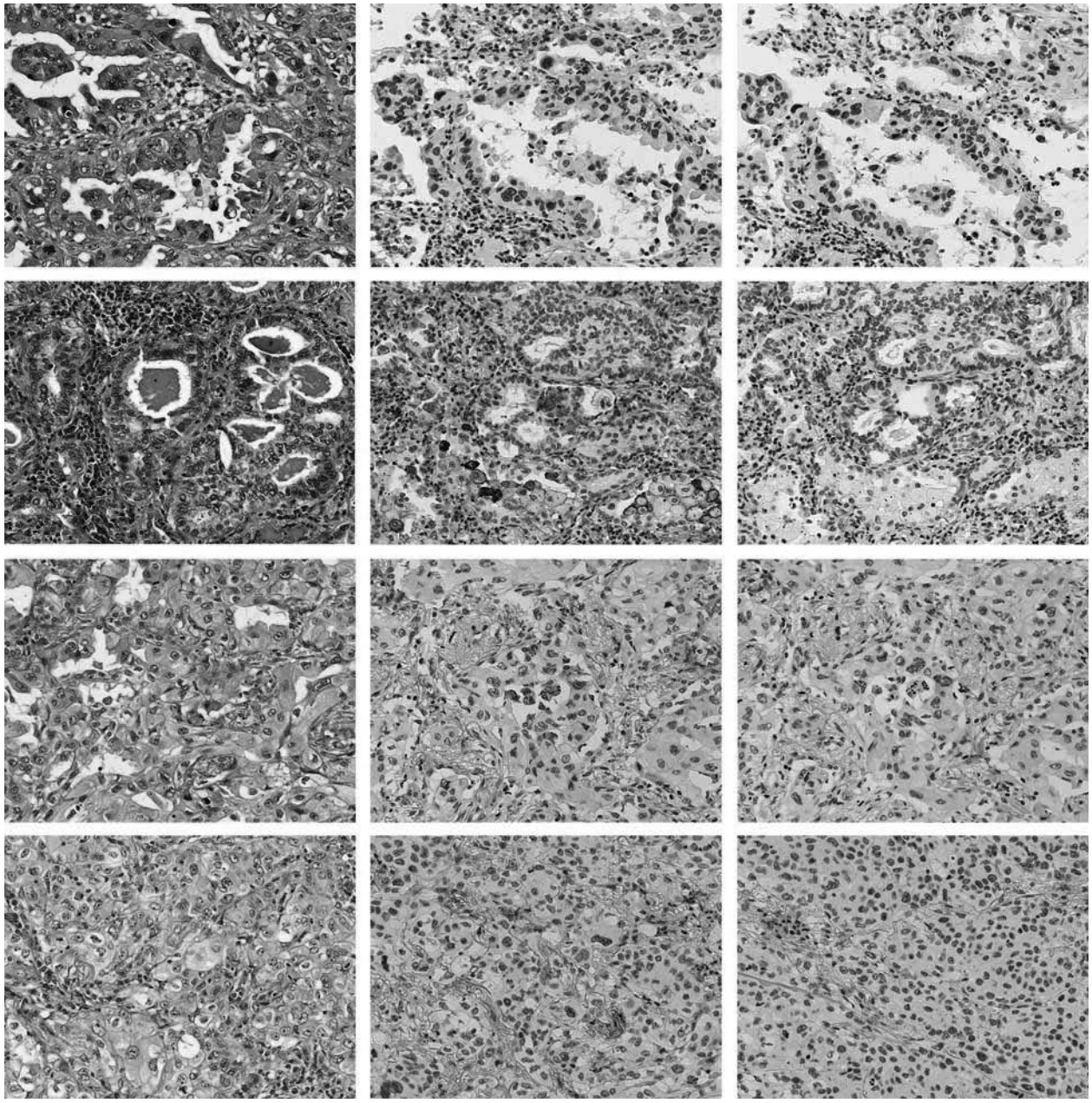

FIGURE 5. DAB2 and Intelectin-1 expression in pulmonary adenocarcinoma. Various histomorphologic patterns of pulmonary adenocarcinoma showing no expression of DAB2 (middle column) and Intelectin-1 (right column). Each row shows pulmonary adenocarcinoma with corresponding DAB2 and Intelectin-1 immunohistochemistry. There is focal reactivity of DAB2 in alveolar macrophages and lymphocytes, which need to interpreted with care.

TABLE 2. Sensitivity and Specificity of Immunohistochemical Positive Markers for Differential Diagnosis of Epithelioid Mesothelioma from Pulmonary Adenocarcinoma

Immunohistochemical Markers	Sensitivity (%)	Specificity
INT-1 +	76.0	100
DAB2 +	80.0	97.0
Calretinin +	98.7	74.6
D2-40 +	94.7	89.6
WT-1 +	82.7	100

(data not shown). No Intelectin-1 expression was recorded in any pulmonary adenocarcinoma cases, confirming its potential as a novel positive mesothelial marker. The functional roles of DAB2 and Intelectin-1 expression in epithelioid mesothelioma need further analysis, which is beyond the scope of this study.

In conclusion, we identified 2 novel positive markers of epithelioid mesothelioma, DAB2 and Intelectin-1, by using gene expression microarray analysis and confirmed their utility to differentiate epithelioid mesothelioma from

pulmonary adenocarcinoma by immunohistochemical study. Further validation of immunohistochemical staining of these markers by other institutes is warranted.

ACKNOWLEDGMENTS

The authors thank Ms Yukari Go of the Technical Center in Hiroshima University for excellent technical assistance and Ms Naomi Fukuhara for editorial assistance.

REFERENCES

1. Robinson BW, Lake RA. Advances in malignant mesothelioma. *N Engl J Med*. 2005;353:1591–1603.
2. Mortality rate due to mesothelioma in Japan: Ministry of Health, Labor & Welfare. Available at: www.mhlw.go.jp/toukei/saikin/hw/jinkou/tokusyu/chuuhisyu15/dl/chuuhisyu.pdf. Accessed January 6, 2017.
3. Mesothelioma statistics: cancer research, UK. 2015. Available at: www.cancerresearchuk.org/health-professional/cancer-statistics/statistics-by-cancer-type/mesothelioma. Accessed January 6, 2017.
4. Delgermaa V, Takahashi K, Park EK, et al. Global mesothelioma deaths reported to the World Health Organization between 1994 and 2008. *Bull World Health Organ*. 2011;89:716–724. 724A–724C.
5. Travis WD, Noguchi M, Yatabe Y, et al. Epithelioid mesothelioma. In: Travis WD, Brambilla E, Burke AP, et al, eds. *WHO Classification of Tumours of the Lung, Pleura, Thymus and Heart*. Lyon: IARC; 2015:156–164.
6. Travis WD, Noguchi M, Yatabe Y, et al. Adenocarcinoma. In: Travis WD, Brambilla E, Burke AP, et al, eds. *WHO Classification of Tumours of the Lung, Pleura, Thymus and Heart*. Lyon: IARC; 2015:26–37.
7. Husain AN, Colby T, Ordonez N, et al. Guidelines for pathologic diagnosis of malignant mesothelioma: 2012 update of the consensus statement from the International Mesothelioma Interest Group. *Arch Pathol Lab Med*. 2013;137:647–667.
8. Amatya VJ, Kushitani K, Mawas AS, et al. MUC4, a novel immunohistochemical marker identified by gene expression profiling, differentiates pleural sarcomatoid mesothelioma from lung sarcomatoid carcinoma. *Mod Pathol*. 2017. Doi:10.1038/modpathol.2016.181.
9. Mok SC, Chan WY, Wong KK, et al. DOC-2, a candidate tumor suppressor gene in human epithelial ovarian cancer. *Oncogene*. 1998;16:2381–2387.
10. Li C, Ding C, Chen T, et al. Micro ribonucleic acid-93 promotes proliferation and migration of esophageal squamous cell carcinoma by targeting disabled 2. *Thorac Cancer*. 2015;6:524–533.
11. Du L, Zhao Z, Ma X, et al. miR-93-directed downregulation of DAB2 defines a novel oncogenic pathway in lung cancer. *Oncogene*. 2014;33:4307–4315.
12. Zhoul J, Hernandez G, Tu SW, et al. The role of DOC-2/DAB2 in modulating androgen receptor-mediated cell growth via the non-genomic c-Src-mediated pathway in normal prostatic epithelium and cancer. *Cancer Res*. 2005;65:9906–9913.
13. Bagadi SA, Prasad CP, Srivastava A, et al. Frequent loss of DAB2 protein and infrequent promoter hypermethylation in breast cancer. *Breast Cancer Res Treat*. 2007;104:277–286.
14. Chao A, Lin CY, Lee YS, et al. Regulation of ovarian cancer progression by microRNA-187 through targeting disabled homolog-2. *Oncogene*. 2012;31:764–775.
15. Li C, Chen J, Chen T, et al. Aberrant hypermethylation at sites 86 to 226 of DAB2 gene in non-small cell lung cancer. *Am J Med Sci*. 2015;349:425–431.
16. Tsuji S, Uehori J, Matsumoto M, et al. Human intelectin is a novel soluble lectin that recognizes galactofuranose in carbohydrate chains of bacterial cell wall. *J Biol Chem*. 2001;276:23456–23463.
17. Washimi K, Yokose T, Yamashita M, et al. Specific expression of human intelectin-1 in malignant pleural mesothelioma and gastrointestinal goblet cells. *PLoS One*. 2012;7:e39889.
18. Tsuji S, Tsuura Y, Morohoshi T, et al. Secretion of intelectin-1 from malignant pleural mesothelioma into pleural effusion. *Br J Cancer*. 2010;103:517–523.
19. Zheng L, Weng M, Qi M, et al. Aberrant expression of intelectin-1 in gastric cancer: its relationship with clinicopathological features and prognosis. *J Cancer Res Clin Oncol*. 2012;138:163–172.

労災疾病等医学研究・両立支援報告３　R3－1

石綿ばく露によるびまん性胸膜肥厚と中皮腫・肺癌発生に関する検討

岸本　卓巳，藤本　伸一

岡山労災病院アスベスト研究センター

（平成29年2月24日受付）

要旨：【目的】職業性石綿ばく露によって発症したびまん性胸膜肥厚に合併する肺癌および中皮腫の頻度と症例の詳細について検討した．

【対象と方法】労災補償あるいは石綿健康被害救済法のびまん性胸膜肥厚の胸部画像の認定基準を満たした224例について，平成22年4月から平成28年2月までに肺癌および中皮腫を発症した症例の頻度と症例の詳細について検討した．対照群として，同時期に低線量CT検査を行った石綿健康管理手帳健診対象者2,130例を選択した．

【結果】びまん性胸膜肥厚224例中，中皮腫を発症した症例はなかったが，肺癌発症例は8例（3.6%）あった．観察期間から人口10万人あたり610.3人/年と高率であった．一方，対照群では56例（2.6%）で，人口10万人あたり443.9人/年であった．

肺癌発症症例はすべて男性で，年齢の中央値は72歳と高齢者が多かった．組織型は小細胞癌4例，腺癌3例，扁平上皮癌1例で，すべてが喫煙者であった．職業性石綿ばく露は中等度以上のばく露者が多く，ばく露期間の中央値33.5年，潜伏期間は54年と長かった．そのうち，著しい呼吸機能障害のある症例は5例で，石綿肺を伴うものが3例，伴わないものが2例であった．

【考察】石綿ばく露によって発症するびまん性胸膜肥厚症例は一定以上の石綿ばく露量を必要とすると言われているが，今回肺癌を発症した症例についても同様で，なおかつ重喫煙者が多かった．肺癌発生頻度は石綿健康管理手帳を有する人々より高く55～74歳で30パック・年以上の喫煙男性を対象としたNational Lung Screening Trial（以下，NLST）の10万対645人年と同等であった．また特に発症頻度が高いと報告されている中皮腫の発症は過去6年間1症例もなかったが，その理由は明らかではなかった．

【結論】6年間の観察期間中，著しい呼吸機能障害を有するびまん性胸膜肥厚に発症した肺癌は労災補償対象とされているがわずか2例（0.89%）であり，喫煙との関連が大きかった．また，中皮腫合併は1例もなかった．

（日職災医誌，65：153—159，2017）

—キーワード—

石綿ばく露，びまん性胸膜肥厚，肺癌

はじめに

石綿ばく露によるびまん性胸膜肥厚とは限局性胸膜肥厚である胸膜プラークに対して，広範囲で肺の一葉以上を巻き込むような胸膜の線維化（臓側胸膜の病変で，通常は壁側胸膜との癒着を来たしている）である．胸膜プラークとの画像上の相違にはcrow's　feetと円形無気肺所見が重要である[1]．日本では平成15年から著しい呼吸機能障害を伴う症例は労災補償対象疾病となり，平成22年からは石綿健康被害救済法（以下，救済法とする）の対象ともなった．びまん性胸膜肥厚は臓側と壁側胸膜あるいは胸膜と横隔膜の癒着から主に拘束性呼吸機能障害を来すとともに拡散能低下が生じると報告されている[2)3)]．しかし，その成因とともに，本疾患に関わる累積石綿ばく露量や，中皮腫や肺癌の合併頻度等不明な点も少なくない．今回，職業性石綿ばく露によるびまん性胸膜肥厚症例のうち中皮腫あるいは肺癌を合併した症例について検討したので報告する．

目　的

職業性石綿ばく露によって発症したびまん性胸膜肥厚に合併する肺癌および中皮腫の頻度と症例の詳細につい

表1　びまん性胸膜肥厚224例中，原発性肺癌を合併した症例

症例	年齢	性別	著しい呼吸機能障害	肺癌組織型	喫煙歴	喫煙指数	職業病	ばく露年数（年）	潜伏期間（年）	両側性片側性	石綿肺の有無	胸膜プラーク		肺内石綿小体数本/g
												限局性	広範囲	
1	64	男性	あり	小細胞癌	30本×15年	450	造船・保温	31	33	両側性	PR2/2		+	198,654
2	74	男性	あり	腺癌	20本×35年	700	造船・配管	45	59	両側性	PR1/1		+	ND
3	71	男性	なし	腺癌	30本×55年	1,650	石綿運搬	3	51	右側片側性	なし		+	ND
4	73	男性	あり	扁平上皮癌	40本×50年	2,000	塗装	35	53	両側性	PR1/1	+		ND
5	68	男性	なし	腺癌	30本×20年	600	ボード成型	45	53	両側性	なし	+		10,601
6	68	男性	なし	小細胞癌	40本×38年	1,320	水道配管	32	43	両側性	なし	+		ND
7	73	男性	あり	小細胞癌	20本×48年	960	建設業	54	67	両側性	なし		+	ND
8	81	男性	あり	小細胞癌	20本×50年	1,000	内装作業	29	55	両側性	なし		+	5,300

て検討する．

対象と方法

平成22年4月1日から平成28年2月1日までに全国労災病院や研究協力者の病院及び石綿健康被害救済法により認定された職業性石綿ばく露によって発症したびまん性胸膜肥厚症例224例を対象とした．対象症例要件として労災補償あるいは石綿健康被害救済法の認定基準である胸部レントゲン写真上の胸膜肥厚の範囲が片側であれば片側胸郭の2分の1以上，両側の場合には両側胸郭の4分の1以上であって，石綿ばく露作業従事期間が3年以上ある症例とした．このうち，著しい呼吸機能障害を伴う症例は176例，そうでない症例が48例であった．すなわち，176例は労災補償あるいは救済法の対象となった症例である．これら症例のうち平成28年2月1日までに病理組織学的に中皮腫と診断された症例あるいは肺癌と確定診断された症例について検討した．

検討項目は年齢，性別，著しい呼吸機能障害の有無，肺癌の組織型，喫煙歴，職業歴・年数・肺癌発生までの潜伏期間，胸部画像所見としてのびまん性胸膜肥厚の範囲，石綿肺，胸膜プラークの有無及び肺内石綿小体数である．なお，肺癌の病期，組織型は肺癌取扱い規約（第7版）に則った．

対照は平成22年4月1日から平成28年2月1日までに岡山労災病院・富山労災病院・千葉労災病院・香川労災病院・北海道中央労災病院・玉野三井病院・近畿中央胸部疾患センター・山口宇部医療センターの8施設における石綿健康管理手帳健診受診者2,080例および，石綿ばく露歴を有する現役労働者のうち低線量CT撮影に文書で同意した50例の計2,130例とした．

結　果

対象224例のうち性別では男性218例（97.3%），女性6例（2.7%）であった．診断時年齢は44歳から91歳（中央値72歳）で，中皮腫を発症した症例は皆無であった．また，肺癌を発症した症例は8例（3.6%）であった．観察期間を考慮した肺癌発生率は人口10万人当たり610.3人/年であった．一方，対照とした低線量CTを撮影した2,130例のうち性別は男性2,048例（96.2%），女性82例（3.8%）であった．診断時年齢は48歳から96歳（中央値72歳）で，胸膜プラークを認めた症例は1,904例（89.4%）であった．また，平成28年2月までの肺癌発生率は56例（2.6%）であった．観察期間を考慮した肺癌発生率は人口10万人当たり433.9人/年であった[4]．一方，中皮腫は7例（0.3%）であった．

びまん性胸膜肥厚に肺癌を発症した8例の詳細は表1に示す．

年齢は64歳から81歳（中央値72歳）で全例男性であった．著しい呼吸機能障害があった症例は5例であった．肺癌組織型では小細胞癌4例，腺癌3例，扁平上皮癌1例であった．8例はすべて喫煙者で，喫煙指数は450から2,000で，中央値は980と重喫煙者が大半であった．職業性石綿ばく露歴では造船，配管，石綿運搬など中等度以上のばく露量を受ける作業歴があり，職業性ばく露期間も3～54年間（中央値33.5年）であった．初回ばく露から肺癌発生までの潜伏期間は33～67年（中央値54年）と長かった．画像上，びまん性胸膜肥厚は1例を除いて両側性で，石綿肺の合併が3例あった．また，全例に胸膜プラークを認め，そのうち3例では胸部レントゲン写真上で胸膜プラークを認めるか胸郭の4分の1以上の広範囲プラークを認めた．また，肺内石綿小体を測定できた3例中全例で肺癌発生頻度を2倍以上にする肺乾燥重量1gあたり5,000本以上[5]が検出された．

上述のごとく肺癌を発生した8例中5例では著しい呼吸機能障害があり，労災あるいは救済法の対象となる症例である．そのうち症例1，2，4は石綿肺合併症例であり，昭和53年の石綿肺癌認定基準の1型以上の石綿肺に合併した肺癌として認定を受けるべき症例である．

また，症例3，5，6は著しい呼吸機能障害がないため，びまん性胸膜肥厚として労災あるいは救済法で認定されない症例である．しかし，他の認定要件である胸膜プラークあるいは広範囲胸膜プラークと職業性石綿ばく露歴があるため石綿肺癌として認定される症例であるため，石綿肺癌認定基準としてのびまん性胸膜肥厚の基準は必要

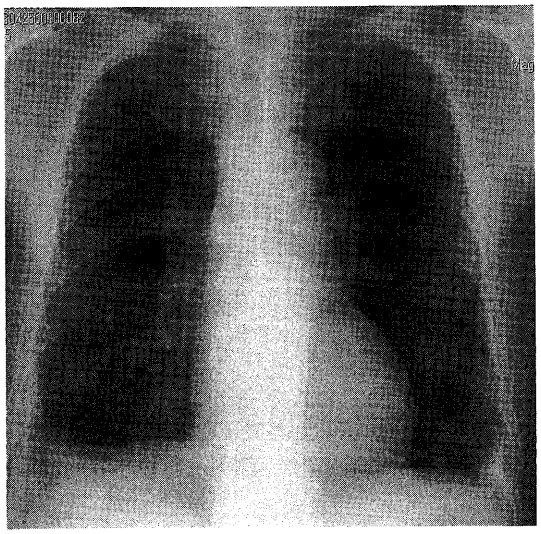

図1　平成X－4年　胸部レントゲン写真正面像で両側びまん性胸膜肥厚を来した症例である．

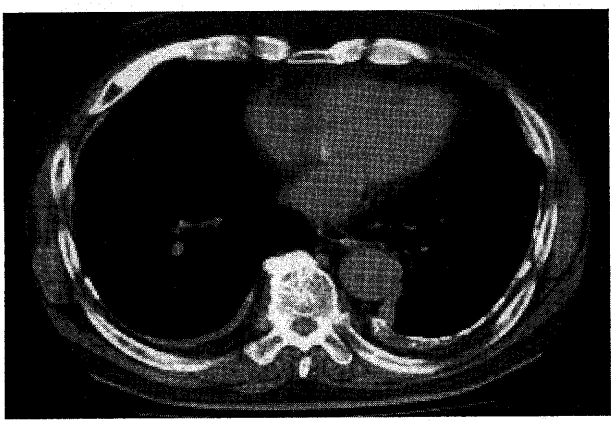

図2　平成X－4年　胸部CT縦隔条件では両側びまん性胸膜肥厚は一部に石灰化胸膜プラークを伴う．

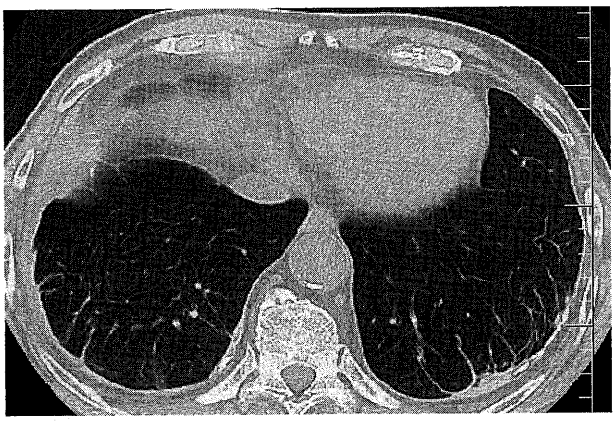

図3　平成X－4年　胸部CT肺野条件で両側胸壁にcrow's feet signを認める．

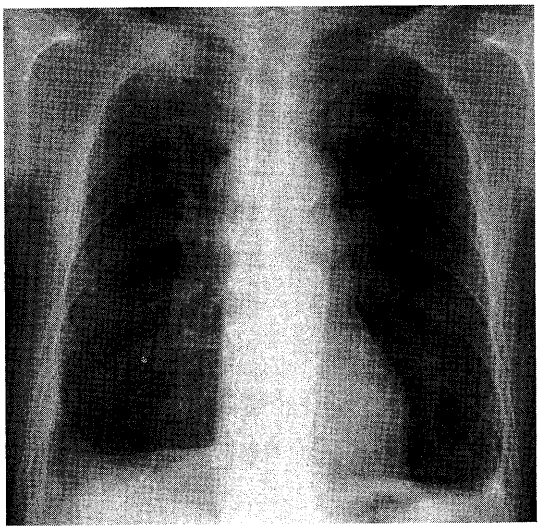

図4　肺癌発生時の胸部レントゲン写真正面像では右肺尖部に腫瘤陰影を認める．

としない．

労災認定基準である著しい呼吸機能障害を伴うびまん性胸膜肥厚症例で石綿肺を伴わない症例は症例7，8の2例のみとなる．そこで，この2例について症例を呈示する．

症例7は73歳，男性で，主訴は体重減少である．職業歴では大工として約54年間の職業性石綿ばく露歴がある．喫煙歴としては20本/日，48年間と重喫煙者である．

現病歴では近医で高血圧と糖尿病を加療中であった．平成X－4年7月にびまん性胸膜肥厚のため労災認定をうけている．診断時の呼吸機能検査は，VC：2.15L，%VC：63.9%，$FEV_{1.0}$：0.97L，1秒率%：45.1%，%1秒量：36.8%であり，著しい混合性呼吸機能障害を伴っていた．動脈血ガス分析においては，PH：7.34，PaO_2：79.4mmHg，$PaCO_2$：43.3mmHgとほぼ正常であった．

診断時の平成X－4年4月の胸部レントゲン写真で(図1)は，両側の肋横角の消失と両側の胸膜肥厚を認め，両側胸壁の4分の1以上のびまん性胸膜肥厚の基準を満たしていた．また，図2，3の如く胸部CTにて胸膜プラークではなく，びまん性胸膜肥厚であることを確認した．平成X年9月に血清CEAの上昇と体重減少のため前医で精査を施行したところ，胸部レントゲン写真にて腫瘤陰影を認め，精査加療目的で平成X年10月に当院に紹介となった．胸部レントゲン写真(図4)では，右肺尖部に腫瘤陰影を認めた．胸部CT（図5）では，右肺S1に38mm大の腫瘤とリンパ節#4R，#7，#10Rに腫大を認めた．経気管支肺生検と超音波気管支鏡ガイド下針生検を施行し，小細胞肺癌と診断した．全身精査の結果，T2aN2M0 cStage IIIA，と診断した．年齢と肺機能を考慮し化学療法単独での治療方針となった．平成X年10月から化学療法を行い奏効しているため生存中である．

症例8は81歳の男性で，主訴は労作時呼吸困難である．喫煙歴は20本/日，50年間の過去喫煙者である．職業歴では，内装作業を26歳から29年間行っており，職業性石綿ばく露歴を有する．

平成X年6月の初診時の胸部レントゲン上（図6）両

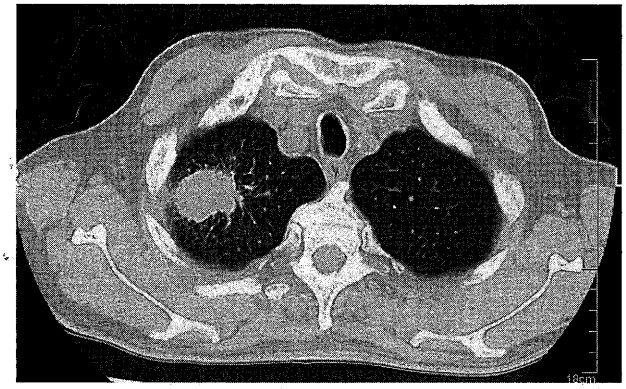

図5　胸部CTでは右肺S1に53×38mm大の辺縁不明瞭な腫瘤陰影を認める.

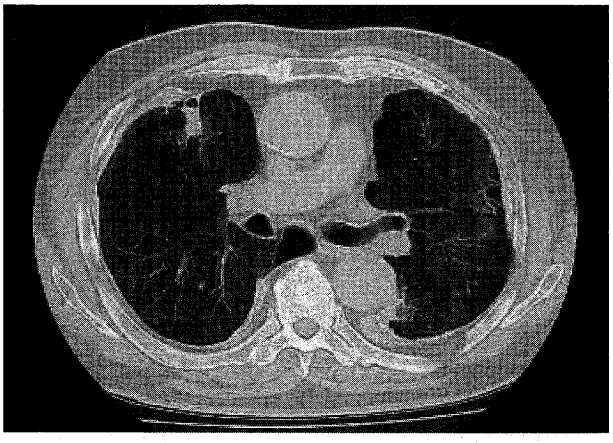

図7　初診時の胸部CT写真　右円形無気肺と左crow's feet signを認める.

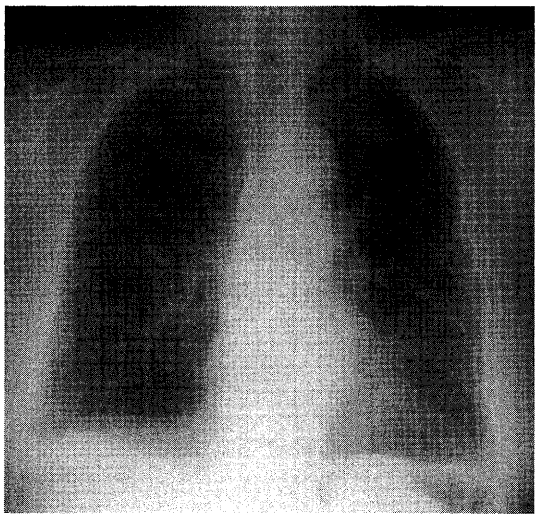

図6　胸部レントゲン写真正面像では両側石灰化胸膜プラークと両側に胸郭の2分の1以上のびまん性胸膜肥厚を認める.

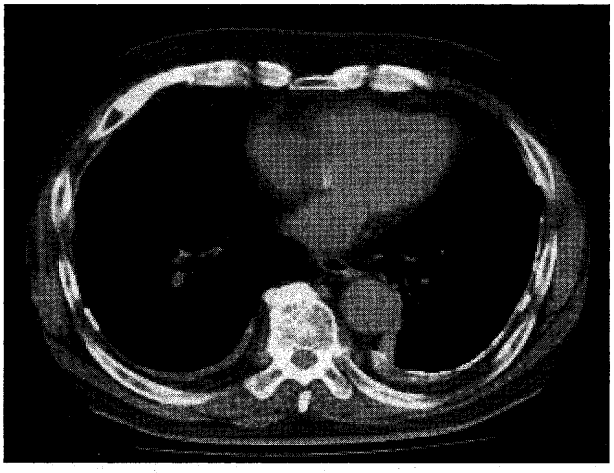

図8　両側に石灰化胸膜プラークを認め,左側石灰化プラークは胸壁内側の2分の1以上を占める.

側びまん性胸膜肥厚があり,肋横角は鈍であり,両側石灰化胸膜プラークを認めた.同日の胸部CT肺野条件では右肺S4に円形無気肺を認めるとともに肺の気腫性変化を伴っていた(図7).肺野に石綿肺を示唆する線維性変化を認めなかった.一方,胸部CT縦隔条件(図8)では左側胸膜に石灰化を伴う広範囲プラークを認めた.

呼吸機能1次検査では,VC:2.29L,$FEV_{1.0}$:1.59L,%VC:70.6%,1秒率:70.98%,%1秒量:65.1%であったが,動脈血ガス分析にてpH:7.367,PaO_2:58.2mmHg,$PaCO_2$:44.3mmHg,A-aDO_2:37.8mmHgと低酸素血症を認めた.PaO_2が60mmHg以下であったため,著しい呼吸機能障害があると認められ,労災認定を受けた.

当初は労作時呼吸困難のみで安静時には呼吸困難がなかったが,その後徐々に呼吸不全が進行し,PaO_2が50mmHg未満となったため在宅酸素療法が導入された.

平成X+3年11月に両側に急性肺炎を合併した.抗生剤による治療を開始したが,完全には回復せず,人工呼吸器による呼吸管理が必要となった.平成X+3年12月に胸部CTを撮影したところ図9に認められるように左肺S3に径2cm大の腫瘤陰影を認め,左肺門部リンパ節腫大を来たしていることが明らかとなった.リンパ節腫大は対側肺門部にも認めたため画像上,T1N3M0の原発性肺癌と診断した.その後,慢性呼吸不全急性増悪により平成X+4年2月に死亡した.剖検にて組織学的に混合型小細胞癌(扁平上皮癌成分を含む)であると診断された.また,肺内石綿小体数を算定したところ5,300本/g肺乾燥重量であった.

考　察

石綿肺のないびまん性胸膜肥厚有所見は石綿肺ほどではないが,中皮腫のリスクが高い.たとえばKarjarainenら[6]は石綿肺1,287例,良性石綿胸膜疾患4,708例を追跡した結果,肺癌リスクは1.3倍(95%CI:1.0〜1.8)で,中皮腫リスクは5.5倍(95%CI:1.5〜14.1)であったと報告している.また,石綿セメント労働者を対象とした検討では,石綿肺ほど頻度は高くないが,びまん性胸膜肥厚

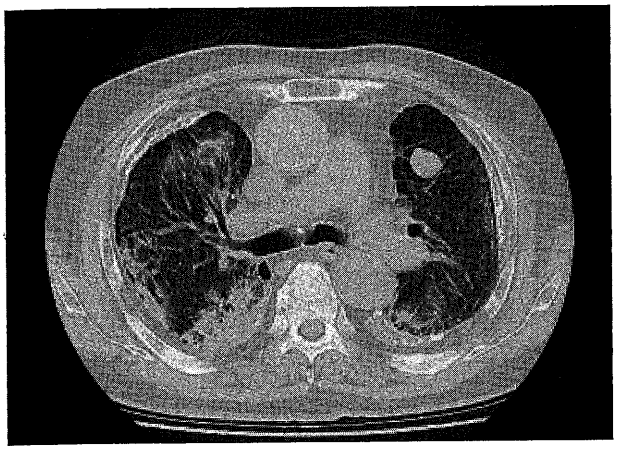

図 9a　左肺 S3 領域に辺縁が明瞭な腫瘤陰影を認める．

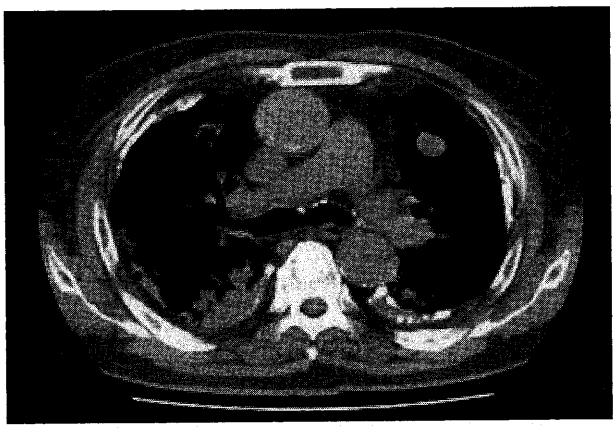

図 9b　左肺 S3 に腫瘤陰影を認める．

の発症頻度は石綿ばく露量が多いほど高いと報告されている[7]．今回，我々は胸部画像上の基準を満たす職業性石綿ばく露のあるびまん性胸膜肥厚 224 例を約 6 年経過観察した．この間，肺癌の発症は 8 例(3.6%)であったが，中皮腫発生例は 1 例もなかった．肺癌発生率は 610.3 人/年であった．これは 55～74 歳で 30 パック・年以上の喫煙者を対象とした NLST の[8]10 万対 645 人/年と同等の肺癌発生率であった．

また，発生頻度が有意に高いと報告されている中皮腫の発生はなく明らかに低発症率であった．その理由としてびまん性胸膜肥厚の本態は臓側胸膜の広範囲な線維化で壁側胸膜との癒着が高頻度で起こっているため，壁側胸膜に発症する胸膜中皮腫の発生母地が癒着により縮小していたために偶然合併がなかった可能性も想定されたが，約 6 年間の経過観察だけでは不十分でもある．

肺癌発生については 224 例中 8 例の 3.6% あったが，石綿肺合併がなく，著しい呼吸機能障害のない症例を除くと労災認定の対象となった症例は 2 例（0.89%）で 1% にも満たなかった．

症例 7 は喫煙指数が 960 であり，呼吸機能検査上も混合性呼吸機能障害を呈し，%1 秒量が 36.8% と著しい低下をきたしており，呼吸機能障害及び肺癌発症と喫煙が大きく関わっていると考えられる．職業歴では 54 年間の職業性石綿ばく露があり，石灰化胸膜プラークが明らかであるため労災での石綿肺癌の認定は容易である．一方，職業性石綿ばく露歴が明らかにならなかった場合でも左下部胸膜には片側の 4 分の 1 を超える石灰化胸膜プラークを認めることにより石綿健康被害救済法においても認定されるべき事案である．

症例 8 は職業性石綿ばく露によりびまん性胸膜肥厚を発症し著しい呼吸機能障害を来たし，約 4 年間の経過で慢性呼吸不全に肺炎を合併し死亡した．剖検によって診断を確定した原発性肺癌である．労災認定上の著しい呼吸機能障害を合併したびまん性胸膜肥厚に合併した原発性肺癌として労災認定の対象ではあった．本症例は石綿健康被害救済法においても広範囲胸膜プラークあるいは肺内石綿に小体数が 5,000 本/g 以上あったことにより，石綿肺癌として認定されるべき症例である．その他の 6 例についても石綿肺合併の 3 例は問題なく補償・救済の対象症例であるとともに，著しい呼吸機能障害のなかった症例においても日本の認定基準は労災補償・救済の対象となっているから社会的な問題はない．

びまん性胸膜肥厚発症に対する石綿ばく露量に関しては，Helsinki クライテリア 2014[9]において，両側性びまん性胸膜肥厚は中等度また高度の石綿ばく露と関連していることが多く，肺癌起因性に関して考慮されるべきであると述べられている．今回報告した 8 例においても職業歴とその期間から考慮した場合，石綿中等度以上ばく露があったであろうと推察している．

症例 7，8 は労災補償における著しい呼吸機能障害と 3 年以上の職業性石綿ばく露があり，画像上の認定基準を満たす肺癌症例である．しかし，その他の認定基準を満たすためこの基準を満たさなくても問題にはならない．石綿健康被害救済法においてもこの 2 例で認められたように広範囲胸膜プラークに合併した肺癌が認定されるようになったため，本症例のような事案についても不利益はなくなった．

一方，石綿ばく露者を対象とした際に肺癌を合併する症例については喫煙との関連が大きいことは様々な疫学研究からも明白である．今回の 8 例全例が喫煙者でその大半は重喫煙者であり，そのうち 5 例は喫煙と関連の深い小細胞癌及び扁平上皮癌であった．Hammond らの疫学調査[10]では石綿ばく露と喫煙は相乗効果を示し，非石綿ばく露の非喫煙者を対照とすると肺癌発生率が 53.2 倍になると報告している．また，日本の認定基準によって石綿肺癌と認定された 252 症例において，その 91.6% が現在あるいは過去喫煙者であったとの我々の報告[11]からも明らかである．以上のような結果から石綿健康管理手帳を取得しているような過去の石綿ばく露者に対する禁煙活動は肺癌発生を抑制する意味でも重要であると思

われる.

利益相反：利益相反基準に該当無し

文 献

1) Gevenois PA, de Maertelaer V, Madani A, et al: Asbestosis, pleural plaques and diffuse pleural thickening: three distinct benign responses to asbestos exposure. Eur Respir J 11: 1021—1027, 1998.
2) Kee ST, Gamsu G, Blance P: Causes of pulmonary impairment in asbestos-exposed individuals with diffuse pleural thickening. Am J Respir Crit care Med 154: 789—793, 1996.
3) Yates DH, Browne K, Stidolph PN, et al: Asbestos-related bilateral diffuse pleural thickening: natural history of radiographic and lung functional abnormalities. Am J Respir Crit Care Med 153: 301—309, 1996.
4) 玄馬顕一, 加藤勝也, 芦澤和人, 他：石綿健康管理手帳健診受診者を対象とした低線量 CT についての検討—CT 撮影により発見された肺癌・中皮腫症例を中心に—, 平成 27 年度労災疾病臨床研究事業報告書. 2016, pp 82—98.
5) Asbestos, asbestosis, and cancer: the Helsinki criteria for diagnosis and attribution. Scand J Work Environ Health 23: 311—316, 1997.
6) Karjalainen A, Pukkala E, Kauppinen T, Partanen T: Incidence of cancer among Finnish patients with asbestos - related pulmonary or pleural fibrosis. Cancer Cause Control 10: 51—57, 1999.
7) Finkelstein MM, Vingilis JJ: Radiographic abnormalities among asbestos cement workers. An exposure-response study. Am Rev Respir Dis 129: 17—22, 1984.
8) National Lung Screening Trial Research Team, Aberle DR, Adams AM, et al: Reduced lung-cancer mortality with low-dose computed tomographic screening. N Engl J Med 365: 395—409, 2011.
9) Wolff H, Vehmas T, Oksa P, et al: Asbestos, asbestosis, and cancer, the Helsinki criteria for diagnosis and attribution 2014:recommendations. Scand J Work Environ Health 41: 5—15, 2015.
10) Hammond EC, Selikoff IJ, Seidman H: Asbestos exposure, cigarette smoking and death rates. ANN NY Acad Sci 330: 473—490, 1979.
11) Kishimoto T, Gemba K, Fujimoto N, et al: Clinical study of asbestos-related lung cancer in Japan with special reference to occupational history. Cancer Sci 101: 1194—1198, 2010.

別刷請求先 〒702-8055 岡山市南区築港緑町 1—10—25
岡山労災病院アスベスト研究センター長
岸本 卓巳

Reprint request:
Takumi Kishimoto, M.D., PhD
Chief of Asbestos Research Center, Okayama Rosai Hospital, 1-10-25, Chikko-midorimachi, Minami-ku, Okayama, 702-8055, Japan

生涯教育シリーズ——93　日本医師会雑誌　第146巻・特別号(2)　平成29(2017)年10月15日発行　昭和23年4月24日第3種郵便物認可

日本医師会雑誌　第146巻・特別号(2)
THE JOURNAL OF THE JAPAN MEDICAL ASSOCIATION

環境による健康リスク

監　修　車谷 典男
編　集　村田 勝敬
　　川本 俊弘
　　五十嵐 隆
編集協力　島　正之

JMA 日本医師会
http://www.med.or.jp/

コラム

アスベストの発がん機序

岸本卓巳

アスベストとは，アスペクト比３以上の繊維性珪酸塩であり，クロシドライト(青石綿)，アモサイト(茶石綿)，クリソタイル(白石綿)のほか３種類の角閃石を称する．

クロシドライト，アモサイトは体内での半減期が20年以上と長く体内に留まって炎症を惹起し，慢性炎症が発がん性につながる．一方，クリソタイルは珪素(Si)とマグネシウム(Mg)の珪酸塩で中空構造のため，もろく崩壊しやすく，マクロファージによって処理され，体外へ排出されやすい．

アスベストによる炎症の機序としては炎症細胞，特に好中球から有意に高い活性酸素の産生を促す．この活性酸素が中皮細胞を障害してがん化の引き金となる．慢性炎症に関係するアディポサイトカイン［たとえば，単球走化性タンパク-1(monocyte chemotactic protein-1; MCP-1)］の産生制御に障害が起こることでアディポサイトカインが大量に放出され，その直接作用あるいは中皮細胞の遊走(migration)に障害が生じることが発がんにつながる．クロシドライト，アモサイトは活性酸素産生能が高く，また4-ヒドロキシ-2-ノネナールにより細胞内タンパクの切断や酸化変異をきたすが，クリソタイルではこのような作用が弱い．一方，クリソタイルは強力な溶血作用を有するとともに，クリソタイルに付着したヘモグロビンが酸化されたDNAにダメージをきたす．そして局所への鉄過剰状態が引き起こされるため中皮細胞のがん化を招来するとともに，ヒストン/DNAに対するアスベストの親和性と中皮細胞へのアスベスト繊維の侵入により遺伝子変異をきたし発がんにつながるとの報告もある．繊維の形状では５μm以上，直径0.25μm未満の長くて細いアスベスト繊維が中皮腫あるいは肺がん頻度を増加させ，特に５～10μmの繊維が肺がんの発生に最も強く関与しているといわれている．

アスベストによる発がんに関する遺伝子異常について以下の報告がある．

①p16染色体のCDKN2A，p19染色体の*ARF*遺伝子はアスベストによる発がんの抑制遺伝子であるため，この両遺伝子の不活化が発がんの要因となる．

②家族内発がんとして重要なBRCA1-associated protein-1(BAP1)のgermline変異は中皮腫発症の重要な因子である．

③neurofibromin 2(*NF2*)遺伝子の欠失，変異によりHippo pathwayが障害され，yes-associated protein(YAP)の核移行や遺伝子制御を行うリン酸化が弱められることが中皮腫発がんに重要である．特にYAPにより高発現された遺伝子のなかでもphospholipase-C beta-4(*PLCB4*)遺伝子が重要である．

④DNA修復遺伝子であるERCC1 N118N，XRCC1 R339Qの存在がアスベストによる発がんに関与している．

アスベストの発がん性および発がん機序については現時点で確認されていることは以上であるが，未だに解明されていない点も多く，今後の研究に委ねられている．

参考文献

1) Chew SH, Okazaki Y, Nagai H, *et al*: Cancer-promoting role of adipocytes in asbestos-induced mesothelial carcinogenesis through dysregulated adipocytokine production. *Carcinogenesis* 2014; 35: 164-172.
2) Altomare DA, Menges CW, Xu J, *et al*: Losses of both products of the Cdkn2a/Arf locus contribute to asbestos-induced mesothelioma development and cooperate to accelerate tumorigenesis. *PLoS One* 2011; 6: e18828.
3) Kakiuchi T, Takahara T, Kasugai Y, *et al*: Modeling mesothelioma utilizing human mesothelial cells reveals involvement of phospholipase-C beta 4 YAP-active mesothelioma cell proliferation. *Carcinogenesis* 2016: bgw084.

Lung Cancer 112 (2017) 188–194

Contents lists available at ScienceDirect

Lung Cancer

journal homepage: www.elsevier.com/locate/lungcan

A phase II trial of carboplatin plus S-1 for elderly patients with advanced non-small-cell lung cancer with wild-type epidermal growth factor receptor: The Okayama Lung Cancer Study Group Trial 1202

Shoichi Kuyama[a,1], Nobuaki Ochi[b,1], Akihiro Bessho[c], Katsuyuki Hotta[d], Genyo Ikeda[e], Daizo Kishino[f], Toshio Kubo[g], Daijiro Harada[h], Nobukazu Fujimoto[i], Masamoto Nakanishi[a], Takahiro Umeno[a,c], Toshiaki Okada[e,j], Kenichi Chikamori[f], Tomoko Yamagishi[b,i], Kadoaki Ohashi[g], Eiki Ichihara[g], Nagio Takigawa[b,*], Mitsune Tanimoto[a,k], Katsuyuki Kiura[g]

[a] *Department of Respiratory Medicine, Iwakuni Clinical Center, Iwakuni, Japan*
[b] *Department of General Internal Medicine 4, Kawasaki Medical School, Okayama, Japan*
[c] *Department of Respiratory Medicine, Japanese Red Cross Okayama Hospital, Okayama, Japan*
[d] *Center for Innovative Clinical Medicine, Okayama University Hospital, Okayama, Japan*
[e] *Department of Respiratory Medicine, Chugoku Central Hospital, Fukuyama, Japan*
[f] *Department of Medical Oncology, Yamaguchi-Ube Medical Center, Ube, Japan*
[g] *Department of Allergy and Respiratory Medicine, Okayama University Hospital, Okayama, Japan*
[h] *Department of Thoracic Oncology and Medicine, Shikoku Cancer Center, Matsuyama, Japan*
[i] *Department of Medical Oncology, Okayama Rosai Hospital, Okayama, Japan*
[j] *Department of Respiratory Medicine, Fukuyama Medical Center, Fukuyama, Japan*
[k] *Graduate School of Medicine, Dentistry, and Pharmaceutical Sciences, Okayama, Japan*

ARTICLE INFO

Keywords:
Carboplatin
Elderly
Non-small cell lung cancer
S-1
Thymidine phosphorylase

ABSTRACT

Introduction: S-1 is an oral fluoropyrimidine-based combination of tegafur, gimeracil, and oteracil potassium. Although the combination of S-1 with carboplatin is a first-line chemotherapy regimen for advanced non-small cell lung cancer (NSCLC), the efficacy and safety of the regimen in the elderly remain unknown.

Methods: The patient inclusion criteria were previously untreated advanced NSCLC, wild-type epidermal growth factor receptor, aged 70 years or more, and a performance status (PS) of 0–2. The patients received oral S-1 (40 mg/m^2, twice daily) for 2 weeks and carboplatin (area under the curve: 5) on day 1 every 4 weeks as induction treatment. After four induction cycles, S-1 alone (40 mg/m^2, twice daily) was administered for 2 weeks every 4 weeks as a maintenance therapy until disease progression. The primary endpoint was the overall response rate (ORR), which was expected to exceed 20%, and the secondary endpoints included the disease control rate (DCR), progression-free survival (PFS), overall survival (OS), and the toxicity profile. The associations between clinical outcomes and expression of genes such as thymidylate synthase and thymidine phosphorylase in the tumors were evaluated.

Results: Thirty-three patients were enrolled between March 2013 and June 2015. The median age was 78 (range 70–89) years, and 51.5% had a PS of 0. The ORR was 30.3% (95% confidence interval (CI): 14.6–46.0) and the DCR 57.6% (95% CI: 40.7–74.4). Grade 3/4 toxicities included thrombocytopenia (42.4%), neutropenia (33.3%), and anemia (27.3%). There was one treatment-related death due to aspiration pneumonia following febrile neutropenia. The median PFS and OS were 134 days (95% CI: 79–173) and 479 days (95% CI: 250–571), respectively. Low thymidine phosphorylase expression was associated with the DCR ($P < 0.01$).

Conclusion: This study met the predesigned primary endpoint, and the regimen seems to be a favorable treatment option.

* Corresponding author.
E-mail addresses: ntakigaw@gmail.com, ntakigaw@med.kawasaki-m.ac.jp (N. Takigawa).
[1] Drs. Kuyama and Ochi equally contributed to this work and they are both first authors.

http://dx.doi.org/10.1016/j.lungcan.2017.08.010
Received 23 February 2017; Received in revised form 30 July 2017; Accepted 9 August 2017

1. Introduction

Lung cancer is the leading cause of cancer-related death worldwide [1]. Non-small cell lung cancer (NSCLC) accounts for approximately 85% of lung cancers [2]. Oncogenic drivers such as epidermal growth factor receptor (EGFR) mutations [3] and echinoderm microtubule-associated protein-like 4–anaplastic lymphoma kinase (EML4–ALK) [4] have been identified in NSCLC. However, only two targeted drugs are available clinically: EGFR-tyrosine kinase inhibitor (TKI) and ALK-TKI [3,5]. Therefore, it is necessary to develop effective chemotherapies without severe adverse effects for patients who do not benefit from targeted therapy.

Lung cancer patients 60 years or older have relatively high cancer mortality rates regardless of sex [1]. Monotherapy using cytotoxic agents is the standard chemotherapy choice in elderly patients without an EGFR mutation or the EML4–ALK fusion gene [6–9]. A subset analysis of a large phase III trial revealed that the survival benefit from chemotherapy was not influenced by age, and the baseline quality of life and functional status were the best indicators for selecting treatment-fitted elderly patients [10]. Some recent phase III trials have evaluated the effectiveness of platinum-doublet chemotherapy in the elderly [11–13]. Their results were controversial because of early termination of the trials and differences in the regimens/schedules; however, combination chemotherapy in fit elderly patients was promising; thus, the decision to use systemic chemotherapy should not be based on age alone [14].

S-1 is an oral fluoropyrimidine anticancer agent combining tegafur, gimeracil, and oteracil potassium. The overall response rate (ORR) and disease control rate (DCR) for S-1 monotherapy were 22.6–27.6% and 65.5–70.0%, respectively. The median progression-free survival (PFS) and overall survival (OS) were 3.1–4.0 and 11.2–12.1 months, respectively [15–17]. Grade 3/4 toxicities were observed in 6.9–16.7% of the patients [15–18]. In a study of long-term S-1 monotherapy following docetaxel plus cisplatin therapy in patients with curatively resected NSCLC, Niho et al. observed grade 3/4 toxicities during S-1 monotherapy, including anemia in 7.3% and neutropenia in 3.7% [18]. S-1 monotherapy appears to be effective and feasible. Two recent phase III trials for advanced NSCLC showed the non-inferiority of S-1 combined with carboplatin or cisplatin compared with standard platinum doublet chemotherapy [19,20]. Although S-1 plus platinum is considered a standard regimen for advanced NSCLC, its efficacy in the elderly remains unclear.

We have reported clinical trials using S-1 for patients with locally advanced NSCLC, including elderly patients (> 70 years old) [21–24]. We also examined the combination of docetaxel and S-1 in patients with previously treated NSCLC, including the elderly [25]. We believe that S-1 is efficacious and safe for NSCLC patients, even the elderly. Therefore, we conducted this phase II study of carboplatin plus S-1 followed by S-1 monotherapy in elderly patients with NSCLC (Clinical trial number: UMIN000009345).

2. Materials and methods

2.1. Patient selection

This multicenter phase II trial was conducted in accordance with the Declaration of Helsinki and was approved by the institutional review board of each participating institution.

Chemotherapy-naïve patients aged ≥70 years old with pathologically confirmed NSCLC harboring stage IIIB or IV wild-type *EGFR*, an Eastern Cooperative Oncology Group performance status (PS) 2 or lower, and a measurable lesion according to the Response Evaluation Criteria in Solid Tumors (RECIST) criteria ver. 1.1 were eligible for this study. EGFR mutations were analyzed in biopsied samples using commercial assays, such as PNA-LNA PCR clamp, PCR-Invader, and Scorpion-ARMS. Additional inclusion criteria were a white blood cell count ≥3000/mm^3, absolute neutrophil count ≥1500/mm^3, platelet count > 150,000/mm^3, hemoglobin level ≥9.0 g/dL, serum bilirubin level ≤1.5 mg/dL, aspartate aminotransferase and alanine aminotransferase levels ≤2.5-fold the normal ranges, creatinine level ≤1.5 mg/dL, and arterial oxygen pressure ≥60 mmHg. Patients were excluded it they had symptomatic brain metastasis, interstitial lung disease, a massive effusion requiring drainage, or severe comorbidities such as uncontrolled diabetes or cardiac disease or if they were taking warfarin sodium or dabigatran etexilate. All patients provided written informed consent.

2.2. Treatment schedule

Carboplatin was given as an intravenous infusion (area under the curve: 5) on day 1, and S-1 (80 mg/m^2 divided into two doses, after breakfast and dinner) was given orally on days 1–14, every 4 weeks. After four cycles of the combination therapy, S-1 monotherapy (same dose and schedule as that used for induction therapy) was continued until disease progression. The S-1 dose was based on the body surface area (BSA) as follows: BSA < 1.25 m^2, 80 mg/day; 1.25 m^2 ≤ BSA < 1.5 m^2, 100 mg/day; and 1.5 m^2 ≤ BSA, 120 mg/day. Although a dose reduction for carboplatin was not permitted, the S-1 dose was reduced from 120 to 100 mg/day, 100–80 mg/day, or 80–60 mg/day based on toxicity. Only one dose reduction was allowed. Second-line chemotherapy or further treatments were given at the physician's discretion.

2.3. Patient assessment

Patient assessment, including a physical examination, chest x-ray, complete blood count, and biochemical profile, was repeated once a week during the first cycle and at least once per subsequent cycle. Tumor response was evaluated by computed tomography using RECIST ver. 1.1 at least once every two cycles until disease progression. A response of at least 4 weeks duration was confirmed as a complete or partial response, and stable disease was defined as disease lasting at least 6 weeks from initiation of the treatment protocol. DCR was defined according to the complete response, partial response, and stable disease rates together. Response was confirmed by an independent extramural review. Toxicities were assessed according to the National Cancer Institute–Common Toxicity Criteria for Adverse Events ver. 4.0.

2.4. Gene profiling analysis

Tissue samples were collected from patients who participated in this study and provided additional written informed consent. For quantification, 10 μm slices from paraffin-embedded specimens were set aside. RNA was isolated from tumor tissues using the RNeasy FFPE Kit (Qiagen, Chatsworth, GA, USA). cDNA was prepared using the High Capacity Reverse Transcription Kit from Life Technologies (Foster City, CA, USA), according to the manufacturer's instruction. The expression levels of the following six genes were determined by TaqMan real-time PCR (TaqMan array card; Life Technologies) after TaqMan assay-based pre-amplification: thymidylate synthase (TS), thymidine phosphorylase (TP), dihydropyrimidine dehydrogenase (DPD), orotate phosphoribosyl transferase (OPRT), vascular endothelial growth factor (VEGF), and excision repair cross-complementing gene 1 (ERCC1). The array card included ACTB, GAPDH, and RPLP0 as reference genes based on their validated roles as housekeeping genes [26,27]. The relationships between gene expression and outcomes, including the response, PFS, and OS rates, were evaluated.

2.5. Statistical analysis

The primary endpoint of this study was the ORR, and secondary endpoints included the DCR, PFS, OS, and toxicity profile. OS was

Table 1
Patient characteristics.

Characteristic	n (%)
Age, median (range), years	78 (70–89)
Sex	
Male	28 (84.9)
Female	5 (15.2)
ECOG performance status	
0/1/2	17/13/3 (51.5/39.4/9.1)
Histology	
Adenocarcinoma	19 (57.6)
Squamous cell carcinoma	13 (39.4)
Not otherwise specified	1 (3.0)
Tumor stage	
Recurrence/IIIB/IV	3/5/25 (9.1/15.2/75.8)
Current/former/never smoker	2/26/5 (6.1/78.8/15.2)
Brinkman Index	
< 400	8 (24.2)
≥400	25 (75.8)
Median (range)	840 (0–1800)

Abbreviations: ECOG, Eastern Cooperative Oncology Group.

evaluated from the date of study entry to death. The final analysis was planned for 1 year after the last patient was registered.

Assuming that an ORR of 20% would support the potential usefulness of the therapy, whereas an ORR of 5% would be at the lower limit of interest, with alpha = 0.10 and beta = 0.20, the estimated accrual was 28 patients for this study. Given the possibility of variance inflation due to censoring or protocol violation, the sample size was set at 32 patients. Survival was estimated using the Kaplan–Meier method. The difference among survival curves was evaluated using the log-rank test. Patient characteristics and gene expression profiles or treatment response were compared between groups using the χ^2 test. The statistical analyses were performed using Stata for Windows, ver. 14.0 (Stata, College Station, TX, USA).

3. Results

3.1. Patient characteristics

We enrolled 33 patients between Mar 2013 and June 2015 in this study. Table 1 shows the baseline patient characteristics. The median age was 78 (range 70–89) years. The proportion of males was 84.8%, and patients with adenocarcinoma and squamous cell carcinoma comprised 57.6% (19/33) and 39.4% (13/33), respectively. Most patients were current or former smokers (84.9%), and the median Brinkman index was 840.

3.2. Treatment

The median number of induction treatment (carboplatin plus S-1) cycles was 3 (range 1–4), and 15 patients (45.5%) subsequently received maintenance S-1 monotherapy. Four cycles of combination chemotherapy were completed by 42.4% (14/33) of the patients. The main reasons for discontinuation during induction were prolonged neutropenia and thrombocytopenia. Dose reduction was necessary during the induction phase in 36.4% (12/33) of the patients, while no reductions were necessary during the maintenance phase. At the time of analysis on July 30, 2016, 21.2% (7/33) of patients were alive and received subsequent chemotherapy, and one patient continued S-1 maintenance therapy.

3.3. Response and survival analyses

The response was assessed in 32 of the 33 enrolled patients; the remaining patient dropped out of the study because of a grade 3 skin toxicity during the first course of treatment before the radiological evaluation. The proportion of patients who achieved a response was 30.3% (10/33; 95% confidence interval [CI]: 14.6–46.0, 90% CI: 17.2–43.4), which met the primary endpoint of an ORR ≥ 20% (lower limit of 90% CI 17.2 > the lower limit of interest 5%). The DCR was 57.6% (95% CI: 40.7–74.4, Table 2). Table 3 shows the subgroup analysis of the treatment responses and survival according to histology. There was no significant difference in the ORR between patients with squamous cell carcinoma and those with adenocarcinoma ($p = 0.94$, χ^2 test). The median follow-up was 808 (range 293–1204) days, the median PFS was 134 days (95% CI: 79–173), and the median survival time (MST) was 479 days (95% CI: 250–571). Fig. 1A and B show the PFS and OS curves for all patients, respectively. The 1-year survival rate was 54.1% (95% CI: 35.7–69.3). The PFS curves were similar between patients with adenocarcinoma and those with squamous cell carcinoma (Fig. 2A). Although the MST was longer in patients with adenocarcinoma than in those with squamous cell carcinoma (571 *vs.* 250 days; Fig. 2B), the difference was not significant ($p = 0.06$).

Table 2
Objective treatment response and survival.

	n	%
Complete response	0	0.0
Partial response	10	30.3
Stable disease	9	27.3
Progressive disease	13	39.4
Not assessable	1	3.0
Overall response rate	10	30.3
(95% CI)		(14.6–46.0)
Disease control rate	19	57.6
(95% CI)		(40.7–74.4)
Survival		
Median PFS (days) (95% CI)	134 (79–173)	
Median OS (days) (95% CI)	479 (250–571)	
1-y survival rate (%) (95% CI)	54.1 (35.7–69.3)	

Abbreviations: CI, confidence interval; OS, overall survival; PFS, progression-free survival.

3.4. Post-study chemotherapy

Overall, 70.0% (23/33) of the patients received subsequent post-study systemic chemotherapy (Table S1). Of these, 14 patients (42.4%) received further chemotherapy. The median post-study treatment line was 1 (range 0–5). Although most of the patients received single-agent chemotherapy, four received combination chemotherapy (amrubicin plus erlotinib, gemcitabine plus vinorelbine, or docetaxel plus bevacizumab). The patients were administered the following agents: docetaxel (31.6%), pemetrexed (31.6%), nab-paclitaxel (23.7%), and

Table 3
Objective response and survival rates according to tumor histology.

	ADC (n = 19)		SCC (n = 13)	
	No.	%	No.	%
Complete response	0	0.0	0	0.0
Partial response	6	31.6	4	30.8
Stable disease	5	26.3	4	30.8
Progressive disease	8	42.1	4	30.8
Not assessable	0	0.0	1	7.7
Overall response rate	6	31.6	4	30.8
(95% CI)	(10.7–52.5)		(0.06–55.9)	
Disease control rate	11	57.9	8	61.5
(95% CI)	(35.7–80.1)		(35.1–88.0)	
Survival				
Median PFS (days) (95% CI)	148 (64–193)		95 (68–244)	
Median OS (days) (95% CI)	571 (317–763)		250 (95–374)	
1-y survival rate (%) (95% CI)	73.3 (47.2–87.9)		30.8 (9.5–55.4)	

Abbreviations: ADC, adenocarcinoma; CI, confidence interval; OS, overall survival; PFS, progression-free survival; SCC, squamous cell carcinoma.

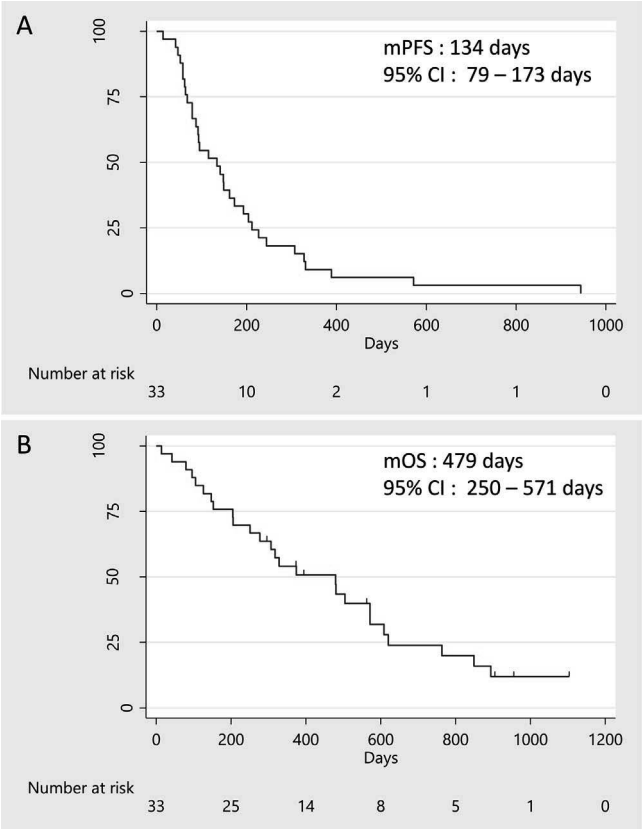

Fig. 1. Progression-free and overall survival curves for all patients.

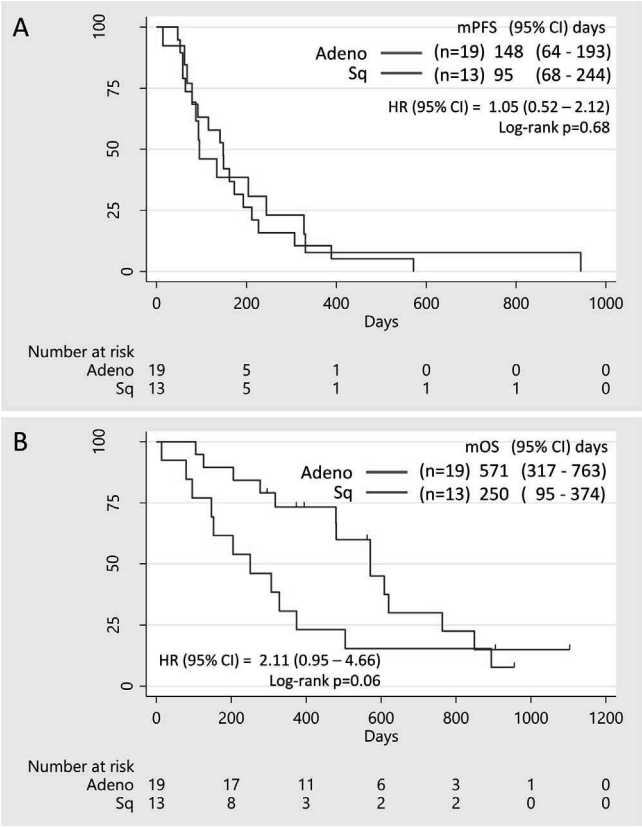

Fig. 2. Progression-free and overall survival curves according to tumor histology.

Table 4
Incidence of adverse events.

Adverse event	Grade 3 (%)	Grade 3 or higher (%)
General		
Fatigue	0.0	0.0
Anorexia	0.0	0.0
Nausea	0.0	0.0
Vomiting	0.0	0.0
Skin rash	0.0	0.0
Febrile neutropenia	9.1	12.1
Pneumothorax	0.0	3.0
Erythema multiforme	0.0	3.0
Hematological		
Neutropenia	24.2	33.3
Anemia	27.3	27.3
Thrombocytopenia	33.3	42.4
Biochemical		
AST/ALT elevation	0.0	0.0
Creatinine elevation	0.0	0.0

Abbreviations: ALT, alanine amino transferase; AST, aspartate amino transferase.

others (13.2%). One patient received alectinib, because the EML4–ALK fusion gene was detected later. One patient received nivolumab.

3.5. Gene profiling analysis

Gene expression analyses were performed in 17 of the 33 patients. The expression of six genes (TS, TP, DPD, OPRT, ERCC1, and VEGF) was successfully measured in these 17 patients. Fig. S1 shows the PFS and OS curves. The cut-off values were based on the median expression level of each gene. In the histological subgroup analysis (Fig. S2), TS expression was higher in the patients with squamous cell carcinoma, albeit not significantly ($p = 0.085$, χ^2 test). Low TP expression was significantly correlated with a better DCR ($p = 0.004$, χ^2 test). Figs. S3 and S4 show the distribution of gene expression stratified according to response. There were no significant differences in the PFS or OS stratified by each gene (Figs. S5 and S6).

3.6. Safety

Table 4 shows the adverse event profile. The majority of the grade 3 or higher adverse events were thrombocytopenia (42.4%), neutropenia (33.3%), and anemia (27.3%). One patient developed grade 3 skin toxicity (erythema multiforme) just before beginning the second cycle of carboplatin/S-1. He recovered fully after discontinuing all suspected drugs, including S-1, and received prednisolone 30 mg/day for several days. Because we could not rule out S-1-related skin toxicity, we decided to discontinue the protocol treatment. Two deaths (6.1%) occurred during the study. One patient died after four cycles of maintenance S-1 monotherapy of a spontaneous pneumothorax due to ruptured bullae in the contralateral lung; death was thus considered to be unrelated to the S-1 treatment. The other died of aspiration pneumonia following febrile neutropenia and was deemed a treatment-related death.

4. Discussion

This phase II trial met the pre-designed primary endpoint (ORR ≥ 20%), with a favorable survival outcome and moderate toxicities, in elderly patients with advanced NSCLC. Low TP expression in tumors might serve as a marker predictive of a better DCR.

Standard chemotherapy regimens have been established for elderly NSCLC patients in the last two decades. In 1999, an Italian group reported the first results from a phase III trial of vinorelbine monotherapy compared with supportive care alone for the elderly. The survival outcome was significantly better in the chemotherapy arm (MST: 6.4

months in the vinorelbine arm *vs*. 4.8 months in the supportive care arm) [7]. Subsequently, a phase III trial comparing vinorelbine, gemcitabine, and both drugs together showed no survival benefit in the combination arm [8]. Thus, single-agent monotherapy was proposed as the standard regimen for the elderly. A Japanese group evaluated the efficacy of docetaxel versus vinorelbine. Previously untreated stage IIIB/IV NSCLC patients, ≥70 years of age with a PS of 2 or lower, were enrolled. Although there was no significant difference in OS between the two treatment arms, PFS and ORR were significantly better in the docetaxel arm than in the vinorelbine arm (median PFS: 5.5 months *vs*. 3.1 months, $p < 0.001$; ORR: 22.7% *vs*. 9.9%, $p = 0.019$) [9]. We also found that docetaxel was effective in select elderly patients (> 75 years old) with advanced NSCLC [28]. Thus, docetaxel monotherapy was proposed as the standard treatment for the elderly in Japan.

Two phase III trials of S-1 combined platinum doublet chemotherapy showed possible survival benefit in patients with squamous cell carcinoma than those with adenocarcinoma [20,29]. On the contrary, possible survival benefit was observed in the adenocarcinoma group in our study (Fig. 2B). Thus, it remains unclear whether the combination of S-1 with platinum has different efficacy between adenocarcinoma and squamous cell carcinoma. Further investigations are warranted.

Chemotherapy-related adverse events are likely to arise in the elderly, probably because of their impaired organ functions and comorbidities compared with younger patients. Grade 3/4 neutropenia is associated with serious complications. The previously reported [9] incidence of grade 3/4 neutropenia (82.9%) caused by docetaxel monotherapy was greater than that in the present study (33.3%). Therefore, the carboplatin/S-1 combination seems to be safer than docetaxel monotherapy in terms of neutropenia.

Age is an important factor when choosing a chemotherapy regimen. Although the benefits of chemotherapy are similar regardless of age, toxicities generally are more common in the elderly [30]. In a randomized phase III trial, Quoix et al. compared carboplatin and weekly paclitaxel with monotherapy in elderly patients with advanced NSCLC [31]. Grade 3/4 hematological toxicities were significantly more frequent in the combination chemotherapy group than in the monotherapy group. The incidence of treatment-related deaths with the combination therapy was also high (4.4% *vs*. 1.3%). However, both PFS and OS were significantly longer in patients treated with the combination therapy (median PFS: 6.0 *vs*. 2.8 months, MST: 10.3 *vs*. 6.2 months) [31]. Table S2 shows the results from representative trials of platinum combination therapy conducted in elderly (≥70 years) patients with NSCLC. The median PFS and MST ranged from 4.7 to 6.2 months and from 10.3 to 17.0 months, respectively. The survival benefit observed in our study was comparable with that in those studies [12,13,31,32]. The efficacy and safety of S-1 plus carboplatin have not been evaluated in the elderly. In addition, no related subset analyses have been reported [19,33–35]. Compared with those studies, the response and survival benefit in our study were comparable or better, but the incidence of adverse events was higher (Tables S2 and S3).

The expression of six genes, TS, TP, DPD, OPRT, VEGF, and ERCC1, were evaluated in this study. High TS expression is often observed in squamous cell carcinoma and is associated with a poor treatment response to fluorouracil [36–38]. However, there were no significant differences in PFS or OS according to TS expression, which might be because of the small sample size. By contrast, lower TP expression was significantly correlated with a better DCR. Low TP expression led to a better response and survival in gastric cancer patients [37,39]. TP is an enzyme involved in pyrimidine nucleotide metabolism, and low TP expression might be advantageous for tumor shrinkage or stabilization by S-1. TP was recently found to be the same molecule as platelet-derived endothelial cell growth factor, which stimulates the chemotaxis of endothelial cells and angiogenesis [40,41], and high TP expression was correlated with increased angiogenesis and a poor prognosis [42–46]. Therefore, the importance of TP expression in NSCLC should be clarified.

There were some limitations to our study. First, this was a single-arm study. Patient selection bias could not be eliminated. Second, the significance of S-1 maintenance has not been established. Only one report has examined S-1 maintenance therapy for advanced NSCLC [47], although it has been evaluated for other malignancies and in an adjuvant setting for NSCLC [48–52]. Suzuki, et al. reported S-1 maintenance therapy following four cycles of carboplatin and S-1 induction therapy in patients with advanced squamous cell lung cancer [47]. The median age was 72 years (range, 57–89 years), and 19 patients (37.3%) were aged > 75 years. The treatment seemed feasible and tolerable even in the population including elderly. Further studies are needed to reveal the efficacy and survival benefit of S-1 maintenance therapy. Third, tissue samples were collected for gene expression analysis in only 52% (33/17) of the subjects. The relationship between TP gene expression and treatment outcome should be verified in future studies. Fourth, we could not evaluate quality of life, comorbidities, number of medications, or functional and cognitive status, which should be evaluated in future studies of NSCLC in the elderly.

In conclusion, carboplatin plus S-1 had favorable efficacy and tolerable toxicity for the elderly with NSCLC. This study met the predesigned primary endpoint, and the regimen seems to be a treatment option. We need to conduct further studies to evaluate whether this combination is superior to the standard first-line treatment for the elderly.

Disclosure

KH received honoraria outside the current work from AstraZeneca, Ono Pharmaceutical, Astellas, Novartis, BMS, MSD, Eli Lilly Japan, Daiichi-Sankyo Pharmaceutical, Boehringer-Ingelheim, Nihon Kayaku, Taiho Pharmaceutical, and Chugai Pharmaceutical. KH also has received research funding outside the current work from AstraZeneca, Boehringer-Ingelheim, Ono Pharmaceutical, Astellas, Novartis, BMS, Eli Lilly Japan, MSD, and Chugai Pharmaceutical. NT has received honoraria from Eli Lilly Japan, AstraZeneca, Daiichi-Sankyo Pharmaceutical, Chugai Pharmaceutical, Taiho Pharmaceutical, Pfizer Inc. Japan, Boehringer-Ingelheim, and Ono Pharmaceutical, and research funding from AstraZeneca, Pfizer Inc. Japan, Kyowa Hakko Kirin, Eli Lilly Japan, Chugai Pharmaceutical, Nippon Kayaku Co. Ltd, Taiho Pharmaceutical, Takeda Pharmaceutical Co. Ltd, Boehringer-Ingelheim, and Ono Pharmaceutical. KK has received honoraria from Chugai Pharmaceutical, Eli Lilly Japan, Pfizer Inc. Japan, Novartis Pharm, and Taiho Pharmaceutical, and research funding from AstraZeneca, Boehringer-Ingelheim, Nippon Kayaku Co. Ltd, Daiichi-Sankyo Pharmaceutical, and Shionogi Co. Ltd. All other authors declare that they have no conflict of interest.

Acknowledgement

Molecular analysis of this study was funded by Taiho Pharmaceutical Co., Ltd.(Tokyo, Japan).

Appendix A. Supplementary data

Supplementary data associated with this article can be found, in the online version, at http://dx.doi.org/10.1016/j.lungcan.2017.08.010.

References

[1] R.L. Siegel, K.D. Miller, A. Jemal, Cancer statistics 2016, CA Cancer J. Clin. 66 (2016) 7–30.
[2] R. Siegel, D. Naishadham, A. Jemal, Cancer statistics 2012, CA Cancer J. Clin. 62 (2012) 10–29.
[3] T.J. Lynch, D.W. Bell, R. Sordella, S. Gurubhagavatula, R.A. Okimoto, B.W. Brannigan, P.L. Harris, S.M. Haserlat, J.G. Supko, F.G. Haluska, D.N. Louis, D.C. Christiani, J. Settleman, D.A. Haber, Activating mutations in the epidermal

growth factor receptor underlying responsiveness of non-small-cell lung cancer to gefitinib, N. Engl. J. Med. 350 (2004) 2129–2139.
[4] M. Soda, Y.L. Choi, M. Enomoto, S. Takada, Y. Yamashita, S. Ishikawa, S. Fujiwara, H. Watanabe, K. Kurashina, H. Hatanaka, M. Bando, S. Ohno, Y. Ishikawa, H. Aburatani, T. Niki, Y. Sohara, Y. Sugiyama, H. Mano, Identification of the transforming EML4-ALK fusion gene in non-small-cell lung cancer, Nature 448 (2007) 561–566.
[5] E.L. Kwak, Y.-J. Bang, D.R. Camidge, A.T. Shaw, B. Solomon, R.G. Maki, S.-H.I. Ou, B.J. Dezube, P.A. Jänne, D.B. Costa, M. Varella-Garcia, W.-H. Kim, T.J. Lynch, P. Fidias, H. Stubbs, J.A. Engelman, L.V. Sequist, W. Tan, L. Gandhi, M. Mino-Kenudson, G.C. Wei, S.M. Shreeve, M.J. Ratain, J. Settleman, J.G. Christensen, D.A. Haber, K. Wilner, R. Salgia, G.I. Shapiro, J.W. Clark, A.J. Iafrate, Anaplastic lymphoma kinase inhibition in non-small-cell lung cancer, N. Engl. J. Med. 363 (2010) 1693–1703.
[6] G. Frasci, V. Lorusso, N. Panza, P. Comella, G. Nicolella, A. Bianco, G. De Cataldis, A. Iannelli, D. Bilancia, M. Belli, B. Massidda, F. Piantedosi, G. Comella, M. De Lena, Gemcitabine plus vinorelbine versus vinorelbine alone in elderly patients with advanced non-small-cell lung cancer, J. Clin. Oncol. 18 (2000) 2529–2536.
[7] C. Gridelli, The ELVIS trial: a phase III study of single-agent vinorelbine as first-line treatment in elderly patients with advanced non-small cell lung cancer. Elderly Lung Cancer Vinorelbine Italian Study, Oncologist 6 (Suppl. 1) (2001) 4–7.
[8] C. Gridelli, F. Perrone, C. Gallo, S. Cigolari, A. Rossi, F. Piantedosi, S. Barbera, F. Ferraù, E. Piazza, F. Rosetti, M. Clerici, O. Bertetto, S.F. Robbiati, L. Frontini, C. Sacco, F. Castiglione, A. Favaretto, S. Novello, M.R. Migliorino, G. Gasparini, D. Galetta, R.V. Iaffaioli, V. Gebbia, MILES Investigators, Chemotherapy for elderly patients with advanced non-small-cell lung cancer: the Multicenter Italian Lung Cancer in the Elderly Study (MILES) phase III randomized trial, J. Natl. Cancer Inst. 95 (2003) 362–372.
[9] S. Kudoh, K. Takeda, K. Nakagawa, M. Takada, N. Katakami, K. Matsui, T. Shinkai, T. Sawa, I. Goto, H. Semba, T. Seto, M. Ando, T. Satoh, N. Yoshimura, S. Negoro, M. Fukuoka, Phase III study of docetaxel compared with vinorelbine in elderly patients with advanced non-small-cell lung cancer: results of the West Japan Thoracic Oncology Group Trial (WJTOG 9904), J. Clin. Oncol. 24 (2006) 3657–3663.
[10] P. Maione, F. Perrone, C. Gallo, L. Manzione, F. Piantedosi, et al., Pretreatment quality of life and functional status assessment significantly predict survival of elderly patients with advanced non-small-cell lung cancer receiving chemotherapy: a prognostic analysis of the multicenter Italian lung cancer in the elderly study, J. Clin. Oncol. 23 (2005) 6865–6872.
[11] E. Quoix, G. Zalcman, J.-P. Oster, V. Westeel, E. Pichon, A. Lavolé, J. Dauba, D. Debieuvre, P.-J. Souquet, L. Bigay-Game, E. Dansin, M. Poudenx, O. Molinier, F. Vaylet, D. Moro-Sibilot, D. Herman, J. Bennouna, J. Tredaniel, A. Ducoloné, M.-P. Lebitasy, L. Baudrin, S. Laporte, B. Milleron, Intergroupe Francophone de Cancérologie Thoracique, Carboplatin and weekly paclitaxel doublet chemotherapy compared with monotherapy in elderly patients with advanced non-small-cell lung cancer: IFCT-0501 randomised, phase 3 trial, Lancet 378 (2011) 1079–1088.
[12] T. Abe, K. Takeda, Y. Ohe, S. Kudoh, Y. Ichinose, H. Okamoto, N. Yamamoto, H. Yoshioka, K. Minato, T. Sawa, Y. Iwamoto, H. Saka, J. Mizusawa, T. Shibata, S. Nakamura, M. Ando, A. Yokoyama, K. Nakagawa, N. Saijo, T. Tamura, Randomized phase III trial comparing weekly docetaxel plus cisplatin versus docetaxel monotherapy every 3 weeks in elderly patients with advanced non-small-cell lung cancer: the intergroup trial JCOG0803/WJOG4307L, J. Clin. Oncol. 33 (2015) 575–581.
[13] H. Tsukada, A. Yokoyama, K. Goto, T. Shinkai, M. Harada, M. Ando, T. Shibata, Y. Ohe, T. Tamura, N. Saijo, Randomized controlled trial comparing docetaxel-cisplatin combination with weekly docetaxel alone in elderly patients with advanced non-small-cell lung cancer: japan Clinical Oncology Group (JCOG) 0207†, Jpn. J. Clin. Oncol. 45 (2015) 88–95.
[14] G.A. Masters, S. Temin, C.G. Azzoli, G. Giaccone, S. Baker, J.R. Brahmer, P.M. Ellis, A. Gajra, N. Rackear, J.H. Schiller, T.J. Smith, J.R. Strawn, D. Trent, D.H. Johnson, American society of clinical oncology clinical practice, systemic therapy for stage IV non-small-cell lung cancer: american society of clinical oncology clinical practice guideline update, J. Clin. Oncol. 33 (2015) 3488–3515.
[15] O. Nishiyama, H. Taniguchi, Y. Kondoh, K. Takada, K. Baba, H. Saito, Y. Sugino, M. Yamamoto, T. Ogasawara, M. Kondo, K. Imaizumi, Y. Hasegawa, R. Suzuki, K. Shimokata, Central Japan Lung Study Group, Phase II study of S-1 monotherapy as a first-line treatment for elderly patients with advanced nonsmall-cell lung cancer: the Central Japan Lung Study Group trial 0404, Anticancer Drugs 22 (2011) 811–816.
[16] M. Wada, M. Yamamoto, S. Ryuge, Y. Nagashima, N. Hayashi, S. Maki, S. Otani, K. Katono, A. Takakura, T. Yanaihara, S. Igawa, M. Yokoba, H. Mitsufuji, M. Kubota, M. Katagiri, N. Masuda, Phase II study of S-1 monotherapy in patients with previously treated, advanced non-small-cell lung cancer, Cancer Chemother. Pharmacol. 69 (2012) 1005–1011.
[17] T. Kasai, Y. Nakamura, M. Fukuda, T. Kitazaki, S. Nagashima, H. Takatani, H. Nakano, K. Nakatomi, T. Ikeda, H. Yamaguchi, K. Tsukamoto, M. Oka, S. Kohno, A phase II study of S-1 for previously untreated elderly patients with advanced non-Small cell lung cancer, Chemotherapy 61 (2016) 93–98.
[18] S. Niho, N. Ikeda, H. Michimae, K. Suzuki, H. Sakai, T. Kaburagi, K. Minato, T. Kato, H. Okamoto, T. Seto, Y. Hosomi, K. Shimizu, F. Oshita, H. Kunitoh, M. Tsuboi, M. Takeuchi, K. Watanabe, Feasibility trial for adjuvant chemotherapy with docetaxel plus cisplatin followed by single agent long-term administration of S-1 chemotherapy in patients with completely resected non-small cell lung cancer: thoracic Oncology Research Group Study 0809, Br. J. Cancer 109 (2013) 545–551.
[19] I. Okamoto, H. Yoshioka, S. Morita, M. Ando, K. Takeda, T. Seto, N. Yamamoto, H. Saka, K. Asami, T. Hirashima, S. Kudoh, M. Satouchi, N. Ikeda, Y. Iwamoto, T. Sawa, M. Miyazaki, K. Tamura, T. Kurata, M. Fukuoka, K. Nakagawa, Phase III trial comparing oral S-1 plus carboplatin with paclitaxel plus carboplatin in chemotherapy-naïve patients with advanced non-small-cell lung cancer: results of a west Japan oncology group study, J. Clin. Oncol. 28 (2010) 5240–5246.
[20] K. Kubota, H. Sakai, N. Katakami, M. Nishio, A. Inoue, H. Okamoto, H. Isobe, H. Kunitoh, Y. Takiguchi, K. Kobayashi, Y. Nakamura, H. Ohmatsu, S. Sugawara, K. Minato, M. Fukuda, A. Yokoyama, M. Takeuchi, H. Michimae, A. Gemma, S. Kudoh, Tokyo Cooperative Oncology Group, A randomized phase III trial of oral S-1 plus cisplatin versus docetaxel plus cisplatin in Japanese patients with advanced non-small-cell lung cancer: TCOG0701 CATS trial, Ann. Oncol. 26 (2015) 1401–1408.
[21] K. Chikamori, D. Kishino, N. Takigawa, K. Hotta, N. Nogami, H. Kamei, S. Kuyama, K. Gemba, M. Takemoto, S. Kanazawa, H. Ueoka, Y. Segawa, S. Takata, M. Tabata, K. Kiura, M. Tanimoto, Okayama Lung Cancer Study Group, A phase I study of combination S-1 plus cisplatin chemotherapy with concurrent thoracic radiation for locally advanced non-small cell lung cancer, Lung Cancer 65 (2009) 74–79.
[22] N. Takigawa, K. Kiura, K. Hotta, S. Hosokawa, N. Nogami, K. Aoe, K. Gemba, K. Fujiwara, S. Harita, M. Takemoto, K. Himei, T. Shinkai, Y. Fujiwara, S. Takata, M. Tabata, S. Kanazawa, M. Tanimoto, Okayama Lung Cancer Study Group, A phase I study of S-1 with concurrent thoracic radiotherapy in elderly patients with localized advanced non-small cell lung cancer, Lung Cancer 71 (2011) 60–64.
[23] K. Aoe, N. Takigawa, K. Hotta, T. Maeda, D. Kishino, N. Nogami, M. Tabata, S. Harita, T. Okada, T. Kubo, S. Hosokawa, K. Fujiwara, K. Gemba, M. Yasugi, T. Kozuki, Y. Kato, K. Katsui, S. Kanazawa, H. Ueoka, M. Tanimoto, K. Kiura, A phase II study of S-1 chemotherapy with concurrent thoracic radiotherapy in elderly patients with locally advanced non-small-cell lung cancer: the Okayama Lung Cancer Study Group Trial 0801, Eur. J. Cancer 50 (2014) 2783–2790.
[24] N. Nogami, N. Takigawa, K. Hotta, Y. Segawa, Y. Kato, T. Kozuki, I. Oze, D. Kishino, K. Aoe, H. Ueoka, S. Kuyama, S. Harita, T. Okada, S. Hosokawa, K. Inoue, K. Gemba, T. Shibayama, M. Tabata, M. Takemoto, S. Kanazawa, M. Tanimoto, K. Kiura, A phase II study of cisplatin plus S-1 with concurrent thoracic radiotherapy for locally advanced non-small-cell lung cancer: the Okayama Lung Cancer Study Group Trial 0501, Lung Cancer 87 (2015) 141–147.
[25] Y. Segawa, K. Kiura, K. Hotta, N. Takigawa, M. Tabata, K. Matsuo, H. Yoshioka, H. Hayashi, H. Kawai, K. Aoe, T. Maeda, H. Ueoka, M. Tanimoto, A randomized phase II study of a combination of docetaxel and S-1 versus docetaxel monotherapy in patients with non-small cell lung cancer previously treated with platinum-based chemotherapy: results of Okayama Lung Cancer Study Group (OLCSG) Trial 0503, J. Thorac. Oncol. 5 (2010) 1430–1434.
[26] A. Bonanomi, D. Kojic, B. Giger, Z. Rickenbach, L. Jean-Richard-Dit-Bressel, C. Berger, F.K. Niggli, D. Nadal, Quantitative cytokine gene expression in human tonsils at excision and during histoculture assessed by standardized and calibrated real-time PCR and novel data processing, J. Immunol. Methods 283 (2003) 27–43.
[27] S. Pérez, L.J. Royo, A. Astudillo, D. Escudero, F. Alvarez, A. Rodríguez, E. Gómez, J. Otero, Identifying the most suitable endogenous control for determining gene expression in hearts from organ donors, BMC Mol. Biol. 8 (2007) 114.
[28] N. Takigawa, Y. Segawa, D. Kishino, K. Fujiwara, Y. Tokuda, N. Seki, T. Shinkai, Y. Watanabe, S. Hiraki, T. Kozuki, K. Gemba, M. Tabata, K. Kiura, H. Ueoka, M. Tanimoto, Clinical and pharmacokinetic study of docetaxel in elderly non-small-cell lung cancer patients, Cancer Chemother. Pharmacol. 54 (2004) 230–236.
[29] H. Yoshioka, I. Okamoto, S. Morita, M. Ando, K. Takeda, T. Seto, N. Yamamoto, H. Saka, S. Atagi, T. Hirashima, S. Kudoh, M. Satouchi, N. Ikeda, Y. Iwamoto, T. Sawa, Y. Nakanishi, K. Nakagawa, Efficacy and safety analysis according to histology for S-1 in combination with carboplatin as first-line chemotherapy in patients with advanced non-small-cell lung cancer: updated results of the West Japan Oncology Group LETS study, Ann. Oncol. 24 (2013) 1326–1331.
[30] G.A. Masters, S. Temin, C.G. Azzoli, G. Giaccone, S. Baker, J.R. Brahmer, P.M. Ellis, A. Gajra, N. Rackear, J.H. Schiller, T.J. Smith, J.R. Strawn, D. Trent, D.H. Johnson, American society of clinical oncology clinical practice, systemic therapy for stage IV non-small-cell lung cancer: american society of clinical oncology clinical practice guideline update, J. Clin. Oncol. 33 (2015) 3488–3515.
[31] E. Quoix, G. Zalcman, J.-P. Oster, V. Westeel, E. Pichon, A. Lavolé, J. Dauba, D. Debieuvre, P.-J. Souquet, L. Bigay-Game, E. Dansin, M. Poudenx, O. Molinier, F. Vaylet, D. Moro-Sibilot, D. Herman, J. Bennouna, J. Tredaniel, A. Ducoloné, M.-P. Lebitasy, L. Baudrin, S. Laporte, B. Milleron, Intergroupe Francophone de Cancérologie Thoracique, Carboplatin and weekly paclitaxel doublet chemotherapy compared with monotherapy in elderly patients with advanced non-small-cell lung cancer: IFCT-0501 randomised, phase 3 trial, Lancet 378 (2011) 1079–1088.
[32] Y.-M. Chen, R.-P. Perng, J.-F. Shih, J. Whang-Peng, A phase II randomized study of vinorelbine alone or with cisplatin against chemo-naïve inoperable non-small cell lung cancer in the elderly, Lung Cancer 61 (2008) 214–219.
[33] K. Tamura, I. Okamoto, T. Ozaki, T. Kashii, K. Takeda, M. Kobayashi, K. Matsui, T. Shibata, T. Kurata, K. Nakagawa, M. Fukuoka, Phase I/II study of S-1 plus carboplatin in patients with advanced non-small cell lung cancer, Eur. J. Cancer 45 (2009) 2132–2137.
[34] K. Kaira, N. Sunaga, N. Yanagitani, H. Imai, M. Utsugi, Y. Iwasaki, K. Shimizu, H. Iijima, H. Tsurumaki, Y. Tomizawa, T. Hisada, T. Ishizuka, R. Saito, M. Mori, Phase 2 study of S-1 plus carboplatin in patients with advanced non-small cell lung cancer, Lung Cancer 68 (2010) 253–257.
[35] A. Sekine, H. Satoh, T. Baba, S. Ikeda, R. Okuda, T. Shinohara, S. Komatsu, E. Hagiwara, T. Iwasawa, T. Ogura, T. Kato, Safety and efficacy of S-1 in combination with carboplatin in non-small cell lung cancer patients with interstitial lung disease: a pilot study, Cancer Chemother. Pharmacol. 77 (2016) 1245–1252.
[36] T. Miyoshi, K. Kondo, H. Toba, M. Yoshida, H. Fujino, K. Kenzaki, S. Sakiyama, M. Takehisa, A. Tangoku, Predictive value of thymidylate synthase and dihydropyrimidine dehydrogenase expression in tumor tissue, regarding the efficacy of

postoperatively administered UFT (tegafur + uracil) in patients with non-small cell lung cancer, Anticancer Res. 27 (2007) 2641–2648.
[37] P.P. Grimminger, P.M. Schneider, R. Metzger, D. Vallböhmer, A.H. Hölscher, P.V. Danenberg, J. Brabender, Low thymidylate synthase, thymidine phosphorylase, and dihydropyrimidine dehydrogenase mRNA expression correlate with prolonged survival in resected non-small-cell lung cancer, Clin. Lung Cancer 11 (2010) 328–334.
[38] M. Takeda, I. Okamoto, N. Hirabayashi, M. Kitano, K. Nakagawa, Thymidylate synthase and dihydropyrimidine dehydrogenase expression levels are associated with response to S-1 plus carboplatin in advanced non-small cell lung cancer, Lung Cancer 73 (2011) 103–109.
[39] W. Ichikawa, T. Takahashi, K. Suto, Y. Shirota, Z. Nihei, M. Shimizu, Y. Sasaki, R. Hirayama, Simple combinations of 5-FU pathway genes predict the outcome of metastatic gastric cancer patients treated by S-1, Int. J. Cancer 119 (2006) 1927–1933.
[40] T. Sumizawa, T. Furukawa, M. Haraguchi, A. Yoshimura, A. Takeyasu, M. Ishizawa, Y. Yamada, S. Akiyama, Thymidine phosphorylase activity associated with platelet-derived endothelial cell growth factor, J. Biochem. 114 (1993) 9–14.
[41] K. Miyadera, T. Sumizawa, M. Haraguchi, H. Yoshida, W. Konstanty, Y. Yamada, S. Akiyama, Role of thymidine phosphorylase activity in the angiogenic effect of platelet derived endothelial cell growth factor/thymidine phosphorylase, Cancer Res. 55 (1995) 1687–1690.
[42] K. Reynolds, F. Farzaneh, W.P. Collins, S. Campbell, T.H. Bourne, F. Lawton, A. Moghaddam, A.L. Harris, R. Bicknell, Association of ovarian malignancy with expression of platelet-derived endothelial cell growth factor, J. Natl. Cancer Inst. 86 (1994) 1234–1238.
[43] K. Maeda, Y.S. Chung, Y. Ogawa, S. Takatsuka, S.M. Kang, M. Ogawa, T. Sawada, N. Onoda, Y. Kato, M. Sowa, Thymidine phosphorylase/platelet-derived endothelial cell growth factor expression associated with hepatic metastasis in gastric carcinoma, Br. J. Cancer 73 (1996) 884–888.
[44] Y. Takebayashi, S. Akiyama, S. Akiba, K. Yamada, K. Miyadera, T. Sumizawa, Y. Yamada, F. Murata, T. Aikou, Clinicopathologic and prognostic significance of an angiogenic factor thymidine phosphorylase, in human colorectal carcinoma, J. Natl. Cancer Inst. 88 (1996) 1110–1117.
[45] T.S. O'Brien, S.B. Fox, A.J. Dickinson, H. Turley, M. Westwood, A. Moghaddam, K.C. Gatter, R. Bicknell, A.L. Harris, Expression of the angiogenic factor thymidine phosphorylase/platelet-derived endothelial cell growth factor in primary bladder cancers, Cancer Res. 56 (1996) 4799–4804.
[46] Y. Imazano, Y. Takebayashi, K. Nishiyama, S. Akiba, K. Miyadera, Y. Yamada, S. Akiyama, Y. Ohi, Correlation between thymidine phosphorylase expression and prognosis in human renal cell carcinoma, J. Clin. Oncol. 15 (1997) 2570–2578.
[47] S. Suzuki, M. Karayama, N. Inui, T. Fujisawa, N. Enomoto, Y. Nakamura, S. Kuroishi, H. Matsuda, K. Yokomura, N. Koshimizu, M. Toyoshima, S. Imokawa, K. Asada, M. Masuda, T. Yamada, H. Watanabe, T. Suda, Continuation maintenance therapy with S-1 in chemotherapy-naïve patients with advanced squamous cell lung cancer, Invest. New Drugs 34 (2016) 490–496.
[48] G. Nakayama, Y. Kodera, H. Yokoyama, N. Okuda, T. Watanabe, C. Tanaka, N. Iwata, N. Ohashi, M. Koike, M. Fujiwara, A. Nakao, Modified FOLFOX6 with oxaliplatin stop-and-go strategy and oral S-1 maintenance therapy in advanced colorectal cancer: CCOG-0704 study, Int. J. Clin. Oncol. 16 (2011) 506–511.
[49] H. Shinchi, K. Maemura, Y. Mataki, H. Kurahara, M. Sakoda, S. Ueno, Y. Hiraki, M. Nakajo, S. Natsugoe, S. Takao, A phase II study of oral S-1 with concurrent radiotherapy followed by chemotherapy with S-1 alone for locally advanced pancreatic cancer, J. Hepatobiliary Pancreat. Sci. 19 (2012) 152–158.
[50] Y. Urata, I. Okamoto, M. Takeda, Y. Hattori, K. Okuno, T. Shimada, T. Kurata, H. Kaneda, M. Miyazaki, M. Terashima, K. Tanaka, S. Morita, K. Nakagawa, S. Negoro, M. Satouchi, Phase 2 study of S-1 and carboplatin plus bevacizumab followed by maintenance S-1 and bevacizumab for chemotherapy-naive patients with advanced nonsquamous non-small cell lung cancer, Cancer 119 (2013) 2275–2281.
[51] Q.H. Ke, S.Q. Zhou, J.Y. Yang, W. Du, G. Liang, Y. Lei, F. Luo, S-1 plus gemcitabine chemotherapy followed by concurrent radiotherapy and maintenance therapy with S-1 for unresectable pancreatic cancer, World J. Gastroenterol. 20 (2014) 13987–13992.
[52] N. Okumura, M. Sonobe, K. Okabe, H. Nakamura, M. Kataoka, M. Yamashita, M. Nakata, K. Kataoka, Y. Yamashita, J. Soh, H. Yoshioka, K. Hotta, K. Matsuo, J. Sakamoto, S. Toyooka, H. Date, Feasibility of adjuvant chemotherapy with S-1 plus carboplatin followed by single-agent maintenance therapy with S-1 for completely resected non-small-cell lung cancer: results of the Setouchi Lung Cancer Group Study 1001, Int. J. Clin. Oncol. 22 (2017) 274–282.

Case Reports in Oncology

Case Rep Oncol 2017;10:553–557

DOI: 10.1159/000477659
Published online: June 22, 2017

Case Report

Esophagobronchial Fistula in a Patient with Squamous Cell Carcinoma of the Lung: A Case Report

Taichi Ozeki[a] Michiko Asano[b] Nobukazu Fujimoto[c] Jun Nishimura[a] Kenji Takada[a] Yosuke Miyamoto[b] Yasuko Fuchimoto[b] Sae Wada[b] Shinji Ozaki[b] Takumi Kishimoto[a]

[a]Department of Medicine, Okayama Rosai Hospital, Okayama, Japan; [b]Department of Pulmonary Medicine, Okayama Rosai Hospital, Okayama, Japan; [c]Department of Medical Oncology, Okayama Rosai Hospital, Okayama, Japan

Keywords
Fistula · Squamous cell carcinoma · Chemoradiotherapy · Cisplatin · Docetaxel · Lung tumor

Abstract
A 73-year-old man was referred to our hospital after a 2-week history of bloody sputum and cough. Computed tomography (CT) images of the chest showed a mass grouped with mediastinal lymph nodes, and bronchoscopy showed a projecting mass in the right main bronchus. After a transbronchial biopsy, the patient was diagnosed with squamous cell carcinoma (T4N2M0 stage IIIB). The patient was treated with systemic chemotherapy, consisting of cisplatin (40 mg/m^2, days 1 and 8) and docetaxel (30 mg/m^2, days 1 and 8), and concurrent thoracic irradiation at a daily dose of 2 Gy. On day 35 of treatment, the patient complained of a sore throat and cough. A CT of the chest showed punctate low-attenuation foci between the esophagus and bronchus. Gastrointestinal endoscopy and bronchoscopy demonstrated a fistula in the middle intrathoracic esophagus and the left main bronchus. The patient's symptoms gradually improved, and the fistula was closed after the suspension of chemoradiotherapy. Radiotherapy was resumed and completed on day 82. However, on day 108, he developed a fever and cough, and a tumor with fistula was revealed in the right main bronchus. He had an esophageal stent inserted, but he later died of sudden hemoptysis.

KARGER

Nobukazu Fujimoto, MD, PhD
Department of Medical Oncology
Okayama Rosai Hospital
1-10-25 Chikkomidorimachi, Okayama 7028055 (Japan)
E-Mail nobufujimot@gmail.com

Introduction

An esophagobronchial fistula represents a connection between the esophagus and the bronchus, resulting from direct neoplastic infiltration and necrosis between the esophagus, bronchi, and mediastinum [1]. A fistula could also be induced by necrosis or cytoreduction of the tumor, though there is no clear evidence that treatment modalities such as chemotherapy or radiotherapy increase the incidence of fistula formation [2]. We report on a patient with squamous cell carcinoma of the lung who developed an esophagobronchial fistula twice in his clinical course. The first one developed during chemoradiotherapy, and the second one was thought to be due to extension of the tumor.

Case Report

A 72-year-old Japanese man was referred to our hospital after 2 weeks of bloody sputum and cough. He had a history of hypertension but was not treated with medication. He had smoked between the ages of 20 and 72 years, and had been exposed to asbestos at shipyards for 15 years. Physical examination revealed a slight wheeze in the bilateral lungs, and no superficial lymph nodes were palpated. A blood test revealed elevated white blood cells, C-reactive protein, and serum calcium levels. Tumor markers were slightly elevated in carcinoembryonic antigen (13.4 ng/mL) and cytokeratin 19 fragment (12.9 ng/mL). Computed tomography (CT) of the chest showed a 60-mm mass grouped with mediastinal lymph nodes, which invaded the right main bronchus (Fig 1a, b). After a transbronchial biopsy of the mass, the diagnosis of squamous cell carcinoma was made. The staging workup, including magnetic resonance imaging of the brain and whole-body fluorine-18 2-fluoro-2-deoxy-d-glucose positron emission tomography, revealed his disease as cT4N2M0, stage IIIB.

The patient was treated with systemic chemotherapy, consisting of cisplatin (40 mg/m^2, days 1 and 8) and docetaxel (30 mg/m^2, days 1 and 8), and concurrent thoracic irradiation at a daily dose of 2 Gy. On day 35 of treatment, he complained of a sore throat and cough, and a CT of the chest showed punctate low-attenuation foci between the esophagus and bronchus (Fig. 1c). Gastrointestinal endoscopy and bronchoscopy demonstrated a fistula in the middle intrathoracic esophagus and the left main bronchus, respectively (Fig. 2a, b). After the suspension of chemoradiotherapy and abstaining from eating, his symptoms gradually improved and the fistula was closed on day 52 (Fig. 2c). Radiotherapy at 2 Gy was resumed every other day and 60 Gy was completed on day 82. The fistula remained closed and the patient was discharged after the second course of chemotherapy.

However, he was referred to our hospital for a sore throat and fever again on day 108. A CT of the chest showed a clear connection between the esophagus and the right main bronchus (Fig. 3a), and there was ground glass opacity spread in the right lower lung. Bronchoscopy demonstrated a mass with the fistula in the right main bronchus (Fig. 3b). Pathological analyses of the mass showed poorly differentiated squamous cell carcinoma. Based on these findings, the patient was diagnosed with a relapse of the cancer. He had an esophageal stent inserted; however, he died of sudden hemoptysis on day 146. An autopsy was not allowed.

Discussion

The development of an esophagobronchial fistula is a devastating and life-threating complication. The incidence of fistula in lung cancer is rare compared with that in esophageal cancer (0.16 vs. 4.9%). A fistula may occur in lung cancer when the tumor makes contact with the esophagus [2]. In the current case, the tumor was located in the mediastinal space and close to the middle intrathoracic esophagus. The first fistula was considered the result of tumor necrosis and damage to the mucous membrane induced by chemoradiotherapy, because the fistula developed in the left main bronchus and the initial tumor in the right main bronchus disappeared at that time. This speculation was also supported by the finding that the fistula improved after 3 weeks' interruption of chemoradiotherapy. On the other hand, the second fistula was considered the result of tumor progression, because the fistula was associated with a tumor that had the same histology as the initial tumor. To our knowledge, this is the first report of an esophagobronchial fistula developing twice in 1 patient by different mechanisms.

An esophagobronchial fistula is a serious complication and the survival time is around 8 months [3]. Direct surgical closure, chemotherapy, and radiotherapy [4] may be used to close the fistula. However, the utility of these treatments was not established, and stent insertion is currently recommended in such situations for symptomatic relief [5]. An esophageal stent was inserted in the current case; however, long-term symptomatic relief was not obtained due to massive hemoptysis.

Chemoradiotherapy is a standard treatment option for locally advanced lung cancer [6], even in cases where the tumor is located close to or invades the esophagus. In such cases, physicians should be extremely cautious about the development of esophagobronchial fistula during and after treatment. In addition to the CT scanning, gastrointestinal endoscopy, before and during treatment, might be considered for early detection of a fistula. In conclusion, we reported a case of squamous cell carcinoma of the lung in a patient who twice developed an esophagobronchial fistula that was caused by different mechanisms.

Acknowledgement

This study was supported by The Research, Development, and Dissemination of Projects Related to Nine Fields of Occupational Injuries and Illnesses of the Japan Labour Health and Welfare Organization and by grants-in-aid from the Ministry of Health, Labor and Welfare, Japan.

Statement of Ethics

The authors have no ethical conflicts to disclose.

Disclosure Statement

The authors declare that they have no conflict of interest.

References

1 Chan KP, Eng P, Hsu AA, Huat GM, Chow M: Rigid bronchoscopy and stenting for esophageal cancer causing airway obstruction. Chest 2002;122:1069–1072.
2 Martini N, Goodner JT, D'Angio GJ, Beattie EJ Jr: Tracheoesophageal fistula due to cancer. J Thorac Cardiovasc Surg 1970;59:319–324.
3 Herth FJ, Peter S, Baty F, Eberhardt R, Leuppi JD, Chhajed PN: Combined airway and oesophageal stenting in malignant airway-oesophageal fistulas: a prospective study. Eur Respir J 2010;36:1370–1374.
4 Yamada S, Takai Y, Ogawa Y, Kakuto Y, Sakamoto K: Radiotherapy for malignant fistula to other tract. Cancer 1989;64:1026–1028.
5 Kvale PA, Simoff M, Prakash UB; American College of Chest Physicians: Lung cancer. Palliative care. Chest 2003;123(suppl):284S–311S.
6 Segawa Y, Kiura K, Takigawa N, Kamei H, Harita S, Hiraki S, Watanabe Y, Sugimoto K, Shibayama T, Yonei T, Ueoka H, Takemoto M, Kanazawa S, Takata I, Nogami N, Hotta K, Hiraki A, Tabata M, Matsuo K, Tanimoto M: Phase III trial comparing docetaxel and cisplatin combination chemotherapy with mitomycin, vindesine, and cisplatin combination chemotherapy with concurrent thoracic radiotherapy in locally advanced non-small-cell lung cancer: OLCSG 0007. J Clin Oncol 2010;28:3299–3306.

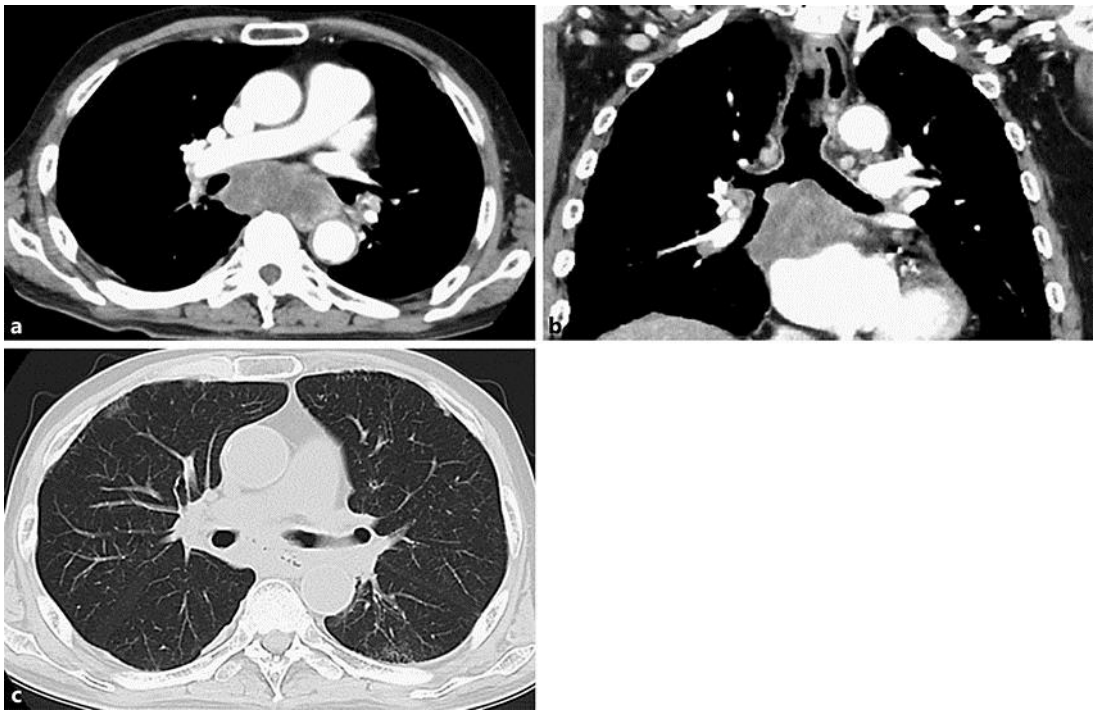

Fig. 1. Computed tomography (CT) of the chest at the initial presentation showing a mass grouped with mediastinal lymph nodes, which invaded the right main bronchus: axial view (**a**) and coronal view (**b**). **c** The CT of the chest on day 35 of treatment demonstrated punctate low-attenuation foci between the esophagus and bronchus.

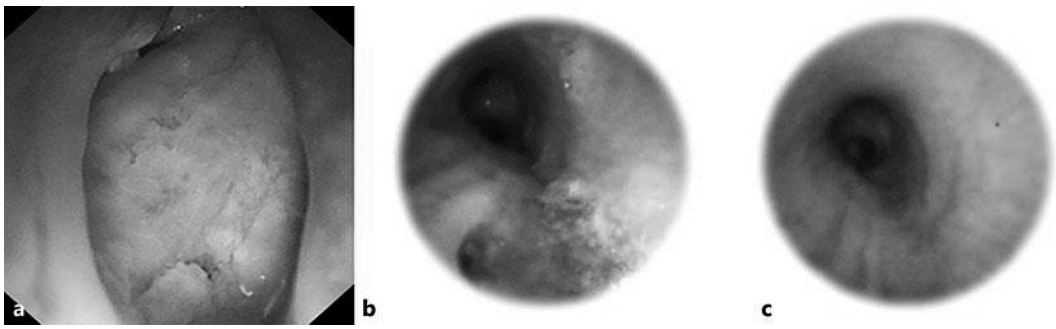

Fig. 2. Gastrointestinal endoscopy and bronchoscopy demonstrated a fistula in the middle intrathoracic esophagus (**a**) and the left main bronchus (**b**), respectively. After the suspension of chemoradiotherapy and abstaining from eating, the fistula was closed (**c**).

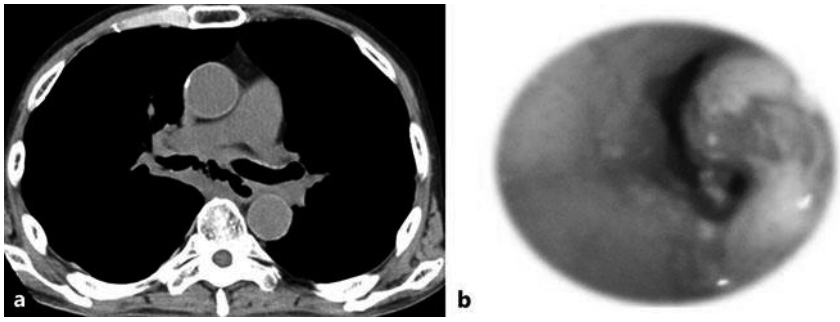

Fig. 3. a Computed tomography of the chest on day 108, showing a connection between the esophagus and the right main bronchus. **b** Bronchoscopy demonstrated a tumor with the fistula in the right main bronchus.

Case Reports in Oncology

Case Rep Oncol 2017;10:666–670

DOI: 10.1159/000479147
Published online: July 21, 2017

Case Report

Adenocarcinoma of the Lung Acquiring Resistance to Afatinib by Transformation to Small Cell Carcinoma: A Case Report

Jun Nishimura[a] Yosuke Miyamoto[b] Nobukazu Fujimoto[c] Taichi Ozeki[a] Kenji Takada[a] Michiko Asano[b] Yasuko Fuchimoto[b] Sae Wada[b] Shinji Ozaki[b] Takumi Kishimoto[a]

[a]Department of Medicine, Okayama Rosai Hospital, Okayama, Japan; [b]Department of Pulmonary Medicine, Okayama Rosai Hospital, Okayama, Japan; [c]Department of Medical Oncology, Okayama Rosai Hospital, Okayama, Japan

Keywords
Adenocarcinoma · Afatinib · Small cell carcinoma · Irinotecan · Drug resistance · Transformation

Abstract
A 65-year-old woman visited our hospital due to right chest pain and dyspnea on exertion. Chest radiography revealed decreased permeability of the right lung. Computed tomography demonstrated a huge mass in the right upper lobe and right pleural effusion. Right pleural effusion cytology yielded a diagnosis of adenocarcinoma and was positive for mutation of epidermal growth factor receptor (EGFR; exon 21 L858R). Afatinib was selected for the initial treatment. Multiple tumors regressed remarkably, but then rapidly progressed 3 months later. We performed re-biopsy to detect the mechanism of resistance to afatinib. Histopathology revealed a mixture of small cell carcinoma (SCC) and adenocarcinoma harboring same EGFR mutation. To the best of our knowledge, this is the first report of transformation to SCC after treatment with afatinib.

KARGER

Nobukazu Fujimoto, MD, PhD
Department of Medical Oncology
Okayama Rosai Hospital
1-10-25 Chikkomidorimachi, Okayama 7028055 (Japan)
E-Mail nobufujimot@gmail.com

Introduction

Lung cancers harboring epidermal growth factor receptor (EGFR) mutations usually respond to EGFR tyrosine kinase inhibitors (TKIs), but most acquire resistance [1, 2]. Transformation of the tumor has been reported to be one of the mechanisms of acquired resistance after treatment with first-generation EGFR-TKIs [3]. However, few reports have described transformation during treatment with the second-generation EGFR-TKI afatinib [4]. We report a case of adenocarcinoma of the lung that acquired resistance to afatinib via transformation to small cell carcinoma (SCC).

Case Report

A 65-year-old woman visited our hospital due to right chest pain and dyspnea on exertion. A chest radiograph revealed decreased permeability of the right lung (Fig. 1a). Computed tomography (CT) demonstrated a huge mass in the right upper lobe (Fig. 1b) and right pleural effusion. In addition, multiple masses were detected on the left lung, liver, and left adrenal grand, as well as mediastinal lymphadenopathy. Pathological examination of the right pleural effusion and a transbronchial biopsy from the right upper bronchus yielded a diagnosis of adenocarcinoma of the lung. Because an EGFR mutation (exon 21 L858R) was detected, treatment with afatinib was initiated.

Multiple tumors remarkably regressed in 1 month, but paronychia (grade 3) appeared in 2 months. Due to difficulties in daily life, the treatment was interrupted for 2 weeks. CT images 3 months after the initial treatment demonstrated growth of the tumors in the lung. We performed another transbronchial biopsy to determine the mechanisms of resistance to afatinib. Histopathological examination revealed a mixture of SCC and adenocarcinoma (Fig. 2) harboring the same EGFR mutation as the initial biopsy specimen. Systemic chemotherapy consisting of cisplatin and irinotecan was administered, but no tumor regression was evident and carcinomatous pericarditis occurred. In addition, the patient complained of consciousness disorder and convulsions. Lumbar puncture identified adenocarcinoma cells in the cerebrospinal fluid. The patient was diagnosed with carcinomatous meningitis and erlotinib treatment was administered. However, no symptomatic improvement occurred and the patient died 5 months after the initial diagnosis. Autopsy was not allowed.

Discussion

In lung cancers harboring EGFR mutations, EGFR-TKIs demonstrate a favorable response, but drug resistance emerges in most cases. A transformation of adenocarcinoma to SCC is one of the resistance mechanisms in first-generation EGFR-TKIs and occurs in 14% of resistant cases, in which the same EGFR mutation is found before and after the changes [5]. An amplification of MET, a high affinity tyrosine kinase receptor for hepatocyte growth factor, and a T790M mutation have been reported as resistance mechanisms of the second-generation EGFR-TKI afatinib [4]. However, to the best of our knowledge, this is the first report of transformation to SCC after afatinib treatment.

In the current case, SCC cells were found 3 months after the initial treatment with afatinib. After the chemotherapy for SCC, the carcinomatous meningitis progressed rapidly. Thus, we hypothesized that a very early stage of SCC development was observed in the cur-

rent case. Although there is a possibility that adenocarcinoma and SCC coexisted from the initial diagnosis, a transbronchial biopsy from the same spot demonstrated adenocarcinoma alone at the time of the initial diagnosis and adenocarcinoma and SCC at the re-biopsy. We consider these findings to support our hypothesis.

When resistance to an EGFR-TKI occurs in lung cancer harboring an EGFR mutation, re-biopsy is recommended to reveal the resistance mechanisms. For cases with a T790M mutation in exon 20, osimertinib has been reported to be a promising treatment option [6]. Recently, the utility of liquid biopsy has been reported for the detection of the T790M mutation [7]. However, to date, SCC transformation cannot be detected by liquid biopsy. In cases in which EGFR-TKI treatment fails, re-biopsy should be applied to reveal the resistance mechanisms and aid in the selection an appropriate treatment.

Favorable results of systemic chemotherapy consisting of platinum and etoposide or irinotecan have been reported in cases of SCC transformation [8], but little response was observed in the current case and the adenocarcinoma progressed rapidly. The effect of EGFR-TKIs for transformed SCC is reported to be limited [9]. A treatment strategy for transformed SCC and existing adenocarcinoma should be established.

In conclusion, we reported a case of EGFR-mutated adenocarcinoma of the lung that transformed to SCC.

Acknowledgments

This work was supported by “the research and development and the dissemination projects related to the 9 fields of occupational injuries and illnesses” of the Japan Labour Health and Welfare Organization and by grants-in-aid from the Ministry of Health, Labor and Welfare, Japan.

Statement of Ethics

The authors have no ethical conflicts to disclose.

Disclosure Statement

The authors have no conflicts of interest to declare.

References

1 Maemondo M, Minegishi Y, Inoue A, Kobayashi K, Harada M, Okinaga S, Morikawa N, Oizumi S, Tanaka T, Isobe H, Kudoh S, Hagiwara K, Nukiwa T, Gemma A: First-line gefitinib in patients aged 75 or older with advanced non-small cell lung cancer harboring epidermal growth factor receptor mutations: NEJ 003 study. J Thorac Oncol 2012;7:1417–1422.

2 Rosell R, Carcereny E, Gervais R, Vergnenegre A, Massuti B, Felip E, Palmero R, Garcia-Gomez R, Pallares C, Sanchez JM, Porta R, Cobo M, Garrido P, Longo F, Moran T, Insa A, De Marinis F, Corre R, Bover I, Illiano A, Dansin E, de Castro J, Milella M, Reguart N, Altavilla G, Jimenez U, Provencio M, Moreno MA, Terrasa J, Munoz-Langa J, Valdivia J, Isla D, Domine M, Molinier O, Mazieres J, Baize N, Garcia-Campelo R, Robinet G, Rodriguez-Abreu D, Lopez-Vivanco G, Gebbia V, Ferrera-Delgado L, Bombaron P, Bernabe R, Bearz A, Artal A, Cortesi E, Rolfo C, Sanchez-Ronco M, Drozdowskyj A, Queralt C, de Aguirre I, Ramirez JL, Sanchez JJ, Molina MA, Taron M, Paz-Ares L: Erlotinib versus standard chemotherapy as

first-line treatment for European patients with advanced EGFR mutation-positive non-small-cell lung cancer (EURTAC): a multicentre, open-label, randomised phase 3 trial. Lancet Oncol 2012;13:239–246.

3 Yu HA, Arcila ME, Rekhtman N, Sima CS, Zakowski MF, Pao W, Kris MG, Miller VA, Ladanyi M, Riely GJ: Analysis of tumor specimens at the time of acquired resistance to EGFR-TKI therapy in 155 patients with EGFR-mutant lung cancers. Clin Cancer Res 2013;19:2240–2247.

4 Wu SG, Liu YN, Tsai MF, Chang YL, Yu CJ, Yang PC, Yang JC, Wen YF, Shih JY: The mechanism of acquired resistance to irreversible EGFR tyrosine kinase inhibitor-afatinib in lung adenocarcinoma patients. Oncotarget 2016;7:12404–12413.

5 Sequist LV, Waltman BA, Dias-Santagata D, Digumarthy S, Turke AB, Fidias P, Bergethon K, Shaw AT, Gettinger S, Cosper AK, Akhavanfard S, Heist RS, Temel J, Christensen JG, Wain JC, Lynch TJ, Vernovsky K, Mark EJ, Lanuti M, Iafrate AJ, Mino-Kenudson M, Engelman JA: Genotypic and histological evolution of lung cancers acquiring resistance to EGFR inhibitors. Sci Transl Med 2011;3:75ra26.

6 Mok TS, Wu YL, Ahn MJ, Garassino MC, Kim HR, Ramalingam SS, Shepherd FA, He Y, Akamatsu H, Theelen WS, Lee CK, Sebastian M, Templeton A, Mann H, Marotti M, Ghiorghiu S, Papadimitrakopoulou VA: Osimertinib or platinum-pemetrexed in EGFR T790M-positive lung cancer. N Engl J Med 2017;376:629–640.

7 Sueoka-Aragane N, Katakami N, Satouchi M, Yokota S, Aoe K, Iwanaga K, Otsuka K, Morita S, Kimura S, Negoro S: Monitoring EGFR T790M with plasma DNA from lung cancer patients in a prospective observational study. Cancer Sci 2016;107:162–167.

8 Oser MG, Niederst MJ, Sequist LV, Engelman JA: Transformation from non-small-cell lung cancer to small-cell lung cancer: molecular drivers and cells of origin. Lancet Oncol 2015;16:e165–e172.

9 Niederst MJ, Sequist LV, Poirier JT, Mermel CH, Lockerman EL, Garcia AR, Katayama R, Costa C, Ross KN, Moran T, Howe E, Fulton LE, Mulvey HE, Bernardo LA, Mohamoud F, Miyoshi N, VanderLaan PA, Costa DB, Janne PA, Borger DR, Ramaswamy S, Shioda T, Iafrate AJ, Getz G, Rudin CM, Mino-Kenudson M, Engelman JA: RB loss in resistant EGFR mutant lung adenocarcinomas that transform to small-cell lung cancer. Nat Commun 2015;6:6377.

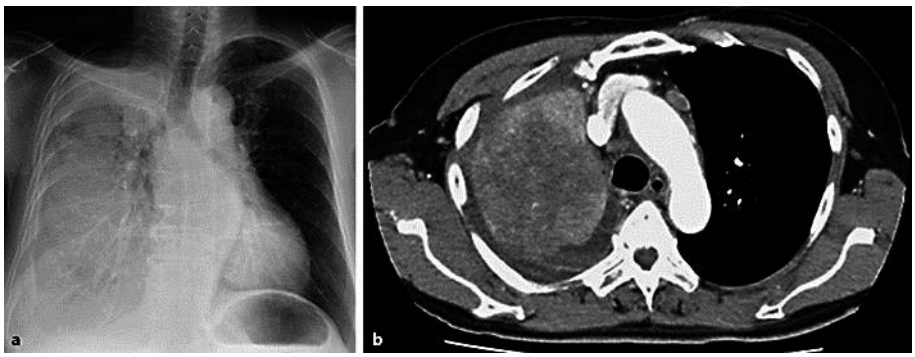

Fig. 1. **a** Chest radiograph showing decreased permeability of the right lung. **b** CT image of the chest demonstrating a huge mass in the right lung and right pleural effusion.

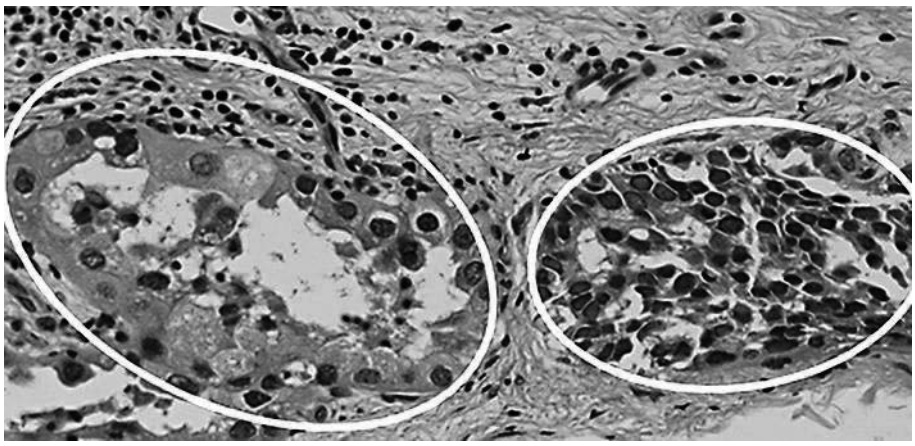

Fig. 2. Pathological analysis of the transbronchial re-biopsy specimen revealed adenocarcinoma (left circle) and small cell carcinoma (right circle).

Clinical & Experimental Immunology
The Journal of Translational Immunology

Clinical and Experimental Immunology ORIGINAL ARTICLE doi:10.1111/cei.12999

Association of immunoglobulin G4 and free light chain with idiopathic pleural effusion

Y. Murata,*†‡ K. Aoe,* Y. Mimura-Kimura ,* T. Murakami,* K. Oishi,*†‡ T. Matsumoto,* H. Ueoka,* K. Matsunaga,§ M. Yano‡ and Y. Mimura *

*The Department of Clinical Research, †The Department of Respiratory Medicine, National Hospital Organization Yamaguchi-Ube Medical Center, Ube, Japan, ‡Division of Cardiology, The Department of Medicine and Clinical Science, and §The Department of Respiratory Medicine and Infectious Disease, Yamaguchi University Graduate School of Medicine, Ube, Japan

Accepted for publication 13 June 2017
Correspondence: Y. Mimura, Department of Clinical Research, NHO Yamaguchi-Ube Medical Center, 685 Higashi-Kiwa, Ube, 755-0241, Japan.
E-mail: mimuray@yamaguchi-hosp.jp

Summary

The cause of pleural effusion remains uncertain in approximately 15% of patients despite exhaustive evaluation. As recently described immunoglobulin (Ig)G4-related disease is a fibroinflammatory disorder that can affect various organs, including the lungs, we investigate whether idiopathic pleural effusion includes IgG4-associated etiology. Between 2000 and 2012, we collected 830 pleural fluid samples and reviewed 35 patients with pleural effusions undiagnosed after pleural biopsy at Yamaguchi-Ube Medical Center. Importantly, IgG4 immunostaining revealed infiltration of IgG4-positive plasma cells in the pleura of 12 patients (34%, $IgG4^+$ group). The median effusion IgG4 level was 41 mg/dl in the $IgG4^+$ group and 27 mg/dl in the $IgG4^-$ group ($P < 0{\cdot}01$). The light and heavy chains of effusion IgG4 antibodies of patients in the $IgG4^+$ group were heterogeneous by two-dimensional electrophoresis, indicating the absence of clonality of the IgG4 antibodies. Interestingly, the κ light chains were more heterogeneous than the λ light chains. The measurement of the κ and λ free light chain (FLC) levels in the pleural fluids showed significantly different κ FLC levels (median: 28·0 *versus* 9·1 mg/dl, $P < 0{\cdot}01$) and κ/λ ratios (median: 2·0 *versus* 1·2, $P < 0{\cdot}001$) between the $IgG4^+$ and $IgG4^-$ groups. Furthermore, the κ/λ ratios were correlated with the $IgG4^+/IgG^+$ plasma cell ratios in the pleura of the $IgG4^+$ group. Taken together, these results demonstrate the involvement of IgG4 in certain idiopathic pleural effusions and provide insights into the diagnosis, pathogenesis and therapeutic opportunities of IgG4-associated pleural effusion.

Keywords: fibrinous pleuritis, free light chain, IgG4-related disease, pleural effusion

Introduction

Pleural effusion remains common, originating from a wide range of pathologies including congestive heart failure, pneumonia and cancer [1]. A diagnostic algorithm for the differentiation of a pleural effusion proposed by Light *et al.* has been widely accepted [2] and recommended in the British Thoracic Society pleural disease guideline [3]. Nonetheless, the cause of the pleural effusion remains unclear in a substantial percentage of patients with persistently exudative effusions after the history, physical examination and biochemical and cytological tests of pleural fluid [4–6]. No diagnosis has been established for up to 15% of patients, despite invasive procedures such as thoracoscopy or open pleural biopsy [4,6,7]. Therefore, a new approach is needed to detect the cause(s) of undiagnosed pleural effusions [8–11]. Because immunoglobulin G4 (IgG4)-related disease is recognized as a fibroinflammatory condition of unknown cause that can affect multiple organs including the lungs and pleura [12,13], IgG4 might be related to certain idiopathic pleural effusions.

Hamano *et al.* originally reported elevated serum IgG4 concentrations in patients with autoimmune pancreatitis [14], and IgG4-related autoimmune disease has been proposed as a new clinicopathological entity characterized by $IgG4^+$ plasma cell infiltration [15]. High serum IgG4 levels and infiltration of $IgG4^+$ plasma cells have also been reported in other organs, including salivary and lacrimal glands [15–18]. Although the criteria for diagnosis of

IgG4-related disease in the lung have not been established, elevated serum IgG4 concentrations and histopathological examinations, such as marked lymphoplasmacytic infiltration including $IgG4^+$ cells and fibrosis, have been recommended [19–21]. Taniguchi *et al.* have reported interstitial pneumonia associated with autoimmune pancreatitis and marked infiltration of $IgG4^+$ plasma cells in the pulmonary alveolar septum [22]. Common radiological findings of IgG4-related lung disease include hilar and mediastinal lymphadenopathy, thickening of perilymphatic interstitium with or without subpleural and/or peribronchovascular consolidation, and the pathological examination reveals lymphoplasmacytic infiltration with fibrosis, which correlates well with the radiological manifestations [23].

It has been reported that pleural effusion may occur in association with systemic IgG4-related disease [16,24–30]. Conversely, there have been a few case reports on isolated IgG4-related pleural effusion [26,31,32], but little is known about the involvement of IgG4 in the pleural effusion. In this study, we hypothesize that idiopathic pleural effusions include IgG4-associated aetiology and demonstrate pleural infiltration of $IgG4^+$ plasma cells in a substantial percentage of patients with idiopathic pleural effusion.

Methods

Patients

Idiopathic pleural effusion was defined as any persistent, exudative pleural effusion that remains undiagnosed after the history and physical examination, biochemical and cytological studies of pleural fluid, radiographic examinations and histopathological analysis of biopsied specimens [4,6]. Diagnosis of idiopathic pleural effusion was made after a minimum of 1-year follow-up (range = 1–10 years), with detailed exploration including computed tomographic (CT) scanning to exclude other causes of effusion such as malignant pleural mesothelioma and carcinomatous pleuritis, according to previous studies that mainly performed follow-up of 1–2 years [4,7,33–36]. In this retrospective study, we accumulated 830 pleural fluid samples at Yamaguchi-Ube Medical Center between 2000 and 2012 and reviewed 35 patients with undiagnosed pleural effusions who underwent thoracoscopy and pleural biopsy, after excluding three patients who had a malignancy during follow-up. Biochemical data were obtained for the sera and pleural fluids when thoracentesis was conducted. Biological and bacterial analyses of sera and pleural fluids, CT scan, cytological and histological examination did not demonstrate malignancy or infectious disease in patients with pleural effusions. The patients' pleural fluids were stored at −80°C until use. This study was approved by the institutional review board of NHO Yamaguchi-Ube Medical Center (Approval no. 26–2). Written informed consent was obtained from each patient or their family for the use of data and samples.

IgG4 immunohistochemistry

The parietal pleura were obtained from biopsy specimens. Immunostaining for IgG or IgG4 was performed by activation of the pleura with 0·1% trypsin, incubation with rabbit polyclonal anti-human IgG antibody (Dako, Glostrup, Denmark; cat. no. A0423) or biotinylated mouse monoclonal anti-human IgG4 antibody (clone HP-6025; Sigma B3648; Sigma, St Louis, MO, USA) [37,38] and HistoFine® Simple Stain™ Max PO Multi (Nichirei Biosciences, Tokyo, Japan; cat. no. 724152), and development with 3,3'-diaminobenzidine (Nichirei Bioscience; cat. no. 715301). The average number of $IgG4^+$ plasma cells within three high-power fields (HPFs) was calculated, and patients with the presence of > 10 $IgG4^+$ plasma cells/HPF and an $IgG4^+/IgG^+$ cell ratio of $> 40\%$, as described for biopsy specimens [23,38,39], were assigned to the $IgG4^+$ group.

Immunoglobulin analysis of pleural fluids

IgG1, IgG2, IgG3, IgG4, IgM, IgA and IgE in pleural fluids were quantitated with Bio-Plex Pro Assays Human Isotyping 7-Plex (Bio-Rad, Hercules, CA, USA), according to the manufacturer's instructions. Bio-Plex Suspension Array System was operated with Bio-Plex Manager (version 6·0).

Purification of IgG4 antibodies from pleural fluids

IgG4 was purified from pleural fluids by diethylaminoethyl (DEAE)-cellulose ion exchange chromatography and subsequently by affinity chromatography on anti-IgG4 antibody-coupled Sepharose-4. Pleural fluid was dialyzed against 0·01 M phosphate buffer (pH 7·0). DEAE-cellulose (DE52; Whatman Biosystems, Chalfont St Giles, UK) in a column ($\phi 1 \times 30$ cm) was equilibrated with 0·01 M phosphate buffer (pH 7·0). The dialyzed pleural fluid (20 ml) was passed onto the DEAE column and the fall-through fractions containing IgG were collected. IgG4 in the IgG of the fall-through fractions was purified with anti-IgG4-coupled Sepharose-4 that had been prepared by coupling monoclonal anti-IgG4 antibody (clone HP-6025; Sigma) to CNBr-activated Sepharose-4 (GE) according to the manufacturer's instructions. The bound IgG4 was eluted with 0·1 M glycine-HCl (pH 2·7) and neutralized immediately with 1 M Tris.

Two-dimensional electrophoresis (2-DE) of effusion IgG4 antibodies

2-DE of purified IgG4 was performed as described previously [40,41]. Briefly, isoelectric focusing (IEF) gel solution contained 8·5 M urea, acrylamide/Bis (5% T, 3% C), 10% glycerol, 1·3 mM lysine and a mixture of Pharmalyte pH 3–10 (1·25%) and pH 5–8 (1·25%) (GE), which was degassed and polymerized by adding ammonium persulphate and TEMED

to concentrations of 0·05 and 0·1%, respectively. Purified IgG4 was reduced in the presence of 5% β-mercaptoethanol at room temperature for 1 h, and urea was added to a concentration of 8·5 M immediately before loading onto the capillary IEF gel (ϕ1 mm × 5 cm). IEF was run in Mini-PROTEAN 2-D Electrophoresis Cell (Bio-Rad) at 200 V for 15 min, 400 V for 15 min and 750 V for 2·5 h. After IEF, capillary gel was equilibrated with sodium dodecyl sulphate (SDS) sample buffer containing 5% β-mercaptoethanol for 30 min. After washing the capillary gel with SDS running buffer, SDS-polyacrylamide gel electrophoresis (SDS-PAGE) was performed at 25 mA constant per gel. After transferring the proteins onto PVDF membranes, γ4, κ and λ chains on the blots were probed with biotinylated anti-IgG4 (Sigma; cat. no. B3648)/horseradish peroxidase-conjugated Extavidin (Sigma; cat. no. E2886), peroxidase-conjugated anti-κ and anti-λ light chain antibodies (Bio-Rad; cat. nos STAR127P and STAR129P), respectively.

Free light chain (FLC) analysis of pleural fluids

The levels of κ and λ FLCs in pleural fluids were measured by latex-based immunoassay using Freelite kappa kit and Freelite lambda kit (The Binding Site, Birmingham, UK). The measurement with Freelite was performed by The BN II System (Siemens, Munich, Germany) at a qualified clinical laboratory of SRL Inc. (Tokyo, Japan). The diagnostic ranges for serum κ FLC, λ FLC and κ/λ FLC ratio are 3·3–19·4 mg/l, 5·7–26·3 mg/l and 0·26–1·65, respectively [42].

Statistical analysis

The Mann–Whitney *U*-test was used to assess differences in the laboratory data, pleural fluid immunoglobulin levels and FLC levels between the $IgG4^+$ and $IgG4^-$ groups. The immunoglobulin data are expressed as median and interquartile range (IQR) unless stated otherwise. A correlation coefficient was obtained using Pearson's equation. $P < 0·05$ was considered statistically significant. All statistical analyses were conducted using IBM SPSS statistics (version 22·0; IBM, Armonk, NY, USA).

Results

Characteristics of patients' pleural fluids and pleura

Clinical and demographic information of 35 patients with idiopathic pleural effusion was obtained from the medical records (Tables 1 and 2). Biopsies from the parietal pleura of these patients demonstrated diffuse sclerosing inflammation, but no malignant cells were identified. Fibrosis was pronounced on the side of the pleural cavity, while storiform fibrosis was not seen. Diffuse lymphoplasmacytic infiltration was observed in 16 of 35 patients (Fig. 1a,b). No obliterative phlebitis was observed. IgG4 immunostaining was performed to examine whether $IgG4^+$ plasma cells were present in the pleura of the 35 patients (Fig. 1c–h). $IgG4^+$ plasma cells were variably detected, and the cut-off for IgG4 positivity was set to 10 $IgG4^+$ plasma cell counts per HPF, as proposed for biopsy specimens [23,39]. Of 35 patients, 12 patients showing $>$ 10 $IgG4^+$ plasma cells/HPF were assigned to the $IgG4^+$ group (median = 31; range = 20–70; Tables 1 and 2) and 23 patients with $\leq$ 10 $IgG4^+$ plasma cells/HPF to the $IgG4^-$ group (median = 0·3; range = 0–5). All patients in the $IgG4^+$ group showed $IgG4^+/IgG^+$ cell ratios greater than 40% (Table 2). The patients in the $IgG4^+$ group were older men with a median age of 76 years, and biochemical analysis showed lower median effusion LDH and CRP levels for this group (Table 1).

Table 1. Clinical characteristics of patients with pleural effusions of unknown cause

	$IgG4^-$ group ($n = 23$)	$IgG4^+$ group ($n = 12$)	P
Age (years)	70 (63–78)	76 (73–80)	0·092
Sex (male/female)	22/1	12/0	0·851
Serum			
Total protein (g/dl)	7·1 (6·4–7·3)	7·2 (6·7–7·6)	0·420
Albumin/globulin	1·00 (0·80–1·30)	1·05 (0·85–1·20)	0·932
LDH (IU/l)	186 (164–235)	181 (164–227)	0·797
CRP (mg/dl)	1·48 (0·75–2·14)	0·83 (0·27–1·83)	0·161
Pleural fluid			
Total protein (g/dl)	4·3 (3·9–5·0)	4·5 (3·6–5·2)	1·000
LDH (IU/l)	356 (197–577)	221 (145–340)	0·049
CRP (mg/dl)	0·89 (0·51–1·24)	0·34 (0·17–1·31)	0·085
ADA (U/l)	21·7 (16·4–23·5)	21·5 (15·9–29·5)	0·719
LDH in pleural fluid/serum	1·60 (1·29–3·00)	1·19 (0·77–1·95)	0·079

Data are presented as median (interquartile range). LDH = lactate dehydrogenase; CRP = C-reactive protein; ADA = adenosine deaminase. The normal ranges for total protein, albumin/globulin ratio, LDH and CRP in serum are 6·0–8·3 g/dl, 1·0–2·0, 120–240 IU/l and $<$ 0·3 mg/dl, respectively. The normal range for pleural fluid ADA is $<$ 30 U/l [2].

Immunoglobulin analysis of pleural fluids

Effusion IgG4 levels were significantly higher in the $IgG4^+$ group than in the $IgG4^-$ group (median = 41 *versus* 27 mg/dl, $P < 0·01$, Fig. 2d). The proportion of IgG4 to the total IgG was also higher in the $IgG4^+$ group than in the $IgG4^-$ group (median = 3·2 *versus* 1·9%, $P < 0·01$, Fig. 2h), which confirms higher IgG4 production in the pleura of the former group. The pleural fluid IgA levels were also elevated in the $IgG4^+$ group (median = 403 *versus* 193 mg/dl, Fig. 2f), in contrast to those of IgG1, IgG2, IgG3, IgM and IgE (Fig. 2a–c,e,g).

Clonality of the IgG4 antibodies of patients in the $IgG4^+$ group

To exclude the possibility of malignant lymphoma and multiple myeloma, the clonality of the effusion IgG4

Table 2. Clinical features of patients in the immunoglobulin (Ig)G4$^+$ group.

						CT scan findings				
n	Age/sex	Effusion IgG4, mg/dl	IgG4$^+$ PC counts/HPF*	IgG4$^+$/IgG$^+$ PC ratio (%)	Respiratory symptom	Pleura	Pulmonary lesion	Mediastinal lymphadenopathy	Extrapulmonary lesion	Follow-up period (years)
1	75M	1133·1	48	85	Dyspnoea on effort	(–)	(–)	(–)	(–)	6
2	81M	20·3	70	93	Abnormality of X-ray	Pleural plaque	(–)	(–)	(–)	2
3	68M	239·6	45	75	Dyspnoea on effort	Pleural plaque and thickening	Ground glass attenuation	(–)	(–)	5
4	76M	44·1	31	48	Abnormality of X-ray	Pleural thickening	Fibrosis	(–)	(–)	3
5	73M	60·1	24	65	Cough	Pleural thickening	Consolidation	(–)	(–)	9
6	73M	37·6	20	75	Abnormality of X-ray	Pleural plaque	Round atelectasis	(–)	(–)	10
7	73M	36·7	22	70	Abnormality of X-ray	(–)	Pneumoconiosis nodule	(–)	(–)	9
8	84M	36·3	26	81	Abnormality of X-ray	Pleural plaque and thickening	(–)	(–)	(–)	3
9	77M	36·5	31	69	Abnormality of X-ray	(–)	Consolidation	(–)	(–)	3
10	78M	36·3	29	54	Abnormality of X-ray	Pleural plaque	(–)	(–)	(–)	5
11	67M	50·7	35	79	Dyspnoea on effort	Pleural plaque	(–)	(–)	(–)	6
12	81M	50·6	57	51	Abnormality of X-ray	(–)	(–)	(–)	(–)	1

*PC = plasma cell; HPF = high-power field (×400); CT = computed tomography.

antibodies of patients in the IgG4$^+$ group was examined by 2-DE (Fig. 3). The control human IgG4, κ myeloma protein, was separated into four γ4 H chain spots with different isoelectric points and one κ L chain spot, but no λ L chain spot (Fig. 3a–c). In contrast, the H and L chains of the IgG4 antibodies of the patients were more heterogeneous in terms of isoelectric point and molecular weight (Fig. 3d–i). In particular, both κ and λ L chains were detected, indicating that their IgG4 antibodies are polyclonal. The numbers of the spots of the κ and λ chains were 10 and 5–6, respectively, which suggests that the κ chain predominates in the effusion IgG4 antibodies of the patients.

Free light chains (FLC) analysis of pleural fluids

As the κ chain was associated predominantly with IgG4 H chain in the patients (Fig. 3), it was presumed that the κ-type was also predominant in the FLCs of the pleural fluids of the IgG4$^+$ group. FLCs are produced in excess of the H chains during immunoglobulin synthesis and secreted into the circulation. The FLC assay was developed originally to support the diagnosis of L chain multiple myeloma, and has been used to assess the excess of one L chain isotype over another by using κ/λ ratio as a surrogate for clonal expansion [43–45]. Interestingly, the κ FLC levels were higher in the patients of the IgG4$^+$ group than in the IgG4$^-$ group (median = 30·1 *versus* 9·1 mg/dl, $P < 0{\cdot}01$) (Fig. 4a), whereas the median λ FLC levels were not significantly different (Fig. 4b). Importantly, the median κ/λ FLC ratio was above the normal range and significantly higher in the IgG4$^+$ group than in the IgG4$^-$ group (2·0 *versus* 1·2, $P < 0{\cdot}001$) (Fig. 4c). In a comparison of patients between the IgG4$^-$ and IgG4$^+$ groups, the receiver operating characteristic (ROC) curve for the κ/λ FLC ratio had a sensitivity of 0·87, a specificity of 0·83 at a cut-off value of 1·42 with an area under the curve (AUC) of 0·88 (Fig. 5). In addition, the κ/λ FLC ratios were found to be correlated with the IgG4$^+$ plasma cell counts/HPF and the IgG4$^+$/IgG$^+$ cell ratios in the pleura of the IgG4$^+$ group (Fig. 6). These results are consistent with the predominance of the κ chain in the 2-DE patterns of the effusion IgG4 antibodies (Fig. 3).

Discussion

The aetiology of exudative pleural effusion sometimes remains unknown, despite thoracoscopy and histological examination of pleural biopsy specimens. In this study, we have shown that 34% of patients with idiopathic pleural effusion are associated with IgG4. To our knowledge, this study is the first to investigate the incidence of IgG4-associated pleural effusion in patients with idiopathic pleural effusion. A pleural marker that might be related to this pleural effusion is also discussed.

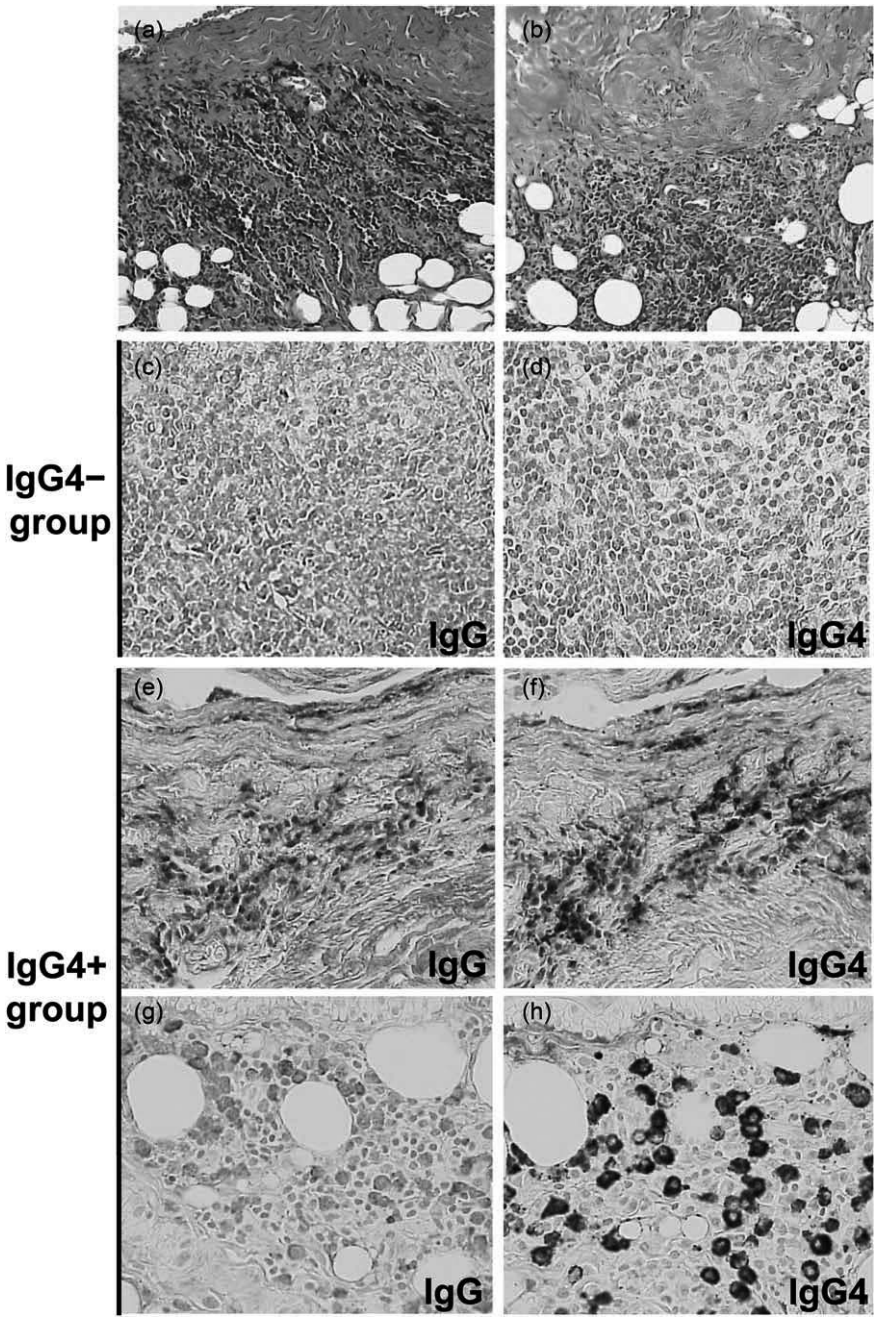

Fig. 1. Histopathological features of the parietal pleura of patients with idiopathic pleural effusion. (a,b) Fibrous thickening of the pleura and prominent lymphoplasmacytic infiltrate in the subpleural fibrous and adipose tissue (haematoxylin and eosin staining, magnification ×100). (c–h) Immunostaining for immunoglobulin (Ig)G or IgG4, magnification ×200. (a,e,f) Case 1, effusion IgG4: 1133·1 mg/dl. (b,g,h). Case 2, effusion IgG4: 20·3 mg/dl (Table 2).

Pleural effusions are manifested in some systemic IgG4-related disease. In previous case reports on IgG4-related disease, pleural effusion occurred as one of the symptoms of the systemic disease involving pancreas, salivary glands, etc. Nodular lesions and bronchovascular involvement are the most common pulmonary manifestations, and various combinations of pulmonary abnormalities are often found in the same patients [23,46,47]. In contrast, the patients in this study did not show multi-organ system involvement other than pleuritis. Considering the elevated effusion IgG4 levels, tissue $IgG4^+$ plasma cell numbers and $IgG4^+/IgG^+$ plasma cell ratios (Table 2), however, the IgG4-associated aetiology is evident for the patients in the $IgG4^+$ group of this study. The patients in the $IgG4^+$ group were elderly men and less inflammatory compared with those in the $IgG4^-$ group (Table 1), which is in agreement with characteristics of IgG4-related disease that affects predominantly older men and progresses slowly with relatively weak inflammation signs [48]. IgG4 antibodies are considered generally to be anti-inflammatory [49,50], but their pathogenic effects have also been reported [51,52]. At present, it is unclear whether the increased production of IgG4 antibody is a causative factor of the pleural effusion or a bystander phenomenon associated with chronic inflammatory reactions.

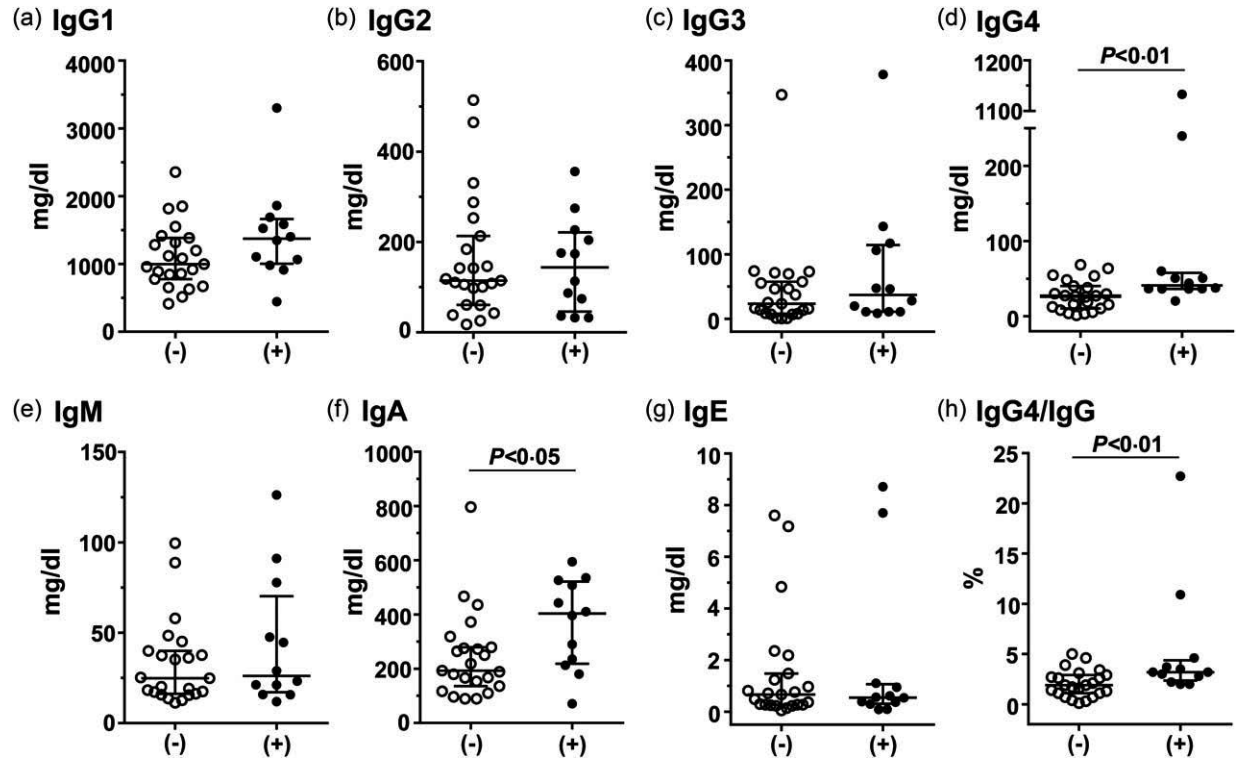

Fig. 2. Comparison of pleural fluid levels of immunoglobulins between the immunoglobulin (Ig)G4$^-$ and IgG4$^+$ groups. (−), IgG4$^-$ group; (+), IgG4$^+$ group. Median and interquartile ranges are shown.

In differential diagnosis, sarcoidosis and multi-centric Castleman's disease were ruled out by clinical and radiological findings, including lack of mediastinal/hilar or extrapulmonary lymphadenopathy in the chest X-ray and CT scan examinations (Table 2). Although lymphoma/myeloma needs to be suspected when the IgG4 levels are markedly high, in this study the IgG4 antibodies were polyclonal and no patient developed malignancy during at least 1-year follow-up (median 5 years, Table 2). Interestingly, the effusion IgG4 levels did not correlate with the extent of pleural infiltration of IgG4$^+$ plasma cells (cases 1 and 2, Fig. 1, Table 2). Although the effusion IgG4 level of case 2

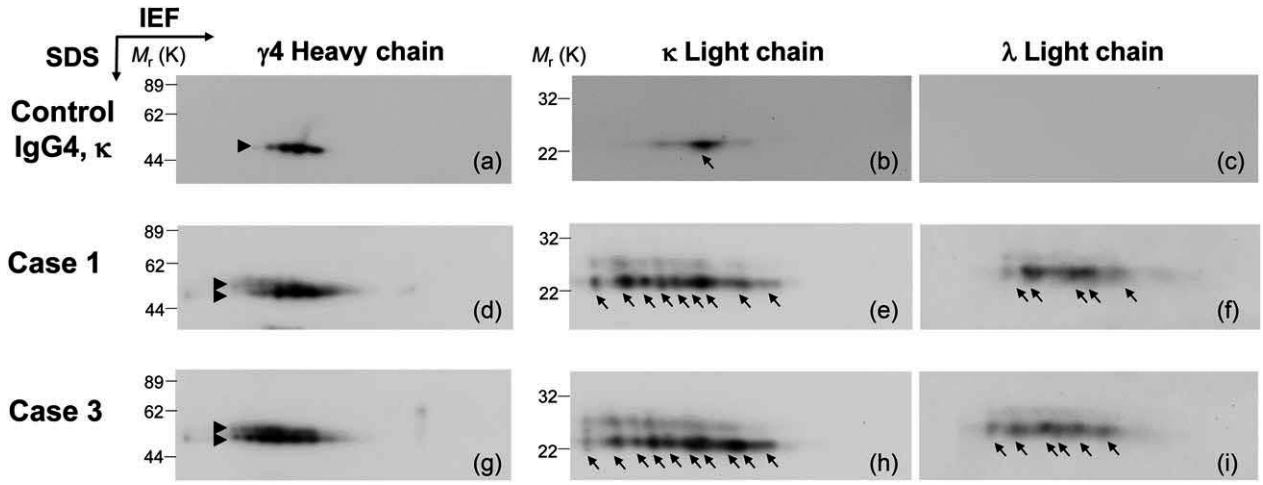

Fig. 3. Analysis of the clonality of the effusion immunoglobulin (Ig)G4 antibodies of patients in the IgG4$^+$ group by two-dimensional electrophoresis (2-DE). Control IgG4 κ myeloma protein from Sigma (cat no. I4639) (a –c). Effusion IgG4 antibodies of representative cases with abnormal IgG4 levels (d–i). The H and L chains were probed with anti-IgG4-Fc (left), anti-κ chain (middle) and anti-λ chain (right) antibodies.

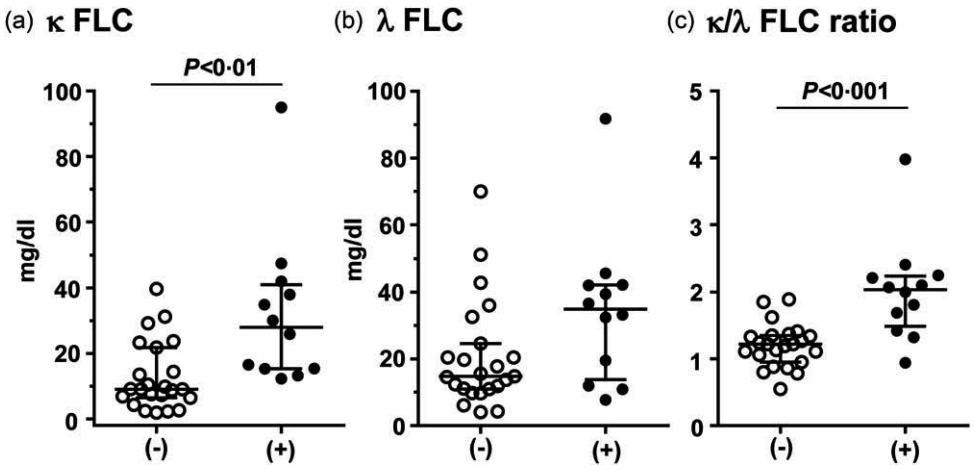

Fig. 4. Comparison of pleural fluid levels of the κ and λ free L chains (FLC) (a,b) and κ/λ ratio (c). Median and interquartile ranges are shown. (−), Immunoglobulin (Ig)G4$^-$ group; (+), IgG4$^+$ group.

in the IgG4$^+$ group was as low as 20·3 mg/dl, IgG4 immunostaining exhibited dense infiltration of IgG4$^+$ plasma cells in the pleura (Fig. 1h). The discrepancy between serum IgG4 concentrations and immunohistochemical findings has also been noted in IgG4-related disease [53]. Therefore, a biomarker other than IgG4 is needed to support the diagnosis of this pleural effusion. The measurements of FLC in the pleural fluid may be considered.

Elevated FLC levels (Fig. 4a,b) are likely to reflect the activation of polyclonal B cells that infiltrate in the pleura. Higher κ FLC levels and κ/λ ratios in the IgG4$^+$ group than in the IgG4$^-$ group may be useful to discriminate the IgG4-associated pleural effusion (Fig. 4). Over-production of serum FLC and high serum κ/λ ratios have been shown recently to correlate with the disease activity of systemic lupus erythematosus [54], rheumatoid arthritis, primary Sjőgren's syndrome [55] and IgG4-related disease [56]. However, the reason for the high κ/λ ratios in these diseases is not known. One possibility to explain the high κ/λ ratios in the IgG4$^+$ group is dominant selection of Vκ genes by possible antigen(s) that elicit pleuritis. It has been reported that the κ/λ ratios of granulocyte–macrophage colony-stimulating factor (GM-CSF) autoantibodies in the sera of patients with autoimmune pulmonary alveolar proteinosis are correlated with disease severity [57]. The study suggests the occurrence of selective expansion of λ-type anti-GM-CSF antibody-positive B cell clones in the peripheral lymphatic tissues. However, neither autoantigens nor disease-specific IgG4 autoantibodies have been identified in IgG4-related disease [12]. A second possibility is a preferential association of the κ L chains with the γ4 and α H chains because the levels of IgG4 and IgA were elevated in the pleural fluids (Fig. 2). The κ L chains have been shown to be associated preferentially with IgG4 and IgA H chains from the analyses of subclass distribution in 659 IgG myeloma sera [58] and 176 IgG and 62 IgA myeloma proteins [59]. These studies show the mean κ/λ ratios for the IgG4 myeloma proteins as 3·0 ($n = 24$ [58]) and 2·7 ($n = 11$ [59]) and that for IgA as 2·1 ($n = 42$ [59]). The correlations of the effusion κ/λ FLC ratios with the IgG4$^+$ cell counts and IgG4$^+$/IgG$^+$ cell ratios in the pleura are in agreement with this notion (Fig. 6). It has been reported that FLC can confer mast cell-dependent hypersensitivity in mice and that increased κ FLC monomer and dimer levels and high κ/λ ratios are often found in the cerebrospinal fluid of patients with multiple sclerosis [60,61]. The pleural effusions in the IgG4$^+$ group may be attributable to the accumulation of κ FLCs.

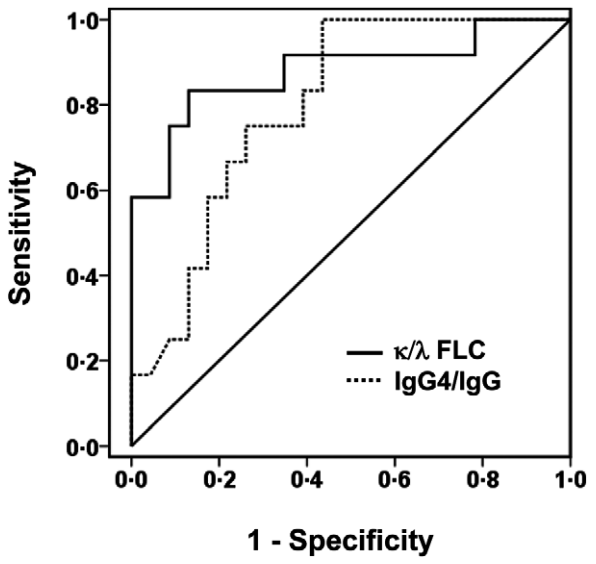

Fig. 5. Receiver operating characteristic (ROC) analysis on diagnostic utility of immunoglobulin (Ig)G4 and κ/λ ratio for distinguishing patients between the IgG4$^-$ and IgG$^+$ groups. Cut-off value for κ/λ ratio, 1·42; sensitivity, 0·87; specificity, 0·83. Area under the curve (AUC), 0·88; 95% confidence interval (CI) for the AUC, 0·74 – 1·00. Cut-off value for IgG4/IgG ratio, 2·75%; sensitivity, 0·75; specificity, 0·74; AUC, 0·80; 95% CI for the AUC, 0·66–0·94.

IgG4-related pleural lesions are reported to be steroid-responsive [26,32,62]. Considering B cell activation as a

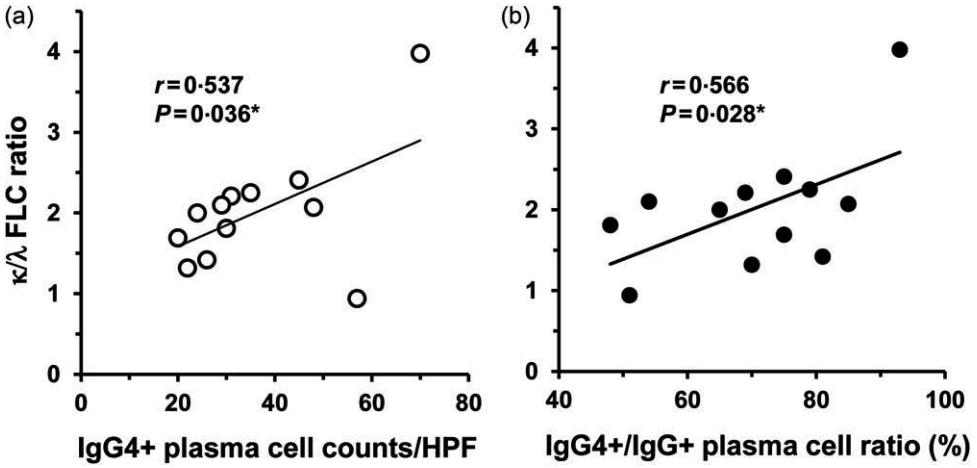

Fig. 6. Correlation of the effusion κ/λ free L chains (FLC) ratio with immunoglobulin (Ig)G4$^+$ plasma cell counts (a) and IgG4$^+$/IgG$^+$ plasma cell ratio (b) in the pleura of patients in the IgG4$^+$ group. *One-tailed *P*-value.

possible mechanism for the pleural effusion in our study, the same therapeutic strategy with immunosuppressive agents may be applicable to our cases. One patient in the IgG4$^+$ group who had suffered recurrent pleural effusions (Case 1, Table 2) received corticosteroids, which ameliorated the pleural effusion. Conversely, pleural effusions resolved spontaneously in a subset of patients, and so watchful waiting may be appropriate in some patients with mild pleural effusion or asymptomatic pleuritis, as described for IgG4-related disease in other organs [63]. However, criteria to justify treatment of IgG4-related pleural lesions need to be established by future prospective studies.

This study has several limitations. This is a retrospective study with a small number of patients. One patient was followed-up for 1 year, although more than 1-year follow-up is recommended for detection of occult pleural malignancy [7,33,36]. It was not possible in all patients to assess the development of an extra-pleural IgG4-related lesion during follow-up. As serum samples were not available, the serum levels of IgG4, κ and λ FLCs could not be analysed. Immunoglobulins including IgG4 were quantitated by a capture sandwich immunoassay, which is different from nephelometry used in the literature, and so the IgG4 concentrations in this study cannot be compared directly with those in the previous reports on IgG4-related disease.

Acknowledgements

We thank Masami Murakami and Masazumi Tanaka for technical assistance. This study was supported in part by Japan Society for the Promotion of Science under JSPS KAKENHI Grant no. 23590578 (Y. M.).

Disclosure

The authors declare no conflicts of interest.

References

1 Porcel JM, Azzopardi M, Koegelenberg CF, Maldonado F, Rahman NM, Lee YC. The diagnosis of pleural effusions. Expert Rev Respir Med 2015; **9**:801–15.
2 Light RW. Pleural diseases, 6th edn. Philadelphia, PA: Lippincott Williams & Wilkins, 2013.
3 Hooper C, Lee YC, Maskell N, BTS Pleural Guideline Group. Investigation of a unilateral pleural effusion in adults: British Thoracic Society Pleural Disease Guideline 2010. Thorax 2010; **65**: ii4–17.
4 Ferrer JS, Munoz XG, Orriols RM, Light RW, Morell FB. Evolution of idiopathic pleural effusion: a prospective, long-term follow-up study. Chest 1996; **109**:1508–13.
5 Light RW. The undiagnosed pleural effusion. Clin Chest Med 2006; **27**:309–19.
6 Aleman C, Sanchez L, Alegre J *et al*. Differentiating between malignant and idiopathic pleural effusions: the value of diagnostic procedures. Q J Med 2007; **100**:351–9.
7 Davies HE, Nicholson JE, Rahman NM, Wilkinson EM, Davies RJ, Lee YC. Outcome of patients with nonspecific pleuritis/fibrosis on thoracoscopic pleural biopsies. Eur J Cardiothorac Surg 2010; **38**:472–7.
8 Aoe K, Hiraki A, Murakami T *et al*. Diagnostic significance of interferon-gamma in tuberculous pleural effusions. Chest 2003; **123**:740–4.
9 Aoe K, Hiraki A, Murakami T *et al*. Relative abundance and patterns of correlation among six cytokines in pleural fluid measured by cytometric bead array. Int J Mol Med 2003; **12**: 193–8.
10 Aoe K, Hiraki A, Maeda T *et al*. Soluble receptor-binding cancer antigen expressed on SiSo cells in pleural fluid: a potential diagnostic marker for malignant pleural effusion. Chest 2004; **126**: 1195–7.
11 Porcel JM. Pleural fluid biomarkers: beyond the Light criteria. Clin Chest Med 2013; **34**:27–37.
12 Stone JH, Zen Y, Deshpande V. IgG4-related disease. N Engl J Med 2012; **366**:539–51.
13 Della-Torre E, Lanzillotta M, Doglioni C. Immunology of IgG4-related disease. Clin Exp Immunol 2015; **181**:191–206.
14 Hamano H, Kawa S, Horiuchi A *et al*. High serum IgG4 concentrations in patients with sclerosing pancreatitis. N Engl J Med 2001; **344**:732–8.

15 Kamisawa T, Funata N, Hayashi Y *et al.* A new clinicopathological entity of IgG4-related autoimmune disease. J Gastroenterol 2003; **38**:982–4.
16 Zen Y, Inoue D, Kitao A *et al.* IgG4-related lung and pleural disease: a clinicopathologic study of 21 cases. Am J Surg Pathol 2009; **33**:1886–93.
17 Stone JH, Khosroshahi A, Hilgenberg A, Spooner A, Isselbacher EM, Stone JR. IgG4-related systemic disease and lymphoplasmacytic aortitis. Arthritis Rheum 2009; **60**:3139–45.
18 Yamamoto M, Ohara M, Suzuki C *et al.* Elevated IgG4 concentrations in serum of patients with Mikulicz's disease. Scand J Rheumatol 2004; **33**:432–3.
19 Masaki Y, Dong L, Kurose N *et al.* Proposal for a new clinical entity, IgG4-positive multiorgan lymphoproliferative syndrome: analysis of 64 cases of IgG4-related disorders. Ann Rheum Dis 2009; **68**:1310–5.
20 Umehara H, Okazaki K, Masaki Y *et al.* A novel clinical entity, IgG4-related disease (IgG4RD): general concept and details. Mod Rheumatol 2012; **22**:1–14.
21 Matsui S, Yamamoto H, Minamoto S, Waseda Y, Mishima M, Kubo K. Proposed diagnostic criteria for IgG4-related respiratory disease. Respir Investig 2016; **54**:130–2.
22 Taniguchi T, Ko M, Seko S *et al.* Interstitial pneumonia associated with autoimmune pancreatitis. Gut 2004; **53**:770; author reply 770–1.
23 Matsui S, Hebisawa A, Sakai F *et al.* Immunoglobulin G4-related lung disease: clinicoradiological and pathological features. Respirology 2013; **18**:480–7.
24 Miyake K, Moriyama M, Aizawa K *et al.* Peripheral $CD4^+$ T cells showing a Th2 phenotype in a patient with Mikulicz's disease associated with lymphadenopathy and pleural effusion. Mod Rheumatol 2008; **18**:86–90.
25 Rossi G, Marchioni A, Guicciardi N, Cadioli A, Cavazza A. Recurrent pleural and pericardium effusions in a white woman with IgG4-related syndrome. Am J Surg Pathol 2009; **33**:802–3.
26 Yamamoto H, Suzuki T, Yasuo M *et al.* IgG4-related pleural disease diagnosed by a re-evaluation of chronic bilateral pleuritis in a patient who experienced occasional acute left bacterial pleuritis. Intern Med 2011; **50**:893–7.
27 Sekiguchi H, Horie R, Utz JP, Ryu JH. IgG4-related systemic disease presenting with lung entrapment and constrictive pericarditis. Chest 2012; **142**:781–3.
28 Ishida M, Hodohara K, Furuya A *et al.* Concomitant occurrence of IgG4-related pleuritis and periaortitis: a case report with review of the literature. Int J Clin Exp Pathol 2014; **7**:808–14.
29 Choi JH, Sim JK, Oh JY *et al.* A case of IgG4-related disease presenting as massive pleural effusion and thrombophlebitis. Tuberc Respir Dis (Seoul) 2014; **76**:179–83.
30 Waheed W, Nickerson J, Ambaye AB, Babi MA, Tandan R. IgG4-related neuromyopathy associated with recurrent pleural effusion. J Clin Neuromuscul Dis 2015; **16**:210–9.
31 Kojima M, Nakazato Y, Kaneko Y, Sugihara S, Masawa N, Nakamura N. Cytological findings of IgG4-related pleural effusion: a case report. Cytopathology 2013; **24**:338–40.
32 Corcoran JP, Culver EL, Psallidas I *et al.* A 63-year-old man with a recurrent right-sided pleural effusion. Thorax 2015; **70**: 504–7.
33 El Solh AA, Abdo T, Pineda L, Ramadan F, Berbary E. A longitudinal study of idiopathic exudative lymphocytic pleural effusion in older people. J Am Geriatr Soc 2005; **53**:1957–60.
34 Bintcliffe OJ, Hooper CE, Rider IJ *et al.* Unilateral pleural effusions with more than one apparent etiology. A prospective observational study. Ann Am Thorac Soc 2016; **13**:1050–6.
35 DePew ZS, Verma A, Wigle D, Mullon JJ, Nichols FC, Maldonado F. Nonspecific pleuritis: optimal duration of follow-up. Ann Thorac Surg 2014; **97**:1867–71.
36 Janssen JP, Ramlal S, Mravunac M. The long-term follow up of exudative pleural effusion after nondiagnostic thoracoscopy. J Bronchol 2004; **11**:169–74.
37 Pifferi M, Di Cicco M, Bush A, Caramella D, Chilosi M, Boner AL. Uncommon pulmonary presentation of IgG4-related disease in a 15-year-old boy. Chest 2013; **144**:669–71.
38 Deshpande V, Zen Y, Chan JK *et al.* Consensus statement on the pathology of IgG4-related disease. Mod Pathol 2012; **25**: 1181–92.
39 Chari ST. Diagnosis of autoimmune pancreatitis using its five cardinal features: introducing the Mayo Clinic's HISORt criteria. J Gastroenterol 2007; **42**:39–41.
40 Mimura Y, Kabat EA, Tanaka T, Fujimoto M, Takeo K, Nakamura K. Microheterogeneity of mouse antidextran monoclonal antibodies. Electrophoresis 1995; **16**:116–23.
41 Mimura Y, Nakamura K, Tanaka T, Fujimoto M. Evidence of intra- and extracellular modifications of monoclonal IgG polypeptide chains generating charge heterogeneity. Electrophoresis 1998; **19**:767–75.
42 Katzmann JA, Clark RJ, Abraham RS *et al.* Serum reference intervals and diagnostic ranges for free kappa and free lambda immunoglobulin light chains: relative sensitivity for detection of monoclonal light chains. Clin Chem 2002; **48**:1437–44.
43 Bradwell AR, Carr-Smith HD, Mead GP *et al.* Highly sensitive, automated immunoassay for immunoglobulin free light chains in serum and urine. Clin Chem 2001; **47**:673–80.
44 Drayson M, Tang LX, Drew R, Mead GP, Carr-Smith H, Bradwell AR. Serum free light-chain measurements for identifying and monitoring patients with nonsecretory multiple myeloma. Blood 2001; **97**:2900–2.
45 Bradwell AR, Carr-Smith HD, Mead GP, Harvey TC, Drayson MT. Serum test for assessment of patients with Bence Jones myeloma. Lancet 2003; **361**:489–91.
46 Fujinaga Y, Kadoya M, Kawa S *et al.* Characteristic findings in images of extra-pancreatic lesions associated with autoimmune pancreatitis. Eur J Radiol 2010; **76**:228–38.
47 Hamano H, Arakura N, Muraki T, Ozaki Y, Kiyosawa K, Kawa S. Prevalence and distribution of extrapancreatic lesions complicating autoimmune pancreatitis. J Gastroenterol 2006; **41**:1197–205.
48 Umehara H, Nakajima A, Nakamura T *et al.* IgG4-related disease and its pathogenesis-cross-talk between innate and acquired immunity. Int Immunol 2014; **26**:585–95.
49 Aalberse RC, Stapel SO, Schuurman J, Rispens T. Immunoglobulin G4: an odd antibody. Clin Exp Allergy 2009; **39**: 469–77.
50 van der Neut Kolfschoten M, Schuurman J, Losen M *et al.* Anti-inflammatory activity of human IgG4 antibodies by dynamic Fab arm exchange. Science 2007; **317**:1554–7.
51 Cornell LD, Chicano SL, Deshpande V *et al.* Pseudotumors due to IgG4 immune-complex tubulointerstitial nephritis associated with autoimmune pancreatocentric disease. Am J Surg Pathol 2007; **31**:1586–97.

52 Deshpande V, Chicano S, Finkelberg D *et al*. Autoimmune pancreatitis: a systemic immune complex mediated disease. Am J Surg Pathol 2006; **30**:1537–45.
53 Sah RP, Chari ST. Serologic issues in IgG4-related systemic disease and autoimmune pancreatitis. Curr Opin Rheumatol 2011; **23**:108–13.
54 Aggarwal R, Sequeira W, Kokebie R *et al*. Serum free light chains as biomarkers for systemic lupus erythematosus disease activity. Arthritis Care Res (Hoboken) 2011; **63**:891–8.
55 Gottenberg JE, Aucouturier F, Goetz J *et al*. Serum immunoglobulin free light chain assessment in rheumatoid arthritis and primary Sjogren's syndrome. Ann Rheum Dis 2007; **66**:23–7.
56 Grados A, Ebbo M, Boucraut J *et al*. Serum immunoglobulin free light chain assessment in IgG4-related disease. Int J Rheumatol 2013; **2013**:426759.
57 Nei T, Urano S, Itoh Y *et al*. Light chain (kappa/lambda) ratio of GM-CSF autoantibodies is associated with disease severity in autoimmune pulmonary alveolar proteinosis. Clin Immunol 2013; **149**:357–64.
58 Skvaril F, Morell A, Barandun S. The IgG subclass distribution in 659 myeloma sera. Vox Sang 1972; **23**:546–51.
59 Aucouturier P, Preud'Homme JL. Subclass distribution of human myeloma proteins as determined with monoclonal antibodies. Immunol Lett 1987; **16**:55–7.
60 Redegeld FA, van der Heijden MW, Kool M *et al*. Immunoglobulin-free light chains elicit immediate hypersensitivity-like responses. Nat Med 2002; **8**:694–701.
61 Kaplan B, Livneh A, Sela BA. Immunoglobulin free light chain dimers in human diseases. ScientificWorldJournal 2011; **11**: 726–35.
62 Gajewska ME, Rychwicka-Kielek BA, Sorensen K, Kubik M, Hilberg O, Bendstrup E. Immunoglobulin G4-related pleuritis - a case report. Respir Med Case Rep 2016; **19**: 18–20.
63 Khosroshahi A, Wallace ZS, Crowe JL, *et al*. International consensus guidance statement on the management and treatment of IgG4-related disease. Arthritis Rheumatol 2015; **67**: 1688–99.

労災疾病臨床研究事業費補助金

悪性中皮腫に対するヒト化抗CD26抗体を基盤とする
安全かつ有効な新規併用療法の確立

平成29年度　総括・分担研究報告書

平成 30 年 3 月 31 日発行

発行：研究代表者　森本　幾夫
〒113-8421　東京都文京区本郷 2-1-1
順天堂大学大学院医学研究科　免疫病・がん先端治療学講座
TEL：03-3868-2310